Differential spreading along the NE Atlantic ridge system and post-breakup deformation of the adjacent continental margins

Eline Le Breton

MÉMOIRES GÉOSCIENCES RENNES

Eline LE BRETON

Differential spreading along the NE Atlantic ridge system and post-breakup deformation of the adjacent continental margins

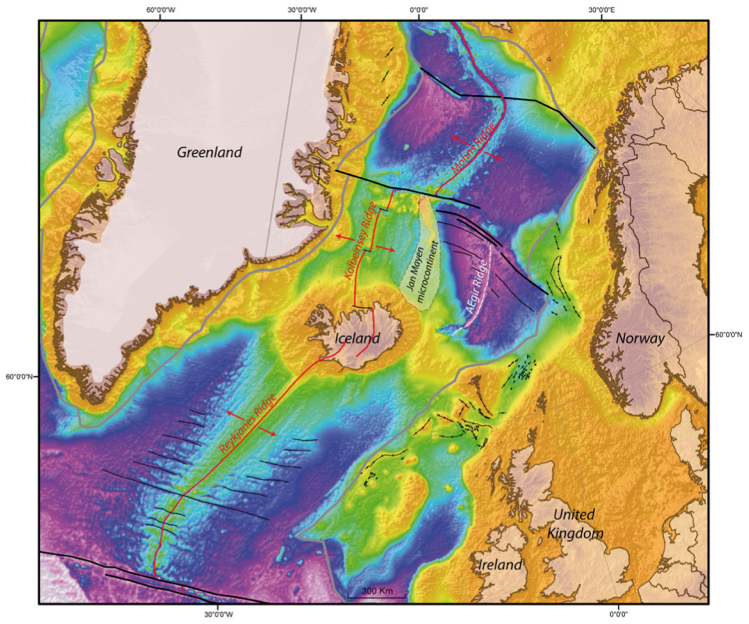

Thèse de l'Université de Rennes 1

n° 141

2012

N° d'ordre : 4435 **ANNÉE 2012**

THÈSE / UNIVERSITÉ DE RENNES 1
sous le sceau de l'Université Européenne de Bretagne

pour le grade de

DOCTEUR DE L'UNIVERSITÉ DE RENNES 1

Mention : Sciences de la Terre

Ecole doctorale Sciences de la Matière, Rennes

présentée par

Eline LE BRETON

préparée à l'unité de recherche UMR 6118
Géosciences Rennes
Université Rennes 1

Differential spreading along the NE Atlantic ridge system and post-breakup deformation of the adjacent continental margins

Thèse soutenue à Rennes le 26.03.2012

devant le jury composé de :

Haakon FOSSEN
Professeur, University of Bergen / *rapporteur*

Jean-Pierre GRATIER
Physicien CNAP, ISTerre, Université de Grenoble / *rapporteur*

Denis GAPAIS
D.R. CNRS, Université Rennes 1 / *examinateur*

Gavin LEWIS
Team Leader, Chevron Onshore Europe / *examinateur*

Peter R. COBBOLD
D.R. Emérite CNRS, Université Rennes 1 / *directeur de thèse*

Olivier DAUTEUIL
D.R. CNRS, Université Rennes 1 / *co-directeur de thèse*

Préface

Cette thèse a été financée par l'entreprise américaine CHEVRON. De ce fait, le manuscrit est rédigé dans son intégralité en anglais. Cependant, un résumé détaillé en français de la problématique de cette thèse, de la méthodologie utilisée et des principaux résultats et perspectives est proposé en début de manuscrit. Les principaux résultats de cette thèse sont présentés sous la forme de deux articles scientifiques, l'un en révision dans la revue *Tectonics* et l'autre en révision dans la revue *Journal of the Geological Society of London*. Je remercie mes co-auteurs pour leurs contributions, sans lesquelles ce travail n'aurait pas été possible.

Remerciements

Je tiens tout d'abord à remercier les membres du jury, Haakon Fossen, Jean-Pierre Gratier, Denis Gapais et Gavin Lewis, d'avoir accepté de juger ce travail.

Je tiens à remercier tout particulièrement mon directeur de thèse, Peter R. Cobbold, de m'avoir proposé ce sujet de thèse. Merci Peter, pour ton enthousiasme et pour ton soutien tout au long de la thèse. J'ai beaucoup apprécié nos discussions, scientifiques mais aussi culturelles tout particulièrement lors de notre mission de terrain en Ecosse. J'ai beaucoup appris et je t'en remercie. Je souhaite remercier également Olivier Dauteuil, mon co-directeur de thèse, qui m'a suivi depuis mon arrivée au sein du laboratoire Géosciences Rennes, en Master 2. Merci Olivier, pour ton soutien et tes conseils.

Je souhaite remercier également Gavin Lewis et Peter Connolly de Chevron, d'avoir financé ce projet de thèse et de m'avoir donné l'opportunité de venir travailler au sein de l'entreprise Chevron, à Houston, pendant trois mois. Cette expérience en entreprise fut très enrichissante. J'en profite pour remercier toutes les personnes que j'ai rencontrées à Chevron et qui m'ont encadrées au cours de mes deux stages, notamment Matt Laroche et Betty Johnson, merci aux collègues et amies qui m'ont permis de passer un excellent séjour (même avec 40°C et 99.9% d'humidité !), merci donc à Anastasia, Kelley et Josie (qui m'ont fait découvrir le rodéo, les ladies night, la danse country à Austin et la Nouvelle Orléans !), merci aussi à Tess, Cherie, Rick, Stewart, Robert, Sara, Julia… et pardon à tous ceux que j'oublie…

J'ai réalisé ma thèse principalement au sein du laboratoire Géosciences Rennes (UMR6118, CNRS et Université Rennes 1). Je tiens donc à remercier tous les membres du laboratoire pour leur aide et la bonne ambiance au labo, ce qui m'a permis de réaliser cette thèse dans les meilleures conditions possibles. Merci à Pierrick Roperch et Delphine Rouby pour leur aide en modélisation et leurs remarques constructives qui m'ont permis d'améliorer significativement mes modèles. Merci également à toute l'équipe enseignante de Géosciences Rennes avec qui j'ai eu le plaisir de travailler au cours de mon monitorat et de mon ATER, merci à Jacques, Cécile, Erwan, Pierre, Philippe B., Jean-Pierre, Pavel, Romain, Thierry, Jean et Michel, sans oublier les gestionnaires de l'enseignement Jean, Aurore et Aline, merci pour

votre gentillesse et votre bonne humeur ! Merci à Marie-Paule et Chantal pour leur efficacité à toute épreuve ! Merci également aux bibliothécaires Isabelle et Catherine, et merci à Eddie. Merci aux permanents avec lesquels j'ai eu le plaisir de discuter de sciences et d'autres à l'occasion de repas ou apéros… merci à Marc P., Marc J., Laurent H., Kerry, Gilles, Christian, François, Stéphane, Annick C., Sylvie, Jean-Noël, Marie-Pierre, Yann, Annick…

Bien sûr, trois ans de thèse c'est aussi trois ans de super moments entre amis, trois ans de rigolades, de super soirées et de coaching pour tenir le coup ! Tout d'abord merci au meilleur bureau qui soit, le 211 forcément : merci aux « anciens » Nuno et Guillaume, merci aux M2, Seb et Lucie, et un merci spécial à Gwen (attention au compactus !) et Alain (je crois que je te dois toujours une guiness pour m'avoir « sauvé la vie » sur cette fameuse « autoroute » en Ecosse!). Merci pour tous ces bons souvenirs et rigolades dans le bureau, on se fera un TLMVPSP avant que je parte quand même ! Un merci spécial à Fabou et Gwen pour votre aide la veille de mon rendu de thèse!! Merci à tous les doctorants, M2, post-docs, ATER et jeunes chercheurs pour tous ces bons souvenirs, un grand merci à Pipo (j'ché pas dire… c'était juste super cheval !) et Marie (vive Jane !) ; merci aux copains de promo : Romain et Jeanne (à quand le prochain karaoke ?), Nathan (on l'a fait, yes!!), Cécile (merci pour le coaching via hotmail !), Dédé, Guigui, Laure ; merci à la tarot team : Cloclo et Gillou, Mélo, J², Romain, Lorraine, Mélanie (on se retrouve sur Toox !) ; merci à Fabou, Anne-Claire, Tits, Justine, Morgane, Gloria, JL, JC, Laurie, Sylvia, Emilie, Sam, Paul, Camille, Roman, Lena ; merci aux « anciens » : Céline, Guilhem, Nico, Dadou, Fabien, Erwan (Linux, mon sauveur !), Nol, Blaise, François, Christelle, Vincent, Antoine; sans oublier les copains du bât 14B et du 3e: *Grazie mille* Pietro, Stéphane, Etienne, Morgane, Reb, Clément, Seb, Laure, Alex, Delphine, Quino, Jo, Sarah, Tanguy, Laurent, Pascal, Jérémy, Thibault, Maria, Antoine, Jérôme… Merci à tous !

Et enfin, un grand merci à ma famille et aux amis de Caen (Cyrielle et JB, Angélique et Romain, Emilie, Sandrine) que la thèse m'a un peu empêché de voir ces derniers temps, mais on va rattraper ça ! Et une spéciale dédicace à Christoff, sans qui je ne me serais jamais lancée dans une telle aventure et qui m'a soutenu pendant toutes ces années, alors merci pour tout !

Résumé en français

L'ouverture différentielle de l'océan Atlantique Nord-Est et ses effets sur les déformations post-break up des marges continentales

---

1- Problématique et objectifs de la thèse

La théorie de la tectonique des plaques est fondée sur l'hypothèse que les déformations de la lithosphère sont induites par la dynamique interne de la Terre. Cette dynamique est à l'origine du découpage de la lithosphère en un certain nombre de plaques rigides qui se déplacent sur l'asthénosphère moins visqueuse (e.g. *Holmes*, 1944 ; *Hess*, 1962 ; *McKenzie and Parker*, 1967 ; *Morgan*, 1968). La frontière divergente entre deux plaques qui s'éloignent l'une de l'autre correspond à une ride océanique, lieu de création de la lithosphère océanique (e.g. *Dietz*, 1961 ; *Hess*, 1962 ; *Vine and Matthews*, 1963). La zone de transition entre la croûte continentale (~40km d'épaisseur) et la croûte océanique (~7km d'épaisseur) est appelée marge continentale. Elle est dite « passive » lorsqu'il n'y a pas de subduction et est considérée comme tectoniquement inactive (e.g. *McKenzie*, 1978). On retrouve ce type de marges aux bordures de l'océan Atlantique (e.g. *Mitchell and Reading*, 1969).

Mais, lorsque l'on étudie l'ouverture de cet océan et la structure de ses marges, on se rend compte des limites de ce modèle dit de plaque « rigide » et de marge « passive ». En effet, les premières reconstructions cinématiques de l'ouverture océanique utilisant de grandes plaques rigides montrent d'importantes anomalies (écarts ou recouvrements des plaques) (e.g. *Bullard et al.,* 1965). Les meilleures reconstructions cinématiques s'obtiennent lorsque (1) l'on prend en compte des déformations continentales intraplaques (e.g. Amérique du Sud/Afrique ; e.g. *Torsvik et al., 2009*) et que (2) l'on subdivise les grandes plaques (e.g. Amérique du Nord/Europe) en plusieurs sous-plaques (Reykjanes/Jan Mayen/Mohns pour l'Atlantique Nord-Est ; e.g. *Gaina et al.*, 2009) séparées par des failles transformantes (**Figure 1**). De plus, des reconstructions cinématiques ont montré que la vitesse d'ouverture

océanique varie de part et d'autre de la zone transformante de Jan Mayen (JMFZ) dans l'Atlantique Nord-Est (*Mosar et al.*, 2002), entrainant des mouvements importants des sous-plaques les unes par rapport aux autres.

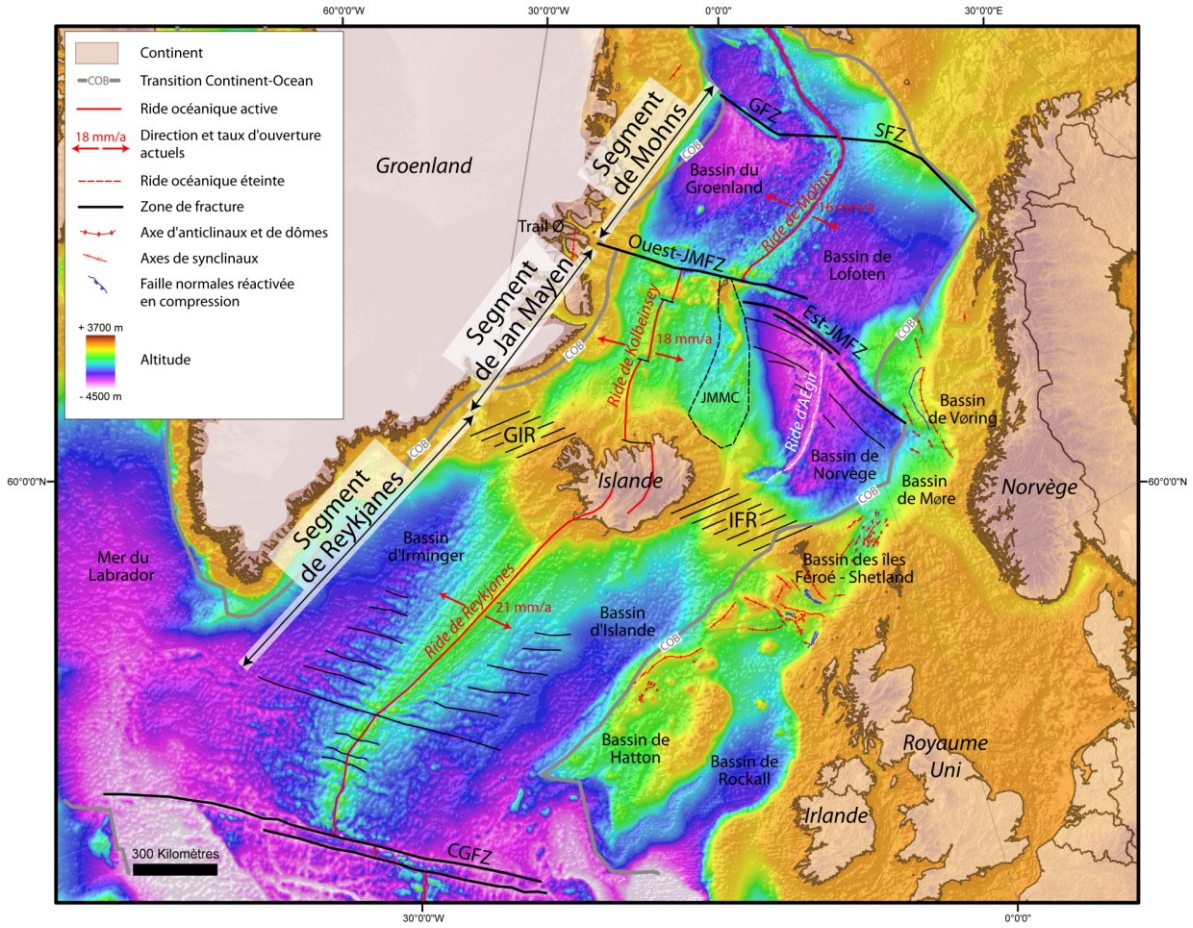

Figure 1. *Principales structures tectoniques de l'Atlantique Nord-Est sur une carte topographique et bathymétrique (ETOPO1). Les directions et taux d'ouverture sont d'après Mosar et al. (2002), la transition continent-océan d'après Olesen et al. (2007) et Gaina et al. (2009), et les déformations compressives sur les marges d'après Jonhson et al. (2005), Doré et al. (2008) et Tuitt et al. (2010). Abréviations du nord au sud : GFZ, Greenland Fracture Zone; SFZ, Senja Fracture Zone; JMFZ, Jan Mayen Fracture Zone; JMMC, Jan Mayen Microcontinent; GIR, Greenland-Iceland Ridge; IFR: Iceland-Faeroe Ridge; CGFZ, Charlie Gibbs Fracture Zone.*

L'océan Atlantique Nord-Est s'est ouvert entre le Groenland et le Nord-Ouest de l'Europe au Cénozoïque. Cette ouverture fut très complexe, notamment entre l'Islande et la zone de fracture de Jan Mayen. En effet, le microcontinent de Jan Mayen (JMMC) s'est formé progressivement au cours de l'ouverture océanique et s'est séparé totalement du Groenland au

cours de l'Oligocène. Ceci a entrainé un étirement important de la croûte continentale entre le microcontinent et le Groenland, qui a atteint l'océanisation au cours de l'Oligocène et ainsi l'extinction de l'ouverture océanique le long de la ride d'Aegir, à l'Est, et la formation d'une nouvelle ride à l'ouest du JMMC, la ride de Kolbeinsey (**Figure 1**). De plus, l'océan Atlantique Nord-Est est en interaction avec le point chaud situé actuellement sous l'Islande, responsable de la formation du fort relief de cette île (**Figure 1**). La position de ce point chaud sous la marge Est-groenlandaise, puis progressivement sous la ride de Reykjanes suggère qu'il a eu rôle important dans la formation du JMMC (e.g. *Müller et al.,* 2001). La marge continentale européenne a, quant à elle, subi des déformations compressives au Cénozoïque pendant l'ouverture océanique (e.g. *Doré et al.*, 2008 ; **Figure 1**). Les mécanismes à l'origine de ces déformations compressives sont sources de nombreux débats au sein de la communauté scientifique. Différentes hypothèses sont proposées telles que (1) la poussée compressive Alpine (e.g. *Boldreel and Andersen*, 1993, 1998), (2) la poussée due à la ride océanique ou « Ridge-Push » (e.g. *Boldreel and Andersen*, 1993, 1998 ; *Doré and Lundin*, 1996), (3) les processus d'isostasie-climat-érosion (e.g. *Nielsen et al.*, 2009), (4) l'interaction avec le point chaud islandais (e.g. *Lundin and Doré*, 2002 ; *Doré et al.*, 2008) et/ou (5) l'ouverture différentielle de l'Atlantique Nord-Est (e.g. *Mosar et al.*, 2002).

L'objectif de cette thèse est d'apporter des informations qualitatives et quantitatives sur les possibles causes et les conséquences d'une ouverture différentielle de l'océan Atlantique Nord-Est, et sa signification en termes de dynamiques lithosphérique et mantellique (développement structural et déformations post-break up des marges; effets des points chauds mantelliques). Les principales questions auxquelles je tâcherai de répondre au travers de cette thèse sont :

- Quelles sont les causes et conséquences d'une ouverture différentielle de l'océan Atlantique Nord-Est ?
- Est-elle responsable des déformations tertiaires observées sur la marge continentale européenne ? Ces déformations se retrouvent-elle dans le continent ?
- Quel est l'impact du point chaud sur l'ouverture océanique et la déformation des marges ?

2- Démarche scientifique et méthodologie

Les chapitres 2 et 3 présentent le contexte géologique de l'étude et la méthode utilisée pour les reconstructions cinématiques de l'ouverture de l'océan Atlantique Nord-Est. Les meilleures reconstructions cinématiques s'obtiennent lorsque l'on subdivise l'Atlantique Nord-Est en segments océaniques (Reykjanes, Jan Mayen et Mohns ; **Figure 1**). J'ai utilisé une méthode de restauration palinspastique afin d'obtenir un modèle cinématique de l'ouverture de cet océan, à partir de données d'anomalies magnétiques et de la géométrie des zones de fracture. Cette méthode fut développée à Rennes pour restaurer des surfaces déformées par des failles délimitant des blocs à l'aide une méthode de minimisation par moindres carrés des vides et recouvrements entre éléments (*Cobbold*, 1979), dans les domaines en extension (*Rouby et al.*, 1993), et en compression (*Arriagada et al.*, 2008). Dans le cas de cette étude, les blocs sont limités par les anomalies magnétiques et les zones de fracture et cette méthode revient à minimiser les écarts entre les anomalies magnétiques conjuguées de part et d'autre de la ride. Ainsi, la méthode prend en compte les déformations géodynamiques qui ont pu affecter les isochrones après leur formation ; de plus elle permet une quantification des mouvements relatifs des plaques les unes par rapport aux autres le long des zones transformantes et des zones de fracture. J'ai mené plusieurs tests (en plan/sur sphère, côté ouest de la ride fixe/ côté est de la ride fixe, chapitre 3) pour valider la méthode, prendre en compte l'effet de la sphéricité de la Terre, et améliorer la construction de carte de blocs afin d'obtenir le meilleur agencement des anomalies magnétiques.

J'ai réalisé une synthèse bibliographique à partir de données publiées sur les marges nord-est atlantiques afin de caractériser les déformations ayant affecté ces marges au Tertiaire. J'ai de plus étudié l'éventuelle réactivation de grande failles décrochantes continentales, au travers d'une campagne de terrain en Ecosse, le long de la faille de la Great Glen.

Au cours de mon doctorat, j'ai aussi effectué un stage au sein de l'entreprise Chevron, au cours duquel j'ai travaillé sur l'ouverture océanique de l'Atlantique Sud et plus particulièrement sur la structure de la marge Sud-Est Brésilienne qui était en interaction avec deux points chauds (Tristan da Cunha et Trindade).

Enfin, la comparaison de l'ensemble des résultats a permis de mettre en évidence les effets de l'ouverture océanique différentielle et des panaches mantelliques sur les déformations compressives des marges et continents adjacents.

3- Résultats majeurs

3.1 Ouverture différentielle de l'océan Atlantique Nord-Est

Le chapitre 4 présente un nouveau modèle cinématique de l'Europe, par rapport au Groenland, au cours de l'ouverture océanique de l'Atlantique Nord-Est. Ce modèle prend en compte la formation du JMMC et les déformations de la marge européenne pendant l'ouverture océanique. Ce modèle assure un bon ajustement des anomalies magnétiques de part et d'autre de chaque ride, notamment pour la zone complexe entre l'Islande et la JMFZ (Segment de Jan Mayen). Ce modèle prédit des directions et des taux d'ouverture différents entre les trois segments océaniques. Notamment entre le Chron 24 (52.9 Ma) et le Chron 13 (33.3 Ma) – Chron 8 (26.4), le JMMC s'individualise progressivement entrainant une rotation anti-horaire de 30° du JMMC et une ouverture en V le long de la ride d'Aegir. Ceci est à l'origine d'une rotation horaire (~10°) du côté est de cette ride. Cette ouverture complexe de ce segment océanique par rapport aux deux segments voisins, entrainent des déplacements importants le long des grandes zones transformantes (JMFZ et la Faeroe Fracture Zone, FFZ ; **Figure 2**).

3.2 Conséquences de l'ouverture différentielle sur les marges et continents

Le chapitre 4 présente les estimations des déplacements relatifs entre les segments le long de la JMFZ et de la FFZ et des rotations relatives entre chaque segment. Le modèle prédit une période majeure de déplacement sénestre le long de la FFZ (jusqu'à 45 km) entre le Chron 21 et le Chron 8 (Eocène Moyen – Oligocène Supérieur) et le long de la JMFZ (jusqu'à 20 km) entre le Chron 17 et le Chron 13 (Eocène Supérieur – Oligocène Inférieur) et entre le Chron 8 et le Chron 5 (Miocène). Ces périodes coïncident avec le développement des structures compressives sur la marge continentale des Féroé-Rockall et sur la marge Norvégienne, respectivement. De plus le déplacement sénestre ainsi que la rotation relative entre les segments sont compatibles avec la localisation, la cinétique et l'orientation des structures compressives sur les marges (**Figure 2**).

Le chapitre 5 présente les résultats de la campagne de terrain effectué au Nord-Est de l'Ecosse, au niveau d'affleurements d'âge Jurassique. Cette mission apporte des preuves supplémentaires d'une réactivation post-Jurassique en dextre de la Great Glen Fault (GGF) avec un déplacement estimé à environ 10-18 km. L'âge de réactivation reste assez peu

contraint, mais je suggère que la GGF ait été réactivée entre l'Eocène Supérieur et l'Oligocène Supérieur (*c.* 37 – 26 Ma). Cette période coïncide avec (1) un épisode d'exhumation de l'Ecosse, (2) une phase compressive induite par de l'orogenèse Alpine, (3) un pulse du point chaud Islandais, et surtout (4) avec un déplacement sénestre le long de la FFZ. En effet, un déplacement sénestre le long de la FFZ est compatible avec une réactivation en dextre de la GGF (**Figure 2**).

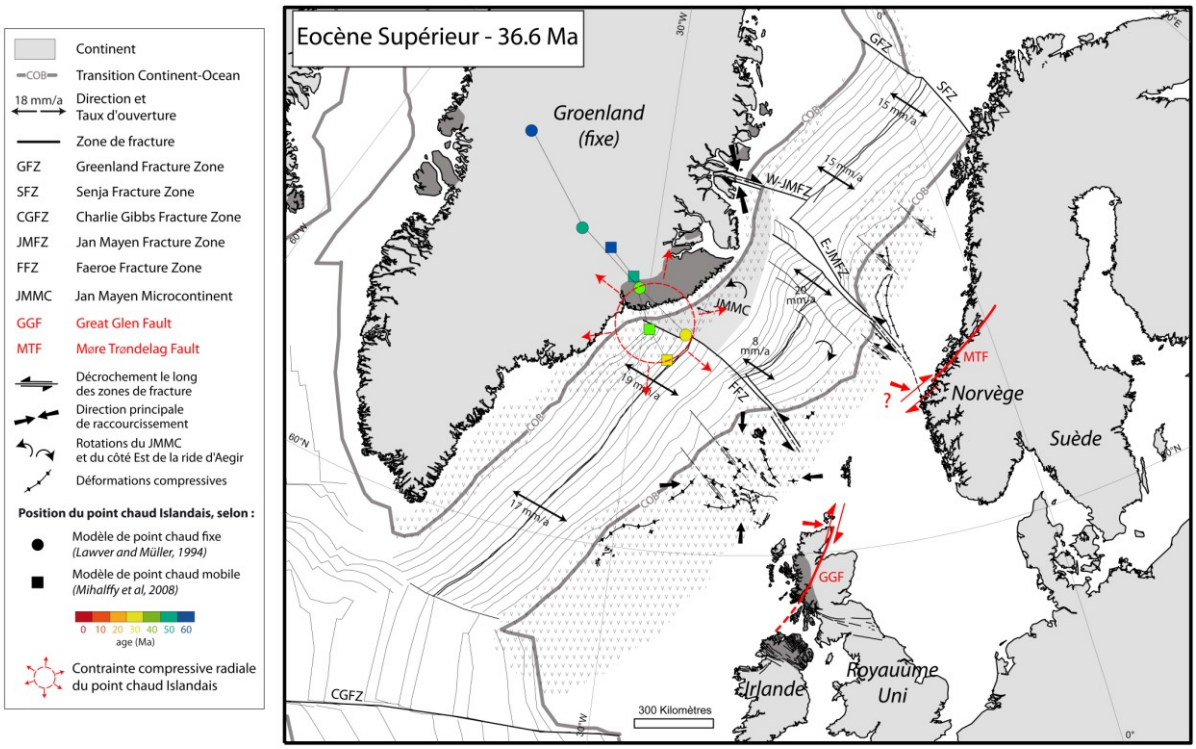

Figure 2. *Positions de l'Europe, du microcontinent de Jan Mayen (JMMC) et du point chaud Islandais, relatives au Groenland fixe, à 36.6 Ma (Eocène Supérieur). Un décrochement sénestre le long de la FFZ et de la JMFZ, est induit par les différences de direction et taux d'ouverture entre les différents segments océaniques et éventuellement par une contrainte radiale compressive du point chaud Islandais, causerait une déformation compressive de la marge Européenne et une réactivation dextre de la GGF, en Ecosse.*

Je suggère donc que l'ouverture océanique différentielle entre les rides de Reykjanes, d'Aegir/Kolbeinsey et de Mohns soit responsable de :

(1) Une réactivation sénestre des zones de fracture orientées NW-SE dans la prolongation de la JMFZ présentes sur la marge norvégienne, entre l'Eocène Supérieur et l'Oligocène

Inférieur et surtout pendant le Miocène, entraînant ainsi le développement de structures compressives sur cette marge.

(2) Une déformation fortement en constriction, dont les directions principales de raccourcissement sont environ NS et EW, un décrochement sénestre le long des zones de fractures orientées NW-SE, et la réactivation de structures préexistantes d'âge Lewisien (de direction NW-SE, NW et EW) et d'âge Calédonien (de direction NE-SW), entre l'Eocène et l'Oligocène Inférieur, entraînant le développement de structures compressives d'orientation variée (NW-SE à NE-SW) au niveau de la marge Féroé-Rockall.

(3) Une réactivation sénestre des zones de fractures orientées NW-SE, subparallèles à la FFZ, permettant très probablement le développement de structures compressives dans le Nord-Est du Bassin des îles Féroés-Sheltland, entre l'Eocène et l'Oligocène.

(4) Une réactivation dextre de la GGF en Ecosse en réponse à un mouvement sénestre le long de la FFZ.

3.3 Comparaison entre Atlantique NE et Atlantique Sud – Influence du point chaud

Les chapitres 4 et 5 discutent de l'influence possible du point chaud Islandais sur l'ouverture différentielle de l'Atlantique Nord-Est. Je suggère en effet que la position de ce point chaud sous la marge Est-Groenlandaise, au voisinage du JMMC à l'Eocène Supérieur et Oligocène, a entraîné la séparation du JMMC du Groenland et les variations résultantes de direction et de taux d'ouverture entre les segments océaniques, provoquant ainsi les déformations compressives des marges. Au Miocène, le point chaud Islandais était sous la ride de Reykjanes, entraînant la formation de l'Islande et du fort relief autour de cette île (Plateau Islandais). Les taux d'ouvertures étaient plus importants le long de la ride de Reykjanes que le long des rides de Kolbeinsey et de Mohns, entraînant des déplacements relatifs le long de la FFZ et de la JMFZ à cette époque. De plus, les contraintes compressives induites par ce point chaud et par le développement du Plateau Islandais ont pu réactiver en sénestre les zones de fracture océaniques et ainsi déformer la marge Européenne au Miocène.

Le chapitre 6 présente une comparaison entre l'Atlantique Nord-Est et l'Atlantique Sud (à l'Est des bassins de Santos et Campos) (**Figure 3**). J'y discute de façon plus générale les impacts possibles des points chauds sur (1) la localisation des rides océaniques, (2) les variations de taux d'ouverture, et (3) la réactivation de structures préexistantes sur les marges continentales. En effet, l'activité magmatique d'un point chaud en interaction avec une marge

continentale semble affaiblir la résistance de cette marge. Ainsi lorsque celle-ci est soumise à des contraintes, ceci favorise la réactivation de structures préexistantes et la déformation de la marge (e.g. Marge sud-est Brésilienne). De plus, l'apport magmatique du point chaud entraîne des augmentations de taux d'ouverture océanique et pourrait localiser l'axe de la ride et provoquer ainsi d'éventuel transfert de ride ou 'ridge-jump' (e.g. entre la ride d'Aegir et la ride de Kolbeinsey dans l'Atlantique Nord-Est). Enfin, les forces d'un panache mantellique pourraient générer des contraintes compressives qui se transmettraient le long de la plaque, réactivant ainsi des structures préexistantes sur la marge continentale adjacente (e.g. contraintes compressives radiales du point chaud Islandais et déformation compressive de la marge Nord-Ouest Européenne).

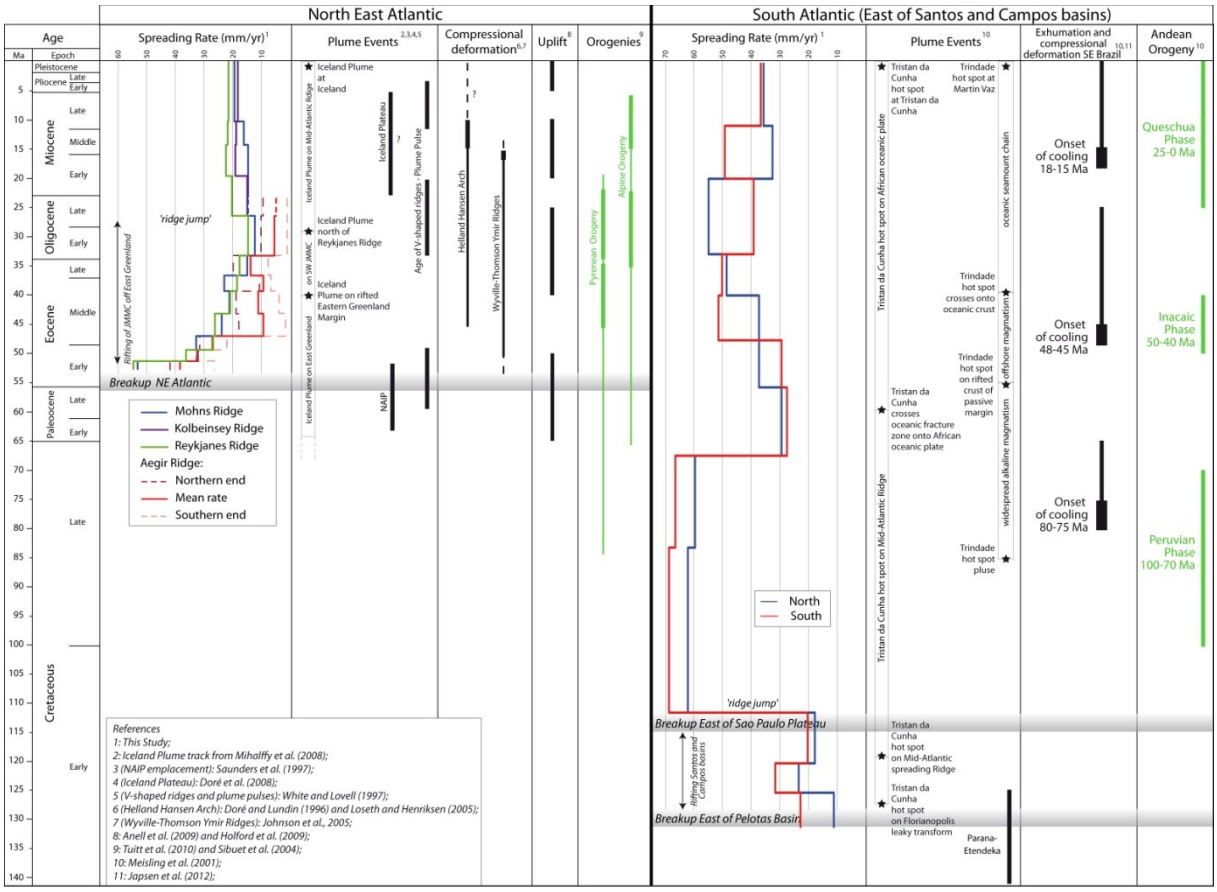

Figure 3. *Diagramme illustrant les variations, au cours du temps, des taux d'ouverture océanique dans l'Atlantique Nord-Est et l'Atlantique Sud (à l'est des bassins de Santos et Campos) et le timing des évènements régionaux (point chaud, déformation compressive, exhumation et orogènes).*

4- Conclusions et Perspectives

Les résultats de cette thèse sont importants pour les études portant sur les mouvements des plaques, les déformations intraplaques et les forces motrices, ainsi que pour l'exploration pétrolière des marges continentales. En effet, ce travail montre que les plaques lithosphériques, notamment leur partie océanique, ne sont pas parfaitement rigides, et que les points chauds et l'expansion des fonds océaniques peuvent avoir une influence significative sur la déformation compressive des marges continentales.

Les marges nord-est Atlantique représentent des cibles pour l'exploration d'hydrocarbures. Cette étude fournit un nouveau modèle cinématique de l'ouverture de l'océan Atlantique Nord-Est et donc une nouvelle interprétation de la paléo-position de l'Europe par rapport au Groenland au moment de la rupture continentale, qui, tous deux, ont des implications pour l'exploration pétrolière des marges conjuguées. De plus, cette étude fournit de nouvelles interprétations des mécanismes à l'origine de la déformation compressive des marges, ces déformations pouvant être responsables de la formation de pièges pétroliers sur la marge européenne ou pouvant modifier la géométrie des pièges préexistants. D'autres études seraient nécessaires pour améliorer pour mieux contraindre la chronologie du développement de ces structures compressives et le taux de raccourcissement. L'activité magmatique des points chauds peut également avoir influencé de façon significative l'histoire thermique des marges, ce qui peut influer sur la production de pétrole dans les bassins. Par conséquent, des études complémentaires seraient utiles pour estimer les influences spatiales et temporelles d'un panache mantellique sur une marge continentale.

Cette étude montre également que l'ouverture océanique différentielle peut avoir réactivé des structures lithosphériques continentales telles que la faille de la Great Glen (GGF) en Ecosse. A l'avenir, des études géochronologiques de basse température permettront de mieux contraindre l'âge de cette réactivation. Un travail similaire le long de la faille de Møre Trøndelag (MTF) en Norvège apporterait de meilleures contraintes sur la relation entre l'ouverture différentielle de l'Atlantique Nord-Est et la réactivation tertiaire de la GGF et de la MTF.

De nombreuses questions émergent de cette étude, telles que : jusqu'où l'ouverture océanique différentielle de l'Atlantique Nord-Est a-t-elle affecté le continent européen ? Quelles sont et d'où viennent les forces exactes à l'origine de la déformation compressive et

l'exhumation des marges continentales ? Quelles sont les forces générées par les panaches mantelliques ? Et enfin, quelle est l'échelle spatiale d'influence des points chauds sur les processus lithosphériques et de surface ?

Références

Anell, I., H. Thybo, and I. M. Artemieva (2009), Cenozoic uplift and subsidence in the North Atlantic region: Geological evidence revisited, *Tectonophysics*, *474*(1-2), 78-105, doi:10.1016/j.tecto.2009.04.006.

Arriagada, C., P. Roperch, C. Mpodozis, and P. R. Cobbold (2008), Paleogene building of the Bolivian Orocline: Tectonic restoration of the central Andes in 2-D map view, *Tectonics*, *27*(6), 1-14, doi:10.1029/2008TC002269.

Boldreel, L. O., and M. S. Andersen (1993), Late Pliocene to Miocene compression in the Faeroe-Rockall area, in *Petroleum Geology of Northwest Europe: Proceedings of the 4th Conference*, edited by J. R. Parker, pp. 1025-1034, Geological Society, London, Petroleum Geology Conference series.

Boldreel, L. O., and M. S. Andersen (1998), Tertiary compressional structures on the Faroe – Rockall Plateau in relation to northeast Atlantic ridge-push and Alpine foreland stresses, *Tectonophysics*, *300*, 13-28.

Bullard, E., J. E. Everett, and a. G. Smith (1965), The Fit of the Continents around the Atlantic, *Philosophical Transactions of the Royal Society A: Mathematical, Physical and Engineering Sciences*, *258*(1088), 41-51, doi:10.1098/rsta.1965.0020.

Cobbold, P. R. (1979), Removal of finite deformation using strain trajectories, *Journal of Structural Geology*, *1*(1), 67-72, doi:10.1016/0191-8141(79)90022-1.

Dietz, R. S. (1961), Evolution by spreading of the sea floor, *Nature, 190*, 854.

Doré, A. G., and E. R. Lundin (1996), Cenozoic compressional structures o n the NE Atlantic margin: nature, origin and potential significance for hydrocarbon exploration, *Petroleum Geology*, *2*, 299-311.

Doré, A. G., E. R. Lundin, N. J. Kusznir, and C. Pascal (2008), Potential mechanisms for the genesis of Cenozoic domal structures on the NE Atlantic margin: pros, cons and some new ideas, in *The Nature and Origin of Compression in Passive Margins*, vol. 306, edited by H. Johnson, A. G. Doré, R. W. Gatliff, R. Holdsworth, E. R. Lundin, and J. D. Ritchie, Geological Society, London, Special Publications, *306*, 1-26.

Gaina, C., L. Gernigon, and P. Ball (2009), Palaeocene – Recent plate boundaries in the NE Atlantic and the formation of the Jan Mayen microcontinent, *Journal of the Geolocal Society, London*, *166*, 601-616, doi:10.1144/0016-76492008-112.

Hess, H. H. (1962), History of ocean basins. *Geological Society of America Bulletin; Petrologic Studies: A Volume to Honour A.F. Buddington*, 559-620.

Holford, S. P., P. F. Green, I. R. Duddy, J. P. Turner, R. R. Hillis, and M. S. Stoker (2009), Regional intraplate exhumation episodes related to plate-boundary deformation, *Geological Society of America Bulletin*, *121*(11-12), 1611-1628, doi:10.1130/B26481.1.

Holmes, Arthur (1944). *Principles of Physical Geology* (1 ed.). Edinburgh: Thomas Nelson & Sons.

Japsen, P., J. M. Bonow, P. F. Green, P. R. Cobbold, D. Chiossi, R. Lilletveit, L. P. Magnavita, and A. Pedreira (2012), Episodic burial and exhumation in NE Brazil after

opening of the South Atlantic, Geological Society of America Bulletin, published online on 13 January 2012 as doi:10.1130/B30515.1.

Johnson, H., J. D. Ritchie, K. Hitchen, D. B. Mcinroy, and G. S. Kimbell (2005), Aspects of the Cenozoic deformational history of the Northeast Faroe − Shetland Basin , Wyville − Thomson Ridge and Hatton Bank areas, in *Petroleum Geology: North-West Europe and Global Perspectives - Proceedings of the 6th Petroleum Geology Conference*, edited by A. G. Doré and B. A. Vining, Geological Society, London, Petroleum Geology Conference series, 6, 993-1007.

Lawver, L. A., and R. D. Müller (1994), Iceland Hotspot track, *Geology*, *22*, 311-314.

Løseth, H., and S. Henriksen (2005), A Middle to Late Miocene compression phase along the Norwegian passive margin, in *Petroleum Geology: North-West Europe and Global Perspectives - Proceedings of the 6th Petroleum Geology Conference*, edited by A. G. Doré and B. A. Vining, Geological Society, London, Petroleum Geology Conference series, *6*, 845 -859.

Lundin, E. R., and A. G. Doré (2002), Mid-Cenozoic post-breakup deformation in the "passive" margins bordering the Norwegian - Greenland Sea, *Marine and Petroleum Geology*, *19*, 79-93.

McKenzie, D. P., and R. L. Parker (1967), The north Pacific, an example of tectonics on a sphere, *Nature, 216*, 1276–80.

McKenzie, D. (1978), Some remarks on the development of sedimentary basins, *Earth and Planetary Science Letters*, *40*, 25-32.

Meisling, K. E., P. R. Cobbold, and V. S. Mount (2001), Segmentation of an obliquely rifted margin, Campos and Santos basins, southeastern Brazil, *AAPG Bull., 85***,** 1903–1924.

Mihalffy, P., B. Steinberger, and H. Schmeling (2008), The effect of the large-scale mantle flow field on the Iceland hotspot track, *Tectonophysics*, *447*(1-4), 5-18, doi:10.1016/j.tecto.2006.12.012.

Mitchell, A. H., and H. G. Reading (1969), Continental margins, geosynclines, and ocean floor spreading, *The Journal of Geology*, *77*(6), 29-646.

Morgan, W. J. (1968), Rises, trenches, great faults, and crustal blocks, *Journal of Geophysical Research, 73,* 1959–82

Mosar, J., G. Lewis, and T. Torsvik (2002), North Atlantic sea-floor spreading rates: implications for the Tertiary development of inversion structures of the Norwegian – Greenland Sea, *Journal of the Geological Society*, *159*, 503-515, doi:110.1144/0016-764901-135.

Müller, R. D., C. Gaina, W. R. Roest, and D. L. Hansen (2001), A recipe for microcontinent formation, *Geology*, *29*(3), 203.

Nielsen, S, K. Gallagher, C. Leighton, N. Balling, L. Svenningsen, B. H. Jacobsen, E. Thomsen, O. B. Nielsen, C. Heilmann-Clausen, D. L. Egholm, M. A. Summerfield, O. R. Clausen, J. A. Piotrowski, M. R. Thorsen, M. Huuse, N. Abrahamsen, C. King, H. Lykke-Andersen (2009) ,The evolution of western Scandinavian topography: A review of Neogene uplift versus the ICE (isostasy–climate–erosion) hypothesis, *Journal of Geodynamics, 47*(2-3), 72-95.

Olesen, O., J. Ebbing, E. Lundin, E. Mauring, J. R. Skilbrei, and T. H. Torsvik (2007), An improved tectonic model for the Eocene opening of the Norwegian – Greenland Sea: Use of modern magnetic data, *Marine and Petroleum Geology*, *24*, 53-66, doi:10.1016/j.marpetgeo.2006.10.008.

Rouby, D., P. R. Cobbold, P. Szatmari, S. Demercian, D. Coelho, and J. A. Rici (1993a), Least-squares palinspastic restoration of regions of normal faulting - application to the

Campos Basin (Brazil), *Tectonophysics*, *221*(3-4), 439-452, doi:10.1016/0040-1951(93)90172-G.

Saunders, A. D., J. G. Fitton, A. C. Kerr, M. J. Norry, and R. W. Kent (1997), The North Atlantic Igneous Province, in *Large Igneous Provinces Continental, Oceanic, and Planetary Flood Volcanism*, edited by J. J. Mahoney and M. F. Coffin, American Geophysical Union, Geophysical Monograph Series, *100*, 45-93.

Sibuet, J-C., S.P. Srivastava, and W. Spakman (2004), Pyrenean orogeny and plate kinematics, *Journal of Geophysical Research*, *109*, B08104.

Torsvik, T.H., S. Rousse, C. Labails, and M. A. Smethurst (2009), A new scheme for the opening of the South Atlantic Ocean and the dissection of an Aptian salt basin. *Geophysical Journal International, 177*, 1315–1333.

Tuitt, A., J. R. Underhill, J. D. Ritchie, H. Johnson, and K. Hitchen (2010), Timing , controls and consequences of compression in the Rockall – Faroe area of the NE Atlantic Margin, in *Petroleum Geology: From Mature Basins to New Frontiers - Proceedings of the 7th Petroleum Geology Conference*, edited by B. A. Vining and S. C. Pickering, Geological Society, London, Petroleum Geology Conference series, *7*, 963-977.

Vine, F. J., and D. H. Matthews (1963). Magnetic anomalies over oceanic ridges. *Nature*, *199*, 947–9.

White, N., and B. Lovell (1997), Measuring the pulse of a plume with the sedimentary record, *Nature*, *387*, 888-891.

Abstract

One of the main assumptions of the theory of plate tectonics is that all lithospheric plates are rigid. However, reconstructions of the opening of the NE Atlantic Ocean, on the basis of two rigid plates (Eurasia and Greenland), lead to gaps and overlaps between the plates. The area between Iceland and the Jan Mayen Fracture Zone (JMFZ) had a complex spreading history, including progressive separation of the Jan Mayen Microcontinent (JMMC) and a ridge jump from the Aegir Ridge to the Kolbeinsey Ridge. Moreover, post-breakup compressional structures developed along the continental margin of NW Europe, but apparently not on the East Greenland Margin. We therefore investigate how compressional deformation of the NW European Margin may have resulted from variations in the direction and rate of sea-floor spreading along the various ridges. In order to reconstruct the complex spreading history of the NE Atlantic and to study the evolution of the European Margin during sea-floor spreading, we have developed a method for palinspastic reconstructions of the opening of an ocean, using magnetic anomalies and fracture zones. The best kinematic reconstructions result from subdividing the NE Atlantic into three oceanic segments: Reykjanes, Jan Mayen and Mohns. The method allows all oceanic segments to spread at a different rate and results in accurate determinations of spreading rates and relative displacements between the segments. The model ensures a good fit of the magnetic anomalies and predicts differences in direction and rate of spreading between the Reykjanes, Kolbeinsey/Aegir and Mohns ridges. This differential sea-floor spreading generated left-lateral slip between the oceanic segments: (1) from Early Eocene to Late Oligocene, along the Faeroe Fracture Zone (FFZ); and (2) from Late Eocene to Early Oligocene, as well as during the Miocene, along the JMFZ. Such left-lateral motion and the relative rotation between the oceanic segments are compatible with the development of inversion structures on the NW European Margin at these times. Field observations of Jurassic outcrops in NE Scotland have provided additional evidences for post-Jurassic right-lateral reactivation of the Great Glen Fault (GGF), under transpression. The period of reactivation may be from Late Eocene to Late Oligocene, which coincides with (1) an exhumation episode in Scotland, (2) intraplate stress from the Alpine Orogeny (3) a pulse of the Iceland Mantle Plume, and (3) left-lateral slip along the FFZ. Such left-lateral slip along the FFZ is compatible with right-lateral reactivation of the GGF. The driving forces may have come from the Iceland Mantle Plume, which was in a suitable position to generate differential sea-floor spreading along the NE Atlantic and resulting deformation of the NW European margin.

Table of contents

Chapter 1

Introduction

1.1 Notions of Plate Tectonics

The theory of plate tectonics provides a framework for large-scale motions of the Earth's upper layer, the lithosphere, and tectonic processes. This theory developed in the 20th century from the concept of continental drift (e.g. *Taylor*, 1910; *Wegener*, 1912), *i.e.* the movement of the Earth's continents relative to each other, but gained acceptance by of the geoscientific community in the 1960s when the concepts of mantle convection (e.g. *Holmes*, 1944; *Hess*, 1962) and sea-floor spreading (e.g. *Dietz*, 1961; *Hess*, 1962) helped to explain continental drift. One of the main assumptions of the theory of plate tectonics is that the outer part of the Earth is in two layers, lithosphere and asthenosphere, these having different mechanical and rheological properties. The lithosphere is cooler, more rigid and loses heat by conduction; while the asthenosphere is hotter, low viscous and transfers heat by convection (*Hess*, 1962). The concept of sea-floor spreading (e.g. *Dietz*, 1961; *Hess*, 1962) implies that a new sea-floor forms at mid-oceanic ridges, spreads away from the ridges as it ages, and subducts at subduction zones. Convection currents in the asthenosphere (*Hess*, 1962) explain the movements of the lithosphere, involving accretion of new lithosphere at mid-oceanic ridges and disappearance of old lithosphere by subduction at ocean trenches (**Figure 1.1**).

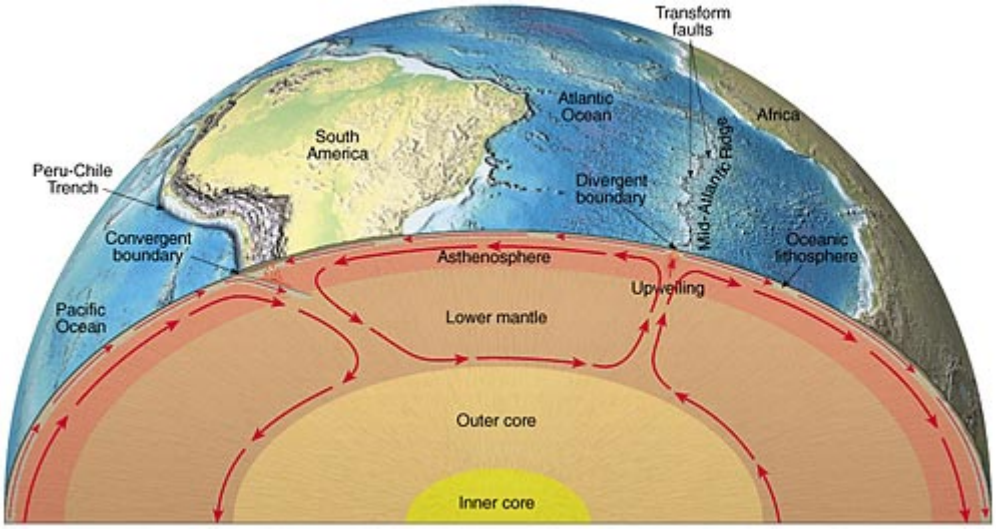

Figure 1.1 *Schematic representation of internal structure of the Earth, mantle convection and plate tectonics (https://sites.google.com/site/reifkecare/).*

The concept of sea-floor spreading became popular after the discovery of magnetic anomalies and their interpretation as markers of sea-floor spreading (*Vine and Matthews*, 1963). Magnetic anomalies are local variations in the Earth's magnetic field compared to a mean field. The Earth's magnetic field is recorded in rocks, which contain magnetic minerals, during their cooling when the temperature drops below the Curie temperature (e.g. basaltic rocks of the oceanic crust) (*Vine and Matthews*, 1963). On the oceanic floor, bands of normal and inverse polarity alternate, parallel to the ridge axis, and age away from the ridge. Chronological scale of magnetic inversions allows calculation of spreading rates and dating of the oceanic crust (*Vine and Wilson*, 1965; *Müller et al.*, 2008) (**Figures 1.2, 1.3**). *Wilson* (1965) also introduced the concept of transform faults that offset magnetic anomalies. The appearance of seismic studies, with the analysis of earthquakes and their mechanisms, also reinforced concept of sea-floor spreading and more generally of plate tectonics (*Isack et al.*, 1968). Earthquakes were observed in the first 100 km of depth confirming that the first layer of the Earth, the lithosphere, had a rigid behaviour and overlies the ductile asthenosphere. Exceptions are for oceanic trenches, where deep earthquakes follow inclined planes (*Wadati*, 1928; *Benioff*, 1949). *Oliver and Isacks* (1967) interpreted these zones as the track of the oceanic lithosphere dipping into the mantle, confirming the concept of sea-floor spreading and movements of the lithosphere.

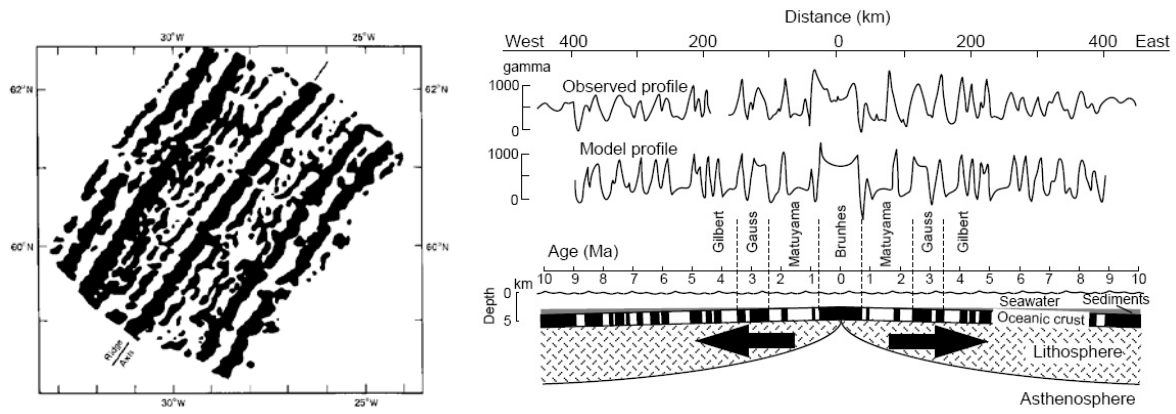

Figure 1.2 *Map of symmetrical magnetic anomalies on both sides of the Reykjanes Ridge (from Vine and Matthews, 1963). Formation of marine magnetic anomalies at an oceanic ridge undergoing sea-floor spreading (from Butler, 1992).*

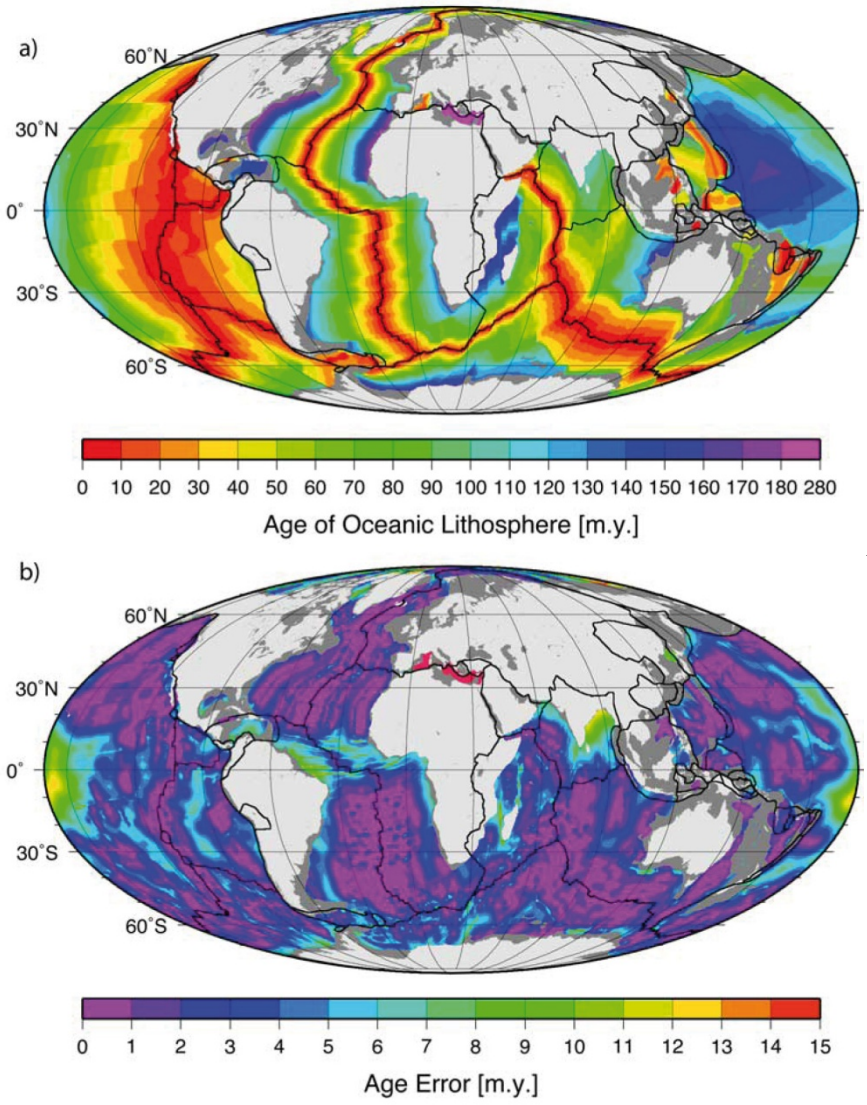

Figure 1.3 ***(****a) Age-area distribution of the ocean floor and (b) gridded age uncertainties, Mollweide projection. Continental margins are medium gray, and continents are light gray. From Müller et al. (2008).*

Wilson (1965), *McKenzie and Parker* (1967), *Morgan* (1968) and *Le Pichon* (1968) introduced the idea of a subdivision of the lithosphere into plates that are perfectly rigid, moving relative to one another. The seven large plates are the Pacific, North American, Eurasian, African, Antarctic, Indo-Australian, and South American (**Figure 1.4**). Smaller plates are the Arabian Plate, the Caribbean Plate, the Nazca Plate off the west coast of South America and the Scotia Plate in the southern Atlantic Ocean. All these plates are rigid shells that move in relation to one another at one of three types of plate boundaries (**Figure 1.4**): (1) Convergent boundaries, at which two plates come together, (2) Divergent boundaries, at which two plates separate, and (3) Transform boundaries, at which two plates slide past one another laterally. The tectonic plates ride on top of the asthenosphere, the solid but less-viscous part of the upper mantle that can flow, and their motion is strongly coupled with convection patterns inside the Earth's mantle (*Hess*, 1962).

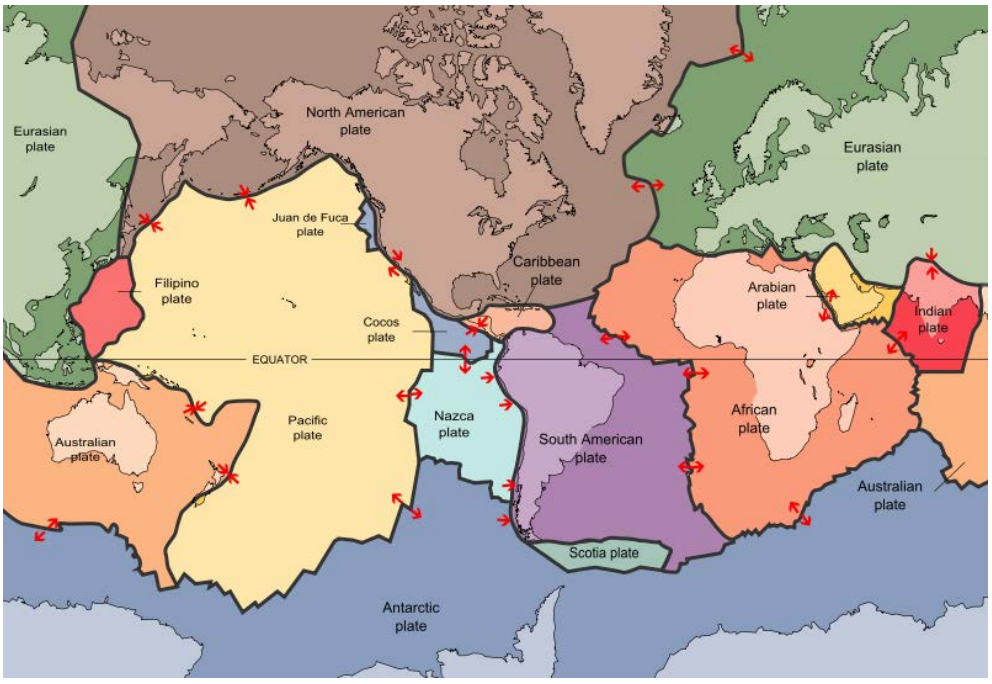

Figure 1.4 *Tectonic plates. Arrows indicate divergent or convergent plate boundaries (from United States Geological Survey).*

Determining the driving forces of plate motion is one of the most important scientific problems and is a subject for debate. *Ziegler* (1993) argues for the dominance of basal shear traction, while others argue that basal shear only plays a small role due to weak coupling between the lithosphere and asthenosphere. *Forsyth and Uyeda* (1975), *Carlson et al.* (1983) and *Richardson* (1992) argue that plate boundary forces are the main driving mechanisms of

plate motion. A major debate concerns a "top-down" versus mantle-driven mechanism for driving the organization of plates (*Anderson*, 2001). Five main forces are suggested to drive plate motion (e.g. *Wessel and Müller*, 2007).

(1) Basal shear traction or basal drag (e.g. *Ziegler*, 1993), shear forces acting at the base of the plates, while popular in the past, this notion has fallen out of favour in preference to other plate-driving mechanisms.

(2) Ridge Push (e.g. *Meijer and Wortel*, 1992; *Richardson*, 1992; *Coblentz and Richardson*, 1995), which originates from a lateral distribution pressure gradient that acts on the entire plate normal to the strike of a mid-oceanic ridge and arises from the isostatic sinking of the oceanic lithosphere away from the mid-oceanic ridge as it cools and densifies (*Wilson*, 1993).

(3) Slab Pull (e.g. *Forsyth and Uyeda*, 1975), which originates from the negative buoyancy of the downgoing dense oceanic lithosphere at subduction zones.

(4) Trench suction (e.g. *Stevenson and Turner*, 1997), a lifting pressure or suction on the upper surface of the downgoing plate caused by an asthenospheric corner flow that is induced by the motion of the descending plate.

(5) Collisional Forces (e.g. *Bott*, 1982), which arises as a result of the frictional forces between the two colliding plates and impede rather than drive plate motions.

In order to understand possible driving forces for plate motions, it may be useful to reconstruct past plate motions.

1.2 Kinematic Reconstructions of Relative Plate Motions and Unsolved Problems

A kinematic reconstruction is a representation of the relative position of one plate relative to another at a given time. A plate is chosen and assumed "stationary" and the position of the surrounding plates is reconstructed for a given time relatively to the stationary plate. In map projection, the stationary plate is represented in its present-day position while the position of the mobile plates is reconstructed using the calculated rotation parameters. We thus measure the relative motion. Because all plates are likely to move on the Earth surface, including the one chosen as a stationary referential, this reference frame is arbitrary.

Bullard et al. (1965) presented the classic work on continental fits around the Atlantic Ocean (**Figure 1.5**). They solved the fit of the circum-Atlantic using a least-squares technique that minimized the overlap and gap between isobaths of previously contiguous continental shelves. This work introduced the use of Eulerian geometry for describing motions of

spherical shells on the Earth. The discovery of magnetic anomalies and transform faults helped in understanding studies of relative plate motions. *Morgan* (1968) described the motion of one plate by a simple rotation between its initial position to its final position. This rotation is defined by an axis passing through the centre of the Earth and an angular velocity (Euler axis and angle; see Chapter 3). Transform faults correspond to small circles centred on the Euler axis, allowing determination of their position.

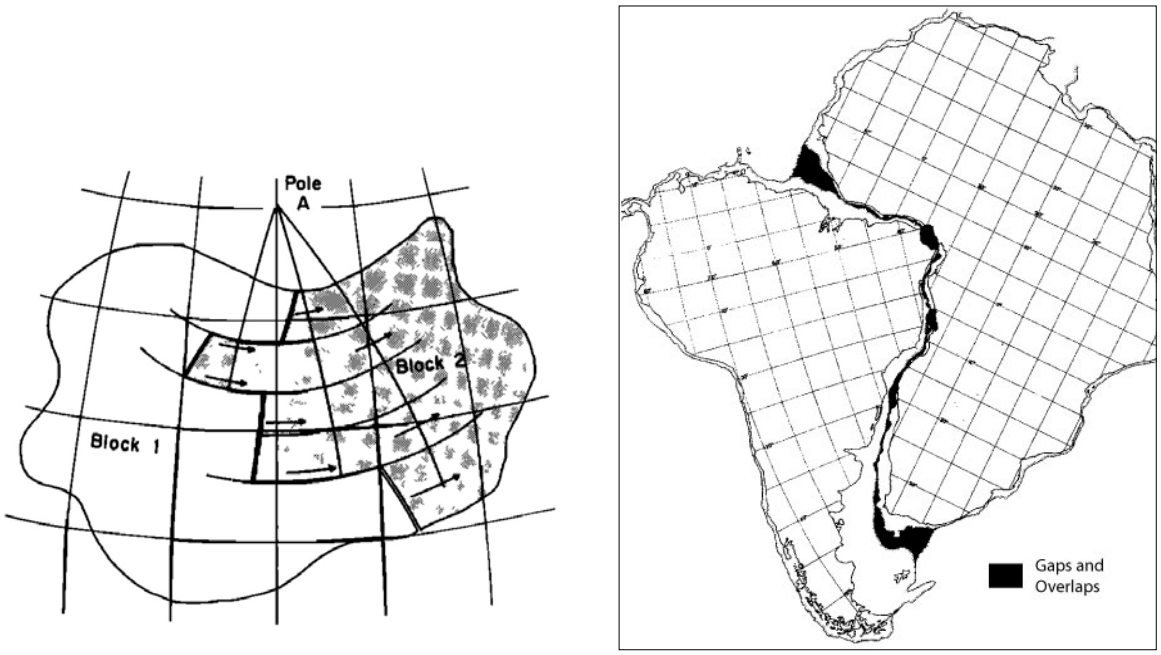

Figure 1.5. *Motion of a block relative to another on sphere is a rotation about a pole; all transform faults on boundary between two blocks are small circles concentric about the pole (Morgan, 1968). Reconstruction of the South Atlantic using two rigid plates shows gaps and overlaps of South American and African plates (Bullard et al., 1965).*

The relative motion of a lithospheric plate relative to another can therefore be described as a rotation that best fits the two plates at a given time. On the basis that magnetic anomalies do not deform since their formation and assuming perfectly rigid plates, *Le Pichon* (1968) and *Pitman and Talwani* (1972) proposed to superpose the conjugate magnetic anomalies of two different plates and calculate from this superposition the position of the rotation axis at the time of their formation. The calculated rotation, which describes the superposition of the conjugate magnetic anomalies, allows reconstructing the relative position of the two plates at this age. This methodology allows reconstructing the position of one plate relative to another for a given age, a stage, and following its trajectory between each stage. The direction of the relative motion between two plates is described locally by fracture zones: they are the geological representation of the trajectories of the plates (*Morgan*, 1968; *Le*

Pichon et al., 1973). The relative motion between two diverging plates can thus be estimated from magnetic anomalies and fracture zones.

One of the main assumptions of the theory of plate tectonics is that all plates are rigid. However, kinematic reconstructions using a rigid-plate system and Euler rotation poles for rotating plates, show overlaps and gaps of the plates (e.g. *Bullard et al.*, 1965) (**Figure 1.5**). Several studies of the North Atlantic opening (e.g. *Unternehr*, 1982; *Srivastava and Tapscott*, 1986; *Rowley and Lottes*, 1988; *Gaina et al.*, 2009) showed that in order to improve the fit, it was necessary to subdivide the main plates. *Bird* (2003) distinguished up to 52 tectonic plates. But even inside microplates, diffuse deformations exist on the continental part of the plates (deformation of sedimentary basins, e.g. *Ziegler*, 1987), and less known on the oceanic part (e.g. *Bull and Scrutton*, 1992). Continental margins appear to be the privileged places for such deformation. Indeed, several studies have shown that post-breakup deformation affects the Atlantic continental passive margins (e.g. *Cobbold et al.*, 2001, 2007; *Leroy et al.*, 2004; *Doré et al.*, 2008; *Japsen et al.*, 2010, 2012;).

In accepting the hypothesis of plate rigidity, we neglect the intraplate deformations. In this thesis, I will focus on the question of non-rigidity of tectonic plates, on the deformation of continental margins and on how to quantify intraplate deformation by kinematic reconstructions of relative plate motion. For this purpose, I have studied the opening of the North East Atlantic Ocean.

1.3 The Studied Area: The North East Atlantic

The NE Atlantic Ocean opened progressively between Greenland and NW Europe during the Cenozoic. Sea-floor spreading occurred along three ridge systems: the Reykjanes Ridge south of Iceland, the Mohns Ridge north of the Jan Mayen Fracture Zone (JMFZ), and the Aegir and Kolbeinsey ridges between Iceland and the JMFZ (**Figure 1.6**). The NE Atlantic Ridge is also in interaction with the Iceland Mantle Plume. Magmatic activity from the plume resulted in the formation of Iceland and significant relief around Iceland.

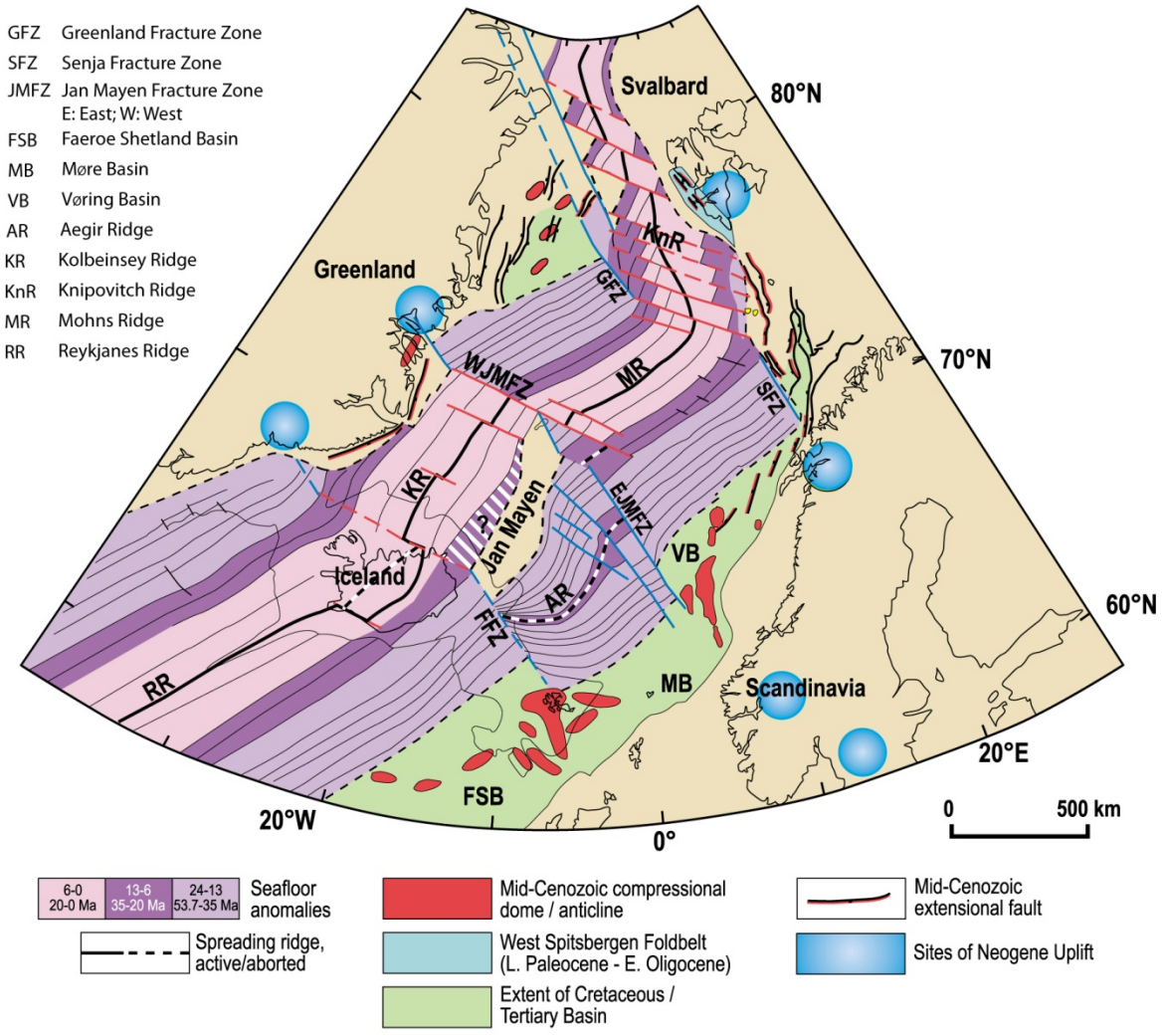

Figure 1.6. *Main tectonic features of NE Atlantic Ocean (Present). Blue fracture zones refer to opening between Chron 24B (53.7 Ma) and Chron 13 (35 Ma), while red fracture zones refer to post-Chron 13 opening. The hachured area west of the Jan Mayen microcontinent indicates possible seafloor. Modified after Lundin and Doré (2002).*

The NE Atlantic had a complex spreading history, especially north of Iceland and south of the JMFZ, where the Jan Mayen Microcontinent (JMMC) formed during sea-floor spreading. Sea-floor spreading progressively ceased along the Aegir Ridge and developed south and west of the JMMC along the Kolbeinsey Ridge (**Figure 1.6**). The Iceland Mantle Plume, south-west of the JMMC and progressively underneath the Reykjanes Ridge (*Lawver and Müller*, 1994), may have had a significant influence on the formation of the microcontinent and on the subsequent ridge transfer from the Aegir Ridge to the Kolbeinsey Ridge (e.g. *Müller et al.*, 2001).

Due to this complex spreading history, kinematic reconstructions using two rigid plates (Europe and Greenland plates) have led to gaps and overlaps between the plates (e.g. *Bullard et al.*, 1965). As described in an earlier section, several authors (e.g. *Unternehr*, 1982; *Srivastava and Tapscott*, 1986; *Rowley and Lottes*, 1988; *Gaina et al.*, 2009) were able to improve the quality of the fit by dividing the ridge system into segments and increasing the number of plates. It remains however difficult to reconstruct a simple spreading history for the Jan Mayen Segment using Euler rotation poles alone.

Moreover, the Faeroe-Rockall Plateau and the Vøring Basin, along the NW European Margin, contains various compressional structures (folds and reverse faults), which formed after continental break-up (*Boldreel and Andersen*, 1993; *Brekke*, 2000; *Davies et al.*, 2004; *Doré et al.*, 2008; *Doré and Lundin*, 1996; *Hitchen*, 2004; *Johnson et al.*, 2005; *Lundin and Doré*, 2002; *Løseth and Henriksen*, 2005; *Ritchie et al.*, 2003, 2008; *Smallwood*, 2004; *Stoker et al.*, 2005; *Tuitt et al.*, 2010). In contrast, along the Greenland margin, there is little evidence for post-breakup deformation, other than some folds of low amplitude (e.g. *Price et al.*, 1997).

The NE Atlantic Ocean is therefore a good area to study the notions of micro-plates and intraplate deformations. Moreover, good magnetic and gravity datasets are available for the NE Atlantic, which allow one to test various methods of kinematic reconstructions.

1.4 Problems and Objectives

The main topic of this thesis is the question of non-rigidity of plate tectonics, intraplate deformation and the influence of mantle plume on sea-floor spreading. The NE Atlantic is a good candidate to study complex spreading history, interaction between a ridge and a mantle plume (the Iceland Mantle Plume) and intraplate deformation such as post-breakup deformation of the NW European Margin.

Mosar et al. (2002) calculated spreading rates along each of the Reykjanes, Aegir and Mohns ridges, showing that there is a significant variation in spreading rates across the JMFZ. They suggested that this differential spreading was responsible for compressional inversion of the Vøring and Faeroe-Shetland Basins rather than the Møre Basin.

Following these observations, the main questions of this thesis are:

- What are the causes and consequences of differential spreading?
- Could it be responsible for Tertiary deformation on the continental margins and continental interiors?

- What is the influence of mantle plumes on sea-floor spreading and on continental margins?

So as to answer these questions, I use a method for palinspastic reconstruction of the opening of the NE Atlantic. This iterative least-squares method minimizes the gaps or overlaps between conjugate magnetic anomalies. In this method, all segments of the NE Atlantic are free to spread at different rates. It also takes into account the possible deformation that occurred since the formation of the magnetic anomalies, and allows calculation of spreading rates and relative displacements between micro-plates during sea-floor spreading. I investigate the possible effect of differential sea-floor spreading on compressional deformation of the NW European continental Margin, obtained from published studies, and of continental interiors. For the latter, I realize a structural analysis along a major lithospheric structure, the Great Glen Fault, Scotland.

I will first present the geological context of this study in Chapter 2, then the method and tests of its application to the opening of the NE Atlantic in Chapter 3. The main results of this thesis are a new kinematic model of the NE Atlantic and a characterization of differential sea-floor spreading along the NE Atlantic ridges and resulting deformation of the adjacent NW European Margin (Chapter 4) and reactivation of continental faults (Chapter 5). Moreover, during this thesis I had the opportunity to work as a trainee at Chevron offices on the opening of the South Atlantic and on the rifting of the Santos Basin that was influenced by magmatic activity from mantle plumes. Therefore, from a comparison of the NE Atlantic and the South Atlantic, I will discuss in Chapter 6 the possible influence of mantle plumes on variation of sea-floor spreading rates and on the structural development of continental margins.

Chapter 2

Geological Context

2.1 North East Atlantic Ocean

The NE Atlantic Ocean lies between Greenland and NW Europe (**Figure 2.1**). As in other oceanic areas, relief of the sea-floor has resulted mainly from spreading along a system of oceanic ridges. In comparison to other oceanic areas, the NE Atlantic shows an atypical wide (thousandth of km) topographic dome (**Figure 2.1**). Significant relief has resulted also from volcanic activity, especially on and around two islands, Iceland and Jan Mayen. This bathymetric-topographic high and the volcanic activity result from the Iceland Mantle Plume, which is presently located beneath Iceland. Another feature, which is specific to the NE Atlantic Ocean, is that its ridge system is complex. For descriptive purposes, we consider it in three parts. From SW to NE, these are the Reykjanes, Jan Mayen and Mohns segments. Of the Reykjanes and Mohns segments, each consists of one ridge only, whereas the Jan Mayen Segment consists of two ridges (Kolbeinsey and Aegir). Between the three segments are systems of transform faults, the Jan Mayen Fracture Zone (JMFZ) in the North and the Greenland-Iceland-Faeroe Fault Zone in the South. The latter, more than the former, is responsible for a notable topographic feature, the Greenland-Iceland-Faeroe Ridge (GIFR). The spreading history of the Jan Mayen Segment is rather complex, due to (1) the cessation of sea-floor spreading along the Aegir Ridge; (2) the development of a new spreading centre, the Kolbeinsey Ridge; and (3) the formation of a microcontinent, the Jan Mayen Microcontinent (JMMC), between these two ridges (**Figure 2.1**).

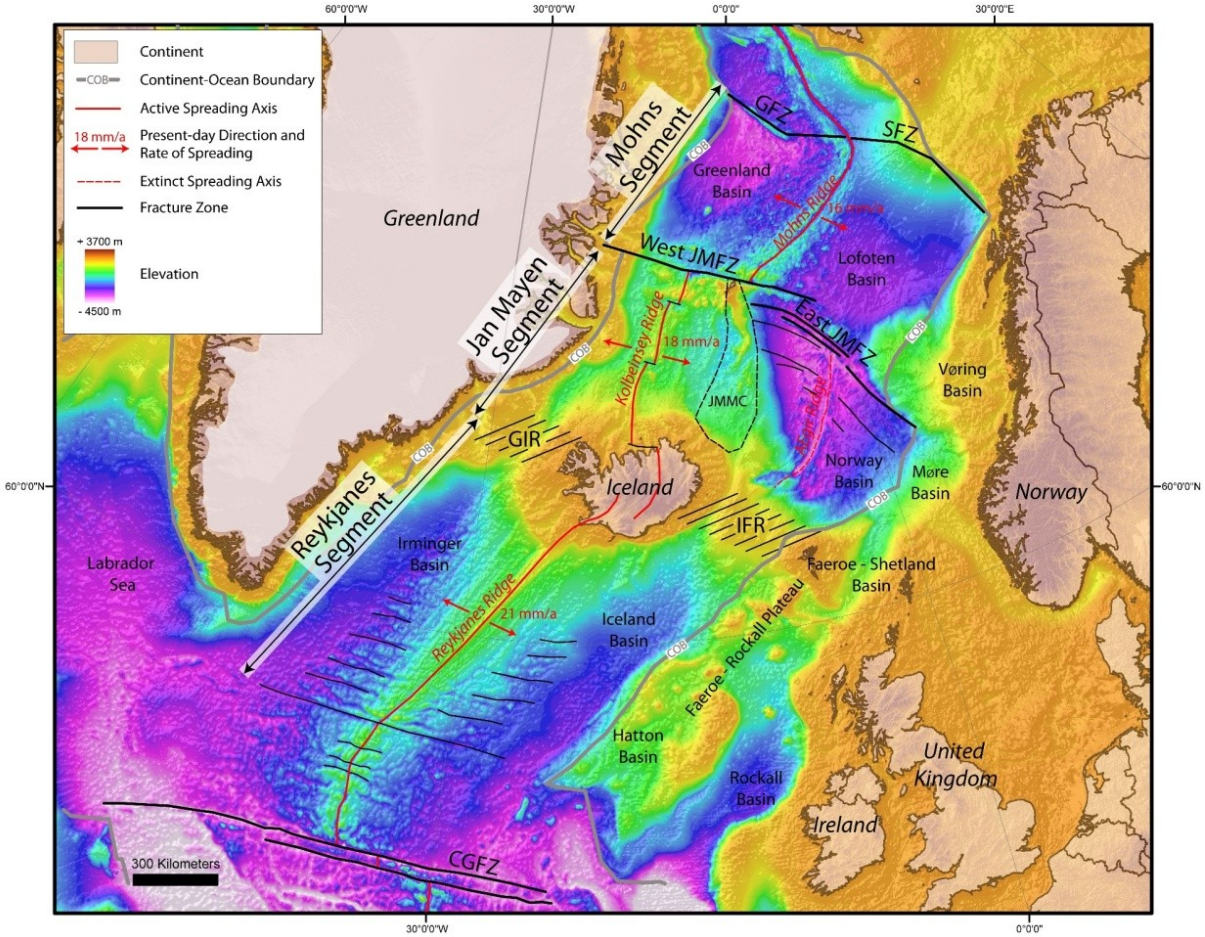

Figure 2.1. *Main tectonic features of the NE Atlantic Ocean on a bathymetric and topographic map (ETOPO1). Present-day spreading rates along Reykjavik, Kolbeinsey and Mohns ridges are from Mosar et al. (2002). Continent-Ocean Boundaries of Europe and Greenland are from Gaina et al. (2009) and Olesen et al. (2007). Abbreviations (North to South): GFZ, Greenland Fracture Zone; SFZ, Senja Fracture Zone; JMFZ, Jan Mayen Fracture Zone (West and East); JMMC, Jan Mayen Microcontinent; GIR, Greenland-Iceland Ridge; IFR: Iceland-Faeroe Ridge; CGFZ, Charlie Gibbs Fracture Zone. Map projection is Universal Transverse Mercator (UTM, WGS 1984, zone 27N).*

2.1.1 Ridge system of North East Atlantic

Sea-floor spreading along the Reykjanes Ridge resulted in the formation of the Irminger and Iceland basins, south of Iceland (**Figure 2.1**), Greenland and Lofoten basins along the Mohns Ridge, north of the JMFZ and south of the Greenland and Senja Fracture Zones. This sea-floor spreading generated characteristic pattern of magnetic anomalies, symmetric and parallel to the ridges since the onset of sea-floor spreading at the end of the Paleocene., The oldest magnetic anomaly is Chron 24 (52.9 Ma, mean age, **Figures 2.2**).

Present-day spreading rates are about 2.1 cm/yr along the Reykjanes Ridge and 1.6 cm/yr along the Mohns Ridge (*Mosar et al.*, 2002). These spreading rates are much slower than those in mid-oceanic ridges in the Pacific where they reach 10 cm/yr (*Herron*, 1972). Therefore, the NE Atlantic ridge system, like the whole mid-Atlantic Ridge, is an example of a slow-spreading mid-oceanic ridge system.

The Aegir Ridge is an extinct ridge of the Jan Mayen Segment, north of the Iceland-Faeroe Ridge and east of the JMMC (**Figure 2.1**). Sea-floor spreading along this ridge resulted in the formation of the Norway Basin, south of the East-JMFZ. Magnetic anomalies along this ridge show significant curvature. Magnetic anomalies are well defined on the eastern side of the ridge than on its western side, close to the JMMC, where it is more difficult to identify the isochrons. The oldest magnetic anomaly identifiable in the Norway Basin is Chron 24 (52.9 Ma) (**Figure 2.2**). The youngest well-identifiable magnetic anomaly is Chron 13 (33.3 Ma) and a younger one, more difficult to distinguish, could be Chron 8 (26.4 Ma). Sea-floor spreading therefore ceased about that time along the Aegir Ridge.

The Kolbeinsey Ridge is the present-day active spreading centre of the Jan Mayen Segment, east of Greenland, west of the JMMC, north of Iceland and south of the JMFZ (**Figure 2.1**). The oldest magnetic anomaly identifiable on both sides of the Kolbeinsey Ridge, from Iceland to the JMFZ, is Chron 6 (19.6 Ma) (**Figure 2.2**). Sea-floor spreading along the Kolbeinsey Ridge started at least since that time, but magnetic anomalies are not well identifiable around Iceland and along the GIFR, which makes it difficult to determine the chronology of sea-floor spreading in these areas. Sea-floor spreading started north of the Reykjanes Ridge, southwest of the JMMC, and propagated progressively northward, toward the JMFZ, separating progressively the JMMC from the Greenland plate (*Bott*, 1985, 1987; *Gaina et al.*, 2009; *Nunns*, 1983; *Unternehr*, 1982, see section 2.4).

Slow spreading ridges, like those in the NE Atlantic, have generally large central rift valleys (*Choukroune et al.*, 1984). Such axial valleys are visible along the Mohns Ridge (e.g. *Dauteuil and Brun,* 1996). However, there is no axial valley in the northern part of the Reykjanes Ridge; this probably results from hot asthenospheric flow southward from the Iceland plume (*Vogt*, 1971).

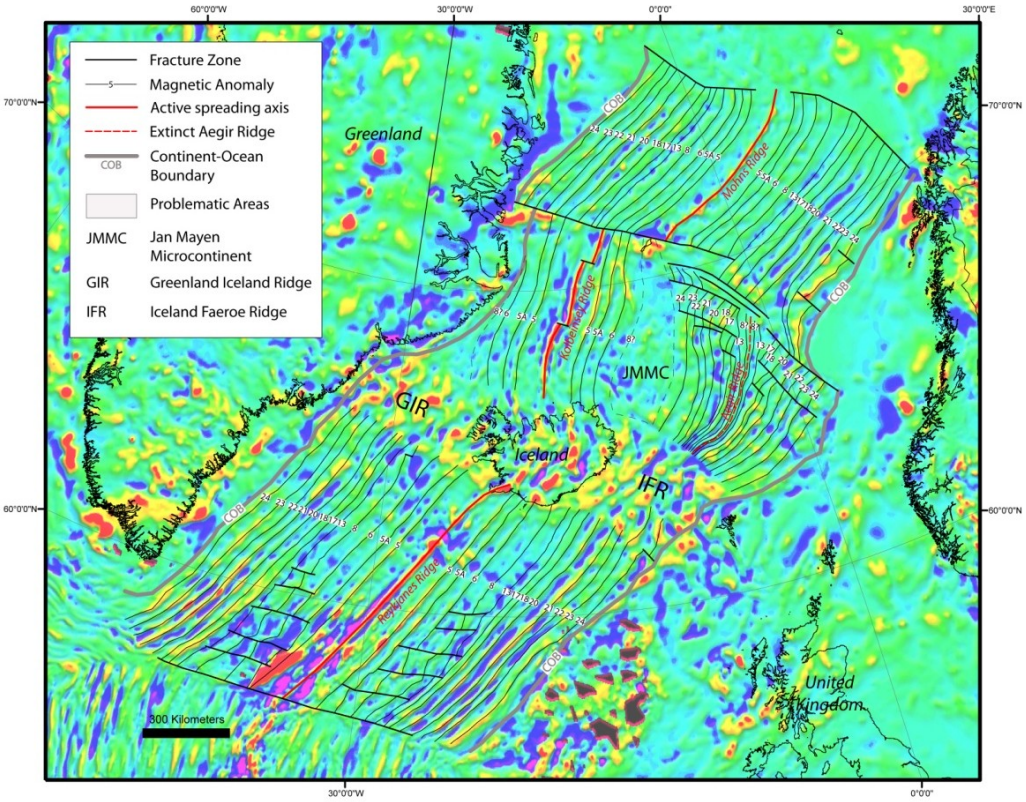

Figure 2.2A. *Map of magnetic anomalies, NE Atlantic Ocean, compilation of data from Macnab et al. (1989), Skogseid et al. (2000), Gaina et al. (2002), Jones et al. (2002b), Olesen et al. (2007), Gernigon et al. (2009), and Maus et al. (2009). Background image is recent model EMAG2 of crustal magnetic anomalies (Maus et al., 2009). Map projection is Universal Transverse Mercator (UTM, WGS 1984, zone 27N).*

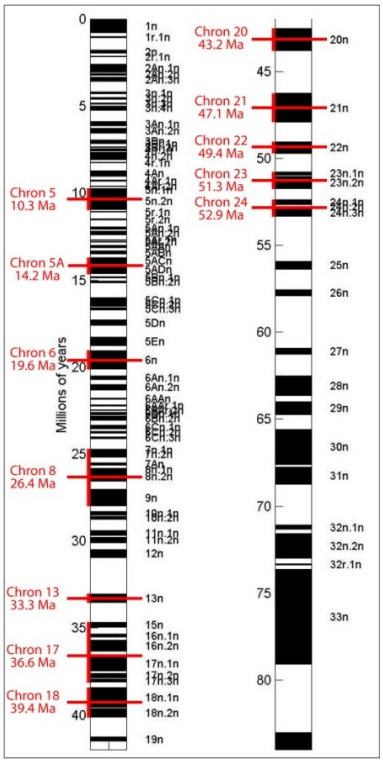

Figure 2.2B. *Ages of magnetic anomalies, from Cande and Kent (1995).*

The Reykjanes Ridge can be divided into two structural types (*Jones*, 2003): (1) south of Iceland, the topography and gravity show V-shaped lineations oriented sub-parallel to the Reykjanes Ridge (**Figure 2.1**), whereas (2) further south, the oceanic crust is segmented and magnetic anomalies are offset by fracture zones (**Figure 2.2A**), this being typical of a slow-spreading ridge away from the influence of a mantle plume. Magmatic activity from the Iceland Mantle Plume, interacting with the ridge, resulted in the formation of Iceland and strong relief around it (**Figure 2.1**). It also modified the magnetic signature of the crust, so that magnetic anomalies are not simple over these areas (**Figure 2.2**).

2.1.2 Iceland Plateau and Greenland-Iceland-Faeroe Ridge

Iceland is the largest part of the mid-NE Atlantic ridge system that emerged above sea level. Iceland and the significant bathymetric-topographic high around it, the Iceland Plateau, and the GIFR, developed as a result of intense magmatic activity, when the NE Atlantic Ridge interacted with a major thermal and compositional anomaly, the Iceland Mantle Plume (e.g. *Saunders et al.*, 1997). Many of the features of the NE Atlantic, such as the Iceland Plateau and the GIFR, can be attributed to the interaction of a mantle plume under Iceland and the mid-Atlantic Ridge (*Ito et al.*, 2003). This interaction will be discussed in more detail in section 2.2.

The Iceland Plateau is a roughly circular plateau encompassing Iceland. It is bounded by a sharp topographic step and forms the central segment of the GIFR (**Figure 2.1**). It stands 4000 m above the sea floor and its emergent part reaches an elevation of 2110 m. Iceland consists of basaltic material, so that values for velocities of P-wave, (Vp) are typical of oceanic crust (e.g. *Fedorova et al.*, 2005). The crustal thickness, however, is 4–5 times thicker than normal oceanic crust (7-10 km). The thickest crust (~40 km) is directly above the centre of the plume, under central Iceland (e.g. *Darbyshire et al.*, 2000; *Foulger et al.*, 2003 *Federova et al.*, 2005; **Figure 2.3**). *Foulger et al.* (2003) proposed a structural model of the Icelandic crust, including (1) an upper crust of 7 ± 1 km thick, heterogeneous and with high velocity gradients; (2) a lower crust of 15-30 ± 5 km thick that begins where the velocity gradient decreases radically (generally at Vp~6.5 km/s); and (3) a crust-mantle boundary, which is a transition zone ~5 ± 3 km thick throughout where Vp increases progressively from ~7.2 to ~8.0 km/s.

The Iceland Plateau, some 500 km wide, may have originated from lower crustal flow above the Iceland plume (*Jones and Maclennan*, 2005). Another possibility is that the plateau represents a major phase of subaerial basalt lava flows, over pre-existing oceanic crust (*Foulger et al.*, 2003; *Doré et al.*, 2008). The oldest onshore basalts, in northwest Iceland, are of lower Miocene age (*Johannesson and Sæmundsson*, 1998). The approximate age of the Iceland Plateau is thus Miocene (*Ellen*, 2002) but remains difficult to constrain due to the lack of age- dated cores.

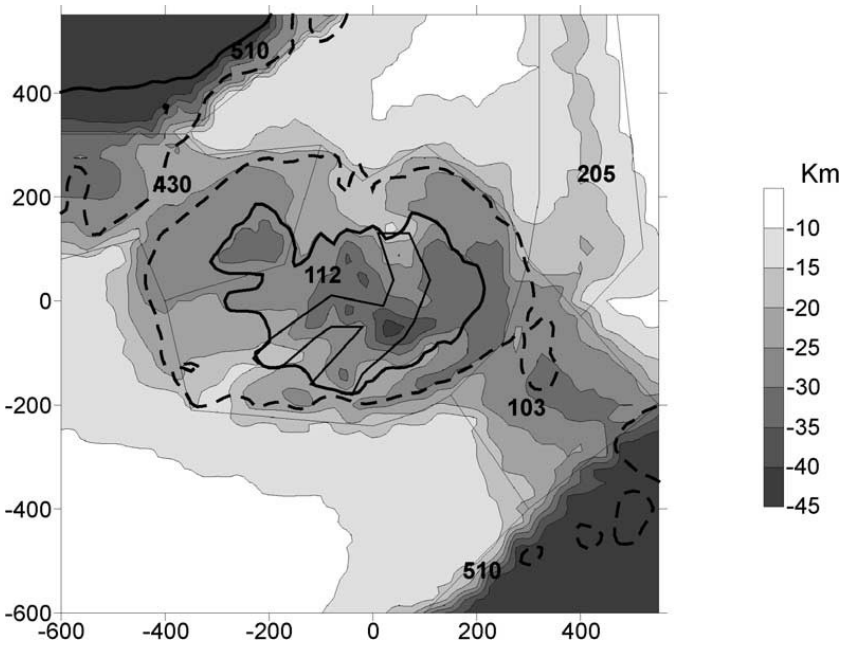

Figure 2.3. *Map of Moho depth in Iceland and surroundings, from Fedorova et al. (2005). Thin polygons are schematic boundaries of tectonic regions. Some corresponding density contrasts between mantle and crust are shown in kg/m3. Solid line is: approximate coast; dashed line: 400 m depth contour representing shelf break.*

The GIFR is an anomalous shallow bathymetric feature, reaching 400m above sea level, which crosses the NE Atlantic from Greenland to the north Scottish shelf (**Figure 2.1**). It forms an aseismic transverse ridge across the ocean, except where it is crossed by the active spreading centre in Iceland (e.g. *Bott*, 1983). The whole ridge is underlain by unusually thick crust for an oceanic region, approx. 30 km thick (*Bott*, 1983; *Foulger et al*., 2003; *Bonhoff and Makris,* 2004; *Fedorova et al.,* 2005; **Figures 2.3 and 2.4**). *Bonhoff and Makris* (2004) identified, from a wide aperture seismic survey, a Moho depth of 23 km below the crest of the Iceland-Faeroe Ridge (IFR) (**Figure 2.4**). The crust is subdivided into an upper part (Vp = 5.7–6.3 km/s) and a lower part (Vp = 6.6–7.0 km/s) by a first order discontinuity with a

velocity increase of 0.3–0.5 km/s. The Moho depth decreases to about 15 km towards the south and north of the IFR.

The GIFR is regarded as a hotspot track due to persistent volcanism caused by the tail of the Iceland Mantle Plume in interaction with the Mid-Atlantic Ridge (e.g. *Morgan*, 1971; *Bott*, 1983; *Lawver and Müller*, 1994; *Eldholm et al.*, 2000; **see section 2.2**). Thus the GIFR appears to be of central importance in reconstructing the opening of the NE Atlantic Ocean.

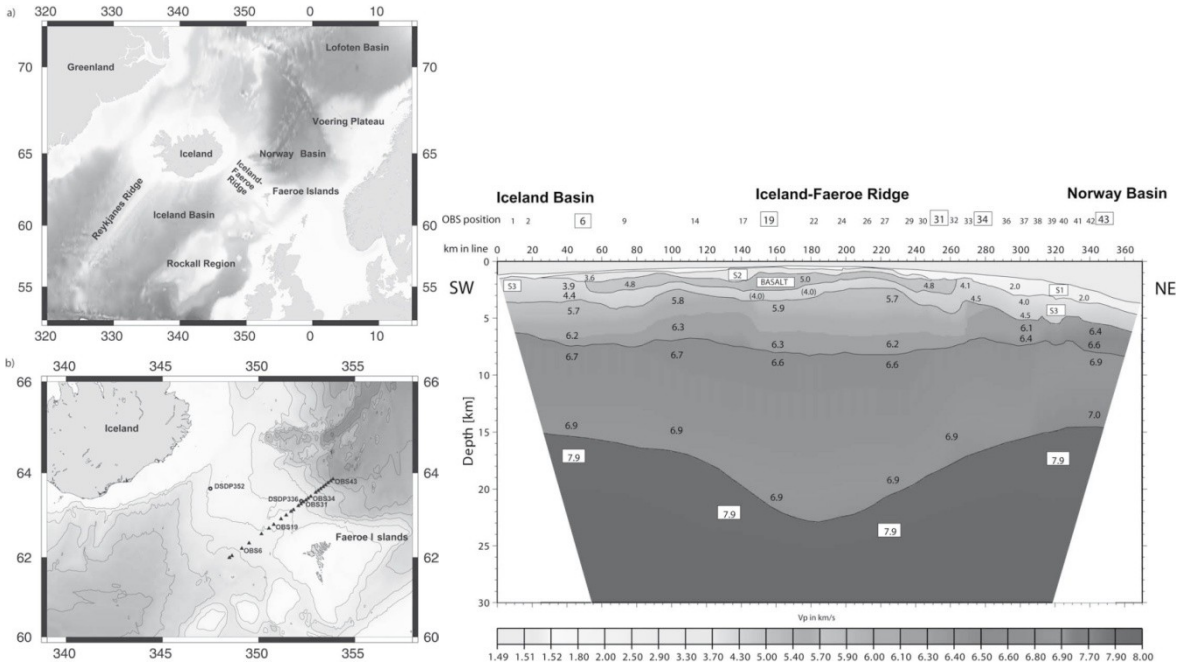

Figure 2.4. *2D- P-wave velocity depth model for the seismic line across the southeastern part of the Iceland-Faeroe-Ridge, from Bohnoff and Markris (2004).*

2.1.3 Jan Mayen Microcontinent

The Jan Mayen Microcontinent (JMMC) was identified originally on the basis of being a bathymetric high, the Jan Mayen Ridge, a positive free-air gravity anomaly and due to the lack of magnetic anomalies, all indicating that it consisted of continental crust. Seismic reflection and refraction data confirmed this interpretation (*Kodaira et al.*, 1998). The JMMC extends about 500 km southwards from the JMFZ and is up to 160 km wide. The Jan Mayen Ridge can be divided into two main components, the main ridge in the north and the southern ridge complex (**Figure 2.5A**). The main ridge reaches from the JMFZ in the north to the Jan Mayen trough, which separates the two main features, in the south. The northern main ridge is well defined, continuous and stands higher than the southern part. The southern part consists

of several smaller ridges which become indistinct to the south and disappear beneath sediments and lavas closer to Iceland. The crustal thickness reaches a maximum of 16 km on the eastern side of the main ridge (*Breivik et al.*, 2003).

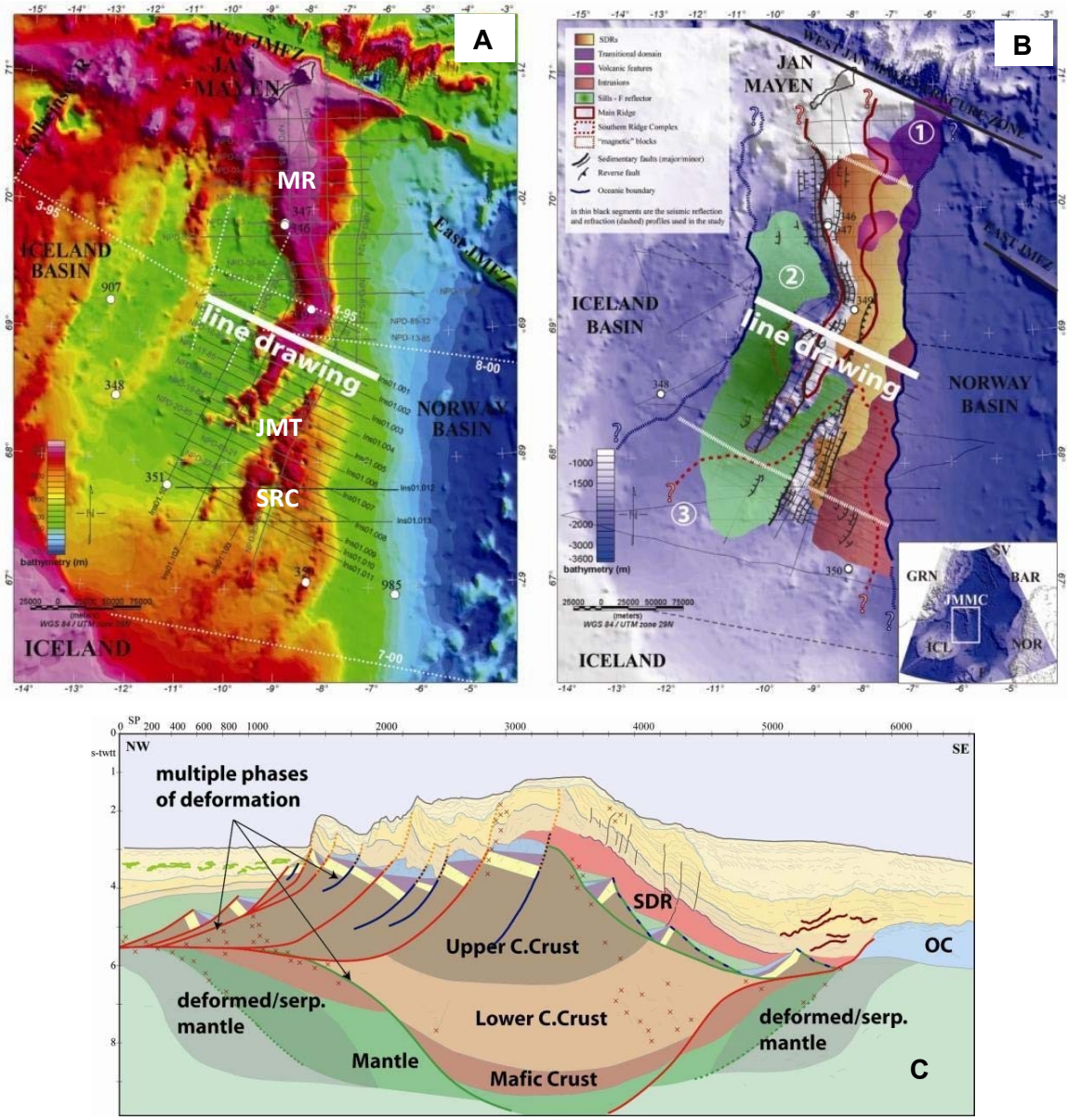

Figure 2.5 *Structure of the Jan Mayen Microcontinent (JMMC): A) Bathymetric map, B) Structural map, and C) Schematic interpretation. Abbreviations: MR, Main Ridge; JMT, Jan Mayen Trough; SRC, Southern Ridge Complex. Modified from Péron-Pinvidic et al. (2010).*

The JMMC is strongly affected by normal faulting and the number of fault blocks and the general structural complexity increase southward (*Gudlaugsson et al.*, 1988, **Figure 2.5B**). Faults mapped on seismic reflection data are roughly N-S trending in the northern part

and NNE-SSW trending to the south (*Gudlaugsson et al.*, 1988; *Scott et al.,* 2005). *Gaina et al.* (2009) and *Peron-Pindivic et al.* (2010) have suggested that the southern part of the JMMC is a zone of high extension where continental crust has been highly thinned. Post-magmatic block faulting occurs on the western margin of the JMMC (conjugate to the East Greenland margin), whereas its eastern margin (conjugate to the Vøring margin) consists of a seaward-dipping basaltic succession (*Gudlaugsson et al.*, 1988, **Figure 2.5C**). These authors ascribed this block faulting, on the western margin of the JMMC, to rifting and separation of the JMMC from East Greenland (**see section 2.4**). The volcanic island of Jan Mayen, in the northern part of the JMMC, is a very young feature which formed in the Pleistocene (*Imsland, P.,* 1978).

2.2 North Atlantic Igneous Province and Iceland Mantle Plume

Magmatism was widespread throughout the NE Atlantic during breakup between Eurasia and Greenland in the Paleocene, accounting for a large Cenozoic igneous province (e.g. *Saunders et al.*, 1997). This North Atlantic Igneous Province (NAIP) extends from eastern Canada to the British Isles. Within this NAIP are basaltic and picritic lavas of Baffin Island and West Greenland, basaltic lavas of East Greenland, seaward-dipping reflectors and offshore lavas along the Greenland and NW European volcanic rifted margins, Iceland, the GIFR and Faeroe Islands, and basaltic lavas and dyke swarms of the British Isles (e.g. *White*, 1988; *Lawver and Müller*, 1994; *Saunders et al.*, 1997; *Storey et al.*, 2007; *Upton*, 1988) (**Figure 2.6**).

Saunders et al. (1997) discerned two major phases of igneous activity: (1) a first phase around 62 Ma with continent-based magmatism in Baffin Islands, W Greenland, the British Isles, and possibly central E Greenland; and (2) a second phase, starting approx. 56 Ma, represented by seaward-dipping reflector sequences (SDRS) along the continental margins, basalts in central E Greenland, the GIFR, the Faeroe Islands and Iceland. Quantitative calculations of NAIP dimensions reveal an areal extent of 1.3×10^6 km², a length of 2600 km, a volume of extrusive basalt of 1.8×10^6 km^3 and a total crustal volume ranging from 6.2 to 9.6×10^6 km^3, which makes the NAIP one of the largest igneous provinces in the world (*Eldholm and Grue*, 1994; *Coffin and Eldholm*, 1994; *Holbrook et al.*, 2001).

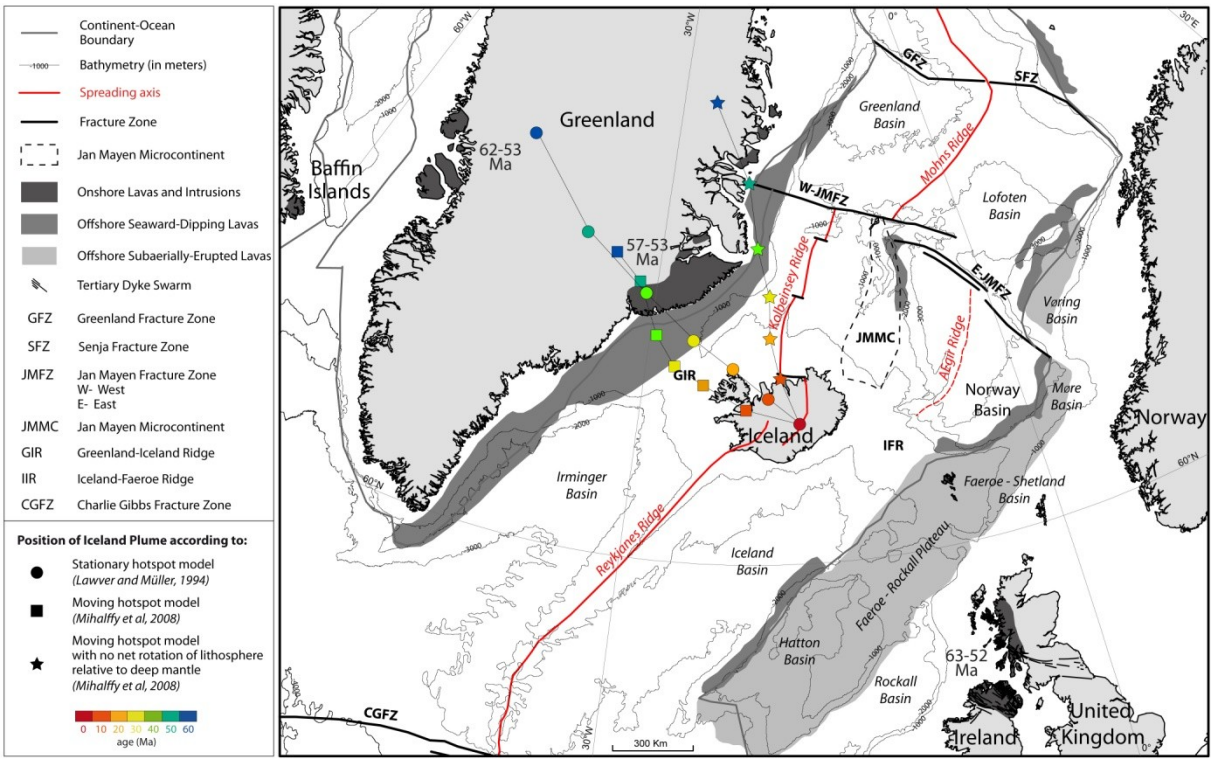

Figure 2.6. *Map of the NE Atlantic showing distribution of igneous rocks in the North Atlantic Igneous Province and location of Iceland Mantle Plume, relative to Greenland, at intervals of 10 Ma according to stationary hotspot model of Lawver and Müller (1994) and moving hotspot model of Mihalffy et al. (2008). Onshore and offshore Tertiary lavas are from Storey et al. (2007) and dyke swarms from Upton (1988). Ages of onshore lavas and intrusions are from White and McKenzie (1989). Map projection is Universal Transverse Mercator (UTM, WGS 1984, zone 27N).*

Morgan (1971) argued that Iceland formed due to a ridge-centered mantle plume under the island and that hotspots are anomalously hot material rising from deeper levels in the mantle. *Courtillot et al.* (2003) proposed three distinct types of hotspots in the Earth's mantle: (1) 'primary' deeper plumes possibly coming from the lowermost mantle boundary layer (D"); (2) 'secondary' plumes possibly coming from the top of domes near the depth of the transition zone at the locations of superswells; and (3) 'tertiary' hotspots that may have a superficial origin, linked to tensile stresses in the lithosphere and decompression melting (**Figure 2.7**). They classified the Iceland hotspot as a 'primary' deep plume.

White and McKenzie (1989) proposed a relationship between mantle plumes and the formation of large igneous provinces (**Figure 2.8**). If a plume reaches the base of the lithosphere in a region under extension, or in a region with pre-existing thinned lithosphere, melting will be amplified and the excess melts may result in an igneous province (e.g. *White*

and McKenzie, 1989; *Eldholm et al.*, 2000). *Saunders et al.* (1997) argued that the Iceland Mantle Plume played a major role in the formation of the NAIP because (1) the simultaneous and widespread initiation of activity requires a major thermal event in the mantle; (2) some of the magmas associated with the first phase of magmatic activity were highly magnesian, indicating that the mantle source regions were unusually hot; (3) the SDRs emplaced subaerially or into shallow water, indicating buoyant support by the mantle during rifting and breakup; and (4) the isotopic and compositional diversity of present-day Icelandic basalts is observed in many of the Paleocene sequences, after crustal contamination and pressure of melt segregation are taken into account.

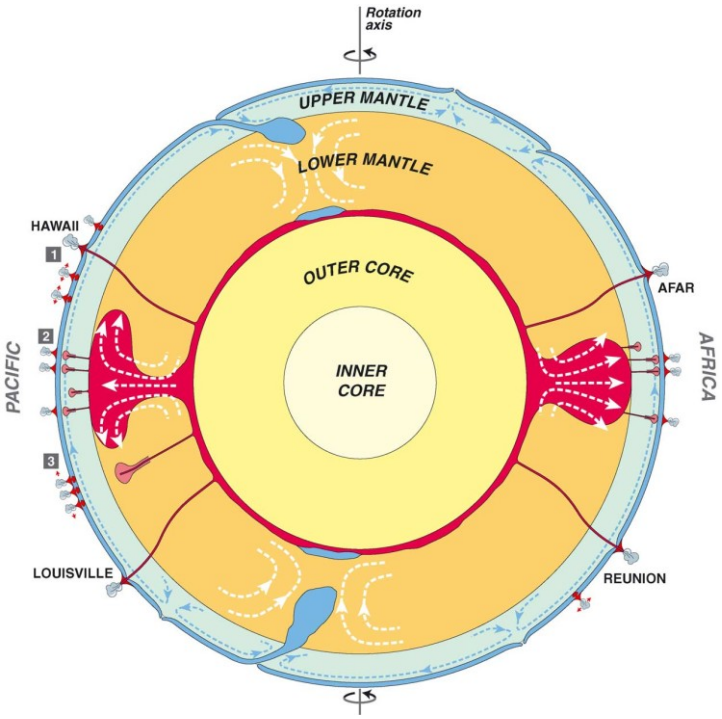

Figure 2.7. *Schematic cross-section through rotation axis of dynamic Earth, outlining sources of three types of plumes/hotspots according to Courtillot et al. (2003).*

This hypothesis has encouraged workers to estimate the position of the Iceland plume through time (*e.g. Lawver & Müller*, 1994; *Torsvik et al.*, 2001a). Several models of Iceland Mantle Plume track exist (**Figure 2.6**): (1) Model 1, the stationary hotspot model of *Lawver and Müller* (1994), using the absolute plate motion reference frames from *Müller et al.* (1993); (2) Model 2, the moving hotspot model of *Mihalffy et al.* (2008), using absolute plate model reference frames from *Steinberger et al.* (2004); and (3) Model 3, the moving hotspot model of *Mihalffy et al.* (2008) with no net rotation of the lithosphere relative to the mantle. Between 60 and 50 Ma, a period of igneous activity in the NE Atlantic, the mantle plume was

beneath Greenland according to the three models. However, its location differs in the three models. According to Model 1, the plume head was beneath Greenland; according to Model 2, the plume head was under eastern Greenland; and according to Model 3, the plume head was under northeastern Greenland. Model 1 and 2 would therefore be more appropriate to explain the NAIP magmatism (**Figure 2.8**). *Ganerød et al.* (2010) have provided a model of 60 Ma paleolatitudinal position of the NAIP in line with current apparent polar wander paths. They have argued that a deep mantle plume is a plausible cause for NAIP volcanism. However, their model predicts that the paleolatitude of the NAIP was *c.* 1500 km south of modern Iceland, challenging correlations of the NAIP and the Icelandic hotspot. They therefore speculate that the NAIP either formed from a different plume, located more southerly during the Early Paleogene, or, alternatively, that the Icelandic plume migrated north. This would be in favor of the moving hotspot model of *Mihalffy et al.* (2008) (Model 2; **Figure 2.6**).

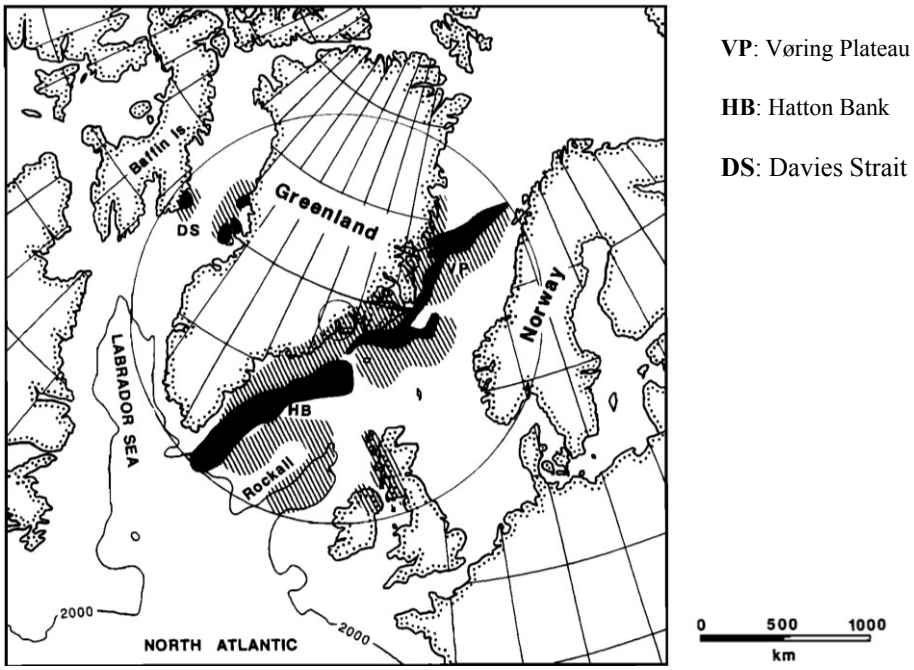

Figure 2.8. *Reconstruction of the North Atlantic region at magnetic anomaly 23 time (51.3 Ma), just after onset of oceanic spreading, by White and McKenzie (1989). Black shading shows position of extrusive rocks, whereas hatching shows the extent of early Tertiary igneous activity in the region. Notice inferred position of mantle plume under eastern Greenland (small circle) and extent of plume head (large circle). This figure highlights that the plume may affect a large area including margins.*

However, an alternative model which does not invoke a mantle plume has been proposed to explain the voluminous NAIP magmatism (e.g. *Foulger and Anderson*, 2005; *Foulger et al.*, 2005). *Foulger et al.* (2000, 2001) argue that, while there are evidences from seismic tomography for an upper mantle velocity reduction beneath Iceland, the anomaly cannot be proven to reach the Earth's core. *Foulger and Anderson* (2005) argue for a 'cool' model for the Iceland 'hotspot' and for compositional rather than a thermal origin for 'hotspots'. Fundamental differences between a mantle plume model and this alternative model are the depth extent of the anomalous mantle structure beneath Iceland, as well as mantle temperatures. The alternative model attributes enhanced magmatism in the Iceland region to high local mantle fertility leading to anomalously large volumes of melt on this part of the ridge. The source of the fertile region according to this model is eclogitized oceanic crust subducted during the Caledonian collision (*Foulger and Anderson*, 2005; *Foulger et al.*, 2005).

2.3 Continental Margins of North East Atlantic

The NW European and E Greenland continental margins mark the transition between the NE Atlantic oceanic crust and the Eurasian and Greenland continental crusts, respectively (**Figure 2.1**). These margins formed during rifting between Greenland and Eurasia before the onset of sea-floor spreading. They consist of stretched continental crust and magmatic rocks, due to intense magmatic activity during rifting and are classified as volcanic passive margins (**Figure 2.9**; *Geoffroy*, 2005).

Volcanic passive margins form part of large igneous provinces, characterized by massive emplacements of mafic extrusive and intrusive rocks over very short time periods (e.g. *White and McKenzie*, 1989; **section 2.2**). Volcanic passive margins are distinguished from non-volcanic margins (or "cold" margins, e.g. the Iberian margin) which do not contain large amounts of extrusive and/or intrusive rocks (*Wilson et al.*, 2001).

The main characteristics of volcanic passive margins are (**Figure 2.10**; *Callot et al.*, 2001; *Gernigon et al.*, 2004): (1) thick sequences of flood basalt onshore, continuing offshore as sequences of thick seaward-dipping reflectors (SDRs); (2) numerous sill/dyke and vent complexes intruding sedimentary basin of the margins; (3) lack of strong passive margin subsidence during and after breakup; and (4) zones of anomalously high P-wave velocities (7.1-7.8 km/s) in the lower crust, so-called Lower Crustal Bodies (LCBs) or High Velocity

Zone (HVZs) (*Eldholm and Grue*, 1994; *Coffin and Eldholm*, 1994; *Eldholm et al.*, 2000). LCBs often occur along the continent-ocean transition but can extend beneath the continental part of the crust. They are interpreted as due to underplating (e.g. *Mjelde et al.*, 2008) or igneous intrusion in the lower crust (e.g. *White and Smith*, 2009)

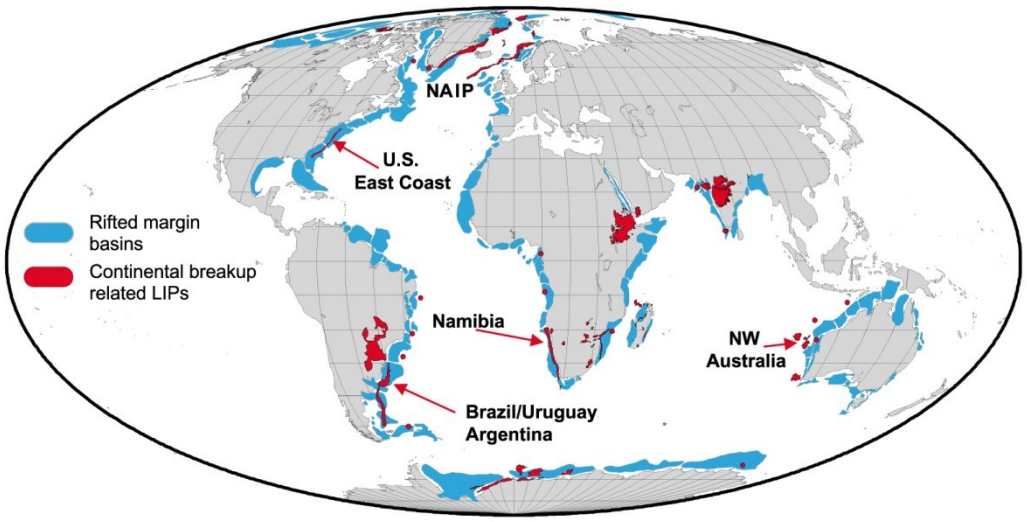

Figure 2.9. *Global distribution of rifted margin basins and breakup related large igneous provinces (LIPs), such as the North Atlantic Igneous Province (NAIP). From Skogseid (2001).*

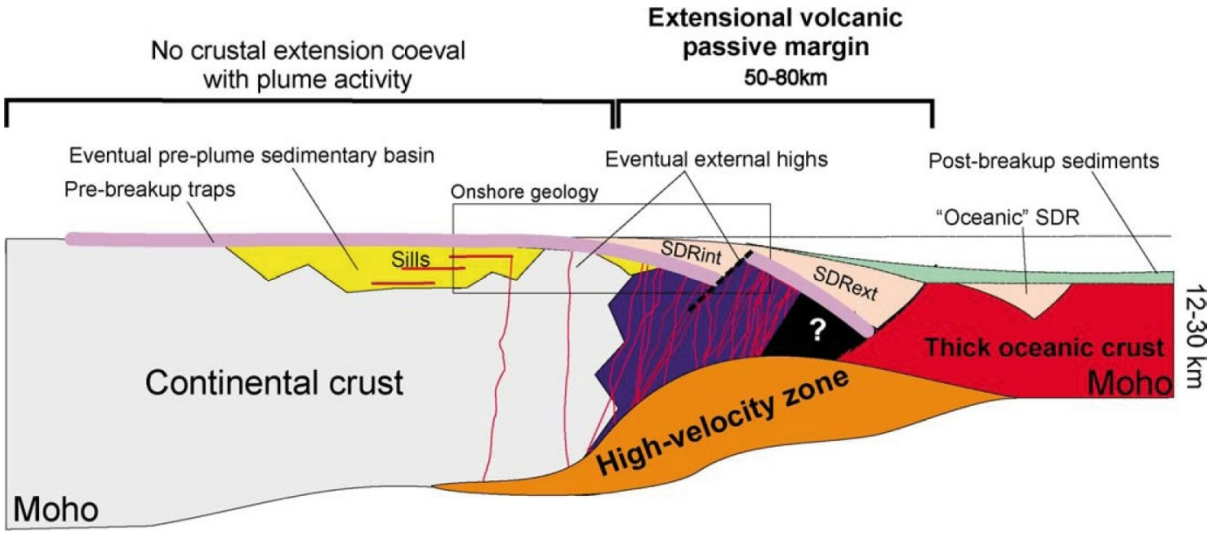

Figure 2.10. *Across-strike section of a volcanic passive margin. The presence of inner sedimentary basins is not the rule. SDRint and SDRext: respectively, internal and external seaward-dipping lavas and volcanic projections (i.e. "Seaward-Dipping Reflectors" in offshore studies), (from Geoffroy, 2005).*

Rifting and sea-floor spreading along the NE Atlantic during the Cenozoic resulted in the formation of two conjugate volcanic continental margins: the NW European and East Greenland margins. Extensional events forming the NW European and East Greenland margins occurred during the Late Palaeozoic (Early-Middle Devonian, Carboniferous, Late Permian-Early Triassic), Late Jurassic - Early Cretaceous and Late Cretaceous-Early Tertiary times. An extensional pulse leading to continental separation, major volcanism and subsequent sea-floor spreading along the NE Atlantic occurred in the early Eocene at approx. 55 Ma (e.g *Ziegler*, 1988, 1989a; *Doré et al.*, 1999; *Brekke*, 2000; *Nielsen et al.*, 2009; **Figure 2.11**).

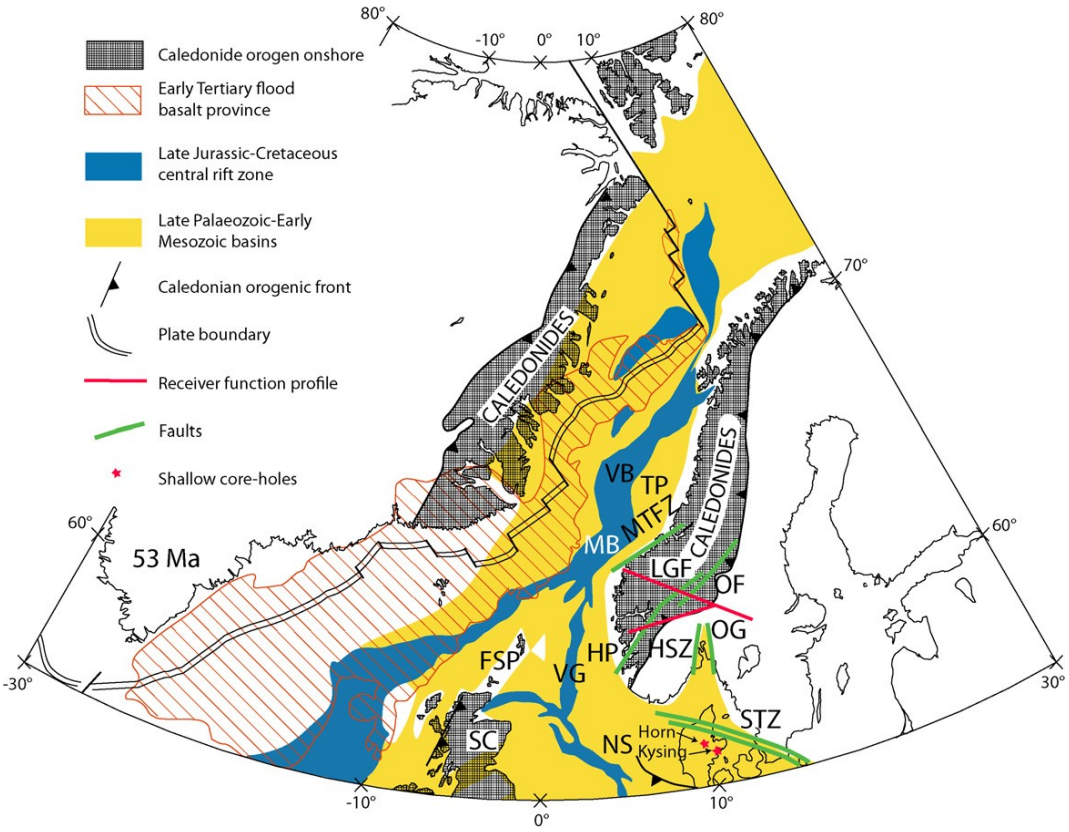

Figure 2.11. *Plate configuration at the time of NE Atlantic breakup with main structural elements after Skogseid et al. (2000). The sedimentary basins separating the onshore remains of the Caledonides are the result of Late Palaeozoic through Mesozoic episodes of post-orogenic continental extension. FSP: Faeroe-Shetland Platform; HP: Horda Platform; HSZ: Hardangerfjorden Shear Zone; LGF: Lærdal-Gjende Fault; MB: Møre Basin; MTFZ: Møre-Trøndelag Fault Zone; NS: North Sea; OF: Olestøl Fault; OG: Oslo Graben; TP: Trøndelag Platform; VB: Vøring Basin; VG: Viking Graben; SC: Scotland; STZ: Sorgenfrei-Tornquist Zone. From Nielsen et al. (2009)*

The Late Jurassic to early Tertiary rifting and breakup phases were governed by the stepwise northward propagation of Central Atlantic sea-floor spreading (e.g. *Ziegler*, 1988). The Mesozoic rifts and breakup axis between Greenland and NW Europe follow pre-existing Caledonian and Hercynian fold belts (*Ziegler*, 1989a).

2.3.1 North West European Margin

The NW European Continental Margin lies between the European continent and the NE Atlantic. It is *c.* 2650 km long, *c*. 880 km wide in the south, east of Ireland, and *c.* 50 km wide in the north, east of northern Norway (**Figure 2.12**).

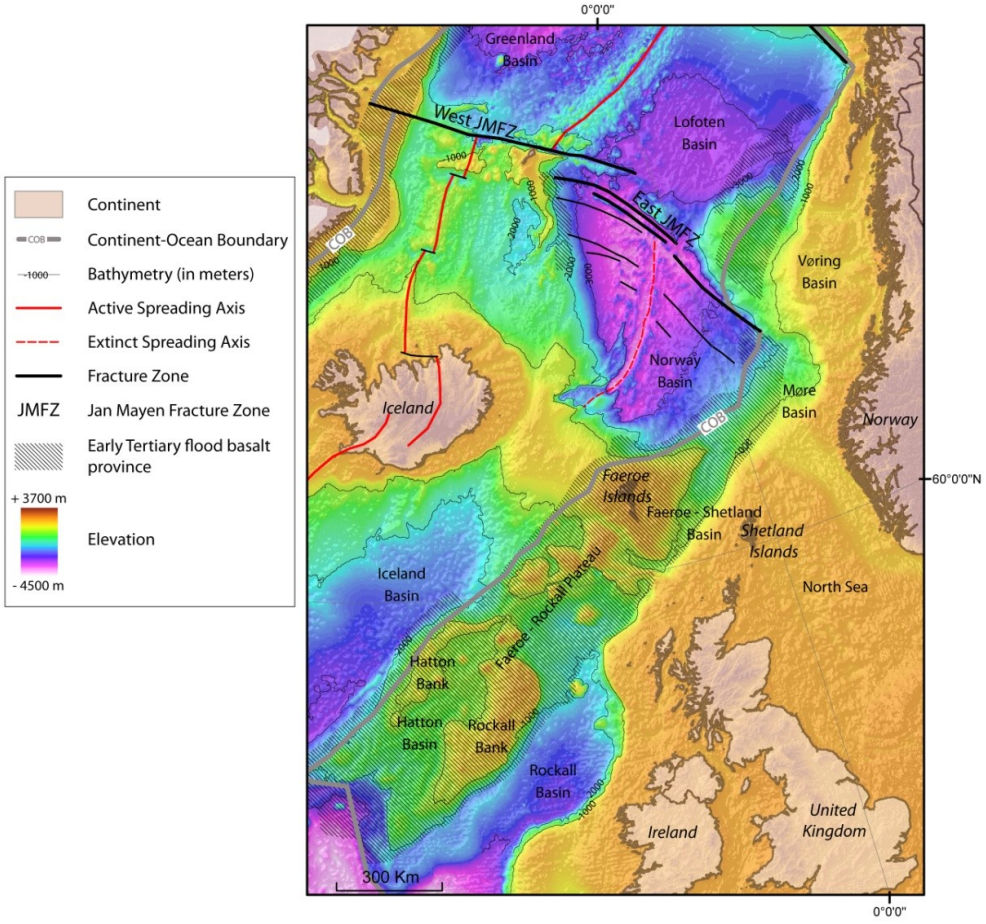

Figure 2.12. *Topographic-bathymetric map of the North West Continental Margin, showing two main regions: 1) the Norwegian Margin to the north, comprising the Vøring and Møre basins, and 2) the Faeroe-Rockall Margin to the south, comprising Hatton Basin, Hatton Bank, Rockall Basin, Rockall Bank, Faeroe-Rockall Plateau, Faeroe Islands and Faeroe-Shetland Basin. Tertiary flood basalt provinces are from Storey et al. (2007). Continent-Ocean Boundary is from Olesen et al. (2007) and Gaina et al. (2009). Map projection is Universal Transverse Mercator (UTM, WGS 1984, zone 27N).*

The European Continental Margin was subject to several phases of extension. Collapse of the Caledonian Orogeny an the NE Atlantic rifting resulted in a wide rifted region (e.g. *Ziegler*, 1988; *Lundin and Doré*, 2005), wider than the Greenland Margin (**Figure 2.1**). Several sedimentary basins formed on the European Margin as a result of rifting: the Vøring and Møre basins in the north, the Faeroe-Shetland Basin in the centre and the Hatton and Rockall basins in the south. We will refer to the Norwegian Margin as the area comprising the Vøring and Møre basins, and the Faeroe-Rockall Margin as the area between the Hatton/Rockall and Faeroe-Shetland basins (**Figure 2.12.**).

Gravity modelling data showed a segmentation of the NW European margin (*Kimbell et al.*, 2004, 2005). These authors interpret the numerous NW-trending lineaments as pre-Caledonian structures that were reactivated as transfer zones during phases of Mesozoic extension (**Figure 2.13**).

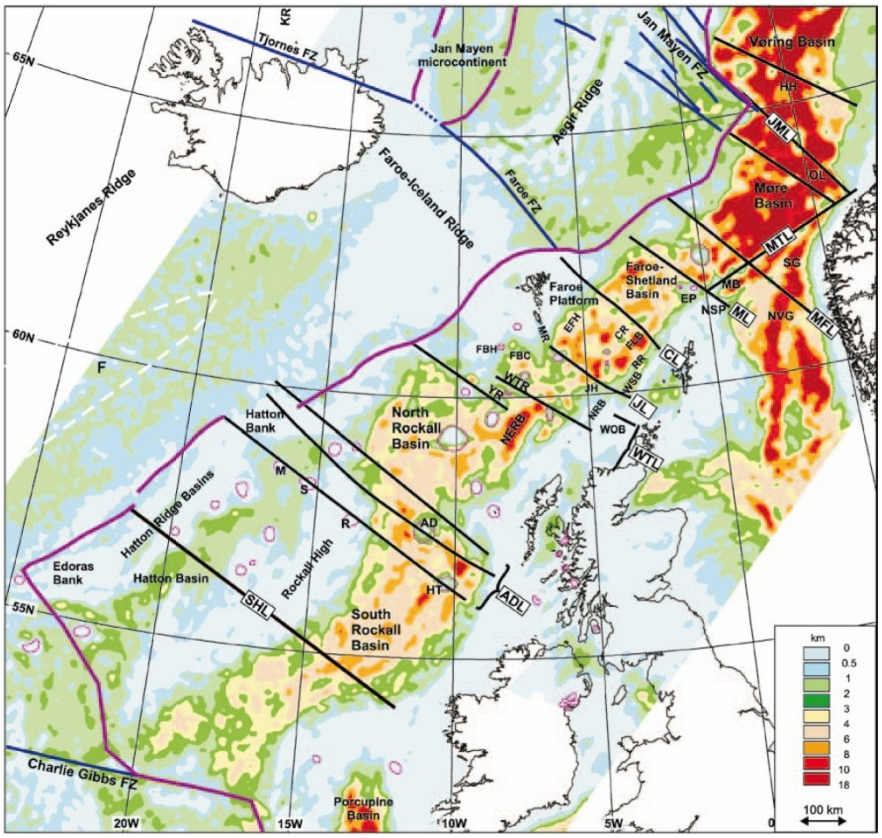

Figure 2.13. *NW-trending lineaments segmenting the NE Atlantic Margin and apparent sediment thickness based on regional 3D gravity modelling (Kimbell et al., 2004). Abbreviations for lineaments: ADL, Anton Dohrn Lineament Complex; CL, Clair Lineament; JL, Judd Lineament; JML, Jan Mayen Lineament; MFL, Marflo Lineament; ML, Magnus Lineament; MTL, Møre–Trøndelag Lineament; SHL, South Hatton Lineament; WTL, Wyville–Thomson Lineament Complex. From Kimbell et al. (2005).*

Some of the lineaments appear to have influenced the early evolution of the oceanic crust by providing the precursors to transform offsets (*Kimbell et al.*, 2005). These authors also showed some evidence of Cenozoic deformation due to transpressive reactivation of the lineaments (**section 2.3.3**).

2.3.1.1 Norwegian Margin

The structural configuration of the Norwegian Continental Margin reflects the overprinting of a complex network of Jurassic and older basins by a continuous NE-SW chain of deep Cretaceous-Cenozoic basins (*Doré et al.*, 2008). Two major basins dominate this margin, with a very thick Cretaceous fill: the Vøring and Møre Basins (*Brekke*, 2000; **Figure 2.14).**

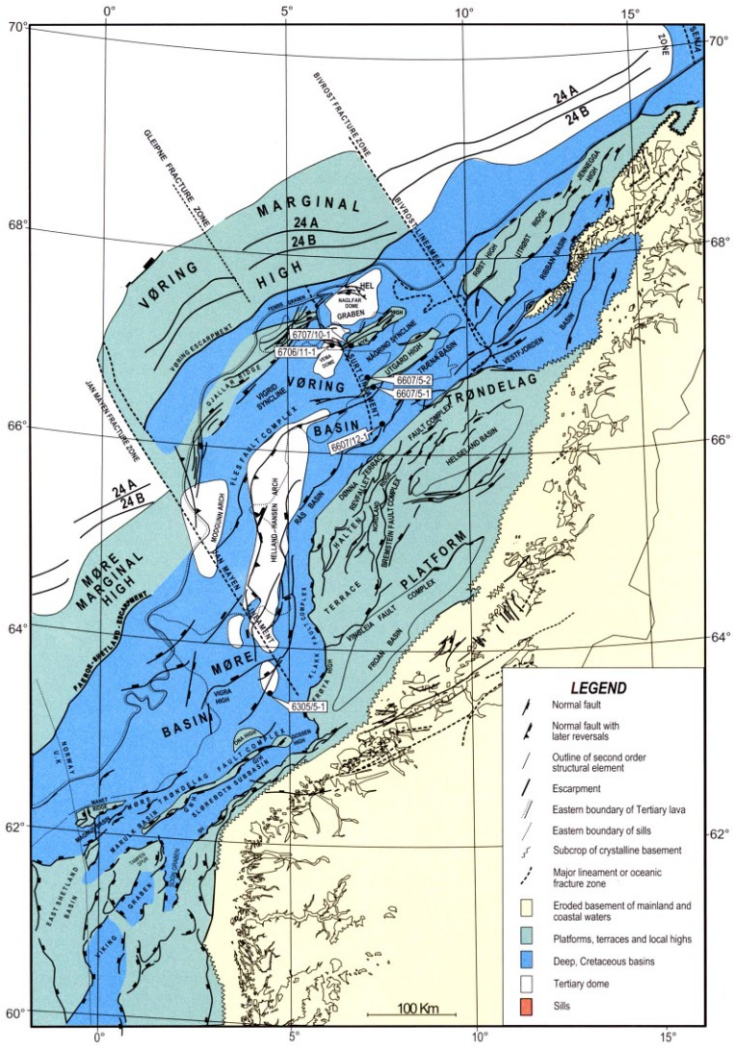

Figure 2.14. *Simplified structural map of the Norwegian Margin from Brekke (2000). Abbreviations: GIH, Giske High; GNH, Gnausen High; SH, Selje High.*

Several NW-trending lineaments segment the Norwegian Margin. A major one, the Jan Mayen Lineament, separates the Vøring Basin from the Møre Basin and prolongs the oceanic JMFZ onto the margin. The Vøring and Møre basins are flanked by the Cretaceous Trøndelag Platform to the east and by the Møre and Vøring Marginal Highs capped by Eocene lavas to the west. The tectonic development of the area is controlled by two structural trends: NE-SW and NW-SE (*Brekke*, 2000; **Figure 2.14**). The typical feature of both the Vøring and Møre basins is the large thickness of the Cretaceous sequence, of which the base in the central parts of the basins lies at depths between 9 and 13 km (*Brekke*, 2000; **Figure 2.15**). The crust beneath the basins stretched and thinned significantly over a wide rift area in the late Mid-Jurassic-Early Cretaceous rifting episode (*Brekke*, 2000).

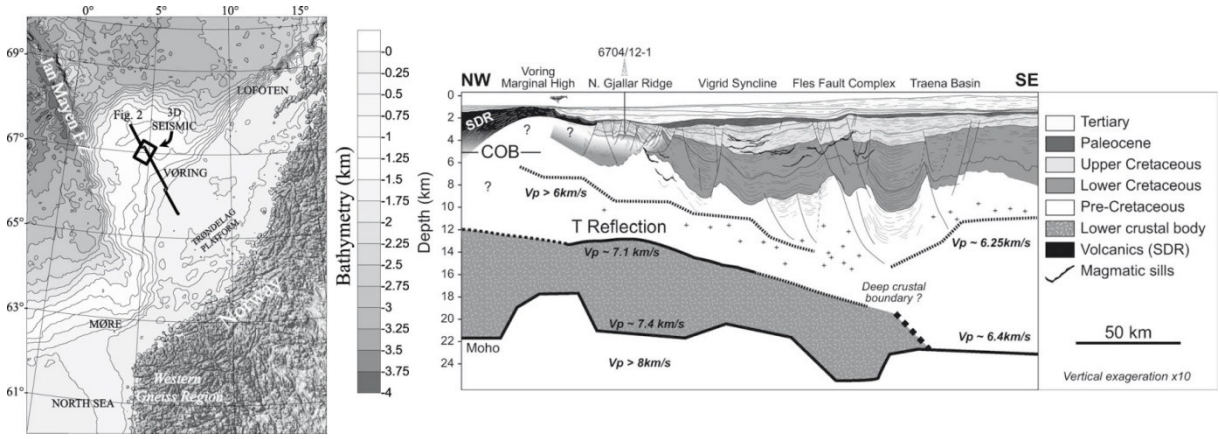

Figure 2.15. Crustal-scale cross section of the Norwegian Margin across the Vøring Basin, from *Gernigon et al.* (2004)

The Norwegian Margin is a typical volcanic margin, including emplacement of SDRs and LCBs (**Figure 2.10**), well visible particularly in the outer Vøring Basin (**Figure 2.3.5**). The outer Vøring Basin is a complex system of faulted ridges defined at the base Tertiary unconformity surface (*Gernigon et al.*, 2004). It is located between a deep Cretaceous basin to the east and the Vøring Marginal High to the west near the ocean-continent transition (*Brekke, 2000; Gernigon et al.*, 2004; *Mjelde et al.*, 2007; *Olesen et al.*, 2007; **Figure 2.14**). As part of the polyrifted system, the outer Vøring Basin was particularly affected by Late Cretaceous-Palaeocene rifting leading to breakup and SDR emplacement at approx. 54-55 Ma (*Gernigon et al.*, 2004).

The Vøring Basin was tectonically active also during Tertiary time and contains a series of Cenozoic domes that affects the sedimentary cover (**section 2.3.3**). In contrast, the Møre Basin was generally tectonically quiet throughout the Cretaceous and Tertiary periods,

experiencing mainly continuous subsidence. Only minor activity occurred in Tertiary time; involving reactivations of the Jan Mayen lineament and minor faulting along the Faeroe-Shetland Escarpment (*Brekke*, 2000).

2.3.1.2 Faeroe-Rockall Margin

The Faeroe-Rockall Margin comprises the Rockall and the Hatton basins separated from each other by bathymetric highs: 1) the Rockall Bank, between the Rockall and Hatton basins; and 2) the Hatton Bank, between the Hatton and the Iceland basins (**Figures 2.12 and 2.16**). The Faeroe-Shetland Basin separates the Faeroe Islands to the west from the British Isles to the east. The area between the Rockall/Hatton basins and the Faeroe Islands is the Faeroe-Rockall Plateau (**Figure 2.12**). Northward propagation of the Central Atlantic in late Mesozoic time led to high Early Cretaceous crustal stretching on the southern NW European Margin that may have locally progressed during the Albian to crustal separation and the onset of limited sea-floor spreading in the Rockall Basin (*Ziegler*, 1989a).

Continental crust underlains the plateau (*e.g. Bott et al*., 1974) and is thicker beneath the banks (~25 km) and the Faeroe Islands (~28 km) and thinner under the Hatton Basin (~20km) and Faeroe-Rockall Basin (~18-20 km) (*White et al.*, 2008; **Figure 2.16**). The continental-ocean crustal transition occurs beneath the western flank of the Hatton Bank where seaward-dipping reflectors emplaced (*Hitchen*, 2004; *White et al*., 2008*;* **Figures 2.12 and 2.16**).

Cenozoic sediments fill the basins and overlie early Tertiary plateau basalts (e.g. *Boldreel and Andersen*, 1998). On the banks, thin layer of Quaternary and Neogene sediments cover the lower Tertiary volcanic rocks, which locally crop out at the seafloor, in the Faeroe Islands. Seismic data do not clearly image the base of the Paleogene volcanic, the thickness of basalts is therefore very difficult to predict, though seismic data suggest 6 km of basalt below the Faeroe Islands (*Davison et al.*, 2010). Gravity data suggests significant differences between the upper crustal composition and structure of the Rockall Bank (high gravity anomaly) and Hatton Bank (low gravity anomaly) (*Hitchen*, 2004). Samples of the Rockall Bank showed metamorphic basement of Early Proterozoic age, however no metamorphic basement were sampled on the Hatton Bank where there is a cover of Palaeozoic, Mesozoic and/or Cenozoic sediments and lavas (*Hitchen*, 2004). The Rockall Basin contains on average 4-7 km of Mesozoic units, which deposited on rifted continental crust, involving rotated fault blocks throughout the basin (*Davison et al.*, 2010).

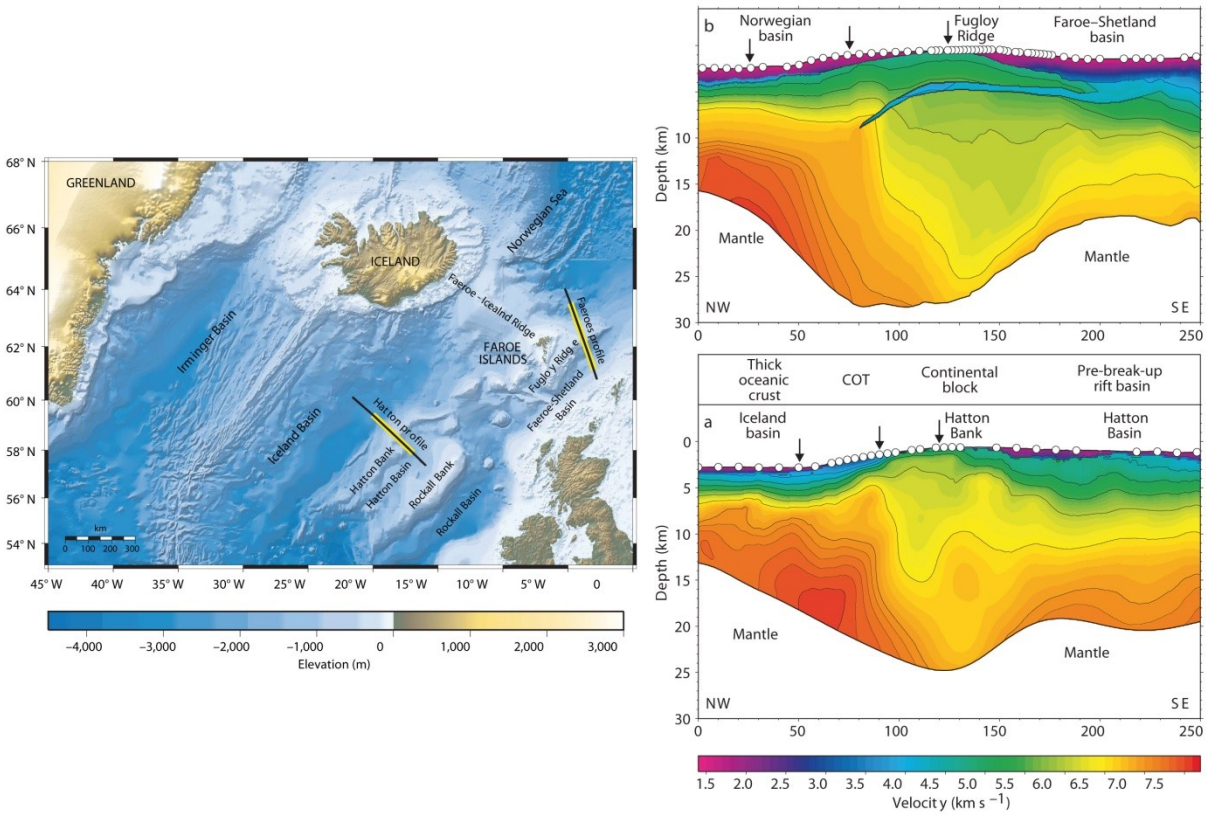

Figure 2.16. *Location of seismic profiles across NW European Margin (A) and seismic velocity structure of crust across continent-ocean transition near Faeroe Islands (B) and Hatton Bank (C). Lower-crustal layering (high velocities >7.0 km s^{-1}), due to igneous intrusions, lies beneath the basalts on the continent–ocean transition, ending at 90 km against continental crust with markedly lower velocities. Post-rift Cenozoic sediments are in purple. Profiles are aligned with 0 km distance at seafloor spreading magnetic anomaly Chron 22. Colour bands are at 0.1 km s^{-1} intervals, with contours above 7.0 km s^{-1} spaced every 0.1 km s^{-1} to highlight the lower-crustal velocity. From White et al. (2008).*

The Faeroe–Rockall Plateau comprises numerous compressional structures, postdating the early Tertiary volcanic activity (e.g. *Boldreel and Andersen*, 1998; *Johnson et al.*, 2005; *Tuitt et al.*, 2010). The folds have resulted from a post-breakup compressional tectonic phase that affected the margin (section 2.3.3).

2.3.2 East Greenland Margin

The East Greenland Margin extends approx. 2500 km long, approx. 80 km wide in the southernmost part and approx. 300 km wide in the northernmost part. It can be divided into

two regions: 1) the northeast Greenland Margin, north of Iceland, and 2) the southeast Greenland Margin, south of Iceland (**Figure 2.17**). Sea-ice, icebergs and ice on almost all the shelf makes studies of the margin difficult. However, the onshore part of East Greenland provides very good outcrops to study the interactions between Tertiary faulting and magmatism, related to the NAIP emplacement (**section 2.2**) (e.g. *Price et al.*, 1997).

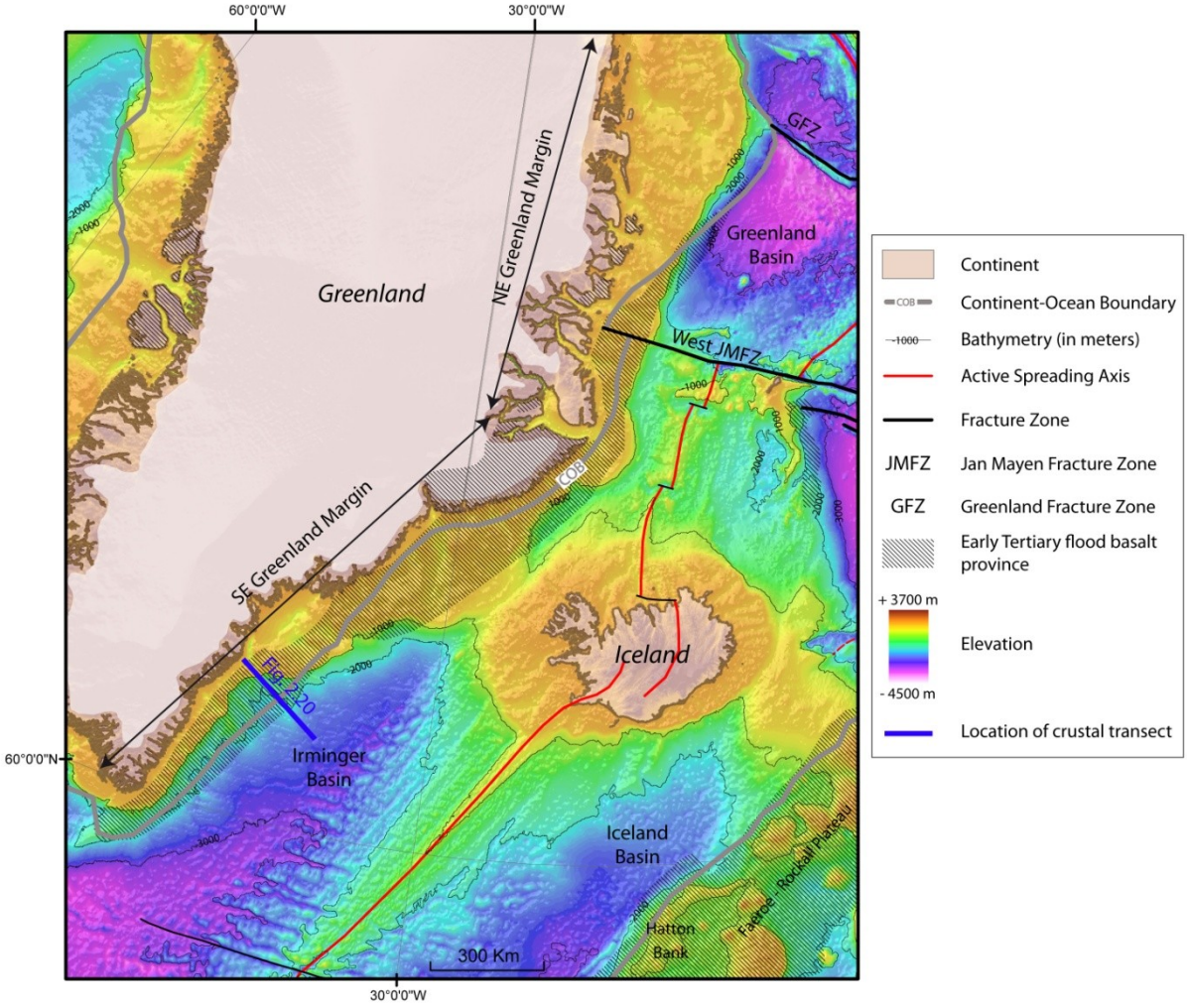

Figure 2.17. *Topographic-bathymetric map of East Greenland Continental Margin, showing two main regions: northeast (NE), and southeast (SE) Greenland Margin. Tertiary flood basalt provinces are from Storey et al. (2007). Continent-Ocean Boundary is from Olesen et al. (2007) and Gaina et al. (2009). Blue lines indicate crustal transect of Figure 2.20. Map projection is Universal Transverse Mercator (UTM, WGS 1984, zone 27N).*

The East Greenland Margin comprises (*Johnson and Gallagher*, 2000; **Figures 2.17.**): 1) an Achaean-Caledonian crystalline interior, with a mid-Devonian to Tertiary sedimentary succession (*Escher and Pulvertaft*, 1995; *Hamann et al.*, 2005); 2) a near-shore continent-

ocean boundary (COB) of Palaeocene age (e.g. *Scott*, 2000), except on the northeast margin where it is approx. 300 km from the shoreline; and 3) a discontinuous early Paleogene flood basalt sequence, both onshore and offshore (e.g. *Saunders et al.*, 1997; *Storey et al*., 2007).

2.3.2.1 North East Greenland Margin

As for the NW European Margin, so for the NE Greenland Margin, a long history of post-Caledonian extension, with similar extension phases, has resulted in syn-rift sedimentation within rift basins (**Figure 2.18**).

The most prominent feature on the Northeast Greenland Margin is a large, very deep (>13 km) sedimentary basin, the Danmarkshavn Basin (*Hamann et al.*, 2005; **Figure 2.18A**). The Koldewey Platform defines the western margin of the basin, whereas on the eastern margin, a series of NE-trending structural highs form the Danmarkshavn Ridge. The sedimentary succession in Danmarkshavn Basin is supposed of Devonian to Paleogene age and presents numerous unconformities along the basin margins. The Thetis Basin, east of the Danmarkshavn Ridge, is a relatively young basin that comprises a thick Cretaceous and Tertiary succession (*Hamann et al.*, 2005; **Figure 2.18A**).

The East Greenland volcanic province, between the JMFZ and Bivrost Fracture Zone, consists in Tertiary plateau basalts and offshore volcanic rocks that obscure seismic data (**Figure 2.18**).

South of the JMFZ, the structural style differs from the areas to the north. It is characterized by few but large faults blocks. The amount of extension, however, appears to be similar in the two areas. The thickness of the Devonian-Jurassic succession in the Jameson Land Basin (approx. 17 km) is similar to that of the Danmarkshavn Basin (approx. 13 km) (*Hamann et al.*, 2005; **Figure 2.18B**). The Liverpool Land Basin, to the east, is younger and contains Tertiary successions (*Hamann et al.*, 2005; **Figure 2.18B**). Tertiary plateau basalts cover a large proportion of this area. The outer part of the shelf, oceanic crust occurs beneath a thick Tertiary wedge. In this area, a series of pseudo-escarpments and seaward-dipping reflectors mark the ocean–continent transition zone (*Larsen,* 1990).

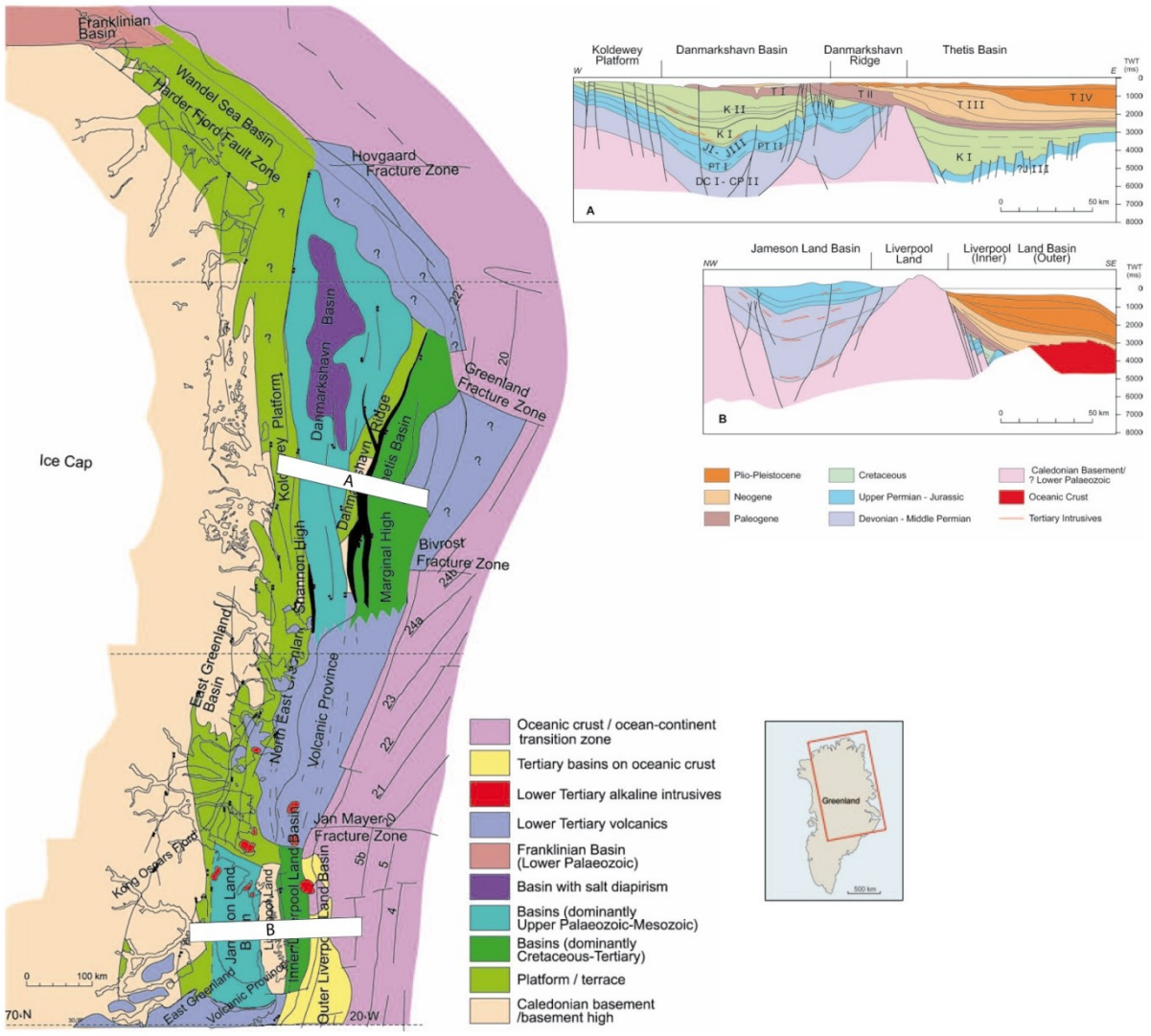

Figure 2.18. *Tectonic map of the Northeast Greenland Shelf, showing main structural elements: the Koldewey Platform, Danmarkshavn Basin, Danmarkshavn Ridge, Thetis Basin and Marginal High. Geo-seismic cross sections of (A) the Northeast Greenland Shelf (north of 75°N) and (B) the Jameson Land Basin – Liverpool Land Shelf (c. 71°N). Age of seismic mega-sequences: DC, Devonian-mid-Carboniferous; CP, Late carboniferous-Early Permian; PT, mid-Permian-Triassic; J, Jurassic; KI, Upper Jurassic-Lower Cretaceous; KII, Late Cretaceous; TI, Palaeocene; TII, Eocene-Late Oligocene; TIII, Early Miocene-Late Miocene; TIV, Early Pliocene-Holocene. From Hamann et al. (2005).*

The part of the Greenland Margin between Iceland and the JMFZ underwent extension and magmatism during mid-Cenozoic time due to the separation of the Jan Mayen Microcontinent and the relocation of the spreading centre from the now extinct Aegir Ridge to the present-day active Kolbeinsey Ridge (**section 2.1**; e.g. *Talwani and Eldholm*, 1977; *Nunns*, 1983; *Noble et al.*, 1988; *Upton et al.*, 1995; *Price et al.*, 1997; *Saunders et al.*, 1997;

Müller et al., 2001; *Gaina et al.*, 2009). Formation of major half-graben took place along the central East Greenland margin and overprinted the initial breakup structure along this part of the margin (*Larsen*, 2002). *Mjelde et al.* (2008) provided an integrated 1580 km long crustal transect across the JMMC, the present-day active Kolbeinsey Ridge and extinct Aegir Ridge based on crustal model derived from ocean bottom seismographic surveys (**Figure 2.19**). This crustal transect shows (1) a thick oceanic crust, especially between the JMMC and East Greenland, which is interpreted as the influence of the Iceland Mantle Plume on sea-floor spreading along the Kolbeinsey Ridge; (2) a lower crustal high-velocity layer underlying the More Basin; and (3) a west-dipping COB detachment (*Mjelde et al.*, 2008).

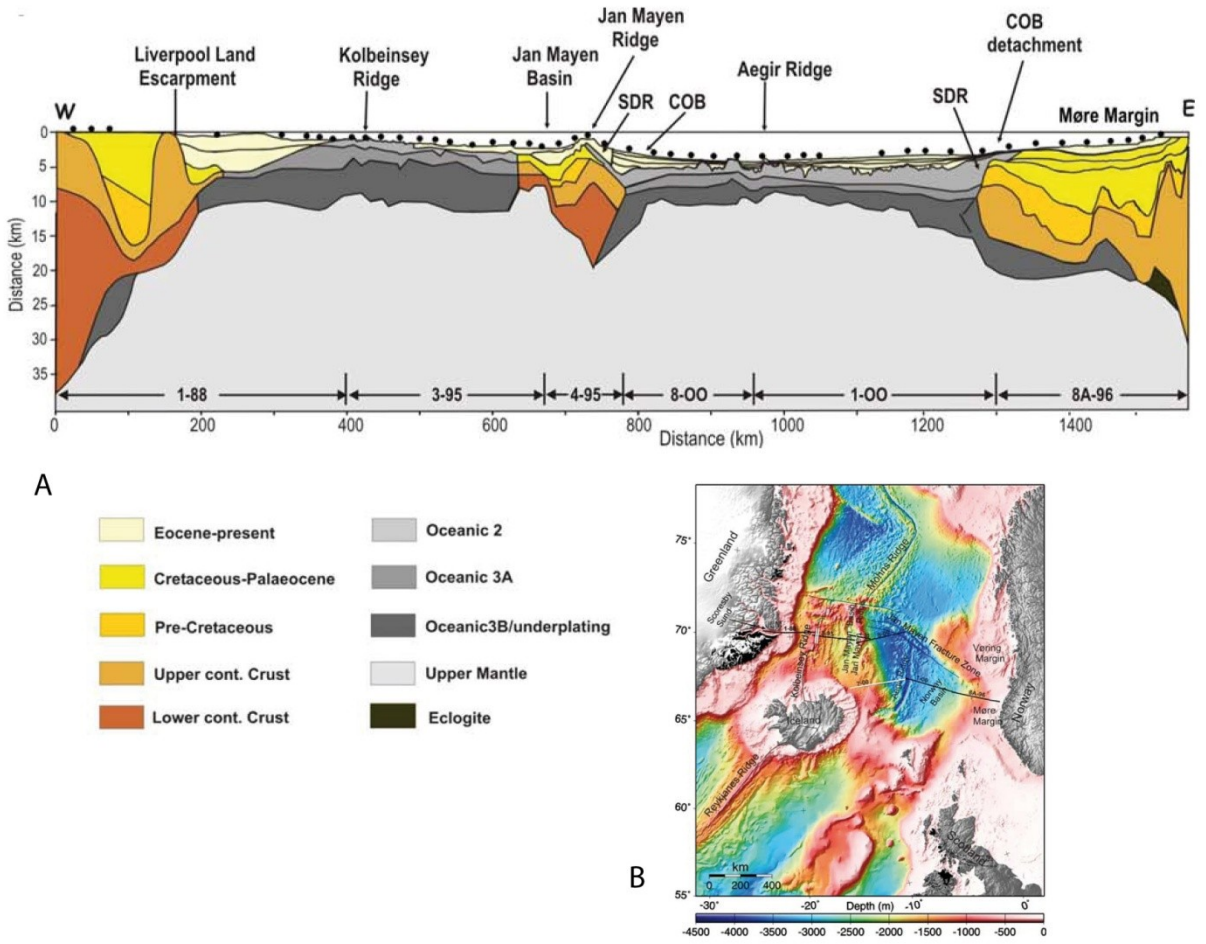

Figure 2.19. *(A) Interpreted present-day transect across the NE Atlantic, passing through Jan Mayen Microcontinent and Kolbeinsey and Aegir ridges. Brown lower crustal layer is non-intruded lower crust, whereas dark grey lower crustal layer is a mixture of mafic, lower crustal intrusions, (B) Bathymetric map of NE Atlantic and indication of ocean bottom seismometer profiles, in black, included in the transect. From Mjelde et al., (2008).*

2.3.2.2 South East Greenland Margin

The southeast Greenland Margin is very narrow in comparison to the conjugate Faeroe-Rockall Margin, which experienced more Mesozoic extension prior to Tertiary breakup and developed several basins separated by banks (**section 2.3.1.2**). The widespread magmatism associated with the NAIP widely affected the southeast Greenland Margin during the Late Palaeocene-Early Eocene. Magmatism occurred both onshore on the East coast of Greenland and offshore along the rifted margin, including emplacement of SDR sequences (e.g. *Larsen and Jakobsdóttir*, 1988; *Noble et al.*, 1988; *Larsen*, 2002; *Hopper et al.*, 2003; *White and Smith*, 2009 **Figure 2.17**).

Hopper et al. (2003) have provided a crustal transect across the southeast Greenland Margin obtained from seismic data from the SE Greenland Margin (**Figure 2.20**). The crustal transect shows (1) the margin structure from the Achaean continental crust to oceanic crust, (4) an abrupt transition between the continental and oceanic crusts (COB <50 km wide), (2) a high velocity zone in the lower crust (>7.3 km/s), (3) SDR sequences that underlie the oceanic crust, and (4) a small amount of crustal thinning, which occurred prior to final breakup.

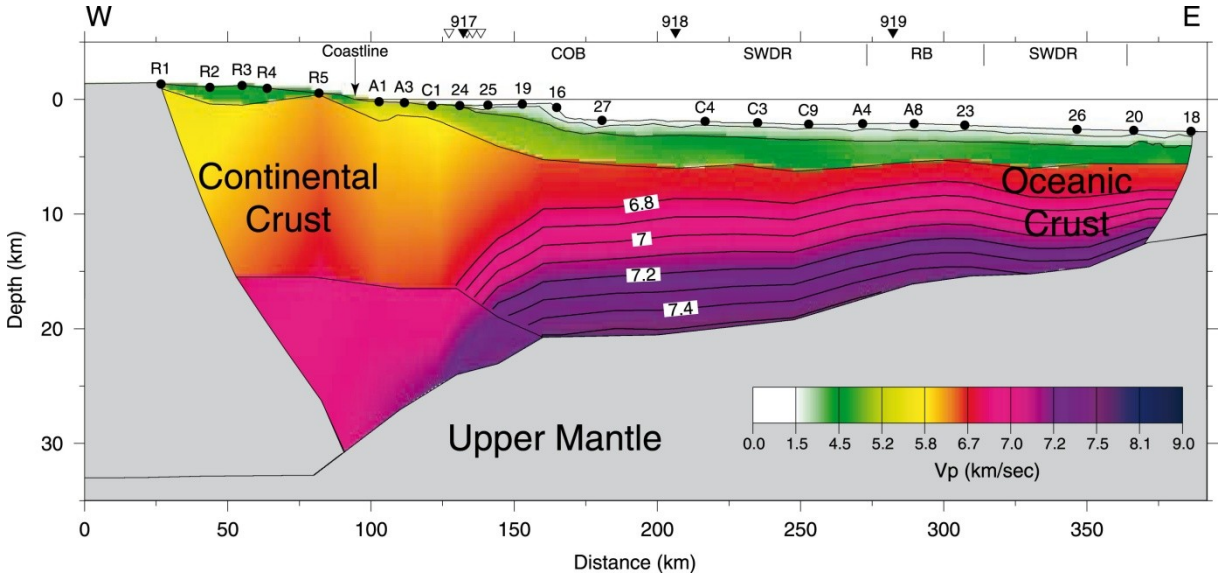

Figure 2.20. *Velocity Model of the SE Greenland Margin, approx. 600 km south of the GIFR (location of the transect on Figure 2.3.9). The oceanic crustal section shows velocity contours from 6.8 to 7.4 km/s. Triangles along the top line are the ODP drill sites. Areas not constrained by modelled arrivals are grey. Abbreviations: COB, Continent-Ocean Boundary; SWDR, Seaward Dipping Reflectors; RB, Rough Basement). From Hopper et al. (2003).*

ODP drilling and seismic surveys off southeast Greenland show that the upper part of the oceanic crust consists of 4-6 km thick sequences of SDR sequences (e.g. *Larsen*, 2002). SDR sequences are present along the whole rifted Greenland margin, parallel to the coast (**Figure 2.17.**).

A comparison of the southeast Greenland Margin to the conjugate Hatton Bank shows a clear asymmetry in the early accretion history of North Atlantic oceanic crust (**Figure 2.21.**). (*Hopper et al*., 2003). This asymmetry may indicate:
(1) an east directed ridge migration during initial opening (*Hopper et al*., 2003);
(2) a difference in accretional process due to a different thermal structure of the plates. Faster accretion are predicted on cooler plate, which is consistent with Greenland margin being bounded by thick Archean lithosphere; whereas the Hatton Bank is bounded by younger and presumably warmer lithosphere beneath the Faeroe-Rockall Plateau (*Hopper et al.*, 2003);
and/or (3) an initial phase of stretching creating asymmetric thinned continental crust. This thinned crust was then buried by the extensive volcanism. Repeated Mesozoic stretching events prior to the Tertiary break up occurred along the European Margin. Thus, breakup would have occurred on the western side of the Mesozoic regions of extension on the European side (*White and Smith*, 2009).

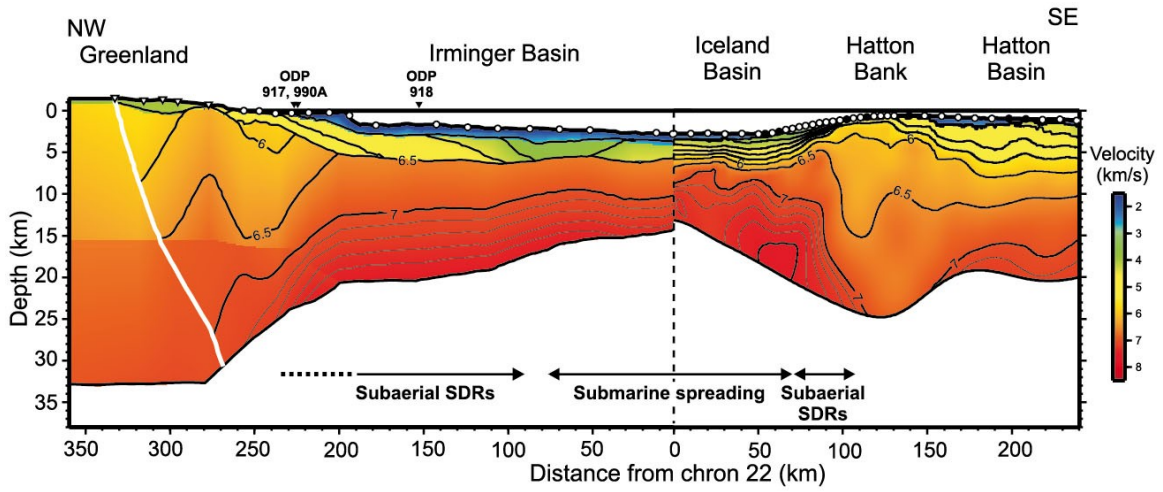

Figure 2.21. *Comparison of velocity models from the Hatton profile and the East Greenland conjugate profile (Hopper et al., 2003). Models are aligned at Chron 22 (~ 49.4 Ma). Contours are drawn every 0.5 km/s from 3.5 to 7.0 km/s and every 0.1 km/s for velocities >0.1 km/s. White line marks the limit of ray coverage in the Greenland velocity model. From White and Smith (2009).*

2.3.3 Post-break up deformation of the margins

Seismic stratigraphic interpretation, geomorphological analysis and thermal history studies (apatite fission track and vitrinite reflectance analyses) have revealed episodes of uplift and exhumation of Scandinavia, British Isles and Greenland during the Cenozoic (e.g. *Stuevold et al.*, 1992; *Thomson et al.*, 1999; *Chalmers*, 2000; *Green*, 2002; *Praeg et al*., 2005; *Redfield et al.*, 2005; *Bonow et al.*, 2007; *Hendriks et al.*, 2007; *Jolivet*, 2007; *Holford et al.*, 2009; *Japsen et al.*, 2005, 2007, 2010; *Anell et al.* 2009; *Nielsen et al.*, 2009; *Redfield*, 2010;).

(1) A first major phase of regional uplift occurred in the Palaeocene to Early Eocene (approx. 65–50 Ma). This uplift, of approx. 2 km, is probably due to rift-flank uplift during the break-up of the NE Atlantic between Europe and Greenland, as indicated by the northward propagation of uplift, and to mantle processes. Possible mantle processes are thermal effects and magmatic underplating in connection with the emplacement of the NAIP, pulse and temperature changes of the Iceland Mantle Plume (e.g. *Anell et al.*, 2009; *Green,* 1989*; Rohrman and Van Der Beek*, 1996; *White and Lovell*, 1997; *Jones et al.*, 2002a; *Nielsen et al.*, 2002; *Storey et al.*, 2007; *Holford et al.*, 2009; *Hartley et al.*, 2011).

(2) Two phases of local uplift, of kilometre scale, occurred during the late Eocene to late Oligocene (approx. 40-25 Ma) and in the Miocene (approx 20-10 Ma) probably due to intraplate stress regime, such as changes in spreading dynamics (including the transfer of spreading from the Aegir to Kolbeinsey ridges and the separation of the JMMC from E Greenland) and the Alpine compressional stress (e.g. *Doré et al.*, 1999; *Thomson et al.*, 1999; *Hansen et al.*, 2001; *Anell et al.*, 2009; *Holford et al.*, 2009; *Japsen et al.*, 2005, 2010).

(3) A second main phase of regional uplift occurred in the Plio-Pleistocene (5–0 Ma), of magnitude of approx. 1- 2 km (e.g. *Green et al.*, 1989; *Rohrman et al.*, 1995; *Doré et al.*, 1999; *Anell et al*., 2009). This uplift was probably due to glacial erosion and isostatic readjustment (e.g. *Riis and Fjedlskaar*, 1992; *Doré et al.*, 1999; *Nielsen et al.*, 2009).

However, the mechanisms (mantle driven, compression, or isostasy processes) at the origin of these uplift and exhumation episodes remain subject to debate, and this summary is not exhaustive. In what follow, we will focus on the offshore compressional deformation that affected the NE Atlantic continental margins during the Cenozoic.

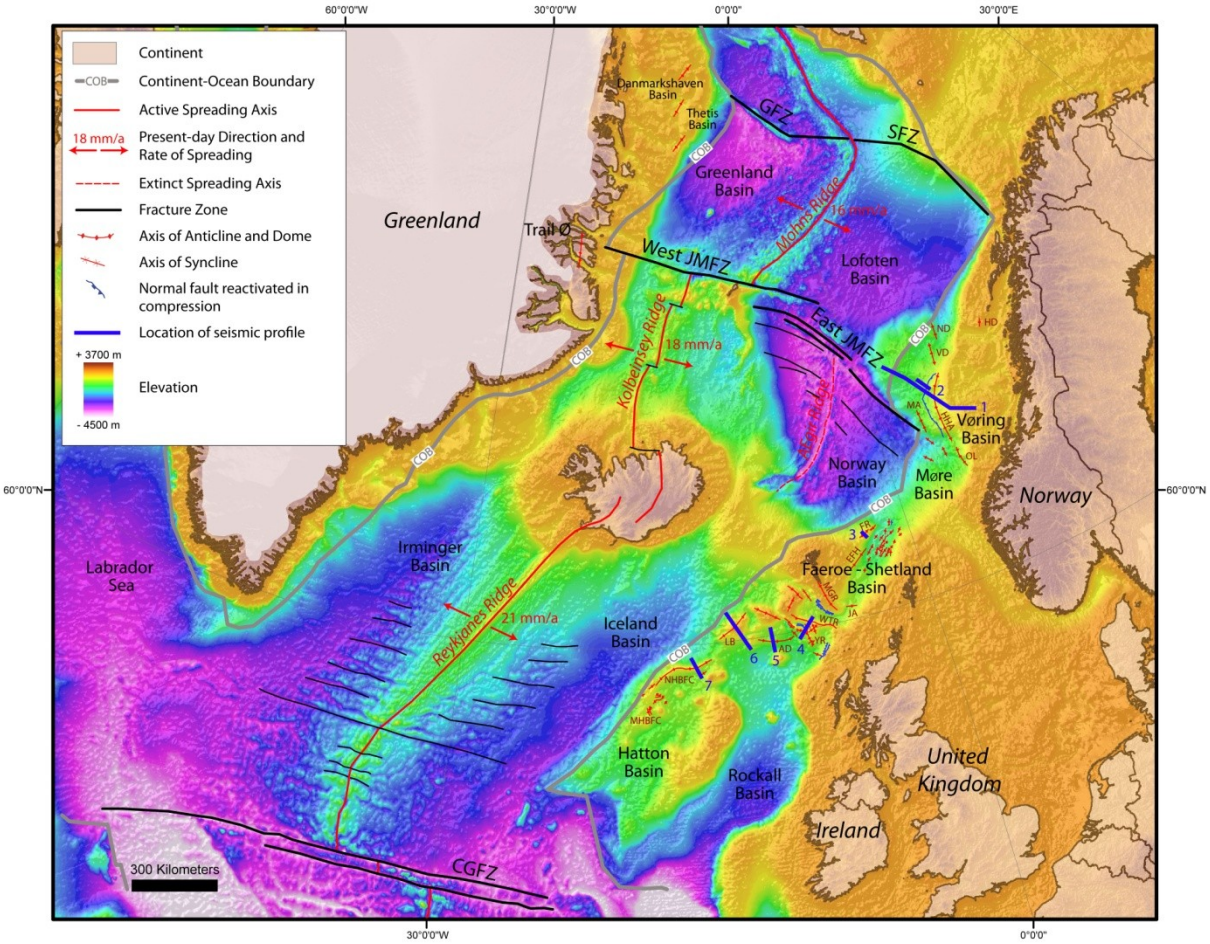

Figure 2.22. *Principal tectonic features of the NE Atlantic Ocean on a bathymetric and topographic map (ETOPO1). Compressional structures (folds and reverse faults) on NW European Continental Margin are from Johnson et al. (2005); Doré et al. (2008), and Tuitt et al. (2010). Present-day spreading rates along ridges are from Mosar et al. (2002). Continent-Ocean Boundaries of Europe and Greenland are from Olesen et al. (2007)and Gaina et al. (2009). Blue lines indicate cross-sections of Figures 2.23 and 2.24. Abbreviations (North to South): GFZ, Greenland Fracture Zone; SFZ, Senja Fracture Zone; JMFZ, Jan Mayen Fracture Zone (West and East); HD, Hedda Dome; ND, Naglfar Dome; VD, Vema Dome; MA, Modgunn HHA, Helland Hansen Arch; OL, Ormen Lange Dome; FR, Fugløy Ridge; EFH, East Faeroe High; MGR, Munkagrunnar Ridge; JA, Judd Anticline; WTR, Wyville Thomson Ridge; YR, Ymir Ridge; AD, Alpine Dome; LB, Lousy Bank; NHBFC, North Hatton Bank Fold Complex; MHBFC, Mid Hatton Bank Fold Complex; CGFZ, Charlie Gibbs Fracture Zone. Map projection is Universal Transverse Mercator (UTM, WGS 1984, zone 27N).*

Numerous folds, inverted basins and normal faults reactivated in compression, are widely observed along the NW European Margin. These structures are interpreted as episodes of compressional post-breakup deformation of the continental margin (*Boldreel and Andersen*, 1993; *Doré and Lundin*, 1996; *Brekke*, 2000; *Lundin and Doré*, 2002; *Davies et al.*, 2004; *Hitchen*, 2004; *Smallwood*, 2004; *Stoker et al.*, 2005; *Johnson et al.*, 2005; *Løseth and Henriksen*, 2005; *Ritchie et al.*, 2003, 2008; *Doré et al.*, 2008; *Tuitt et al.*, 2010) (**Figure 2.22**). Along the East Greenland Margin, little evidence of post-breakup compressional deformation exists on the northeast part of the margin (*Price et al.*, 1997; *Hamann et al.*, 2005).

2.3.3.1 Deformation on Norwegian Margin

On the Norwegian Margin, compressional doming, basin inversion and reverse faulting occurred during the Cenozoic, predominantly within deep Cretaceous depocentres in the Vøring Basin (*Lundin and Doré*, 2002) and north of the Møre Basin along the Jan Mayen lineament (*Brekke*, 2000). This compressional deformation is responsible for the development of arches and domes, such as the Ormen Lange, Vema and Naglfar Domes and the Modgunn and Helland-Hansen Arches (**Figures 2.22**). These structures generally have N-S to NNE-SSW trends. The largest structure is the Helland-Hansen Arch with an axial trace of approx. 280 km, maximal amplitude of approx. 1 km and maximal wavelength in the order of 60 km (*Vågnes et al.*, 1998, **Figures 2.22 and 2.23**). *Vågnes et al.*, 1998 estimated that the total shortening is in the order of 2-3 %.

Lundin and Doré (2002) described two main phases of strike-slip-compression and of formation of large N- and NNE-trending domes and arches (e.g. the Ormen Lange Dome and the Helland Hansen Arch): in (1) the Middle Eocene to Early Oligocene and (2) the Early Miocene. *Løseth and Henriksen* (2005) determined, from seismic data of the syn-tectonic Kai Formation in the area of the Helland Hansen Arch, a Mid- to Late Miocene (15-10 Ma) compression phase. *Doré and Lundin* (1996) suggested that the compressional domes were formed by left-lateral reactivation of NW-SE trending lineaments, subparallel to or directly in the continuation of the JMFZ.

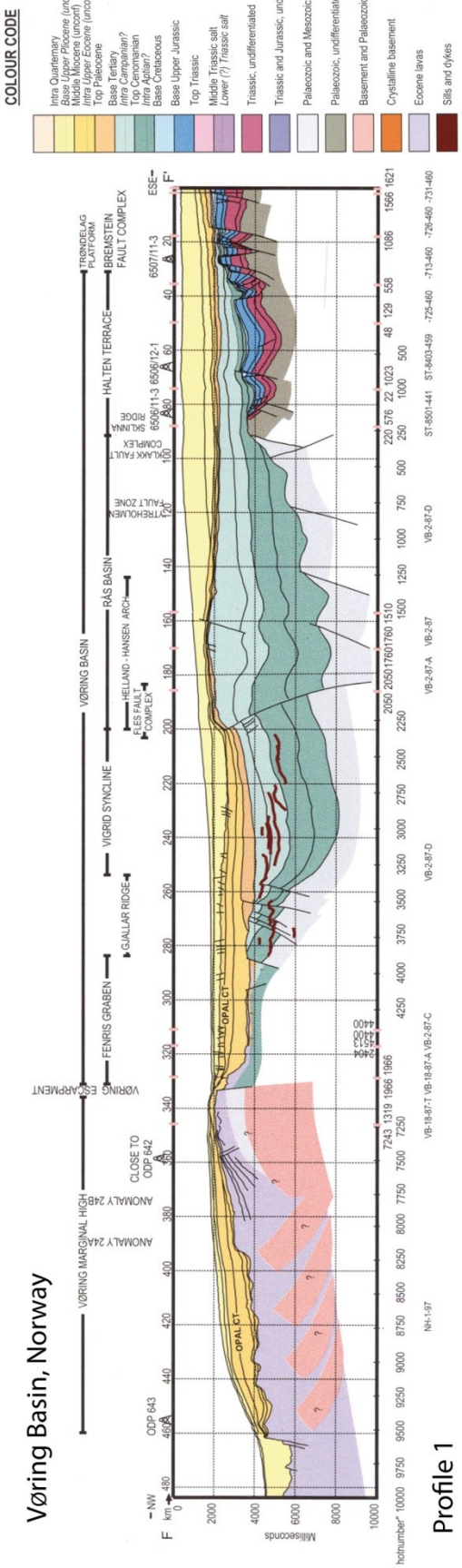
Vøring Basin, Norway
COLOUR CODE
Intra Quaternary
Base Upper Pliocene (unconf)
Middle Miocene (unconf)
Intra Upper Eocene (unconf)
Top Paleocene
Basa Tertiary
Intra Campanian?
Top Cenomanian
Intra Aptian?
Base Cretaceous
Base Upper Jurassic
Top Triassic
Middle Triassic salt
Lower (?) Triassic salt
Triassic, undifferentiated
Triassic and Jurassic, undifferentiated
Palaeozoic and Mesozoic, undifferentiated
Palaeozoic, undifferentiated
Basement and Palaeozoic, undifferentiated
Crystalline basement
Eocene lavas
Sills and dykes
TRØNDELAG PLATFORM
VØRING BASIN
BREMSTEIN FAULT COMPLEX
HALTEN TERRACE
RÅS BASIN
VIGRID SYNCLINE
HELLAND - HANSEN ARCH
FENRIS GRABEN
GJALLAR RIDGE
VØRING MARGINAL HIGH
VØRING ESCARPMENT
ANOMALY 24B
ANOMALY 24A
CLOSE TO ODP 642
ODP 643
OPAL CT
NW
ESE
F
F'
Millisecconds
km
Profile 1

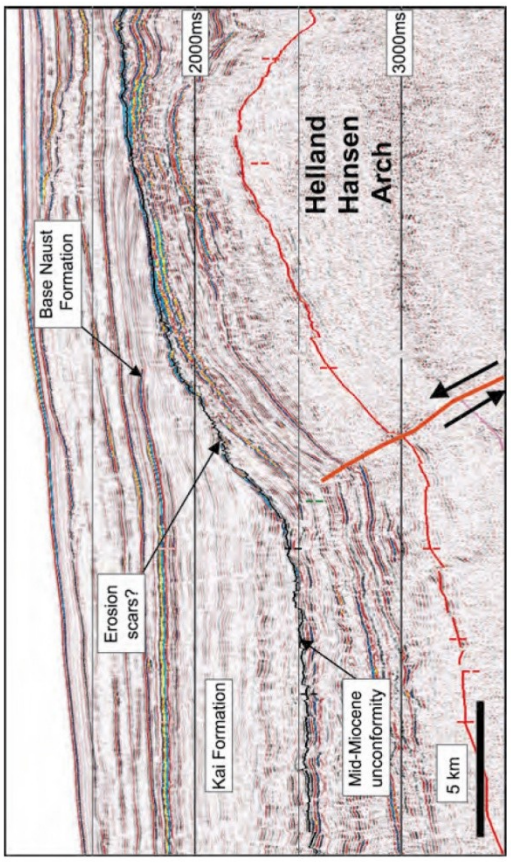
Base Naust Formation
Erosion scars?
Kai Formation
Mid-Miocene unconformity
Helland Hansen Arch
2000ms
3000ms
5 km
Profile 2

Figure 2.23. (previous page) *Interpreted seismic profiles across the Helland-Hansen Arch, in Vøring Basin, Norway, from Brekke (2000) for Profile 1 and Løseth and Henriksen (2005) for Profile 2, showing reactivation of a normal fault in compression on the western flank of the Helland-Hansen Arch. Locations of profiles are on Figure 2.22.*

2.3.3.2 Deformation on Faeroe-Rockall Plateau and Faeroe-Shetland Basin

On the Faeroe-Rockall Plateau, the compressional structures are different from those on the Norwegian Margin and they vary in size, trend and shape (*Tuitt et al.*, 2010). North of the Faeroe-Shetland Basin, the trend of anticlines is predominantly NE-SW (e.g. the Fugløy Ridge), whereas in the south, their trend is mainly NW-SE (e.g. the Munkagrunnar Ridge) (**Figures 2.22. and 2.24**). On the southern part of the plateau, on the Hatton Bank, the trend of the compressional structures varies from mostly NE-SW (e.g. the Mid-Hatton Bank Fold Complex) to NNE-SSW (e.g. the North Hatton Bank Fold Complex) (**Figures 2.22 and 2.24**). In all areas, the folds reach approx. 2 to 4 km in amplitude and 40 km in wavelength (*Johnson et al.*, 2005).

Boldreel and Andersen (1998) proposed three main phases of compressional deformation, each resulting in a distinct structural trend: (1) In the Palaeocene – Early Eocene, when WNW-trending (e.g. the Wyville-Thomson Ridge), NNW-trending (e.g. Munkagrunnar Ridge) and ENE-trending (e.g. Fugløy Ridge) structures developed; (2) In the Oligocene, when NE-ENE-trending folds grew, east of the Faeroe Islands and between the Faeroe Islands and the Hatton Bank; (3) In the Miocene, when NW-trending anticlines developed perpendicularly to the continental margin. More recent studies, using seismic reflection data, have shown that the NE-ENE-trending structures in the NE Faeroe-Shetland Basin developed mainly during the Early Miocene to Middle Miocene and may have continue to grow during Early Pliocene to Recent times (*Johnson et al.*, 2005; *Ritchie et al.*, 2003, 2008). Though, *Johnson et al.* (2005) and *Ritchie et al.* (2003, 2008) have suggested an older phase of deformation in the Fugløy Ridge, during the Eocene and Oligocene. South of the WTYR area, the Alpine dome formed during the Oligocene, whereas further south, the North Hatton Bank Fold Complex formed in the Middle-Late Eocene to Early Oligocene (*Johnson et al.*, 2005; *Ritchie et al.*, 2003, 2008). *Tuitt et al.* (2010) described several compressional unconformities on the Faeroe-Rockall Plateau, varying from Late Palaeocene to Early Oligocene ages.

Faeroe-Rockall Margin

Profile 3

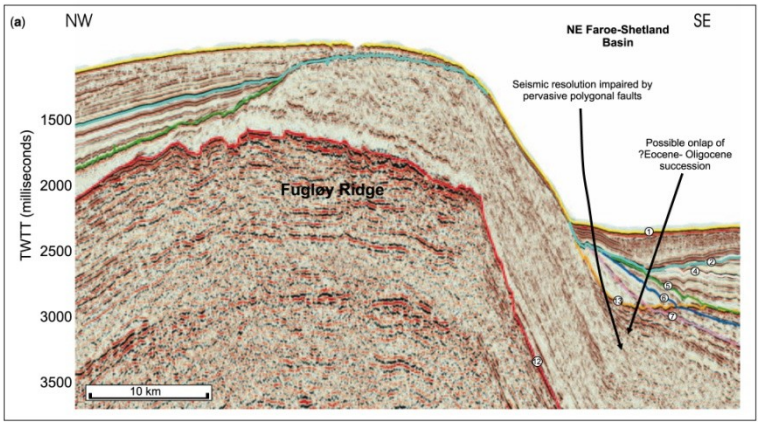

Profile 4

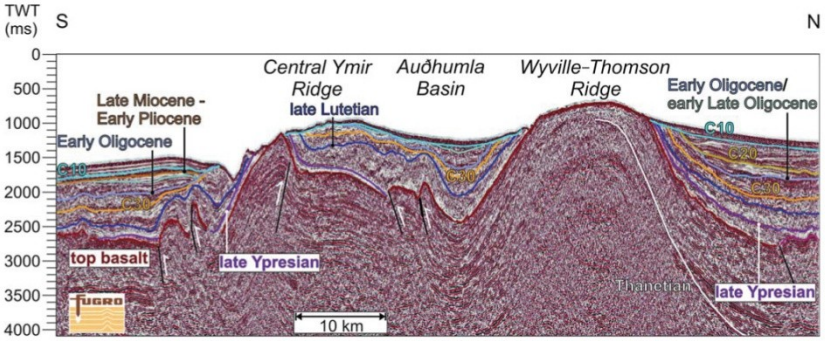

Profile 5

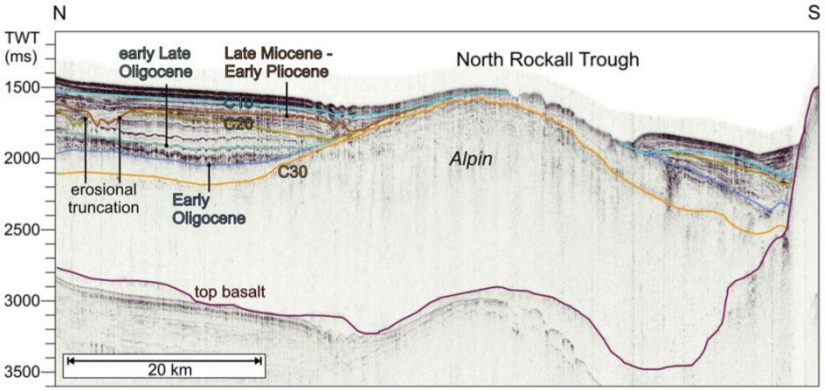

Profile 6

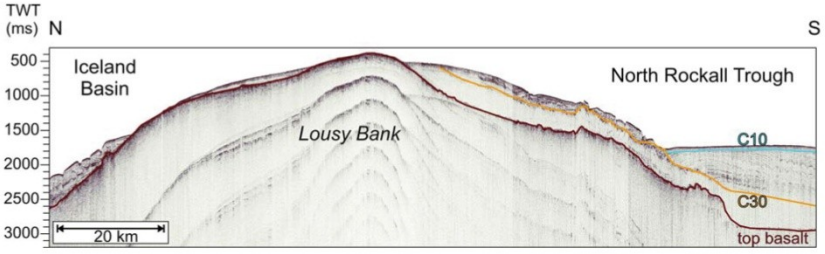

Profile 7

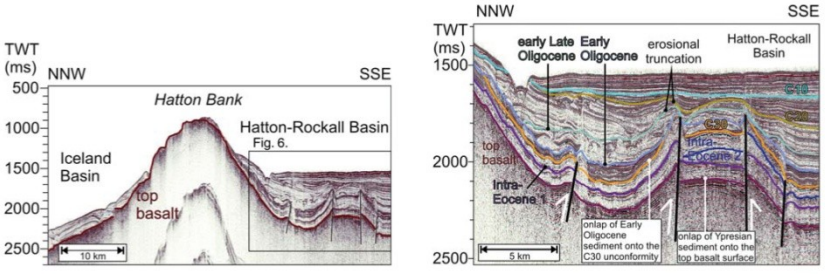

Figure 2.24. (previous page) *Interpreted seismic profiles across the Fugløy Ridge (Profile 3), the Ymir and Wyville-Thomson Ridges (Profile 4), the Alpine Dome (Profile 5), the Lousy Bank (Profile 6) and the North Hatton Bank Fold Complex (Profile 7), showing post-breakup compressional structures on the Faeroe-Rockall Margin, NW Europe. Profile 3 is from Johnson et al. (2005) and profiles 4 to 7 are from Tuitt et al. (2010). Locations of profiles are on Figure 2.22.*

2.3.3.3 Deformation on North East Greenland Margin

Similar, although less studied, features have been identified onshore East Greenland (*Price et al.*, 1997) and offshore NE Greenland (*Hamann et al.*, 2005)

Price et al. (1997) have described a post-54 Ma period of compression of the Trail Ø region (**Figure 2.22**), indicated by the development of folds that affect Tertiary dolerite sills. These folds have wavelengths in the order of 5-10 km and axes trending approximately N-S (**Figure 2.22**). They have also described a post-54 Ma period of extension and magmatism around 36 Ma that they interpret as related to the separation of the JMMC from East Greenland. They furthermore suggest that the extension of East Greenland ended when the Kolbeinsey Ridge totally separated Greenland from the JMMC, between anomalies Chron 7 and Chron 6 (26.4-19.4 Ma, **section 2.4**), and that the compression post-dated the extension and occurred in Late Miocene time, as in the Vøring Basin and Faeroe-Shetland Basin.

Furthermore, seismic data, of the NE Greenland Margin, show low-amplitude folds in the upper part of a Late Oligocene to Miocene sedimentary sequence in the Thetis Basin (mega-sequence TIII, **Figure 2.18**) and faults that occur throughout the shelf area, in NE trending zones about 10-20 km wide (*Hamann et al.*, 2005). These faults are steeply dipping and convergent, and have reversal component and throws of up to approx. 200 m along the Danmarkshavn Basin, which is characteristic of strike-slip movement. *Hamann et al.* (2005) therefore suggest a period of compression affecting the NE Greenland Margin during the Late Miocene.

Figure 2.25 summarizes the timing and possible mechanisms of development of the main compressional structures of the NW European and NE Greenland margins. I discuss in next section the possible mechanisms at the origin of these post-breakup deformations.

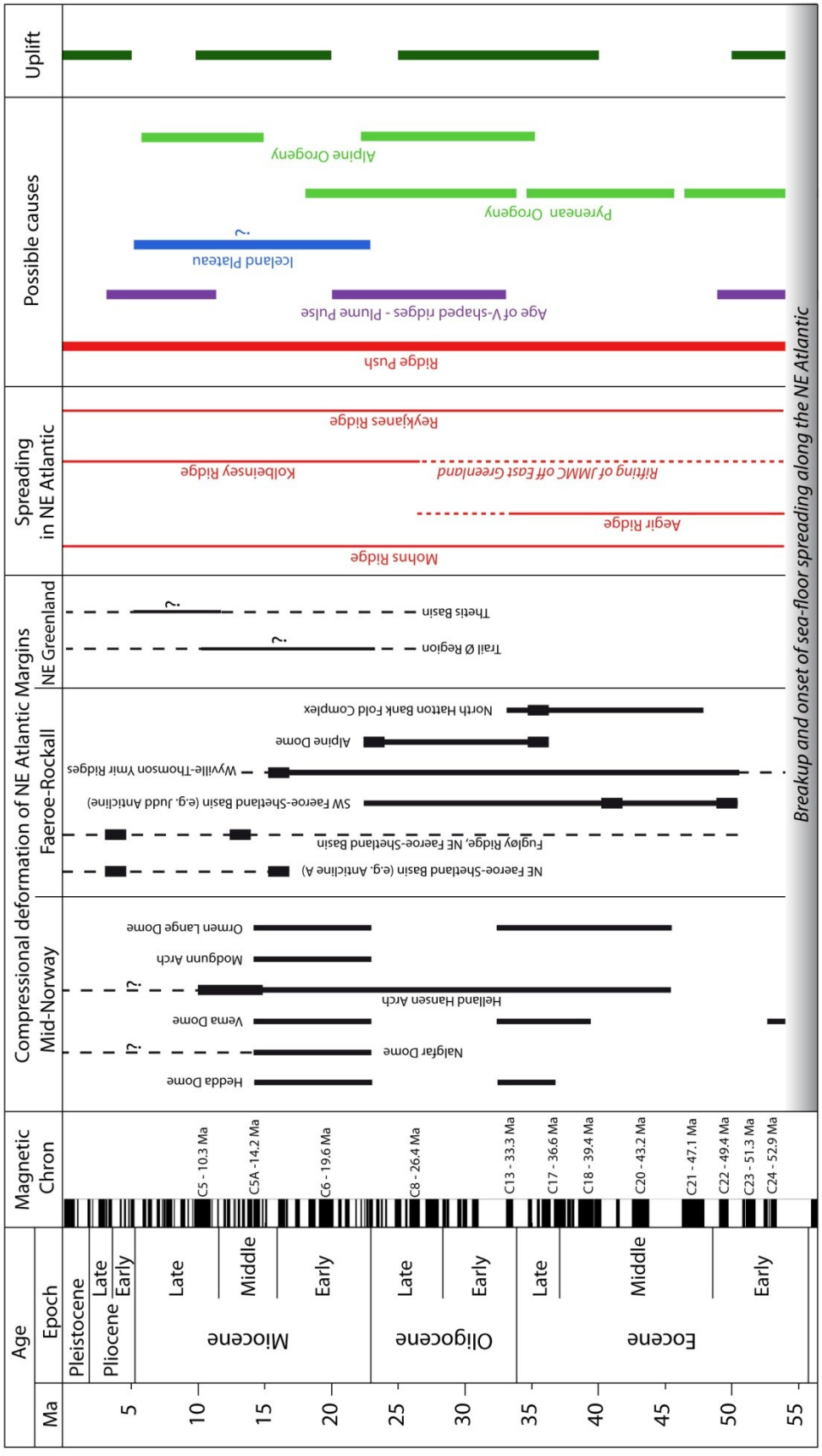

Figure 2.25. *Chronological summary of (1) compressional deformation that affected Mid-Norwegian Margin (from Doré and Lundin, 1996; Brekke, 2000; Løseth and Henriksen, 2005; Doré et al., 2008), Faeroe-Rockall Margin (from Smallwood et al., 2004; Johnson et al., 2005; Ritchie et al., 2003, 2008; Tuitt et al., 2010) and NE Greenland Margin (from Price et al., 1997; Hamann et al., 2005); (2) sea-floor spreading along NE Atlantic; (3) possible mechanisms causing compressional deformation: ridge push, Iceland Mantle Plume pulse enhancing ridge-push (correlation between age of V-shaped ridges and plume pulse from White and Lovell, 1997), formation of Iceland Plateau (from Doré et al., 2008), and compressional Alpine and Pyrenean stress field (from Tuitt et al., 2010); and (4) main phases of uplift that affected NE Atlantic Region during Cenozoic time (from Anell et al., 2009; Holford et al., 2009).*

2.3.3.4 Mechanisms of post-breakup compressional deformation

Numerous mechanisms for the formation of theses compressional structures have been suggested and are still subject of debate (**Figure 2.25**). I summarize the principal proposed mechanisms below.

(1) Sedimentary flank loading and differential compaction

Stuevold et al. (1992) have suggested that intra-basinal arching, such as the Helland-Hansen Arch in the Vøring Basin, is a result of differential subsidence during the Eocene and Oligocene, and of Neogene differential loading and compaction of thick Cretaceous clays that reactivated Late Cretaceous to Paleogene faults. However, this mechanism is unlikely a primary cause of the structures; an initial tectonic impulse is necessary (*Doré et al.*, 2008).

(2) Alpine stress field

Several authors have suggested that the stress from the Alpine Orogeny was responsible for the formation of Cenozoic inversion structures on the NW European Continental Margin (e.g. *Roberts*, 1989; *Boldreel and Andersen*, 1993, 1998; *Vågnes et al.*, 1998; *Brekke*, 2000). This idea has been applied to inversion features observed in the North Sea (*Ziegler*, 1989b) and there is reasonable correspondence in age between period of compressive phases on the NE European Margin and the Alpine events. However, to explain the compressional deformation on the Norwegian and the E Greenland margins, other authors argue against this hypothesis (e.g. *Doré et al.*, 1999; *Mosar et al.*, 2002; *Doré et al.*, 2008). Indeed, the Norwegian Margin lies on the Scandinavian craton and the Sorgenfrei-Tornquist Zone separates it from the North Sea area and Central Europe (**Figure 2.11**). Therefore, the far-field stresses from the Alpine Orogeny may strongly deflect across this lithospheric boundary and may not act significantly on the Norwegian Margin (e.g. *Mosar et al.*, 2002). The East Greenland Margin was decoupled from the Alpine stress by a spreading ridge, and thus the development of folds in this area cannot be attributed to direct propagation of the Alpine stress (*Doré et al*., 1999; 2008).

(3) Ridge Push

The Ridge Push force from the NE Atlantic Ridge, roughly perpendicular to the ridge axis, may explain the formation, or at least the initiation, of inversion structures on the NE Atlantic Margin (e.g. *Boldreel and Andersen*, 1993, 1998; *Doré and Lundin*, 1996; *Price et al.*, 1997;

Vågnes et al., 1998; *Pascal and Gabrielsen*, 2001). Ridge Push is generally thought to be the dominant force acting on passive margins, and can in some circumstances generate enough stress to cause mild deformation (e.g. *Doré et al.*, 2008). It originates from a lateral distribution pressure gradient that acts on the entire plate normal to the strike of a mid-oceanic ridge and arises from the isostatic sinking of the oceanic lithosphere away from the mid-oceanic ridge as it cools and densifies (*Wilson*, 1993). Ridge push force may be effective only after the newly formed oceanic lithosphere has cooled and contracted for more that 30 Ma (*Mosar et al.*, 2002) and estimates of its magnitude are 2.8 10^{12} N/m for 80 Ma oceanic crust (*Dahlen*, 1981). However, the time elapsed between onset of sea-floor spreading in the NE Atlantic and compressional deformation on the adjacent margin is very little, it is therefore difficult to invoke ridge push force alone as the cause of the deformation (*Lundin and Doré*, 2002). Moreover, this mechanism alone does not seem to be able to explain either the episodic timing or the location of the structures in the Vøring Basin, rather than in the Møre Basin (*Mosar et al.*, 2002; *Doré et al.*, 2008).

(4) Pulses of the Iceland Mantle Plume and plume-enhanced ridge push

Lundin and Doré (2002) have suggested that a plume-enhanced ridge push was the main driving force for compressional deformation of the Norwegian Margin. Model of *Bott* (1991) have shown that double of the ridge push force (6.2 10^{12} N/m) should develop as a result of a ridge being underlain by an anomalously hot upper mantle such as in the NE Atlantic. Therefore, the force may be sufficient to deform the margin. Moreover, *Lundin and Doré* (2002) have suggested that plume-enhanced ridge push would explain both the episodic timing of the deformation and the location of deformation on both sides of the ridge. Indeed, the Iceland Plume appears to have been pulsating, since at least the Early Palaeocene, and periods of high plume activity have been correlated with pulses in sedimentation both in the North Sea and in the Faeroe-Shetland Basin (*White and Lovell*, 1997). *White and Lovell* (1997) have associated prominent V-shaped topographic ridges along the Reykjanes Ridge with periods of high plume flux. Based on the work of *White and Lovell* (1997), *Lundin and Doré* (2002) distinguished three periods of more concentrated plume activity: (1) Late Palaeocene – Early Eocene, approx. 60-48 Ma; (2) Late Eocene to Early Miocene, approx. 33-20 Ma; (3) Mid Miocene to Pliocene, approx. 11-4 Ma. These periods correlate reasonably well with compressional events on the Faeroe-Rockall area but less with well with the compressional deformation on the Norwegian Margin. Despite the uncertainties, these authors have suggested that plume-enhanced spreading is a plausible driving force for the mid-

Cenozoic compressional deformation on the margins. *Tuitt et al.* (2010) link the Late Eocene to Early Oligocene compressional event affecting the Faeroe-Rockall area with plume-enhanced ridge push. They moreover suggest that the Alpine and Pyrenean compression amplified the effects of plume-enhanced ridge push, which is coherent with the fact that the NE Greenland Margin that was not affected by the Alpine stress displays milder deformation in comparison with that on the NE Atlantic Margin.

(5) Stress associated with the development of the Iceland Plateau

Doré et al. (2008) proposed that the primary agent generating the body force acting on NE Atlantic passive margins was the development of the Iceland Plateau in Miocene times, but the age remains poorly constrained. They have estimated the difference in gravitational potential energy between the Iceland Plateau and the adjacent Norwegian Margin, and thus the force applied to the margin, to be about 5 10^{12} N/m . They have moreover estimated the horizontal stress between 50 and 150 MPa, which may have been enough to deform adjacent margins. This process may explain the episodic development, specifically the pulse in the early middle Miocene, and the location of the compressional structures around Iceland. However, this does not seem to explain the earlier phases of compressional deformation.

(6) Differential sea-floor spreading, mantle drag and upper v. lower plate geometry

Mosar et al. (2002) have suggested that the variations in spreading rates between the Mohns, Aegir and Reykjanes ridges (with greater spreading rates along the Mohns and Reykjanes ridges than along the Aegir Ridge) was responsible for the development of inversion structures in the Vøring Basin and Faeroes-Rockall Plateau rather than in the Møre Basin. Moreover, they have shown that spreading along the Aegir Ridge was asymmetric and suggested that this asymmetry caused differential mantle drag at the base of the lithosphere, with less mantle drag in the Møre Basin. Furthermore, they have suggested that upper plate margins such as the Vøring Basin and probably the Faeroe Basin have a lower compressional strength than lower plate margins such as the Møre Basin, and therefore developed inversion structures more readily.

Not one of these mechanisms appears to be sufficient to explain alone the development of compressional post-breakup deformation of the NE Atlantic margins. Therefore, complementary research is necessary to test these hypotheses. Indeed, the NE Atlantic margins represent attractive hydrocarbon exploration targets for the petroleum

industry due to the presence of source rocks in the deep Mesozoic basins and potential traps in the mid-Cenozoic anticlines (e.g. *Doré and Lundin*, 1996; *Lundin and Doré*, 2002; *Davison et al.*, 2010; *Japsen et al.*, 2010; *Tuitt et al.*, 2010). Therefore, it is useful to understand the structure and evolution of the margins, more particularly the timing, location and causes of the development of post-breakup deformation on the margins, and to restore at best the sea-floor spreading history of the NE Atlantic and its impact on the adjacent continental margins.

2.4 Kinematic models for opening of North East Atlantic

Since the work of *Bullard et al.* (1965) on continental fits around the Atlantic, numerous kinematic reconstructions of the NE Atlantic have been proposed, e.g. by *Pitman and Talwani* (1972); *Vogt and Avery* (1974); *Talwani and Eldholm* (1977); *Le Pichon et al.* (1977); *Unternehr* (1982); *Nunns* (1983); *Archambault* (1984); *Bott* (1985); *Srivastava and Tapscott* (1986); *Bott* (1987); *Rowley and Lottes* (1988); *Fidalgo Gonzales* (2001); *Torsvik et al.* (2001b); *Gaina et al.* (2002); *Lundin and Doré* (2002); *Scott et al*. (2005); *Gaina et al.* (2009).

Early reconstructions using a two rigid plates (Eurasia and Greenland) led to gaps and overlaps between them (e.g. *Bullard et al.*, 1965; *Rowley and Lottes*, 1988) especially due to the complex spreading history of the Jan Mayen Segment (e.g. *Unternehr*, 1982; *Nunns*, 1983; *Bott*, 1985, 1987). Through the years, the acquisition of new geophysical and geological data in the NE Atlantic on the Jan Mayen Microcontinent and on the continental margins led to better kinematic reconstructions of the NE Atlantic. Several models include a subdivision of the plates that improves the fit (e.g. *Lundin and Doré*, 2002; *Gaina et al.*, 2009). The global geodynamic evolution of the NE Atlantic since sea-floor spreading is well established and can be summarized as below. However, when looking in detail, some problems in kinematic reconstruction remain unsolved, especially concerning the complex spreading history of the Jan Mayen Segment.

In the Late Palaeocene, Greenland and Eurasia separated by northward propagation of sea-floor spreading from the central North Atlantic (e.g. *Pitman and Talwani*, 1972; *Vogt and Avery*, 1974; *Srivastava and Tapscott*, 1986). A triple-junction existed between the North Atlantic and the Labrador Sea ridges until the extinction of the latter at about 35 Ma (e.g. *Vogt and Avery*, 1974). This extinction triggered a change in spreading direction between Europe and Greenland at about that time (e.g. *Vogt and Avery*, 1974*; Srivastava and Tapscott*, 1986;

Srivastava and Roest, 1999). After continental break up (~56 Ma) (e.g. *Nunns*, 1983), the mid-oceanic ridge between the Greenland and the Eurasian margins became offset to the east along the northern flank of the GIFR (*Nunns*, 1983; *Bott*, 1985, 1987; *Lundin and Doré*, 2002). Sea-floor spreading occurred along the Aegir Ridge on the eastern side of the JMMC, which was part of Greenland at that time (e.g. *Nunns*, 1983). During the Eocene, continental extension occurred in the south-western part of the JMMC, in the prolongation of the Reykjanes Ridge (*Unternehr*, 1982; *Nunns*, 1983; *Bott*, 1985, 1987; *Kodaira et al.*, 1998; *Gaina et al.*, 2009; *Gernigon et al.*, 2011; *Peron-Pinvidic et al.*, 2011). *Gernigon et al.* (2011) have suggested that a major phase of extension of the JMMC occurred around Chron 21 (47.1 Ma) and that a complementary fan-shaped spreading initiated at that time along the Aegir Ridge. This continental extension reached break-up southwest of the JMMC around Chron 17 and Chron 13 (36.6 – 33.3 Ma) and a new spreading centre, the Kolbeinsey Ridge, formed north of the Reykjanes Ridge and progressively propagated northward (*Talwani and Eldholm*, 1977; *Unternehr*, 1982; *Nunns*, 1983; *Bott*, 1985, 1987; *Skogseid et al.*, 2000; *Müller et al.*, 2001; *Scott et al.*, 2005; *Gaina et al.*, 2009;). The JMMC drifted off Greenland, progressively from south to north, and underwent a 30° counter-clockwise rotation (*Nunns*, 1983; *Bott*, 1987). The Kolbeinsey Ridge reached the JMFZ and therefore totally separated the JMMC from Greenland, between Chron 8 and Chron 6 (26.4 – 19.6 Ma) (e.g *Gaina et al.*, 2009; *Lundin and Doré*, 2002). Contemporaneously, sea-floor spreading ceased along the Aegir Ridge and the JMMC became part of the Eurasian plate (*Unternehr*, 1982; *Talwani and Eldholm*, 1977; *Nunns*, 1983; *Bott*, 1985, 1987; *Skogseid et al.*, 2000; *Müller et al.*, 2001; *Lundin and Doré*, 2002; *Scott et al.*, 2005; *Gaina et al.*, 2009). *Müller et al.* (2001) have suggested that the Iceland Mantle Plume was responsible for rifting on the edge of the eastern Greenland margin, subsequent formation of the JMMC and establishment of the Kolbeinsey Ridge west of the JMMC. According to the stationary hot spot model of *Lawver and Müller* (1994), the Iceland Plume head was underneath the eastern Greenland Margin at that time (40-30 Ma). Then in Miocene time, the plume head was beneath the Reykjanes Ridge axis and created the Iceland Plateau (*Doré et al.*, 2008). Since Chron 6 (19.6 Ma), the Kolbeinsey Ridge has been the only active spreading centre in the Jan Mayen Segment (e.g. *Gaina et al.*, 2009).

If we compare two kinematic reconstructions of the NE Atlantic, one from *Lundin and Doré* (2002) and the other from *Gaina et al.* (2009), we can see that these authors interpret differently the evolution of the European continent-ocean boundary. Indeed, the model of

Lundin and Doré (2002, **Figure 2.26**) predicts a significant offset between the Reykjanes and Jan Mayen segments, along the Faeroe Fracture Zone (FFZ), and between the Jan Mayen and Mohns segments, along the JMFZ, at Chron 24 and these offsets diminish during sea-floor spreading; whereas in the model of *Gaina et al.* (2009, **Figure 2.27**), these authors assume that the Greenland and Eurasian continents are rigid and that the ocean-continent boundary does not change through time. They accommodate the fan-shaped spreading along the Aegir Ridge by the progressive separation of the JMMC from Greenland.

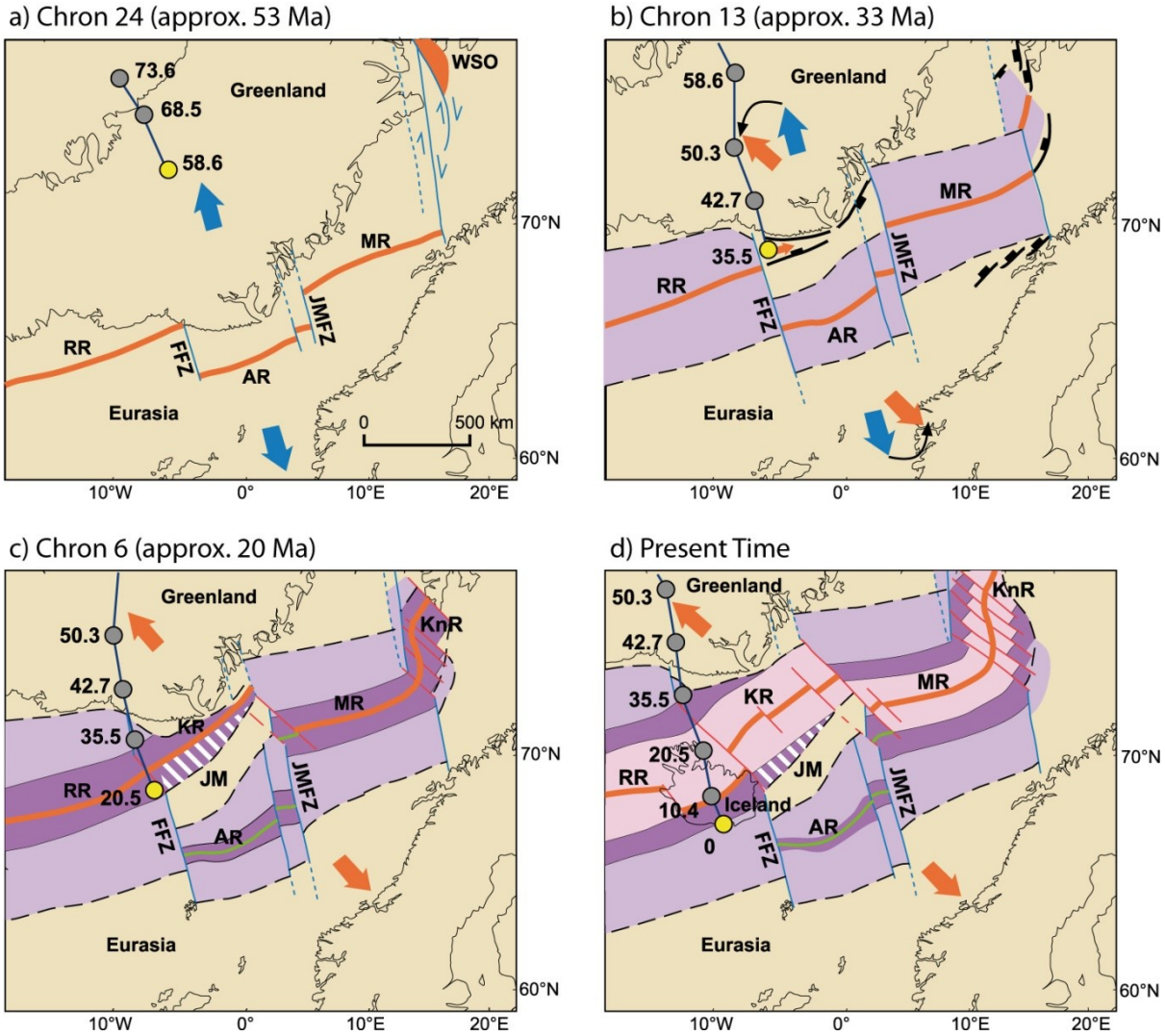

Figure 2.26. *Plate tectonic evolution of NE Atlantic from Lundin and Doré (2002, modified). Grey and yellow dots mark position of Iceland Plume centre; grey dots mark previous positions and yellow dots approximate position at each reconstruction. Position of Iceland Plume centre is from Torsvik et al. (2001a). Bold red lines indicate active spreading ridge, red line represents extinct ridge. Blue and red arrows show relative plate motion, with a*

change in direction at Chron 13. Abbreviations: AR, Aegir Ridge; FFZ, Faeroe Fracture Zone; JM, Jan Mayen Microcontinent; JMFZ, Jan Mayen Fracture Zone; KR, Kolbeinsey Ridge; KnR, Knipovitch Ridge; MR, Mohns Ridge; RR, Reykjanes Ridge; WSO, West Spitsbergen Orogeny.

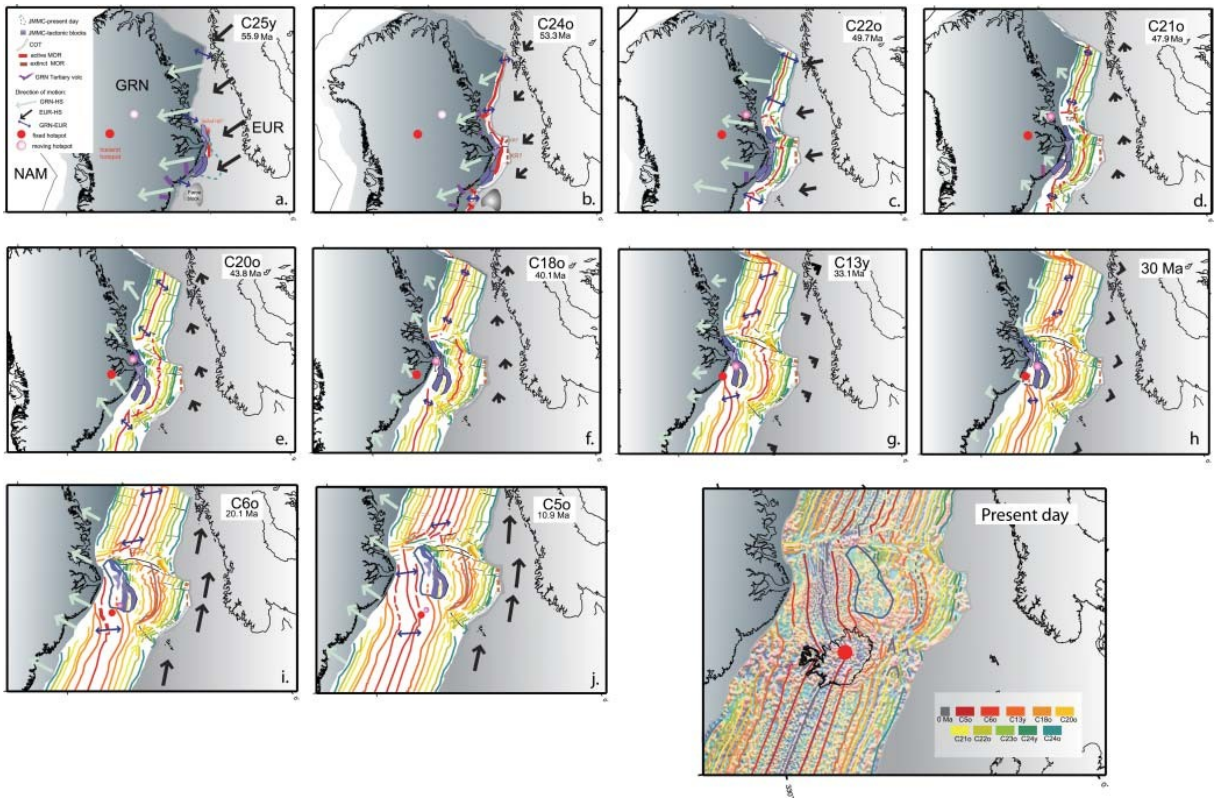

Figure 2.27. *Kinematic reconstruction of NE Atlantic and Jan Mayen Microcontinent in an absolute reference frame from Gaina et al. (2009). Abbreviations: JMMC, Jan Mayen Microcontinent; COB, Continent-Ocean Boundary; MOR, Mid-Oceanic Ridge; GRN, Greenland; NAM, North America; EUR, Eurasia; HS, Hotspot.*

However, when comparing the rotation poles of *Gaina et al.* (2009) with our magnetic dataset (compilation from *Macnab et al.*, 1989; *Skogseid et al.*, 2000; *Gaina et al.*, 2002; *Jones et al.*, 2002b; *Olesen et al.*, 2007; *Gernigon et al.*, 2009; *Maus et al.*, 2009), we see that there are misfits in reconstruction of the conjugate magnetic anomalies of the Aegir Ridge (**Figure 2.28.**). This suggests that relative displacements along the FFZ and JMFZ may have occurred during sea-floor spreading, as suggested by the model of *Lundin and Doré* (2002). This relative displacement may be due to differential spreading along the Aegir Ridge, visible by the fan-shaped of the conjugate anomalies, and between the Reykjanes, Aegir and Mohns ridges, as suggested by *Mosar et al.* (2002).

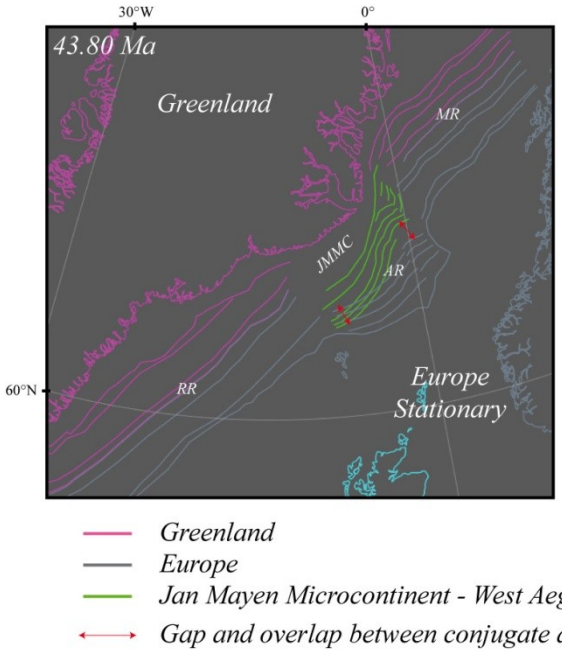

Finite rotations of the northern Jan Mayen microcontinent relative to a fixed Eurasia plate

Chron	Age	Latitude	Longitude	Angle
	30.0	0.00	0.00	0.00
13y	33.1	67.11	129.15	0.62
18o	40.1	−58.90	157.90	8.52
20o	43.8	−60.03	158.66	13.22
21o	47.9	−56.49	153.68	12.89
22o	49.7	−54.60	154.09	13.57
23o	50.9	−55.44	154.43	15.99
24o	53.3	−27.28	136.06	7.11
25y (fit)	55.9	−40.00	145.00	11.40

Figure 2.28. *Gap and overlap (in red arrows) of conjugate anomalies of the Aegir Ridge in kinematic reconstruction of the NE Atlantic at 43.80 Ma. Rotation poles are from Gaina et al (2009). Abbreviation: AR, Aegir Ridge; JMMC, Jan Mayen Microcontinent; MR, Mohns Ridge; RR, Reykjanes Ridge.*

In this thesis, I will investigate more fully this idea of differential sea-floor spreading along the NE Atlantic ridge system. I have used a palinspastic reconstruction method in order to obtain a best fit of the conjugate anomalies of the Aegir Ridge and to calculate spreading rates of each ridge system and relative displacement along the main oceanic fracture zones (Chapters 3). I will investigate furthermore the role of this differential spreading on post-breakup compressional deformation of the adjacent continental margins, following *Mosar et al.* (2002), and the influence of the Iceland Plume on differential sea-floor spreading (Chapter 4).

Chapter 3

Restoration Method and Application to opening of NE Atlantic

3.1 Plate Motion Reconstructions using Euler's theorem

To reconstruct the paleopositions of continents is one of the major challenges of plate tectonics (**Chapter 1**). Numerous kinematic reconstructions have been published, using Euler's theorem, to reconstruct paleopositions and motions of tectonic plates (e.g. *Bullard et al.*, 1965; *McKenzie and Parker*, 1967; *Morgan*, 1968; *Pitman and Talwani,* 1972; *Vogt and Avery*, 1974; *Talwani and Eldholm*, 1977; *Le Pichon et al.*, 1977; *Srivastava and Tapscott,* 1986; *Rowley and Lottes*, 1988; *Gaina et al.* 2002, 2009; **Chapters 1 and 2**).

The motion of one plate can be described by a rotation on a sphere, from an initial position to a final position, about an axis passing through the centre of the Earth, and at an angular velocity (Euler axis and angle; e.g. *Morgan*, 1968; *Greiner*, 1999; *Wessel and Müller*, 2007; **Figure 3.1**). Finite Euler poles for the fit of continents can be determined from the ancient boundaries of continents (e.g. *Bullard et al.,* 1965). Finite Euler poles and stage poles for the description of sea-floor spreading history of oceans are determined by least-squares fits of magnetic lineations and fracture zone datasets (e.g. *McKenzie and Parker*, 1967; *Morgan*, 1968; *Le Pichon et al.*, 1977; *Hellinger*, 1981; *Srivastava and Tapscott*, 1986; *Rowley and Lottes*, 1988; *Gaina et al.* 2002, 2009; **Figure 3.2**). Indeed, the oceanic crust can be represented as a succession of long magnetized blocks, with vertical edges. The blocks are perpendicular to the direction of spreading, have alternately normal and inverse magnetic polarity, and are distributed symmetrically about the ridge axis (e.g. *Vine and Matthews*,

1963; *Archambault*, 1984; **Chapter 1**). Inversions of the Earth magnetic field are thus registered as frontiers between crustal blocks with opposite polarity. These blocks draw in surface linear magnetic anomalies, which are parallel to the ridge axis. On the basis that magnetic anomalies have not deformed they appeared and assuming that the blocks are rigid, it is possible to superpose conjugate magnetic anomalies of two plates and thereby calculate the position of the rotation axis at the time of their formation.

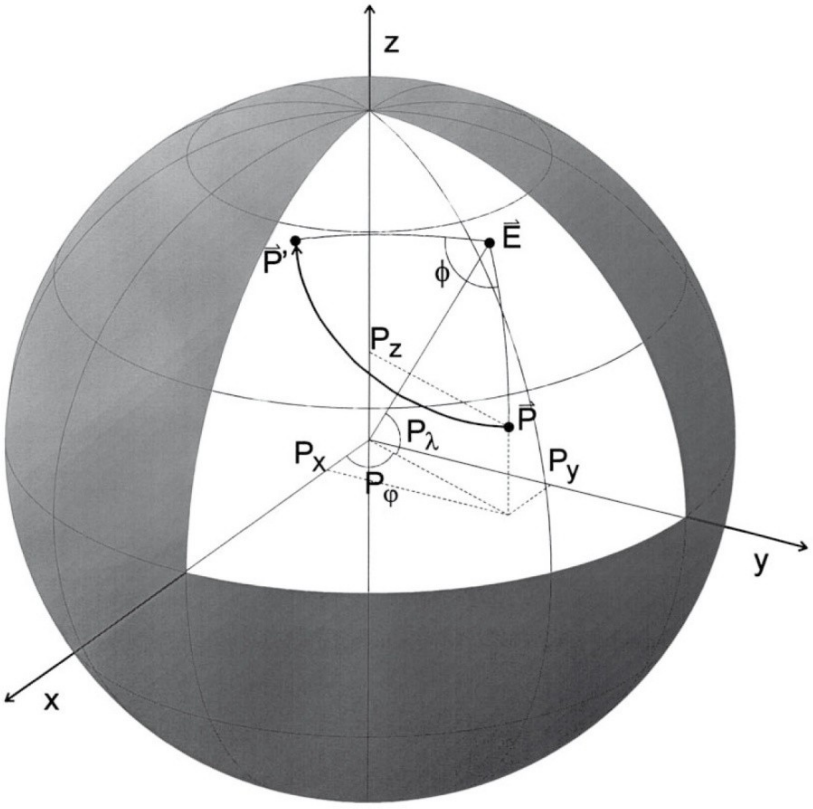

Figure 3.1. *Definition of geographical and Cartesian coordinates of a point and of a rotation angle.* ***P*** *is a point,* ***P'*** *the rotated point,* P_λ *the latitude,* P_φ *the longitude,* ***E*** *the Euler pole and* Φ *the rotation angle (from Greiner, 1999).*

Chang (1987, 1988), *Chang et al.* (1992), *Royer and Chang* (1991) and *Kirkwood et al.* (1999) developed a method, based on the criterion of fit of *Hellinger* (1981), to estimate poles for finite plate motions poles and their uncertainties. In this method, magnetic anomalies and fracture zones data are both regarded as points on two conjugate isochrons, which consist of great circle segments (**Figure 3.2**). The best fit reconstruction is obtained by minimising the sum of the misfits for conjugate sets of data point of magnetic anomalies and fracture zones with respect to individual great circle segments. Consequently, the reconstruction

depends critically on correctly identifying conjugate data points that belong to a common isochron segment (e.g. *Müller et al.*, 1999).

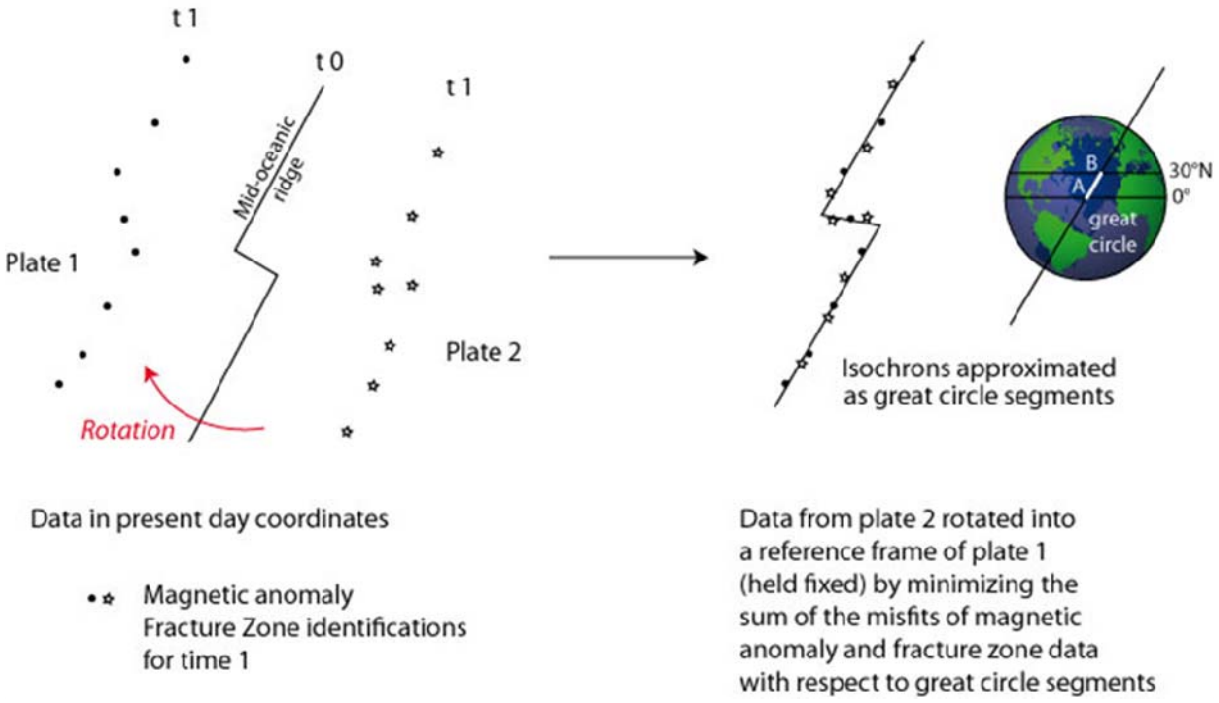

Figure 3.2. *Hellinger*'s (1981) criterion of fit. The rotation of plate 2 to plate 1 is determined by minimizing the sum of misfits for great circle segments (modified from *Wessel and Müller*, 2007).

This method leads to good reconstructions of the spreading history of oceans, at first order. However, at second order, it is difficult to apply this method to the reconstruction complex spreading history of oceanic segment (e.g. the Jan Mayen Segment, **Chapters 1 and 2**) because they may involve fan-shaped ridges and curved magnetic anomalies, such as the conjugate magnetic anomalies of the Aegir Ridge in the NE Atlantic (**Figure 2.28**; **section 2.4**). Therefore, I have used an iterative least-squares method of palinspastic restoration, which minimizes the gaps and overlaps between conjugate magnetic anomalies. This method allows all segments of the NE Atlantic to spread at different rates and takes into account possible deformation on continental margins.

3.2 Palinspastic Restoration Method

In order to take into account possible intraplate deformation (on the European Continental Margin), I have used an iterative least-squares method for palinspastic reconstruction of the opening of the NE Atlantic Ocean. The method proceeds by minimizing gaps or overlaps between adjacent strips of oceanic crust, which follow magnetic anomalies. An early application of this method was to restore deformed surfaces, by minimizing gaps and overlaps between elements (*Cobbold*, 1979). Subsequent applications were to regions of strike-slip faulting (*Audibert*, 1991), normal faulting (*Rouby et al.*, 1993a,b; *Rouby*, 1994) or reverse faulting (*Bourgeois et al.*, 1997; *Arriagada*, 2004; *Arriagada et al.*, 2008).

3.2.1 Principle of restoration method

The method is purely geometric. For example, in a region of normal faulting, where a single fault offsets a stratigraphic horizon, the projection of the fault heave on a map defines a cut-off lens (**Figure 3.3**). The width of the lens is proportional to the fault heave. The least-squares method minimizes the gaps (cut-off lenses) across normal faults on a structure-contour map of a given stratigraphic horizon. The first step before restoration is therefore to determine the positions and heaves of the normal faults. The result is a fault-block map, where faults (real or artificial) surround each block (**Figure 3.4a-b**). The second step is to number the blocks and define a stationary block, for reference purposes (**Figure 3.4c**). An algorithm then minimizes the sum of the squares of the distances across cut-off lenses, with respect to unknown values of rigid translation and rotation for the remaining blocks (**Figure 3.4d, section 3.2.2**). This method is applicable also to regions of reverse faulting, in which the cut-off lenses are overlaps, not gaps (*Bourgeois et al.*, 1997; *Arriagada*, 2004; *Arriagada et al.*, 2008).

In this work, I do not apply the method to restore surfaces between normal or reverse faults, but to fit conjugate magnetic anomalies of an oceanic domain and therefore to restore the opening of the NE Atlantic. The edges of the blocks are magnetic anomalies or fracture zones and the cut-off lenses represent the gaps between conjugate anomalies (**section 3.3.1**). The restoration is in a horizontal plane. To digitize the block map I have used the Universal Transverse Mercator (Zone 27 N) geographic projection, in which coordinates are Cartesian and two dimensional. In a following section (**3.3.3**), I will discuss possible errors that may arise from such restoration in horizontal plane, rather than in spherical coordinates, depending

on the size and location of the studied area. Because the blocks consist of oceanic material, I assume that they are rigid. The restoration yields a full pattern of displacements for all material points, from which one may calculate mean spreading rates and relative displacements along the main fracture zones (**section 3.3.2**).

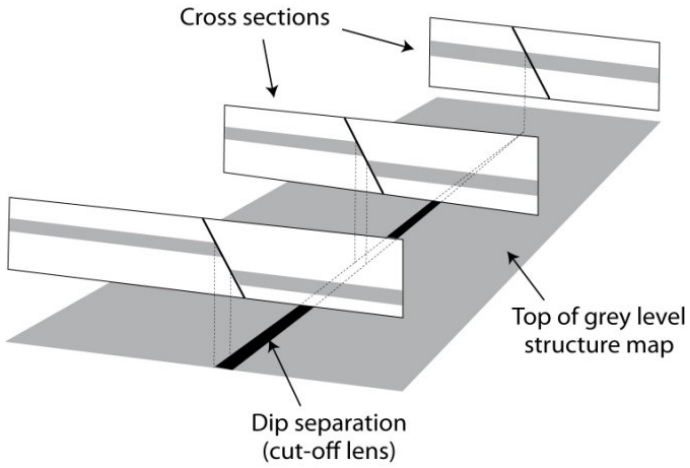

Figure 3.3. *Cut-off lens on a structure-contour map. Sections show grey layer, offset across normal faults. Vertical projection of footwall and hangingwall cut-offs defines cut-off lens (black). Width of lens is proportional to fault heave. Because fault is of normal type, cut-off lens is a gap. For a reverse fault, it would be an overlap. (From Rouby et al., 1993a)*

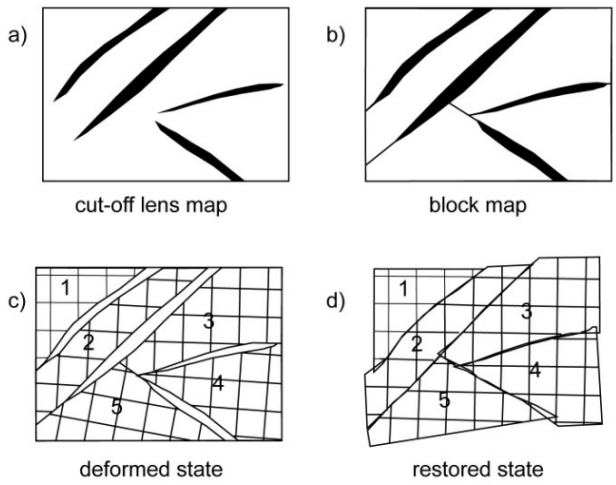

Figure 3.4. *Data processing and restoration in plane view. (a) Vertical projection of footwall and hangingwall cut-offs defines cut-off lens, (b) Construction of Fault-Block map by extrapolation of cut-off lenses (artificial fault), (c) Numbering of blocks, and (d) packing by rigid translations and rotations relative to block 1, which is stationary (From Rouby et al., 1993a).*

3.2.2 Numerical procedure

I have used the restoration program originally written by *Rouby* (1994) after *Audibert* (1991). *Arriagada* (2004) modified the program, so as to impose rotations (from paleomagnetic data) and allow shortening of the blocks. This latest version generates a post-script graphic file every 5 iterations. This makes easier to follow the restoration, especially for long computing times (>1 h). To restore the opening of the NE Atlantic, I considered that all blocks, being oceanic, were rigid. I therefore used the program of *Arriagada* (2004) but did not impose rotations or allow for shortening of the blocks.

The numerical procedure minimizes the sum (D) of the squares of all distances across all cut-off lenses. This minimization generates a set of non-linear equations, in terms of block translations and rotations. To solve these equations, the program uses an iterative method, similar to the Gauss-Seidel method (*Audibert*, 1991; *Rouby et al.*, 1993a). A single iteration includes a sequence of operations (**Figure 3.5**): neighbour seeking, block translation (**Figure 3.6**) and block rotation (**Figure 3.7**). The program repeats the iterations cyclically, until the equations have converged, according to a criterion *G*. In fact, *G* is a non-dimensional parameter that represents the fractional area of gaps and overlaps:

$$G = S_g/S_b$$

where S_g is the total surface area of all gaps and overlaps, and S_b is the total surface area of all the blocks (*Rouby et al.*, 1993a). A good approximation to S_g is:

$$S_g = L^*(D/n)^{1/2}$$

where *L* is the length of a line element, n is the total number of line elements, and $(D/n)^{1/2}$ is the root-mean-square gap width (*Rouby et al.*, 1993a). *G* is calculated and tested for convergence at the end of each iteration. The convergence is considered satisfactory when G reaches a minimal value (*Arriagada*, 2004). For restoration of the opening of the NE Atlantic ocean (results presented in Chapter 4), the criterion of convergence G reaches a minimal value of approx. 0.003.

Reading input files
- file.dig, coordinates of the blocks
- file.voi, neighbours of the blocks (defined before restoration)
- file.tec, implementation of shortening
- file.rot, implementation of rotation

Remark: in restoration of NE Atlantic opening, no shortening and rotation are implemented (file.tec and file.rot defined as null)

↓

Cutting each blocks into line elements (z) of equal distance

↓

ALGORITHM FOR ITERATION

A- Start a new iteration
B- Seeking of neighbourg line elements (zn)
C- Minimization of gaps and overlaps by block translation (***Figure 3.6***)
- **(1)** Select new block, by order of increasing block number;
- **(2)** Calculate translation and apply;
- **(3)** If all blocks have been processed, go to **(4)**, otherwise, return to **(1)**;
- **(4)** Calculate average block translation;
- **(5)** If average block translation is smaller than pre-set critival value, go to **D**, otherwise, return to **(1)**;

D- Minimization of gaps and overlaps by block rotation (***Figure 3.7***)
- **(6)** Select new block, by order of increasing block number;
- **(7)** Define projection of line elements upon neighbours;
- **(8)** Calculate rotation and apply;
- **(9)** If rotation is smaller than pre-set critical value, go to **(10)**, otherwise, return to **(7)**;
- **(10)** If all blocks have been processed, go to **E**, otherwise, return to **(6)**;

E- Minimization of gaps and overlaps by block translation
- **(11)** Select new block, by order of increasing block number;
- **(12)** Calculate translation and apply;
- **(13)** If all blocks have been processed, go to **(14)**, otherwise, return to **(11)**;
- **(14)** Calculate average block translation;
- **(15)** If average block translation is smaller than pre-set critival value, go to **F**, otherwise, return to **(11)**;

F- Check overall convergence
- **(16)** Calculate overall fractional gap area *G;*
- **(17)** if *G* is larger than pre-set critical value, return to **A** for further iterations, otherwise restoration is ended;

=> Every 5 iterations, production of output files:
- -file.fin, new coordinates of the blocks
- -file.dep, coordinates of centroid of each block before and after restoration
- -file.res, value of rotation applied to each block
- -file.eps, post-script graphic file to visualize the restoration

Figure 3.5. (previous page) *Numerical procedure and algorithm for iterations. Each rotation cycle occurs between two translation cycles in order to buffer possible buckling effect of the rotation cycle and make the convergence smoother and faster (Rouby et al., 1993a). Modified from Rouby et al. (1993a), Rouby (1994) and Arriagada (2004).*

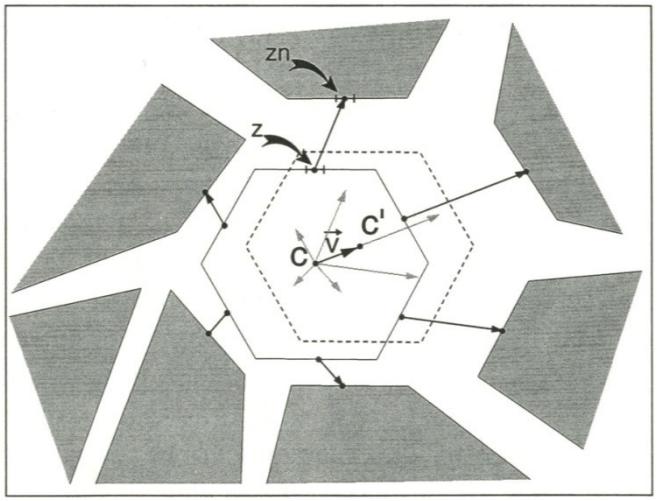

Figure 3.6. *Block translation. Gap vectors span distances between line elements (z) and neighbouring line elements (zn). Vector mean of gap vectors is v. If block translates through v, so that centroid moves from c to c', this minimizes sum of squares of gap distances. From Rouby et al. (1993a).*

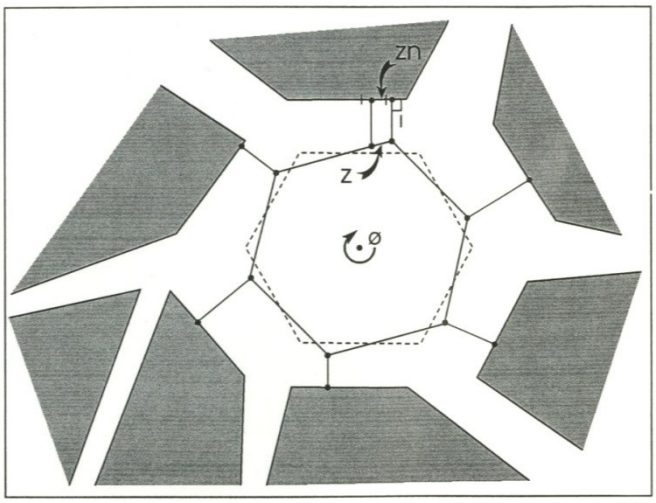

Figure 3.7. *Block rotation. Each line element (z) is projected upon neighbouring line element (zn), defining perpendicular distance l. Rigid rotation through angle f minimizes sum of squares of perpendicular distances for all line elements. Calculation is repeated, with redefinition of perpendicular distances each time, until further adjustments are negligible. From Rouby et al. (1993a).*

3.3 Application to opening of NE Atlantic

In this section, I will describe three tests of the restoration method for the opening of the NE Atlantic Ocean. The purpose of the tests was to improve the block maps and restorations (**section 3.3.1**) and to establish the limits of the method (**section 3.3.3**).

For each test, an appendix illustrates the block map and restoration result at each stage (magnetic anomaly). For each restoration, the main gap to be minimized is the gap between conjugate magnetic anomalies (on opposite sides of the ridge). The restoration program minimizes also gaps and overlaps between the mobile blocks. After one restoration, for example at Anomaly 5, I delete the blocks between anomalies 5 and 6 and digitize a new block map for the second stage of restoration, at Anomaly 6. Therefore a new gap appears between the next pair of conjugate magnetic anomalies (Anomaly 6) that will be restored during the second stage of restoration; and so on, until the blocks of the last magnetic anomaly are restored.

3.3.1 Construction of block maps and restoration tests

3.3.1.1 Dataset

I have used datasets of magnetic anomalies and fracture zones of the NE Atlantic to construct block maps. The most detailed dataset I found for the NE Atlantic, at the beginning of the thesis, was from *Skogseid et al.* (2000). Geographic coordinates for these data are available in the MagLibrary of the GMAP software (*Torsvik and Smethurst*, 1999) (**Figure 3.8**).

I will describe three tests of block maps and restorations: 1) Test 1, restoration of each ridge system independently (Greenland stationary); 2) Test 2, restoration of the whole NE Atlantic relative to a stationary Greenland plate; 3) Test 3, restorations of the whole NE Atlantic relative to a stationary Europe plate.

3.3.1.2 Test 1 – Restoration of each ridge system independently

I have constructed a block map in which the edges of the blocks are magnetic anomalies and fracture zones, except around Iceland, where data are lacking (**Figure 3.9**).

I first tried restoring each ridge system (Reykjanes, Kolbeinsey, Aegir, and Mohns ridges, **Figure 3.10**), independently of the others. Because there is little evidence of post-

break-up deformation on the Greenland Margin, I assume that the western (Greenland) side of each ridge system is rigid and stationary during the restoration. In contrast, the European side of the ridge is mobile and deformable. Restorations are for magnetic anomalies 5, 6, 7, 13 and 15 (**Appendix A)**.

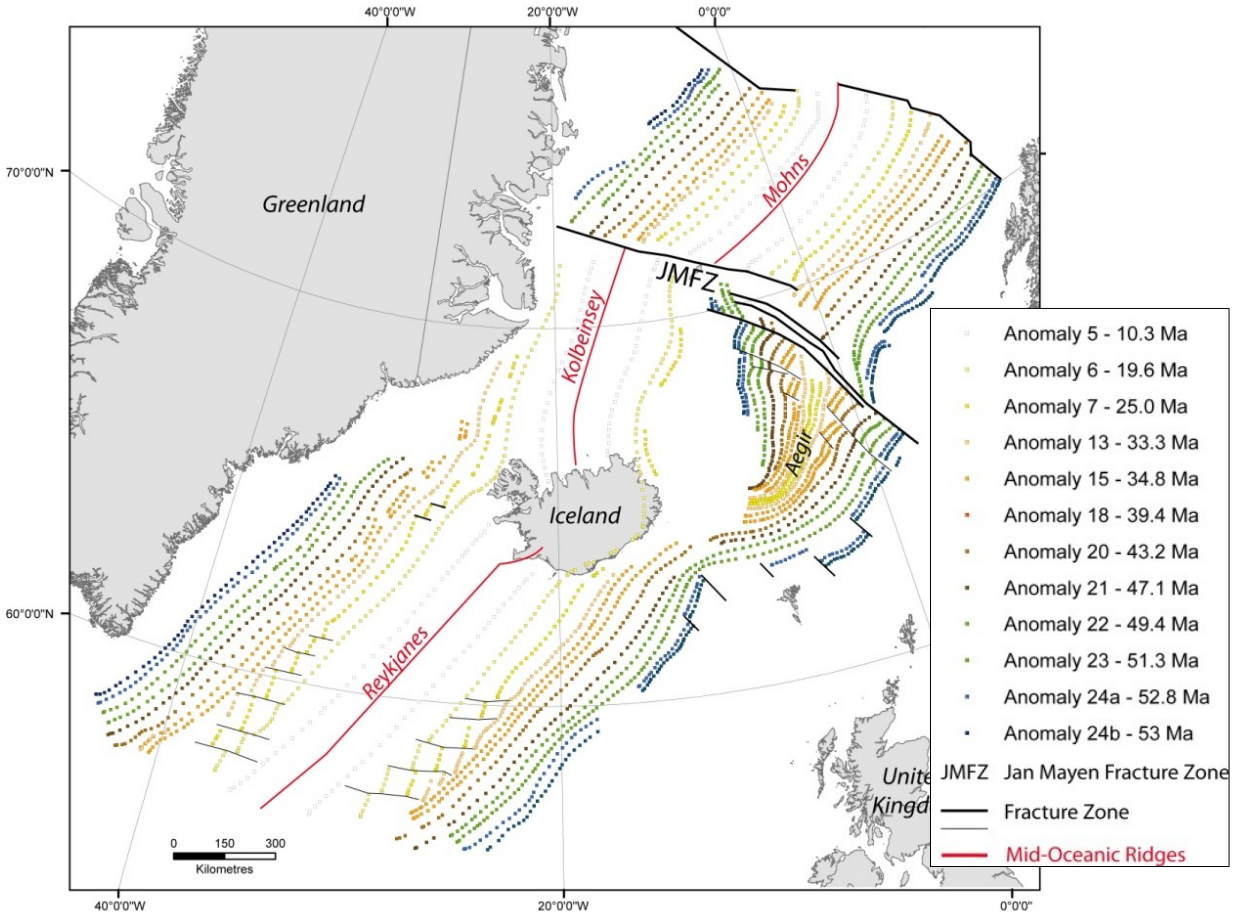

Figure 3.8. *Dataset of magnetic anomalies and fracture zones of the NE Atlantic region, from Skogseid (2000). Modified from Torsvik and Smethurst (1999). Map projection is Universal Transverse Mercator (UTM, WGS 1984, zone 27N).*

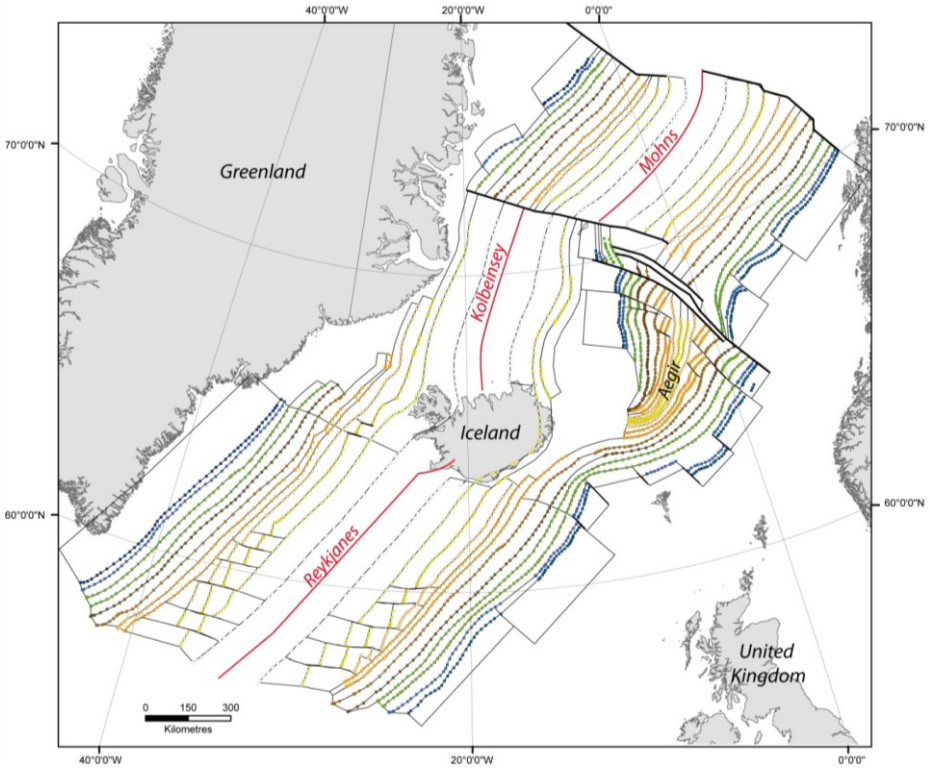

Figure 3.9. *First block map of NE Atlantic. Edges of blocks are mostly magnetic anomalies. Map projection is Universal Transverse Mercator (UTM, WGS 1984, zone 27N).*

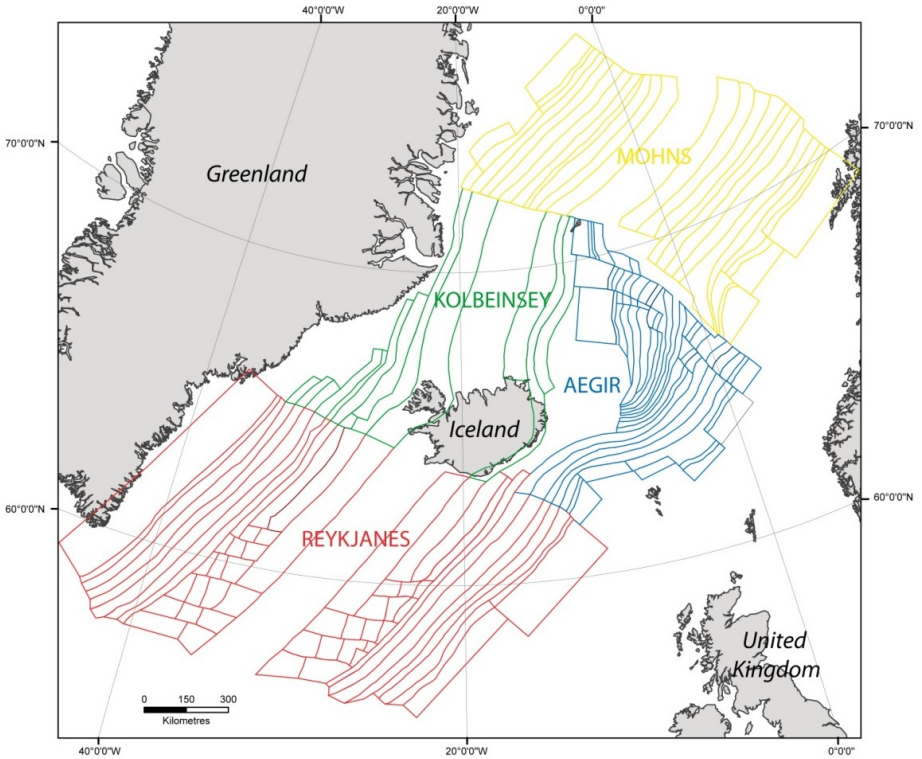

Figure 3.10. *Subdivision of NE Atlantic into four block maps for restoration of each ridge system independently (Reykjanes, Kolbeinsey, Aegir and Mohns ridges). Map projection is Universal Transverse Mercator (UTM, WGS 1984, zone 27N).*

1) Reykjanes and Mohns ridges

These restorations provided good fits between the magnetic anomalies, as one might expect for lines that are nearly straight (**Figures 3.11 and 3.12**). However, conjugate anomalies (on opposite sides of each ridge) did not necessarily have the same initial lengths, so that fits were not possible all along them. Also there were no transverse blocks or other boundaries at the ends of the ridges, so that some (possible unrealistic) strike-slip displacements occurred between conjugate anomalies during restoration.

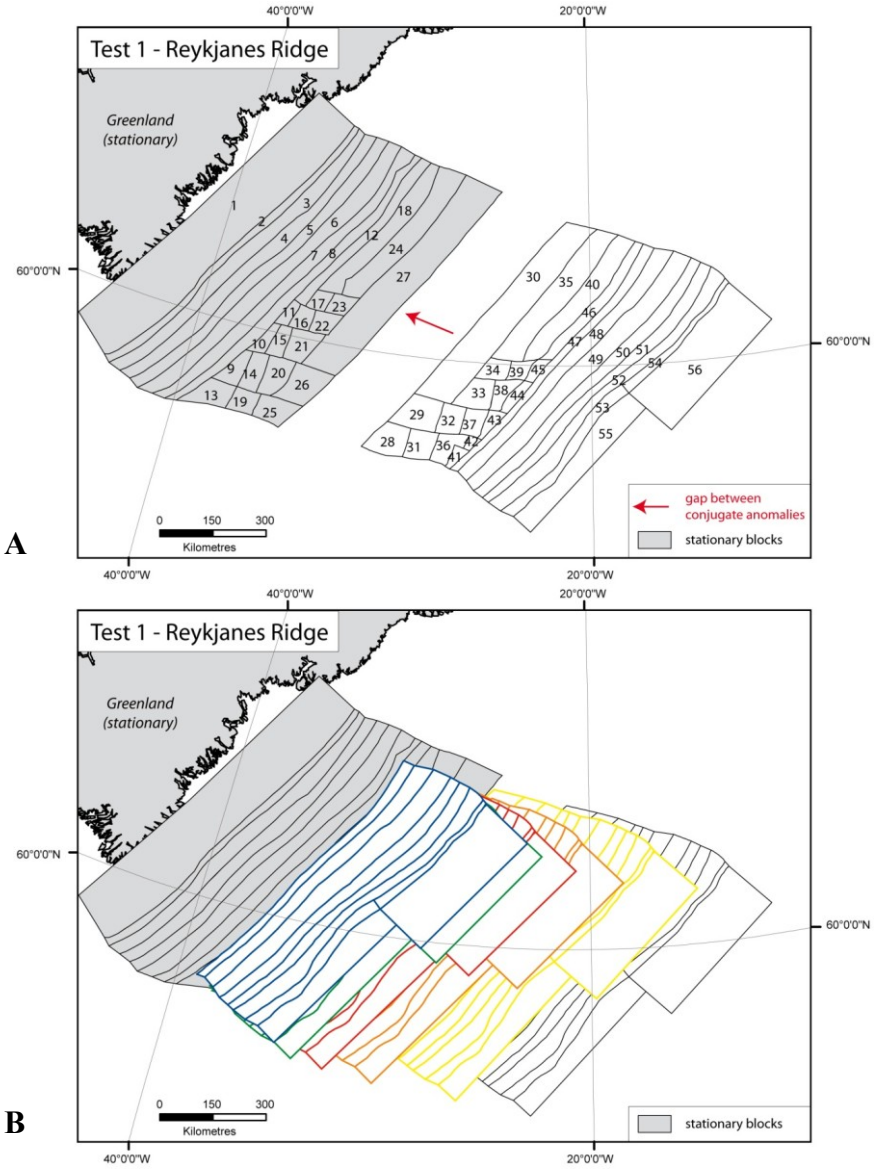

Figure 3.11. *A) Block map for restoration of conjugate anomalies of Reykjanes Ridge (Blocks 1 to 27 are stationary). B) Restoration at anomalies 5 (yellow), 6 (orange), 7 (red), 13 (green) and 15 (blue). Map projection is Universal Transverse Mercator (UTM, WGS 1984, zone 27N).*

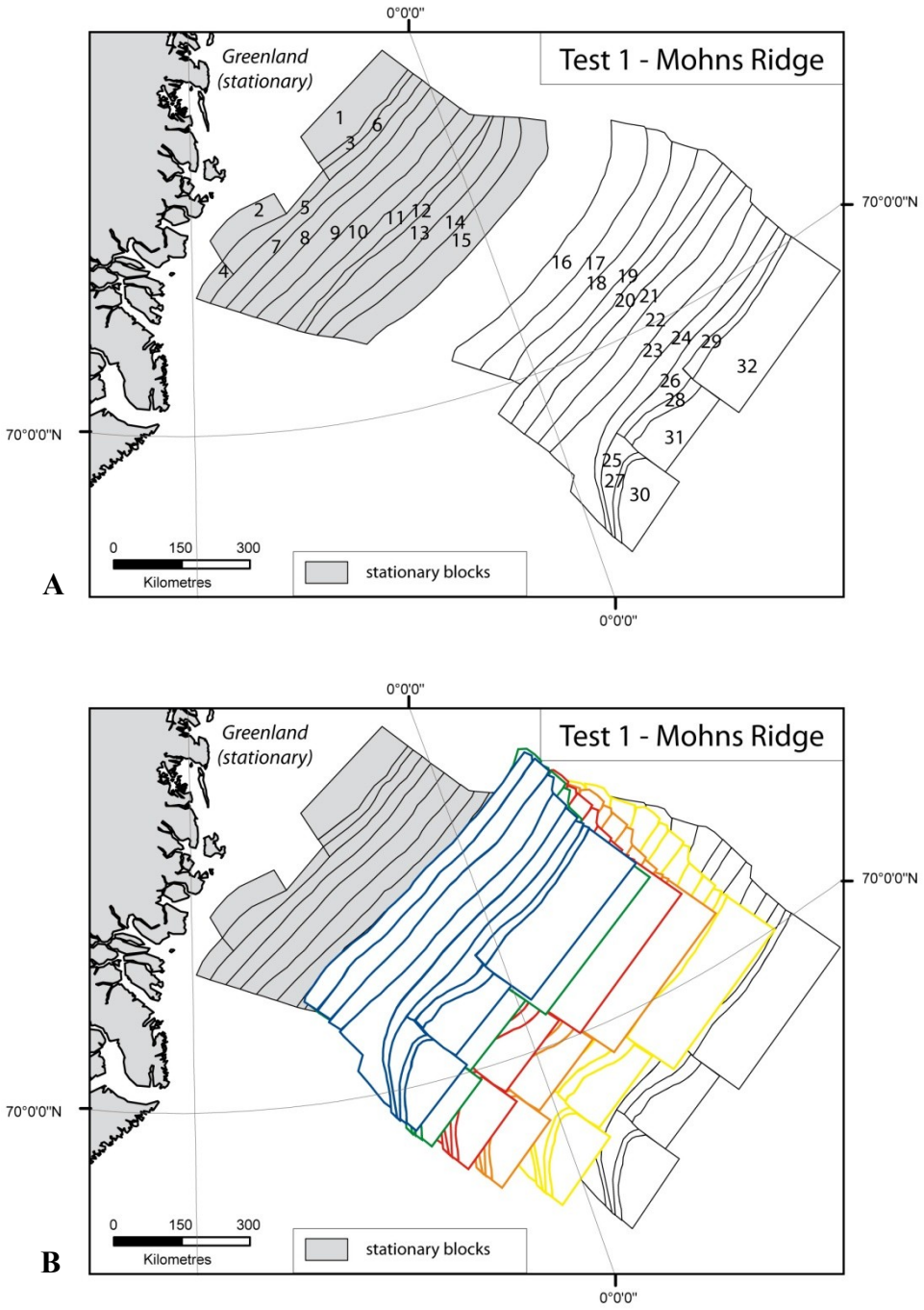

Figure 3.12. *A) Block map for restoration of conjugate anomalies of Mohns Ridge (Blocks 1 to 15 are stationary). B) Restoration at anomalies 5 (yellow), 6 (orange), 7 (red), 13 (green) and 15 (blue). Map projection is Universal Transverse Mercator (UTM, WGS 1984, zone 27N).*

2) Kolbeinsey Ridge

Restoration of the Kolbeinsey ridge yields abnormal overlap of the eastern side on the western side (**Figure 3.13**). This probably results from a lack of magnetic anomaly data around Iceland and a lack of transverse blocks or other boundaries, which would constrain displacements of blocks along the ridge (ridge-long displacements).

3) Aegir Ridge

Restoration of the Aegir ridge starts at Anomaly 7, because the Aegir ridge has been extinct since then. There are problems of block overlapping in the upper central part for restoration at anomaly 15 (**Figure 3.14**). The blocks do not have either southern or northern boundaries. The eastern side thus moves southward, instead of moving northward and rotating toward the western side.

This first test showed that the restoration on the whole produces a good fit of magnetic anomalies. However, the main problems are the lack of magnetic anomalies data, creating gaps in block maps and abnormal overlap of blocks. Moreover, the lack of southern and/or northern boundaries triggers unrealistic ridge-long displacements of the blocks during restoration. Therefore, I decided to restore the whole NE Atlantic to provide southern and/or northern boundaries to each zone (Test 2).

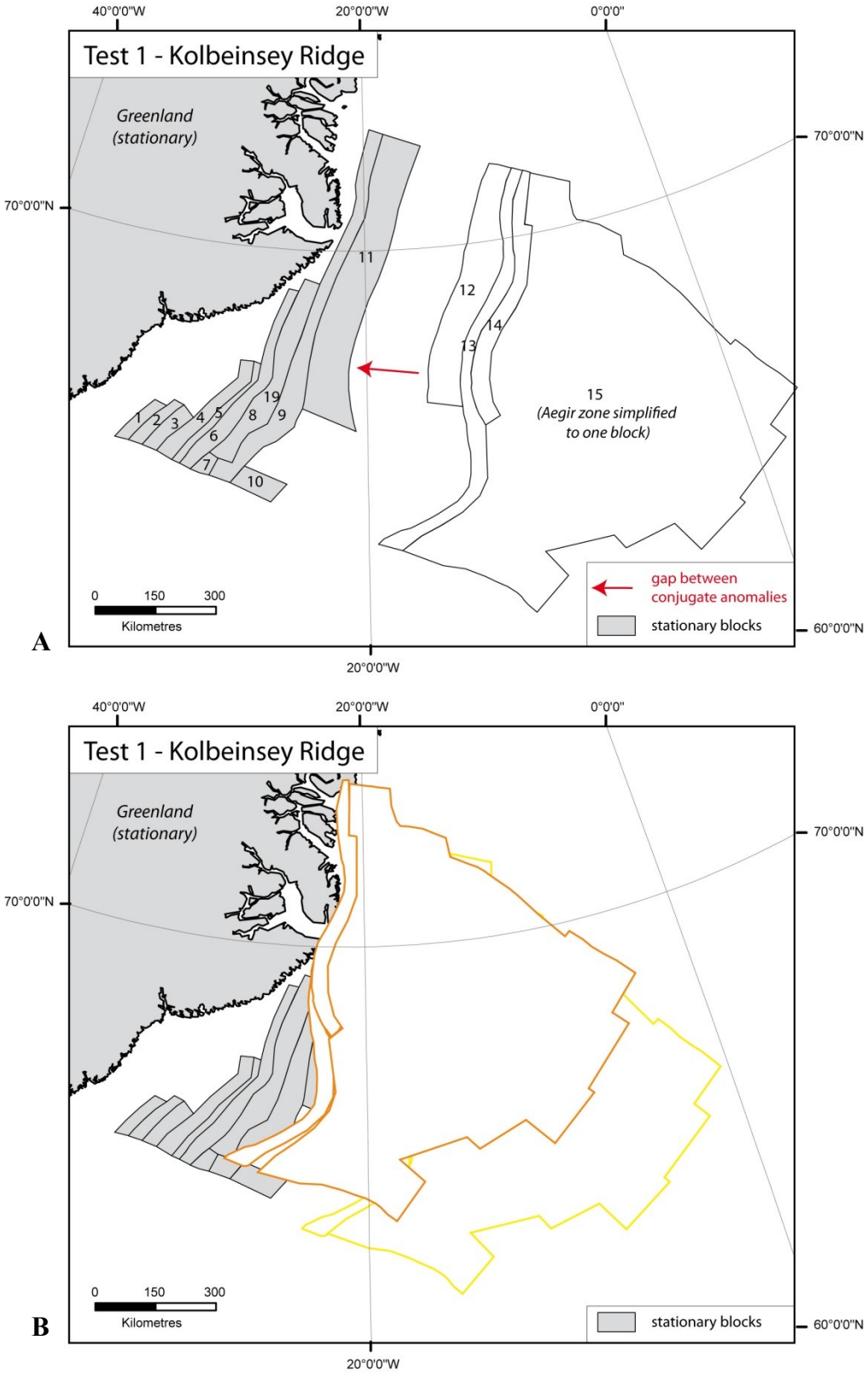

Figure 3.13. *A) Block map for restoration of conjugate anomalies of Kolbeinsey Ridge (Blocks 1 to 11 are stationary). B) Restoration at anomalies 5 (yellow), 6 (orange), 7 (red), 13 (green) and 15 (blue). Map projection is Universal Transverse Mercator (UTM, WGS 1984, zone 27N).*

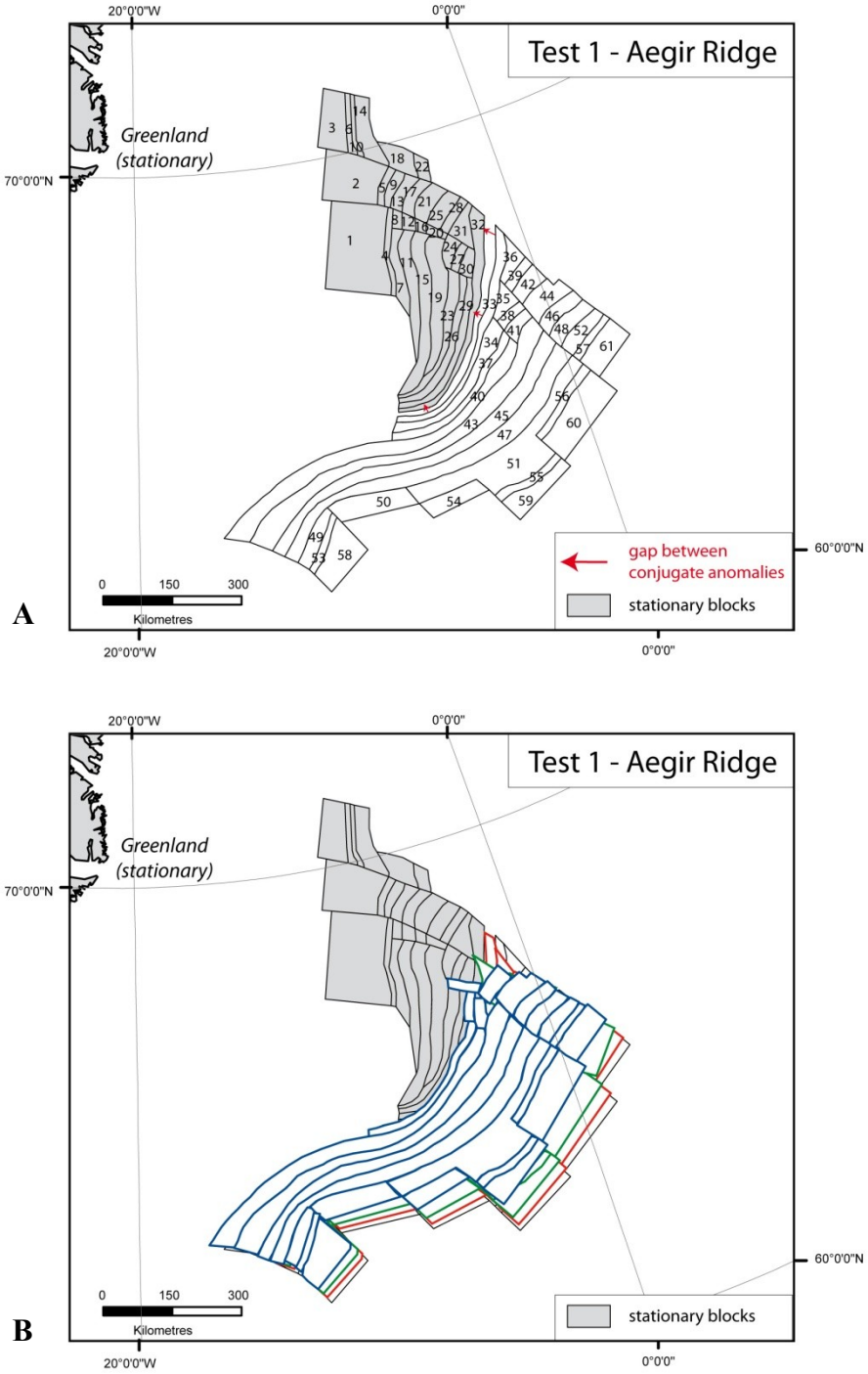

Figure 3.14. *A) Block Map for restoration of conjugate anomalies of Aegir Ridge (Blocks 1 to 32 are stationary). B) Restoration at anomalies 7 (red), 13 (green) and 15 (blue). Map projection is Universal Transverse Mercator (UTM, WGS 1984, zone 27N).*

3.3.1.3 Test 2 – Restoration of whole NE Atlantic relative to a stationary Greenland plate

Restoration of the whole NE Atlantic at Anomaly 5, using the same configuration of blocks as in Test 1, aslo produces abnormal overlap of blocks (**Figure 3.15**).These abnormal overlap of blocks are due to the lack of data, and thus the lack of block, around Iceland.

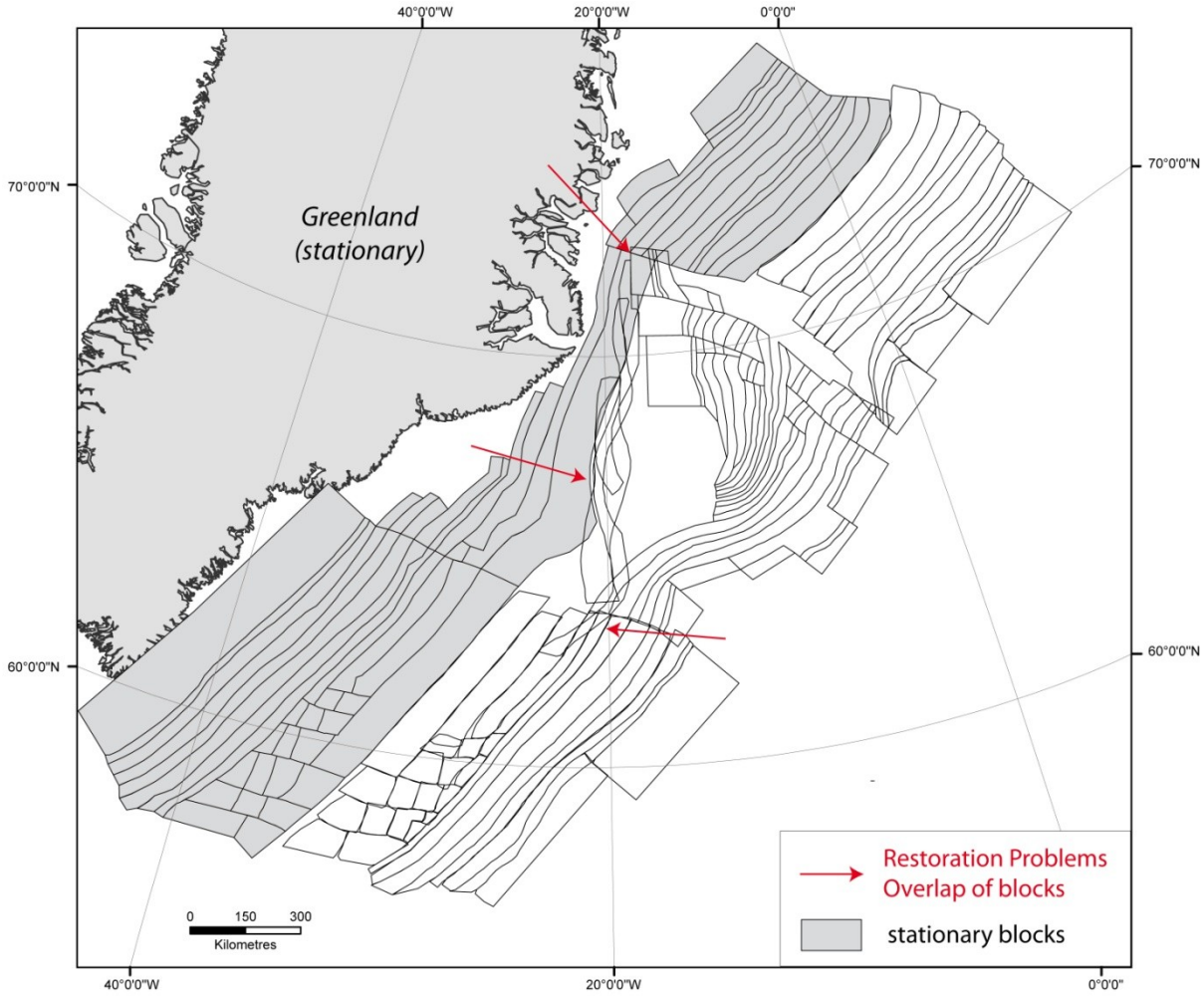

Figure 3.15. *Restoration of the whole NE Atlantic for Anomaly 5. Red arrows indicate overlaps of blocks and unrealistic ridge-long displacements of blocks during the restoration. Map projection is Universal Transverse Mercator (UTM, WGS 1984, zone 27N).*

To obtain a better restoration of the whole NE Atlantic, I made the following modifications to the block map (**Figure 3.16**):

- To compensate for lack of data around Iceland, Jan Mayen and the JMFZ, I filled the gaps with fictitious blocks,
- I drew block boundaries only along magnetic anomalies or transform faults. Therefore the area between the Reykjanes and Jan Mayen segments became a single block.

As in Test 1, the western side of the Reykjanes, Kolbeinsey and Mohns ridge is stationary (Greenland plate). The western side of the Aegir Ridge is mobile for restorations of anomalies 5 and 6. However for anomalies 7 to 24b (when the Aegir Ridge was active) the western side of the Aegir Ridge is stationary.

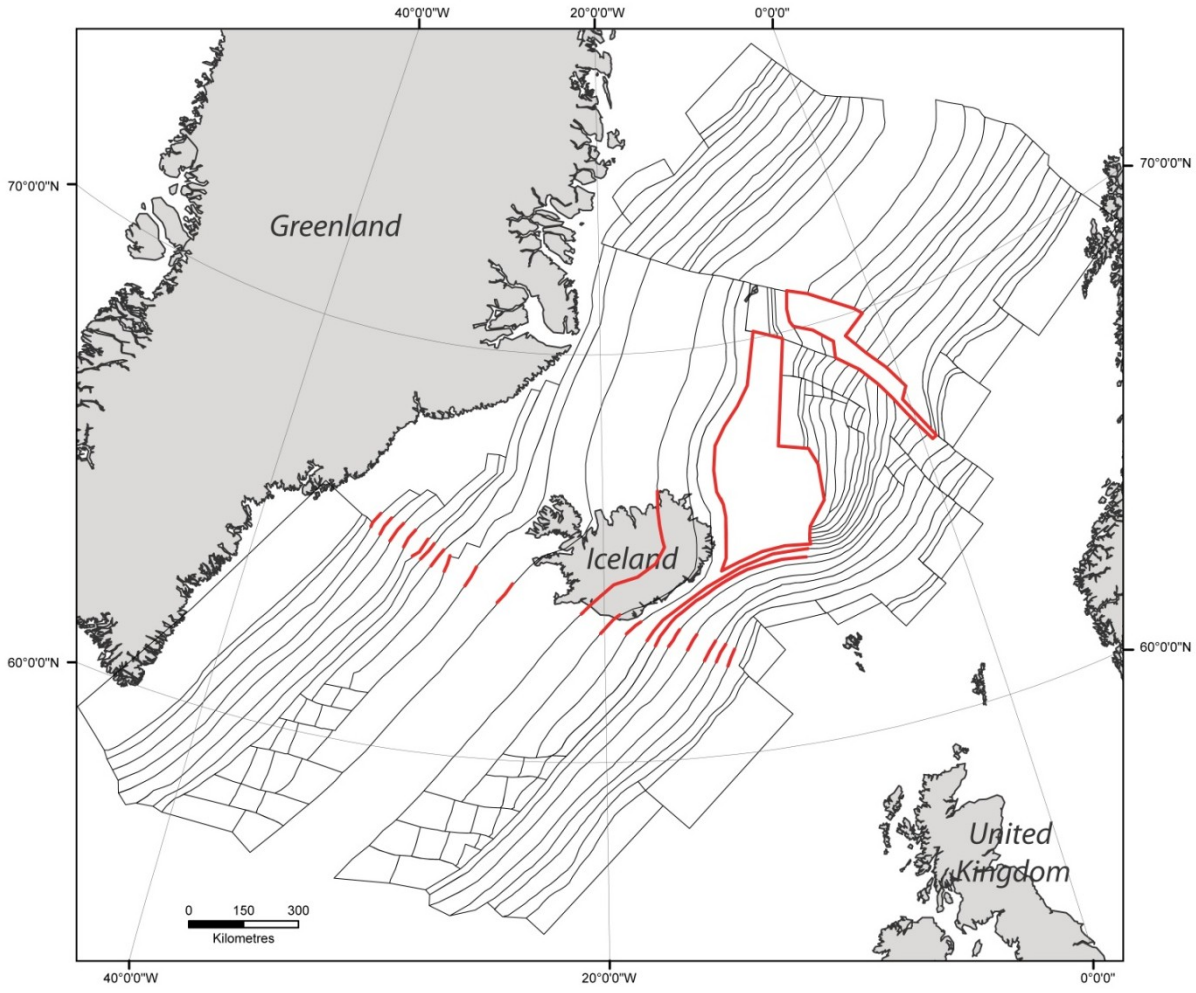

Figure 3.16. *Red lines show modifications to block map for better restoration of whole NE Atlantic. Map projection is Universal Transverse Mercator (UTM, WGS 1984, zone 27N).*

The quality of restoration is good for anomalies 5 and 6, during which the Aegir Ridge was not active. However, at Anomaly 7, the Aegir Ridge was active and its spreading direction was different from those of the Reykjanes and Kolbeinsey ridges (**Figure 3.17**). This caused a major problem during restoration. To solve the problem, I introduced a new boundary between the Reykjanes and Jan Mayen segments (**Figure 3.18**), following the Faeroe Fracture Zone (e.g. *Kimbell et al.*, 2005). Restorations, using this new configuration of blocks, are for magnetic anomalies 5, 6, 7, 13, 15, 18, 20, 21, 22, 23, 24a and 24b (**Appendix B)**.

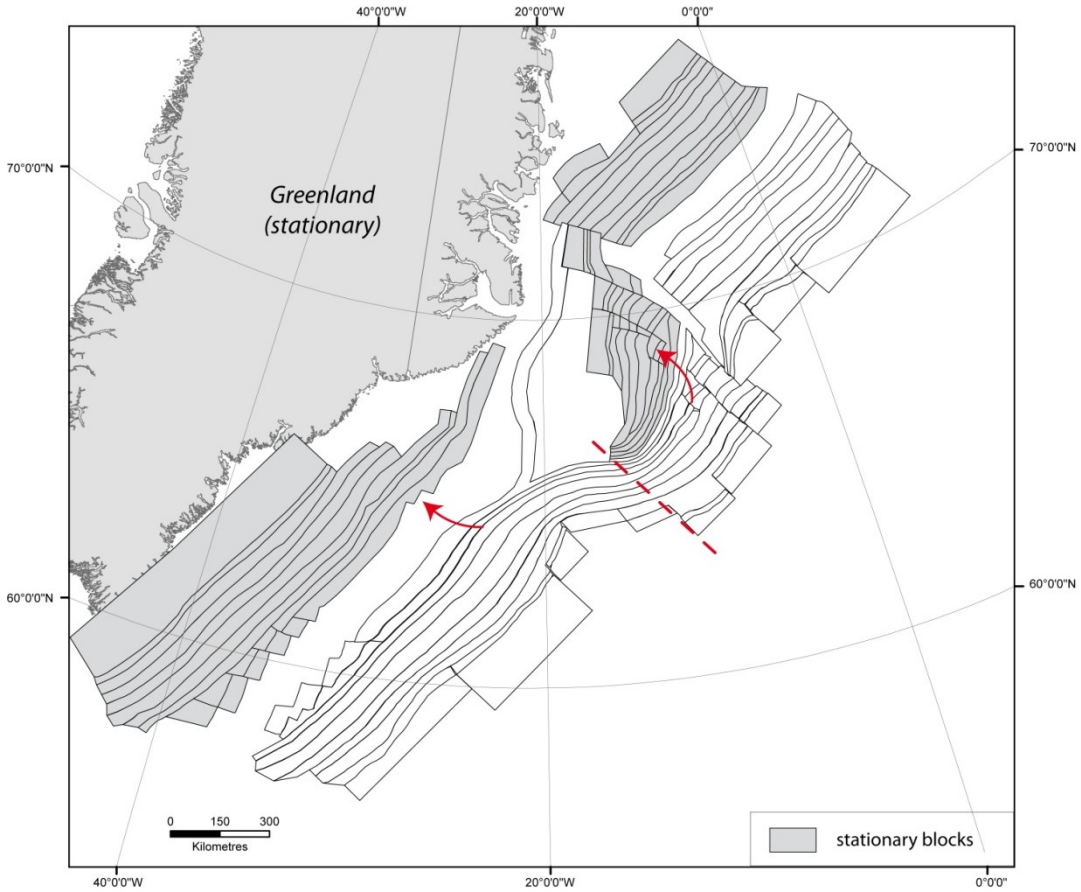

Figure 3.17. *Problem in block map for restoration at Anomaly 7: Reykjanes and Aegir ridges have different spreading directions. Restoration requires a new boundary between Reykjanes and Aegir zones (dashed red line). Map projection is Universal Transverse Mercator (UTM, WGS 1984, zone 27N).*

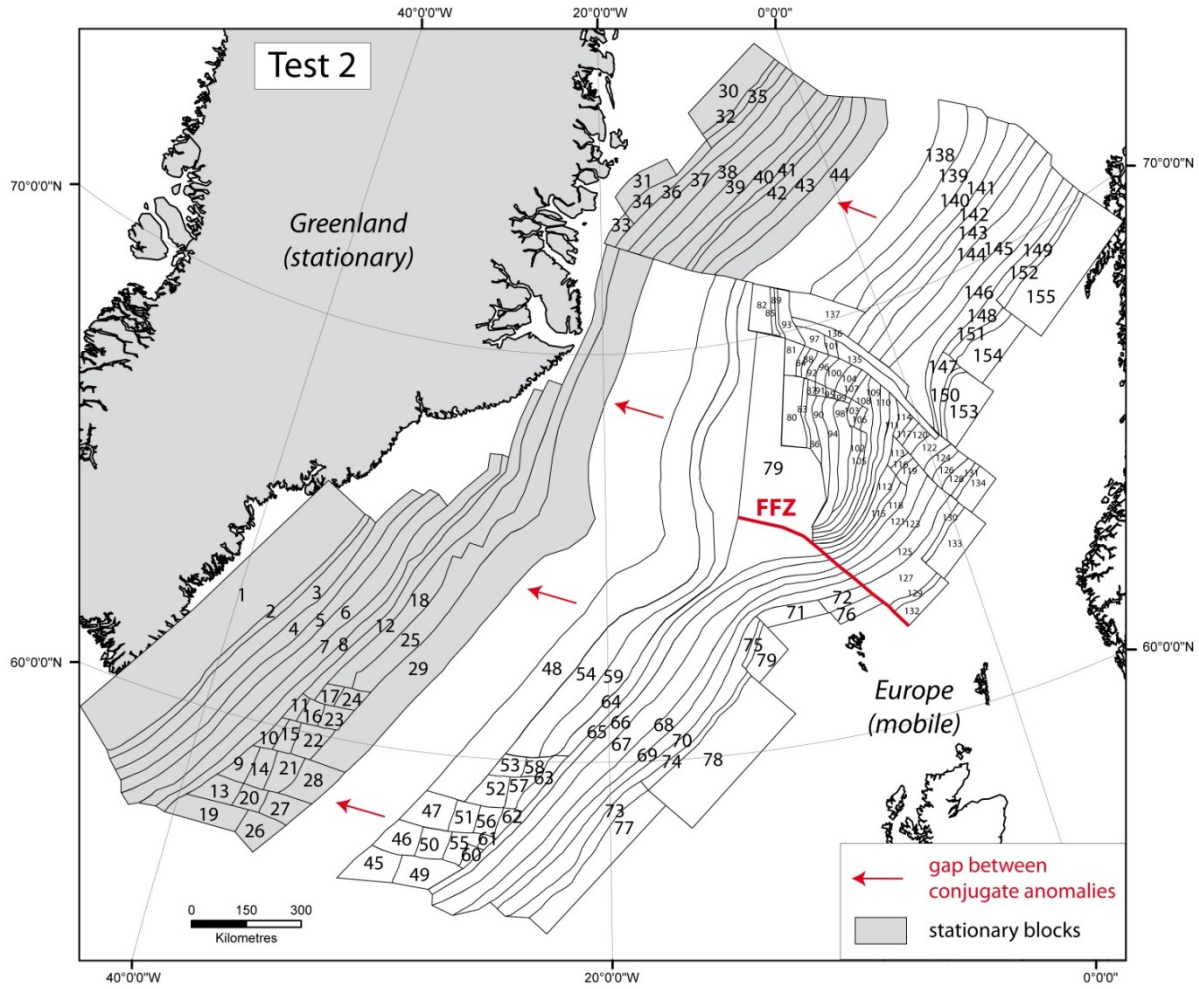

Figure 3.18. *Block Map for Test 2 that includes a boundary between Reykjanes and Jan Mayen segments along Faeroe Fracture Zone (FFZ). Greenland plate is stationary. Map projection is Universal Transverse Mercator (UTM, WGS 1984, zone 27N).*

On the whole, the fits of the magnetic anomalies are satisfactory (G ≈ 0.005). However, the fits of anomalies 6, 7 and 13 around Iceland are not so good (**Figure 3.19A**; **Appendix B**). Restoring the whole NE Atlantic gives better results than restoring each oceanic segment separately, because it constrains the motions along the ridges. If we compare the results of this test with those of Test 1, we see that in Test 2 the Reykjanes segment moves more northward and the Mohns segment moves slightly southward.

The spreading directions of the Reykjanes, Kolbeinsey and Mohns ridges are almost the same, so that the Reykjanes and Mohns segments translate and rotate in approximately the same way. In contrast, the Aegir Ridge has significant curvature and its eastern side rotates more than the sides of the other segments. This tends to create a gap around the FFZ, a

northward translation of the blocks of the Reykjanes Segment to minimize this gap and an overlap around the JMFZ (**Figure 3.19B**; **Appendix B**).

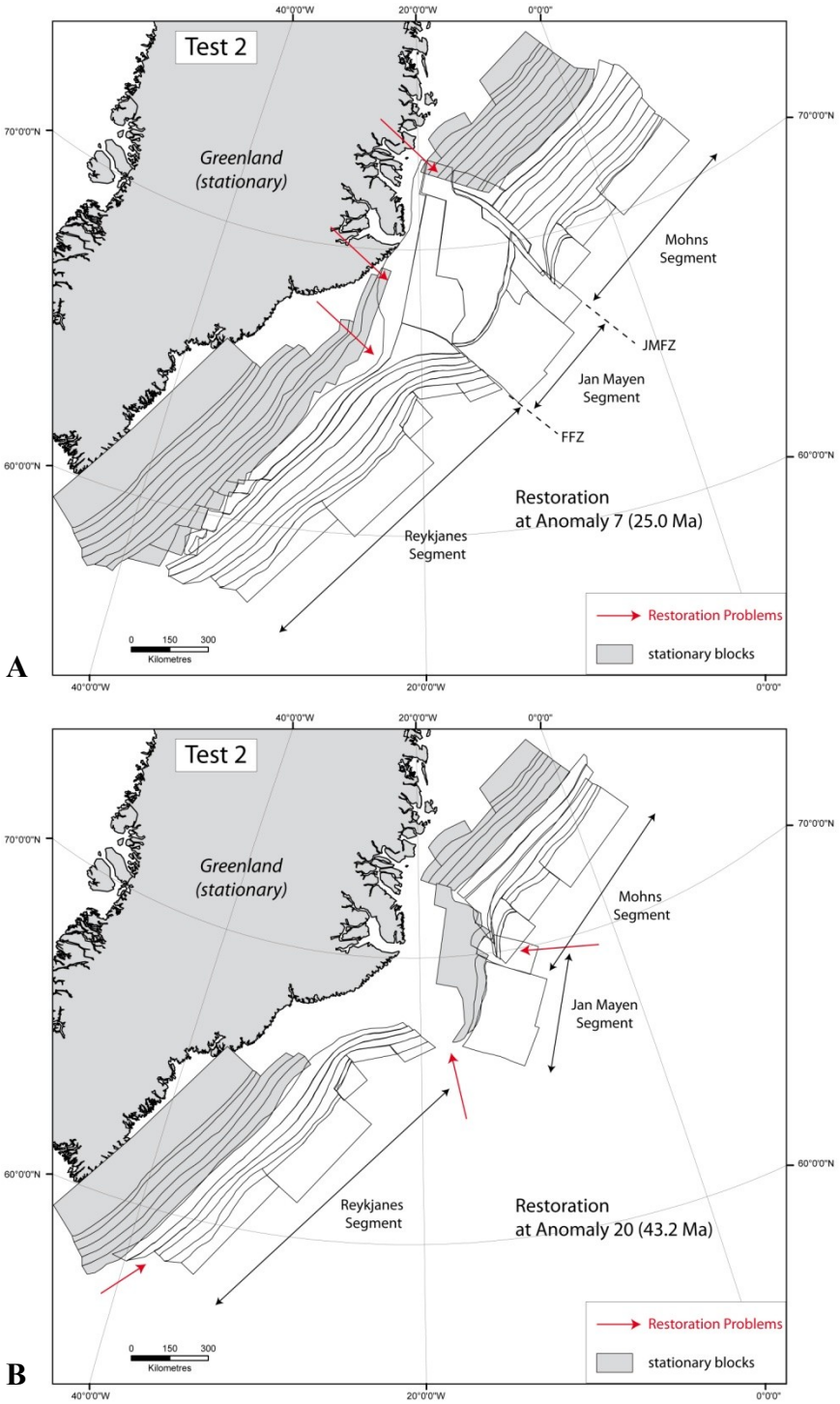

Figure 3.19. *Gap and overlap between blocks during restoration: A) at Anomaly 7 (25.0 Ma), gap and overlap between blocks around Iceland and Jan Mayen Fracture Zone (JMFZ); and B) at Anomaly 20 (43.2 Ma), gap around Faeroe Fracture Zone (FFZ), northward translation of Reykjanes Segment and overlap around JMFZ. Map projection is Universal Transverse Mercator (UTM, WGS 1984, zone 27N).*

In this test, the restoration method gives a good fit of conjugate magnetic anomalies and therefore its application to the NE Atlantic opening is satisfactory. Moreover, the test shows that the Aegir Ridge had a complex spreading history, by comparison with the nearby Mohns and Reykjanes ridges, and that relative displacements along both the FFZ and JMFZ are significant. However, the gaps and overlaps around the FFZ and JMFZ may be due to omissions such as the separation and rotation of the JMMC off Greenland, therefore the gap around the FFZ and overlap between JMFZ may be exaggerated. Moreover, the fits of conjugate magnetic anomalies are not so good around Iceland. The dataset used to draw the blocks around Iceland is not satisfactory for this area needs revising.

Before modifying the block map, I tested the same configuration but relative to a stationary Europe plate.

3.3.1.4 Test 3 – Restoration of whole NE Atlantic relative to a stationary Europe plate

In Test 3, I used the same block map as in Test 2, but assumed that the European side of the ridge was stationary during the restoration, in order to test the restoration method and compare the results with Test 2 (**Figure 3.20**). For anomalies 5 and 6, the western side of the Aegir Ridge was assumed stationary, however from anomalies 7 to 24b (when the Aegir Ridge was active), the western side of the Aegir Ridge was mobile (**see Appendix C**).

Firstly, the fits of the magnetic anomalies globally were satisfactory ($G \approx 0.005$). However, as for Test 2, some problems of gaps and overlaps of blocks occurred especially around Iceland (**Figure 3.21A**). This confirms that the dataset around Iceland and the JMMC needs revising and the block map modified. In Test 3, the blocks on the western side of the Aegir Ridge rotated significantly relatively to the northern Mohns and southern Reykjanes segments (**Appendix C**). This rotation is a consequence of fan-shaped spreading along the Aegir Ridge, visible in the curvature of the magnetic anomalies. In previous studies, this fan-shaped spreading along the Aegir Ridge was interpreted as a result of the separation of the JMMC off Greenland (e.g. *Gaina et al.,* 2009; **section 2.4**).

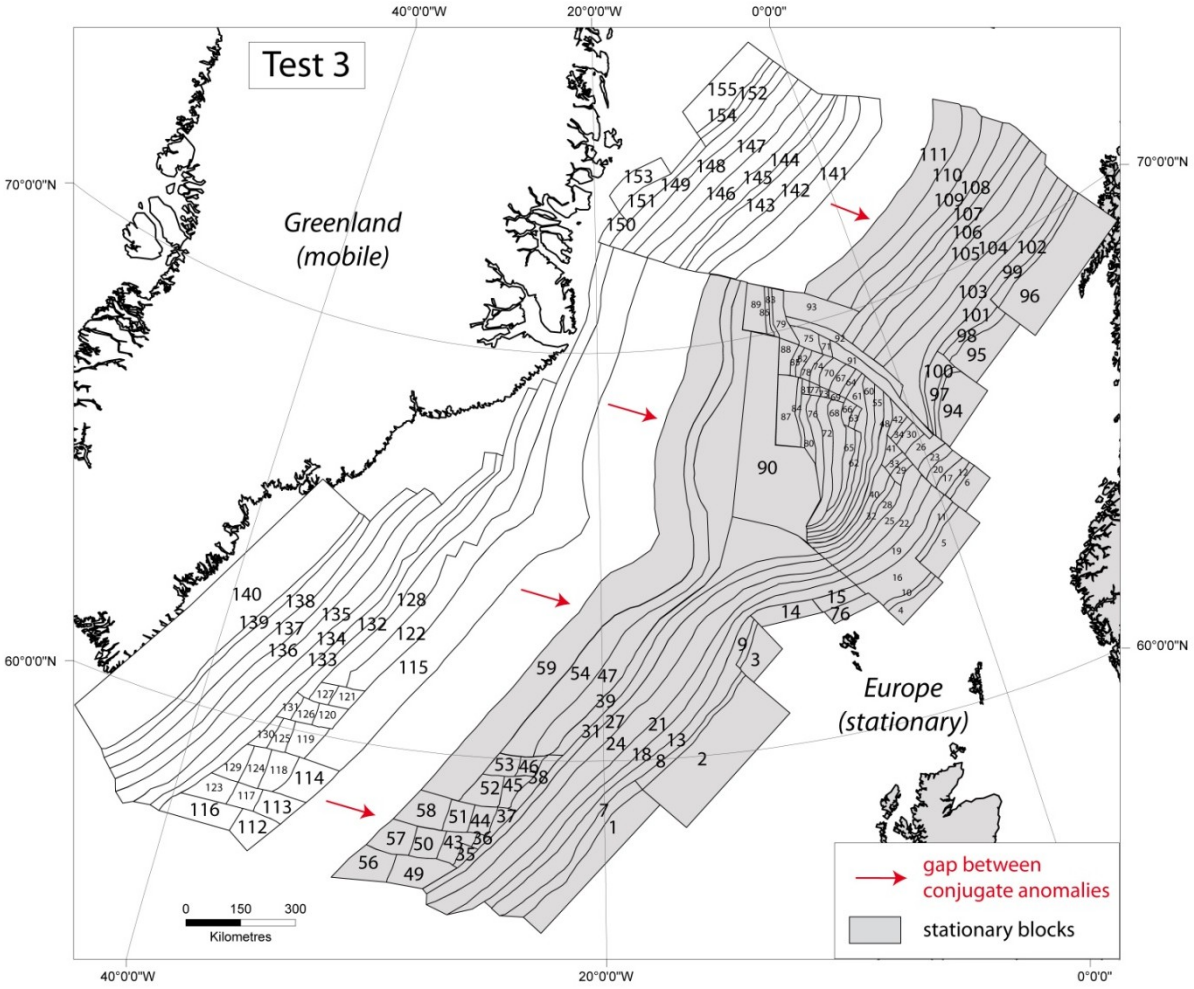

Figure 3.20. *Block map for Test 3 that includes a boundary between Reykjanes and Jan Mayen segments along Faeroe Fracture Zone (FFZ). European plate is assumed stationary. Map projection is Universal Transverse Mercator (UTM, WGS 1984, zone 27N).*

However, results of Test 3 results in some misfits of conjugate anomalies along the Aegir Ridge and overlaps of blocks around the JMFZ (**Figure 3.21B**). Therefore, the fan-shaped spreading along the Aegir Ridge, not only may be due to the separation of the JMMC, but also may have generated relative displacement along both the eastern JMFZ and along the FFZ. In order to test this hypothesis and better restore the NE Atlantic opening relative to a stationary Greenland plate, I decided to revise the dataset of magnetic anomalies for the area around Iceland and to improve the block map in order to take into account the separation of the JMMC from Greenland.

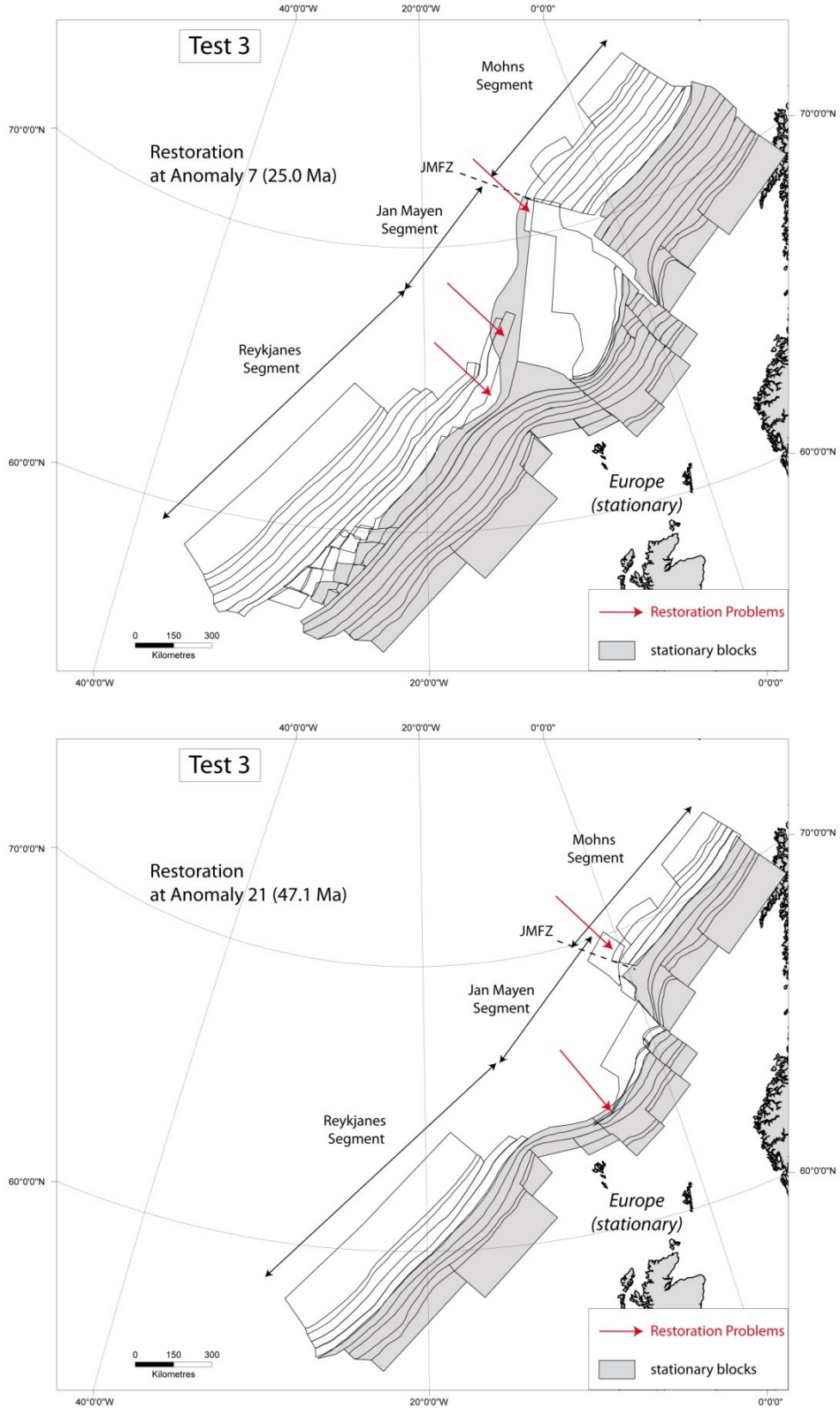

Figure 3.21. *Gaps and overlaps between blocks during restoration: A) at Anomaly 7 (25.0 Ma), gaps and overlaps between blocks around Iceland and Jan Mayen Fracture Zone (JMFZ); and B) at Anomaly 21 (47.1 Ma), overlaps of blocks along Aegir Ridge (misfit of conjugate magnetic anomalies) and around JMFZ. Map projection is Universal Transverse Mercator (UTM, WGS 1984, zone 27N).*

3.3.1.5 Revised dataset and improved block map

Tests of the restoration method to the opening of the NE Atlantic highlighted some problems in the dataset and therefore in the block configuration. The main problems were: (1) the lack of magnetic anomalies data around Iceland and the JMMC, creating gaps and overlaps between blocks; and (2) the lack of northern and/or southern boundaries (e.g. for the Reykjanes Segment in Test 2) triggering ridge-long displacements of blocks during restoration.

Therefore, in order to obtain a best fit of conjugate anomalies and therefore quantify at best spreading rates and relative slip along fracture zones, it was necessary to revise the initial dataset of magnetic anomalies and fracture zones. For this purpose, I compiled all available data for magnetic anomalies (from *Macnab et al. (1989), Skogseid et al. (2000), Gaina et al. (2002), Jones et al. (2002a), Olesen et al. (2007), Gernigon et al. (2009), and Maus et al. (2009)*) and accurate location and shape of fracture zones (from *Kimbell et al.*, 2004; 2005; *Andersen et al.*, 2010). I redrew the magnetic anomalies and determined their ages from the magnetic scale of *Cande and Kent* (1985) (**Figure 3.22**).

I then modified the block map of the NE Atlantic (**Figure 3.23**) using this revised dataset. Furthermore, I integrated information on the structural development of the JMMC from *Unternehr* (1982), *Nunns* (1983), *Bott* (1985, 1987), *Mjelde et al.* (2008), *Gaina et al.* (2009), *Gernigon et al.* (2009, 2011), so as to define the blocks around the JMMC. From these studies, I estimated that approximately 50% of the JMMC consisted of stretched continental crust, especially in the southern part of the JMMC and in its conjugate part on the Greenland margin. I therefore defined 8 thin continental blocks on the western side of the JMMC and 8 others on the eastern side of Greenland, between the magnetic anomaly at Anomaly 8 and the COB, in order to take into account progressive continental stretching along the JMMC, and its subsequent counter clockwise rotation (e.g. *Nunns*, 1983; *Bott*, 1985, 1987; *Gaina et al.*, 2009) (**Figure 3.23**). These 16 blocks thus mimic the stretched continental crust of the JMMC, rather than the oceanic crust (as do the other blocks).

I furthermore added two large stationary blocks to bound the block map on its northern and southern sides (**Figure 3.23**), a first one, north of the Mohns Segment, along the Greenland and Senja FZ, and a second one, south of the Reykjanes Segment, along the Charlie Gibbs FZ. These blocks constrained the opening of the NE Atlantic, coherently with the opening of the Central Atlantic Ocean in the south and the Boreas Basin in the north. I determined the successive positions of these two constraining blocks, relative to a stationary

Greenland plate, using the EarthByte model (rotation poles are from *Gaina et al.*, 2002) and the Gplates software (*Boyden et al.*, 2011). During each stage of restoration, the two stationary blocks impeded any northward or southward displacement of the mobile blocks along the ridge. The JMFZ separated the Mohns and Jan Mayen segments, and the FFZ separated the Jan Mayen and the Reykjanes segments, as in previous block map. Any relative displacements between segments occurred exclusively along these two oceanic fracture zones.

Using this method, I tested two new models. In Model 1, the algorithm minimizes the gaps between adjacent magnetic anomalies of each segment, but not the gaps or overlaps between oceanic fracture zones; whereas, in Model 2, the algorithm minimizes the gaps between adjacent anomalies and also the gaps or overlaps along oceanic fracture zones. The results of these models are presented in Chapter 4.

Figure 3.22. (next page) *Left: Revisied dataset of magnetic anomalies for NE Atlantic Ocean. Data from Macnab et al. (1989), Skogseid et al. (2000), Gaina et al. (2002), Jones et al. (2002a), Olesen et al. (2007) ; Gernigon et al. (2009), and Maus et al. (2009). Background image is recent model EMAG2 of crustal magnetic anomalies (Maus et al., 2009). Right: Revisited ages of magnetic anomalies, from Cande and Kent (1995). Map projection is Universal Transverse Mercator (UTM, WGS 1984, zone 27N).*

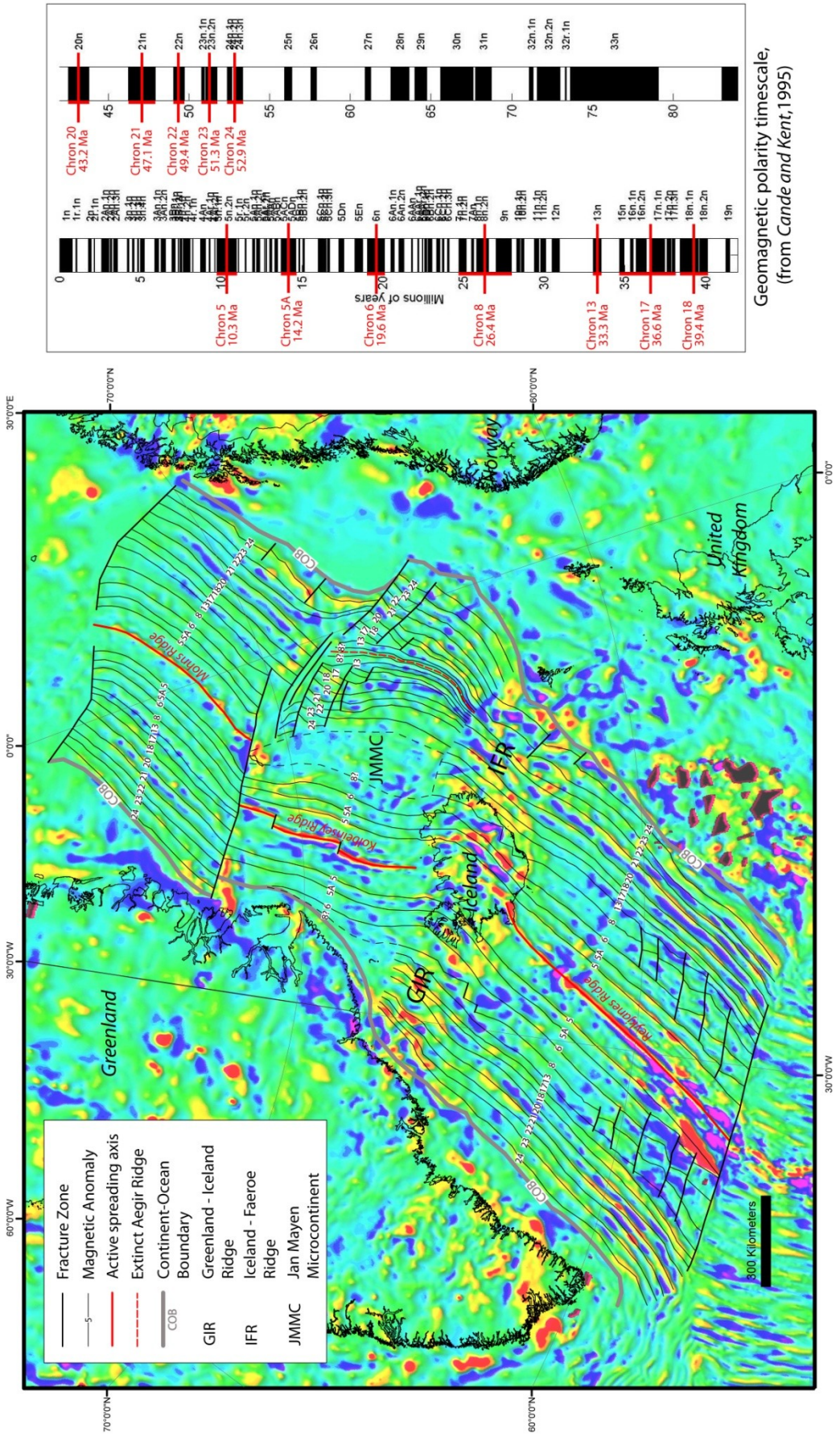
Chron 20 43.2 Ma
Chron 21 47.1 Ma
Chron 22 49.4 Ma
Chron 23 51.3 Ma
Chron 24 52.9 Ma
Chron 5 10.3 Ma
Chron 5A 14.2 Ma
Chron 6 19.6 Ma
Chron 8 26.4 Ma
Chron 13 33.3 Ma
Chron 17 36.6 Ma
Chron 18 39.4 Ma
Millions of years
Geomagnetic polarity timescale, (from Cande and Kent, 1995)
Greenland
Iceland
Norway
United Kingdom
JMMC
GIR
IFR
COB
Mohns Ridge
Kolbeinsey Ridge
Reykjanes Ridge
Fracture Zone
Magnetic Anomaly
Active spreading axis
Extinct Aegir Ridge
Continent-Ocean Boundary
Greenland - Iceland Ridge
Iceland - Faeroe Ridge
Jan Mayen Microcontinent
800 Kilometers

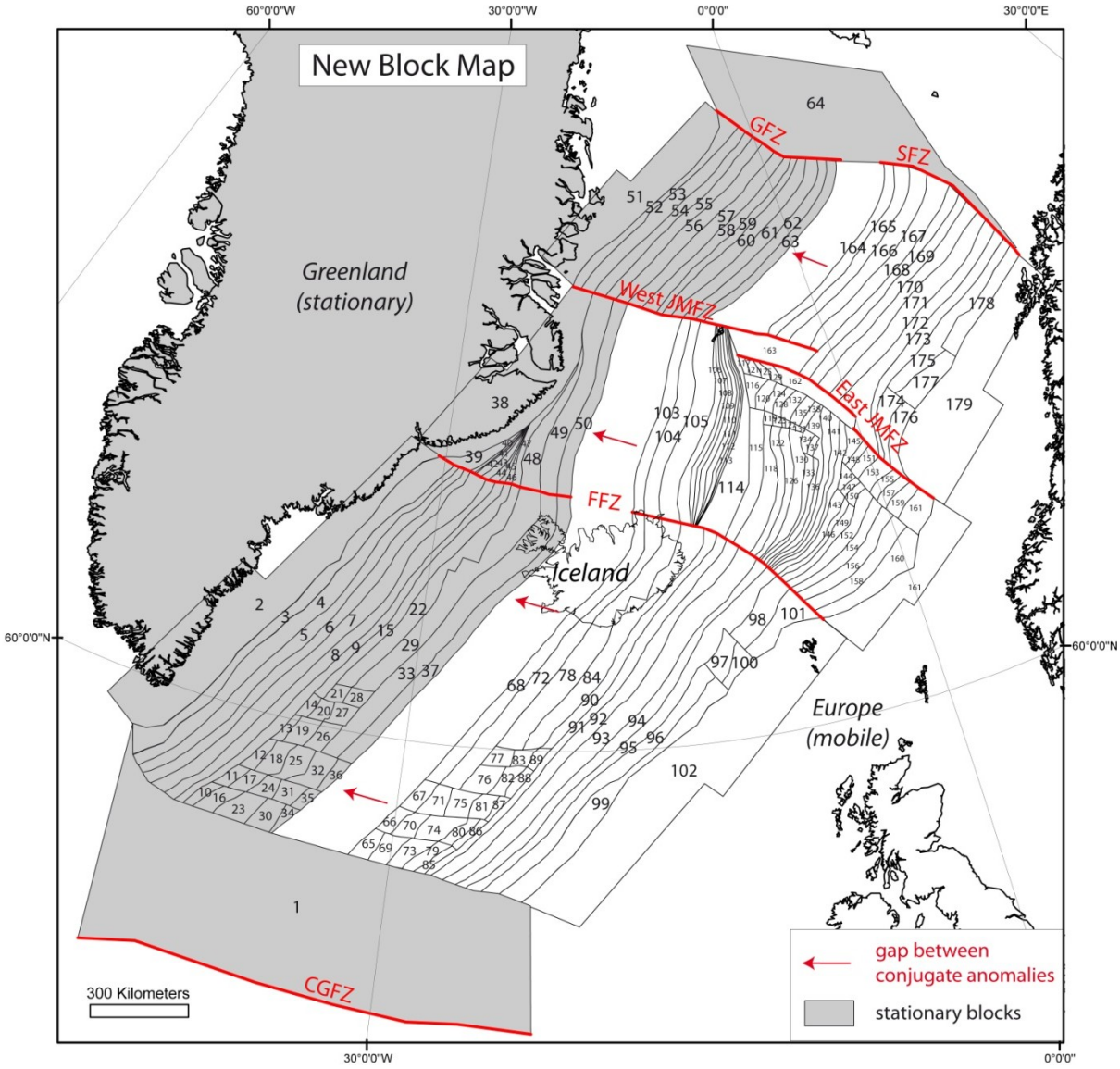

Figure 3.23. *Improved block map from revisied dataset (results of restoration are presented in Chapter 4). Map projection is Universal Transverse Mercator (UTM, WGS 1984, zone 27N).*

3.3.2 Analysis of results: calculation of spreading rates, slip along fracture zones and rotation poles

This section explains the method for calculating of spreading rates, slip along fracture zones and rotation poles from the restoration results. I did these calculations for all restoration tests and will present in this section example of calculation from Test 2 (restoration of the NE Atlantic relative to a stationary Greenland plate). The results of the improved block map (**Figure 3.24**) are presented and discussed in Chapter 4.

At each stage of the restoration, I used the easternmost (external) blocks to calculate mean displacement rates of mobile blocks (**Figure 3.24**). The displacement vectors of the corners of each external block give the direction and the amount of displacement (**Figure 3.25**). This yields spreading rates along each ridge (**Figure 3.26**).

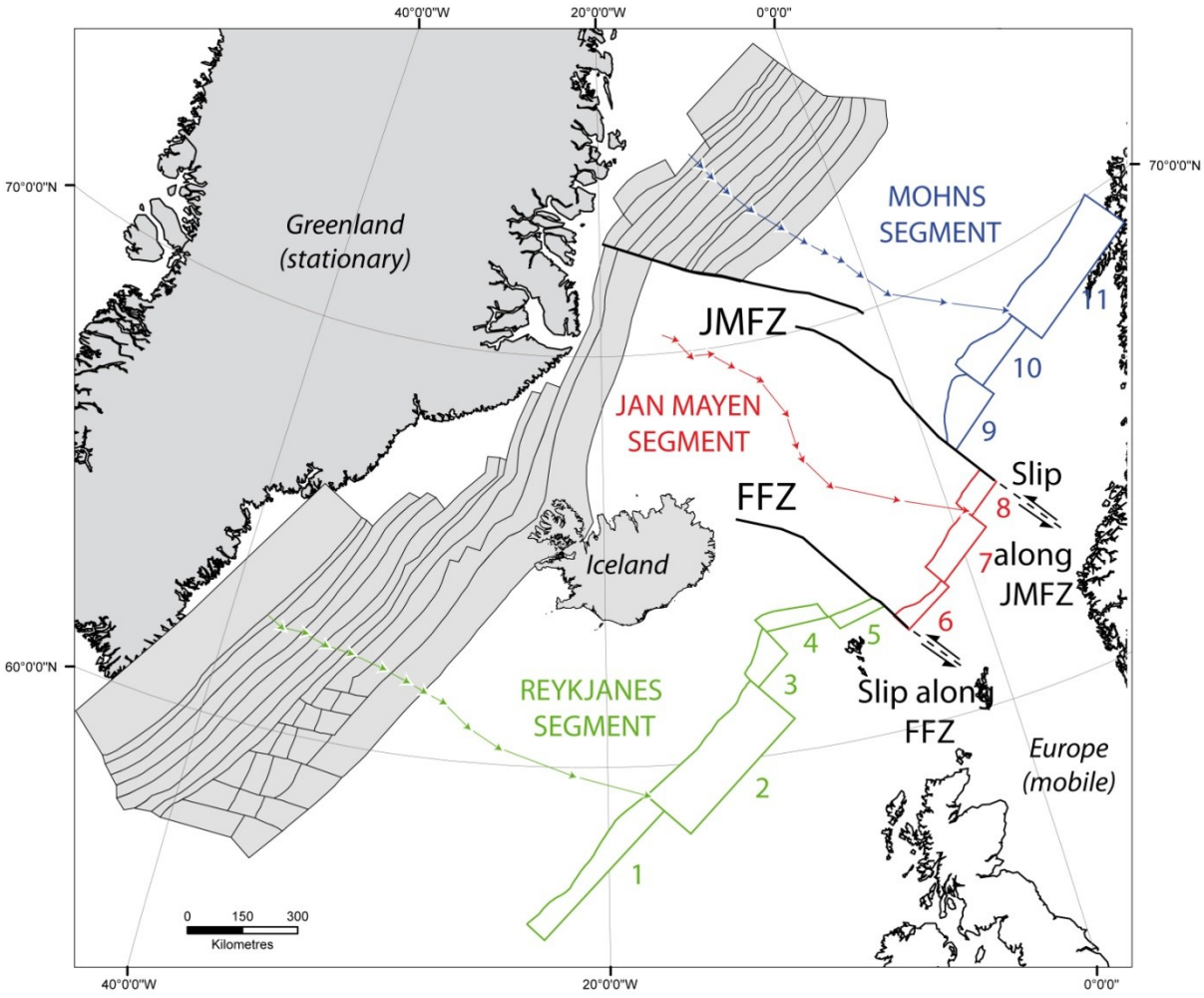

Figure 3.24. *Analysis of restoration results for Test 2. Numbering of external (easternmost) blocks (from 1 to 11) and calculation of average displacements of external blocks during restoration from displacement vectors of each corner of external blocks (green colour for Reykjanes Segment, red colour for Jan Mayen Segment and blue colour for Mohns Segment). Map projection is Universal Transverse Mercator (UTM, WGS 1984, zone 27N).*

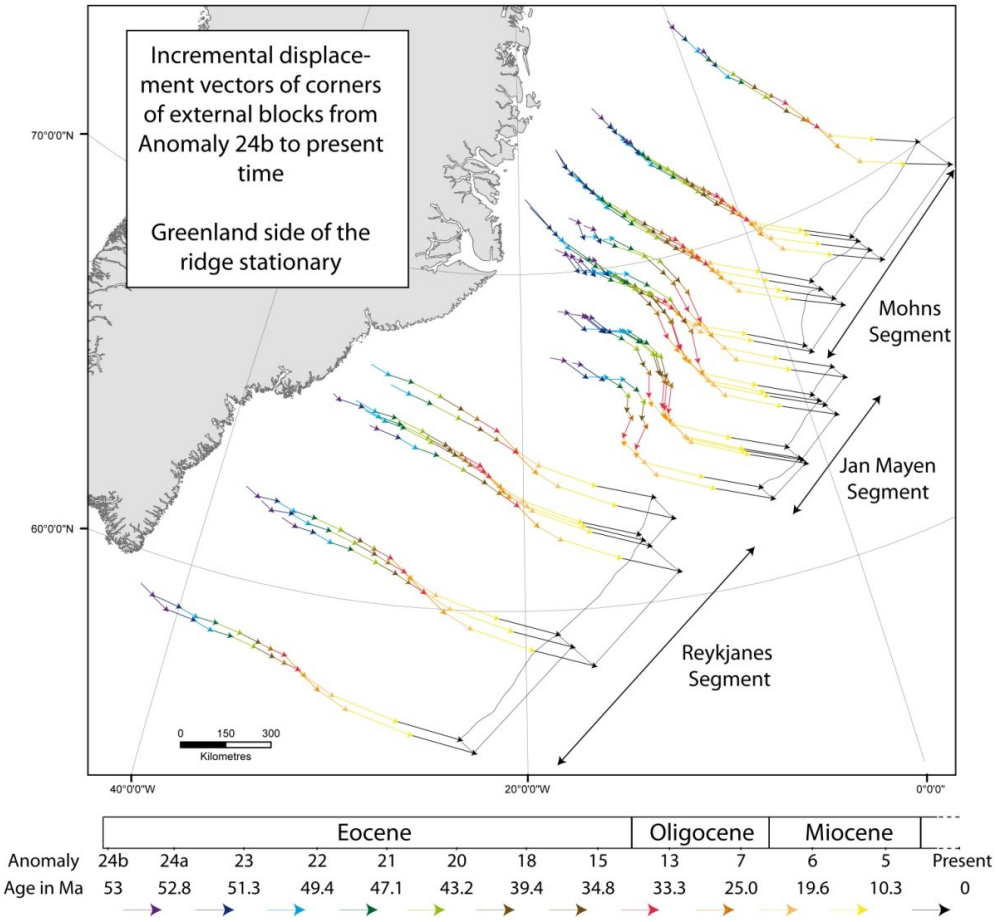

Figure 3.25. *Incremental displacement vectors of external blocks, from Anomaly 24b to present time, for Test 2. These displacement vectors are used to determine displacement rate of each segment, which correspond to spreading rates. Map projection is Universal Transverse Mercator (UTM, WGS 1984, zone 27N).*

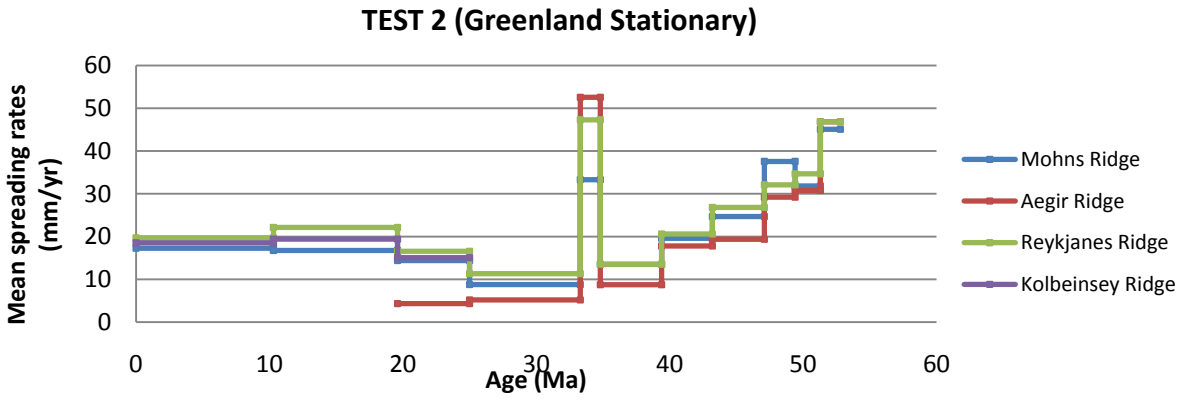

Figure 3.26. *Mean spreading rates (average along each ridge) for Test 2, calculated from incremental displacement vectors. Note, the significant increase in spreading rates is due to the short time interval between anomalies 15 and 13 (34.8 - 33.3 Ma) in the first dataset, however this peak is not observed in spreading rates calculated from restoration using the revised dataset (Chapter 4).*

For each stage in the restoration, I have determined the relative displacement vectors of each segment (**Figure 3.27**). Then, from the distance of these vectors, I have estimated the total and incremental relative displacements between the three oceanic segments, along the JMFZ and FFZ (**Figure 3.28**).

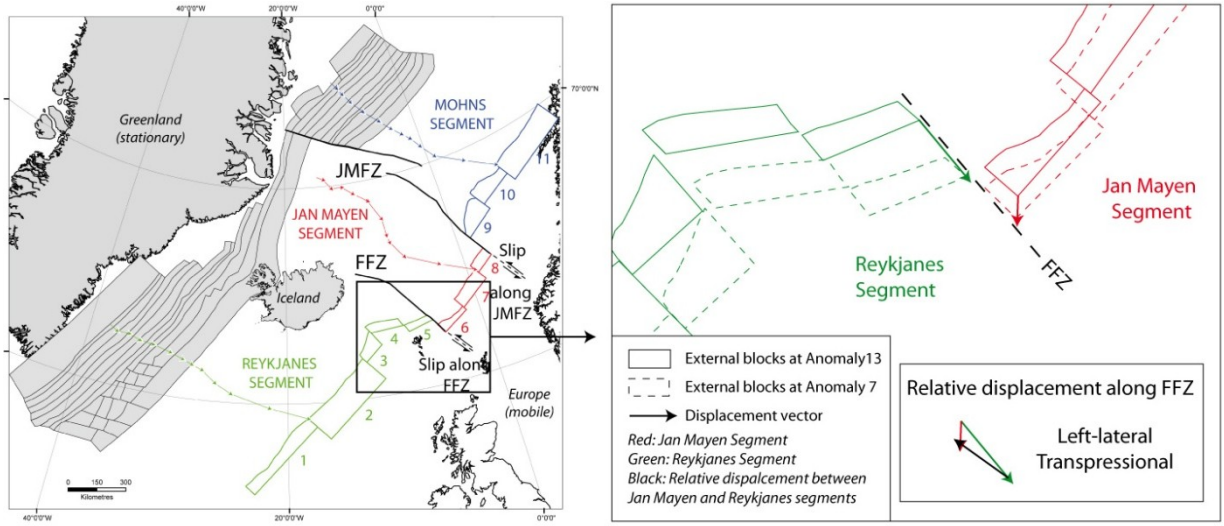

Figure 3.27. *Relative displacement vectors between segments along fracture zones, for example along FFZ, between Anomaly 13 and Anomaly 7, for Test 2. Map projection is Universal Transverse Mercator (UTM, WGS 1984, zone 27N).*

	Eocene								Oligocene		Miocene			
Anomaly	24b	24a	23	22	21	20	18	15	13	7	6	5	Present	
Age (in Ma)	53-52.8	52.8-51.3	51.3-49.4	49.4-47.1	47.1-43.2	43.2-39.4	39.4-34.8	34.8-33.3	33.3-25	25-19.6	19.6-10.3	10.3-0		
Slip along the Jan Mayen Fracture Zone														
Test 2 - Greenland stationary:														
Amount of slip	-	72 km	36 km	48 km	1 km	10 km	12 km	40 km	1 km	50 km	8 km	18 km		
Sense of slip	-	right lateral			-	left lateral	right lateral	left lateral	-	left lateral	-	right lateral		
Slip along the Faeroe Fracture zone														
Test 2 - Greenland stationary:														
Amount of slip	-	5 km	26 km	74 km	71 km	43 km	84 km	73 km	17 km	6 km	0			
Sense of slip	-	-	left lateral						right lateral	-	-			

Figure 3.28. *Relative displacements between oceanic segments along FFZ and JMFZ, for Test 2.*

The external blocks have artificial edges, which serve to calculate, after the restorations, best-fit rotation poles for each ridge and for each magnetic anomaly, using the method of *Kirkwood et al.* (1999) and the criterion of fit of *Hellinger* (1981) (**section 3.1**; **Figure 3.29**). With these rotation poles, I reconstructed the position of the magnetic

anomalies using Gplates Software (*Boyden et al.*, 2011). They represent the best-fit of a whole segment at one stage; therefore they do not represent the exact restoration and do not integrate possible displacements between mobile blocks of one segment.

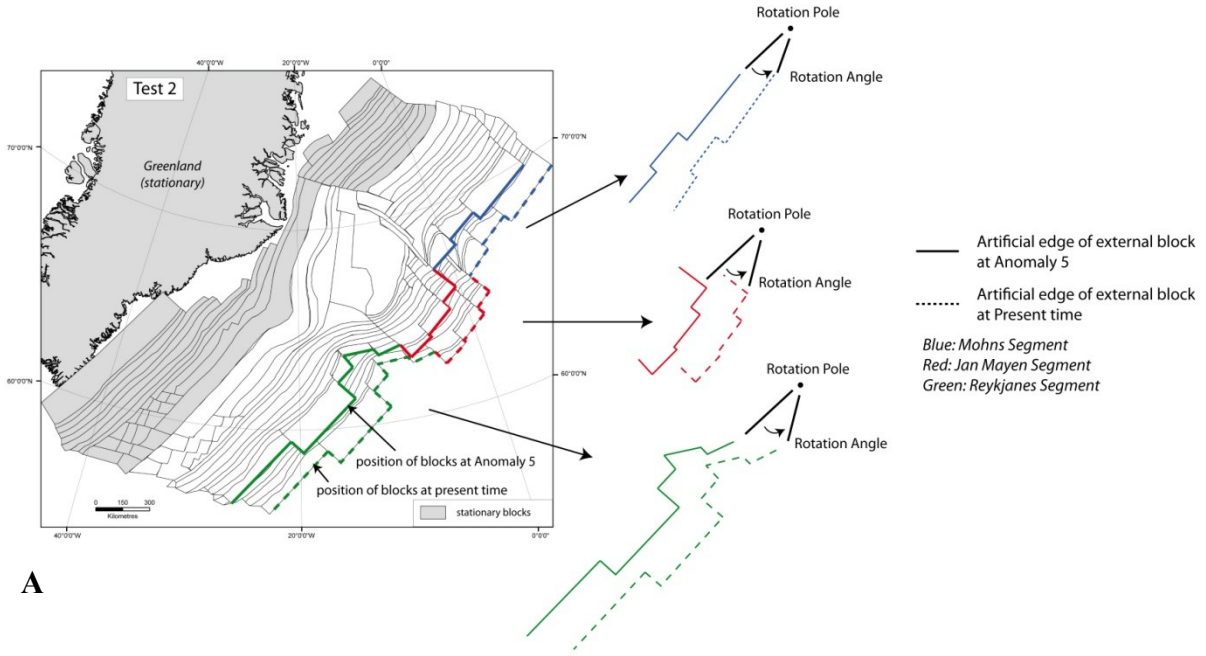

A

```
Results from Hellinger1 using Reykjanes_ano5

 Fitted rotation--alat,along,rho:
   61.447336597524682        131.75607628302370        2.2506256156042741
 conf. level, conf. interval for kappa:
  0.99000001       39.918582114405538        69.604322598380662
 kappahat, degrees of freedom,xchi,flag
   53.598997973193619        173.00000      0.21811111       0.0000000
 Number of points, sections
         198          11
 ahat:
  0.99930676440969501      -3.4582096726632306E-002
1.3786583455583796E-002
  3.4406999294039820E-002  0.99932667662874275
1.2741733701956322E-002
 -1.4217911400961162E-002 -1.2258546575409077E-002  0.99982377398782252
 covariance matrix
  1.9189779907017377E-006 -5.5729213380993649E-007
3.5885683752840347E-006
 -5.5729213380993649E-007  1.8680568834882494E-007 -
1.0443872712495488E-006
  3.5885683752840347E-006 -1.0443872712495488E-006
6.8325910216603460E-006
 H11.2 matrix:
   31862043.000477858        10280824.970050486       -15162909.183113074
   10280824.970050486        40126428.271240778        733848.63105999993
  -15162909.183113074        733848.63105999993        8222292.0065065678
```

B

Figure 3.29. A) *Method of calculation of rotation poles for each segment, for example Anomaly 5 using artificial edges of external blocks (Test 2). B) Rotation poles for Reykjanes Segment and for reconstruction at Anomaly 5, Test 2, using the method of Kirkwood et al. (1999) and criterion of fit of Hellinger (1981). Covariance matrix expresses uncertainties in rotation.*

3.3.3 Limits of the method

The restoration provides a good fit of magnetic anomalies (G ≈ 0.005 for Tests 2 and 3 and G ≈ 0.003 for model presented in Chapter 4). Moreover, the calculation of spreading rates and rotation poles, at least for recent ages (e.g. Anomaly 5), are in good agreement with previous studies (e.g. *Mosar et al.*, 2002; *Gaina et al.*, 2009). For older ages, our restoration method allows relative displacements between the oceanic segments and therefore differences arise in spreading rates and rotation poles. The restorations depend on the hypothesis made in the construction of the block map. Various tests of the method were necessary to improve the block configuration and to restore at best the NE Atlantic. In the improved version of the block map (**Figure 3.23; Chapter 4**), the restoration of the Jan Mayen Segment depends on the choice of configuration of the blocks around the JMMC. This block configuration seems the most accurate with respect to available data on the structural evolution of the JMMC. With this block map, it is possible to restore both the separation of the JMMC and sea-floor spreading along the Aegir Ridge.

The restoration is in a horizontal plane, rather than a spherical surface, and therefore some errors may arise due to the size of the studied area (approx. 2800 km from north to south and 1400 km from west to east) and its proximity to the North Pole. Indeed, distances close to the pole may be biased due to map projection.

In order to take into account the sphericity of the Earth, I modified the restoration program (written in C language). The main modification is a conversion of block translation into rotation. Indeed, a translation between two points on a sphere can be described by a rotation about an axis passing through the centre of the Earth. In the modified algorithm, the input coordinates of the blocks are in geographic coordinate system (latitude, longitude). For each block, in the Translation Cycle (C and E, **Figure 3.5**), I added a conversion of the coordinates into Cartesian coordinates and those of the map projection, so the program calculates the translation of the block on a plane as in the earlier version, then it calculates the rotation pole and angle equivalent to this translation and applies this rotation to the points, in geographic coordinates, of the block. The calculations to convert the coordinates of the blocks and to calculate the rotation, equivalent to the translation, are detailed in **Appendix D**.

I tested this modified version of the restoration program with block maps of Test 2 (Greenland stationary) and Test 3 (Europe stationary), for restoration at Anomaly 5. This modified version of the program worked, however the time of calculation of each iteration

increased significantly (at least x10) and the restoration results did not show significant differences (less than 10%) from those obtained on a plane (**Figure 3.30**). Furthermore, for restorations of Test 2 (Greenland stationary), the fit of conjugate anomalies of the Reykjanes Segment is better in plane restoration than on a sphere (**Figure 3.31**).

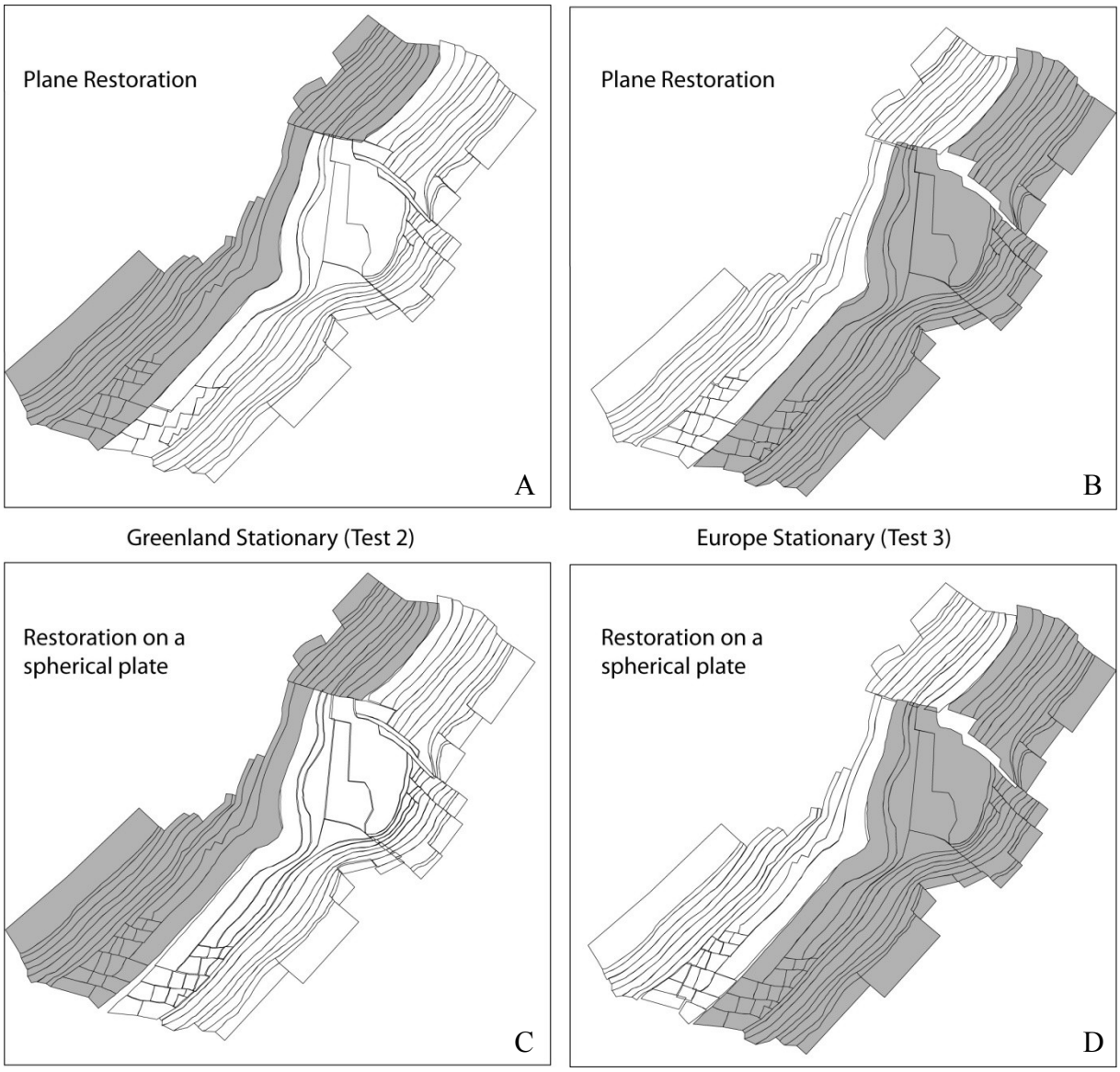

Figure 3.30. *Comparison of restoration results at Anomaly 5 for Test 2 (Greenland stationary in gray) and Test 3 (Europe stationary in gray): A) restoration for Test 2 on a plane, B) restoration for Test 3 on a plane, C) restoration for Test 2 on a sphere, D) restoration for Test 3 on a sphere. Both restoration methods (on a plane or on a sphere) give similar results (differing by less than 10%, mostly due to misfit in spherical restoration of southern*

Reykjanes Segment, see Figure 3.31). Map projection is Universal Transverse Mercator (UTM, WGS 1984, zone 27N).

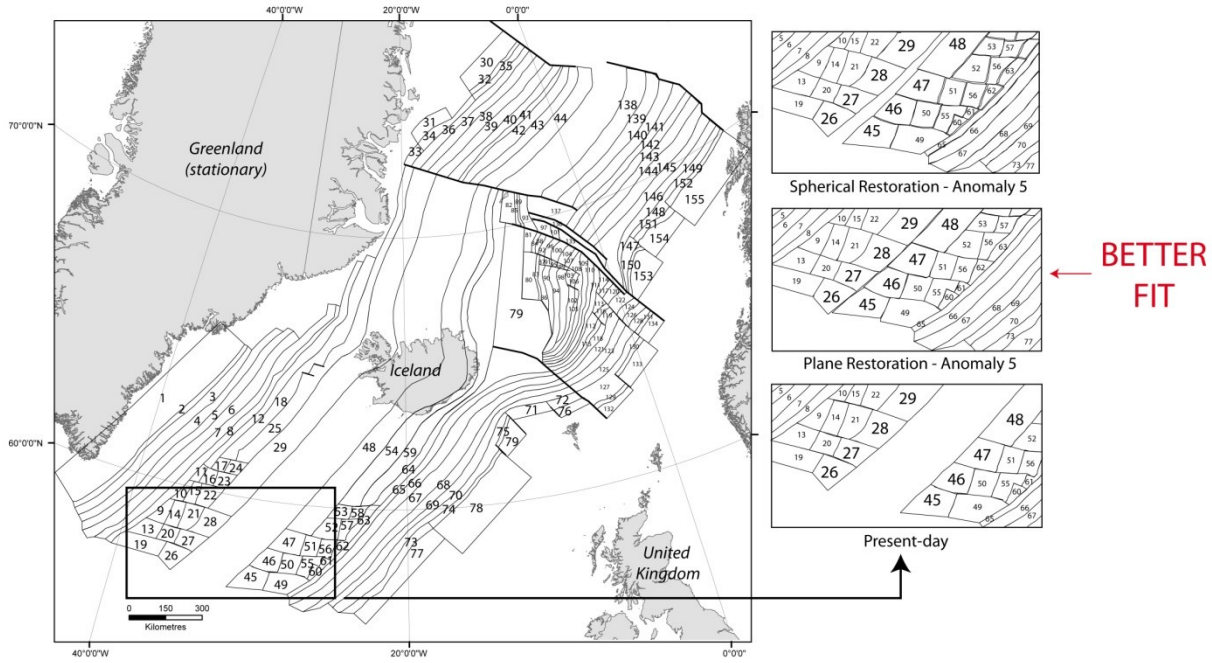

Figure 3.31. *Restoration of southern Reykjanes Ridge, at Anomaly 5 (10.3 Ma), with Greenland side stationary (Test 2). Fit is better for plane restoration. Map projection is Universal Transverse Mercator (UTM, WGS 1984, zone 27N).*

This misfit may result from programming problems in the modified version. Indeed, the modifications complicated the numerical procedure; it would have been best to rewrite the program entirely. However, I did not have time for this. Because the differences between restorations on a plane and on a sphere were not significant, I kept the first version of the program for the restoration of the improved block map (**Chapter 4**). Moreover, calculations are made on small distances (between corners of external blocks), therefore the error due to map projection are small. I estimated these uncertainties, due to non-spherical restoration and map projection, by comparing the initial and final length of the external segments of easternmost blocks. For this purpose, I used the Gplates software (*Boyden et al.*, 2011), which takes into account the sphericity of the Earth in calculation of distances and allows superposition of the segments. I estimated these uncertainties to be, at most, 9 km for the Mohns Segment, 5 km for the Jan Mayen Segment and 4.5 km for the Reykjanes Segment.

I moreover estimated a spatial uncertainty of 5 km for the positions of both magnetic anomalies and fracture zones from previous studies (e.g. *Müller et al.*, 1999; *Gaina et al.*,

2009). Therefore, I considered an error of ± 10 km at most for the calculation of displacements and spreading rates. Thus, relative displacements less than 10 km, between oceanic segments along the fracture zones, are not significant.

In the following chapter, I will present the results of two new models, using the improved block map (section 3.3.15) and calculations of spreading rates and relative displacements between oceanic segments.

Chapter 4

Differential sea-floor spreading and compressional deformation of adjacent continental margin

4.1 Introduction

In the last two chapters, I presented a method of palinspastic restoration and its application for the restoration of opening of the NE Atlantic. Several problems arose from the different tests of this method, that are mostly due to the difficult identification of magnetic anomalies in some areas (around the Jan Mayen Microcontinent, JMMC, and around Iceland) and the rifting of the JMMC off Greenland during sea-floor spreading, that is not taken into account in block maps in which blocks are only delimited by magnetic anomalies (see Chapter 3). Therefore, I improved the block map in order to avoid those problems. In this Chapter, I present the results of two models of kinematic reconstructions of opening of the NE Atlantic Ocean using this new block map, in the form of an article submitted to *Tectonics*.

During the Cenozoic, compressional structures developed along the European Continental Margin. However there is little evidence of such deformation along the Greenland continental margin (see Chapter 2). Mechanisms for the development of this deformation on the continental shelf of NW Europe remain a matter of debate. *Mosar et al.* (2002) suggested that differential sea-floor spreading between the Mohns, Aegir and Reykjanes ridges, as well as mantle drag, were responsible for the development of inversion structures along the Vøring Basin, Norway, and the Faeroe-Rockall Plateau, rather than in the Møre Basin, Norway (see Chapter 2). Therefore, in the kinematic models, I assume that Greenland is rigid and stationary; whereas the European margin is mobile and deformable in order to investigate how these compressional structures may have resulted from variations in the direction and rate of

sea-floor spreading along the ridge system. From these models, I calculate spreading rates along the Reykjanes, Mohns, Aegir and Kolbeinsey ridges and relative displacements along oceanic transform faults, the Jan Mayen Fracture Zone (JMFZ) and the Faeroe Fracture Zone (FFZ), during sea-floor spreading. I demonstrate that these relative displacements and the relative rotation between oceanic segments are compatible, in time and space, with the development of inversion structures along the NW European Continental Margin. Furthermore, I discuss, in the paper and in the general discussion at the end of this chapter, the influence of the Iceland Mantle Plume on the variation in the direction and rate of sea-floor spreading along the NE Atlantic and the resulting deformation on the adjacent European margin.

4.2 Variation in amount and direction of sea-floor spreading along the North East Atlantic Ocean and resulting deformation of the continental margin of North West Europe

Le Breton et al., in review in Tectonics

Variations in amount and direction of sea-floor spreading along the North East Atlantic Ocean and resulting deformation of the continental margin of North West Europe

E. Le Breton[1*], P.R. Cobbold[1], O. Dauteuil[1], G. Lewis[2]

[1] Geosciences Rennes, Université de Rennes 1, CNRS, 263 Avenue du Général Leclerc, 35042 Rennes, France

[2] Chevron Onshore Europe, Seafield House, Hill of Rubislaw, Aberdeen, AB10 6XL, United Kingdom

*Corresponding author, eline.lebreton@univ-rennes1.fr

Abstract

The NE Atlantic Ocean opened progressively between Greenland and NW Europe during the Cenozoic. Sea-floor spreading occurred along three ridge systems: the Reykjanes Ridge south of Iceland, the Mohns Ridge north of the Jan Mayen Fracture Zone (JMFZ), and the Aegir and Kolbeinsey ridges between Iceland and the JMFZ. At the same time, compressional structures developed along the continental margin of NW Europe. We investigate how these compressional structures may have resulted from variations in the amount and direction of sea-floor spreading along the ridge system. Assuming that Greenland is rigid and stationary, we have used a least-squares method of palinspastic restoration to calculate differences in direction and rate of spreading along the Reykjanes, Kolbeinsey/Aegir and Mohns ridges. This differential sea-floor spreading generated relative rotations and displacements between the oceanic segments. We have determined two main periods of left-lateral strike-slip deformation along the main oceanic fracture zones: (1) from Early-Eocene to Late Oligocene, along the Faeroe Fracture Zone; and (2) from Late Eocene to Early Oligocene and during the Miocene, along the JMFZ. Such left-lateral motion and the relative rotation between the oceanic segments are compatible with the development of inversion structures on the Faeroe-Rockall Plateau and Norwegian Margin at those times and probably with the initiation of the Fugløy Ridge in the Faeroe-Shetland Basin during the Eocene and Oligocene. The Iceland Mantle Plume appears to have been in a position to generate differential sea-floor spreading along the NE Atlantic and resulting deformation of the European margin.

Keywords

NE Atlantic, Sea-floor spreading, Fracture Zones, Compression, European Margin, Iceland Plume

1. Introduction

The NE Atlantic Ocean lies between Greenland and NW Europe (**Figure 1**). As in other oceanic areas, relief at the seafloor has resulted mainly from spreading along a system of oceanic ridges. Locally, strong relief has resulted also from volcanic activity, especially on and around two islands, Iceland and Jan Mayen. Another feature, which is specific to the NE Atlantic Ocean, is that its ridge system is complex. For descriptive purposes, we consider it in three parts. From SW to NE, these are the Reykjanes, Jan Mayen and Mohns segments. Of the Reykjanes and Mohns segments, each consists of one ridge only, whereas the Jan Mayen Segment consists of two ridges (Kolbeinsey and Aegir). Between the three segments are systems of transform faults, the Jan Mayen Fracture Zone (JMFZ) in the North and the Greenland-Iceland-Faeroe Fault Zone in the South. The latter, more than the former, is responsible for a notable topographic feature, the Greenland-Iceland-Faeroe Ridge (GIFR).

Seafloor spreading and opening of the NE Atlantic Ocean occurred during the Tertiary period and resulted in a characteristic pattern of magnetic anomalies (**Figure 2**). From the polarity of the geomagnetic data, *Cande and Kent* [1995] defined a time scale, which is in general acceptance. Definition of the anomalies is good over most of the sea bottom, except for a swath along the GIFR and an area to the South of Jan Mayen (**Figure 2**). Ocean drilling and geophysical investigations have revealed that the latter is a small continental plate, the Jan Mayen Micro-Continent (JMMC, **Figure 1**), which rifted off the coast of Greenland during the Eocene [*Bott*, 1985, 1987; *Gaina et al.*, 2009; *Kodaira et al.*, 1998; *Nunns*, 1983; *Unternehr*, 1982]. The significant bathymetric-topographic highs around Iceland and Jan Mayen and along the GIFR developed as a result of intense magmatic activity, when the NE Atlantic Ridge interacted with a major thermal and compositional anomaly, the Iceland Mantle Plume [e.g. *Saunders et al.*, 1997]. The magmatic activity modified the magnetic signature of the crust, so that magnetic anomalies are not simple over these areas (**Figure 2**).

Assuming that Greenland and Eurasia were rigid plates and using the Euler rotation poles to rotate them, *Bullard et al.* [1965] reconstructed the opening of the North Atlantic. However, this led to some gaps and overlaps between the plates. By dividing the ridge system into segments and increasing the number of plates, *Gaina et al.* [2009] were able to improve the quality of the fit. The Jan Mayen Segment, with two spreading centers and a micro-continent, is however more complex than the Reykjanes and Mohns segments (**Figure 1**). Moreover the pattern of magnetic anomalies around the Aegir Ridge has significant curvature

(**Figure 2**). In other words, it is difficult to reconstruct a simple spreading history for the Jan Mayen Segment using the Euler rotation poles alone.

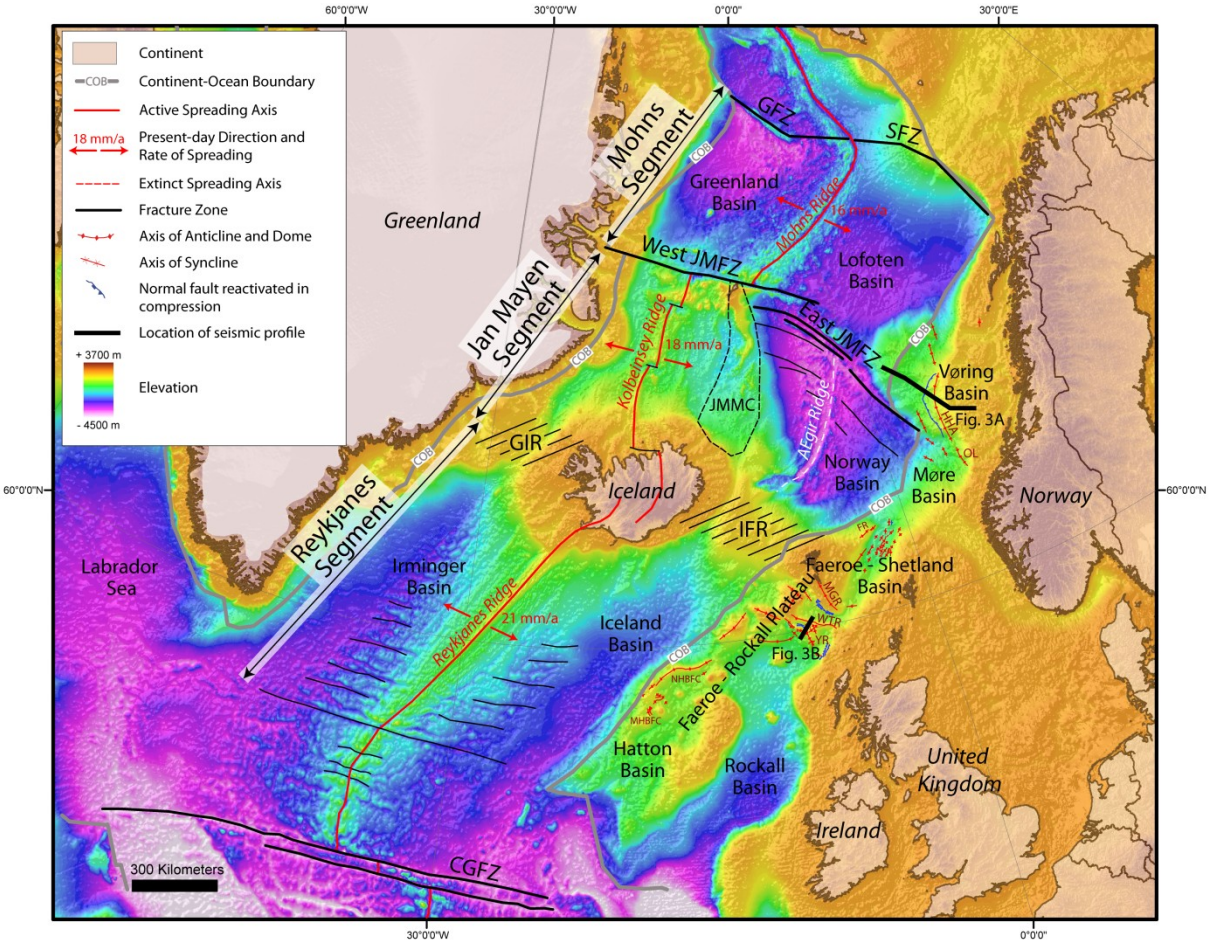

Figure 1. *Principal tectonic features of the NE Atlantic Ocean on a bathymetric and topographic map (ETOPO1). Compressional structures (folds and reverse faults) on NW European Continental Margin are from Doré et al. [2008], Johnson et al. [2005] and Tuitt et al. [2010]. Present-day spreading rates along Reykjavik, Kolbeinsey and Mohns ridges are from Mosar et al. [2002]. Continent-Ocean Boundaries of Europe and Greenland are from Gaina et al. [2009] and Olesen et al. [2007]. Black thick lines indicate seismic profiles of Figure 3. Abbreviations (North to South): GFZ, Greenland Fracture Zone; SFZ, Senja Fracture Zone; JMFZ, Jan Mayen Fracture Zone (West and East); JMMC, Jan Mayen Microcontinent; HHA, Helland Hansen Arch; OL, Ormen Lange Dome; FR, Fugløy Ridge; GIR, Greenland-Iceland Ridge; IFR: Iceland-Faeroe Ridge; MGR, Munkagrunnar Ridge; WTR, Wyville Thomson Ridge; YR, Ymir Ridge; NHBFC, North Hatton Bank Fold Complex; MHBFC, Mid Hatton Bank Fold Complex; CGFZ, Charlie Gibbs Fracture Zone. Map projection is Universal Transverse Mercator (UTM, WGS 1984, zone 27N).*

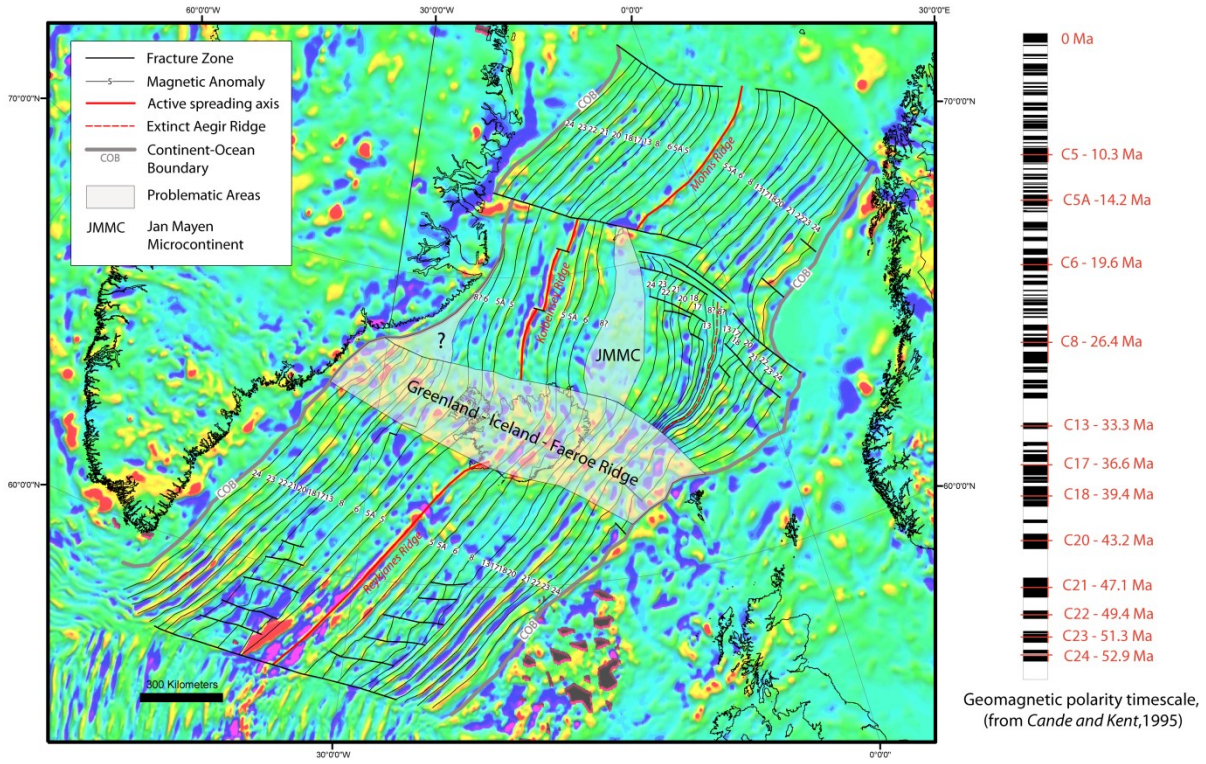

Figure 2. *Map of magnetic anomalies, NE Atlantic Ocean. Background image is recent model EMAG2 of crustal magnetic anomalies [Maus et al., 2009]. Ages of magnetic anomalies are from Cande and Kent [1995]. Map projection is Universal Transverse Mercator (UTM, WGS 1984, zone 27N).*

The continental margins of NW Europe and East Greenland formed by rifting between Greenland and Eurasia, before the onset of sea-floor spreading. The margins consist of stretched continental crust and coeval magmatic rocks, and thus belong to the category of volcanic passive margins [*Geoffroy*, 2005]. The European Margin was subject to several phases of extension after collapse of the Caledonian Orogeny [e.g. *Lundin and Doré*, 2005; *Ziegler*, 1988] and it is therefore wider than the Greenland Margin (**Figure 1**). Several sedimentary basins formed on the European margin as a result of rifting: the Vøring and Møre basins in the north, the Faeroe-Shetland Basin in the centre and the Hatton and Rockall basins in the south. The area between the Hatton/Rockall and Faeroe-Shetland basins we shall refer to as the Faeroe-Rockall Plateau. This plateau, as well as the Vøring Basin, contains various compressional structures (folds and reverse faults), which formed after continental break-up [*Boldreel and Andersen*, 1993; *Brekke*, 2000; *Davies et al.*, 2004; *Doré et al.*, 2008; *Doré and Lundin*, 1996; *Hitchen*, 2004; *Johnson et al.*, 2005; *Lundin and Doré*, 2002; *Løseth and Henriksen*, 2005; *Ritchie et al.*, 2003, 2008; *Smallwood*, 2004; *Stoker et al.*, 2005; *Tuitt et al.*,

2010]. In contrast, along the Greenland margin, there is little evidence for post-breakup deformation, other than some folds of low amplitude [e.g. *Price et al.,* 1997]. *Mosar et al.* [2002] calculated spreading rates along each of the Reykjanes, Aegir and Mohns ridges, showing that there is a significant variation in spreading rates across the JMFZ. They suggested that this differential spreading was responsible for compressional inversion of the Vøring and Faeroe-Shetland Basins rather than the Møre Basin.

So as to investigate this idea more fully, we have developed a method for palinspastic reconstruction of the opening of the NE Atlantic. Our model represents the position of Europe, relative to a stationary and rigid Greenland plate, in order to study the evolution of the European Margin during sea-floor spreading. Instead of traditional Euler rotation poles, we have used an iterative least-squares method, which minimizes the gaps or overlaps between conjugate magnetic anomalies. In this method, all segments of the NE Atlantic are free to spread at different rates. Our models provide new constraints on the style and timing of deformation along major oceanic fracture zones during sea-floor spreading, as well as on the European Continental Margin.

2. Geological setting

2.1 Kinematics of the NE Atlantic Ocean

During the Late Paleocene, Greenland and Eurasia separated, as sea-floor spreading propagated northward out of the central North Atlantic [e.g. *Pitman and Talwani*, 1972; *Srivastava and Tapscott*, 1986; *Vogt and Avery*, 1974]. A triple junction existed between the North Atlantic and the Labrador Sea ridges until the extinction of the latter at about 35 Ma [e.g. *Vogt and Avery*, 1974]. This extinction triggered a change in spreading direction between Europe and Greenland at about that time [e.g. *Srivastava and Roest*, 1999; *Srivastava and Tapscott*, 1986; *Vogt and Avery*, 1974]. After continental break up (~56 Ma) [e.g. *Nunns*, 1983], the mid-oceanic ridge between the margins of Greenland and Eurasia became offset to the east along the northern flank of the GIFR [*Bott*, 1985, 1987; *Nunns*, 1983]. Sea-floor spreading occurred along the Aegir Ridge on the eastern side of the JMMC, which was part of Greenland at that time [e.g. *Nunns*, 1983]. However, rifting propagated northward from the Reykjanes Ridge into the south-western part of the JMMC, after at least Chron 20 (~44 Ma), leading to significant stretching of this microcontinent [*Bott*, 1985, 1987; *Gaina et al.*, 2009; *Müller et al.*, 2001; *Nunns*, 1983]. Between Chron 13 (~33Ma) and Chron 6 (~20Ma), the Aegir Ridge became extinct and a new spreading center, the Kolbeinsey Ridge, formed on the

western side of the highly stretched JMMC, which separated totally from Greenland [*Bott*, 1985, 1987; *Gaina et al.*, 2009; *Müller et al.*, 2001; *Nunns*, 1983; *Scott et al.*, 2005; *Skogseid et al.*, 2000; *Talwani and Eldholm*, 1977; *Unternehr*, 1982]. According to the stationary hot spot model of *Lawver and Müller* [1994], the head of the Iceland Plume was beneath the eastern Greenland Margin at that time (40-30 Ma). *Müller et al.* [2001] suggested that the Iceland Mantle Plume was responsible for (1) rifting at the edge of the eastern Greenland margin, (2) formation of the Kolbeinsey Ridge west of Jan Mayen, (3) subsequent cessation of the Aegir Ridge and (4) separation of the JMMC from Greenland. Later, in Miocene times, the plume head was beneath the Reykjanes Ridge and resulting volcanic activity formed the Iceland Plateau [*Doré et al.*, 2008]. Since Chron 6, the Kolbeinsey Ridge has been the only active spreading centre in the Jan Mayen Segment [e.g. *Gaina et al.*, 2009]. There have been several models for the complex spreading history of the Jan Mayen Segment [*Bott*, 1985, 1987; *Gaina et al.*, 2009; *Nunns*, 1983; *Scott et al.*, 2005; *Unternehr*, 1982]. According to various authors, as the JMMC separated from Greenland, it rotated counter-clockwise by about 30° and this resulted in fan-shaped sea-floor spreading along the Aegir Ridge [*Bott*, 1987; *Gaina et al.*, 2009]. However, misfits remain in reconstructions of conjugate magnetic anomalies of the fan-shaped Aegir Ridge [e.g. *Gaina et al.,* 2009]. We have therefore used a palinspastic method of restoration in order to improve the fit between conjugate magnetic anomalies on this ridge. We discuss the development of the Jan Mayen Segment, in comparison with the Reykjanes and Mohns segments, and the structural history of the adjacent European margin.

2.2 The NW European Continental Margin

Mitchell and Reading [1969] distinguished between (1) an Atlantic-type continental margin ("passive" margin), where there is no differential movement between ocean floor and continent, and (2) an Andean-type margin ("active" margin), where the oceanic floor subducts beneath a submarine trench and a continental arc. Accordingly, a truly "passive" margin, such as the NW European Continental Margin, develops in two stages. First, stretching of continental lithosphere leads to block faulting and subsidence. Second, the margin undergoes long-term thermal subsidence, but no more extensional faulting [*McKenzie*, 1978]. However, many authors have described post-rift compressional structures (folds, reverse faults and reactivated normal faults) along the NW European Margin [*Boldreel and Andersen*, 1993; *Brekke*, 2000; *Davies et al.*, 2004; *Doré et al.*, 2008; *Doré and Lundin*, 1996; *Hitchen*, 2004;

Johnson et al., 2005; *Lundin and Doré*, 2002; *Løseth and Henriksen*, 2005; *Ritchie et al.*, 2003, 2008; *Smallwood*, 2004; *Stoker et al.*, 2005; *Tuitt et al.*, 2010]. Moreover, studies of fission tracks in apatite or zircon have revealed various Cenozoic episodes of uplift and exhumation in NW Europe [e.g. *Anell et al.*, 2009; *Hendriks et al.*, 2007; *Holford et al.*, 2009; *Japsen et al.*, 2010]. In contrast, there is little evidence of post-break up deformation, on the Greenland Margin, except for low- amplitude folds [e.g. *Price et al.,* 1997]. The post-breakup compressional structures developed at the SE ends of the JMFZ in the Vøring Basin, Norwegian Margin, and more widely on the Faeroe-Rockall Plateau (**Figures 1 and 3**) [e.g. *Doré and Lundin*, 1996; *Johnson et al.*, 2005].

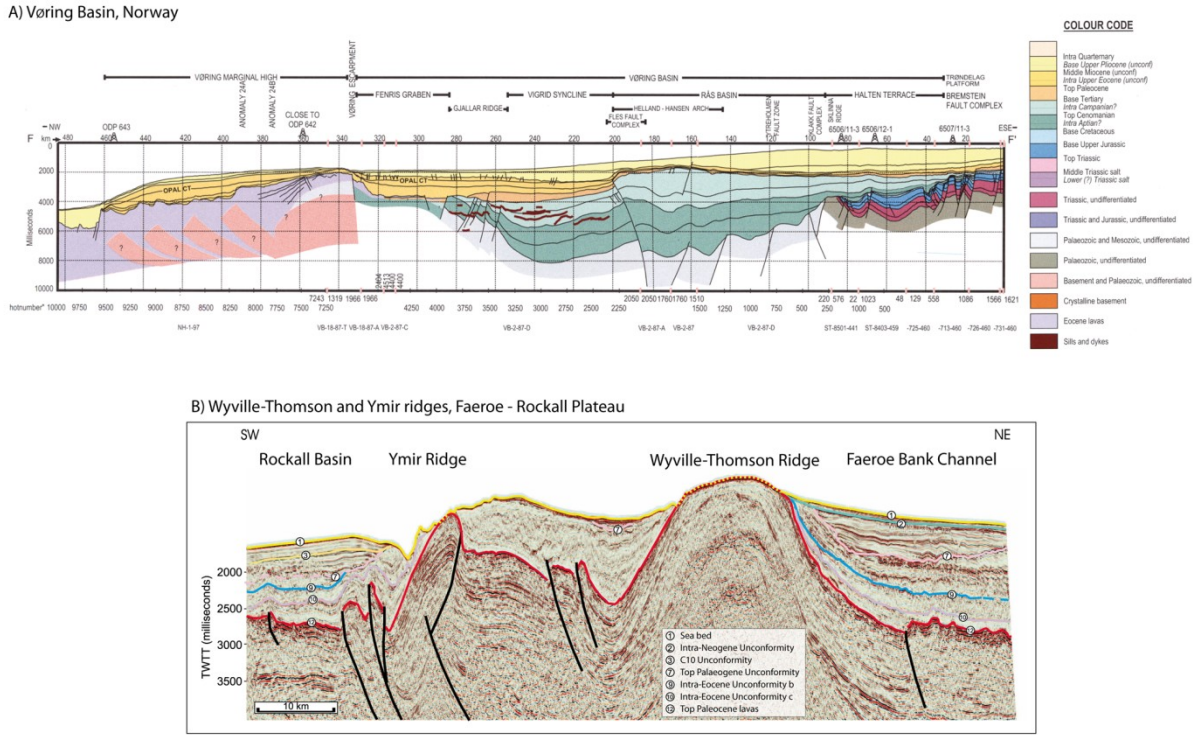

Figure 3. *Interpreted seismic profiles across (A) Helland-Hansen Arch, in Vøring Basin, Norway, from Brekke [2000] and (B) Wyville-Thomson and Ymir ridges, in Faeroe-Rockall Plateau, from Johnson et al. [2005]. Locations of profiles are on Figure 1.*

On the Norwegian Margin, compressional doming, basin inversion and reverse faulting occurred predominantly within deep Cretaceous depocentres, which may have been more susceptible to deformation than other areas [*Lundin and Doré*, 2002]. In the Vøring Basin, *Lundin and Doré* [2002] described two phases of transpression (combination of strike-slip and transverse shortening) in (1) the Middle Eocene to Early Oligocene and (2) the Early Miocene. These phases the authors held responsible for large domes and arches (e.g. the

Ormen Lange Dome and Helland Hansen Arch), trending N or NNE (**Figures 1 and 3**). In the area of the Helland Hansen Arch, *Løseth and Henriksen* [2005] inferred a phase of compression in the Middle to Late Miocene (15- 10 Ma), from seismic interpretation of the syn-tectonic Kai Fm. *Doré and Lundin* [1996] suggested that compressional domes formed by left-lateral reactivation of lineaments trending NW-SE, subparallel to the JMFZ or along it. In contrast, the Møre Basin contains no Cenozoic compressional structures [*Brekke*, 2000]. *Mosar et al.* [2002] suggested that a difference in spreading rates among the Mohns, Aegir and Reykjanes ridges was responsible for the development of inversion structures in the Vøring Basin and on the Faeroes-Rockall Plateau, rather than in the Møre Basin.

On the Faeroe-Rockall Plateau, compressional structures are different from those on the Norwegian Margin and they also vary in size, trend and shape [*Tuitt et al.*, 2010]. North of the Faeroe-Shetland Basin, the trend of anticlines is predominantly NE-SW (e.g. the Fugløy Ridge), whereas in the south, their trend is mainly NW-SE (e.g. the Munkagrunnar Ridge) (**Figures 1 and 3**). On the southern part of the plateau (Hatton Bank), the trend of the compressional structures varies from NE-SW (e.g. the Mid-Hatton Bank Fold Complex) to NNE-SSW (e.g. the North Hatton Bank Fold Complex) (**Figure 1**). *Boldreel and Andersen* [1998] inferred three main phases of compressional deformation, each resulting in a distinct structural trend: (1) a Paleocene to Early Eocene phase, for structures trending WNW (e.g. the Wyville-Thomson Ridge), NNW (e.g. Munkagrunnar Ridge) or ENE (e.g. Fugløy Ridge); (2) an Oligocene phase, for folds trending NE to ENE, to the east of the Faeroe Islands and between the Faeroe Islands and Hatton Bank; (3) a Miocene phase, for anticlines trending NW, perpendicular to the continental margin. More recent studies of seismic reflection data have shown that structures trending NE to ENE across the NE Faeroe-Shetland Basin developed mainly during the Early Miocene to Middle Miocene and may have continued to grow during Early Pliocene to Recent times [*Johnson et al.*, 2005; *Ritchie et al.*, 2008, 2003]. However, there may have been an older (Eocene to Oligocene) phase of deformation on the Fugløy Ridge. South of the WTYR area, the Alpine dome formed during the Oligocene, whereas the North Hatton Bank Fold Complex grew in the Middle Eocene to Early Oligocene [*Johnson et al.*, 2005; *Ritchie et al.*, 2008, 2003]. *Tuitt et al.* [2010] described several compressional unconformities on the Faeroe-Rockall Plateau, their ages varying from Late Paleocene to Early Oligocene.

Amongst the mechanisms which may have accounted for the formation of these compressional structures are (1) the Alpine stress field [e.g. *Brekke*, 2000], (2) ridge push [*Boldreel and Andersen*, 1998; *Doré and Lundin*, 1996], (3) plume-enhanced ridge push

[*Lundin and Doré*, 2002], (4) differential sea-floor spreading and mantle drag [*Mosar et al.*, 2002], (5) differential compaction [e.g. *Stuevold et al.*, 1992] and (6) development of the Iceland Insular Margin [*Doré et al.*, 2008]. These mechanisms are still subject to debate. In this paper, we will investigate the possible effects of differential sea-floor spreading.

3. Data and methods

3.1 Dataset

In the NE Atlantic there have been numerous geophysical surveys. Magnetic datasets are of good quality, but the identification of magnetic anomalies is problematic in some areas, such as around Iceland and along the GIFR, where the ridge interacted with the Iceland mantle plume during sea-floor spreading [e.g. *Saunders et al.*, 1997] (**Figure 2**). We determined the positions of fracture zones from the gravity data of *Andersen et al.* [2010] and *Kimbell et al.* [2005] and of the positions of isochrons from *Gaina et al.* [2009], *Gernigon et al.* [2009], *Jones et al.* [2002], *Macnab et al.* [1989], *Maus et al.* [2009], *Olesen et al.* [2007] and *Skogseid et al.* [2000].

We assign a spatial uncertainty of 5 km for the positions of both magnetic anomalies and fracture zones, as in previous studies [e.g. *Gaina et al.*, 2009; *Müller et al.*, 1999]. The positions and age (55.9 Ma) of the Continent-Ocean Boundaries (COB) of Greenland and Europe are from *Gaina et al.* [2009] and *Olesen et al.* [2007]. Ages of magnetic anomalies are mean values for each identifiable isochron, according to the magnetic time scale of *Cande and Kent* [1995].

3.2 Restoration Method

We have used an iterative least-squares method for palinspastic reconstruction of the opening of the NE Atlantic Ocean. The method proceeds by minimizing gaps or overlaps between adjacent strips of oceanic crust, which follow magnetic anomalies. An early application of this method was to restore deformed surfaces, by minimizing gaps and overlaps between rigid elements [*Cobbold*, 1979]. Subsequent applications were to regions of strike-slip faulting [*Audibert*, 1991], normal faulting [*Rouby et al.*, 1993] or reverse faulting [*Arriagada et al.*, 2008; *Bourgeois et al.*, 1997]. The method is purely geometric. For example, in a region of normal faulting, where a single fault offsets a stratigraphic horizon, the projection of the fault heave on a map defines a cut-off lens (**Figure 4A**). The width of the

lens is proportional to the fault heave. The least-squares method minimizes the gaps (cut-off lenses) across normal faults on a structure-contour map of a given stratigraphic horizon. The first step before restoration is therefore to determine the positions and heaves of the normal faults. The result is a fault-block map, where faults (real or artificial) surround each block (**Figure 4B**), and each block is internally rigid. The second step is to define a stationary block, for reference purposes, An algorithm then minimizes the sum of the squares of the distances across cut-off lenses, with respect to unknown values of rigid translation and rotation for the remaining blocks (**Figure 4B**). This method is applicable also to regions of reverse faulting, in which the cut-off lenses are overlaps, not gaps [*Arriagada et al.*, 2008].

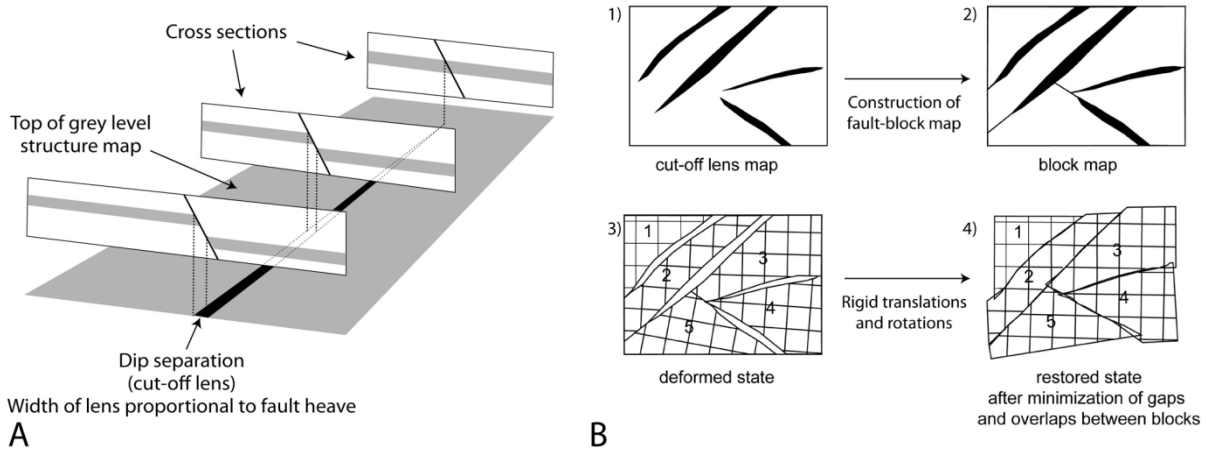

Figure 4. *Principle of restoration method: (A) cut-off lens on a structure contour map and (B) data processing and restoration in plane view (modified after Rouby, 1994).*

The numerical procedure minimizes the sum (D) of the squares of all distances across all cut-off lenses. This minimization generates a set of non-linear equations, in terms of block translations and rotations. To solve these equations, the program uses an iterative method similar to the Gauss-Seidel method [*Audibert*, 1991; *Rouby et al.*, 1993]. A single iteration includes a sequence of operations: neighbor seeking, block translation and block rotation. The program repeats the iterations cyclically, until the equations have converged, according to a criterion G, a non-dimensional parameter that represents the fractional area of gaps and overlaps:

$$G = S_g/S_b \quad (1)$$

where S_g is the total surface area of all gaps and overlaps, and S_b is the total surface area of all the blocks (*Rouby et al.*, 1993). A good approximation to S_g is:

$$S_g = L^*(D/n)^{1/2} \quad (2)$$

where L is the length of a line element, n is the total number of line elements, and $(D/n)^{1/2}$ is the root-mean-square gap width [*Rouby et al.*, 1993]. G is calculated and tested for convergence at the end of each iteration. The convergence is considered satisfactory when G reaches a minimal value [*Arriagada*, 2004].

In this study, we do not apply the method to restore surfaces between normal or reverse faults, but to fit conjugate magnetic anomalies of an oceanic domain and therefore to restore the opening of the NE Atlantic [*Le Breton*, 2012]. The edges of the blocks are magnetic anomalies or fracture zones and the cut-off lenses represent the gaps between conjugate anomalies. The restoration is in a horizontal plane, rather than a spherical surface, and therefore some errors will arise [*Le Breton*, 2012]. We estimate them by comparing the initial and final lengths of blocks. For this purpose we use Gplates software [*Boyden et al.*, 2011], which takes into account the sphericity of the Earth in calculation of distances and allows superposition of the blocks. We estimate these uncertainties to be, at most, 9 km for the Mohns Segment, 5 km for the Jan Mayen Segment and 4.5 km for the Reykjanes Segment. Because there is little evidence of post-break-up deformation on the Greenland Margin [e.g. *Lundin and Doré*, 2002; *Price et al.*, 1997], we assume that the Greenland plate is rigid and stationary. In contrast, we allow the European plate to be mobile and deformable.

3.3 Block Map of the NE Atlantic

We have subdivided the NE Atlantic region into a finite number of rigid oceanic blocks, between magnetic anomalies and fracture zones (**Figure 5**). In the Mohns and Reykjanes segments, the pattern of magnetic anomalies and fracture zones is easily identifiable from Chron 5 to Chron 24. In the Jan Mayen Segment, the pattern of magnetic anomalies is identifiable on the eastern side of the Aegir Ridge, from Chron 13 to Chron 24, and along the Kolbeinsey Ridge, from Chron 6 to the present day. However, it is more difficult to identify the magnetic anomaly of Chron 8 in these two areas (see question marks on Figure 2). Magnetic anomalies are also more difficult to interpret around the JMMC. We therefore used information on the structural development of the JMMC from *Bott* [1985, 1987], *Gaina et al.* [2009], *Gernigon et al.* [2009], *Mjelde et al.* [2008], *Nunns* [1983], and *Unternehr* [1982], so as to define the blocks around the JMMC. From these studies, we estimated that approximately 50% of the JMMC consists of stretched continental crust, especially in the southern part of the JMMC and in its conjugate part on the Greenland margin. We therefore defined 8 thin continental blocks on the western side of the JMMC and

8 others on the eastern side of Greenland, between the magnetic anomaly at Chron 8 and the COB, in order to take into account the progressive continental stretching along the JMMC, and its subsequent counter clockwise rotation, during the restoration [e.g. *Bott*, 1985, 1987; *Gaina et al.*, 2009; *Nunns*, 1983] (**Figure 5**). The 16 blocks thus mimic the stretched continental crust of the JMMC, rather than the oceanic crust (as do the other blocks).

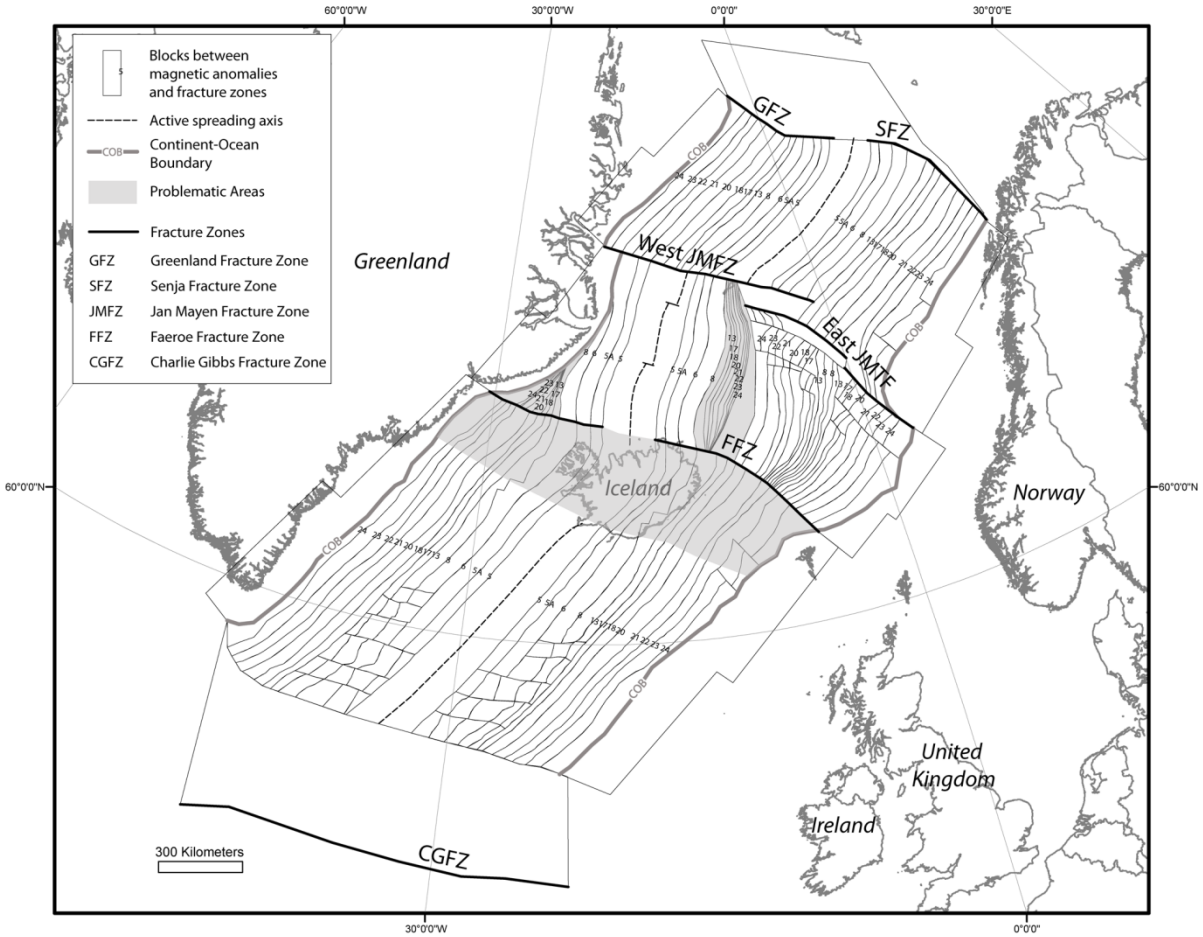

Figure 5. *Block map for restoration of NE Atlantic. Isochrons and fracture zones bound blocks. Map projection is Universal Transverse Mercator (UTM, WGS 1984, zone 27N).*

Two large stationary blocks bound the block map on its northern and southern sides (**Figure 5**), a first one, north of the Mohns Segment, along the Greenland and Senja FZ, and a second one, south of the Reykjanes Segment, along the Charlie Gibbs FZ. Their purpose was to constrain the opening of the NE Atlantic, coherently with the opening of the Central Atlantic Ocean in the south and the Boreas Basin in the north. We determined the successive positions of these two constraining blocks, relative to a stationary Greenland plate, using the EarthByte model (rotations poles are from *Gaina et al.* [2002]) and the Gplates software [*Boyden et al.*, 2011]. During each stage of restoration, the two stationary blocks impeded any

northward or southward displacement of the mobile blocks along the ridge. The JMFZ separates the Mohns and Jan Mayen segments, and the FFZ separates the Jan Mayen and the Reykjanes segments (**Figure 5**). In this method, all segments of the NE Atlantic are free to spread at different rates and in different directions, so that any relative displacements between segments will occur exclusively along the two oceanic fracture zones (JMFZ and FFZ).

At each stage of the restoration, we used the easternmost (external) blocks of each zone to calculate mean displacement rates. This yielded spreading rates along each ridge and relative displacements between each segment through time, along the JMFZ and FFZ. The external blocks along the COB have artificial edges (**Figure 5**), which serve to calculate, after the reconstructions, best-fit rotation poles for each ridge and for each magnetic anomaly (**Figure 6**). *Chang* [1987], *Chang et al.* [1990], *Jurdy and Stefanick* [198] and *Kirkwood et al.* [1999] developed a method, based on the criterion of fit of *Hellinger* [1981], to estimate poles for finite plate motions and their uncertainties. In our study, we used the program *Hellinger1* from *Kirkwood et al.* [1999] to estimate best-fit rotation poles.

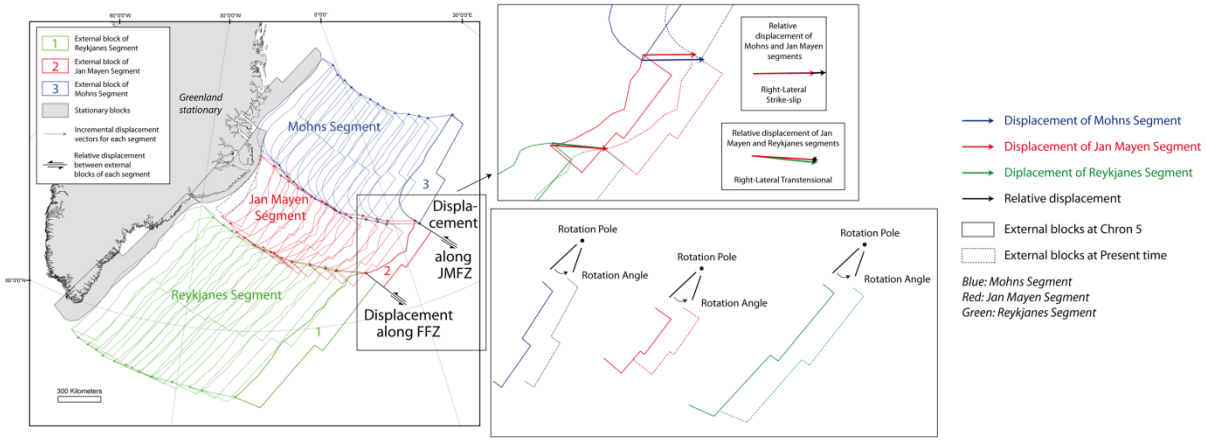

Figure 6. *Method for determining relative displacement vectors between segments along JMFZ and FFZ and rotation poles for each ridge system, for example between Chron 5 and present time. Map projection is Universal Transverse Mercator (UTM, WGS 1984, zone 27N).*

Using this method, we tested two models. The algorithm is the same for both models; however we modified the input parameter that defined which blocks are "neighboring". The algorithm will then minimize the gaps and overlaps between those blocks. In Model 1, the neighboring blocks are those between adjacent magnetic anomalies of each segment, but not between oceanic fracture zones; whereas in Model 2, all blocks are neighboring. Thus, in Model 1, the algorithm minimizes the gaps between adjacent magnetic anomalies of each segment, but not the gaps or overlaps between oceanic fracture zones; whereas, in Model 2,

the algorithm minimizes the gaps between adjacent anomalies and also the gaps or overlaps along oceanic fracture zones.

4. Results

4.1 Reconstruction of the NE Atlantic relative to a stationary Greenland plate

We describe two kinematic models of Europe, relative to a stationary Greenland plate. These models allow displacements on both sides of the Aegir Ridge during the reconstructions in order (1) to take into account the formation and the clockwise rotation of the JMMC, as described by *Bott* [1987], *Gaina et al.* [2009], *Nunns* [1983] and *Unternehr* [1982], and (2) to obtain a good fit between adjacent magnetic anomalies on the Aegir Ridge. For both models, the 13 stages of restoration (including *G* values for each restoration), from 55.9 Ma to Chron 5 (10.3Ma), and the best-fit rotation poles, and their uncertainties, for each spreading system are all in **Appendix 1**.

Both models display good fits of magnetic anomalies for all ridge segments (*G* values range from 0.0016 to 0.0043 for Model 1 and from 0.0007 to 0.0058 for Model 2). Model 1 provides better fits of magnetic anomalies (mean $G = 0.0025$), but allows significant gaps and overlaps across transform faults (~2.4% of the whole surface). Model 2 minimizes the gaps and overlaps across transform faults (~1.4% of the whole surface), but this reduces the goodness of fit between magnetic anomalies (mean $G = 0.0035$). However, we consider that the fit is acceptable, by comparison with the uncertainties in the dataset and the errors in the restoration method. Restorations from Chron 5 (10.3 Ma) to Chron 13 (33.3 Ma) are very similar for models 1 and 2, the main difference between them being for restorations between Chron 13 (33.3 Ma) and Chron 24 (52.69 Ma), when the Aegir Ridge was active. For both models, the JMMC rotates counter clockwise (~25° in Model 1 and ~30° in Model 2) from break-up to Chron 13 (33.3 Ma) (**Appendix 1**). However, between Chron 13 (33.3 Ma) and Chron 24 (52.69 Ma), the eastern side of the Aegir Ridge rotates clockwise more in Model 1 then in Model 2, resulting in significant gaps and overlaps across transform faults in Model 1. The final restorations at 55.9 Ma are very similar for both models and generate significant offsets between oceanic segments along the FFZ and the JMFZ. Previous studies [*Bott*, 1985, 1987; *Nunns*, 1983; *Scott et al.*, 2005] also predicted such offsets along the FFZ and JMFZ

4.2 Direction of Spreading

The incremental displacement vectors of the eastern external blocks, which represent the European COB, illustrate the motion of Europe relative to Greenland for 13 stages, from 55.9 Ma to the present time (**Figure 7**). Both Model 1 and Model 2 produce offsets of the COB at 55.9 Ma: approximately 140 km along the FFZ, between the Reykjanes and Jan Mayen segments, and 70 km along the JMTZ, between the Jan Mayen and Mohns segments.

For both models also, the directions of spreading of the Reykjanes and Mohns segments are relatively similar (**Figure 7**). In Model 1, the main changes in spreading direction are at Chron 21 (47.1 Ma) and Chron 20 (43.2Ma), along the Reykjanes Ridge, and at Chron 8 (26.4 Ma) and Chron 5 (10.3 Ma), along the Mohns Ridge. In Model 2, the main changes in spreading direction are at Chron 18 (39.4 Ma), along the Reykjanes Ridge, and at Chron 24 (52.9 Ma), Chron 8 (26.4 Ma) and Chron 5 (10.3 Ma), along the Mohns Ridge. For both models, the Reykjanes and Mohns ridges have similar spreading histories.

The main difference between the two models is the direction of spreading in the Jan Mayen Segment, between Chron 24 (52.9 Ma) and Chron 13 (33.3 Ma), when the Aegir Ridge was active. In Model 1, the spreading direction of the Jan Mayen Segment varies through time and is significantly different from those of the nearby Reykjanes and Mohns segments, between Chron 24 (52.9 Ma) and Chron 13 (33.3 Ma) (**Figure 7**). Also, the displacements are greater in the northern part of the segment, than they are in the southern part, especially between Chron 20 (43.2 Ma) and Chron 13 (33.3 Ma). Seafloor spreading is thus asymmetric along the Jan Mayen Segment and results in significant clockwise rotation (~20°) of the European COB of the Jan Mayen segment at that time. The differences in spreading directions between the three segments generated significant gaps and overlaps along the FFZ and JMFZ (**Figure 7**).

In Model 2, the direction of spreading of the Jan Mayen Segment is also different from those of the Reykjanes and Mohns segments between Chron 23 (51.3 Ma) and Chron 13 (33.3 Ma), but less so than in Model 1. Spreading is asymmetric along the Jan Mayen Segment, but the resulting clockwise rotation of the European COB of this segment is small (~10°), by comparison with that of Model 1 (~20°). Therefore in Model 2, relative displacements along the FFZ and JMFZ are smaller and more purely strike-slip than they are in Model 1 (**Figure 7**).

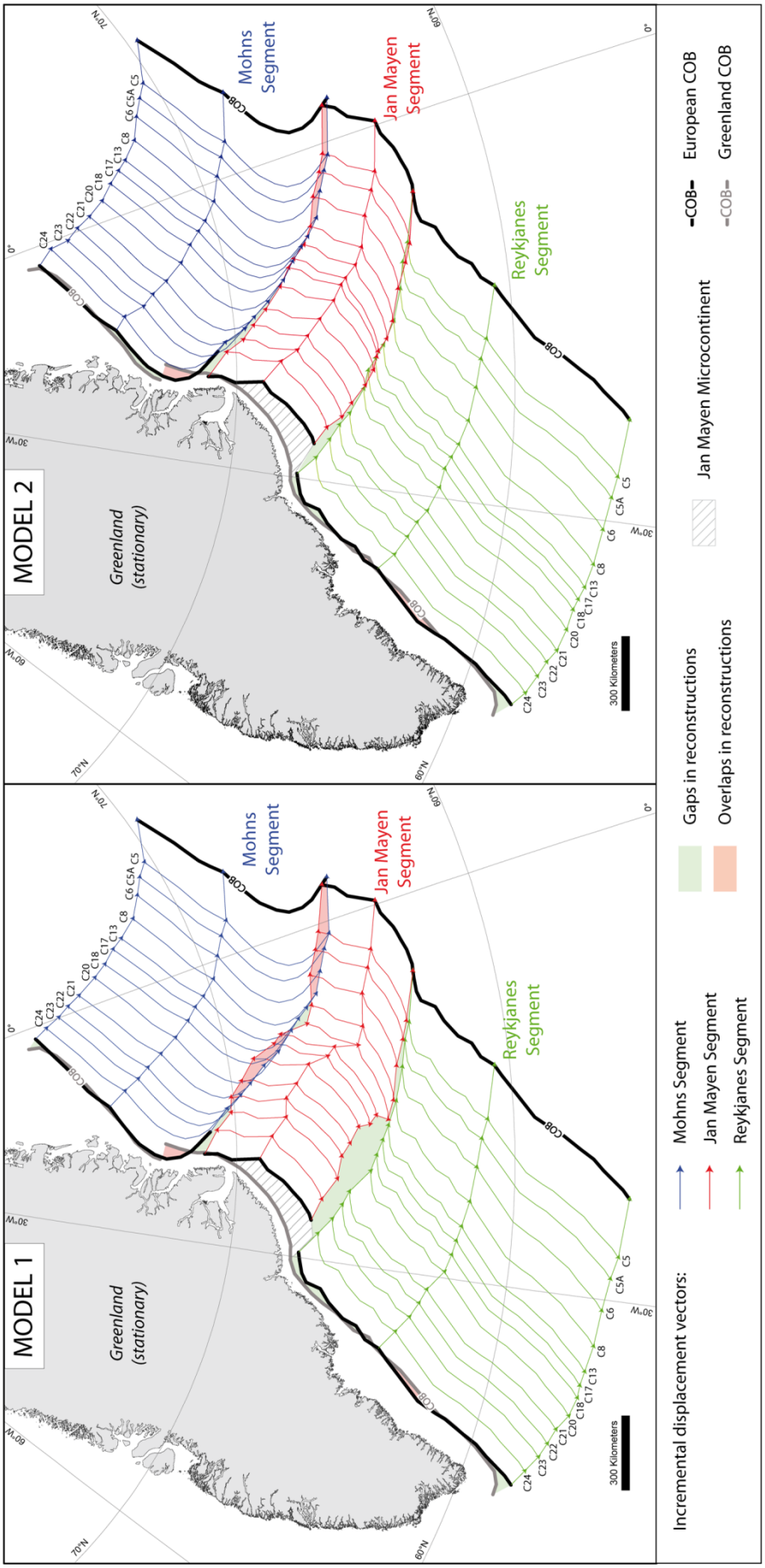
MODEL 1
MODEL 2
Greenland (stationary)
Mohns Segment
Jan Mayen Segment
Reykjanes Segment
COB
C24
C23
C22
C21
C20
C18
C17
C13
C8
C6
C5A
C5
70°N
60°N
40°N
30°W
0°
300 Kilometers
Incremental displacement vectors:
Mohns Segment
Jan Mayen Segment
Reykjanes Segment
Gaps in reconstructions
Overlaps in reconstructions
Jan Mayen Microcontinent
European COB
Greenland COB

Figure 7 (previous page). *Incremental displacement vectors for material points at ends of segments (Mohns, Jan Mayen and Reykjanes) and positions of European Continent-Ocean Boundary relative to stationary Greenland plate, from 55.9 Ma to present time, for Model 1 (involving minimization of gaps between conjugate anomalies) and Model 2 (involving minimization of gaps between conjugate anomalies and between segments). Notice remaining gaps and overlaps along fracture zones. Map projection is Universal Transverse Mercator (UTM, WGS 1984, zone 27N). For ages, see Figure 2.*

Gaps in reconstructions imply that compressional deformation should have occurred during sea-floor spreading; conversely, overlaps imply that deformation was extensional. Thus, Model 1 predicts large compressional deformation (at most, 170 km of shortening) along the FFZ, but extensional deformation (at most, 80 km of stretching) along the JMFZ. However previous studies of these fracture zones, using geophysical data, have not revealed such styles of deformation [e.g. *Bohnhoff*, 2004; *Gernigon et al.*, 2009]. Deformation is smaller in Model 2 (at most, 25 km and 10 km of shortening along the FFZ and JMFZ, respectively). Therefore in what follows we will focus the discussion on the results of Model 2.

4.3 Spreading Rates

For Model 2, we have calculated spreading rates for each ridge system, from the mean displacement rates of external blocks (**Figure 8**). Since 10.3 Ma, the average spreading rates are 21 mm/yr for the Reykjanes Ridge, 18 mm/yr for the Kolbeinsey Ridge and 20 mm/yr for the Mohns Ridge (**Figure 8**). These values are in good agreement with the previous estimates of Mosar et al. [2002] of 21 mm/yr for the Reykjanes Ridge and 18 mm/yr for the Kolbeinsey Ridge, but are slightly higher than their estimate of 16 mm/yr for the Mohns Ridge.

Spreading rates for the Reykjanes and Mohns ridges are high (55 and 53 mm/yr respectively), when sea-floor spreading began in the Early Eocene. They progressively decrease (to 15 and 12 mm/yr respectively) until Chron 8, in the Late Oligocene, before increasing again, during the Late Oligocene and Miocene, up to the present-day rates of 21 and 20 mm/yr, respectively (**Figure 8**). *Mosar et al.* [2002] have described such a spreading history for all ridges and *Torsvik et al.* [2001] noticed the decrease in spreading rate from the Early Eocene to Chrons 13/8 in absolute plate velocities for the North Atlantic. In our Model 2, spreading along the Aegir Ridge has a similar history. Spreading rates are high (up to 38

mm/yr) in the Early Eocene, decrease significantly (down to 9 mm/yr) between Chron 20 (47.1 Ma) and Chron 21 (43.2 Ma), and finally increase (up to 14 mm/yr) between Chron 17 (36.6 Ma) and Chron 13 (33.3 Ma) (**Figure 8**). Sea-floor spreading ceased along the Aegir Ridge between Chron 13 and Chrons 8 to 6 and started along the Kolbeinsey Ridge. Spreading rates progressively increased along the Kolbeinsey Ridge, up to the present-day rate of 18 mm/yr.

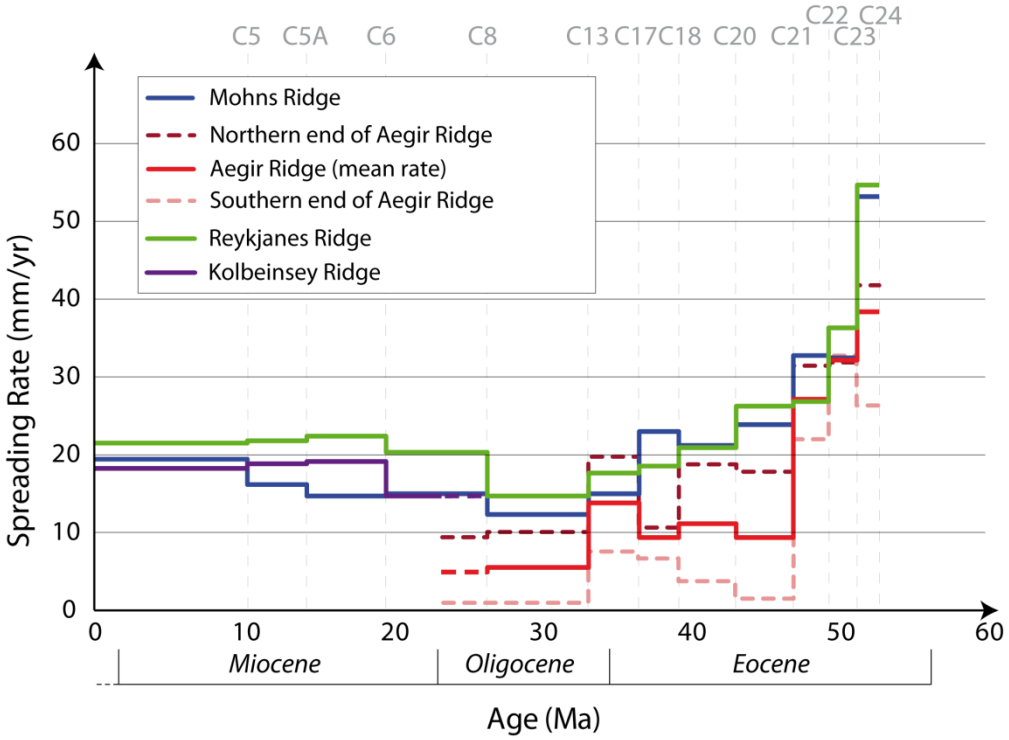

Figure 8. *Spreading rates for Mohns Ridge, Aegir Ridge, Reykjanes Ridge and Kolbeinsey Ridge (Model 2). Dashed lines represent rates of spreading for northern and southern ends of Aegir Ridge.*

The mean spreading rate (average value along the ridge) is lower for the Aegir Ridge than it is for the Reykjanes and Mohns ridges. As we mentioned before, the displacement vectors of the Jan Mayen Segment indicate asymmetric spreading between Chron 23 (51.3 Ma) and Chron 13 (33.3 Ma) (**Figure 7**). At that time, only the Aegir Ridge is active in this segment, so we calculated spreading rates at the northern and southern ends of this ridge (**Figure 8**). Spreading rates were up to 16 mm/yr higher at the northern end of the Aegir Ridge than they were at the southern end (**Figure 8**). *Mosar et al.* [2002] described such a difference in spreading rates across the Aegir Ridge. They correlated it with counter-clockwise rotation of the JMMC during its separation from Greenland. In contrast, our Model

2 predicts both counter-clockwise rotation (~30°) of the JMMC and clockwise rotation (~10°) of the eastern side of the Aegir Ridge (**Appendix 1**, **Figure 7**).

4.4 Intraplate deformation around transfer zones during seafloor spreading

In Model 2, differences in direction and rate of spreading along the Reykjanes, Mohns and Aegir/Kolbeinsey ridges generate relative displacements along the JMFZ and FFZ (**Figure 7**). To analyze deformation on the margin, we have plotted the European COB at 55.9 Ma relative to the present day European COB (**Figure 9**). The region of interest is north of the Mohns Segment and south of the Reykjanes Segment, where the fracture zones (JMFZ and FFZ) about the margin. Neglecting components of rigid motion, we have made the European COB at 55.9 Ma coincide in position and average orientation with the present-day European COB. This allows for better visualization of deformation on the European margin. The Reykjanes, Jan Mayen and Mohns segments have undergone differential displacements and rotations, which reach maximal values against the transfer faults (~47 km for the Reykjanes Segment and ~93 km for the Jan Mayen Segment, against the FFZ; ~126 km for the Jan Mayen Segment and ~52 km for the Mohns Segment, against the JMFZ). Along the Jan Mayen Segment, the direction of relative displacement reverses, from eastward in the north to westward in the south, confirming that sea-floor spreading was asymmetric along that segment. Relative rotations were clockwise (~5°) for the Reykjanes Segment, clockwise for the Jan Mayen Segment (~15° for the northern part, ~5° for the southern part) and counter-clockwise (~5°) for the Mohns Segment. Relative displacements along the FFZ (~140 km) and JMFZ (~74 km) imply left-lateral slip (**Figure 9**).

For each stage in the restoration, we have drawn the relative displacement vectors between each segment (**Figure 6**). Then, from these vectors, we have estimated the total and incremental relative displacements between the three oceanic segments, in other words, along the JMFZ and FFZ (**Figure 10**). Displacements of less than 10 km are smaller than the uncertainties in the dataset and the restoration method. The total relative displacements between the three oceanic segments imply left-lateral transpressional deformation around both the JMFZ (72 km) and the FFZ (144 km), from 55.9 Ma to the present day. The amount of relative displacement, the sense of slip and the style of deformation along the JMFZ and FFZ varied through time (**Figure 10**).

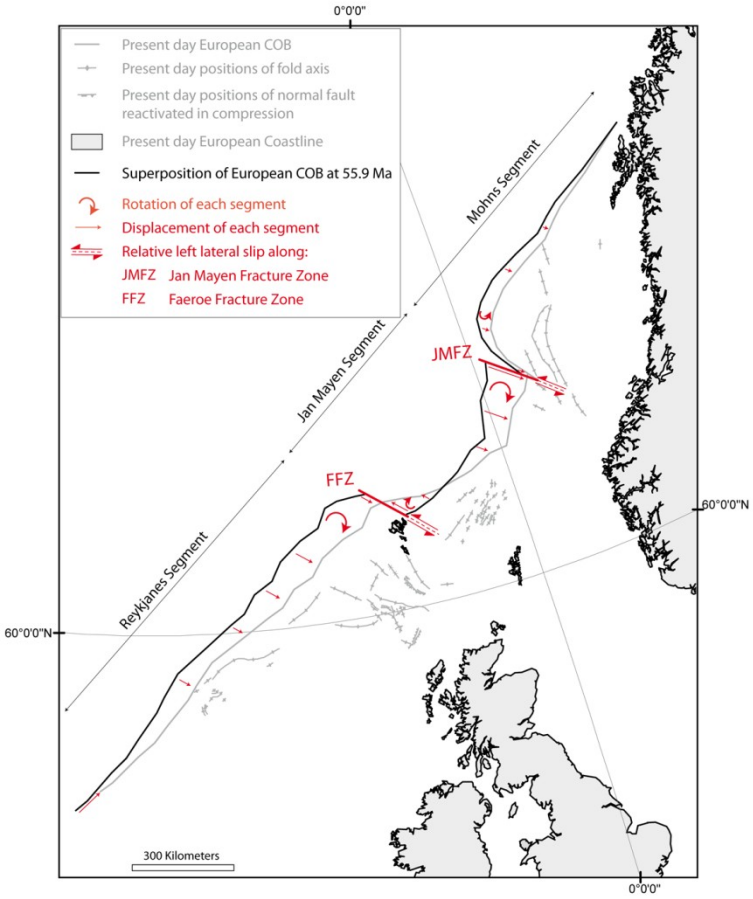

Figure 9. *Relative shapes of (1) European COB at 55.9 Ma (Model 2) and (2) present-day European COB, margin and coastline. For visual comparison of shapes, we have made ends of COB segments to coincide. Arrows indicate relative rotation of each segment, varying displacement vectors along it, and amount of left-lateral slip along JMFZ and FFZ. These boundary displacements may account for patterns of compressional structures on European margin, next to COB (see text for details). Names of inversion structures are in legend of Figure 1. Map projection is Universal Transverse Mercator (UTM, WGS 1984, zone 27N).*

Figure 10 (next page). *Relative displacement, sense of slip and style of deformation along JMFZ and FFZ from 55.9 Ma to present time, from relative displacement vectors between segments (Model 2). Timing of compressional deformation on Norwegian Margin is from Brekke [2000], Doré et al. [2008], Doré and Lundin [1996], Løseth and Henriksen [2005] and on Faeroe-Rockall Plateau from Johnson et al. [2005], Ritchie et al. [2008, 2003], Tuitt et al. [2010]. Positions of inversion structures are on Figure 11.*

	Paleocene	Eocene						Oligocene		Miocene				
Chron		24	23	22	21	20	18	17	13	8	6	5A	5	0
Age (Ma)	55.9-52.9	52.9-51.3	51.3-49.4	49.4-47.1	47.1-43.2	43.2-39.4	39.4-36.6	36.6-33.3	33.3-26.4	26.4-19.6	19.6-14.2	14.2-10.3	10.3-0	

Relative displacement along Jan Mayen Transform Zone

Amount	75 km	13 km	12 km	*(7 km)*	*(6 km)*	*(3 km)*	26 km	20 km	10 km	12 km	19 km	10 km	35 km
Sense of slip	*left lateral*	*right lateral*	*left lateral*	-	-	-	*right lateral*	*left lateral*	*right lateral*	*left lateral*			*right lateral*
Style of deformation	*strike slip*			-	-	-	*strike slip*		*transpressional*	*strike slip*			

Timing of compressional deformation on Norwegian Margin

Doré and Lundin, 1996
Brekke, 2000
Loseth and Henriksen, 2005
Doré et al., 2008

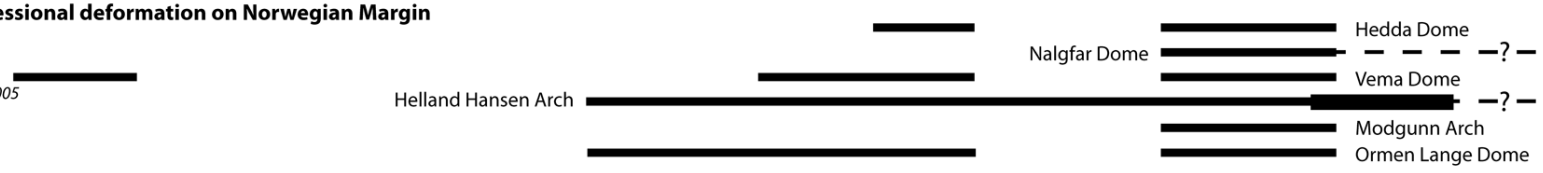

Relative displacement along Faeroe Fracture Zone

Amount	25 km	31 km	*(4 km)*	29 km	45 km	20 km	36 km	*(4 km)*	32 km	*(3 km)*	21 km	*(4 km)*	10 km
Sense of slip	*left lateral*		-	*right lateral*	*left lateral*			-	*left lateral*	-	-	-	*right lateral*
Style of deformation	*transtensional*	*transpressional*	-	*strike slip*				-	*strike slip*	-	*transpressional*	-	*transtensional*

Timing of compressional deformation on Faeroe-Rockall Plateau

Ritchie et al., 2003
Johnson et al., 2005
Ritchie et al., 2008
Tuitt et al., 2010

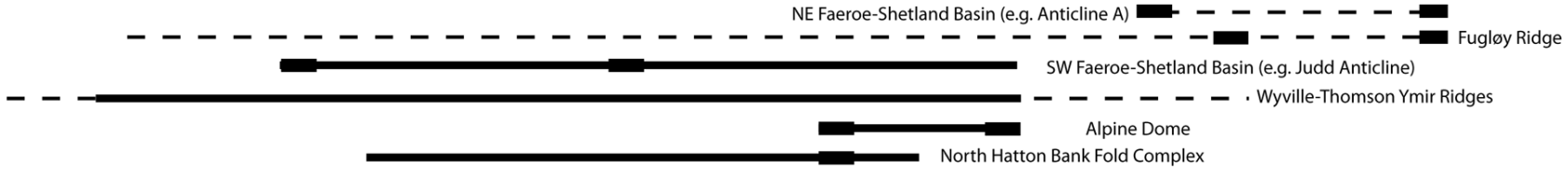

Along the JMFZ, a long period of left-lateral strike-slip occurs between Chron 8 (26.4 Ma) and Chron 5 (10.3 Ma). The style of deformation is dominantly strike-slip, except between Chron 13 (33.3 Ma) and Chron 8 (26.4 Ma), when it is transpressional. The amount of displacement varies from 10 km to 75 km. Model 2 predicts two periods of strike slip: (1) during the Early Eocene, between 55.9 Ma and Chron 22 (49.4 Ma) and (2) from the Late Eocene (39.4 Ma) to the present time.

Along the FFZ, Model 2 predicts (1) 25 to 31 km of left-lateral displacement during the Early Eocene, from 55.9 Ma to Chron 23 (51.3 Ma); and (2) 20 to 45 km of mainly left lateral strike slip from Middle Eocene (Chron 22, 49.4 Ma) to Late Oligocene (Chron 8, 26.4 Ma). Relative displacement occurs also during the Mio-Pliocene but more episodically: 21 km of transpressional displacement between Chron 6 (19.6 Ma) and Chron 5A (14.2 Ma), and 10 km of right-lateral transtensional (combination of strike-slip and transverse stretching) displacement from Chron 5 (10.3 Ma) to the present time. The sense of slip along the FFZ is mostly left-lateral and the style of deformation varies through time. However, Model 2 predicts a long period of strike-slip deformation between Chron 22 (49.4 Ma) and Chron 8 (26.4 Ma).

In summary, Model 2 predicts (1) a period of mainly left-lateral slip along both the JMFZ and the FFZ, at the beginning of sea-floor spreading during the Early Eocene (from 55.9 Ma to 51.3/49.4 Ma); and (2) a longer period of left-lateral slip along the FFZ, between Chron 21 (47.1 Ma, Mid-Eocene) and Chron 8 (26.6 Ma, Late Oligocene), and along the JMFZ between Chron 17 (36.6 Ma, Late Eocene) and Chron 5 (10.3 Ma, Late Miocene) (**Figure 10**).

5. Discussion

5.1 Differential sea-floor spreading and deformation on the adjacent continental margin

Mosar et al. [2002] attributed asymmetric sea-floor spreading to an asymmetric flow pattern in the asthenosphere that causes differential mantle drag [*Forsyth and Uyeda*, 1975]. Our Model 2 predicts differences in direction and rate of spreading between the Reykjanes, Aegir/Kolbeinsey and Mohns ridges. The resulting slip along the FFZ and JMFZ and relative rotation between ridge segments may have deformed the adjacent continental margin (**Figures 9 and 10**).

We have compared the timing of displacements along the JMFZ and FFZ, according to Model 2, with the history of inversion structures on the Norwegian Margin and the Faeroe-Rockall Plateau, respectively (**Figure 10**). In general, periods of relative displacements along the JMFZ and FFZ correlate well with periods of development of the inversion structures on the NW European Margin (**Figure 10**).

On the Norwegian Margin, compressional structures developed during the Late Eocene and Early Oligocene and mainly during the Miocene. These two periods coincide with the main periods of left-lateral strike slip along the JMFZ, between Chron 17 and Chron 13 (Late Eocene to Early Oligocene) and between Chron 8 and Chron 5 (Miocene) (**Figure 10**). Our results are consistent with the hypothesis of *Doré and Lundin* [1996], that compressional domes in the Vøring Basin formed by left-lateral reactivation of NW-SE trending lineaments at the SE end of the JMTZ. We infer from our Model 2 that this left-lateral deformation was due to differential spreading between the Mohns and Jan Mayen segments.

On the Faeroe-Rockall Plateau, compressional structures developed mainly during the Eocene to Late Oligocene [*Johnson et al.*, 2005; *Tuitt et al.*, 2010], when Model 2 predicts left-lateral strike slip along the FFZ between Chron 21 and Chron 8 (47.1 to 26.6 Ma, Mid-Eocene to Late Oligocene) (**Figure 10**). Rotation and northward displacement of the Reykjanes Segment and left-lateral strike-slip along the FFZ **(Figure 9**) may have generated a constrictional deformation, for which the principal directions of shortening trend approximately N-S and E-W in the area south of the Faeroe Islands. Moreover, a series of NW-trending transfer zones, sub-parallel to the FFZ, segment the NE Atlantic margin [*Kimbell et al.*, 2005]. Left-lateral slip along the FFZ may have propagated also along these fracture zones. Constrictional deformation and left-lateral strike slip along NW-trending fracture zones could have generated inversion structures of various trends (from NW-SE to NE-SW), as observed on the Faeroe-Rockall Plateau (**Figures 1 and 9**). Moreover, this deformation may have reactivated pre-existing structures on the Faeroe-Rockall Plateau, either of Lewisian age (trending NW-SE, N-S and E-W) or of Caledonian age (trending NE-SW) [e.g. *Tuitt et al.*, 2010].

On the NE Faeroe-Shetland Basin, compressional structures trend NE to ENE (**Figures 1 and 9**). *Ritchie et al.* [2003] suggested that left-lateral slip along NW-trending transfer zones, sub-parallel to the FFZ, was responsible for the development of NE- to NNE-trending folds in the NE Faeroe-Shetland Basin. However, Model 2 predicts left-lateral displacement along the FFZ during the Eocene and Oligocene, but not during the Miocene, whereas the inversion structures in this area developed mainly during the Early Miocene to

Middle Miocene and from Early Pliocene to Recent times (**Figure 10**) [*Johnson et al.*, 2005; *Ritchie et al.*, 2008, 2003]. Model 2 predicts instead transpressional deformation along the FFZ in the Early Miocene (Chrons 6 – 5A, 19.6-14.2 Ma) and right-lateral transtensional deformation along the FFZ in the Late Miocene and Pliocene (Chron 5A, 10.3 Ma, to present time) (**Figure 10**). The significant period of left-lateral displacement along the FFZ during the Eocene and the Oligocene has probably initiated some of the NE-trending structures in this area, such as the Fugløy Ridge (**Figures 1 and 10**). However, during the Miocene and the Pliocene, there is no clear relationship between the relative displacement along the FFZ and the development of the NE- to ENE- trending structures in the NE Faeroe-Shetland Basin.

5.2 Influence of the Iceland Mantle Plume

In this section, we will examine the possible influence of the Iceland Mantle Plume on differential sea-floor spreading along the NE Atlantic. To this purpose, we have reconstructed the positions of the Iceland Mantle Plume, the NW European Continental Shelf and the JMMC, relative to a stationary Greenland plate and according to the stationary hotspot model of *Lawver and Müller* [1994] or the moving hotspot model of *Mihalffy et al.* [2008]. This we have done for four periods: (1) Late Paleocene (55.9 Ma, and **Figure 11A**), (2) Late Eocene to Early Oligocene (Chron 17, 36.6 Ma, and **Figure 11B**), (3) Early Miocene (Chron 6, 19.6 Ma, and **Figure 11C**) and (4) present time (**Figure 11D**).

Magmatism was widespread throughout the North Atlantic during the Paleogene, accounting for a large Cenozoic igneous province [e.g. *Saunders et al.*, 1997]. Within this North Atlantic Igneous Province (NAIP) are basaltic and picritic lavas of Baffin Island and West Greenland, basaltic lavas of East Greenland, seaward-dipping reflectors and offshore lavas along the Greenland and NW European volcanic rifted margins, the GIFR and Iceland and basaltic lavas and dyke swarms of the British Isles (**Figure 11D**) [e.g. *Lawver and Müller*, 1994; *Saunders et al.*, 1997; *Storey et al.*, 2007]. The Iceland plume is an obvious candidate for explaining the NAIP [e.g. *White and McKenzie*, 1989]. We have illustrated the track of the Iceland mantle plume for two models (**Figure 11**): (1) the stationary hotspot model of *Lawver and Müller* [1994] (using absolute plate motion reference frames from *Müller et al.* [1993]); (2) the moving hotspot model of *Mihalffy et al.* [2008] (using absolute plate motion reference frames from *Steinberger et al.* [2004]). According to the model of *Lawver and Müller* [1994], the Icelandic hotspot was beneath Greenland after breakup at Chron 24 (52.9 Ma, and **Figure 11A**), then beneath the eastern Greenland Margin, west of the

JMMC, around 35 Ma, and afterwards beneath the axis of the Reykjanes Ridge, since approximately 25 Ma. The mantle plume was closer to the NE Atlantic Ridge according to the moving hotspot models of *Mihalffy et al.* [2008], than it was according to the stationary hotspot model (**Figure 11D**).

The Jan Mayen Segment had a complex spreading history in the Eocene and the Oligocene and went through several stages: (1) progressive separation of the JMMC; (2) counter-clockwise rotation of the JMMC; (3) clockwise rotation of the eastern side of the Aegir Ridge (**Figure 11B**); and (4) later ridge jump from the Aegir Ridge to the Kolbeinsey Ridge in the Late Oligocene to Early Miocene (**Figure 11C**). We follow previous studies [e.g. *Gaina et al.*, 2009; *Müller et al.*, 2001] in suggesting that the position of the Iceland Mantle Plume head in the vicinity of the Jan Mayen Segment (**Figure 11B**) generated this plate readjustment. During the Miocene, the plume head was beneath the Reykjanes Ridge (**Figure 11C**) and the resulting volcanic activity formed the Iceland Plateau [*Doré et al.*, 2008]. *Doré et al.* [2008] suggested that this high plateau generated enough stress to deform adjacent margins in the Miocene, and that the Aegir Ridge would have behaved as a shield for the Møre Basin between the Iceland Plateau and the Vøring Basin, where inversion features developed. We suggest moreover that the Iceland Mantle Plume could have generated a radial pattern of compressive stress trajectories, responsible for shear stress along transform faults. In the model of *Lawver and Müller* [1994] and the moving hotspot model of *Mihalffy et al.* [2008], the Iceland Plume Head is south of the FFZ, therefore shear stress should be left-lateral along both the FFZ and JMFZ. By comparison with Model 2, the two main periods of left-lateral relative displacement along the FFZ and the JMFZ are compatible with the shear stress that arises when the Iceland Mantle Plume is south of the FFZ. We suggest moreover that interaction between the Iceland Mantle Plume and the Reykjanes Ridge is responsible for (1) the increase in spreading rates along this ridge at around 25 Ma (**Figure 8**) and (2) resulting differential spreading between the Reykjanes, Kolbeinsey and Mohns ridges and relative displacements along the FFZ and JMFZ during the Miocene (**Figure 10**). Both the stress due to development of the Icelandic Plateau [*Doré et al.*, 2008] and the relative displacement along fracture zones, due to differential spreading, could explain the Miocene phase of deformation in the Vøring Basin and in the NE Faeroe-Shetland Basin, along pre-existing inversion features, domes and anticlines that formed during the Late Eocene to Early Oligocene.

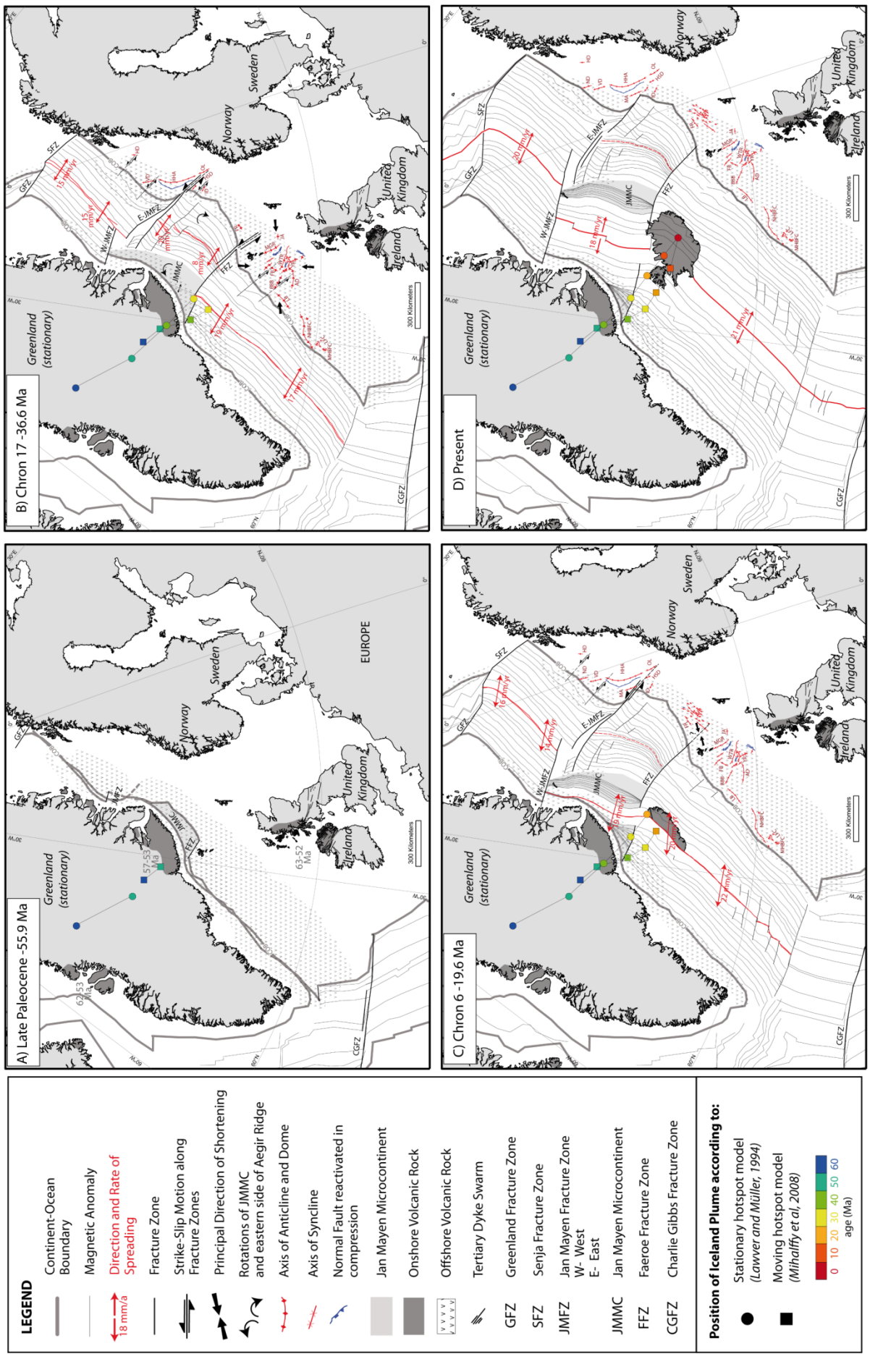
A) Late Paleocene -55.9 Ma
B) Chron 17 -36.6 Ma
C) Chron 6 -19.6 Ma
D) Present
Greenland (stationary)
Norway
Sweden
United Kingdom
Ireland
EUROPE
GFZ
SFZ
JMFZ
W.-JMFZ
E.-JMFZ
JMMC
FFZ
CGFZ
300 Kilometers
LEGEND
Continent-Ocean Boundary
Magnetic Anomaly
Direction and Rate of Spreading
18 mm/a
Fracture Zone
Strike-Slip Motion along Fracture Zones
Principal Direction of Shortening
Rotations of JMMC and eastern side of Aegir Ridge
Axis of Anticline and Dome
Axis of Syncline
Normal Fault reactivated in compression
Jan Mayen Microcontinent
Onshore Volcanic Rock
Offshore Volcanic Rock
Tertiary Dyke Swarm
Greenland Fracture Zone
Senja Fracture Zone
Jan Mayen Fracture Zone
W- West
E- East
Jan Mayen Microcontinent
Faeroe Fracture Zone
Charlie Gibbs Fracture Zone
Position of Iceland Plume according to:
Stationary hotspot model (Lawver and Müller, 1994)
Moving hotspot model (Mihalffy et al, 2008)
0 10 20 30 40 50 60
age (Ma)

Figure 11. *Positions relative to stationary Greenland plate of Europe, Jan Mayen Microcontinent (JMMC) and Iceland Mantle Plume at intervals of 10 My, according to stationary hotspot model of Lawver and Müller [1994] and moving hotspot model of Mihalffy et al. [2008]. Timing is A) Late Paleocene, 55.9 Ma; B) Late Eocene, 36.6 Ma ; C) Early Miocene, 19.6 Ma ; and D) Present. Relative positions of magnetic anomalies and Continent-Ocean Boundaries (COB) in NE Atlantic are from our Model 2. Relative positions of European coastline and magnetic anomalies of oceanic domains other than the NE Atlantic are from Global EarthByte Gplates Model (rotation poles from Gaina et al. [2002]) . Inversion structures are from Doré et al. [2008], Johnson et al. [2005] and Tuitt et al. [2010] and their relative positions from Global EarthByte Model (rotation poles from Gaina et al. [2002]). Onshore and offshore Tertiary lavas are from Storey et al. [2007] and dyke swarms from Upton [1988]. Ages of magmatic activity (Figure 11A) in West and East Greenland and in the British Isles are from White and McKenzie [1989]. Map projection is Universal Transverse Mercator (UTM, WGS 1984, zone 27N).*

5. Conclusions

1) Our new kinematic model of Europe, relative to a stationary Greenland plate during the opening of the NE Atlantic, ensures a good fit of the magnetic anomalies for the complex Jan Mayen Segment, especially around the Aegir Ridge.

2) The model predicts differences in direction and rate of spreading among the Reykjanes, Jan Mayen and Mohns segments. Between Chron 24 and Chrons 13 to 8, the Jan Mayen Segment had a complex spreading history. Rifting of the JMMC off Greenland generated counter-clockwise rotation (~30°) of the JMMC, fan-shaped spreading along the Aegir Ridge and clockwise rotation (~10°) of the eastern side of the Aegir Ridge.

3) Differential sea-floor spreading of the Reykjanes, Mohns and Aegir/Kolbeinsey ridges generated relative displacements along the FFZ and JMFZ and relative rotation of each segment. Our model predicts a main period of left-lateral slip, of up to 45 km along the FFZ between Chron 21 and Chron 8 (47.1 to 26.6 Ma, Mid-Eocene to Late Oligocene) and up to 20 km along the JMFZ, between Chron 17 and Chron 13 (Late Eocene to Early Oligocene) and between Chron 8 and Chron 5 (Miocene). These two periods coincide with the development of compressional structures on the Faeroe-Rockall Plateau and Norwegian Margin, respectively.

4) We suggest that differential spreading was responsible for (1) left-lateral reactivation of NW-SE trending lineaments along the line of the JMFZ, in the Late Eocene to Early Oligocene and mostly during the Miocene, and resulting development of inversion structures on the Norwegian Margin; (2) a constrictional strain, for which the principal directions of shortening trend approximately N-S and E-W, left-lateral strike-slip along NW-trending transfer zones and reactivation of pre-existing structures of Lewisian age (trending NW-SE, N-S and E-W) and Caledonian age (trending NE-SW) in the Eocene and Early Oligocene, resulting in the development of inversion structures of various trends (NW-SE to NE-SW) on the Faeroe-Rockall Plateau; and (3) left-lateral reactivation of NW-trending transfer zones sub-parallel to the FFZ that probably initiated the Fugløy Ridge in the NE Faeroe-Shetland Basin during the Eocene and Oligocene. However, we have not identified a clear relationship between relative displacement along the FFZ and the development of NE- NNE-trending structures in the NE Faeroe-Shetland Basin during the Miocene and Pliocene.

5) We suggest that the position of the Iceland Mantle Plume beneath the eastern Greenland margin, in the vicinity of the JMMC, in the Late Eocene and Oligocene, generated major plate readjustments within the Jan Mayen Segment, separation of the JMMC and subsequent differential spreading and deformation along the European Margin. During the Miocene, the Iceland Mantle Plume remained beneath the Reykjanes Ridge, and the resulting volcanic activity formed the Iceland Plateau. Spreading rates were greater along the Reykjanes Ridge, triggering relative displacements along the FFZ and JMFZ during the Miocene. We therefore suggest that the Icelandic Mantle Plume, together with the NE Atlantic Ridge, were responsible for (1) differential seafloor spreading in the NE Atlantic, and (2) post-rift deformation on the Norwegian Margin and Faeroe-Rockall Plateau.

Acknowledgements

We would like to thank Chevron USA for funding the PhD of E. Le Breton and in particular Peter Connolly for backing the project. We also thank Pierrick Roperch of the University of Rennes 1 for his help with the numerical restorations.

References

Andersen, O. B., P. Knudsen, and P. A. M. Berry (2010), The DNSC08GRA global marine gravity field from double retracked satellite altimetry, *Journal of Geodesy*, *84*(3), 191-199, doi:10.1007/s00190-009-0355-9.

Anell, I., H. Thybo, and I. M. Artemieva (2009), Cenozoic uplift and subsidence in the North Atlantic region: Geological evidence revisited, *Tectonophysics*, *474*(1-2), 78-105, doi:10.1016/j.tecto.2009.04.006.

Arriagada, C., P. Roperch, C. Mpodozis, and P. R. Cobbold (2008), Paleogene building of the Bolivian Orocline: Tectonic restoration of the central Andes in 2-D map view, *Tectonics*, *27*(6), 1-14, doi:10.1029/2008TC002269.

Audibert, M. (1991), Déformation discontinue et rotations de blocs, PhD Thesis, 250 pp., Université Rennes 1.

Bohnhoff, M. (2004), Crustal structure of the southeastern Iceland-Faeroe Ridge (IFR) from wide aperture seismic data, *Journal of Geodynamics*, *37*(2), 233-252, doi:10.1016/j.jog.2004.02.004.

Boldreel, L. O., and M. S. Andersen (1993), Late Pliocene to Miocene compression in the Faeroe-Rockall area, in *Petroleum Geology of Northwest Europe: Proceedings of the 4th Conference*, edited by J. R. Parker, pp. 1025-1034, Geological Society, London.

Boldreel, L. O., and M. S. Andersen (1998), Tertiary compressional structures on the Faroe – Rockall Plateau in relation to northeast Atlantic ridge-push and Alpine foreland stresses, *Tectonophysics*, *300*, 13-28.

Bott, M. H. P. (1985), Plate tectonic evolution of the Icelandic Transverse Ridge and adjacent regions, *Journal of Geophysical Research*, *90*(B12), 9953-9960, doi:0148-0227/85/004B-116850.

Bott, M. H. P. (1987), The continental margin of central East Greenland in relation to North Atlantic plate tectonic evolution, *Journal of the Geological Society*, *144*(4), 561-568, doi:10.1144/gsjgs.144.4.0561.

Bourgeois, O., P. R. Cobbold, D. Rouby, and J.-charles Thomas (1997), Least squares restoration of Tertiary thrust sheets in map view, Tajik depression, central Asia, *Journal of Geophysical Research*, *102*(B12), 24553-27573, doi:10.1029/97JB02477.

Boyden, J. A., R. D. Müller, M. Gurnis, T. H. Torsvik, J. A. Clark, M. Turner, H. Ivey-Law, J. Watson, and J. S. Cannon (2011), Next-generation plate-tectonic reconstructions using GPlates, in *Geoinformatics: Cyberinfrastructure for the Solid Earth Sciences*, edited by G. R. Keller and C. Baru, pp. 95-114, Cambridge University Press.

Brekke, H. (2000), The tectonic evolution of the Norwegian Sea Continental Margin with emphasis on the Voring and More Basins, in *Dynamics of the Norwegian Margin*, vol. 167, edited by A. Nottvedt, pp. 327-378, Geological Society, London, Special Publications.

Bullard, E., J. E. Everett, and a. G. Smith (1965), The Fit of the Continents around the Atlantic, *Philosophical Transactions of the Royal Society A: Mathematical, Physical and Engineering Sciences*, *258*(1088), 41-51, doi:10.1098/rsta.1965.0020.

Cande, S. C., and D. V. Kent (1995), Revised calibration of the geomagnetic polarity timescale for the Late Cretaceous and Cenozoic, *Journal of Geophysical Research*, *100*(B4), 6093-6095, doi:10.1029/94JB03098.

Chang, T. (1987), On the statistical properties of estimated rotations, *Journal of Geophysical Research, 92*, 6319-6329.

Chang, T., J. Stock, and P. Molnar (1990), The rotation group in plate tectonics and the representation of uncertainties of plate reconstructions, *Geophysical Journal International*, *101*, 649–661. DOI: 10.1111/j.1365-246X.1990.tb05576.x

Cobbold, P. R. (1979), Removal of finite deformation using strain trajectories, *Journal of Structural Geology*, *1*(1), 67-72, doi:10.1016/0191-8141(79)90022-1.

Davies, R., I. Cloke, J. Cartwright, A. Robinson, and C. Ferrero (2004), Post-breakup compression of a passive margin and its impact on hydrocarbon prospectivity: An example from the Tertiary of the Faeroe-Shetland Basin, United Kingdom, *AAPG Bulletin*, *88*(1), 1-20, doi:10.1306/09030303008.

Doré, A. G., E. R. Lundin, N. J. Kusznir, and C. Pascal (2008), Potential mechanisms for the genesis of Cenozoic domal structures on the NE Atlantic margin: pros, cons and some new ideas, in *The Nature and Origin of Compression in Passive Margins*, vol. 306, edited by H. Johnson, A. G. Doré, R. W. Gatliff, R. Holdsworth, E. R. Lundin, and J. D. Ritchie, pp. 1-26, Geological Society, London, Special Publications.

Doré, A. G., and E. R. Lundin (1996), Cenozoic compressional structures o n the NE Atlantic margin: nature, origin and potential significance for hydrocarbon exploration, *Petroleum Geology*, *2*, 299-311.

Forsyth, D., and S. Uyeda (1975), On the Relative Importance of the Driving Forces of Plate Motion, *Geophysical Journal of the Royal Astronomical Society*, *43*, 163-200.

Gaina, C., L. Gernigon, and P. Ball (2009), Palaeocene – Recent plate boundaries in the NE Atlantic and the formation of the Jan Mayen microcontinent, *Journal of the Geological Society, London*, *166*, 601-616, doi:10.1144/0016-76492008-112.

Gaina, C., W. . Roest, and R. . Müller (2002), Late Cretaceous–Cenozoic deformation of northeast Asia, *Earth and Planetary Science Letters*, *197*(3-4), 273-286, doi:10.1016/S0012-821X(02)00499-5.

Geoffroy, L. (2005), Volcanic passive margins, *Comptes Rendus Geosciences*, *337*(16), 1395-1408, doi:10.1016/j.crte.2005.10.006.

Gernigon, L., O. Olesen, J. Ebbing, S. Wienecke, C. Gaina, J. O. Mogaard, M. Sand, and R. Myklebust (2009), Geophysical insights and early spreading history in the vicinity of the

Jan Mayen Fracture Zone, Norwegian–Greenland Sea, *Tectonophysics*, *468*(1-4), 185-205, doi:10.1016/j.tecto.2008.04.025.

Hellinger, S. J. (1981), The Uncertainties of Finite Rotations in Plate Tectonics, *Journal of Geophysical Research*, *86*(B10), 9312-9318.

Hendriks, B., P. Andriessen, Y. Huigen, C. Leighton, T. Redfield, G. Murrell, K. Gallagher, S. B. Nielsen, and S. B. N. A (2007), A Fission Track Data Compilation for Fennoscandia 227 A Fission Track Data Compilation for Fennoscandia, *Atlantic*, 227-239.

Hillis, R. R., S. P. Holford, P. F. Green, A. G. Doré, R. W. Gatliff, M. S. Stoker, K. Thomson, J. P. Turner, J. R. Underhill, and G. A. Williams (2008), Cenozoic exhumation of the southern British Isles, *Geology*, *36*(5), 371, doi:10.1130/G24699A.1.

Hitchen, K. (2004), The geology of the UK Hatton-Rockall margin, *Marine and Petroleum Geology*, *21*, 993-1012, doi:10.1016/j.marpetgeo.2004.05.004.

Holford, S. P., P. F. Green, I. R. Duddy, J. P. Turner, R. R. Hillis, and M. S. Stoker (2009), Regional intraplate exhumation episodes related to plate-boundary deformation, *Geological Society of America Bulletin*, *121*(11-12), 1611-1628, doi:10.1130/B26481.1.

Japsen, P., P. F. Green, J. M. Bonow, E. S. Rasmussen, and J. A. Chalmers (2010), Episodic uplift and exhumation along North Atlantic passive margins: implications for hydrocarbon prospectivity, in *Petroleum Geology: From Mature Basins to New Frontiers - Proceedings of the 7th Petroleum Geology Conference*, edited by B. A. Vinning and S. C. Pickering, pp. 979-1004, Geological Society, London.

Johnson, H., J. D. Ritchie, K. Hitchen, D. B. Mcinroy, and G. S. Kimbell (2005), Aspects of the Cenozoic deformational history of the Northeast Faroe − Shetland Basin , Wyville − Thomson Ridge and Hatton Bank areas, in *Petroleum Geology: North-West Europe and Global Perspectives - Proceedings of the 6th Petroleum Geology Conference*, edited by A. G. Doré and B. A. Vining, pp. 993-1007, Geological Society, London.

Jones, S. M., N. White, and J. Maclenna (2002), V-shaped ridges around Iceland: Implications for spatial and temporal patterns of mantle convection, *Geochemistry Geophysics Geosystems*, *3*(10), doi:10.1029/2002GC000361.

Jurdy, D. M. And M. Stefanick (1987), Errors in Plate Rotations as described by covariance matrices and their combination in reconstructions, *Journal of Geophysical Research*, *92*(B7), 6310-6318, doi:0148-0227/87/006B-6262.

Kimbell, G. S., J. D. Ritchie, H. Johnson, and R. W. Gatliff (2005), Controls on the structure and evolution of the NE Atlantic margin revealed by regional potential field imaging and 3D modelling, in *Petroleum Geology: North-West Europe and Global Perspectives - Proceedings of the 6th Petroleum Geology Conference*, edited by A. G. Doré and B. A. Vining, pp. 933-945, Geological Society, London.

Kirkwood, B. H., J.-Y. Royer, T. C. Chang, and R. G. Gordon (1999), Statistical tools for estimating and combining finite rotations and their uncertainties, *Geophysical Journal International*, *137*(2), 408-428, doi:10.1046/j.1365-246X.1999.00787.x.

Kodaira, S., R. Mjelde, K. Gunnarsson, H. Shiobara, and H. Shimamura (1998), Structure of the Jan Mayen microcontinent and implications for its evolution, *Geophysical Journal International*, (132), 383-400.

Lawver, L. A., and R. D. Müller (1994), Iceland Hotspot track, *Geology*, *22*, 311-314.

Le Breton, E. (2012), Differential spreading along the NE Atlantic ridge system and post-breakup deformation of the adjacent continental margins. PhD Thesis, 316 pp., Université Rennes 1.

Lundin, E. R., and A. G. Doré (2002), Mid-Cenozoic post-breakup deformation in the "passive" margins bordering the Norwegian - Greenland Sea, *Marine and Petroleum Geology*, *19*, 79-93.

Lundin, E. R., and A. G. Doré (2005), NE Atlantic break-up: a re-examination of the Iceland mantle plume model and the Atlantic – Arctic linkage, in *Petroleum Geology: North-West Europe and Global Perspectives - Proceedings of the 6th Petroleum Geology Conference*, edited by A. G. Doré and B. A. Vining, pp. 739-754, Geological Society, London.

Løseth, H., and S. Henriksen (2005), A Middle to Late Miocene compression phase along the Norwegian passive margin, in *Petroleum Geology: North-West Europe and Global Perspectives - Proceedings of the 6th Petroleum Geology Conference*, edited by A. G. Doré and B. A. Vining, pp. 845 -859, Geological Society, London.

Macnab, R., J. Verhoef, W. Roest, and J. Arkani-Hamed (1989), New Database Documents the Magnetic Character of the Artic and North Atlantic, *Eos Trans. AGU*, *76*(45), 449-458.

Maus, S. et al. (2009), EMAG2: A 2–arc min resolution Earth Magnetic Anomaly Grid compiled from satellite, airborne, and marine magnetic measurements, *Geochemistry Geophysics Geosystems*, *10*(8), doi:10.1029/2009GC002471.

McKenzie, D. (1978), Some remarks on the development of sedimentary basins, *Earth and Planetary Science Letters*, *40*, 25-32.

Mihalffy, P., B. Steinberger, and H. Schmeling (2008), The effect of the large-scale mantle flow field on the Iceland hotspot track, *Tectonophysics*, *447*(1-4), 5-18, doi:10.1016/j.tecto.2006.12.012.

Mitchell, A. H., and H. G. Reading (1969), Continental margins, geosynclines, and ocean floor spreading, *The Journal of Geology*, *77*(6), 29-646.

Mjelde, R., T. Raum, a. J. Breivik, and J. I. Faleide (2008), Crustal transect across the North Atlantic, *Marine Geophysical Researches*, *29*(2), 73-87, doi:10.1007/s11001-008-9046-9.

Mosar, J., G. Lewis, and T. Torsvik (2002), North Atlantic sea-floor spreading rates: implications for the Tertiary development of inversion structures of the Norwegian – Greenland Sea, *Journal of the Geological Society*, *159*, 503-515, doi:110.1144/0016-764901-135.

Müller, R. D., C. Gaina, W. R. Roest, and D. L. Hansen (2001), A recipe for microcontinent formation, *Geology*, *29*(3), 203, doi:10.1130/0091-7613(2001)029<0203:ARFMF>2.0.CO;2.

Müller, R. D., J.-Y. Royer, S. C. Cande, W. R. Roest and S. Maschenkov (1999), New constraints on the Late Cretaceous/Tertiary plate tectonic evolution of the Caribbean, in Caribbean Basins, in *Sedimentary Basins of the World series*, edited by P. Mann, Elsevier Science B.V., Amsterdam, *4*, 33–59.

Müller, R. D., J.-Y. Royer, and L. A. Lawver (1993), Revised plate motions relative to the hotspots from combined Atlantic and Indian Ocean hotspot tracks, *Geology*, *21*, 275-278.

Nunns, A. G. (1983), Plate tectonic evolution of the Greenland-Scotland Ridge and surrounding regions, in *Structure and development of the Greenland-Scotland Ridge New methods and concepts*, edited by M. H. P. Bott, S. S., M. Talwani, and J. Thiede, pp. 11-30, Plenum Press.

Olesen, O., J. Ebbing, E. Lundin, E. Mauring, J. R. Skilbrei, and T. H. Torsvik (2007), An improved tectonic model for the Eocene opening of the Norwegian – Greenland Sea: Use of modern magnetic data, *Marine and Petroleum Geology*, *24*, 53-66, doi:10.1016/j.marpetgeo.2006.10.008.

Pitman, W. C., and M. Talwani (1972), Sea-Floor Spreading in the North Atlantic, *Geological Society of America Bulletin*, *83*(3), 619-646, doi:10.1130/0016-7606(1972)83[619:SSITNA]2.0.CO;2.

Price, S., J. Brodie, A. Whitiam, and R.A.Y. Kent, (1997), Mid-Tertiary rifting and magmatism in the Traill Ø region, East Greenland, *Journal of the Geological Society, 154*, 419-434, doi:110.1144/gsjgs.154.3.0419.

Ritchie, J. D., H. Johnson, M. F. Quinn, and R. W. Gatliff (2008), The effects of Cenozoic compression within the Faroe-Shetland Basin and adjacent areas, in *The Nature and Origin of Compression in Passive Margins*, edited by H. Johnson, A. G. Doré, R. W. Gatliff, R. Holdsworth, E. R. Lundin, and J. D. Ritchie, pp. 121-136, Geological Society, London, Special Publications.

Ritchie, J. D., H. Johnson, and G. S. Kimbell (2003), The nature and age of Cenozoic contractional deformation within the NE Faroe–Shetland Basin, *Marine and Petroleum Geology*, *20*(5), 399-409, doi:10.1016/S0264-8172(03)00075-8.

Rouby, D. (1994), *Restauration en carte des domaines faillés en extension : Méthode et Application*, PhD Thesis, Mémoires de Geosciences Rennes, No. 58, 230 p.

Rouby, D., P. R. Cobbold, P. Szatmari, S. Demercian, D. Coelho, and J. A. Rici (1993), Least-squares palinspastic restoration of regions of normal faulting - application to the Campos Basin (Brazil), *Tectonophysics*, *221*(3-4), 439-452, doi:10.1016/0040-1951(93)90172-G.

Saunders, A. D., J. G. Fitton, A. C. Kerr, M. J. Norry, and R. W. Kent (1997), The North Atlantic Igneous Province, in *Large Igneous Provinces Continental, Oceanic, and*

Planetary Flood Volcanism, edited by J. J. Mahoney and M. F. Coffin, pp. 45-93, American Geophysical Union.

Scott, R. A., L. A. Ramsey, S. M. Jones, S. Sinclair, and C. S. Pickles (2005), Development of the Jan Mayen microcontinent by linked propagation and retreat of spreading ridges, in *Onshore-Offshore Relationships on the North Atlantic Margin*, vol. 12, edited by B. T. G. Wandas, J. P. Nystuen, E. Eide, and F. M. Gradstein, pp. 69-82, Norwegian Petroleum Society Special Publications.

Skogseid, J., S. Planke, J. I. Faleide, T. Pedersen, O. Eldholm, and F. Neverdal (2000), NE Atlantic rifting and volcanic margin formation, in *Dynamics of the Norwegian Margin*, edited by A. Nottvedt, B. T. Larsen, R. H. Gabrielsen, S. Olaussen, H. Brekke, B. Torudbakken, O. Birkeland, and J. Skogseid, pp. 295-326, Geological Society, London, Special Publications.

Smallwood, J. R. (2004), Tertiary Inversion in the Faroe-Shetland Channel and the Development of Major Erosional Scarps, *Geological Society, London, Memoirs*, *29*(1), 187-198, doi:10.1144/GSL.MEM.2004.029.01.18.

Srivastava, S. P., and W. R. Roest (1999), Extent of oceanic crust in the Labrador Sea, *Marine and Petroleum Geology*, *16*(1), 65-84, doi:10.1016/S0264-8172(98)00041-5.

Srivastava, S. P., and C. R. Tapscott (1986), Plate Kinematics of the North Atlantic, in *The Geology of North America, The Western North Atlantic Region*, edited by P. R. Vogt and B. E. Tucholke, pp. 379-404, Geological Society of America.

Steinberger, B., R. Sutherland, and R. J. O'Connell (2004), Prediction of Emperor-Hawaii semount locations from a revised model of global plate motion and mantle flow, *Nature*, *430*, 167-173, doi:10.1038/nature02660.

Stoker, M. S., R. J. Hoult, T. Nielsen, B. O. Hjelstuen, J. S. Laberg, and P. M. Shannon (2005), Sedimentary and oceanographic responses to early Neogene compression on the NW European margin, *Atlantic*, *22*, 1031-1044, doi:10.1016/j.marpetgeo.2005.01.009.

Storey, M., R. a. Duncan, and C. Tegner (2007), Timing and duration of volcanism in the North Atlantic Igneous Province: Implications for geodynamics and links to the Iceland hotspot, *Chemical Geology*, *241*(3-4), 264-281, doi:10.1016/j.chemgeo.2007.01.016.

Stuevold, L. M., J. Skogseid, and O. Eldholm (1992), Post-Cretaceous uplift events on the Voring continental margin, *Geology*, *20*, 919-922.

Talwani, M., and O. Eldholm (1977), Evolution of the Norwegian-Greenland Sea, *Geological Society of America Bulletin*, *88*(7), 969-999, doi:10.1130/0016-7606(1977)88<969:EOTNS>2.0.CO;2.

Torsvik, T. H., R. Van der Voo, J. G. Meert, J. Mosar, and H. J. Walderhaug (2001), Reconstructions of the continents around the North Atlantic at about the 60th parallel, *Earth and Planetary Science Letters*, *187*(1-2), 55-69, doi:10.1016/S0012-821X(01)00284-9.

Tuitt, A., J. R. Underhill, J. D. Ritchie, H. Johnson, and K. Hitchen (2010), Timing , controls and consequences of compression in the Rockall – Faroe area of the NE Atlantic Margin, in *Petroleum Geology: From Mature Basins to New Frontiers - Proceedings of the 7th Petroleum Geology Conference*, edited by B. A. Vining and S. C. Pickering, pp. 963-977, Geological Society, London.

Unternehr, P. (1982), Etude structurale et cinématique de la mer de Norvège et du Groenland. Evolution du microcontinent de Jan Mayen, PhD Thesis, 228 pp., Université de Bretagne occidentale (Brest).

Upton, B. G. J. (1988), History of Tertiary igneous activity in the N Atlantic borderlands, in *Early Tertiary Volcanism and the Opening of the NE Atlantic*, vol. 39, edited by A. C. Morton and L. M. Parson, pp. 429-453, Geological Society, London, Special Publications.

Vogt, P. R., and O. E. Avery (1974), Detailed Magnetic Surveys in the Northeast Atlantic and Labrador Sea, *Journal of Geophysical Research*, *79*(2), 363-389, doi:10.1029/JB079i002p00363.

White, R., and D. McKenzie (1989), Magmatism at Rift Zones: The Generation of Volcanic Continental Margins and Flood Basalts, *Journal of Geophysical Research*, *94*(B6), 7685-7729, doi:10.1029/JB094iB06p07685.

Ziegler, P. A. (1988), *Evolution of the Arctic-North Atlantic and the Western Tethys*, American Association of Petroleum Geologists Memoir 43.

4.3 General Discussion

Our new kinematic model of Europe, relative to a stationary Greenland plate during the opening of the NE Atlantic, ensures a good fit of the magnetic anomalies for the complex Jan Mayen Segment, especially around the Aegir Ridge. The model predicts differences in the direction and rate of spreading among the Reykjanes, Jan Mayen and Mohns segments. This differential sea-floor spreading of the Reykjanes, Mohns and Aegir/Kolbeinsey ridges generated relative displacements along the FFZ and JMFZ and relative rotation of each segment. I suggest that this differential spreading was responsible for:
(1) left-lateral reactivation of NW-SE trending lineaments along the line of the JMFZ, in the Late Eocene to Early Oligocene and mostly during the Miocene, and resulting development of inversion structures on the Norwegian Margin;
(2) a constrictional strain, for which the principal directions of shortening trend approximately N-S and E-W, left-lateral strike-slip along NW-trending transfer zones and reactivation of pre-existing structures of Lewisian age (trending NW-SE, N-S and E-W) and Caledonian age (trending NE-SW) in the Eocene and Early Oligocene, resulting in the development of inversion structures of trends ranging from NW-SE to NE-SW on the Faeroe-Rockall Plateau;
(3) left-lateral reactivation of NW-trending transfer zones sub-parallel to the FFZ that probably initiated the Fugløy Ridge in the NE Faeroe-Shetland Basin during the Eocene and Oligocene. However, I have not established a clear relationship between relative displacement along the FFZ and the development of NE- NNE-trending structures in the NE Faeroe-Shetland Basin during the Miocene and Pliocene.

In the late Eocene to the Early Oligocene (around 35 Ma), sea-floor spreading rates were greater at the northern end of the Aegir and Reykjanes ridges than they were at their southern ends. This differential spreading generated a clockwise rotation of the eastern side of the Aegir Ridge and left-lateral slip along the FFZ and JMFZ (**Figure 4.1**). Moreover, the JMMC rifted significantly off Greenland and rotated counter-clockwise, and sea-floor spreading ceased in the Labrador Sea, west of Greenland (*Srivastava and Tapscott,* 1986). I suggest that the position of the Iceland mantle plume in the vicinity of the Jan Mayen Segment might have led to more vigorous sea-floor spreading along the northern part of the Aegir and Reykjanes ridges, which would explain the increase of spreading rates at this time and coeval end of sea-floor spreading in the Labrador Sea, around 35 Ma. I suggest moreover that the Iceland Mantle Plume could have generated a radial pattern of compressive stress

trajectories, responsible for left-lateral shear stress along transform faults (**Figure 4.1**), which is compatible with the deformations predicted by our model.

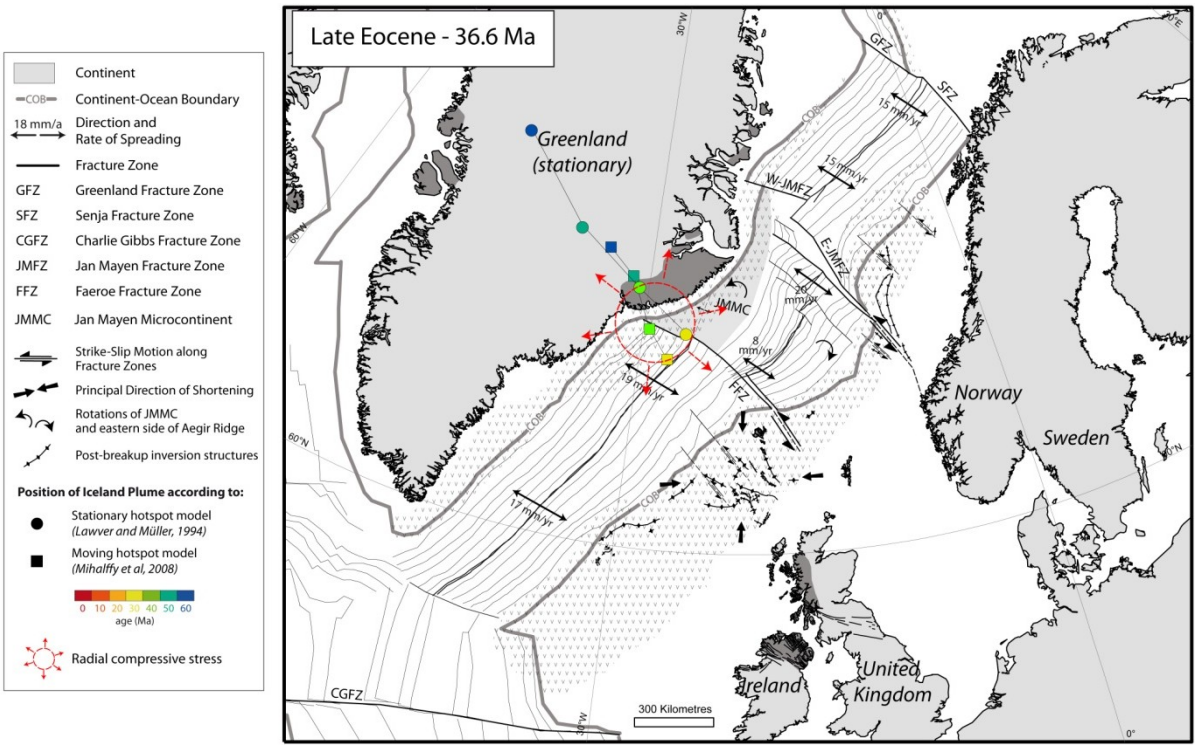

Figure 4.1. *Positions relative to stationary Greenland plate of Europe, Jan Mayen Microcontinent and Iceland Mantle Plume, at 36.6 Ma (Late Eocene). A radial compressive stress from Iceland Mantle Plume could generate compressional shear stress along FFZ and JMFZ.*

During the Miocene, the Iceland Mantle Plume remained beneath the Reykjanes Ridge, and the resulting volcanic activity formed the Iceland Plateau. Sea-floor spreading ceased along the Aegir Ridge around Chron 8 (26.6 Ma) and propagated northwards of the Reykjanes Ridge, forming the Kolbeinsey Ridge. The magma supply from the Iceland plume might have fed more vigorously the Reykjanes Ridge, which would explain the increase in spreading rates along this ridge in the Miocene and the coeval end of sea-floor spreading of the Aegir Ridge. Moreover, spreading rates were greater along the Reykjanes Ridge than they were along the Kolbeinsey and Mohns ridges, which generated relative slip along the FFZ and more particularly along the JMFZ. Both the stress due to growth of the Icelandic Plateau (*Doré et al.* (2008) and the relative displacement along fracture zones, due to differential spreading, could explain the Miocene phase of deformation in the Vøring Basin and in the NE

Faeroe-Shetland Basin, along pre-existing inversion features that formed during the Late Eocene to Early Oligocene.

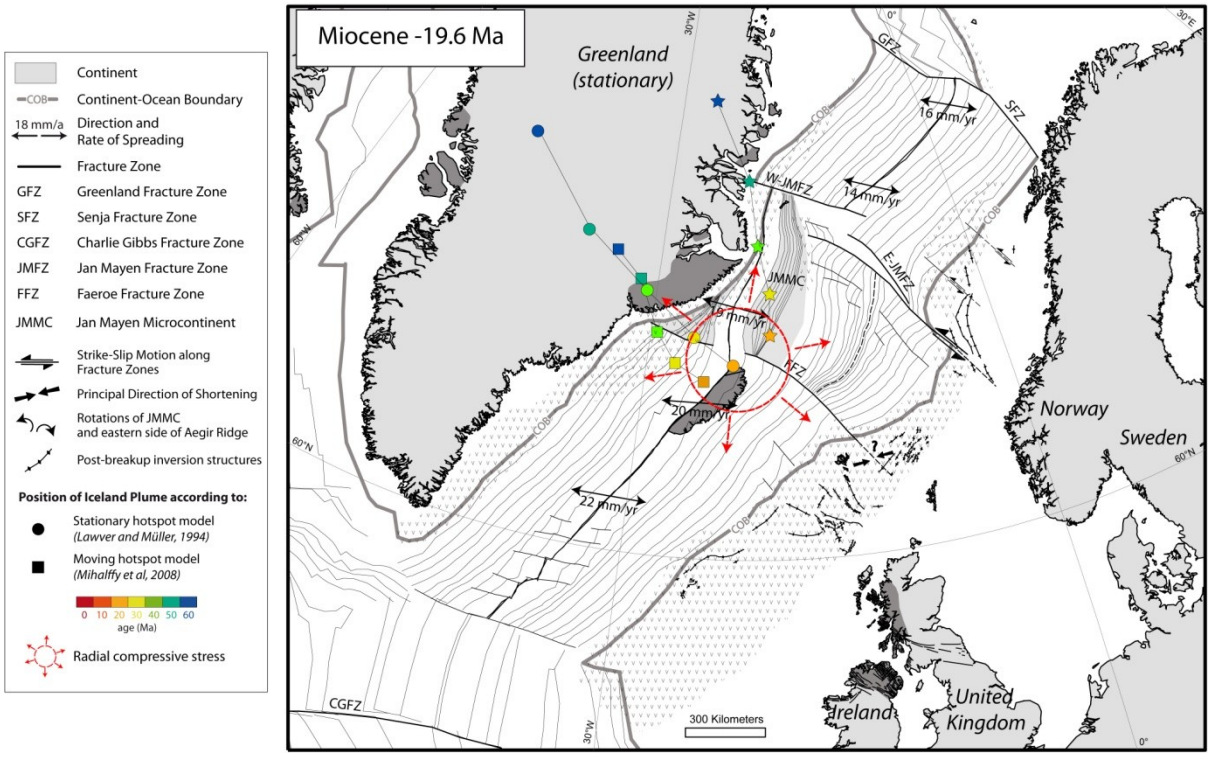

Figure 4.2. *Positions relative to stationary Greenland plate of Europe, Jan Mayen Microcontinent and Iceland Mantle Plume, at 19.6 Ma (Miocene). A radial compressive stress from Iceland Mantle Plume could generate compressional shear stress along FFZ and more particularly along JMFZ.*

In this chapter, I have investigated the role of differential spreading on post breakup deformation of the adjacent continental margin. I have demonstrated that relative slip along the FFZ and JMFZ was compatible with the development compressional deformation along the European margin. However, some questions arise from this study. Could differential spreading along the NE Atlantic also affect the NW European continent? Is there evidence of compressional deformation on the NW European continent during the Cenozoic and could the opening of the NE Atlantic be responsible for such deformation? In the following Chapter, I will focus on these questions and more particularly on the possible reactivation of a Palaeozoic strike-slip fault, the Great Glen Fault in Scotland. In Chapter 6, I will discuss more generally the influence of mantle plume on sea-floor spreading rates and structural development of continental margins.

Chapter 5

Differential sea-floor spreading and reactivation of continental faults

5.1 Introduction

Our Model 2 of kinematic reconstruction of the NE Atlantic, presented in Chapter 4, predicts variations in amount and rates of sea-floor spreading between the Reykjanes, Kolbeinsey/Aegir and Mohns ridges. This differential sea-floor spreading along the NE Atlantic generated left-lateral slip along (1) the Faeroe Fracture Zone (FFZ), up to 45 km, in Mid-Eocene to Late Oligocene, and (2) the Jan Mayen Fracture Zone (JMFZ), up to 20 km, in Late Eocene to Early Oligocene and during the Miocene. I suggested that this deformation was also responsible for the development of inversion structures on the adjacent NW European Continental Margin at those times. In this chapter, I investigate the possible role of differential spreading along the NE Atlantic on the reactivation of lithospheric strike-slip fault on the NW European Continent. A left-lateral slip along the FFZ and the JMFZ could generate perhaps right-lateral reactivation of pre-existing lithospheric structures, such as the Great Glen Fault (GGF) in Scotland and its prolongation in Norway, the Møre Trøndelag Fault (MTF) (**Figure 5.1**).

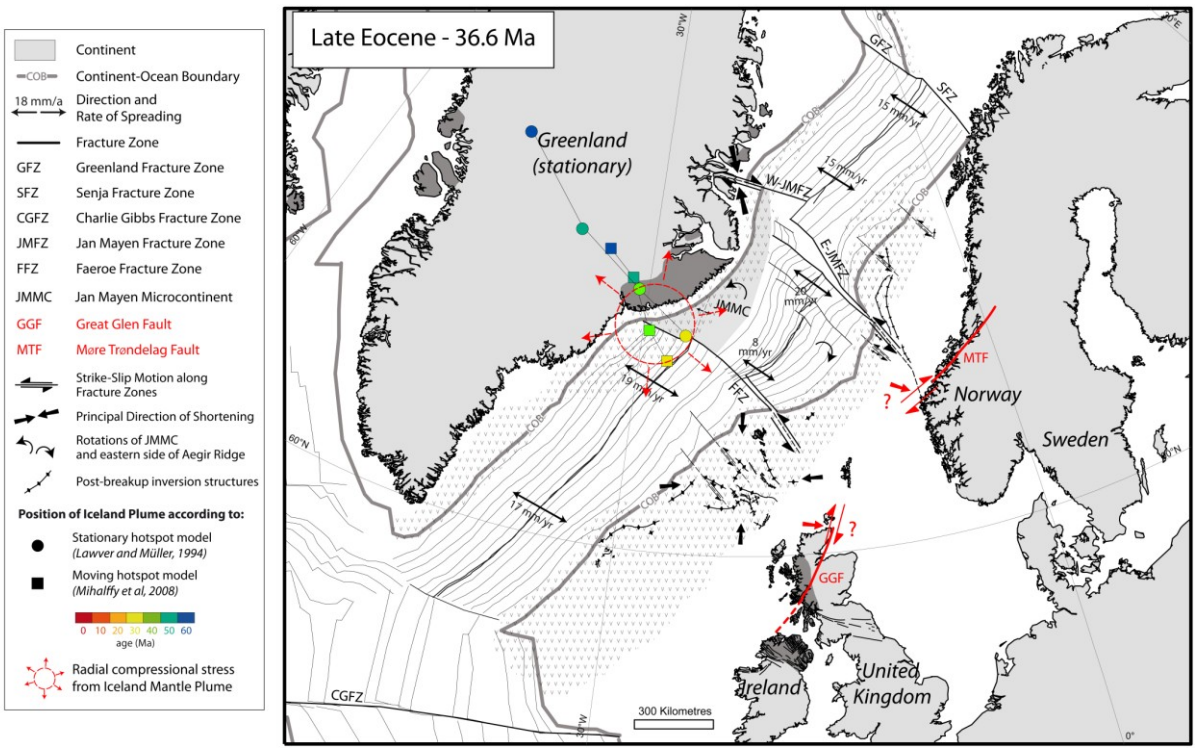

Figure 5.1. *Positions, relative to a stationary Greenland plate, of Europe, Jan Mayen Microcontinent and Iceland Mantle Plume, at 36.6 Ma (Late Eocene). Left-lateral slip along FFZ and JMFZ, due to differential spreading along NE Atlantic and possibly to radial compressional stress from Iceland Mantle Plume, could reactivate right-laterally continental lithospheric faults, such as Great Glen Fault, in Scotland and Møre Trøndelag Fault, in Norway.*

To investigate this idea more fully, we organized fieldwork in Scotland to do structural analysis along the GGF, Scotland. However, we did not have the opportunity to do similar work along the MTF, Norway. Therefore, in what follows I will focus the discussion on the GGF, Scotland. The main results of this work are the subject of an article in preparation for *Journal of the Geological Society of London*.

5.2 Cenozoic reactivation of the Great Glen Fault, Scotland: Additional Evidence and Possible Causes

Le Breton et al., in review in Journal of the Geological Society of London

Cenozoic reactivation of the Great Glen Fault, Scotland: Additional Evidence and Possible Causes

E. Le Breton[1*], P.R. Cobbold[1], A. Zanella[1]

[1] Geosciences Rennes, Université de Rennes 1, CNRS, 263 Avenue du Général Leclerc, 35042 Rennes, France

*Corresponding author, eline.lebreton@univ-rennes1.fr

Abstract

The Great Glen Fault (GGF) trends NNE-SSW across Northern Scotland. According to previous studies, the GGF developed as a left-lateral strike slip fault during the Caledonian Orogeny (Ordovician to Early Devonian). However, it then reactivated right-laterally in the Tertiary. We discuss additional evidence for this later phase. At Eathie and Shandwick, minor folds and faults in fossiliferous Jurassic marine strata indicate post-depositional right-lateral slip. In Jurassic shale, we have found bedding-parallel calcite veins ('beef' and 'cone-in-cone') that may provide evidence for overpressure development and maturation of organic matter at significant depth. Thus, the Jurassic strata at Eathie and Shandwick probably accumulated deeper offshore in the Moray Firth and were subject to Cenozoic exhumation during right-lateral displacement along the GGF. Differential sea-floor spreading along the North East Atlantic ridge system generated left-lateral transpressional displacements along the Faeroe Fracture Zone (FFZ) from the Early Eocene to the Late Oligocene (*c.* 47–26 Ma), a period of uplift and exhumation in Scotland. We suggest that such differential spreading was responsible for reactivation of the GGF. Indeed, left-lateral slip along the FFZ is compatible with right-lateral reactivation of the GGF.

Introduction

Scotland lies between the North East Atlantic Ocean to the west and north, and the North Sea to the east (**Figure 1**). The Great Glen Fault (GGF) is a major Caledonian tectonic structure that trends NNE-SSW across all of Northern Scotland. This strike-slip fault developed left-laterally during the Caledonian Orogeny, in Ordovician to Early Devonian times (e.g. *Hutton & McErlean*, 1991; *Soper et al.*, 1992*; Stewart et al.*, 2000, 2001; *Mendum & Noble*, 2010). However, previous studies of seismic data from the Inner Moray Firth (IMF)

Basin, Mesozoic strata onshore North East Scotland and Tertiary dyke-swarms in North West Scotland, all indicate right-lateral reactivation of the GGF during the Cenozoic (e.g. *Holgate*, 1969; *Underhill & Brodie*, 1993; *Thomson & Underhill*, 1993; *Thomson & Hillis*, 1995). The exact timing and the causes of this reactivation are still uncertain.

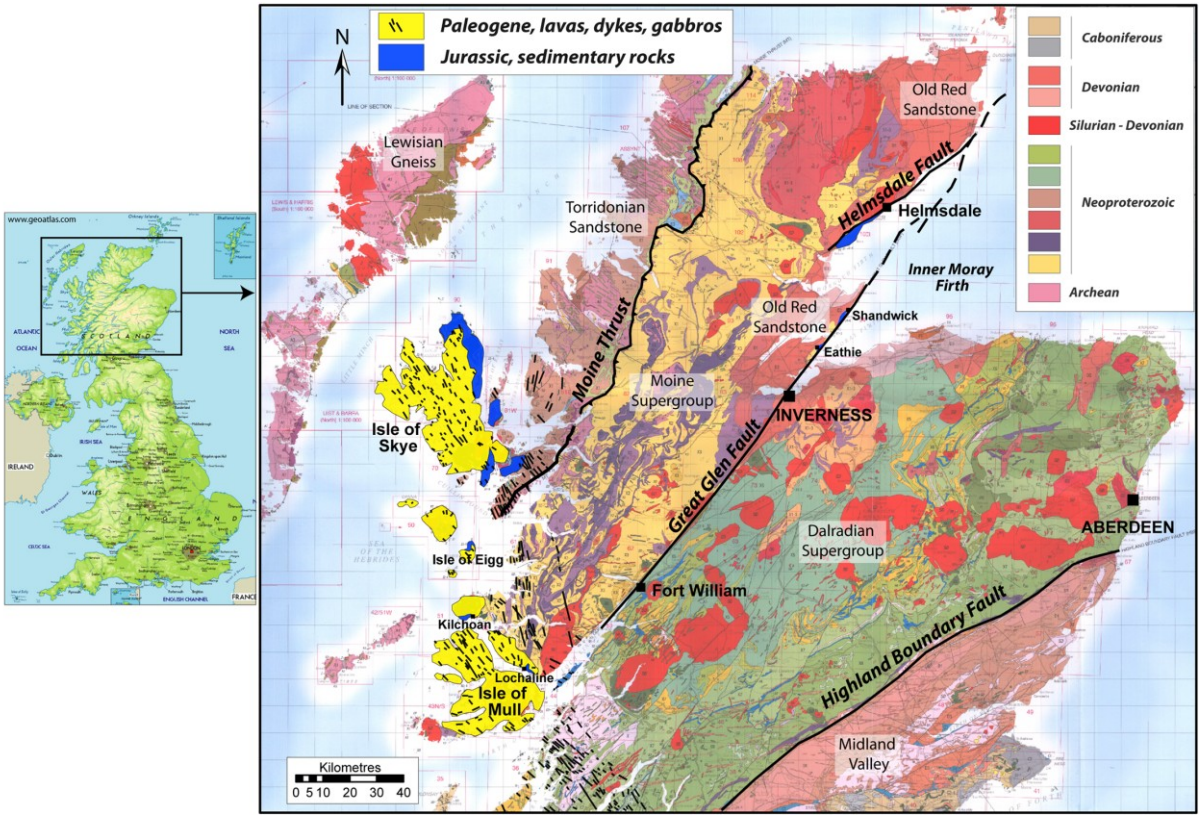

Figure 1. *Geological map of Northern Scotland (modified after Stone, 2007).*

Underhill & Brodie (1993) have shown that the IMF underwent regional uplift during the Cenozoic. This they attribute to reactivation of the GGF. More widely, analyses of sonic velocities, vitrinite reflectance and apatite fission tracks have revealed exhumation and uplift of Scotland during the Cenozoic (e.g *Underhill & Brodie*, 1993; *Thomson & Underhill*, 1993; *Thomson & Hillis*, 1995; *Clift et al.*, 1998; *Jolivet*, 2007; *Holford et al.*, 2009, 2010). In the Early Palaeogene, significant uplift occurred in Scotland. It may have been due to the Iceland Mantle Plume or part of the North Atlantic Igneous Province (NAIP) (e.g. *Brodie & White*, 1994; *Clift et al.*, 1998; *Jones et al.*, 2002). However, Cenozoic uplift of Scotland appears to have been episodic from 65 to 60 Ma, 40 to 25 Ma and 15 to 10 Ma (e.g. *Holford et al.*, 2009, 2010). *Holford et al.* (2010) have suggested that the various episodes of uplift were due to intraplate stress from the Alpine Orogeny and plate reorganisation in the North East Atlantic. *Thomson & Underhill* (1993) and *Thomson & Hillis* (1995) have also attributed uplift of the

IMF to Alpine and North East Atlantic events. *Le Breton et al.* (in review) show that variations in the amount and direction of sea-floor spreading, along and between the ridge systems of the North East Atlantic, generated relative displacements along major oceanic fracture zones, the Faeroe-Fracture Zone (FFZ), between the Reykjanes and Aegir ridges, and the Jan Mayen Fracture Zone (JMFZ), between the Aegir and Mohns ridges. They suggest that this differential sea-floor spreading was responsible for post-breakup compressional deformation of the North West European continental margin.

On this basis, the four main possible causes of reactivation of the GGF and Cenozoic uplift of Scotland are: (1) mantle processes around the Iceland Mantle Plume, (2) intra-plate compression from the Alpine Orogeny, (3) ridge push from the North East Atlantic and (4) variation in the amount and rate of sea-floor spreading and plate reorganisation in the North East Atlantic. In this paper, we investigate the fourth hypothesis. To this purpose, we describe some field observations of Jurassic outcrops in North East Scotland and we discuss possible causes and timing of reactivation of the GGF.

1. Geological Setting

1.1 Onshore rocks of Scotland

Rocks in Scotland have formed over a time span of a billion years. Various orogenies were responsible for a wide variety of rock types (**Figure 1;** *Stone*, 2007). The oldest rocks of Europe (~3 Ga), the Lewisian gneiss, are visible in the Hebrides Islands, NW Scotland, whereas on the mainland along the NW coast they lie under Neoproterozoic sedimentary strata of the Torridonian Sandstone (~1 Ga). The Moine Thrust is a major fault that separates the Lewisian gneiss and Torridonian Sandstone, to the west, from Neoproterozoic metamorphic rocks of the Moine Supergroup, to the east. In North East Scotland, the Moine Supergroup lies under the Devonian Old Red Sandstone, famous for its fossil fish (*Miller*, 1851). Further south, from Fort William to Inverness, the GGF separates the Moine Supergroup from the Dalradian Supergroup. The latter mostly consists of Neoproterozoic metamorphic rocks and late-Caledonian magmatic intrusions (Silurian-Devonian). South of the Highland Boundary Fault, the Midland Valley is a rift valley containing mostly Paleozoic strata. The Moine Thrust, the GGF and the Highland Boundary Fault are major tectonic structures that developed during the Caledonian Orogeny (Ordovician to Early Devonian),

during closure of the Iapetus Ocean and continental collision of Laurentia, Baltica and Avalonia (*Soper et al.*, 1992).

Mesozoic strata, mostly Jurassic, crop out along the North West and North East coasts. On the North West coast, they occur at Ardnamurchan, Loch Aline and more widely across the Inner Hebrides; on the North East coast, at the mouth of the IMF and along the Helmsdale Fault (**Figure 1**). At Eathie and Shandwick, minor faults trending NE-SW, along the GGF, put Jurassic strata against Old Red Sandstone or Neoproterozoic basement (*Judd*, 1873; *Holgate*, 1969; *Underhill & Brodie*, 1993). From fossil evidence, the strata are Kimmeridgian at Eathie and Bathonian to Middle Oxfordian at Shandwick (*Judd*, 1873; *Sykes*, 1975; *Wright & Cox*, 2001). In the Golspie-Helmsdale area, Triassic to Upper Jurassic strata are more widespread (*Stone*, 2007; *Trewin & Hurst*, 2009). The Helmsdale Fault separates them from Neoproterozoic basement or the Late Caledonian Helmsdale Granite, to the west. The Upper Jurassic 'Boulder Beds' accumulated in deep water in the footwall of the Helmsdale Fault, at a time when that fault was active (*Roberts*, 1989; *Trewin & Hurst*, 2009).

Intense volcanic activity occurred along the North East Atlantic margins during continental breakup in early Paleogene time and resulted in the development of the NAIP (*Saunders et al*., 1997). In North West Scotland, this volcanic event was responsible for the development of large gabbroic intrusive centres (e.g. Isles of Skye and Mull), widespread lava flows and dyke swarms (**Figure 1**). Several authors have suggested that the Iceland Mantle Plume was responsible for this widespread magmatic activity (e.g. *White & McKenzi*e, 1989; *Saunders et al.*, 1997).

During the Plio-Pleistocene, glaciation produced U-shaped valleys, such as the Great Glen, and firths. After the last glacial maximum (approx. 18 kyr ago), isostatic readjustment produced Quaternary raised beaches and may still be ongoing (*Firth & Stewart*, 2000).

1.2 Offshore rocks of North East Scotland

The Mesozoic IMF Basin is a western arm of the North Sea rift (**Figure 2**, *Evans et al.*, 2003; *Underhill,* 1991a). However, the IMF Basin did not form in the same way as the Central and Viking Grabens of the North Sea (*McQuillin et al.*, 1982). Numerous seismic surveys have provided good insights into the structural development of the IMF and the North East end of the GGF (**Figure 2**; *Underhill & Brodie*, 1993; *Thomson & Underhill*, 1993; *Thomson & Hills*, 1995). Three major faults have shaped the basin: the Wick Fault at its northern edge, the Banff Fault to the South and the Helmsdale Fault to the West (**Figure 2**).

During Upper Jurassic rifting, fault blocks formed and tilted (*Underhill,* 1991a). However, according to seismic data, well cores and onshore data, the overall structure of the basin was that of a half-graben, the depocentre being next to the Helmsdale Fault (*Thomson & Underhill*, 1993).

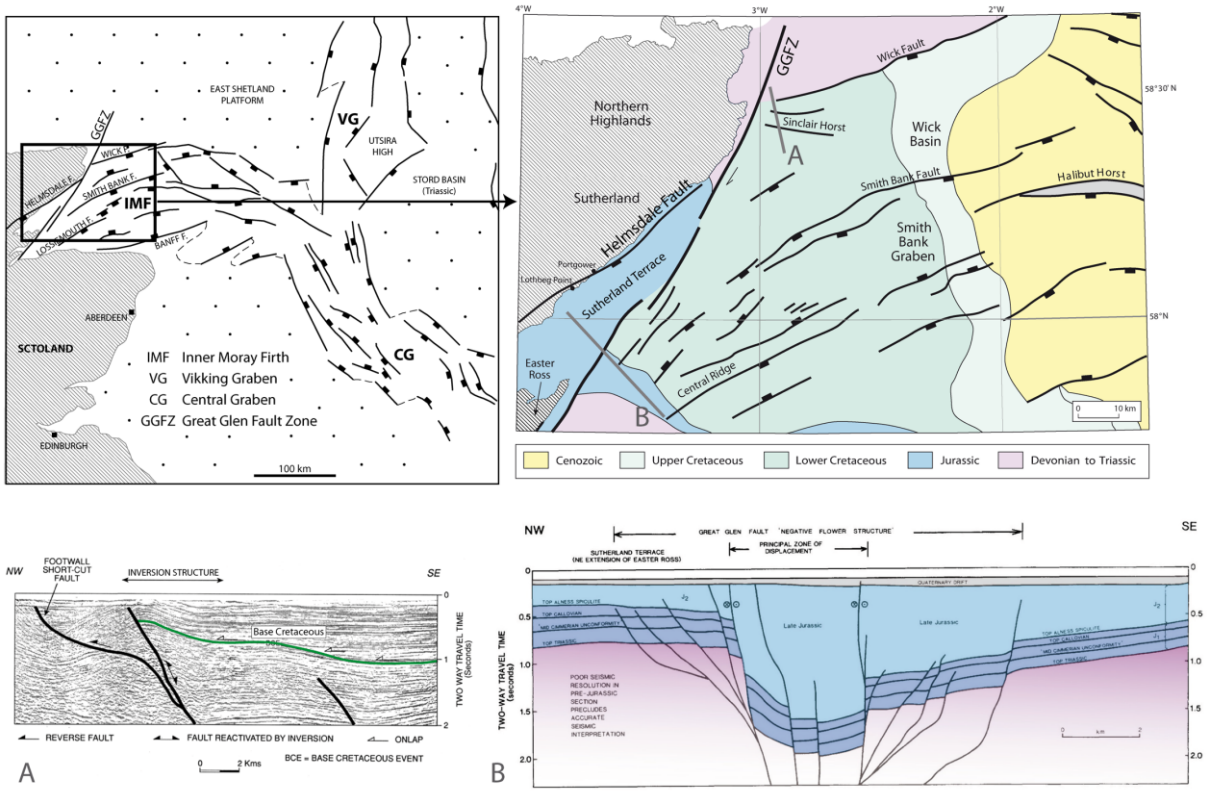

Figure 2. *Top left: structural map of the North Sea Basin and location of the Inner Moray Firth (IMF) Basin (modified after Underhill, 1991a). Top right: structural map of IMF Basin (modified after Evans et al., 2003). Gray lines indicate locations of seismic profiles A and B. A. Seismic profile of IMF Basin showing post-Cretaceous inversion structure along Wick Fault at intersection with Great Glen Fault (from Thomson & Underhill, 1993). B. Geoseismic section, showing typical 'flower structure' of Great Glen Fault (from Underhill & Brodie, 1993).*

McQuillin et al. (1982) have suggested that a post-Carboniferous right-lateral displacement of about 8 km along the GGF was a critical factor in the development of the IMF Basin. On the other hand, *Underhill & Brodie* (1993) have argued that the GGF was inactive as a strike-slip fault, during phases of extension in the IMF, and that the Helmsdale Fault was then the dominant control on the structure. In contrast, the GGF reactivated in the Tertiary and was responsible for regional uplift and basin inversion (*Underhill*, 1991a).

1.3 Evidence for Cenozoic reactivation of the GGF

The GGF developed as a left-lateral fault during the Caledonian Orogeny (*Hutton & McErlean*, 1991; *Stewart et al.*, 2000, 2001). However, according to previous studies, involving seismic data from the IMF Basin and analyses of Mesozoic outcrops and Tertiary dyke swarms, the GGF reactivated right-laterally in the Tertiary (*Holgate*, 1969; *Underhill & Brodie*, 1993; *Thomson & Underhill*, 1993; *Thomson & Hillis*, 1995).

By analysis of the WNW-trending Permo-Carboniferous dyke swarm of northern Argyll, on the North West side of the GGF, *Speight & Mitchell* (1979) inferred a right-lateral displacement of 7-8 km, as well as a considerable downthrow to the SE. Moreover, *Holgate* (1969) deduced 29 km of right-lateral slip along the GGF since the Upper Jurassic, from field observations of Jurassic rocks in Argyll. On the island of Mull, Tertiary dykes are offset right-laterally along the GGF (**Figure 1**; *Thomson & Underhill*, 1993), which is consistent with the previous suggestions of *Holgate* (1969) and *Speight & Mitchell* (1979).

On seismic sections of the IMF Basin, the GGF appears as a 'flower structure' and inversion structures are visible in the North West corner of the basin, along the Wick Fault (**Figure 2**; *Underhill & Brodie*, 1993; *Thomson & Underhill*, 1993). From structural studies along the GGF in Easter Ross (**Figure 2**), onshore well data from Tain and seismic data from the IMF Basin, *Underhill & Brodie* (1993) have identified folds and faults, trending N-S to NNE-SSW, in Devonian strata adjacent to the GGF. Moreover, they have suggested that the Jurassic outcrops in Easter Ross along the GGF (**Figure 2**) may be parts of flower structures that resulted from right-lateral slip along the GGF. In Jurassic strata of the Sutherland Terrace (**Figure 2**), next to the Helmsdale Fault, *Thomson & Underhill* (1993) have described open folds, attributing them to opposing senses of slip on the Helmsdale Fault (left-lateral) and the GGF (right-lateral).

Estimates of right-lateral displacement on the GGF during the Tertiary are small, from 8 km to 29 km, depending on the studies (*Holgate*, 1969; *McQuillin et al.*, 1982; *Rogers et al.*, 1989; *Underhill & Brodie*, 1993). The exact timing of reactivation is uncertain. Several authors have suggested that reactivation was contemporaneous with regional uplift of the Scottish Highlands, during Palaeocene-Eocene events of NE Atlantic rifting or during Oligo-Miocene (Alpine) tectonics (e.g. *Underhill*, 1991b, *Underhill & Brodie*, 1993; *Thomson & Underhill*, 1993; *Thomson & Hillis*, 1995).

1.4 Evidence for Cenozoic exhumation in Scotland

According to seismic and well data, the IMF underwent exhumation during the Cenozoic and the western side of the North Sea tilted to the east (e.g. *Underhill*, 1991b; *Argent et al.*, 2002). Indeed, Jurassic strata in the IMF are *c.* 500-1500 m shallower than they are in the Viking and Central Graben areas to the east. *Thomson & Underhill* (1993) have estimated about 1 km of uplift in the West, decreasing gradually eastwards, whereas *Thomson & Hillis* (1995) inferred that exhumation removed about 1.5 km of basin fill from the IMF.

Several authors have suggested that Scotland experienced a main phase of uplift in the early Paleogene, as a result of igneous underplating or dynamic uplift, associated with the Iceland Mantle Plume and widespread magmatic activity west of Scotland (*White & Lovell*, 1997*; Nadin et al.*, 1997; *Clift et al.*, 1998; *Jones et al.*, 2002; *Mackay et al*., 2005; *Saunders et al.*, 2007; *Persano et al*., 2007). However, fission track analyses on apatite have revealed that Cenozoic exhumation of Scotland was episodic, at 65-60 Ma, 40-25 Ma and 15-10 Ma (*Holford et al.*, 2009, 2010; *Jolivet*, 2007) and may have continued into Late Neogene time (*Hall & Bishop*, 2002; *Stoker*, 2002). *Holford et al.* (2010) have therefore suggested that regional exhumation of Scotland was due mainly to plate-wide horizontal forces, resulting from Alpine orogeny or North East Atlantic events.

Coevally with Cenozoic uplift, widespread compressional folds and reverse faults developed on the North West European continental margin, offshore Scotland, (*Boldreel & Andersen*, 1993, 1998; *Brekke*, 2000; *Hitchen*, 2004; *Johnson et al.*, 2005; *Ritchie et al.*, 2003, 2008; *Smallwood*, 2004; *Stoker et al.*, 2005; *Tuitt et al.*, 2010). South of the Faeroe Islands, such structures (e.g. the Wyville-Thomson ridge, Ymir ridges (WYTR), Alpine Dome and Judd Anticline) formed from the Middle Eocene to the Early Miocene (*Smallwood*, 2004; *Johnson et al.*, 2005; *Ritchie et al.*, 2008; *Tuitt et al.*, 2010). The possible causes of shortening are a subject for ongoing debate: (1) Alpine stress field (e.g. *Boldreel & Andersen*, 1993, 1998), (2) ridge push from the North East Atlantic (e.g. *Boldreel & Andersen*, 1993, 1998), (3) plume-enhanced ridge push (*Lundin & Doré*, 2002), (4) stress associated with the development of the Iceland Plateau (*Doré et al.*, 2008) or (5) differential sea-floor spreading along the North East Atlantic (*Mosar et al.*, 2002; *Le Breton et al.*, in review).

In this paper, we further investigate the structural evidence for Cenozoic right-lateral reactivation of the GGF and we discuss possible causes, such as differential sea-floor spreading along the North East Atlantic.

2. Method

Our data come from observations of Jurassic outcrops along both the GGF and the Helmsdale Fault (**Figure 3**). Upper Jurassic outcrops at Eathie (Kimmeridgian) and South of Shandwick (Port-an-Righ, Lower and Middle Oxfordian, and Cadh'-an-Righ, from Bathonian to Middle Oxfordian) are accessible only at low water. Along the Helmsdale Fault, Jurassic outcrops are more numerous, from Golspie to Helmsdale.

The objectives of our fieldwork were to identify, to measure and to analyse structures within Jurassic strata and the nature of their contact with the Old Red Sandstone or Neoproterozoic/Caledonian basement. We have compared our observations with previous studies and with published seismic data from the IMF, in order to discuss the timing and possible causes of reactivation of the GGF.

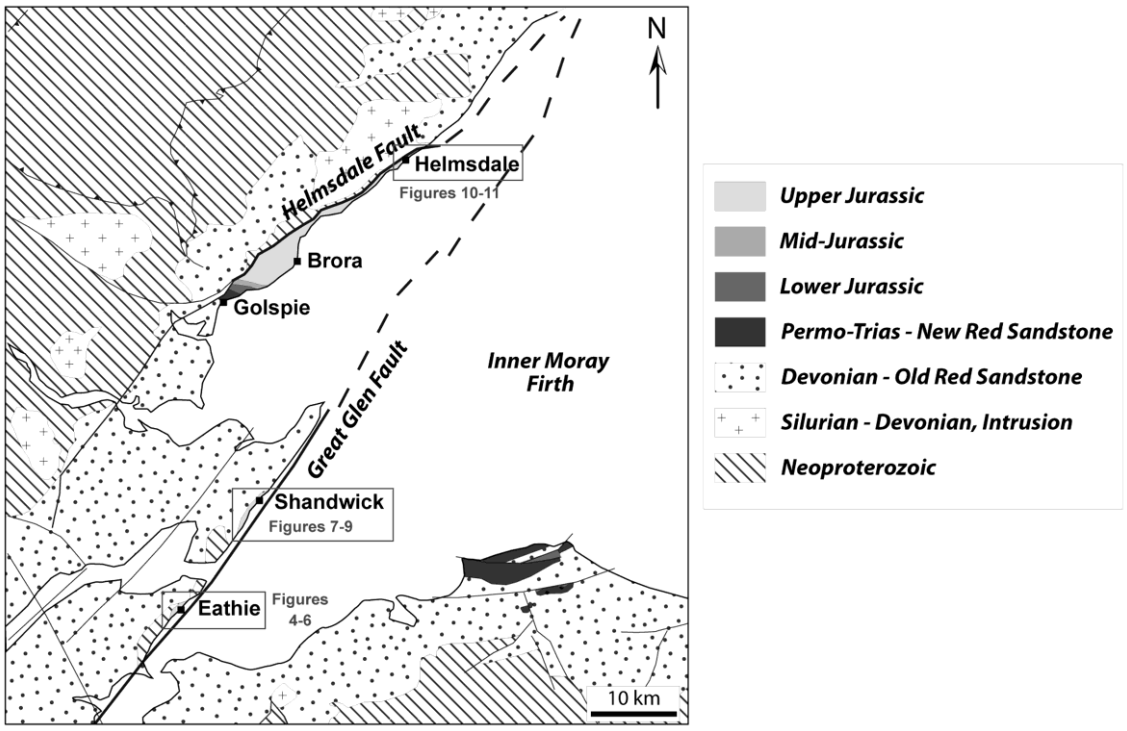

Figure 3. *Geological map of North East Scotland (modified from Stone, 2007). Rectangles indicate locations of figures 4-6, 7-9 and 10-11.*

3. Results

3.1 Eathie

The Jurassic outcrops on the coast at Eathie are easily accessible at low water, via the 'Hugh Miller Trail'. The sequence consists of alternating shale (containing Kimmeridgian

ammonites) and argillaceous limestone, with some sandstone at the North East end of the outcrop. The Upper Jurassic rocks at Eathie are in contact mostly with Neoproterozoic basement, except at the North East end, where they are in contact with the Old Red Sandstone (**Figures 4 and 5**). Previous studies, notably a drilling site for coal exploration, indicate that the Jurassic strata abut a fault, trending NNE-SSW (**Figure 4**; *Miller*, 1851; *Judd,* 1873; *Institute of Geological Sciences, Sheet 94*, 1973). This fault is probably an eastern splay of the GGF (e.g. *Underhill & Brodie*, 1993). We did not see a sharp fault contact; however we did find evidence for faulting, in the form of breccia between Jurassic strata and Neoproterozoic basement.

In the south, the Jurassic strata dip seaward at approx. 40-60°. However towards the North East, the dips vary more strongly (from 10 to 90°) around numerous folds, the axes of which plunge gently and trend from N-S to NE-SW (**Figures 4 and 5**). Moreover, several steep calcite veins, parallel to the GGF, cut the entire Jurassic sequence and their sigmoidal shapes indicate right-lateral slip along the fault (**Figure 5**).

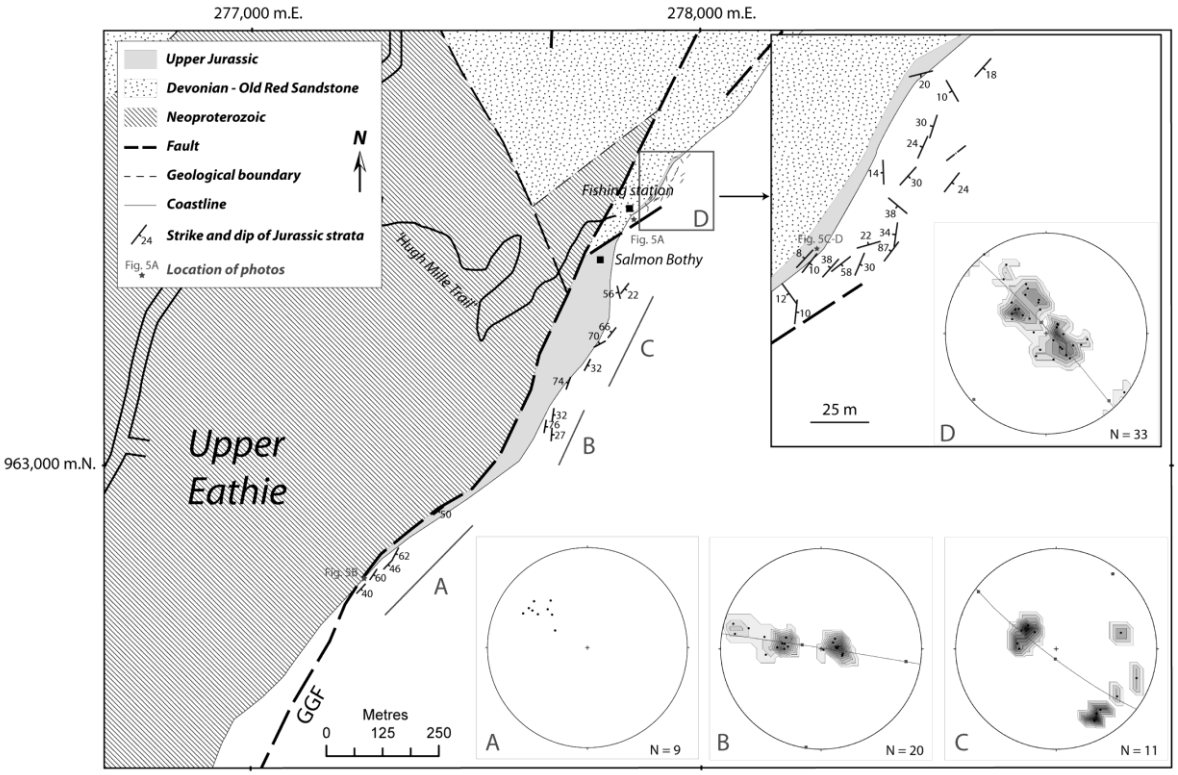

Figure 4. *Geological map of Eathie (modified after Institute of Geological Sciences, Sheet 94, 1973). Strike and dip of Jurassic strata are variable, as a result of folding next to Great Glen Fault (GGF). Stereonets (lower hemisphere) show poles to strata; great circles are perpendicular to fold axes. Stars indicate locations of photographs (Figure 5).*

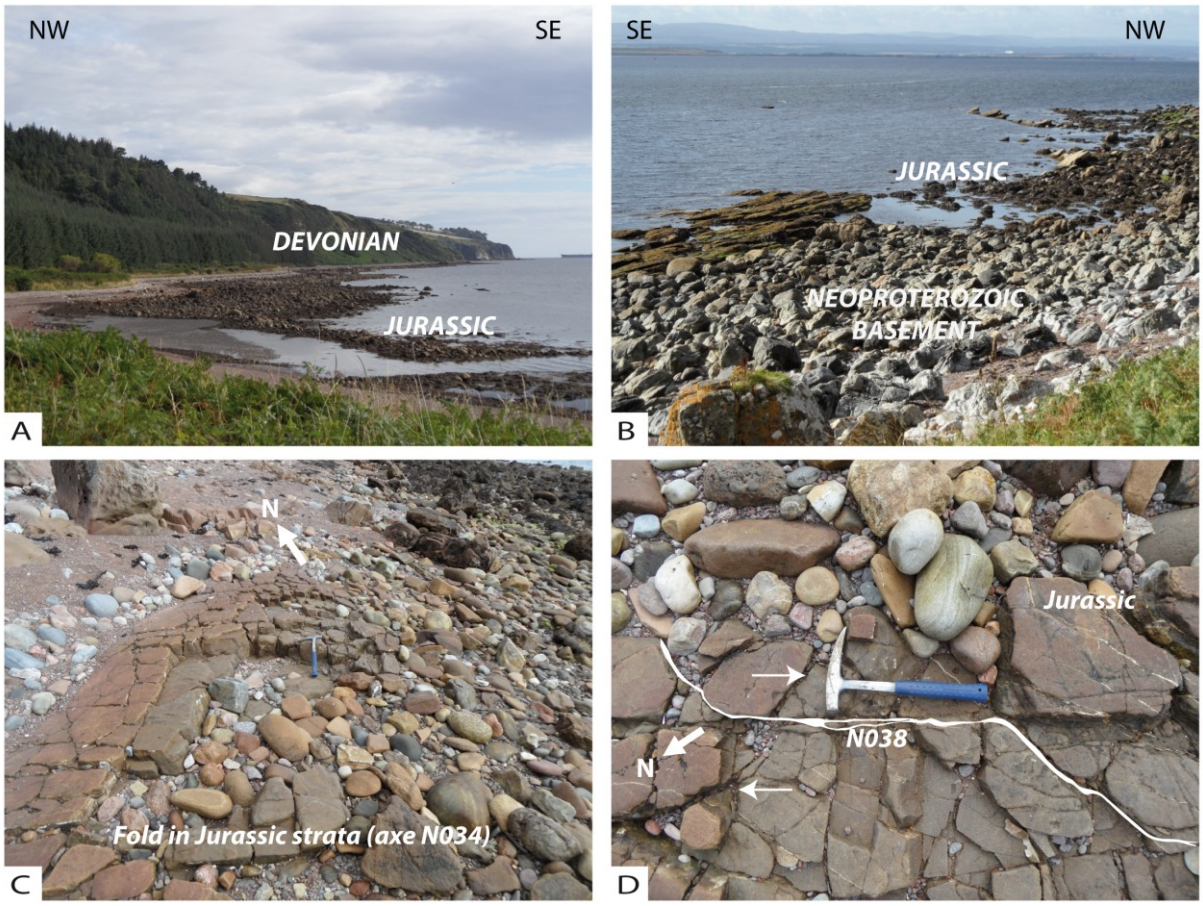

Figure 5. *Photographs of Jurassic outcrop at Eathie. A. Contact between Jurassic strata and Devonian Old Red Sandstone in North East area. B. Contact between Jurassic strata and Neoproterozoic basement in South West area. C. Fold in Jurassic strata adjacent to GGF. D. Calcite veins right-laterally offsetting Jurassic strata. Strike of veins is parallel to Great Glen Fault (approx. N040°).*

Furthermore, we have observed hydraulic fractures in the Jurassic shale that were partially described by *Jonk et al*. (2003; **Figure 6**). In fact, dykes and sills of sandstone occur within Jurassic outcrops (*Jonk et al.*, 2003). Some injectites are similar to 'beef' (bedding-parallel fibrous calcite vein) because they contain fibrous calcite and 'cone-in-cone' (**Figure 6**). In what follows, we will refer to these composite structures as 'beef'. We also noticed that *Hillier & Cosgrove* (2002) described injectites, 'beef' and 'cone-in-cone' within Eocene sandstone at about 2000 m in the Alba oil field of the Outer Moray Firth, attributing these structures to overpressure. In other sedimentary basins (for example the Neuquén Basin of Argentina, or around Charmouth, UK), 'beef' veins provide evidence for overpressure and maturation of organic matter at a depth of several km (*Selley*, 1992; *Rodrigues et al.*, 2009).

Similarly, the Jurassic shale at Eathie may have accumulated deeper offshore in the IMF Basin and then may have been subject to post-Jurassic exhumation. This might have occurred during right-lateral slip along the GGF.

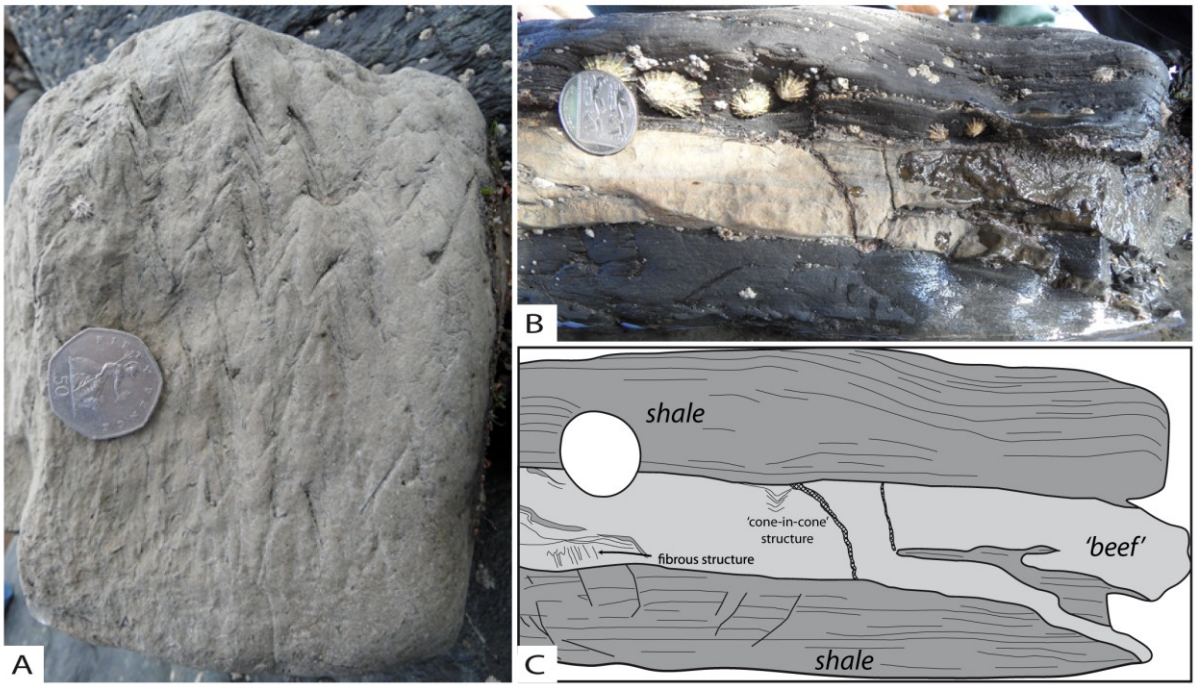

Figure 6. *Photographs of 'cone-in-cone' (A and B) and 'beef' (B) in Jurassic shale at Eathie. C. Interpretation of structures (B).*

3.2 Shandwick

Two outcropping areas of Jurassic strata are accessible on the coast, at low water, south of Shandwick (**Figure 7**). At Port-an-Righ, the strata are Lower to Middle Oxfordian in age; whereas at Cadh'-an-Righ, there is a complete section from Bathonian to Middle Oxfordian (*Sykes*, 1975; *Wright & Cox*, 2001). In both areas, the Jurassic strata abut the Old Red Sandstone. As at Eathie, this contact is a NNE-SSW fault zone, an eastern branch of the GGF (e.g. *Judd*, 1873, *Underhill & Brodie*, 1993).

Port-an-Righ

The Jurassic strata at Port-an-Righ dip generally seaward at approx. 14° to 32° (**Figures 7 and 8**). However, from the top of the cliffs, a large fold is visible on the wave-cut platform, next to the GGF. The fold is asymmetric and sigmoidal. At its North East end, the fold is broadly cylindrical and the fold axis strikes NE-SW, but in the South West the axis

plunges at 16-20° to the South West. Such a domical structure is typical of right-lateral slip within a multilayer (*Richard et al., 1991*). Further towards the North East, the dip of the bedding varies even more (from 12° to the S, through 28-70° to the West, to 10-23°to the East; **Figure 7**). Across the area, steep calcite veins offset the Jurassic strata right-laterally (**Figure 8**). The veins strike at approx. 45° to the GGF. *Jonk et al.* (2003) also described right-lateral strike-slip calcite-cemented faults with NE-SW trends in this area. A fault separates Jurassic from Devonian strata (**Figure 8**; *Jonk et al.*, 2003), but we did not see any striae.

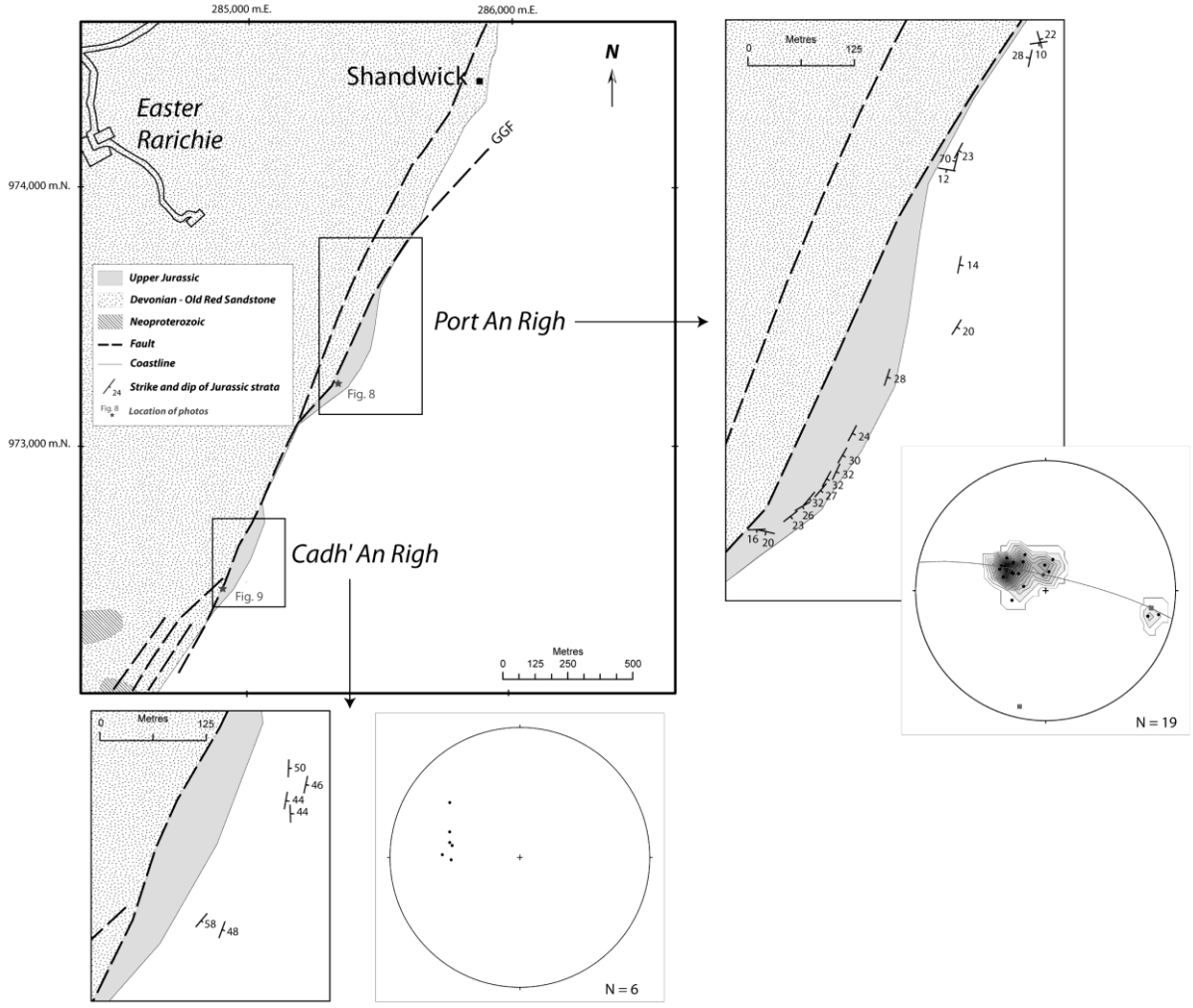

Figure 7. *Geological map of Shandwick (modified after Institute of Geological Sciences, Sheet 94, 1973). Strike and dip of Jurassic strata are variable at Port-an-Righ and Cadh'-an-Righ, as a result of folding next to Great Glen Fault (GGF). Stereonet for Port-an-Righ (lower hemisphere, right) shows poles to strata; great circle is perpendicular to nearly horizontal fold axis, but some data deviate from this. Stereonet for Cadh-an-Righ (lower hemisphere, left) shows great circles (for bedding planes), intersecting at steep fold axis. Stars indicate locations of photographs (Figures 8 and 9).*

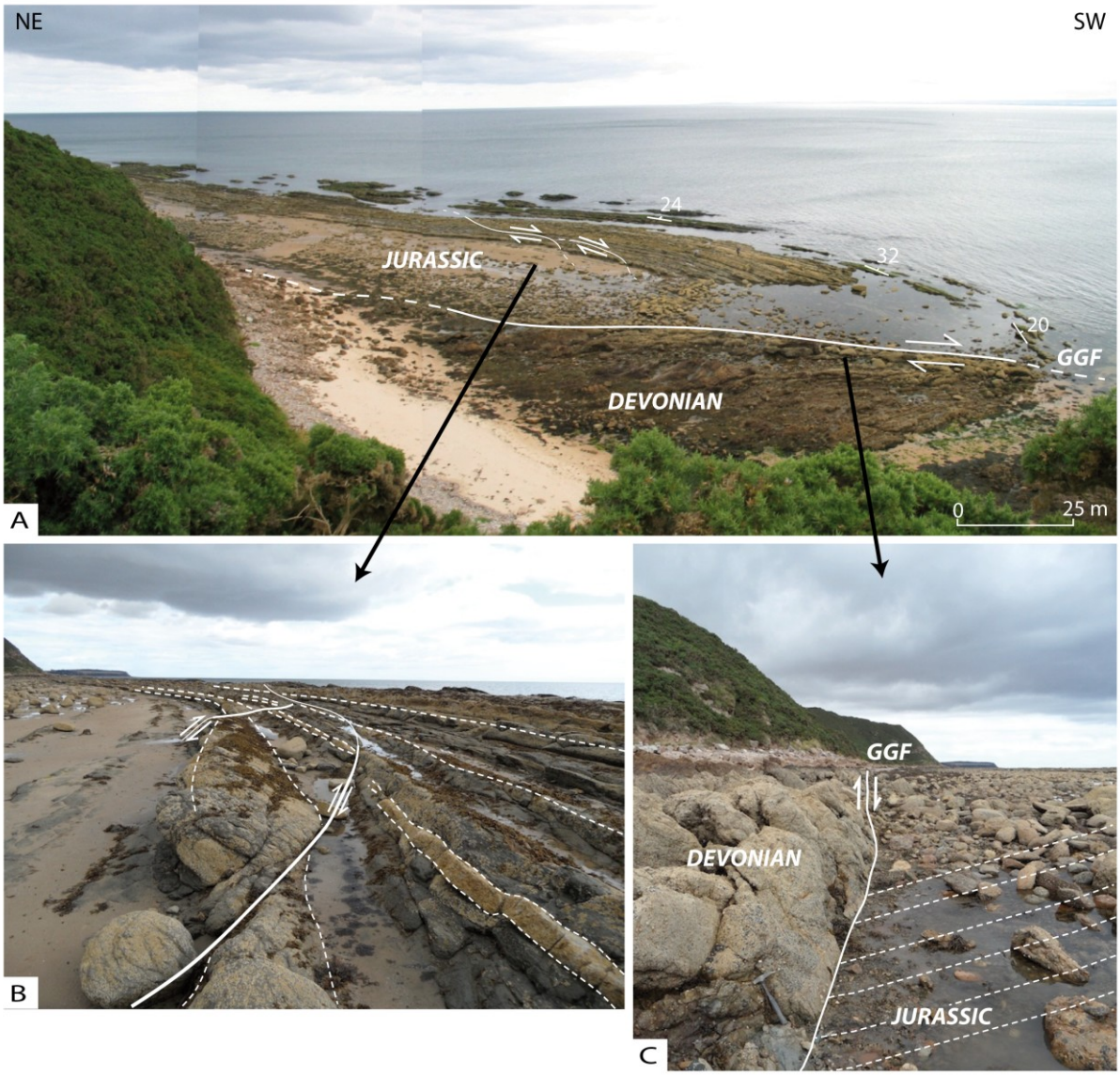

Figure 8. *Photographs of Jurassic outcrop at Port-an-Righ. A. Panoramic view, showing sigmoidal shape of Jurassic fold next to Great Glen Fault (GGF). This shape is diagnostic of right-lateral slip along GGF. B. Calcite veins right-laterally offsetting Jurassic strata. C. Fault contact between Jurassic and Devonian strata.*

Cadh'-an-Righ

Another Jurassic outcrop is visible at Cadh'-an-Righ (**Figure 7**), although access to it is more difficult. In this area, the Devonian strata dip steeply seaward, whereas the Jurassic strata dip generally seaward at 44-58° (**Figure 7**). Once again, we found 'beef' in the Jurassic strata, as well as a coal layer (**Figure 9**).

At Cadh'-an-Righ there is a clear fault contact between Jurassic and Devonian strata (**Figure 9**). The strike of the fault is parallel to the GGF (approx. N040). We found striae,

indicating both right-lateral and reverse slip, which pitch at approx. 8° to the North East. Thus if the 'beef' now at the surface originally formed at a depth of 1500-2500 m, in the oil window (*Rodrigues et al.*, 2009), its exhumation would imply a right-lateral displacement along the GGF of approx. 10-18 km. This amount is consistent with previous estimates (e.g. *Holgate*, 1969; *McQuillin et al.*, 1982; *Rogers et al.*, 1989; *Underhill & Brodie*, 1993).

Figure 9. *Photographs of Jurassic outcrop at Cadh-an-Righ. A. Wide-angle view of fault contact between Jurassic and Devonian strata. B. Close-up view of same, showing reverse and right-lateral slip along GGF. C. 'Beef' in Jurassic shale. D. Fragment of Jurassic coal next to GGF.*

3.3 Helmsdale

Permo-Trias to Upper Jurassic strata crop out along the Helmsdale Fault, between Golspie and Helmsdale (**Figure 10**). At Helmsdale, the Jurassic rocks are in contact with the Helmsdale Granite of Silurian-Devonian age (**Figures 10 and 11**). In this area, the Jurassic strata are of Kimmeridgian age, as at Eathie; however at Helmsdale layers of conglomerate (Helmsdale Boulder Beds) alternate with shale, as a result of syn-tectonic sedimentation in the

footwall of a normal fault (*Thiérault & Steel*, 1995; *Trewin & Hurst*, 2009). The conglomerate contains Devonian clasts, indicating that Devonian strata lay above the Helmsdale Granite at the time of faulting. Moreover, steep calcite veins cut the conglomerate, indicating extension in a direction perpendicular to the Helmsdale Fault (**Figure 11B**). We did not find any 'beef' in the Jurassic strata at Helmsdale and this is consistent with shallow burial, by comparison with the Jurassic strata at Eathie and Shandwick.

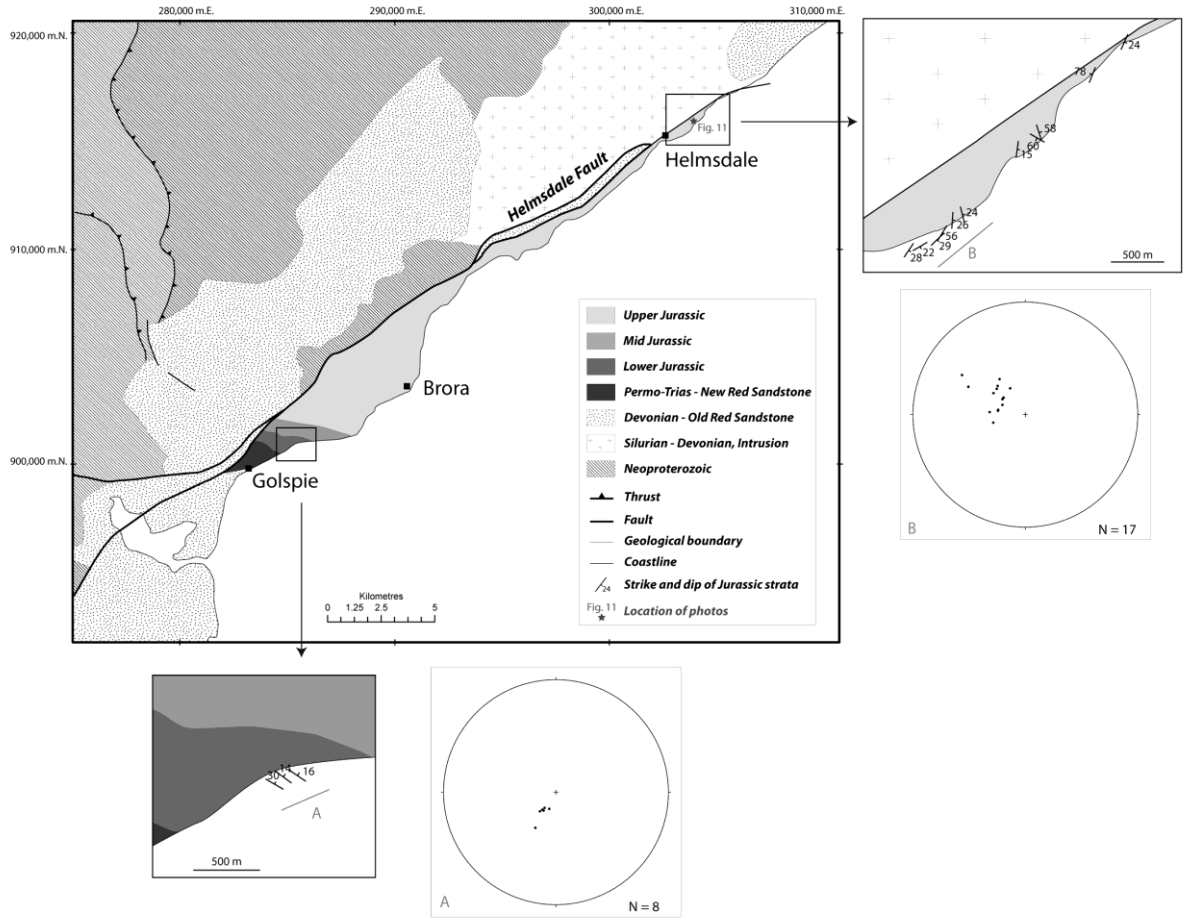

Figure 10. *Geological map of Helmsdale (modified after Stone, 2007). Strike and dip of Jurassic strata are variable, as a result of folding next to Great Glen Fault (GGF). Stereonets for Golspie and Helmsdale (lower hemisphere) show great circles (for bedding planes), intersecting at shallowly plunging fold axes.. Stars indicate locations of photographs (Figure 11).*

Another set of steep calcite veins cuts the entire sequence and therefore post-dates the Jurassic. These veins are sigmoidal, indicating left-lateral slip along the Helmsdale fault zone (**Figure 11**). Such a motion is compatible with right-lateral displacement on the GGF. Indeed, according to previous studies, folds between the Helmsdale Fault and the GGF may have

developed as a result of opposing senses of slip on these two faults (*Thomson & Underhill*, 1993).

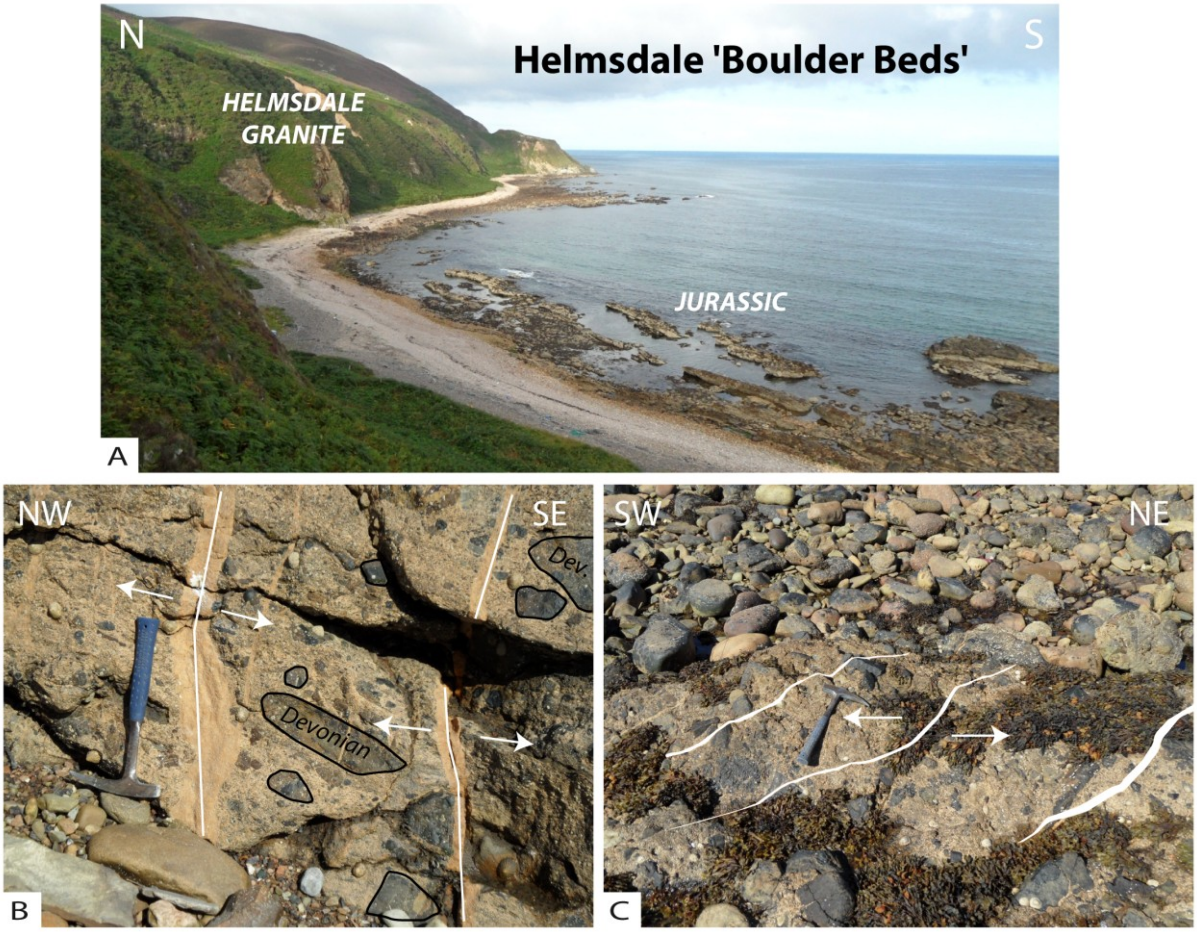

Figure 11. *Photographs of Jurassic outcrop near Helmsdale. A. Jurassic 'Boulder Beds' in contact with Helmsdale Granite. B. Syn-tectonic Jurassic conglomerate containing clasts of Devonian strata and extensional calcite veins. C. Sigmoidal calcite veins left-laterally offsetting Jurassic strata. Strike of calcite veins is parallel to Helmsdale Fault.*

4. Discussion

At Eathie and Shandwick, folds, faults and veins provide structural evidence for post-Jurassic right-lateral reactivation of the GGF. Furthermore, 'beef' at outcrop is one indication that the Mesozoic strata were subject to several km of burial and then to post-Jurassic exhumation. In contrast, at Helmsdale there is no 'beef' and Jurassic conglomerate accumulated at shallower depth, in the footwall of the active Helmsdale Fault. Sigmoidal calcite veins that cut the Jurassic sequence at Helmsdale indicate left-lateral displacement on the Helmsdale Fault. This is compatible with right-lateral displacement along the GGF

(*Underhill & Brodie*, 1993; *Thomson & Underhill*, 1993). At Cadh'-an-Righ, our observations provide further evidence for right-lateral reactivation of the GGF. However, the reverse faulting would indicate a local context of transpression, rather than transtension.

Our observations show clearly that right-lateral reactivation of the GGF was post-Jurassic, but we know of no younger strata onshore, other than Quaternary. Subsurface data from the offshore IMF Basin and the apparent offsets of Palaeocene-Eocene dykes in North West Scotland all indicate that reactivation occurred in Tertiary time (*Holgate*, 1969; *Underhill & Brodie*, 1993; *Thomson & Underhill*, 1993; *Thomson & Hillis*, 1995). However, the exact timing remains uncertain. *Underhill & Brodie* (1993) showed that the IMF Basin underwent regional uplift during the Cenozoic and they attributed this to reactivation of the GGF. More generally, periods of uplift occurred at 65-60 Ma, 40-25 Ma and 15-10 Ma and may have continued into Late Neogene time (*Hall & Bishop*, 2002; *Holford et al.*, 2009, 2010). Therefore, it seems likely that reactivation of the GGF occurred during one of these periods (**Figure 12**).

Amongst the possible causes for reactivation of the GGF and for Cenozoic uplift of Scotland are: (1) mantle processes from the Iceland Plume, (2) intra-plate compression from the Alpine Orogeny, (3) ridge push from the North East Atlantic and (4) variations in the amount and rate of sea-floor spreading in the North East Atlantic. According to recent restorations (*Le Breton et al.,* in review), variations in the amount and direction of sea-floor spreading between the Reykjanes and Aegir ridges of the North East Atlantic (**Figure 13**) generated left-lateral transpressional displacement along the FFZ, first in the Early Eocene (*c.* 56-51 Ma) and then from the Early Eocene to Late Oligocene (*c.* 47–26 Ma). During the latter phase, the Jan Mayen Microcontinent (JMMC) rifted progressively (from south to north) off East Greenland. When these continental areas finally separated, sea-floor spreading transferred from the Aegir Ridge to the Kolbeinsey Ridge (**Figures 12 and 13**). According to the stationary hot spot model of *Lawver & Müller* (1994), the head of the Iceland Plume was beneath the eastern Greenland Margin at that time (*c.* 40-30 Ma). *Müller et al.* (2001) suggested that the Iceland Mantle Plume was responsible for (1) rifting at the edge of the eastern Greenland margin, (2) formation of the Kolbeinsey Ridge west of Jan Mayen, (3) subsequent extinction of the Aegir Ridge and (4) separation of the JMMC from Greenland.

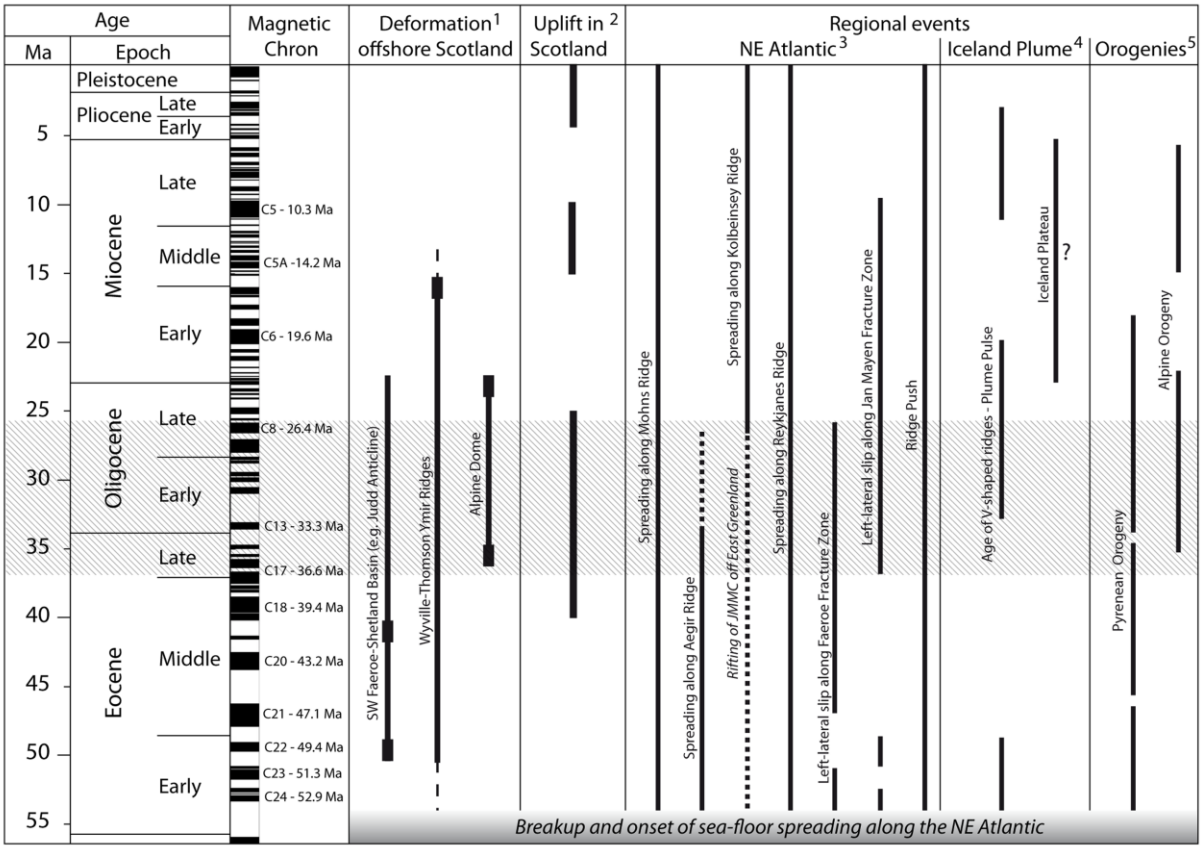

Figure 12. *Summary and correlation of events. Numbers refer to (1) post-breakup compressional deformation offshore Scotland (from Smallwood et al., 2004; Johnson et al., 2005; Ricthie et al., 2008; Tuitt et al., 2010); (2) main phases of uplift in Scotland during Cenozoic time (from Hall & Bishop, 2002; Holford et al., 2009); (3) sea-floor spreading along North East Atlantic ridge system, differential sea-floor spreading along North East Atlantic resulting in left-lateral slip along Faeroe Fracture Zone (FFZ) and Jan Mayen Fracture Zone (JMFZ) (from Le Breton et al., in review), ridge push, Iceland Mantle Plume pulse (correlation between age of V-shaped ridges and plume pulse from White & Lovell, 1997), development of Iceland Plateau, and compressional Alpine and Pyrenean stress field (from Tuitt et al., 2010). Period of synchronous events (hachured) may represent timing of reactivation of Great Glen Fault (GGF). For locations of post-breakup compressional structures offshore Scotland, see Figure 13.*

The Middle Eocene to Late Oligocene was also a period of uplift in Scotland and of compressional deformation on the North West United Kingdom Continental Margin (**Figure 12**). Numerous compressional structures developed offshore Scotland (e.g. the Wyville-Thomson, Ymir ridges (WYTR), the Alpine Dome and the Judd Anticline) from the Middle Eocene to the Early Miocene (**Figure 13**; *Smallwood*, 2004; *Johnson et al.*, 2005; *Ritchie et*

al., 2008; *Tuitt et al.*, 2010). *Le Breton et al.* (in review) have suggested that differential sea-floor spreading of North East Atlantic ridges was responsible for compressional deformation on the continental margin at those times. We suggest furthermore that this differential sea-floor spreading was also responsible for reactivation of the GGF. Indeed, a left-lateral displacement along the FFZ is compatible with a right-lateral reactivation of the GGF (**Figure 13**). The stress field from the Alpine Orogeny and pulses from the Iceland Mantle plume may have amplified the intraplate stress in Scotland, so contributing to reactivation of the GGF. Because all these processes were active simultaneously from the Late Eocene to the Late Oligocene (*c.* 37-26 Ma), we consider that reactivation of the GGF probably occurred in this interval (**Figure 12**).

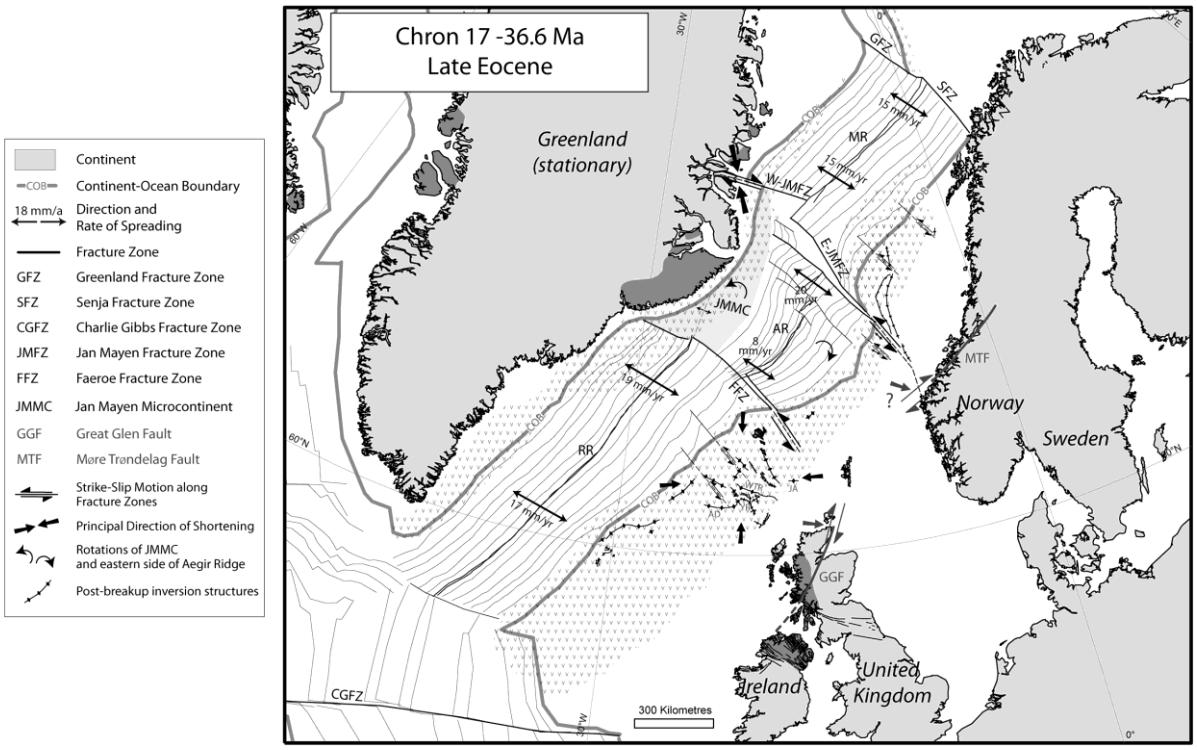

Figure 13. *Position of Europe at 36.6 Ma (Late Eocene), relative to stationary Greenland plate (Le Breton et al., in review). According to a new method of restoration, differential sea-floor spreading along Reykjanes, Aegir and Mohns ridges generated left-lateral displacements along Faeroe and Jan Mayen fracture zones (Le Breton et al,. in review). Such displacements are compatible with right-lateral reactivation of Great Glen Fault and possibly of Møre Trøndelag Fault, respectively. Abbreviations: AD, Alpine Dome; AR, Aegir Ridge; JA, Judd Anticline; MR, Mohns Ridge; RR, Reykjanes Ridge; YR, Ymir Ridge; WTR, Wyville-Thomson Ridge. Map projection is Universal Transverse Mercator (UTM, WGS 1984, zone 27N).*

Conclusions

(1) Our field observations of Jurassic outcrops in Eathie, Shandwick and Helmsdale, North East Scotland, provide additional evidence for post-Jurassic right-lateral reactivation of the GGF, under transpression.

(2) The observation of 'beef' structures in Jurassic shale in Eathie and Shandwick suggest that this formation must have accumulated deeper offshore in the IMF Basin and been subject to post-Jurassic exhumation. This exhumation would be compatible with right-lateral displacement on the GGF. With the hypothesis that 'beef' structures form at approx. 1500-2500 m depth (*Rodrigues et al.*, 2009) and with the 8° pitch of striates observed on fault plan in Cadh'-an-Righ, we estimate the right-lateral displacement along the GGF to be in the order of 10-18 km.

(3) The timing of reactivation of the GGF remains uncertain; however we suggest that the GGF reactivated right-laterally in a time interval from Late Eocene to Late Oligocene, *c*. 37 and 26 Ma. This period coincides with (1) an uplift episode of Scotland, (2) intraplate stress from the Alpine Orogeny (3) Iceland Mantle Plume pulse, and more importantly with (3) a left-lateral slip along FFZ due to differential sea-floor spreading and plate readjustment in the North East Atlantic (separation of the JMMC, 'ridge jump' from the Aegir to the Kolbeinsey ridges). Indeed, a left-lateral slip along the FFZ is compatible with a right-lateral reactivation of the GGF.

(4) Low-temperature geochronological studies may provide in the future better constrain on the timing of reactivation of the GGF. However, the vertical motion along the GGF may not have been significant enough to be visible in such studies. Similar work along the MTF, Norway, would provide better constrain on the relation between differential spreading along the North East Atlantic, left-lateral slip along the FFZ and JMFZ, uplift of Scotland and Norway, and Tertiary reactivation of the GGF and MTF.

Acknowledgements

We would like to thank Chevron USA for funding the PhD of E. Le Breton and in particular Gavin Lewis and Peter Connolly for instigating the project. We are grateful to Andrew Hurst and John Parnell for providing maps, publications, data and encouragement, during our visit to Aberdeen University in August 2011. We also thank Marc Jolivet of the University of Rennes 1 for information on reactivation of the GGF.

References

Argent, J.D., Stewart, S.A., Green, P.F. & Underhill, J.R., 2002. Heterogeneous exhumation in the Inner Moray Firth, UK North Sea: constraints from new AFTA(R) and seismic data. *Journal of the Geological Society*, **159**(6), 715-729, doi:10.1144/0016-764901-141.

Boldreel, L.O., & Andersen, M.S., 1993. Late Pliocene to Miocene compression in the Faeroe-Rockall area. *In*: Parker, J.R. (eds), *Petroleum Geology of Northwest Europe: Proceedings of the 4th Conference*, Geological Society, London, Petroleum Geology Conference series, **4**, 1025-1034.

Boldreel, L.O. & Andersen, M.S., 1998. Tertiary compressional structures on the Faroe – Rockall Plateau in relation to northeast Atlantic ridge-push and Alpine foreland stresses. *Tectonophysics*, **300**, 13-28.

Brekke, H., 2000. The tectonic evolution of the Norwegian Sea Continental Margin with emphasis on the Vøring and More Basins. *In*: Nøttvedt, A. (eds), *Dynamics of the Norwegian Margin*, Geological Society, London, Special Publications, **167**, 327-378.

Brodie, J. & White N., 1994. Sedimentary basin inversion caused by igneous underplating: Northwest European continental shelf. *Geology*, **22**, 147-150.

Clift, P.D., Carter, A. & Hurford, A.J., 1998. The erosional and uplift history of NE Atlantic passive margins: constraints on a passing plume. *Journal of the Geological Society, London*, **155**, 787-800.

Doré, A.G., Lundin, E.R., Kusznir, N.J. & Pascal C., 2008. Potential mechanisms for the genesis of Cenozoic domal structures on the NE Atlantic margin: pros, cons and some new ideas. *In*: Johnson, H., Doré, A.G., Gatliff, R.W., Holdsworth, R., Lundin, E.R. & Ritchie, J.D. (eds), *The Nature and Origin of Compression in Passive Margins*, Geological Society, London, Special Publications, **306**, 1-26.

Evans, D., Graham, C., Armour, A. & Bathurst P., 2003. *The Millennium Atlas: petroleum geology of the central and northern North Sea.* Geological Society, London, 389 p.

Firth, C.R. & Stewart, I.S., 2000. Postglacial tectonics of the Scottish glacio-isostatic uplift centre. *Quaternary Science Reviews*, **19**, 1469-1493.

Hall, A. & Bishop P., 2002. Scotland's denudational history: an integrated view of erosion and sedimentation at an uplifted passive margin. *In*: Doré, A.G., Cartwright, J.A., Stoker, M.S., Turner, J.P. & White, N. (eds), *Exhumation of the North Atlantic Margin: Timing, Mechanisms and Implications for Petroleum Exploration*, Geological Society, London, Special Publications, **196**, 271-290.

Hillier, R.D. & Cosgrove, J.W., 2002. Core and seismic observations of overpressure-related deformation within Eocene sediments of the Outer Moray Firth, UKCS. *Petroleum Geoscience*, **8**, 141-149.

Hitchen, K. 2004. The geology of the UK Hatton-Rockall margin. *Marine and Petroleum Geology*, **21**, 993-1012, doi:10.1016/j.marpetgeo.2004.05.004.

Holford, S.P., Green, P.F., Duddy, I.R., Turner, J.P., Hillis, R.R. & Stoker, M.S., 2009. Regional intraplate exhumation episodes related to plate-boundary deformation. *Geological Society of America Bulletin*, **121**(11-12), 1611-1628, doi:10.1130/B26481.1.

Holford, S. P., Green, P.F., Hillis, R.R., Underhill, J.R., Stoker, M.S. & Duddy, I.R., 2010. Multiple post-Caledonian exhumation episodes across NW Scotland revealed by apatite fission-track analysis. *Journal of the Geological Society*, **167**(4), 675-694, doi:10.1144/0016-76492009-167.

Holgate, N., 1969. Palaeozoic and Tertiary transcurrent movements on the Great Glen Fault. *Scottish Journal of Geology*, **5**(2), 97-139.

Hutton, D.H.W. & McErlean, M., 1991. Silurian and Early Devonian sinistral deformation of the Ratagain granite, Scotland: constraints on the age of Caledonian movements on the Great Glen fault system. *Journal of the Geolocal Society, London*, **148**, 1-4.

Institute of Geological Sciences, 1973. *Geological Map of Cromarty, Sheet 94, 1:50 000*. British Geological Survey.

Johnson, H., Ritchie, J. D., Hitchen, K., Mcinroy, D. B. & Kimbell, G.S., 2005. Aspects of the Cenozoic deformational history of the Northeast Faroe − Shetland Basin, Wyville − Thomson Ridge and Hatton Bank areas. *In*: Doré, A.G. & Vining, B.A. (eds), *Petroleum Geology: North-West Europe and Global Perspectives - Proceedings of the 6th Petroleum Geology Conference*, Geological Society, London, Petroleum Geology Conference series, **6**, 993-1007.

Jolivet, M., 2007. Histoire de la dénudation dans le corridor du loch Ness (Écosse) : mouvements verticaux différentiels le long de la Great Glen Fault. *Comptes Rendus Geosciences*, **339**(2), 121-131, doi:10.1016/j.crte.2006.12.005.

Jones, S.M., White, N., Clarke, B.J., Rowley, E. & Gallagher, K., 2002. Present and past influence of the Iceland Plume on sedimentation. I*n*: Doré, A.G., Cartwright, J.A., Stoker, M.S., Turner, J.P. & White, N. (eds), *Exhumation of the North Atlantic Margin: Timing, Mechanisms and Implications for Petroleum Exploration,* Geological Society, London, Special Publications, **196**, 13-25.

Jonk, R., Duranti, D., Parnell, J., Hurst, A. & Fallick, A.E., 2003. The structural and diagenetic evolution of injected sandstones: examples from the Kimmeridgian of NE Scotland. *Journal of the Geological Society, London*, **160**, 881-894.

Judd, J.W., 1873. The Secondary Rocks of Scotland. *Quarterly Journal of the Geological Society*, **29**(1-2), 97-195, doi:10.1144/GSL.JGS.1873.029.01-02.16.

Lawver, L.A., & Müller, R.D., 1994. Iceland Hotspot track, *Geology*, **22**, 311-314.

Le Breton, E., Cobbold, P.R., Dauteuil, O. & Lewis, G., Variations in amount and direction of sea-floor spreading along the North East Atlantic Ocean and resulting deformation of the continental margin of North West Europe. *Tectonics* (in review).

Lundin, E.R. & Doré, A.G., 2002. Mid-Cenozoic post-breakup deformation in the "passive" margins bordering the Norwegian - Greenland Sea. *Marine and Petroleum Geology*, **19**, 79-93.

Mackay, L.M., Turner, J., Jones, S.M. & White N.J., 2005. Cenozoic vertical motions in the Moray Firth Basin associated with initiation of the Iceland Plume. *Tectonics*, **24**(5), 1-23, doi:10.1029/2004TC001683.

McQuillin, R., Donato, J.A. & Tulstrup J., 1982. Development of basins in the Inner Moray Firth and the North Sea by crustal extension and dextral displacement of the Great Glen Fault, *Earth and Planetary Science Letters*, **60**, 127-139.

Mendum, J.R. & Noble, S.R., 2010. Mid-Devonian sinistral transpressional movements on the Great Glen Fault: the rise of the Rosemarkie Inlier and the Acadian event in Scotland. In: Law, R.D, Butler, R.W.H., Holdsworth, R.E., Krabbendam, M., Strachan, R.A. (eds), *Continental tectonics and mountain building: the legacy of Peach and Horne*, Geological Society, London, Special Publications, **335**, 161-187.

Miller, H., 1851. *The old red sandstone or, New walks in an old field*, published by Gould and Lincoln, Boston, 288 p. From the 4th London Edition.

Mosar, J., Lewis, G. & Torsvik, T., 2002. North Atlantic sea-floor spreading rates: implications for the Tertiary development of inversion structures of the Norwegian – Greenland Sea. *Journal of the Geological Society*, **159**, 503-515, doi:110.1144/0016-764901-135.

Müller, R.D., Gaina, C., Roest, W.R. & Hansen, D.L., 2001. A recipe for microcontinent formation, *Geology*, **29**(3), 203.

Nadin, P.A., Kusznir, N.J. & Cheadle, M.J., 1997. Early Tertiary plume uplift of the North Sea and Faeroe-Shetland Basins. *Earth and Planetary Science Letters*, **148**, 109-127.

Persano, C., Barfod, D.N., Stuart, F.M. & Bishop, P., 2007. Constraints on early Cenozoic underplating-driven uplift and denudation of western Scotland from low temperature thermochronometry. *Earth and Planetary Science Letters*, **263**(3-4), 404-419, doi:10.1016/j.epsl.2007.09.016.

Richard, P., Mocquet, B. & Cobbold, P.R., 1991. Experiments on simultaneous faulting and folding above a basement wrench fault. *Tectonophysics*, **188**, 133-141.

Ritchie, J.D., Johnson, H. & Kimbell G.S., 2003. The nature and age of Cenozoic contractional deformation within the NE Faroe–Shetland Basin. *Marine and Petroleum Geology*, **20**(5), 399-409, doi:10.1016/S0264-8172(03)00075-8.

Ritchie, J.D., Johnson, H., Quinn, M.F. and Gatliff, R.W., 2008. The effects of Cenozoic compression within the Faroe-Shetland Basin and adjacent areas. *In*: Johnson, H., Doré, A.G., Gatliff, R.W., Holdsworth, R., Lundin, E.R. & Ritchie, J.D. (eds), *The Nature and Origin of Compression in Passive Margins*, **306**, 121-136, Geological Society, London, Special Publications.

Roberts, D.G., 1989. Basin inversion in and around the British Isles. *Geological Society, London, Special Publications*, **44**(1), 131-150, doi:10.1144/GSL.SP.1989.044.01.09.

Rodrigues, N., Cobbold, P.R., Loseth, H. & Ruffet, G., 2009. Widespread bedding-parallel veins of fibrous calcite ('beef') in a mature source rock (Vaca Muerta Fm, Neuquen Basin, Argentina): evidence for overpressure and horizontal compression. *Journal of the Geological Society, London*, **166**(4), 695-709.

Rogers, D.A., Marshall, J.E.A. and Austin T.R., 1989. Devonian and later movements on the Great Glen fault system, Scotland. *Journal of the Geolocal Society, London*, **146**, 369-372.

Saunders, A.D., Fitton, J.G., Kerr, A.C., Norry, M.J. & Kent, R.W., 1997. The North Atlantic Igneous Province. *In*: Mahoney, J.J. & Coffin, M.F. *Large Igneous Provinces Continental, Oceanic, and Planetary Flood Volcanism*, Geophysical Monograph, **100**, 45-93.

Saunders, A.D., Jones, S.M., Morgan, L.A., Pierce, K.L., Widdowson, M. & Xu, Y.G., 2007. Regional uplift associated with continental large igneous provinces: The roles of mantle plumes and the lithosphere. *Chemical Geology*, **241**(3-4), 282-318, doi:10.1016/j.chemgeo.2007.01.017.

Selley, R.C., 1992. Petroleum seepages and impregnations in Great Britain. *Marine and Petroleum Geology*, **9**, 226-244.

Smallwood, J.R., 2004. Tertiary Inversion in the Faroe-Shetland Channel and the Development of Major Erosional Scarps. *Geological Society, London, Memoirs*, **29**(1), 187-198, doi:10.1144/GSL.MEM.2004.029.01.18.

Soper, N.J., Strachan, R.A., Holdsworth, R.E., Gayer, R.A. & Geiling R.O., 1992. Sinistral transpression and the Silurian closure of Iapetus. *Journal of the Geolocal Society, London*, **149**, 871-880.

Speight, J.M. & Mitchell, J.G., 1979. The Permo-Carboniferous dyke-swarm of northern Argyll and its bearing on dextral displacement on the Great Glen Fault. *Journal of the Geolocal Society, London*, **139**, 3-11.

Stewart, M., Holdsworth, R.E. & Strachan, R.A., 2000. Deformation processes and weakening mechanisms within the frictional ± viscous transition zone of major crustal-scale faults: insights from the Great Glen Fault Zone, Scotland. *Journal of Structural Geology*, **22**, 543-560.

Stewart, M., Strachan, R.A., Martin, M.W. & Holdsworth, R.E., 2001. Constraints on early sinistral displacements along the Great Glen Fault Zone, Scotland: structural setting, U-Pb geochronology and emplacement of the syn-tectonic Clunes tonalite. *Journal of the Geological Society*, **158**(5), 821-830, doi:10.1144/jgs.158.5.821.

Stoker, M.S., 2002. Mate Neogene development of the UK Atlantic Margin. *In*: Doré, A.G., Cartwright, J.A., Stoker, M.S., Turner, J.P. & White, N. (eds), *Exhumation of the North Atlantic Margin: Timing, Mechanisms and Implications for Petroleum Exploration*, Geological Society, London, Special Publications, **196**, 313-329.

Stoker, M.S., Hoult, R.J., Nielsen, T., Hjelstuen, B.O., Laberg, J.S. & Shannon P.M., 2005. Sedimentary and oceanographic responses to early Neogene compression on the NW European margin. *Atlantic*, **22**, 1031-1044, doi:10.1016/j.marpetgeo.2005.01.009.

Stone, P., 2007. *Bedrock geology UK North, An explanation of the bedrock geology map of Scotland, northern England, Isle of Man and Northern Ireland - 1:625 000*, 5th Edition, British Geological Survey, Natural Environment Research Concil.

Sykes, R.M., 1975. The stratigraphy of the Callovian and Oxfordian stages (Middle-Upper Jurassic) in northern Scotland. *Scottish Journal of Geology*, **11**(1), 51-78.

Thiérault, P. & Steel, R.J., 1995. Syn-rift sedimentation in the Upper Jurassic (Helmsdale Boulder Beds) of the Inner Moray Firth. *In*: Steel, R.J., Felt, V.L., Johannessen, E.P. & Mathieu, C. (eds), *Sequence Stratigraphy on the Northwest European Margin*, **5**, 365-387, Norwegian Petroleum Society Special Publication.

Thomson, K. & Hillis, R.R., 1995. Tertiary structuration and erosion of the Inner Moray Firth. *In*: Scrutton, R.A., Stoker, M.S., Shimmield, G.B. & Tudhope, A.W. (eds), *The Tectonics, Sedimentation and Palaeoceanography of the North Atlantic Region*, Geological Society, London, Special Publications, **90**, 249-269.

Thomson, K., & Underhill J.R., 1993. Controls on the development and evolution of structural styles in the Inner Moray Firth Basin. *In*: Parker, J.R. (eds), *Petroleum Geology of Northwest Europe: Proceedings of the 4th Conference*, Geological Society, London, Petroleum Geology Conference series, **4**, 1167-1178.

Trewin, N.H. & Hurst, A., 2009. *Excursion Guide to the Geology of East Sutherland and Caithness*, 2nd Edition, Aberdeen Geological Society.

Tuitt, A., Underhill, J.R., Ritchie, J.D., Johnson, H. & Hitchen, K., 2010. Timing, controls and consequences of compression in the Rockall – Faroe area of the NE Atlantic Margin. *In*: Vining, B.A. & Pickering, S.C. (eds), *Petroleum Geology: From Mature Basins to New Frontiers - Proceedings of the 7th Petroleum Geology Conference*, Geological Society, London, Petroleum Geology Conference series, **7**, 963-977.

Underhill, J.R., 1991a. Controls on Late Jurassic seismic sequences, Inner Moray Firth, UK North Sea: a critical test of key segments of Exxon's original global cycle chart. *Basin Research*, **3**, 79-98.

Underhill, J.R., 1991b. Implications of Mesozoic-Recent basin development in the western Inner Moray Firth, UK. *Marine and Petroleum Geology*, **8**, 359-369.

Underhill, J.R. & Brodie, J.A., 1993. Structural geology of Easter Ross, Scotland: implications for movement on the Great Glen fault zone. *Journal of the Geological Society*, **150**(3), 515-527, doi:10.1144/gsjgs.150.3.0515.

White, N. & Lovell, B., 1997. Measuring the pulse of a plume with the sedimentary record. *Nature*, **387**, 888-891.

White, R. & McKenzie, D., 1989. Magmatism at Rift Zones: The Generation of Volcanic Continental Margins and Flood Basalts. *Journal of Geophysical Research*, **94**(B6), 7685-7729, doi:10.1029/JB094iB06p07685.

Wright, J.K. & Cox, B.M., 2001. British Upper Jurassic Stratigraphy (Oxfordian to Kimmeridgian), *Geological Conservation Review Series*, Joint Nature Conservation Committee, Peterborough, **21**, 266 p.

5.3 General Discussion

In this Chapter and Chapter 4, I have argued that differential sea-floor spreading in the NE Atlantic generated post-breakup deformation of the adjacent European Continental Margin and possibly a reactivation of major continental structures, such as the GGF in Scotland.

Indeed, our field observations of Jurassic outcrops at Eathie, Shandwick and Helmsdale, NE Scotland, provided additional evidence for post-Jurassic right-lateral reactivation of the GGF, under transpression. We suggest that the GGF reactivated right-laterally in a time interval from Late Eocene to Late Oligocene (approx. 37- 26 Ma) and in response to differential sea-floor spreading and plate readjustments in the NE Atlantic, which generated left-lateral slip along the FFZ at this period (Chapter 4). The timing of reactivation of the GGF remains uncertain. In the future, low-temperature geochronological studies may provide better constraints on the timing. Similar work along the MTF, Norway, might also provide better constraints on the relationship between differential spreading along the NE Atlantic, left-lateral slip along the FFZ and JMFZ, uplift of Scotland and Norway, and Tertiary reactivation of the GGF and MTF.

Another question in this thesis is the possible cause of differential sea-floor spreading. As suggested in this chapter and chapter 4, the position of the Iceland Mantle Plume in the vicinity of the NE Atlantic Ridge and the timing of its pulses could explain variations in the direction and rate of sea-floor spreading and could generate radial compressive stress (**Figure 5.1**). In the following chapter, I will focus on this question and discuss more generally the influence of mantle plume on sea-floor spreading and structural development of continental margins.

Chapter 6

Influence of mantle plumes on sea-floor spreading and structure of continental margins: Comparison of NE Atlantic and South Atlantic

In previous chapters, I presented results on variations in direction and rate of sea-floor spreading along the NE Atlantic ridge system, and the influence of such variations on deformation of the adjacent margin. During my thesis, I also worked for three months as a trainee at Chevron offices in Houston, on the opening of the South Atlantic Ocean and on the rifting of the Santos Basin that was influenced by magmatic activity from mantle plumes. During this internship, I restored the pre-rift structure of the Santos and Campos basins, interpreting seismic data and using the method of Chapter 3, in order to quantify the direction and the amount of extension. Moreover, I reviewed the spreading history of the South Atlantic and the history of magmatism that affected this area. This magmatism may have influenced the opening of the South Atlantic, the rifting style and heat flow history. In this chapter, I will compare results of this internship with those of the NE Atlantic in order to discuss the possible influence of mantle plumes on (1) rates and location of sea-floor spreading and (2) structural development of continental margins (during rifting and after breakup).

Indeed, the SE Brazilian region and the segment of the South Atlantic, east of Santos and Campos basins, have some features in common with the NE Atlantic Ocean and its continental margins:

1) Intense magmatic activity occurred in this area between 138-125 Ma, leading to the emplacement of a magmatic province, the Parana-Etendeka (**Figure 6.1**; e.g. *Hawkesworth et al.*, 2000). This magmatic event was linked to the northward opening of the South Atlantic Ocean over the Tristan da Cunha hotspot (e.g. *Torsvik et al., 2006*).

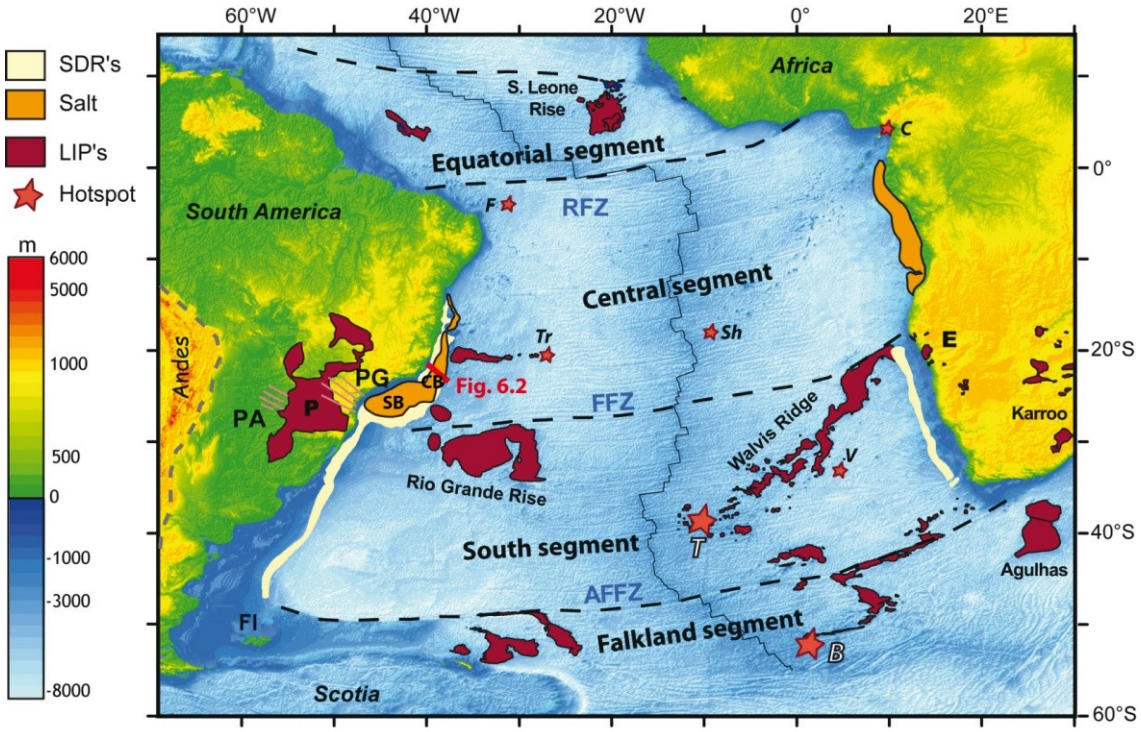

Figure 6.1. *General map of South Atlantic Ocean, on a topographic/bathymetric map from GTOPO 30, and location of cross-section shown in Figure 6.2 (light red line). Fracture zones in dotted line (RFZ, Romanche Fracture Zone; FFZ, Florianopolis Fracture Zone; AFFZ, Agulhas–Falkland Fracture Zone) delimit four segments (Equatorial, Central, South and Falkland). Aptian salt basins are in orange, Large Igneous Provinces in dark red (LIP's; P, Parana; E, Etendeka; Karroo, Sierra Leone Rise and Agulhas) and Seaward Dipping Reflectors (SDRs) in white. Stars represent active hotspots (F, Fernando; C, Cameroon; Tr, Trinidade; Sh, St Helena; T, Tristan; V, Vema; B, Bouvet). Other abbreviations: CB, Campos Basin; FI, Falkland Islands; PG, Ponta Grossa Dyke System; PA, Paraguay Dyke system; SB, Santos Basin. Modified from Torsvik et al. (2009).*

2) Mantle plumes (Tristan da Cunha Plume in the south and Trindade in the north) were present during rifting and opening of the South Atlantic Ocean, in Cretaceous and Tertiary time (**Figures 6.1 and 6.2**; e.g. *Hawkesworth et al.*, 1992; *Peate*, 1997; *Cobbold et al.*, 2001). The Tristan da Cunha hotspot (responsible for the Parana-Etendeka Province and Rio Grande Rise–Walvis Ridge) is considered as a deep plume (e.g. *Torsvik et al.*, 2006).

3) The SE Brazilian Margin is a volcanic continental margin. SDR sequences occur to North and South of it and possibly in the Campos Basin (**Figures 6.1 and 6.3**). The Santos and Campos basins on the SE Brazilian Margin, and their conjugate West African margins, contain significant thicknesses of salt.

4) Phases of exhumation and compressional deformation occurred in SE Brazil in the Late Cretaceous (initiation at *c.* 80-75 Ma), Paleogene (initiation at *c.* 48-45 Ma) and Neogene (initiation at *c.* 18-15 Ma). A possible cause is intraplate stress from ridge push, especially from the Nazca plate (e.g. *Cobbold et al.*, 2001, 2007; *Japsen et al.*, 2012).

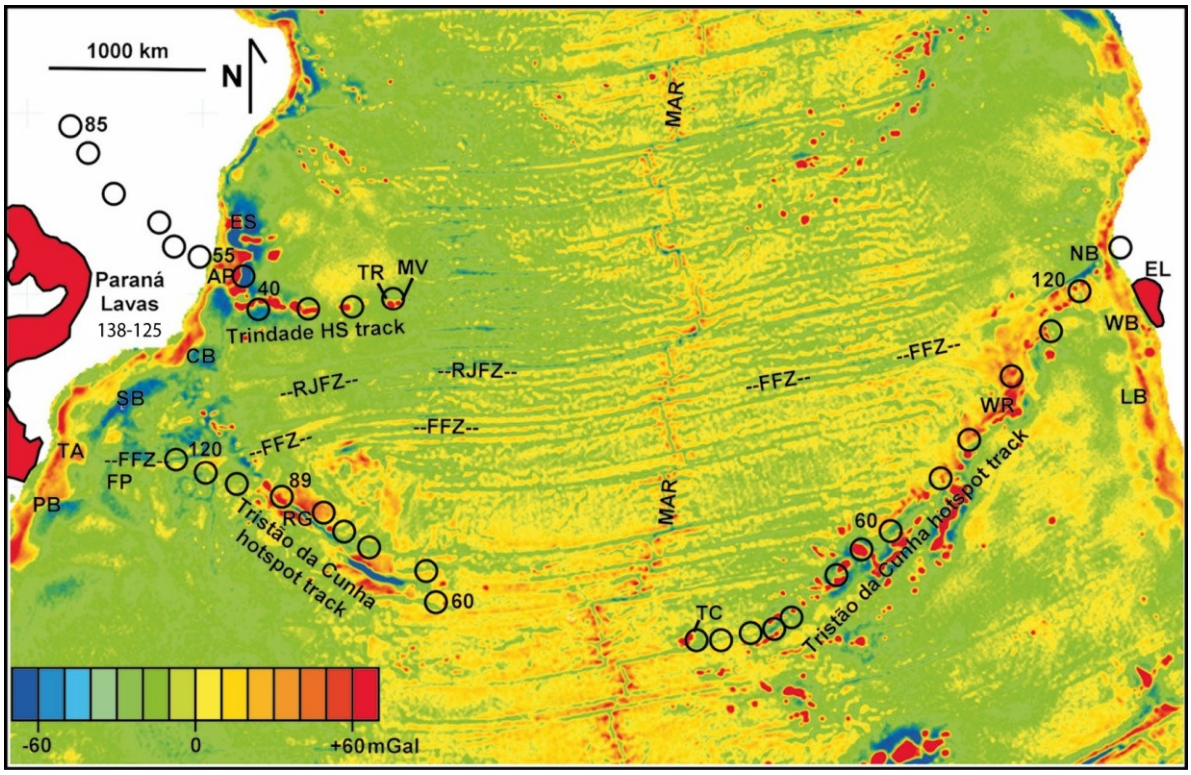

Figure 6.2. *Map of gravity anomalies in South Atlantic. Colour bar shows anomaly values in mGal. Outline of offshore Parana and Etendeka (EL) lavas (age in Ma, from Hawkesworth et al.*, 2000), *Mid-Atlantic Ridge (MAR), major fracture zones (RJFZ, Rio de Janeiro Fracture Zone ; FFZ, Florianopolis Fracture Zone), tracks of Tristan da Cunha and Trindade hot spots (unfilled circles with ages in Ma), resulting seamounts (TR, Trindade; MV, Martin Vaz; TC, Tristan da Cunha), and other offshore features (AP, Abrolhos Plateau; CB, Campos Basin; ES, Esperito Santo Basin; FP, Florianopolis Platform; LB, Luderitz Basin PB; NB, Namib Basin; Pelotas Basin; RG, Rio Grande Rise; SB, Santos Basin; TA, Torres Arches; WB, Walvis Basin;). Modified from Meisling et al. (2001).*

I will first present calculations of spreading rates of the South Atlantic and compare them with those of the NE Atlantic in order to discuss possible influence of mantle plumes on sea-floor spreading. Then, I will present the results of the restoration of pre-rift structure in Santos and Campos basins and a review of the history of magmatism that affected this area

during rifting. I will discuss in this second part, the influence of mantle plumes on structural development and post-breakup reactivation of the margin.

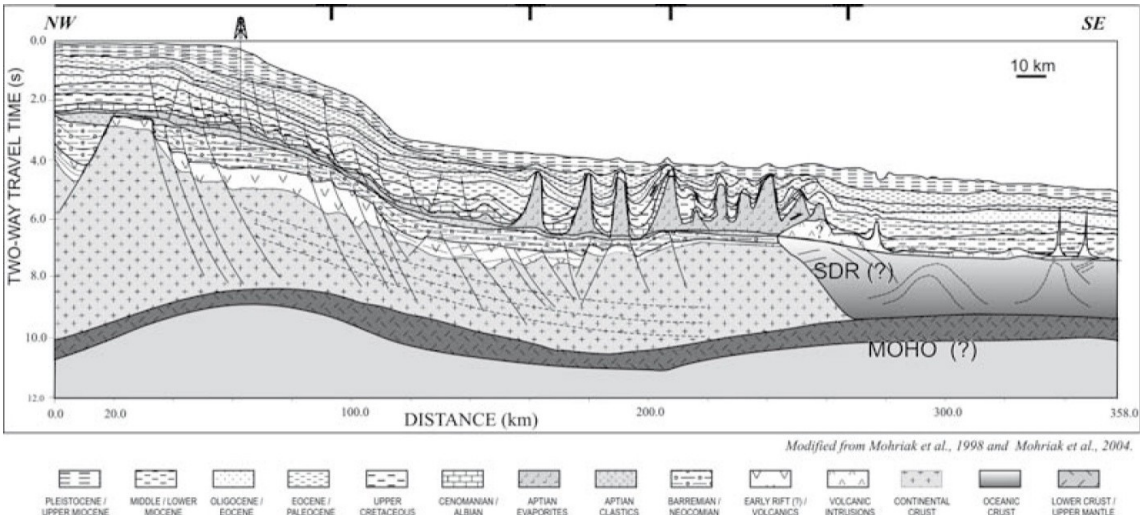

Figure 6.3. *Cross-section of Campos Basin, SE Brazilian Margin from Mohriak et al. (2008). Location is on Figure 6.1.*

6.1 Mantle plumes and variations of sea-floor spreading rates

6.1.1 Spreading rates along South Atlantic, east of Santos and Campos basins

I have calculated spreading rates along the South Atlantic (for the region east of Santos and Campos basins) from isochrons of ages between 83.5 Ma and present time (**Figure 6.4**; *Müller et al.*, 1991). However, for ages older than 83.5 Ma, no isochrons are identifiable due to a long period of normal polarity of the Earth's Magnetic field, in the Early Cretaceous (Chron 34, 120.4-83.5 Ma). Thus, I have used the kinematic model of *Torsvik et al.* (2009) to estimate spreading rates between 83.5 and 131.7 Ma (**Figure 6.5**). Spreading rates are for two reference points, one in the north of the studied area (north of Campos Basin) and another in the south (south of Santos Basin) (**Figure 6.6**).. Sea-floor spreading started at around 112 Ma in this area (e.g. *Scotchman et al*., 2010), so the calculated rates between 112 and 131.7 Ma, correspond to rifting of Santos and Campos basins.

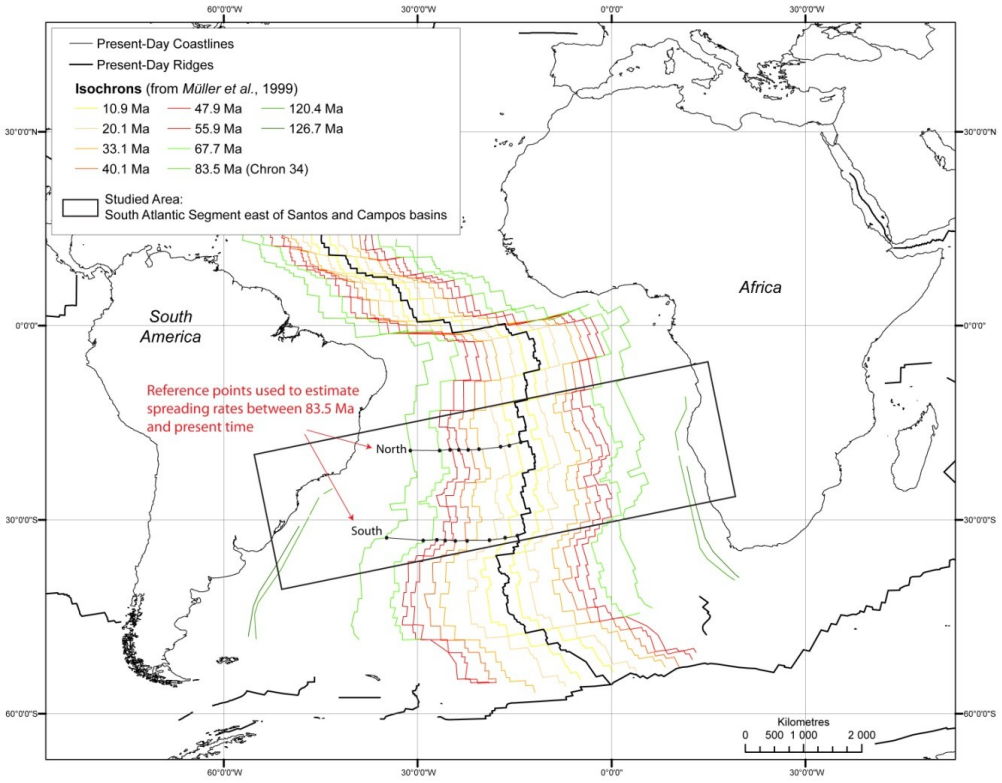

Figure 6.4. *Map of isochrons of South Atlantic Ocean from 83.5 Ma to present time (from Müller et al., 1999, available on Gplates database), used in calculation of spreading rates for two reference points (in black) north and south of studied area (Segment of South Atlantic east of Santos and Campos basins).*

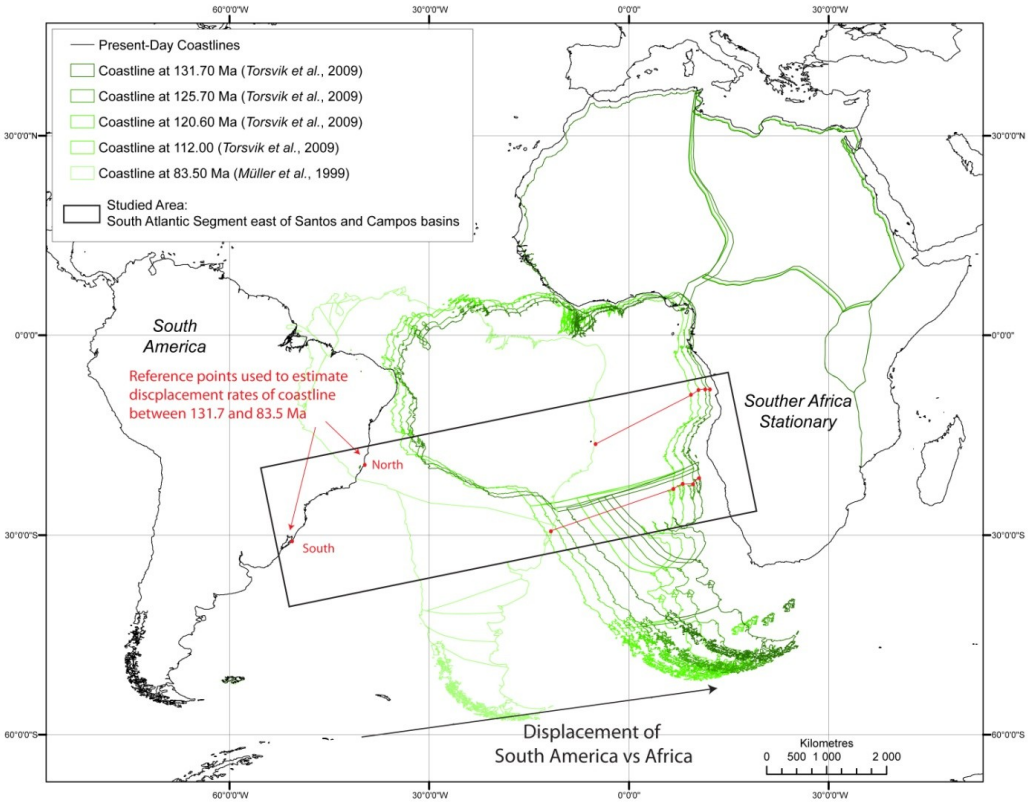

Figure 6.5. (previous page) *Map of position of South America relative to a southern Africa stationary, between 83.5 and 131.7 Ma, used in calculation of spreading rates for two reference points(in red) north and south of studied area (Segment of South Atlantic east of Santos and Campos basins). Rotation poles are from Torsvik et al. (2009).*

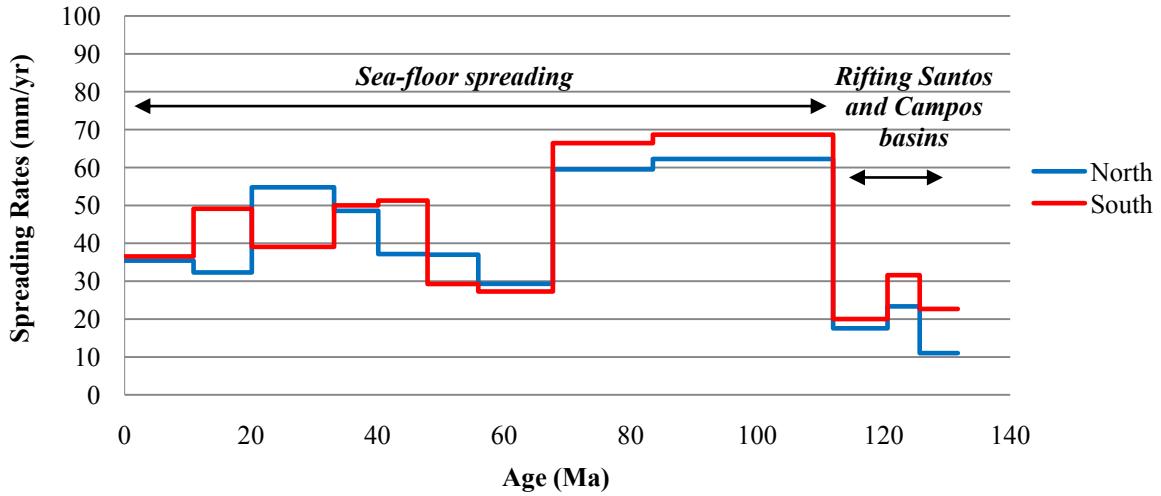

Figure 6.6. *Spreading rates along South Atlantic, east of Santos and Campos basins, from 131.7 Ma to present time.*

Spreading rates along the segment of the South Atlantic east of Santos and Campos basins, varied through time. Spreading rates were greatest just after the onset of sea-floor spreading (at approx. 112 Ma, e.g. *Scotchman et al., 2010*), up to 6.2 to 6.9 cm/yr. They decreased significantly, down to 2.7-2.9 cm/yr, in Late Cretaceous – Early Palaeocene time (around 65 Ma) and increased again up to approx. 5 cm/yr in Eocene, Oligocene and Miocene times. Since the last 10 Ma, spreading rates are in the order of 3.5-3.7 cm/yr.

Spreading rates along this segment of the South Atlantic varied both in time and in space. Indeed, we observe variations between the northern and southern parts of the segment. In Cretaceous time, the southern part spread at approx. 1 cm/yr faster than the northern part. However, during the Tertiary, differences in spreading rates, between the north and the south, were more variable. The northern part spread faster than the southern part in the Early Eocene (3.7 *vs* 2.9 cm/yr) and Oligocene (5.5 *vs* 3.9 cm/yr); whereas the southern part spread faster than the northern part in Middle Eocene time (5.1 *vs* 3.7 cm/yr) and in the Miocene (4.9 *vs* 3.2 cm/yr). This spatial variation could trigger relative displacements along oceanic fracture zones (e.g. Florianopolis Fracture Zone, **Figure 6.1**), as in the NE Atlantic. However, more detailed analysis would be necessary to study such relative displacements.

I have compared these spreading rates with the approximate timing of regional events in the South Atlantic region, as well as with the results of the NE Atlantic (section 6.1.2).

6.1.2 Comparison with NE Atlantic

Figure 6.7 shows spreading rates along the segment of the South Atlantic, east of SE Brazil, and those along the NE Atlantic. For both regions, I have compared the spreading rates with the timing of plume events, exhumation and compressional deformation on the adjacent margin and continent, and main compressional phases of regional orogenies (**Figure 6.7**).

Both in the North East and South Atlantic, sea-floor spreading rates varied through time and show the same trend. After breakup spreading rates are greatest (6-7 cm/yr for the South Atlantic and 4-5.5 cm/yr for the NE Atlantic), then they decrease significantly to reach a minimum (3 cm/yr for the South Atlantic and 0.5-1.5 cm/yr for the NE Atlantic), before increasing again.

There is good correlation between variations in spreading rate and plume events. In both regions, breakup follows a period of widespread magmatism and emplacement of a large igneous province, the Parana-Etendeka in the South Atlantic and the NAIP in the NE Atlantic. In both areas, these large igneous provinces are associated with mantle plume (the Tristan da Cunha Plume and the Iceland Plume, respectively). Magma supply from the plume may explain the fast sea-floor spreading following breakup. Later, the decrease in spreading rates may be related to lower activity of the plume (no Iceland plume pulse in Eocene time) or to an increasing distance between ridge and plume, for example in the South Atlantic, where the Tristan da Cunha plume crosses onto the African plate in Palaeocene time. Then, the increase in spreading rates along the NE Atlantic in Miocene time coincides with the position of the plume head underneath the Reykjanes Ridge. In the South Atlantic, the increase in spreading rates may be related to the arrival of the Trindade hotspot onto oceanic crust and therefore closer to the South Atlantic Ridge.

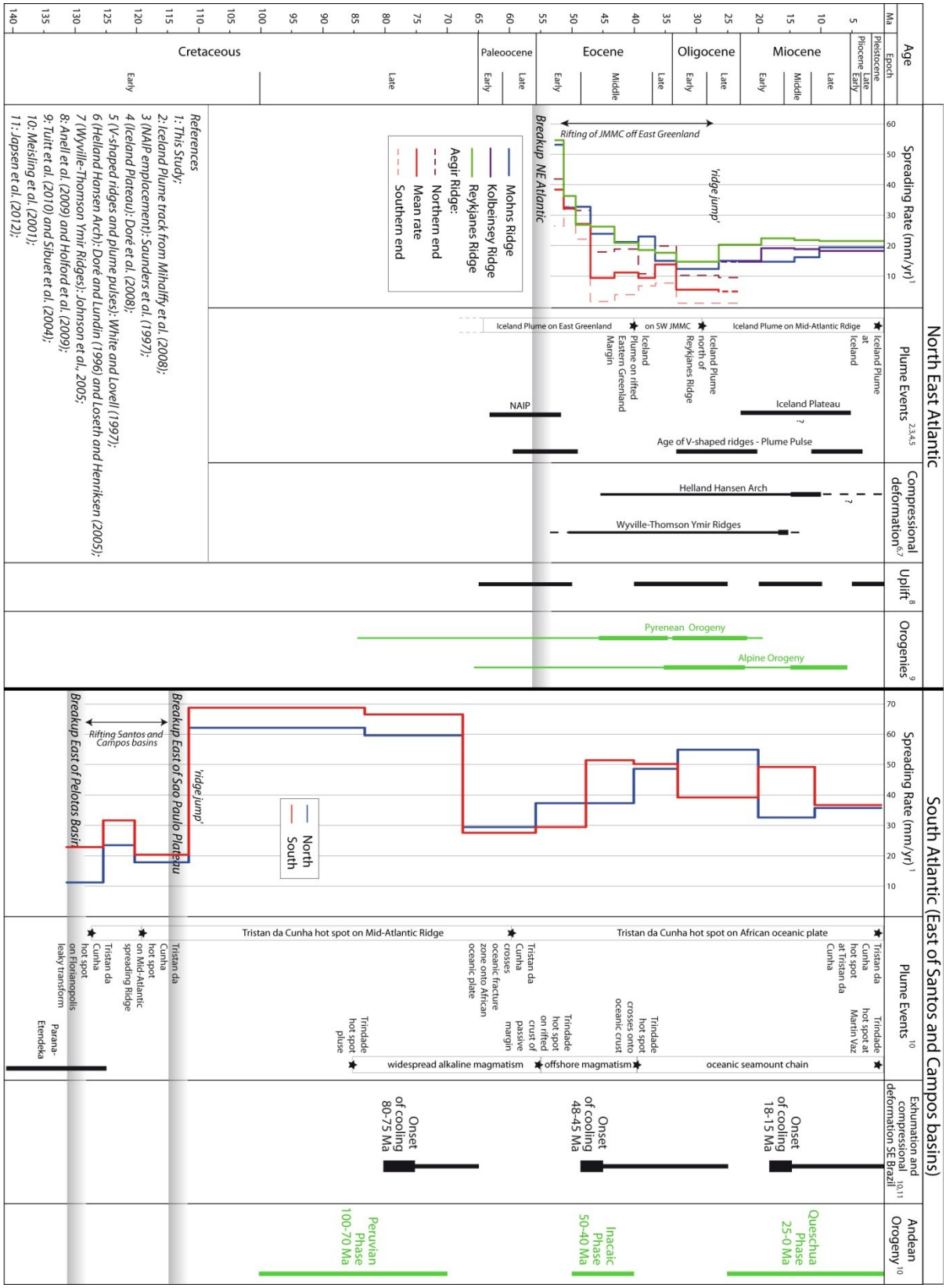

Figure 6.7. *Chronological diagram illustrating the variations in spreading rate along NE Atlantic and for South Atlantic (east of Santos and Campos basins) and approximate timing of regional events (plume events, compressional deformation, exhumation and orogeny).*

In the Late Cretaceous and Paleogene, the SE Brazilian Margin was in interaction with a second mantle plume, the Trindade hot spot (**Figures 6.2 and 6.7**, e.g. *Thompson et al.*, 1998). The plume originated at 90-80 Ma beneath the interior of the South American continent and the hotspot track shows eastward-younging ages of onshore volcanic centres, which is may be due to westward motion of the South American plate (**Figure 6.2**; e.g. *Thompson et al.*, 1998). *Thompson et al.* (1998) suggested that between 80 and 55 Ma, the magma was displaced to the south by a deflection at the base of the subcontinental lithosphere generating volcanic centres 500 km south of the reconstructed hotspot track. These volcanic centres are located along transform zones suggesting that these fracture zones leak igneous rocks originating in the mantle (e.g. *Thompson et al.*, 1998; *Mohriak and Rosendahl*, 2003). Similar leakage of magma from the plume could have happened in the NE Atlantic, along the JMFZ, in Eocene time when the Iceland Plume was beneath the eastern Greenland Margin. Indeed, magma from the Iceland plume could have flowed northward along the JMFZ. This would explain the high sea-floor spreading rates along the northern part of the Aegir Ridge at that time.

Several events inducing compressional deformations and exhumations of the adjacent continental region occurred in both regions (**Figure 6.7**). As already discussed in Chapter 4, differential sea-floor spreading along the NE Atlantic ridge appears to be responsible for compressional deformation of the adjacent continental margin. In the South Atlantic, the periods of variations in spreading rates along the South Atlantic coincide with phases of post-breakup compressional deformation in SE Brazil. However, further studies would be necessary to define the possible effect of variation in spreading rates along the South Atlantic on compressional deformation in SE Brazil.. Possible causes for compressional deformation of SE Brazil are (1) far-field stresses from the Andean Orogeny and ridge push from the Nazca plate and (2) hotspot activity (**section 6.2.2**; e.g. *Cobbold et al.*, 2007, *Japsen et al.*, 2012).

A ‘ridge-jump’ of the spreading axis occurred in both areas, at the time of breakup in the South Atlantic and after breakup in the NE Atlantic. These ‘ridge-jump’ events coincide with arrival of the plume head at the spreading axis, which will be discussed in the following section.

6.1.3 Ridge-jump and location of sea-floor spreading above plume head

A low gravity anomaly prolongs the M0 magnetic anomaly (120.4 Ma) in the Santos Basin (**Figure 6.8**). Seismic data indicate that this zone is underlain by extremely thin continental crust (e.g. *Cobbold et al.*, 2001; *Scotchman et al.*, 2010). *Scotchman et al.* (2010) suggest moreover that this zone is a failed seafloor spreading centre, representing an early attempt at breakup and initiation of seafloor spreading through the centre of the Santos Basin, north of the Florianopolis Fracture Zone (FlFZ), in the early Aptian. The magnetic anomaly at 120.4 Ma (M0), east of the Torres Arch (**Figure 6.8**) indicates the effects of the sea-floor spreading at that time in this area. Sea-floor spreading propagated northward into the Santos Basin. However it occurred more to the east in the Santos Basin in the Late Aptian – Early Albian, around 112 Ma (e.g. *Scotchman et al.*, 2010). A 'ridge jump' to the east of the South Atlantic Ridge thus occurred along the FlFZ, above the Tristan da Cunha plume head (**Figure 6.8**).

In the NE Atlantic, a similar 'ridge-jump' occurred during Tertiary time, after breakup. As described in previous chapters, the sea-floor spreading ended along the Aegir Ridge and initiated north of the Reykjanes Ridge, above the Iceland plume head, forming the Kolbeinsey Ridge around 25 Ma. *Müller et al.* (1998) argue that most of the asymmetry in sea-floor spreading is due to ridge jump around a plume. Indeed, both in the South Atlantic and in the North East Atlantic, a ridge jump occurred and the new spreading centre was located above a plume head (**Figures 6.7 and 6.9**). The magma supply from the plume may explain such a location of the onset of sea-floor spreading.

Thus in both the NE and South Atlantic, mantle plumes have influenced the positions and rates of sea-floor spreading. The position of the Tristan da Cunha plume underneath the Santos Basin during rifting may have also influenced the structural development of this basin (**section 6.2**).

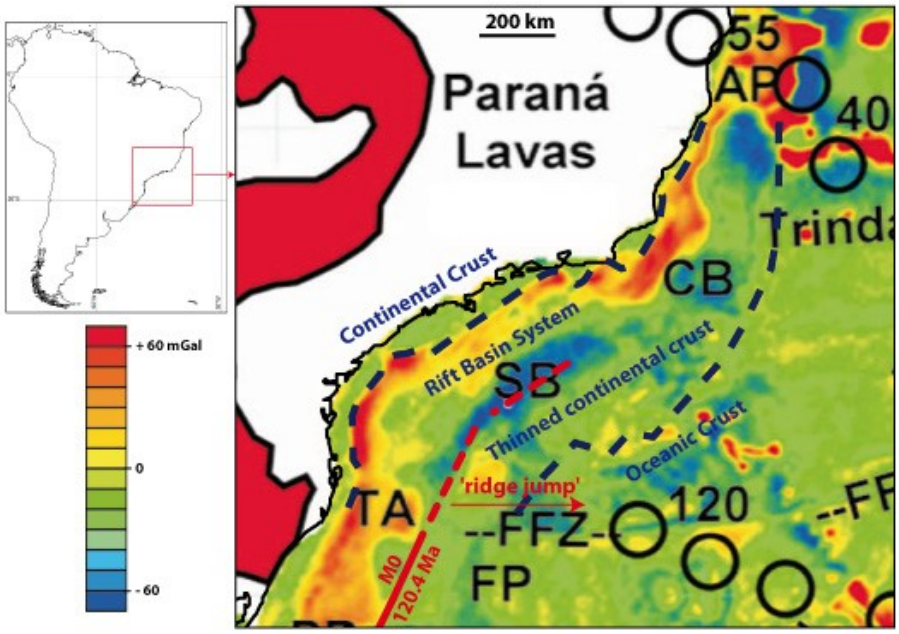

Figure 6.8. *Map of marine gravity anomalies, SE Brazilian Margin. Color bar shows anomaly values in mGal. Offshore Parana lavas are in red. Unfilled circles (with ages in Ma) indicate tracks of Tristan da Cunha (south) and Trindade (north) hot. Magnetic Anomaly at 102.4 Ma (M0) is from Müller et al., 1999). Other abbreviations: AP, Abrolhos Plateau; CB, Campos Basin; FFZ, Florianopolis Fracture Zone; FP, Florianopolis Platform; SB, Santos Basin; TA, Torres Arches. Modified from Meisling et al. (2001).*

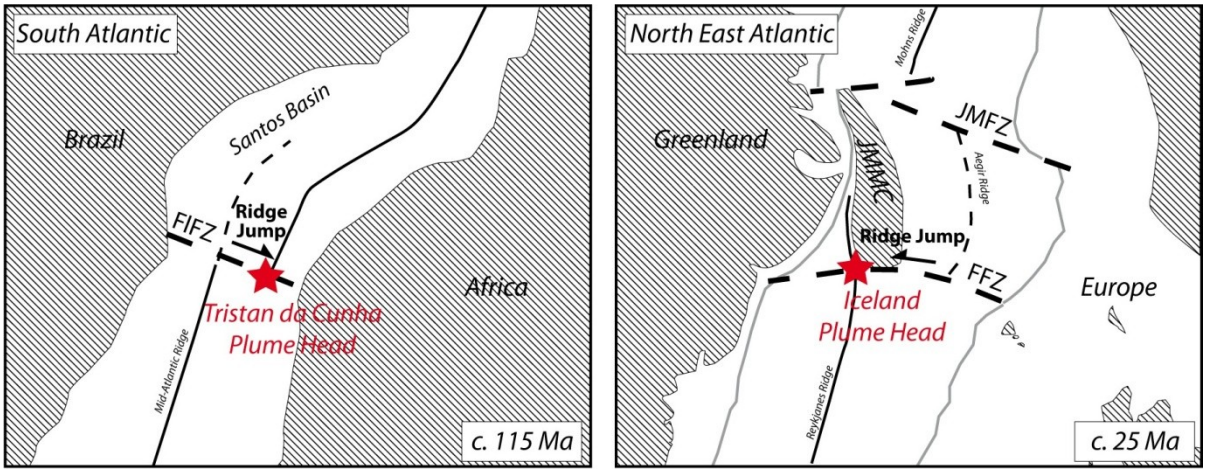

Figure 6.9. *Scheme of ridge jump and position of sea-floor spreading above plume head. A) failure of sea-floor spreading in Santos Basin, South Atlantic, and ridge jump of Mid-Atlantic Ridge to the east, above Tristan da Cunha plume head, at time of breakup (c. 115 Ma), and B) Cessation of sea-floor spreading along Aegir Ridge and ridge-jump to the west, above Iceland plume head, at c. 25 Ma. Abbreviations: FFZ, Faeroe Fracture Zone; FlFZ, Florianopolis Fracture Zone; JMFZ, Jan Mayen Fracture Zone; JMMC, Jan Mayen Microcontinent.*

6.2 Mantle plumes and development of continental margins

6.2.1 Rifting in Santos Basin and role of pre-existing structures

On a structural map of the Santos Basin, for the top of volcanic basement (below the salt layer) rift faults vary in trend, which is sigmoidal in map view (**Figure 6.10**). I restored the pre-rift structure of the Santos Basin (details of restoration are in **Appendix**) predicts two main directions of extension, NNE-SSW and NW-SE, and a small amount of extension (in the order of 0.05-0.16 in the NNE-SSW direction and 0.06 in the NW-SE direction, discussed in **Appendix**). The NW-SE direction of extension corresponds to the main direction of opening of the South Atlantic; however the NNE-SSW direction is perpendicular and thus quite surprising.

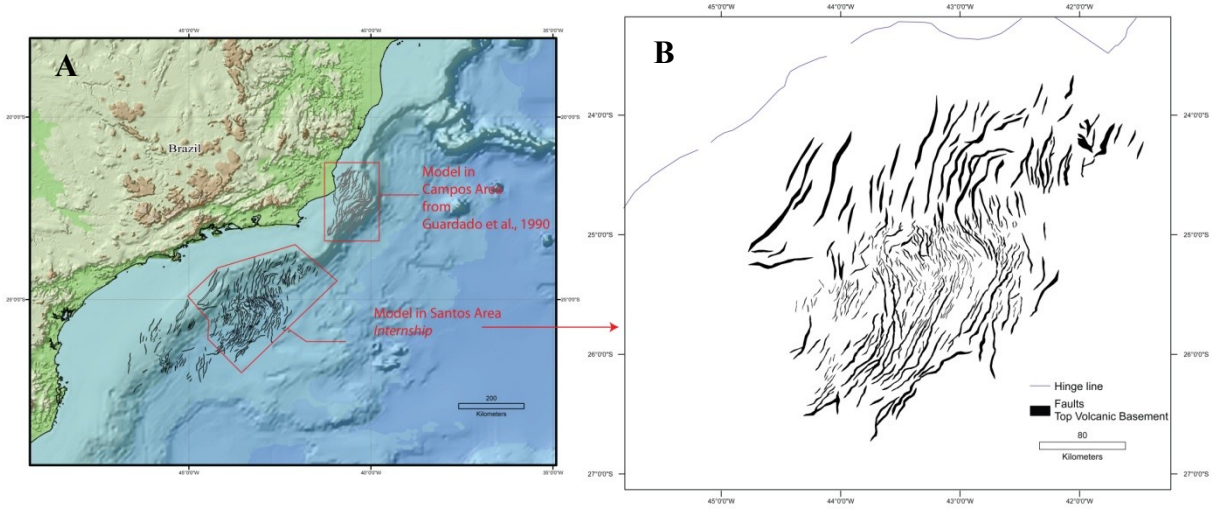

Figure 6.10. *A) Rift framework of Santos and Campos basins on a topographic map (restoration in Appendix). B) Structure map on top volcanic Basement displaying rift framework of Santos Basin and a sigmoid trend of faults. Provided by Chevron.*

These NNE-SSW and NW-SE trends are also visible in the orientations of dykes that intruded in SE Brazil during the widespread magmatism of the Parana-Etendeka Province (**Figure 6.11**). The dykes of the Ponta Grossa Arch trend NW-SE, whereas those of the Sao Paulo – Rio de Janeiro area trend NNE-SSW, parallel to the coast (**Figure 6.11A**; e.g. *Hawkesworth et al.*, 2000; *Guedes et al.*, 2005; *Couthinho*, 2008). Emplacement of these dykes (approx. 138-127 Ma; **Figure 6.12;** e.g. *Hawkesworth et al.*, 2000) was contemporaneous with rifting in the Santos Basin. Coast-parallel dyke swarms are common also in Namibia (**Figure 6.11B;** e.g. *Hawkesworth et al.*, 1992). *Coutinho* (2008) suggested that these dyke swarms represent the arms of a plume-generated triple junction of the opening

of the South Atlantic (**Figure 6.11 B**). The Ponta Grossa Arch dykes swarm would correspond to a failed rift arm (*Coutinho*, 2008).

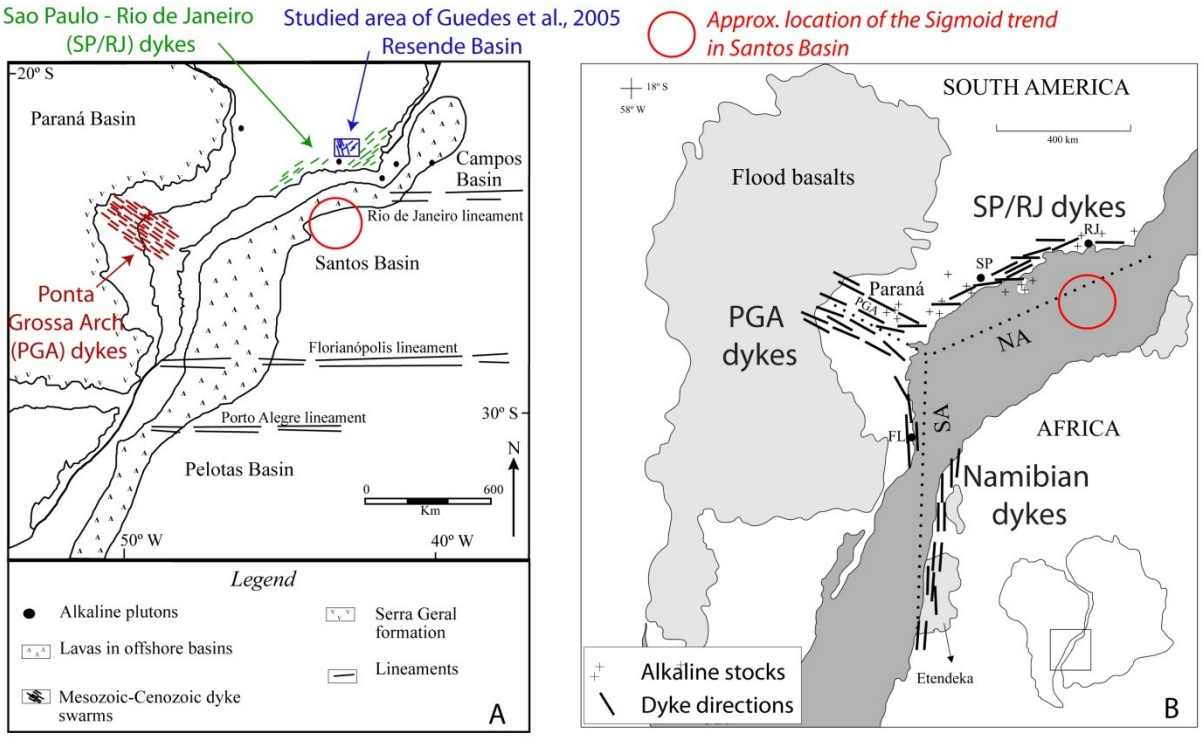

Figure 6.11. *A) Dyke swarm in SE Brazil (timing on Figure 6.11; modified from Guedes et al., 2005) and B) Pre-rift reconstruction of South Atlantic, South America and Africa showing Parana triple junction and correlation of dyke swarms in both continents (modified after Coutinho, 2008). Abbreviations: NA, North Arm; SA, South Arm; PGA, Ponta Grossa Arch (failed arm); RJ, Rio de Janeiro; MT, Montevideo; SP, Sao Paulo; FL, Florianopolis.*

The dykes follow pre-existing Gondwana structures, such as the Curitiba-Maringa and Guapiara fracture zones (**Figure 6.13**). Indeed, the SE Brazil has numerous shear zones, and fractures trending NNE-SSW and NW-SE that developed during the Panafrican Orogeny (**Figure 6.13**; e.g. *Eyes and Eyes*, 1993; *Mohriak and Rosendahl*, 2003). These Precambrian structures may have reactivated during the widespread magmatism of the Parana-Etendeka province and the South Atlantic opening, and so may have been responsible for the orientation of the dyke swarms. Moreover, the rift architecture of the Santos Basin, and of the whole South Atlantic margin, is controlled by NW-SE fracture zones that correspond to Precambrian structures in cratonic regions, such as SE Brazil (**Figure 6.14**; e.g. *Meisling et al.*, 2001; *Mohriak and Rosendahl*, 2003).

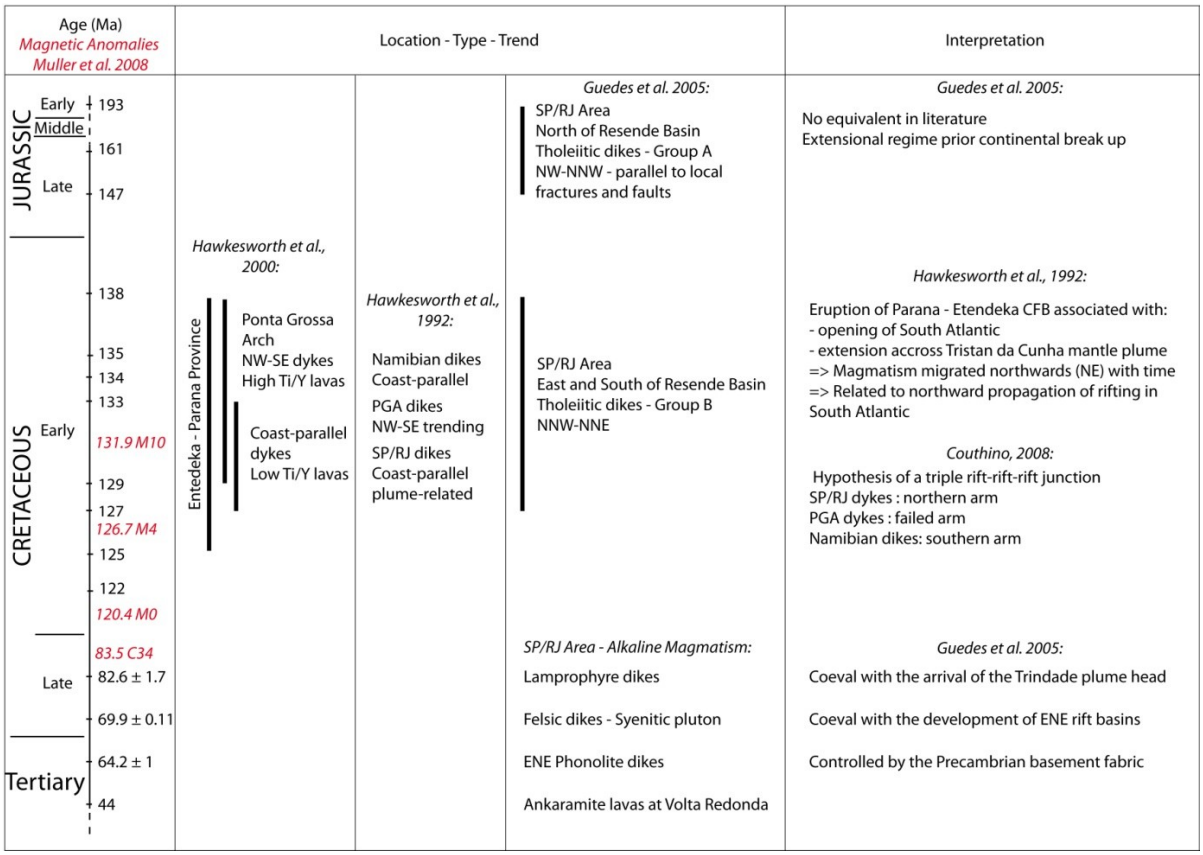

Figure 6.12. *Timing and interpretation of dyke emplacement in Santos Area (from Hawkesworth et al., 1992, 2000; Guedes et al., 2005; Couthino, 2008).*

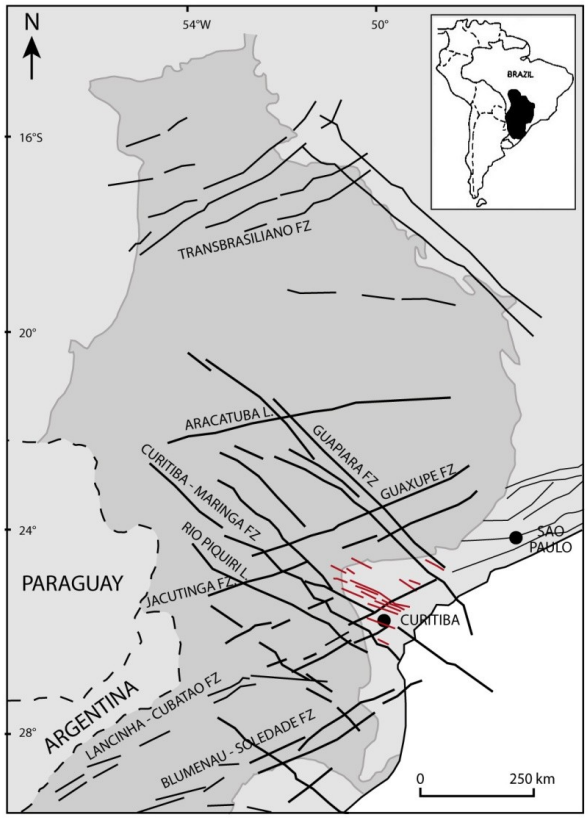

Figure 6.13. *Principal structural lineaments (L) and fault zones (FZ) of SE Brazil. Ponta Grossa Arch dyke swarm is in red. Trends of lineaments and fault zones (NE-SW and NW-SE) coincide with trends of dyke swarm. Modified from Eyes and Eyes (1993).*

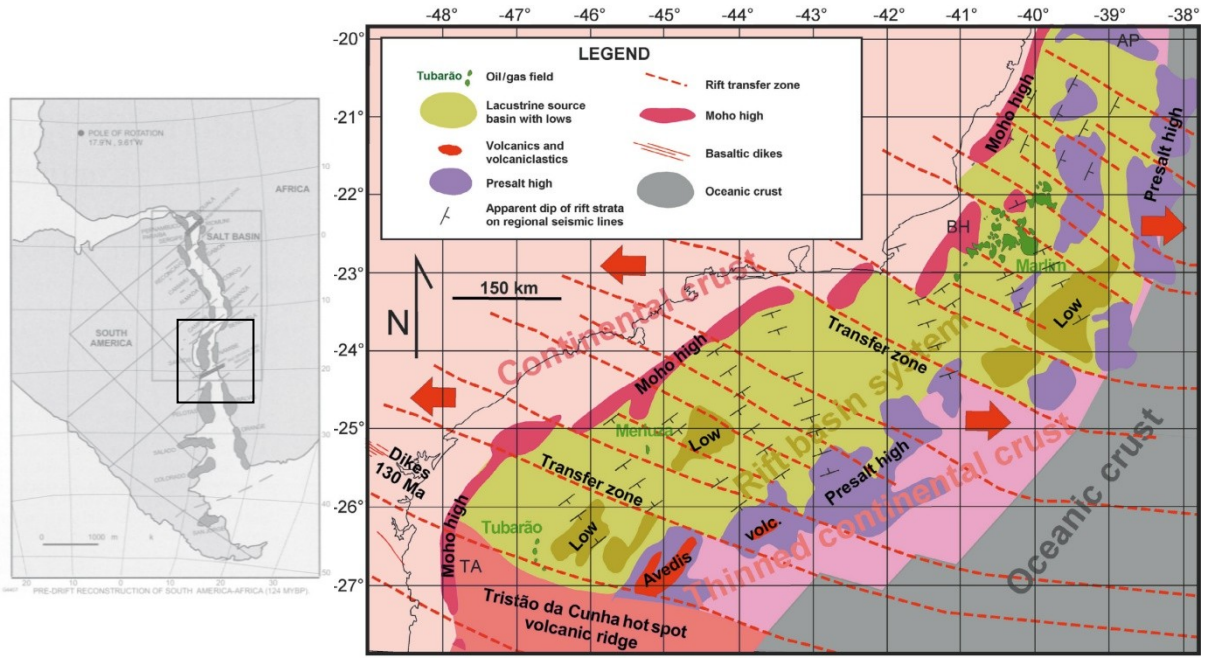

Figure 6.14. *Rift architecture of Santos and Campos basins controlled by NW-SE trending fracture zones. Left: Reconstruction shows conjugate sedimentary basins in the south Atlantic, segmented by fracture zones (from Mohriak and Rosendahl, 2003). Right: Map of main rift-related structural provinces, Campos and Santos basins.*

These pre-existing structures represent some weak lithospheric zones that are reactivated during plume-related magmatic event (emplacement of dyke swarms and Parana-Etendeka province) and during rifting of the South Atlantic. Indeed, the reactivation of pre-existing structures should require less stress than the formation of new structures. Such reactivation occurred on the NE Atlantic continental margin during a post breakup compressional deformation phase (e.g. *Doré and Lundin*, 1996; *Tuitt et al.*, 2010; **Chapter 4**). The SE Brazilian Margin was also subject to a post-breakup reactivation. I will discuss in the following section the possible influence of mantle plumes on post-breakup reactivation.

6.2.2 Mantle plumes and reactivation of pre-existing structures on continental margins

The NW-SE trending fracture zones in the Santos and Campos basins were reactivated in compression during the Late Cretaceous and Cenozoic (**Figure 6.15**, e.g. *Cobbold et al.*, 2001, 2007). *Cobbold et al.* (2001) have suggested that this area was softened by hotspot magmatism and reactivated right-laterally, whereas transfer faults reactivated left-laterally (**Figure 6.15**). The phases of reactivation coincide with phases of Andean Orogeny (**Figure 6.7**). Thus, it appears that the Tristan da Cunha plume influenced the SE Brazilian margin.

Indeed, magmatic activity from the plume appears to have weakened the thinned continental crust, which therefore deformed more easily in response to far-field compressional stress of the Andean Orogeny.

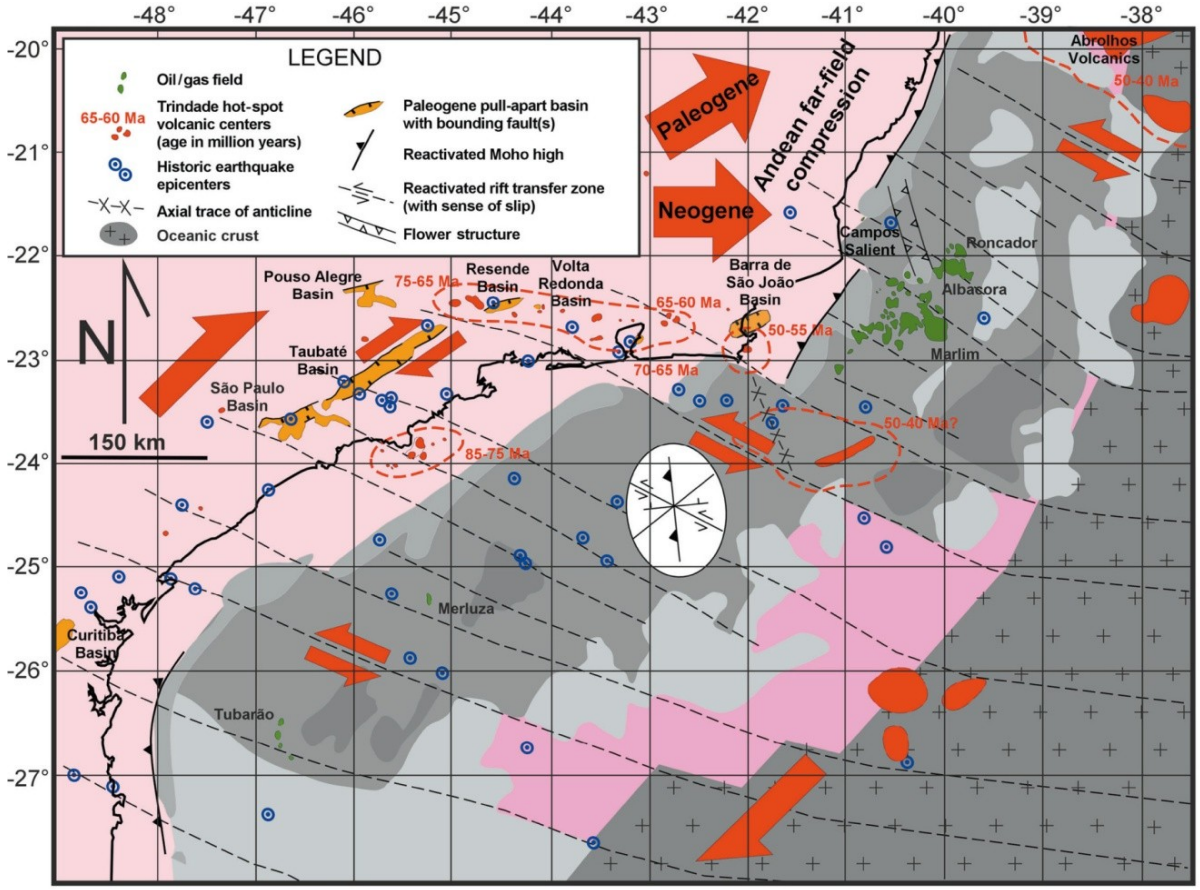

Figure 6.15. *Map showing compressional reactivation of segmented rift system, SE Brazil. From Cobbold et al. (2001).*

In the NE Atlantic, the Iceland Plume was in a position to generate variation of sea-floor spreading and compressional deformation of the NW European Margin (**Chapter 4**). This compressional deformation is mostly located along NW-SE fracture zones that segment the margin (**Figure 6.16**) and has most likely reactivated pre-existing structures of Lewisian and Caledonian ages (**Chapter 4**). Moreover, radial compressional stresses from the Iceland Plume, visible at the present-time on the world stress map (**Figure 6.17;** *Cobbold,* 2008), may reactivated oceanic fracture zones and NW-SE trending fautls on the margin (**Figure 6.16**).

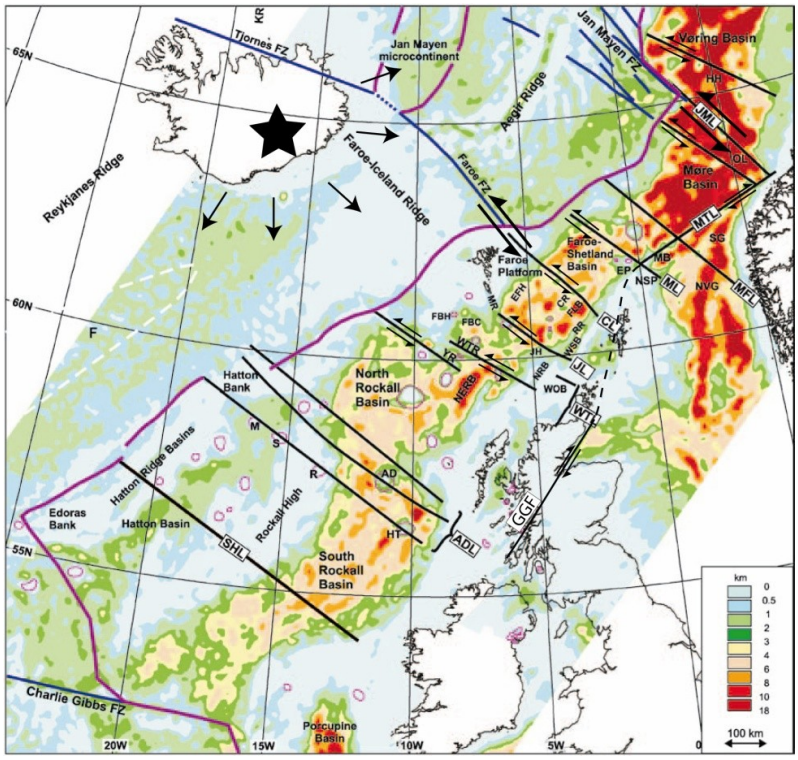

Figure 6.16. *Map of NW-SE lineaments that segment the NW European Margin, modified from Kimbell et al. (2005). Radial compressional stress (arrow) from Iceland Plume may have reactivated these NW-SE faults (Cobbold et al., 2008).*

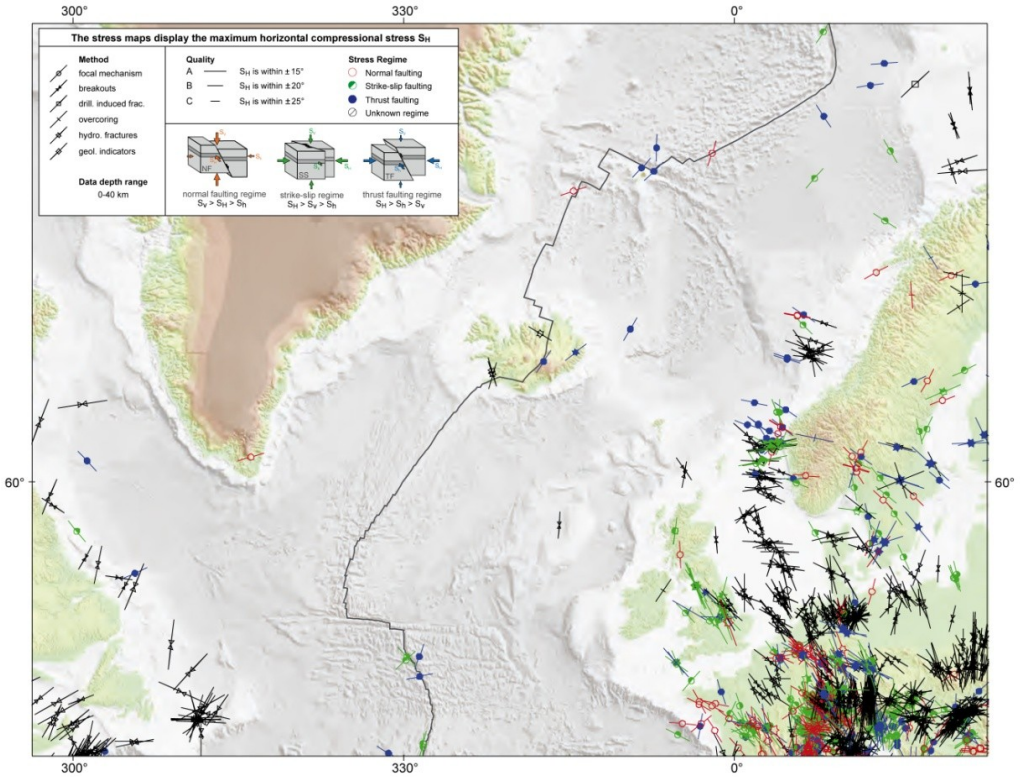

Figure 6.17. *Stress map of NE Atlantic Region (from World Stress Map, Heidbach et al., 2008) showing radial horizontal stress pattern around Iceland Plateau (Cobbold, 2008).*

Therefore, some possible influences of mantle plumes on structural development and evolution of continental margins are: 1) to weaken the continental margin, by intense magmatic activity, and therefore facilitate reactivation and deformation of the margin (e.g. the SE Brazilian Margin); 2) to generate radial stress and reactivate fracture zones on continental margin (e.g. the NW European Margin), and 3) to induce some variations in direction and rate of sea-floor spreading across oceanic fracture zones (e.g. NE Atlantic) and subsequent compressional deformation of the adjacent margin. Other examples of mantle plume influence on plate motion are suggested for example by *Cande and Stegman* (2011) in the Indian Ocean. Push forces of the Reunion plume head is suggested to have driven Indian and African plate motion in Late Cretaceous and Early Cenozoic time and subsequent tectonic events such as the possible cessation of convergence between Africa and Eurasia in the Palaeocene epoch and the bends of the fracture zones on the Southwest Indian Ridge (*Cande and Stegman*, 2011). Mantle plumes may therefore have an important role in plate motions and intraplate deformation.

Chapter 7

Conclusions

In this last part, I will review the main results of each chapter and synthesise them with respect to the main question of this thesis, developed in Chapter 1: What are the cause and consequences of differential sea-floor spreading along the NE Atlantic ridge system? Then, I will discuss the implications of these results and propose some research outlooks that arise from this study.

7.1 Main results

7.1.1 Characterization of differential sea-floor spreading along NE Atlantic

Chapters 2 and 3 present the context of this study and the method used to reconstruct the opening of the NE Atlantic. The best kinematic reconstructions came from subdividing the NE Atlantic into three oceanic segments (Reykjanes, Jan Mayen and Mohns). I have used a method of palinspastic restoration that allows each oceanic segment to spread at a different rate. The method yields the spreading rates and relative displacements between the segments.

Chapter 4 presents a new kinematic reconstruction of Europe, relative to a stationary Greenland plate, during opening of the NE Atlantic. The model takes into account the formation of the JMMC and deformation of the NW European Continental Margin during sea-floor spreading. Moreover it ensures a good fit of magnetic anomalies for the complex Jan Mayen Segment, especially around the Aegir Ridge. The model predicts variations in direction and rate of spreading between the Reykjanes, Jan Mayen and Mohns segments. Between Chron 24 (52.9 Ma) and Chrons 13 (33.3 Ma) to 8 (26.4 Ma), the Jan Mayen Segment had a complex spreading history. Rifting of the JMMC off Greenland generated counter-clockwise rotation (~30°) of the JMMC. Contemporaneous fan-shaped spreading

along the Aegir Ridge generated clockwise rotation (~10°) of the eastern side of the Aegir Ridge.

7.1.2 Consequences of differential spreading on continental margins and interiors

I presented in Chapter 4 the estimates of relative displacements along the FFZ and JMFZ and relative rotation of each segment that resulted from differential sea-floor spreading between the Reykjanes, Aegir/Kolbeinsey and Mohns ridges. The kinematic model predicts a main period of left-lateral slip, of up to 45 km along the FFZ between Chron 21 and Chron 8 (Mid-Eocene to Late Oligocene) and up to 20 km along the JMFZ, between Chron 17 and Chron 13 (Late Eocene to Early Oligocene) and between Chron 8 and Chron 5 (Miocene). These two periods coincide with the development of compressional structures on the Faeroe-Rockall Plateau and Norwegian Margin, respectively.

Chapter 5 presents results of field observations of Jurassic outcrops, NE Scotland. This mission provided additional evidences of post-Jurassic right-lateral reactivation of the GGF under transpression. The amount of right-lateral displacement along the GGF is estimated at approx. 10-18 km. The timing of reactivation of the GGF remains uncertain; however I suggest that it reactivated right-laterally from Late Eocene to Late Oligocene, *c*. 37 and 26 Ma. This period coincides with (1) an exhumation episode in Scotland, (2) intraplate stress from the Alpine Orogeny (3) a pulse of the Iceland Mantle Plume, and more importantly with (3) left-lateral slip along the FFZ. Indeed, left-lateral slip along the FFZ is compatible with right-lateral reactivation of the GGF.

I therefore suggest that differential sea-floor spreading between the Reykjanes, Aegir/Kolbeinsey and Mohns ridges was responsible for:
(1) left-lateral reactivation of NW-SE trending lineaments along the line of the JMFZ, in the Late Eocene to Early Oligocene and mostly during the Miocene, and resulting development of inversion structures on the Norwegian Margin;
(2) a constrictional strain, for which the principal directions of shortening trend approximately N-S and E-W, left-lateral strike-slip along NW-trending transfer zones and reactivation of pre-existing structures of Lewisian age (trending NW-SE, N-S and E-W) and Caledonian age (trending NE-SW) in the Eocene and Early Oligocene, resulting in the development of inversion structures of various trends (NW-SE to NE-SW) on the Faeroe-Rockall Plateau;

(3) left-lateral reactivation of NW-trending transfer zones sub-parallel to the FFZ that probably initiated the Fugløy Ridge in the NE Faeroe-Shetland Basin during the Eocene and Oligocene; and
(4) right-lateral reactivation of the GGF in Scotland, following the left-lateral reactivation of the FFZ.

7.1.3 Cause of differential spreading

I discussed in Chapters 4 and 5, the possible influence of the Iceland Mantle Plume on differential sea-floor spreading along the NE Atlantic. I suggest that the position of the Iceland Mantle Plume beneath the eastern Greenland margin, in the vicinity of the JMMC, in the Late Eocene and Oligocene, generated major plate readjustments within the Jan Mayen Segment, separation of the JMMC and subsequent differential spreading and deformation along the European Margin. During the Miocene, the Iceland Mantle Plume remained beneath the Reykjanes Ridge, and the resulting volcanic activity formed the Iceland Plateau. Spreading rates were greater along the Reykjanes Ridge, triggering relative displacements along the FFZ and JMFZ during the Miocene. Moreover, the radial stress generated from the Iceland Plateau could be responsible for left-lateral reactivation of the main oceanic fracture zones and compressional stress on the continental margin in the Miocene.

Chapter 6 presents a comparison of NE Atlantic and the South Atlantic (east of Santos and Campos basins). I discussed more generally the possible influences of mantle plume on (1) localisation of sea-floor spreading (‘ridge-jump’) and variation in spreading rates and (2) reactivation of pre-existing structures of continental margin. Indeed, it appears that the magmatic activity from the plume in interaction with a rifted continental margin may weaken the thinned continental crust and therefore favours the reactivation and the deformation of the margin in response to far-field compressional stress (e.g. SE Brazilian Margin). Moreover, the magma supply from mantle plume may increase spreading rates and localise sea-floor spreading triggering possible ‘ridge jump’ (e.g. between the Aegir and Kolbeinsey ridges in NE Atlantic). At last, push forces from mantle plume may generate compressional stress that transmit into the plates and may reactivate pre-existing structures of the adjacent continental margin (e.g. radial stress from the Iceland Plume in Miocene and compressional deformation of the NW European Margin).

7.2 Implications and Outlooks

The results of this thesis have implications for studies on plate motions, intraplate deformation and driving forces, as well as for petroleum exploration on continental margins. This work shows that lithospheric plates are not perfectly rigid and that mantle plumes and sea-floor spreading may have significant influences on the compressional post-breakup deformation of adjacent continental margins.

The NE Atlantic margins represent attractive hydrocarbon exploration targets for petroleum industry. This study provides a new kinematic model for the opening of the NE Atlantic and therefore a new interpretation of the paleoposition of Europe relative to Greenland at the time of breakup, both of which have implications for petroleum exploration of conjugate margins. Moreover, this study provides new interpretations of mechanisms at the origin of compressional deformation, which may be responsible for petroleum traps on the European Margin. Further studies would be necessary to improve estimates of the timing of these compressional structures and the amount of shortening. Also, magmatic activity from mantle plumes may have significantly influenced the heat flow history. This has implications for oil production in the basins. Therefore, further studies would be useful to estimate the spatial and temporal influences of a plume on a rifted continental margin.

This study also shows that differential sea-floor spreading may have reactivated continental lithospheric structures such as the Great Glen Fault (GGF) in Scotland. In the future, low-temperature geochronological studies may provide better constraints on the timing of reactivation of the GGF. Similar work along the Møre Trøndelag Fault (MTF), Norway, might provide better constraints on the relationship between differential spreading along the NE Atlantic and Tertiary reactivation of the GGF and MTF.

Several questions arise from this work. How much has differential sea-floor spreading affected the European continent? What are the exact forces that generate compressional deformation and exhumation on continental margins? How do mantle plumes influence continental margins and continental interiors? What are the forces generated by mantle plumes? How widely do mantle plumes influence lithospheric and surface processes?

Appendix Chapter 3

Appendix A: Independent restoration of each ridge system – TEST 1

Restoration of Reykjanes Ridge

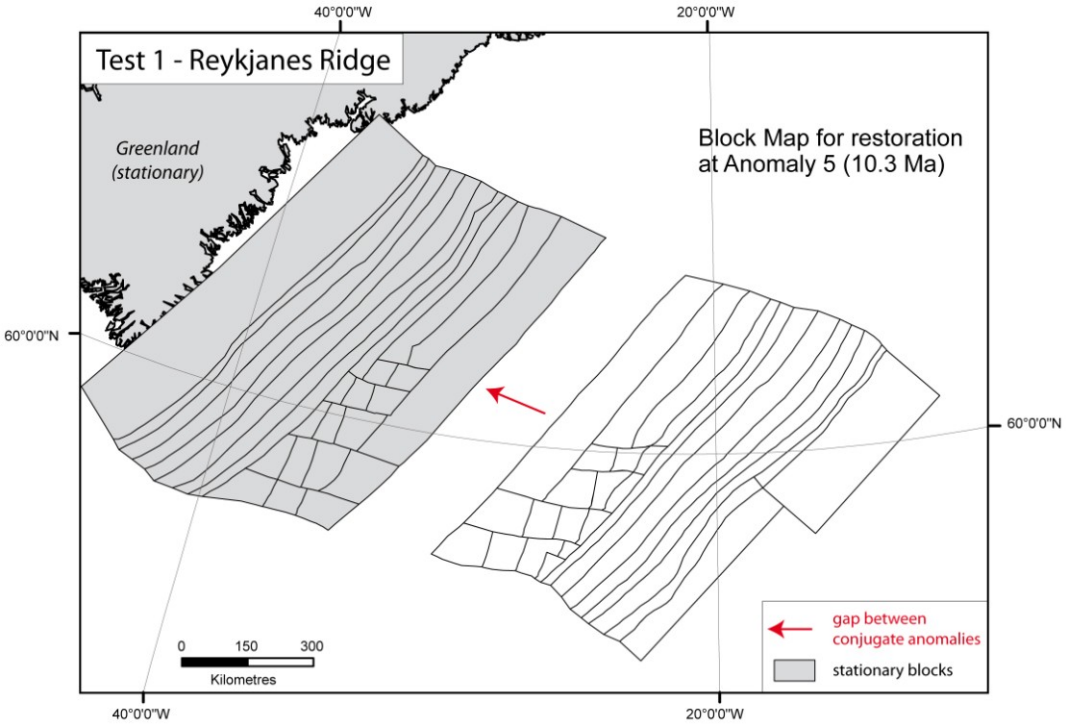

Figure1 *Block map for restoration of Reykjanes Ridge at Anomaly 5 (10.3 Ma)*

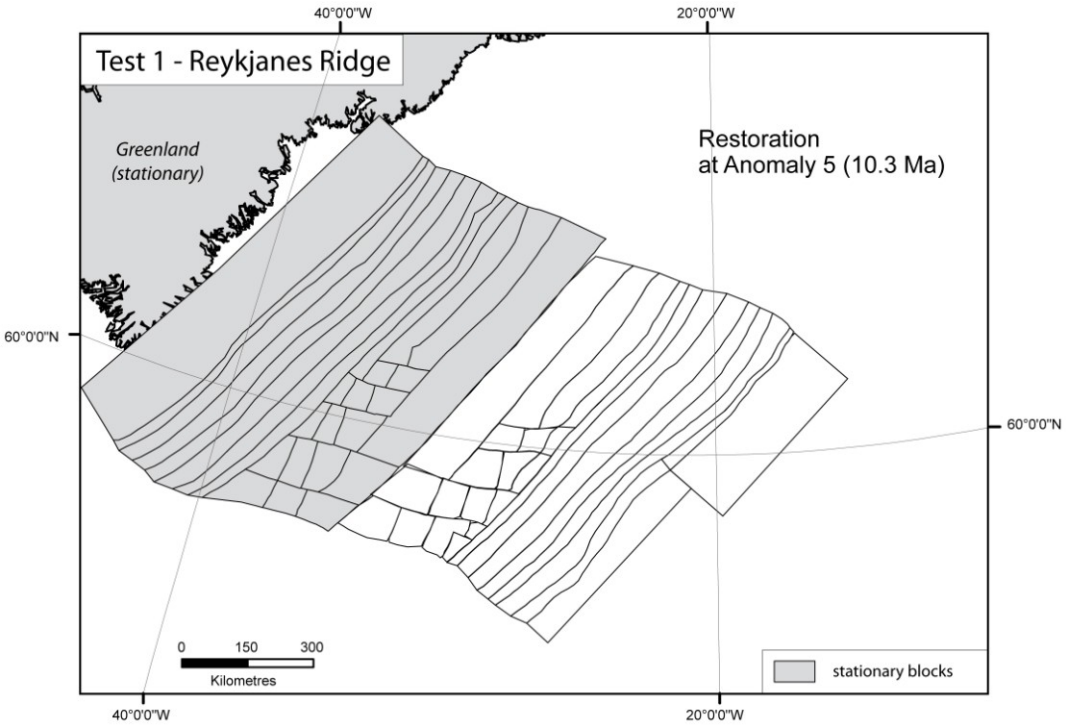

Figure 2 *Restoration of Reykjanes Ridge at Anomaly 5 (10.3 Ma), after 300 iterations*

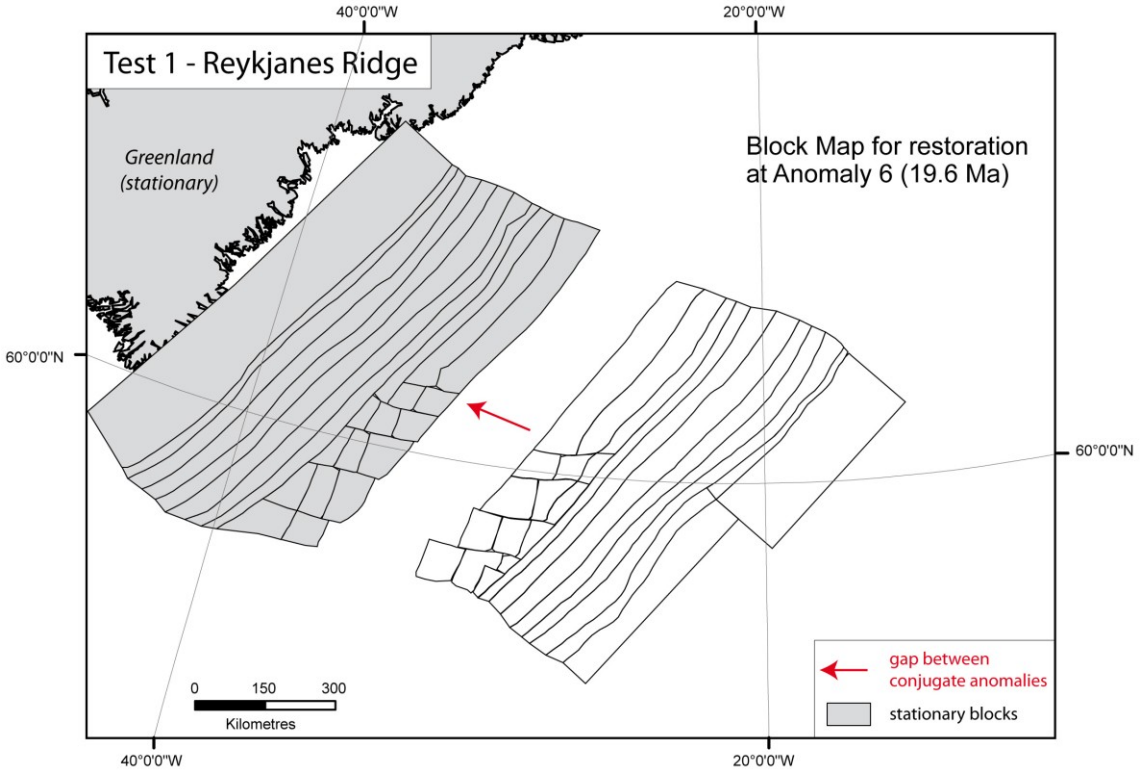

Figure 3 *Block map for restoration of Reykjanes Ridge at Anomaly 6 (19.6 Ma)*

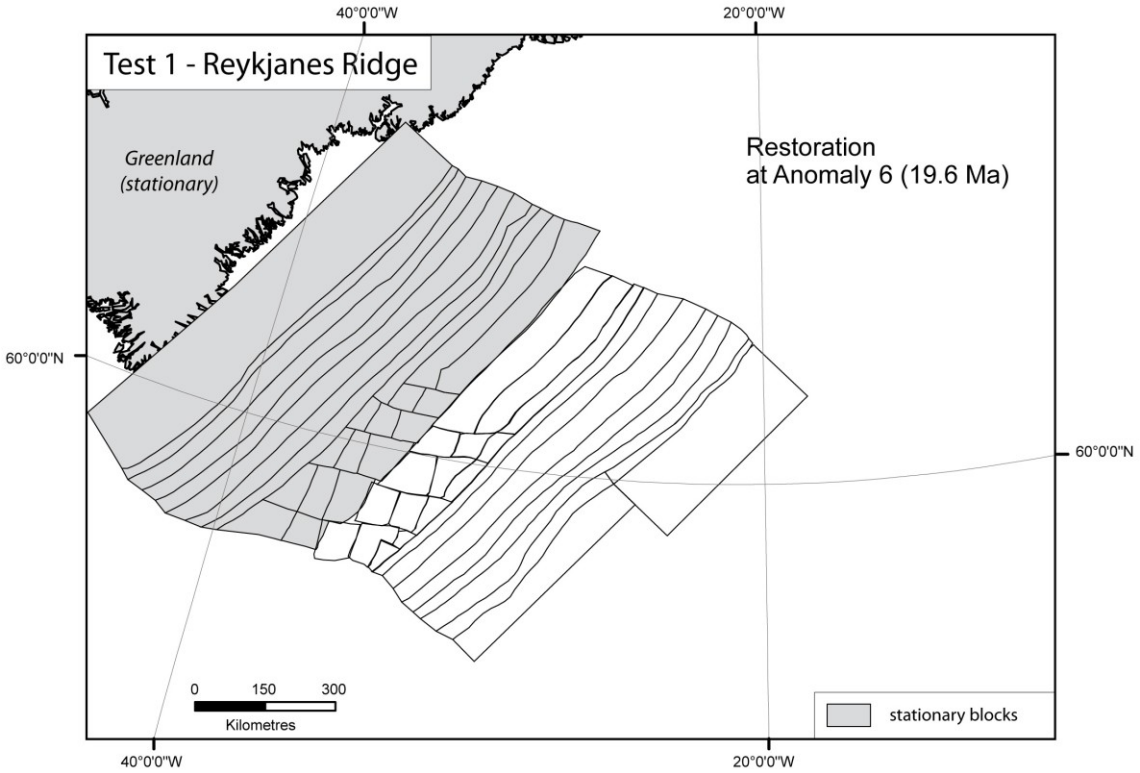

Figure 4 *Restoration of Reykjanes Ridge at Anomaly 6 (19.6 Ma), after 300 iterations*

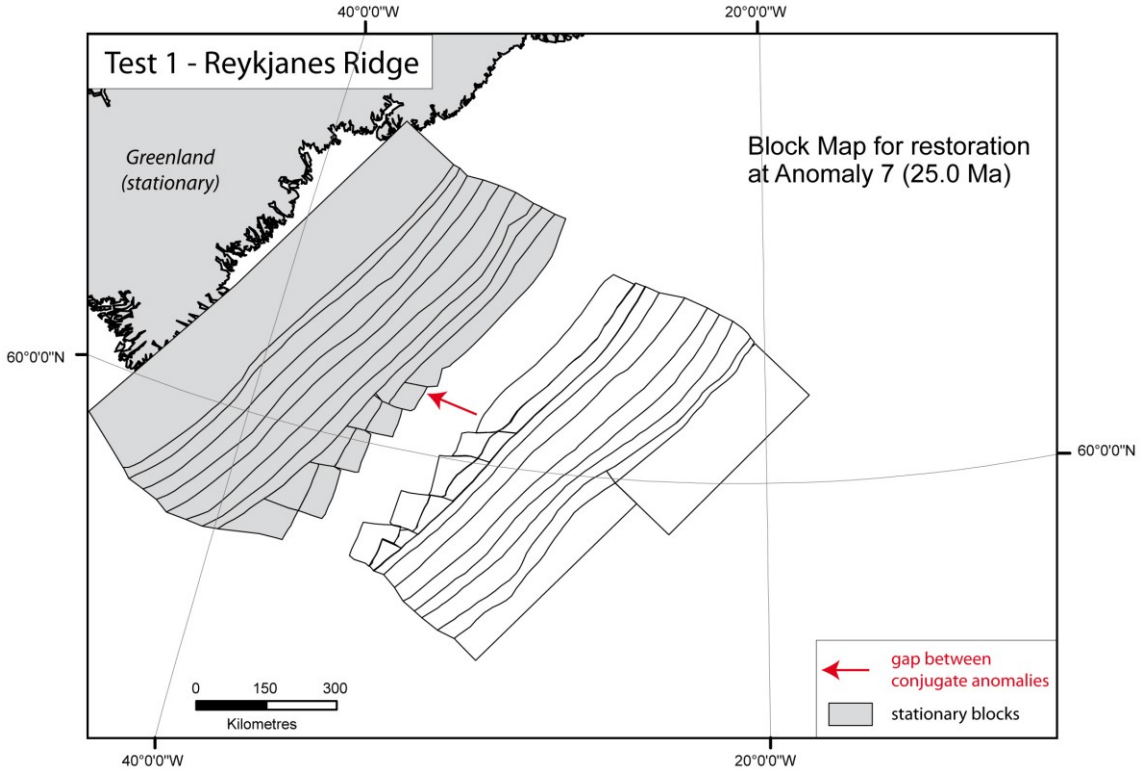

Figure 5 *Block map for restoration of Reykjanes Ridge at Anomaly 7 (25 Ma)*

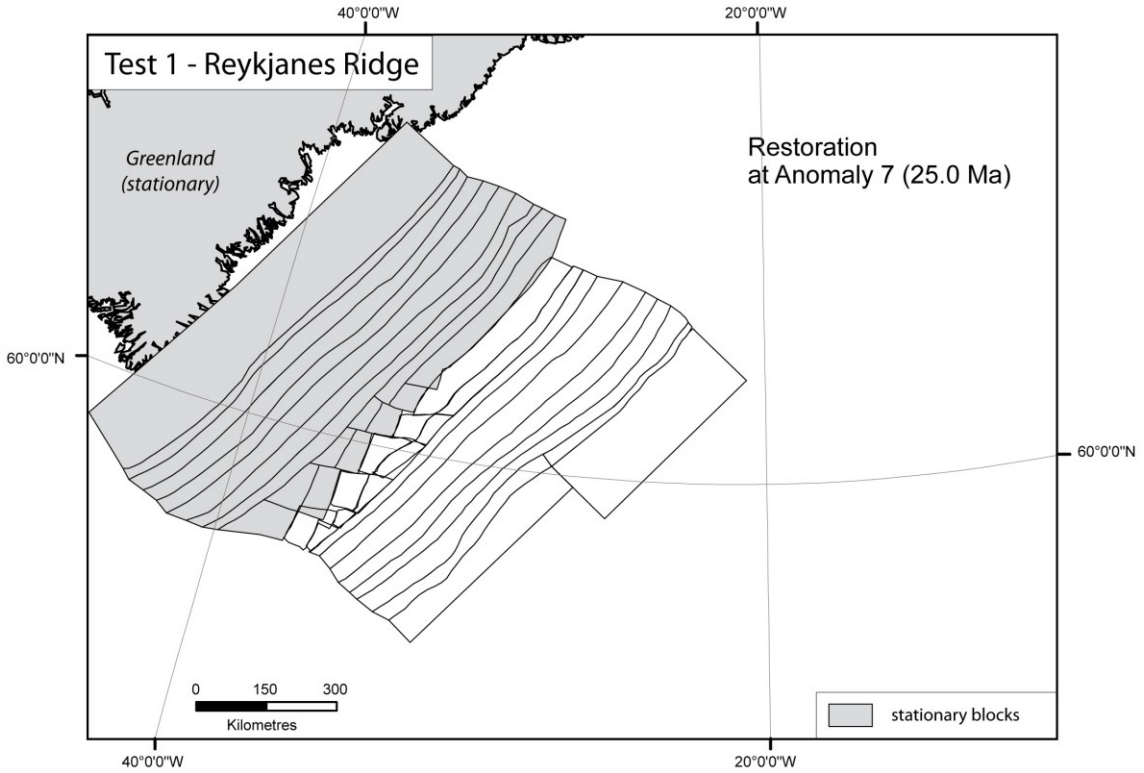

Figure 6 *Restoration of Reykjanes Ridge at Anomaly 7 (25Ma), after 500 iterations*

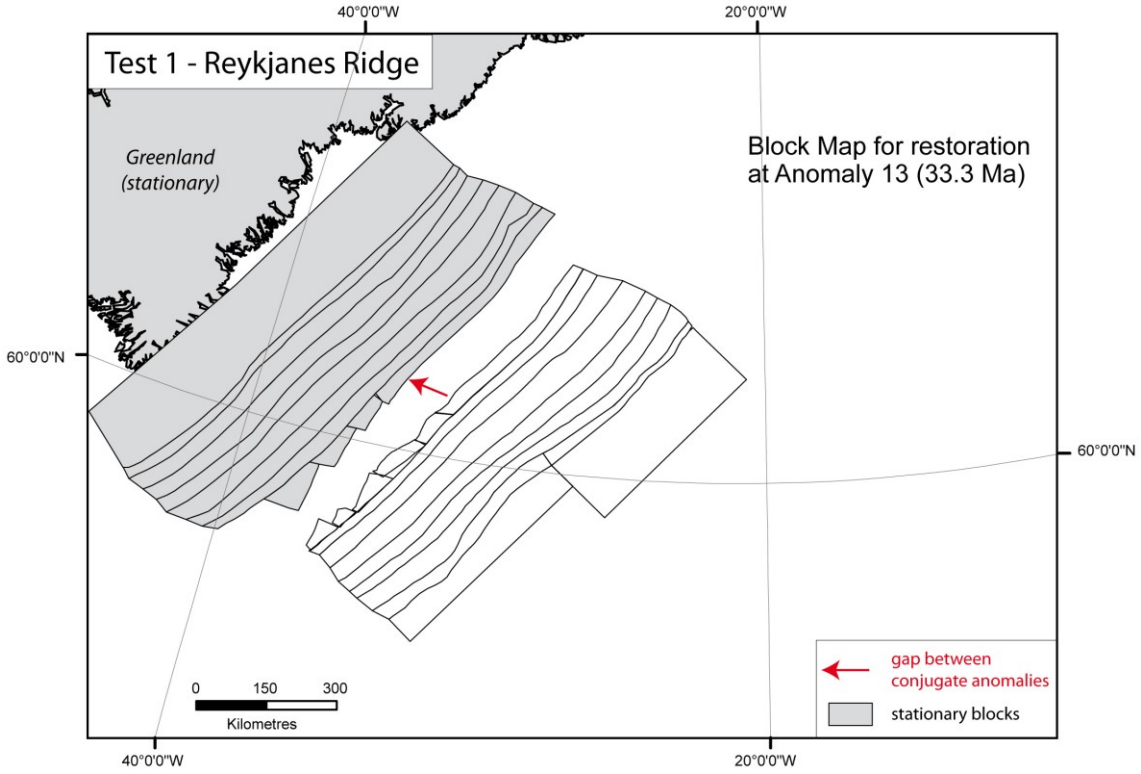

Figure 7 *Block map for restoration of Reykjanes Ridge at Anomaly 13 (33.3 Ma)*

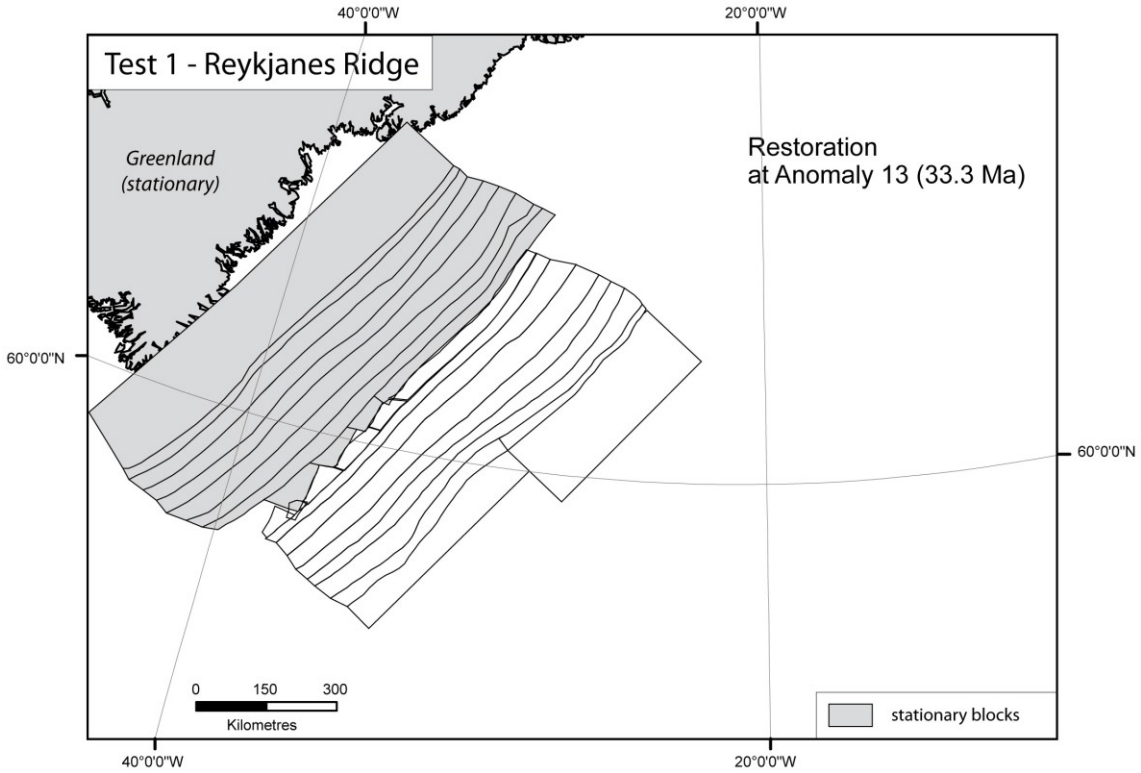

Figure 8 *Restoration of Reykjanes Ridge at Anomaly 13 (33.3 Ma), after 100 iterations*

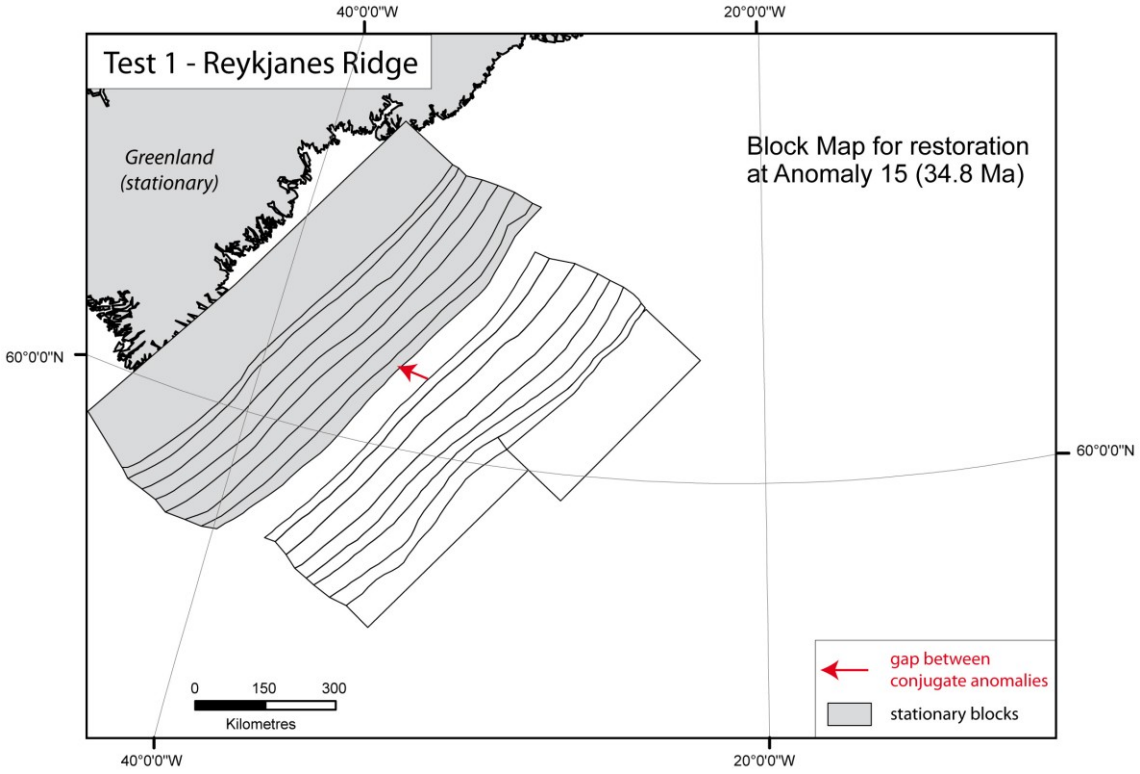

Figure 9 *Block map for restoration of Reykjanes Ridge at Anomaly 15 (34.8 Ma)*

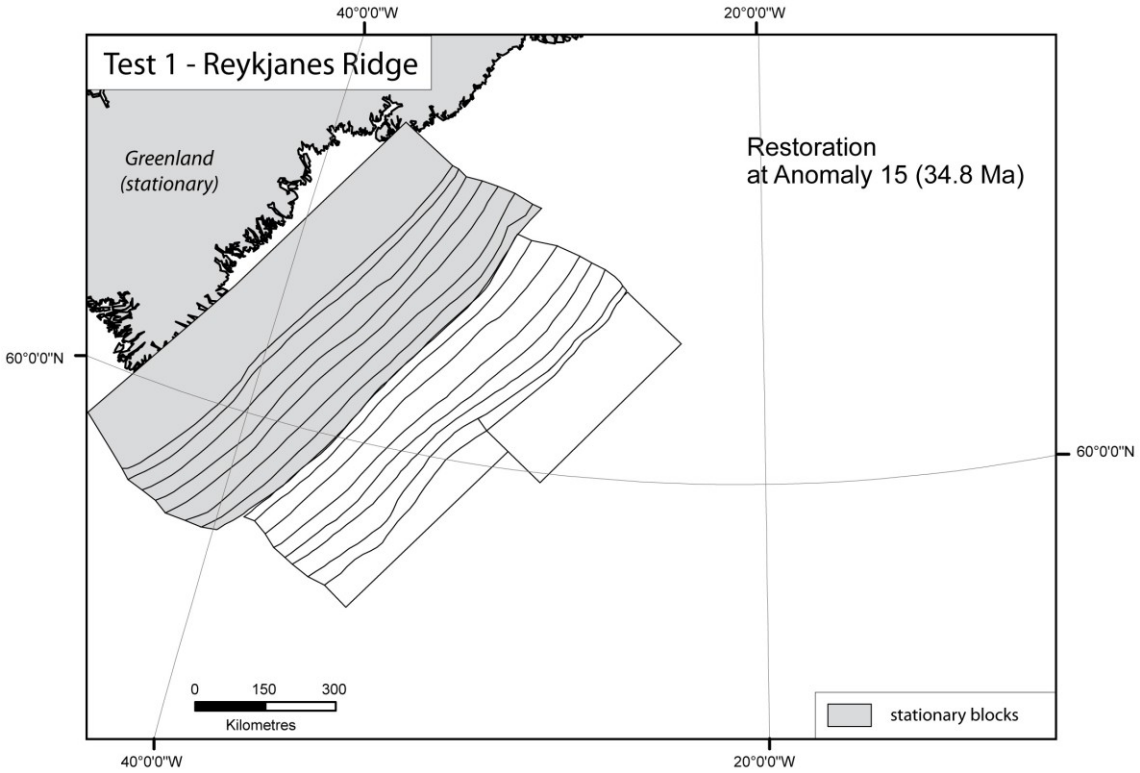

Figure 10 *Restoration of Reykjanes Ridge at Anomaly 15 (34.8 Ma), after 200 iterations*

Restoration of Mohns Ridge

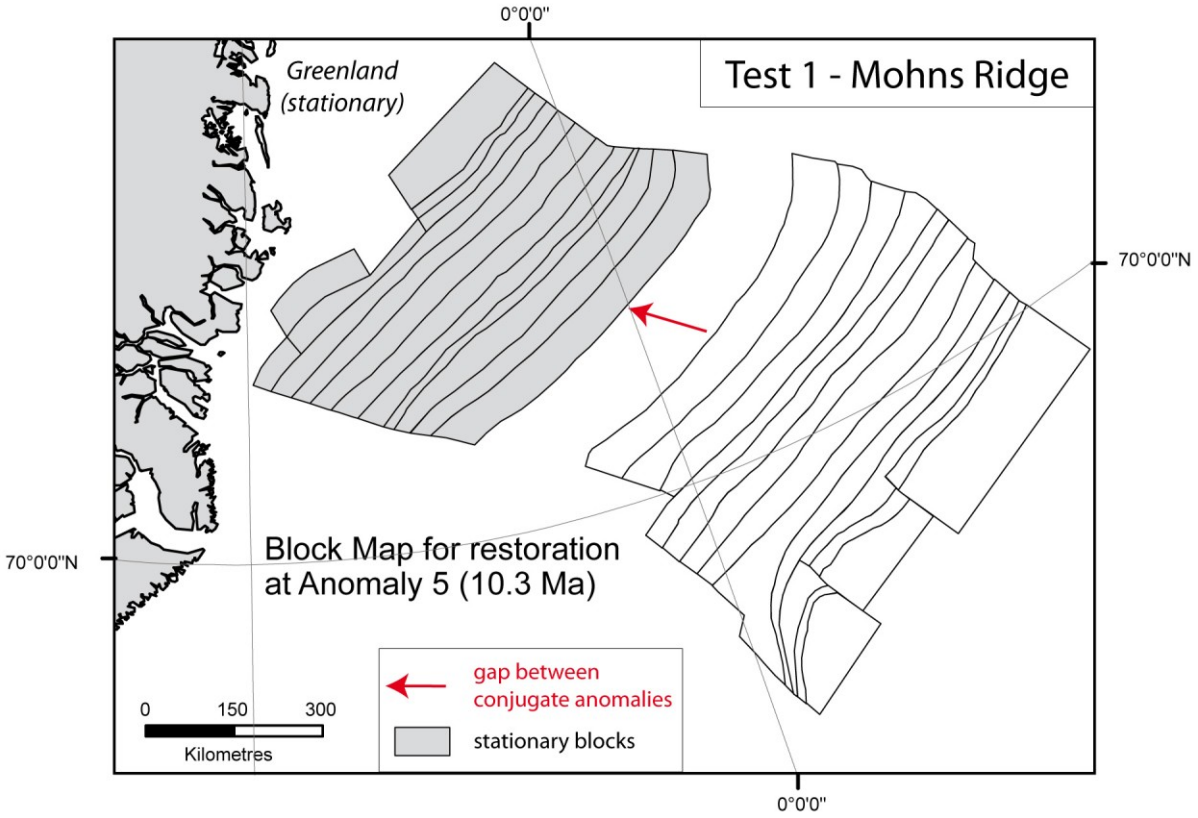

Figure 11 *Block map for restoration of Mohns Ridge at Anomaly 5 (10.3 Ma)*

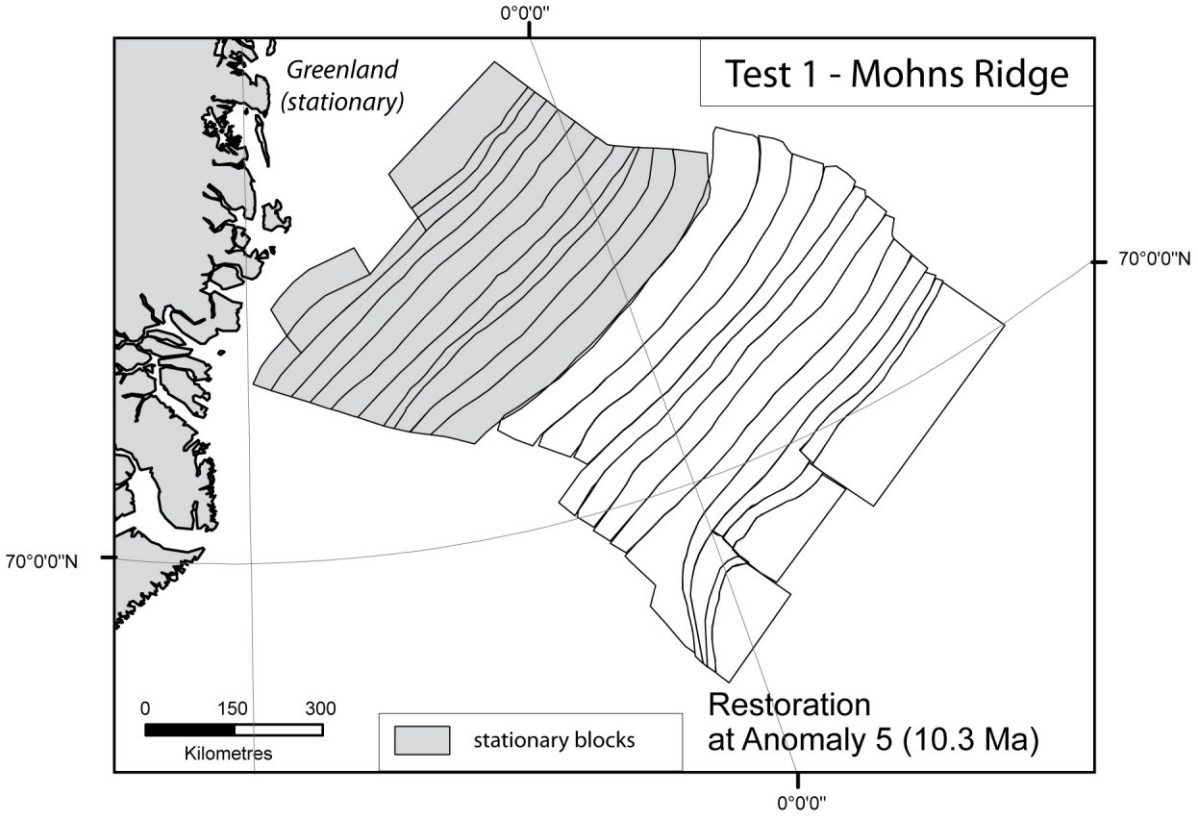

Figure 12 *Restoration of Mohns Ridge at Anomaly 5 (10.3 Ma), after 200 iterations*

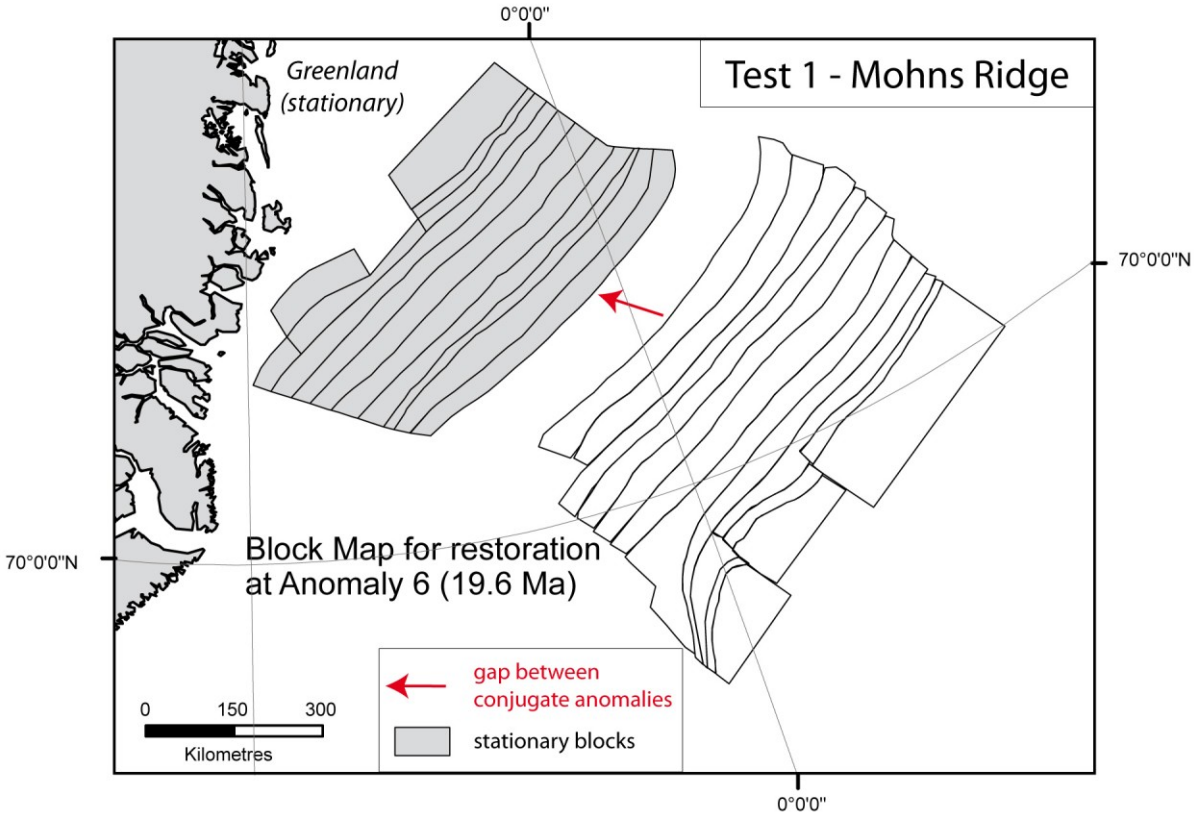

Figure 13 *Block map for restoration of Mohns Ridge at Anomaly 6 (19.6 Ma)*

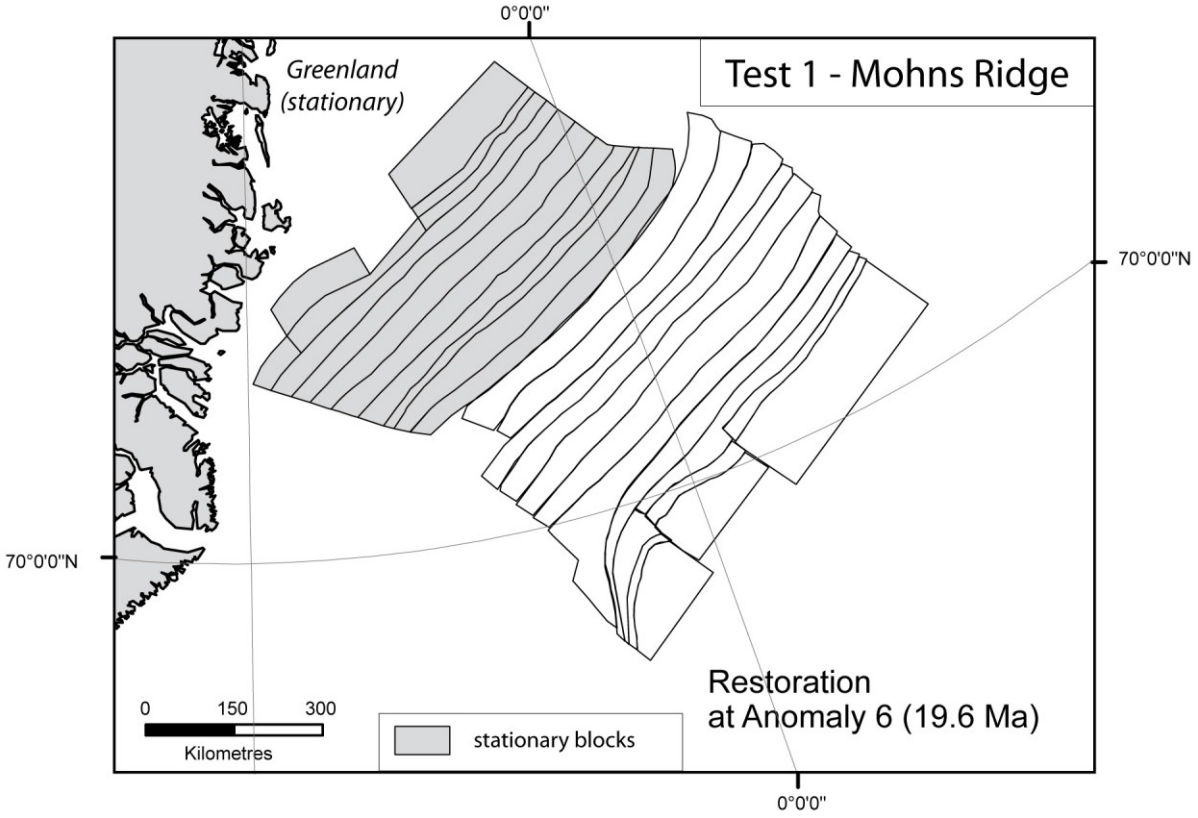

Figure 14 *Restoration of Mohns Ridge at Anomaly 6 (19.6 Ma), after 200 iterations*

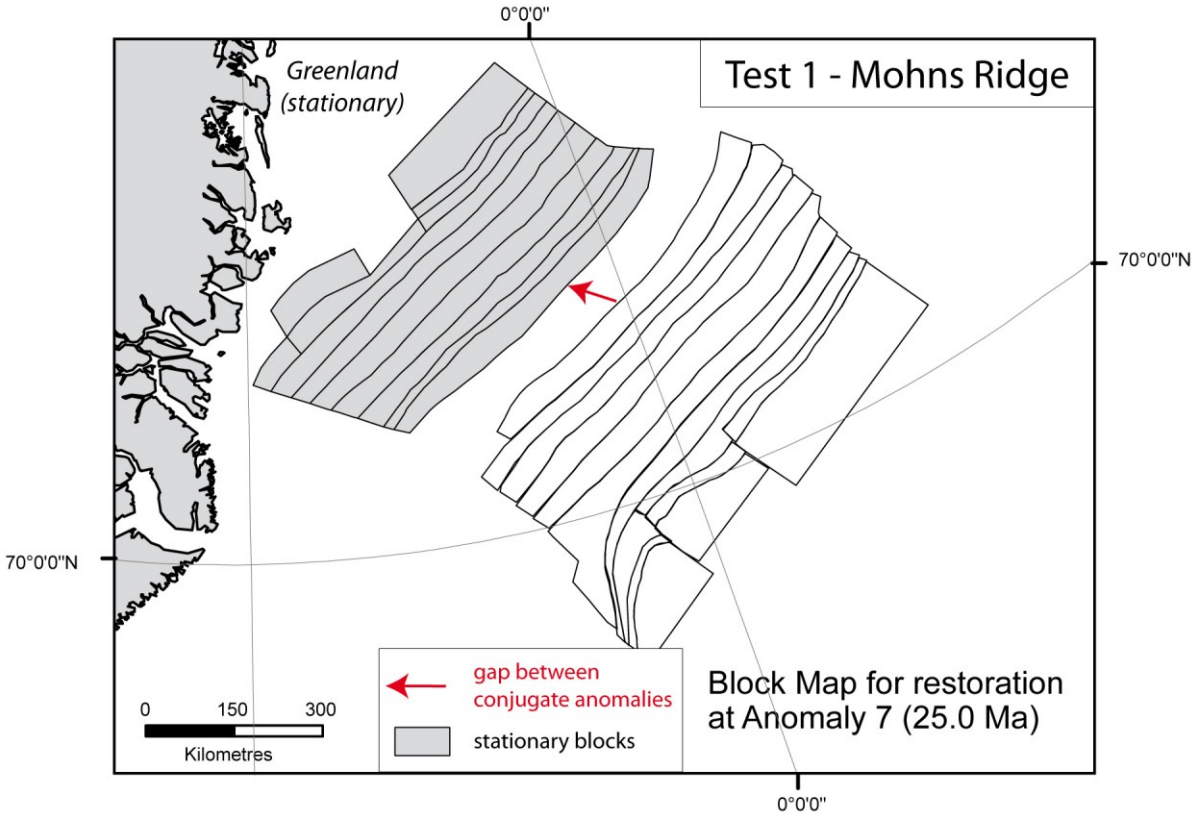

Figure 15 *Block map for restoration of Mohns Ridge at Anomaly 7 (25 Ma)*

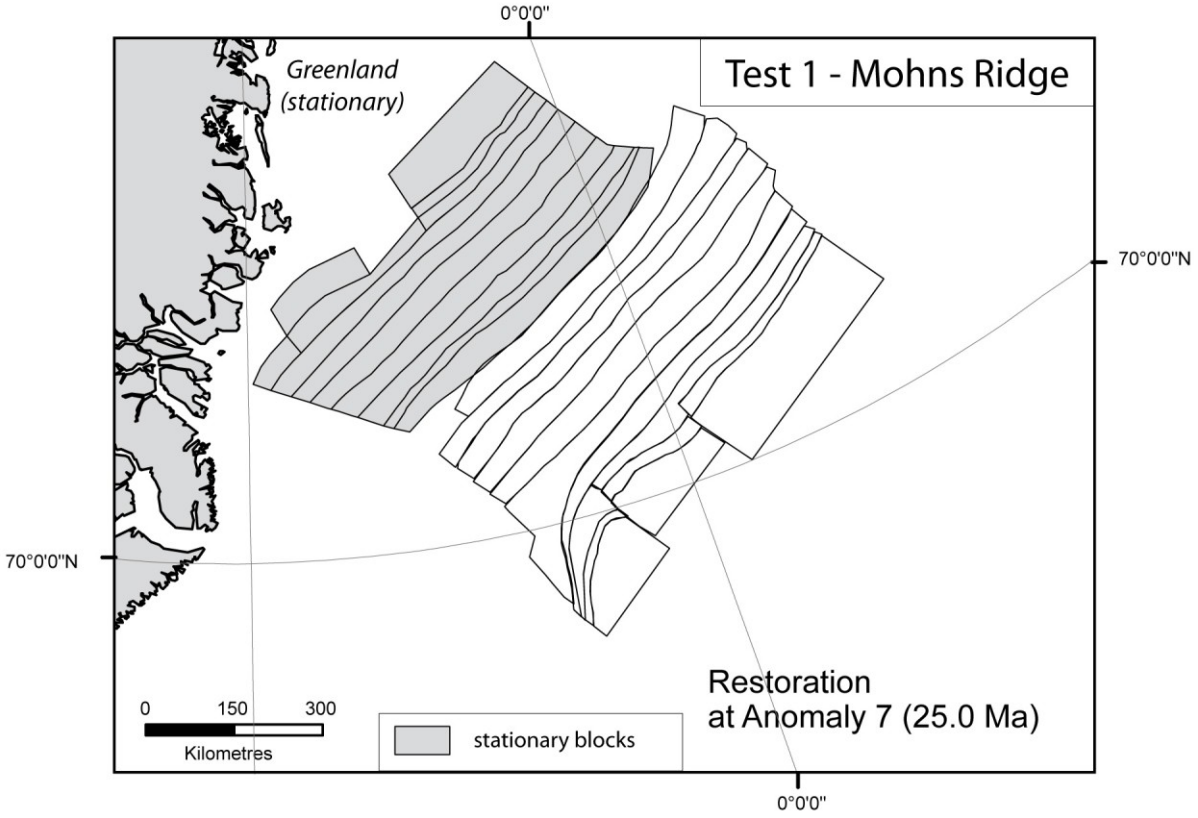

Figure 16 *Restoration of Mohns Ridge at Anomaly 7 (25 Ma), after 200 iterations*

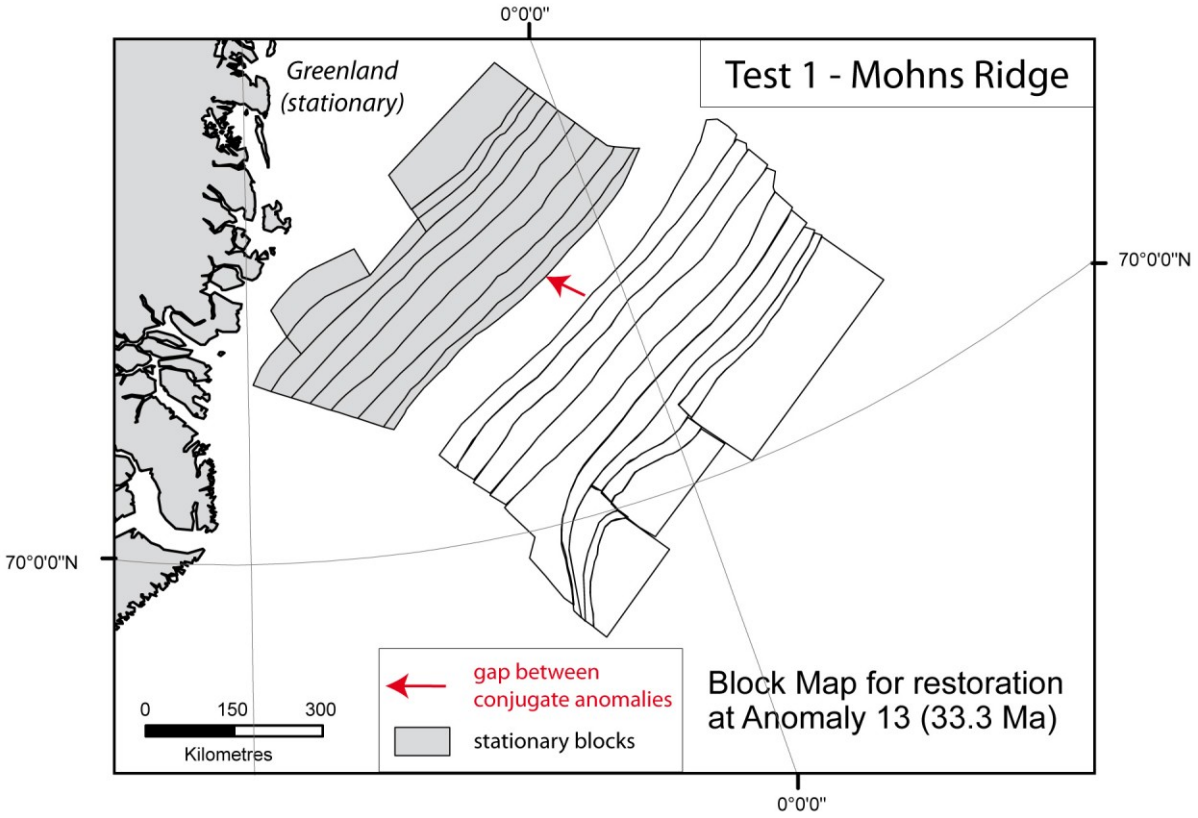

Figure 17 *Block map for restoration of Mohns Ridge at Anomaly 13 (33.3 Ma)*

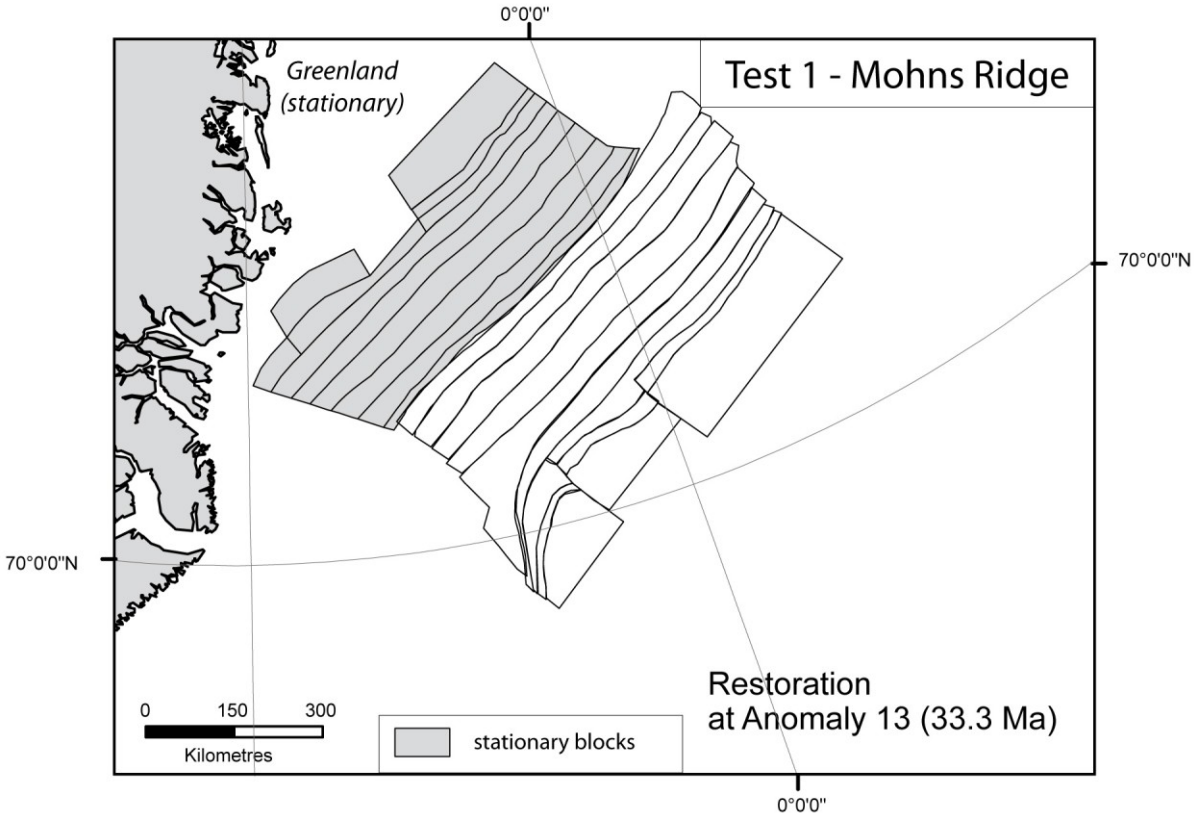

Figure 18 *Restoration of Mohns Ridge at Anomaly 13 (33.3 Ma), after 200 iterations*

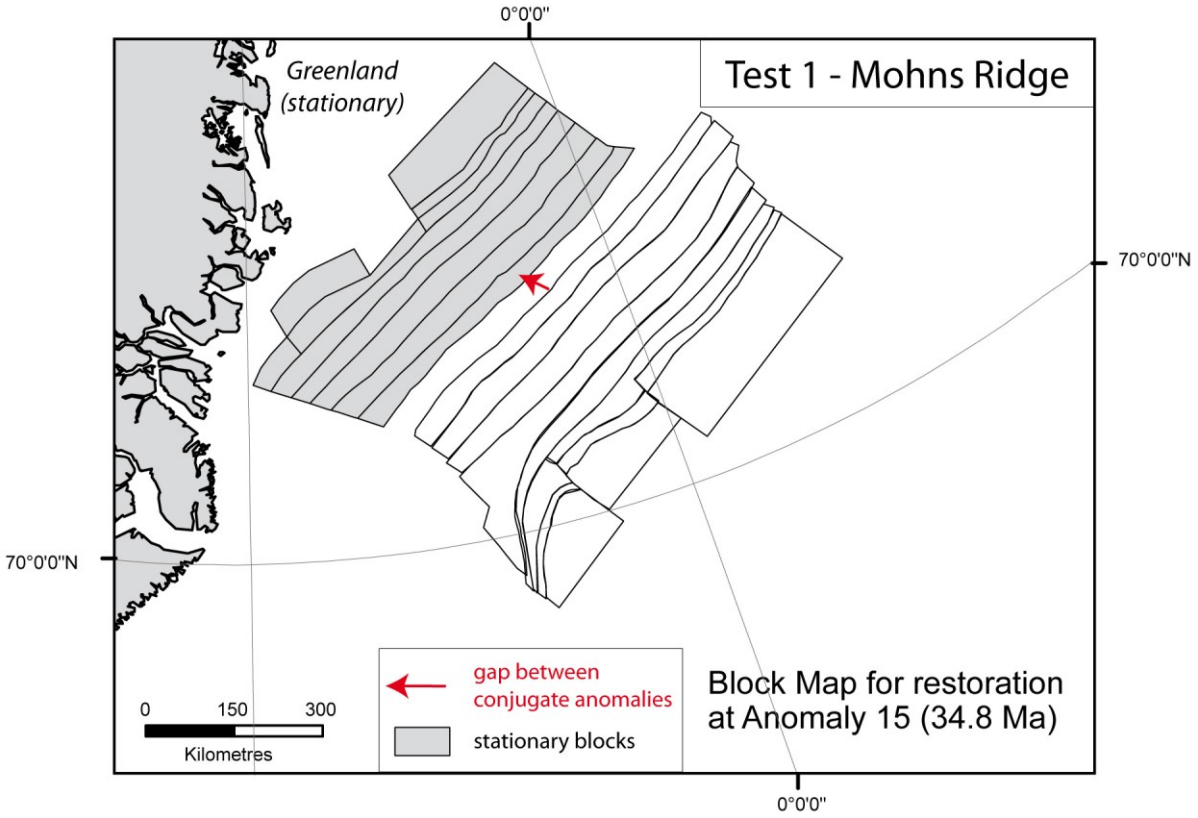

Figure 19 *Block map for restoration of Mohns Ridge at Anomaly 15 (34.8 Ma)*

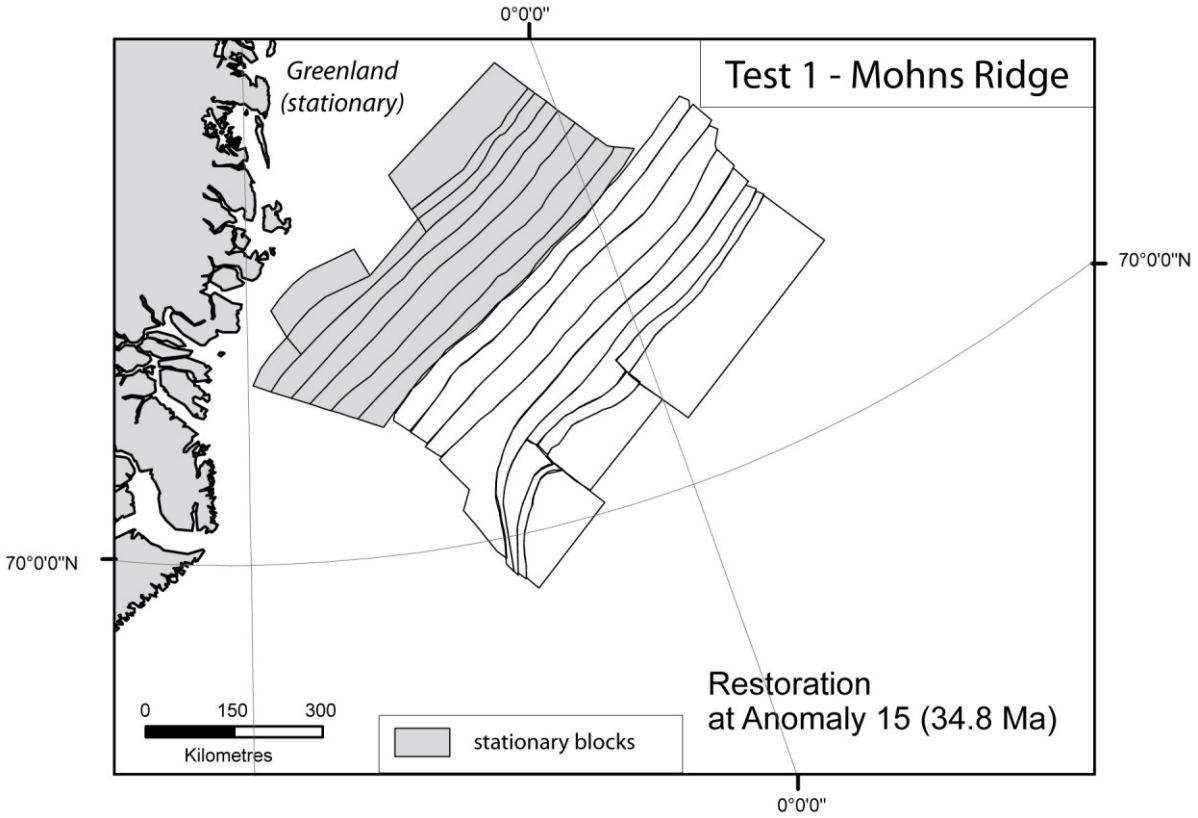

Figure 20 *Restoration of Mohns Ridge at Anomaly 15 (34.8 Ma), after 400 iterations*

Restoration of Kolbeinsey Ridge

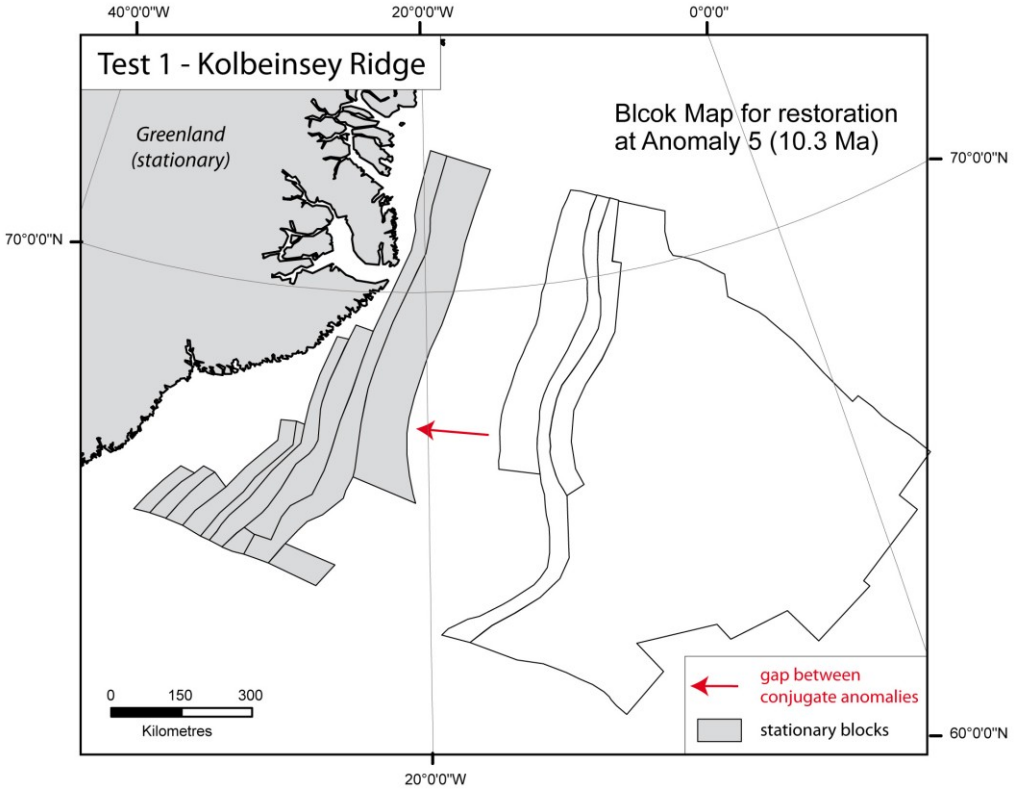

Figure 21 *Block map for restoration of Kolbeinsey Ridge at Anomaly 5 (10.3 Ma)*

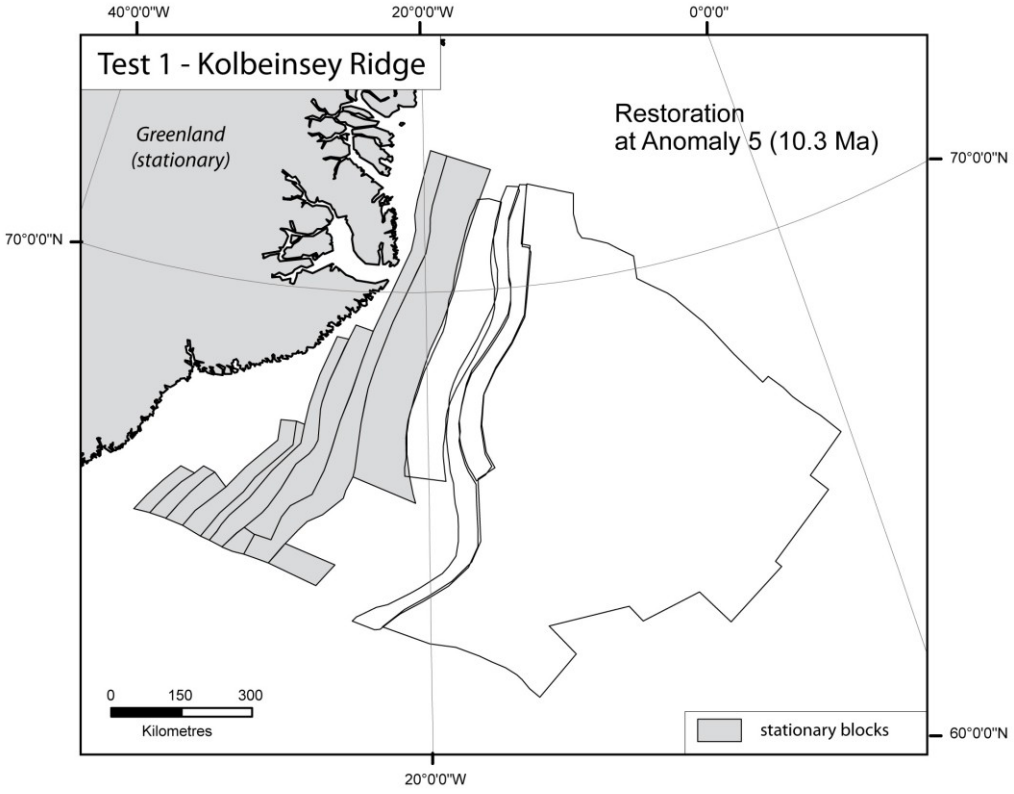

Figure 22 *Restoration of Kolbeinsey Ridge at Anomaly 5 (10.3 Ma), after 200 iterations*

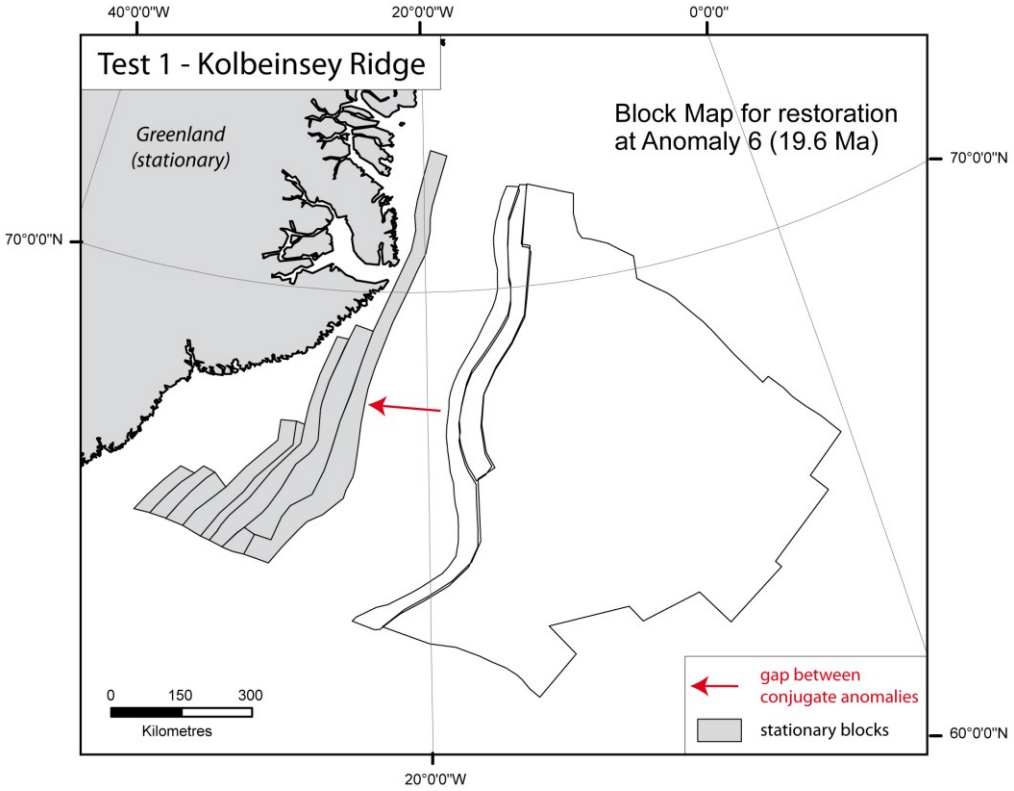

Figure 23 *Block map for restoration of Kolbeinsey Ridge at Anomaly 6 (19.6 Ma)*

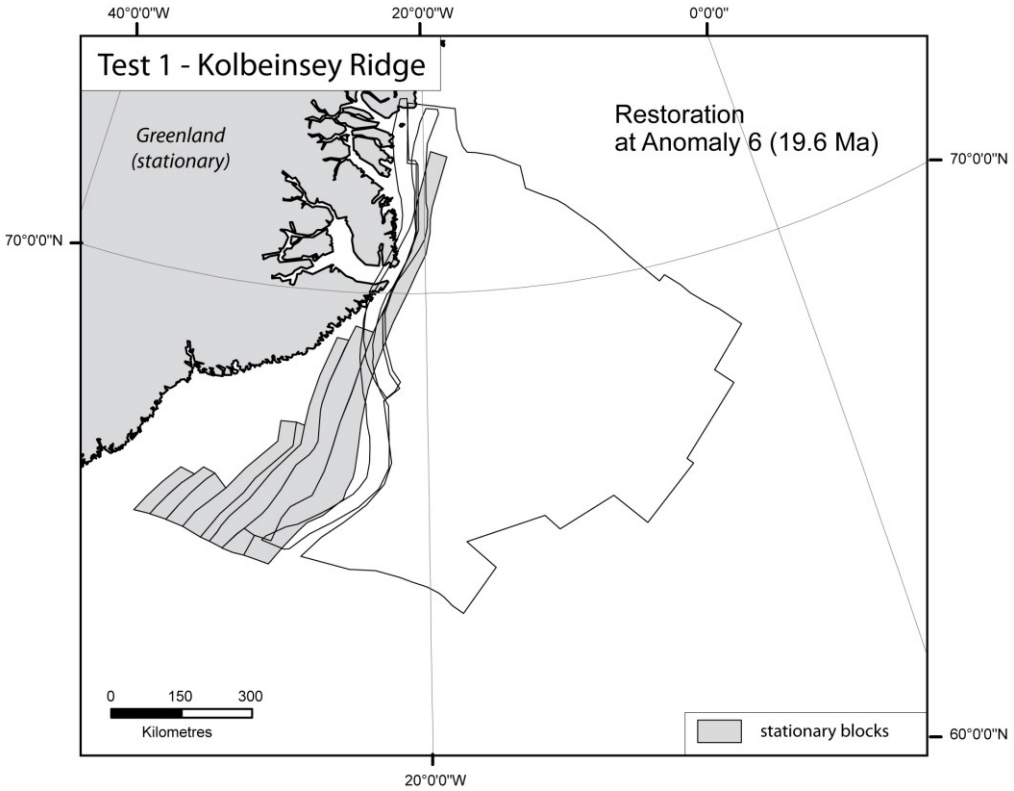

Figure 24 *Restoration of Kolbeinsey Ridge at Anomaly 6 (19.6 Ma), after 200 iterations*

Restoration of Aegir Ridge

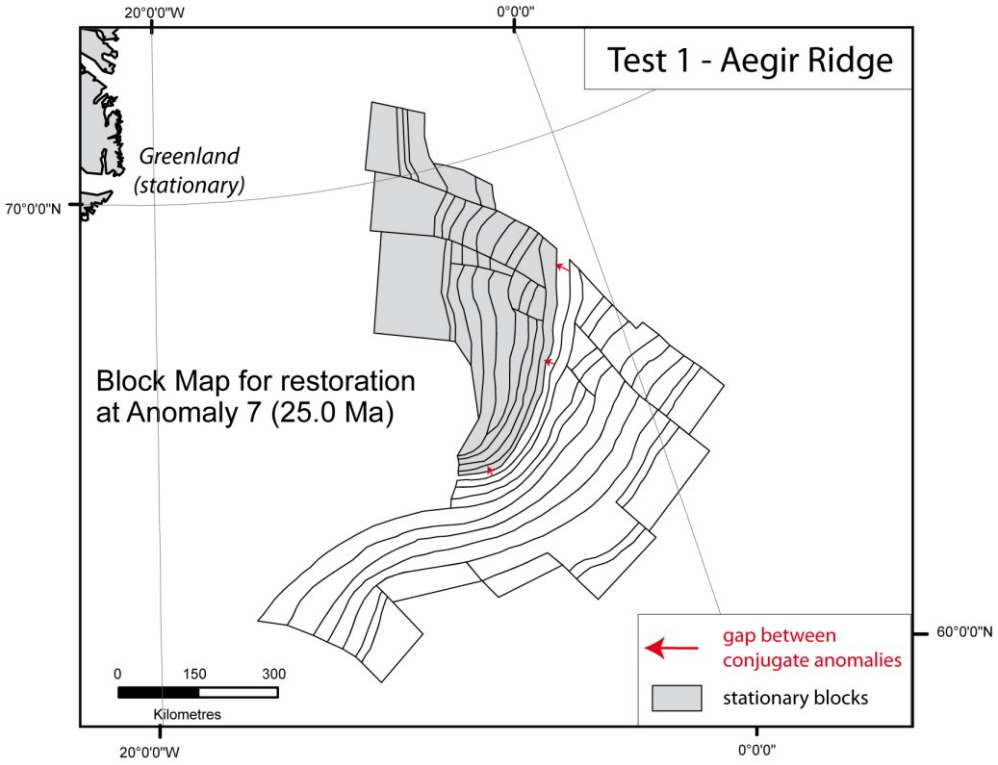

Figure 25 *Block map for restoration of Aegir Ridge at Anomaly 7 (25 Ma)*

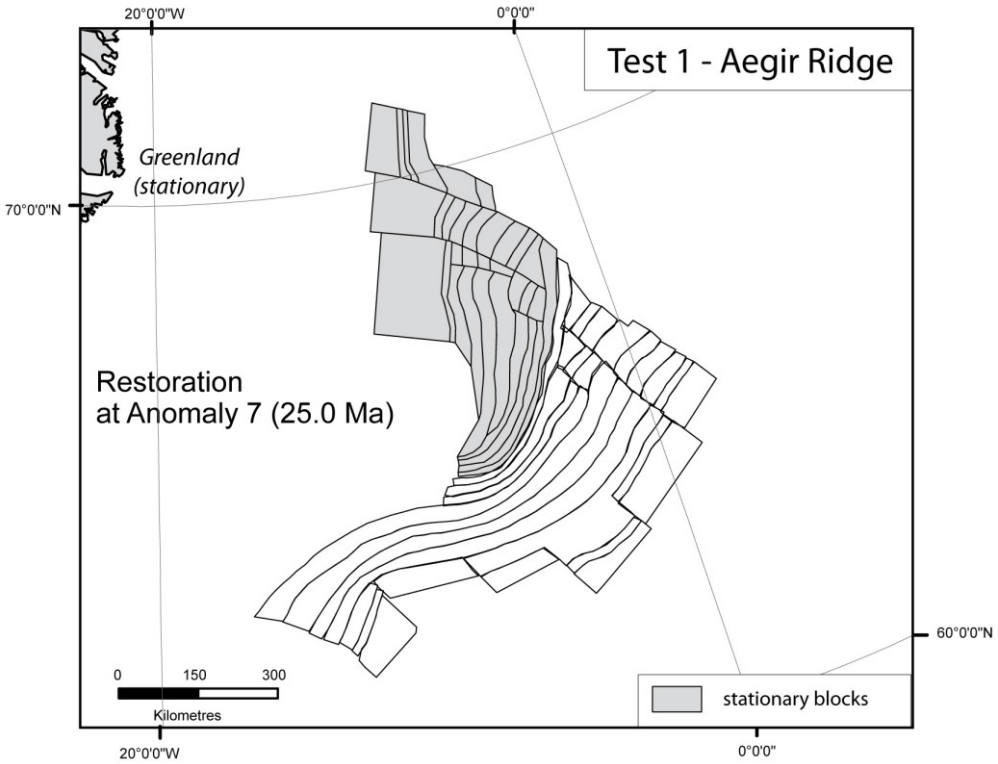

Figure 26 *Restoration of Aegir Ridge at Aegir Ridge at Anomaly 7 (25 Ma), after 200 iterations*

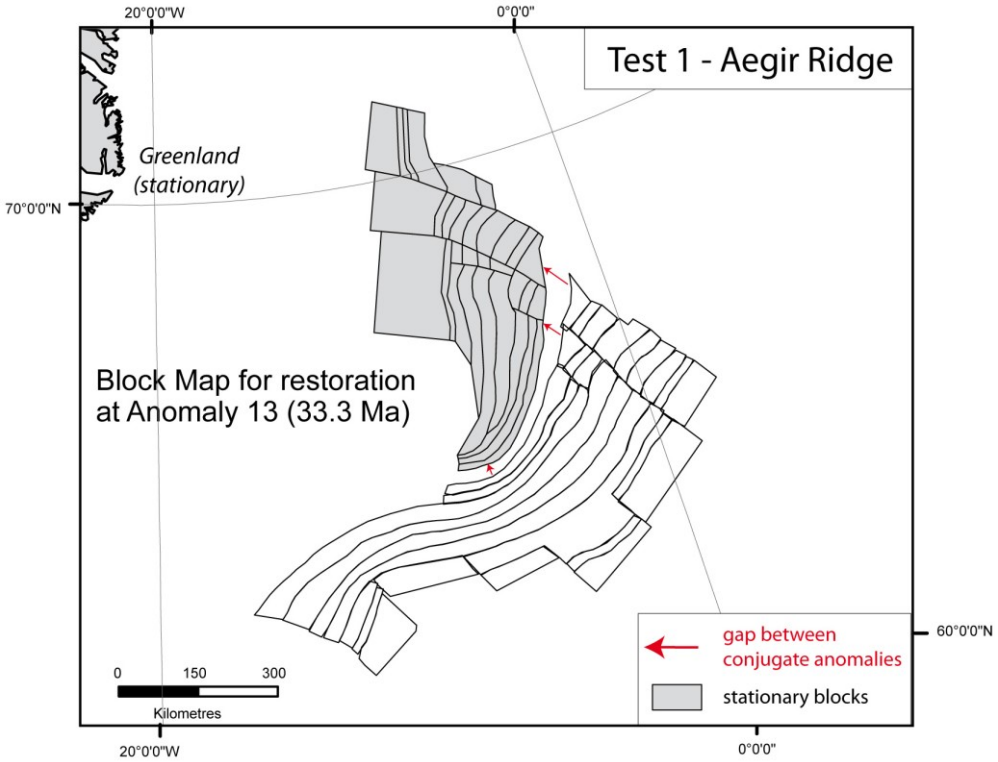

Figure 27 *Block map for restoration of Aegir Ridge at Anomaly 13 (33.3 Ma)*

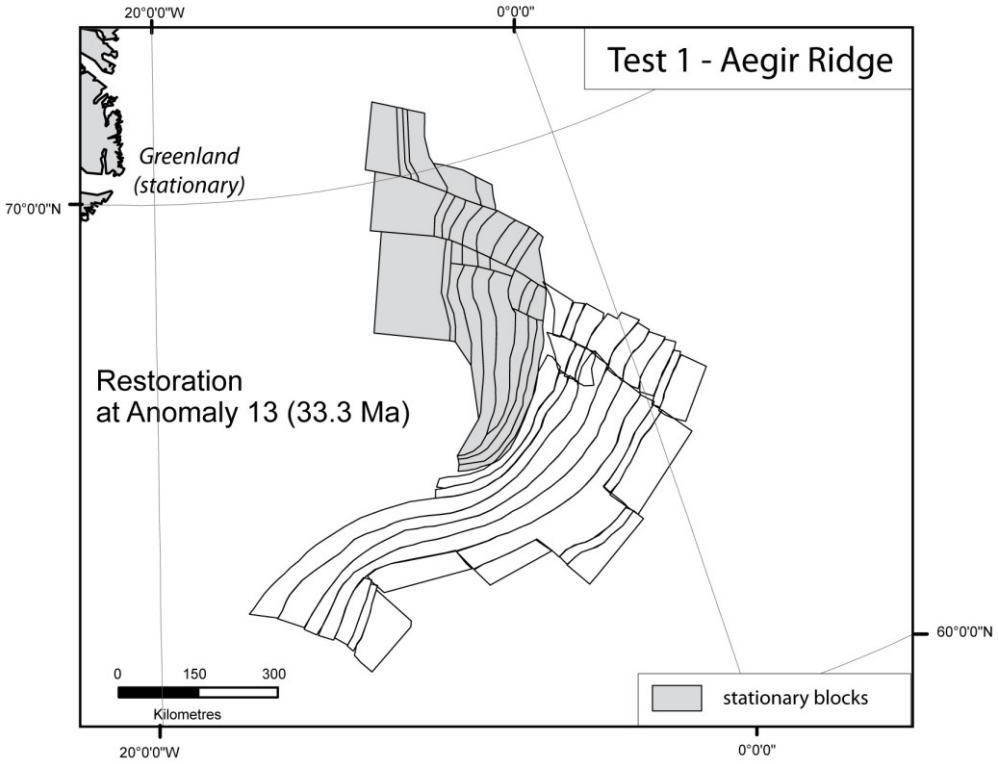

Figure 28 *Restoration of Aegir Ridge at Aegir Ridge at Anomaly 13 (33.3 Ma), after 200 iterations*

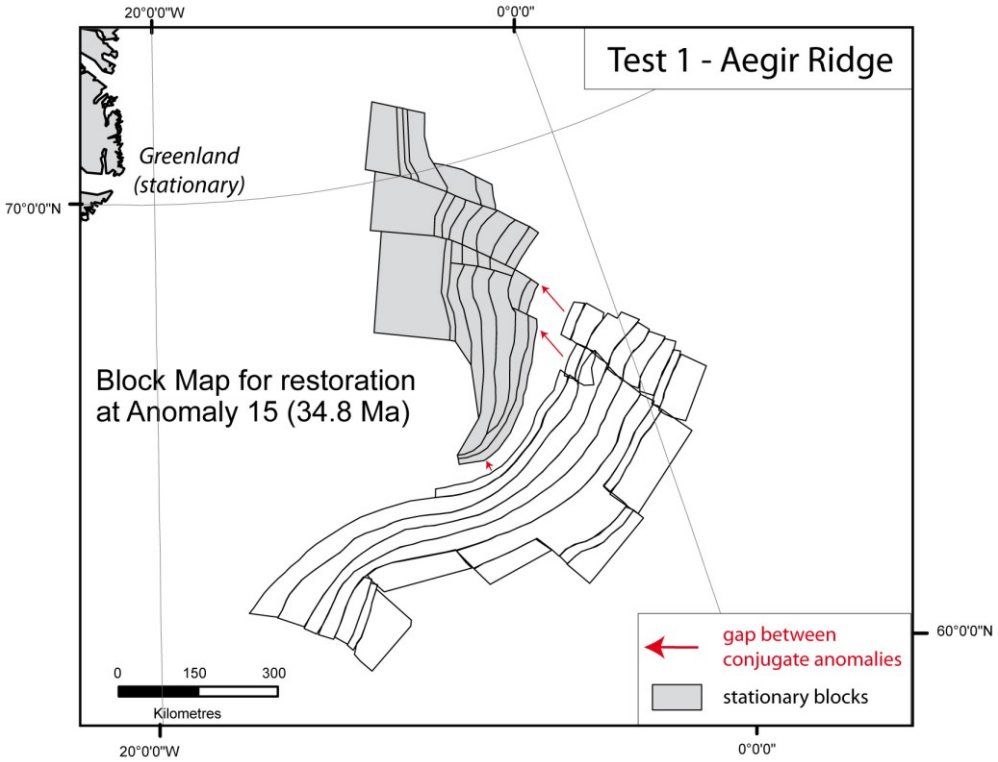

Figure 29 *Block map for restoration of Aegir Ridge at Anomaly 15 (34.8 Ma)*

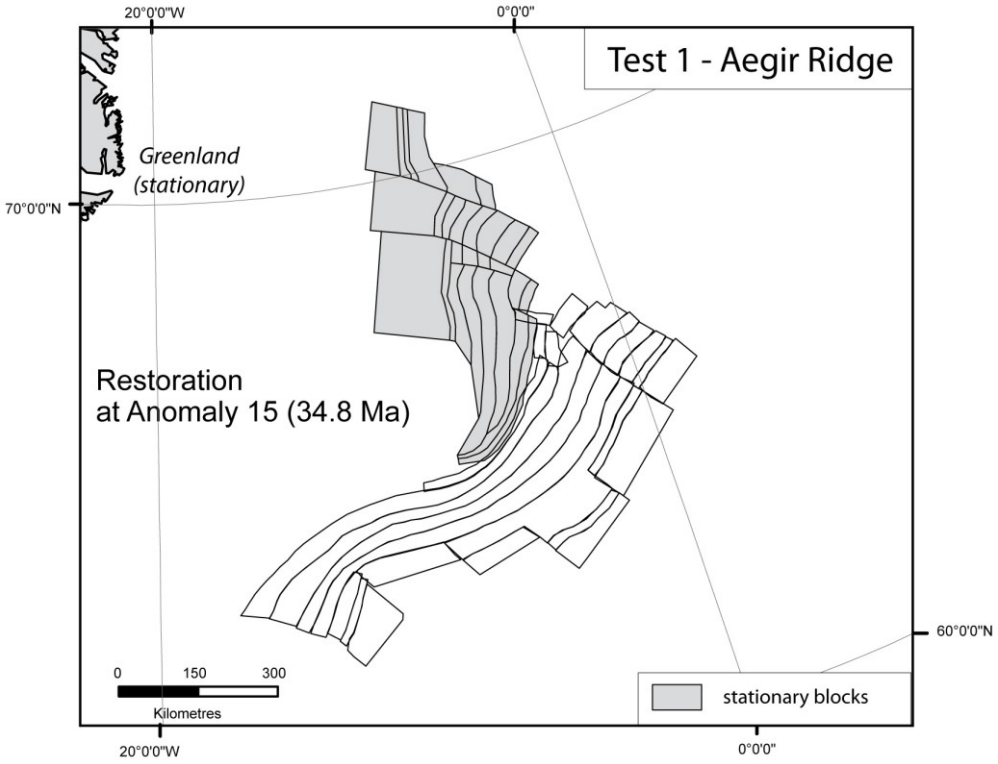

Figure 30 *Restoration of Aegir Ridge at Aegir Ridge at Anomaly 15 (34.8 Ma), after 400 iterations*

Appendix B: Results of restoration of whole NE Atlantic – TEST 2

The block map includes a boundary between the Reykjanes and Jan Mayen Segment, the Faeroe Fracture Zone and the Greenland side of the ridge is assumed stationary

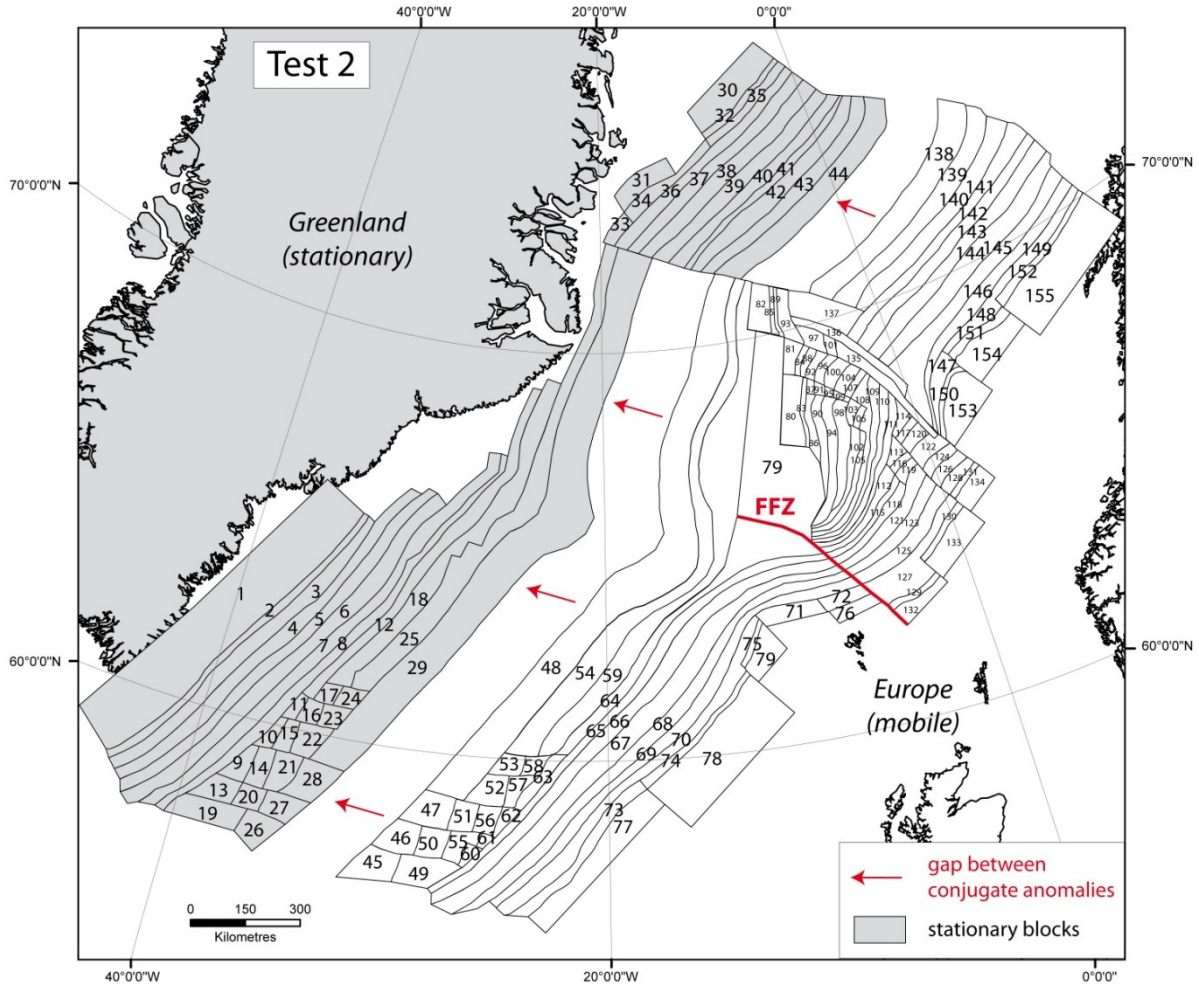

Figure 1 *Initial Block Map of Test 2 that includes a boundary between Reykjanes and Jan Mayen segments along Faeroe Fracture Zone (FFZ). Greenland plate is assumed stationary. Map projection is Universal Transverse Mercator (UTM, WGS 1984, zone 27N).*

I have simplified the block map around the Aegir Ridge and south of the Reykjanes Ridge to avoid displacements of the little blocks in these areas and to reduce the calculation time (by reducing the number of blocks). Indeed, once formed, the oceanic crust is assumed as rigid, only relative displacements along fracture zones are possible. Therefore for restoration, for example at Anomaly 5, the little blocks of older magnetic anomalies are not supposed to move and can be grouped into 'bigger' rigid blocks. These 'bigger' blocks are then redrawn at each restoration stage.

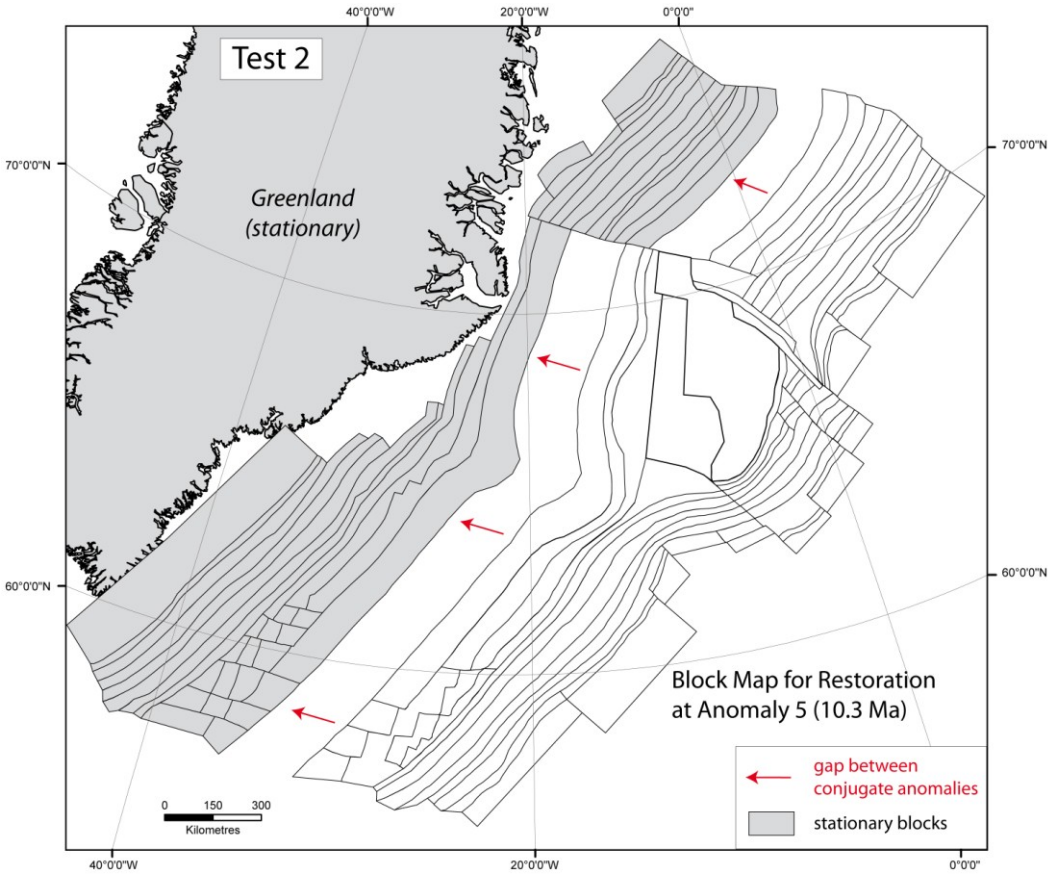

Figure 2 *Block map for restoration at Anomaly 5 (10.3 Ma)*

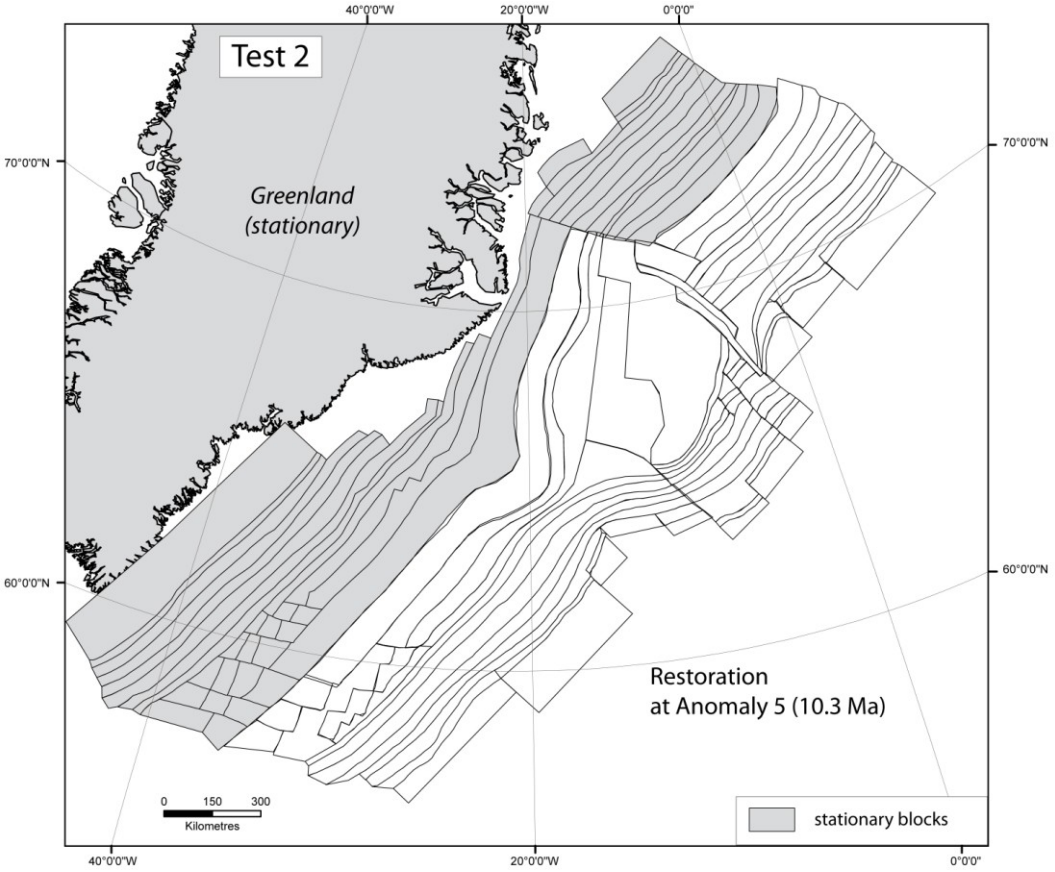

Figure 3 *Restoration at Anomaly 5 (10.3 Ma), after 1200 iterations*

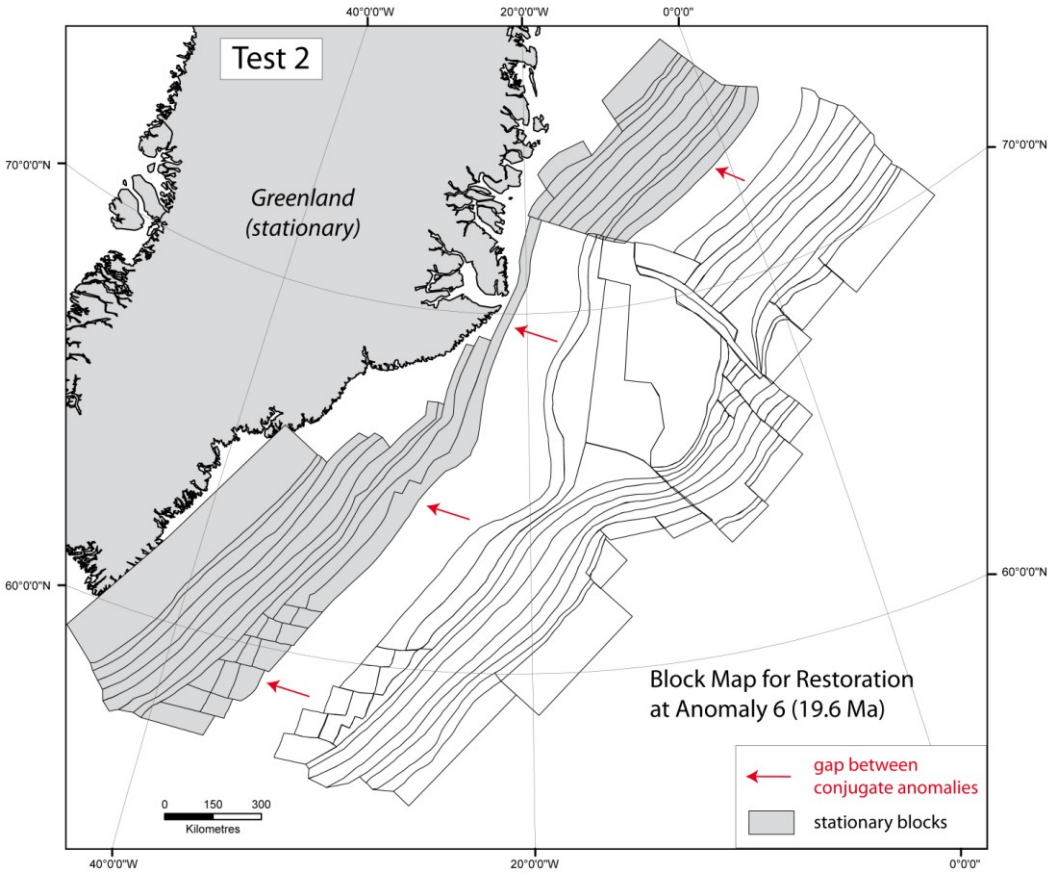

Figure 4 *Block map for restoration at Anomaly 6 (19.6 Ma)*

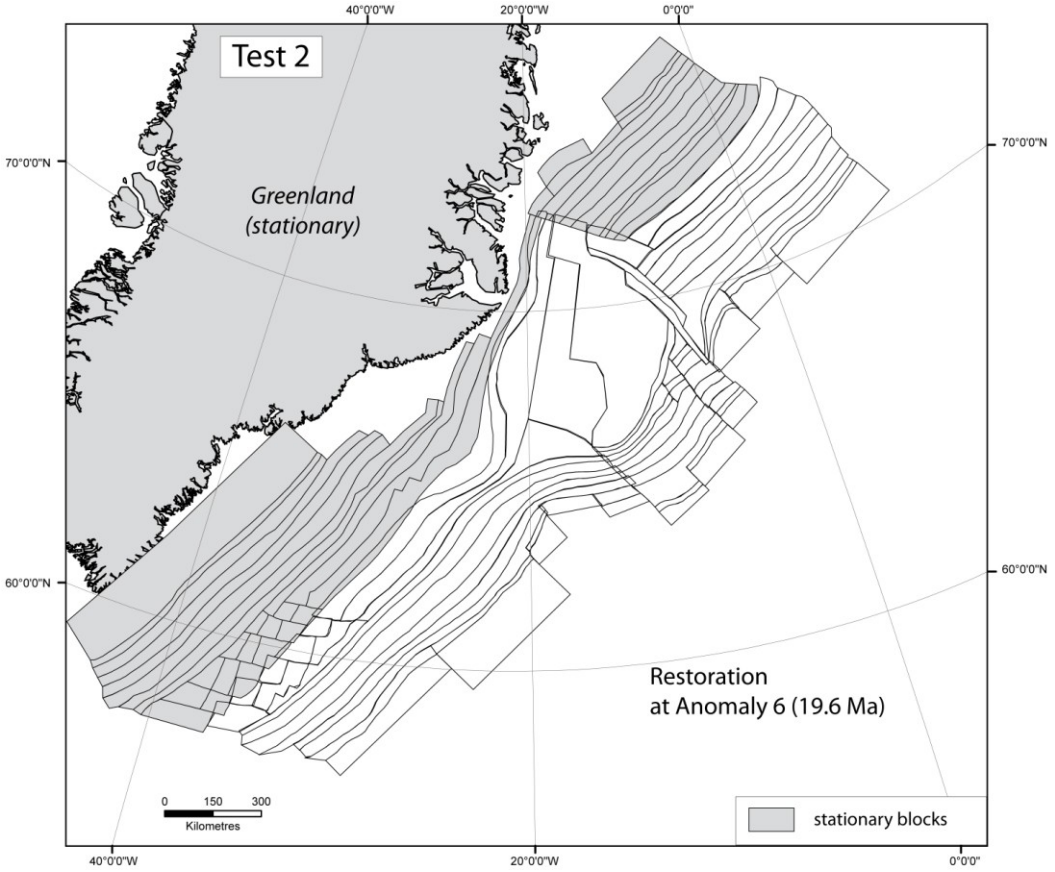

Figure 5 *Restoration at Anomaly 6 (19.6 Ma), after 800 iterations*

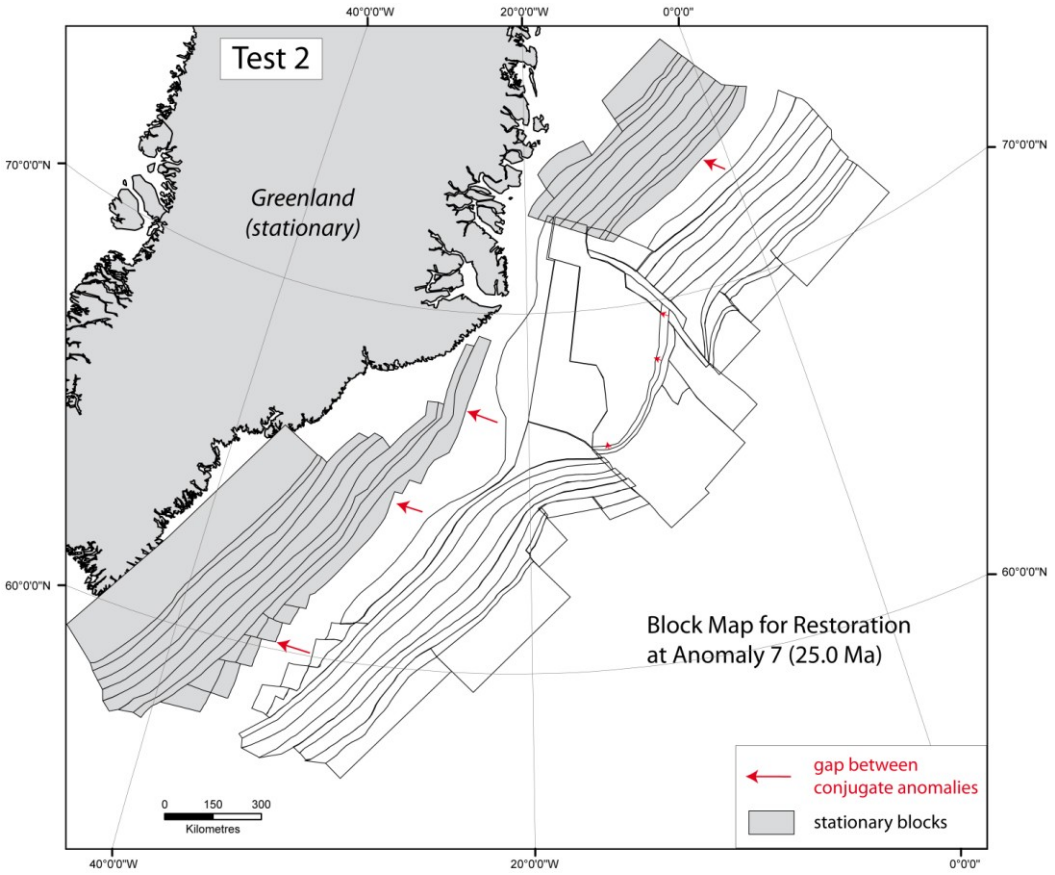

Figure 6 *Block map for restoration at Anomaly 7 (25 Ma)*

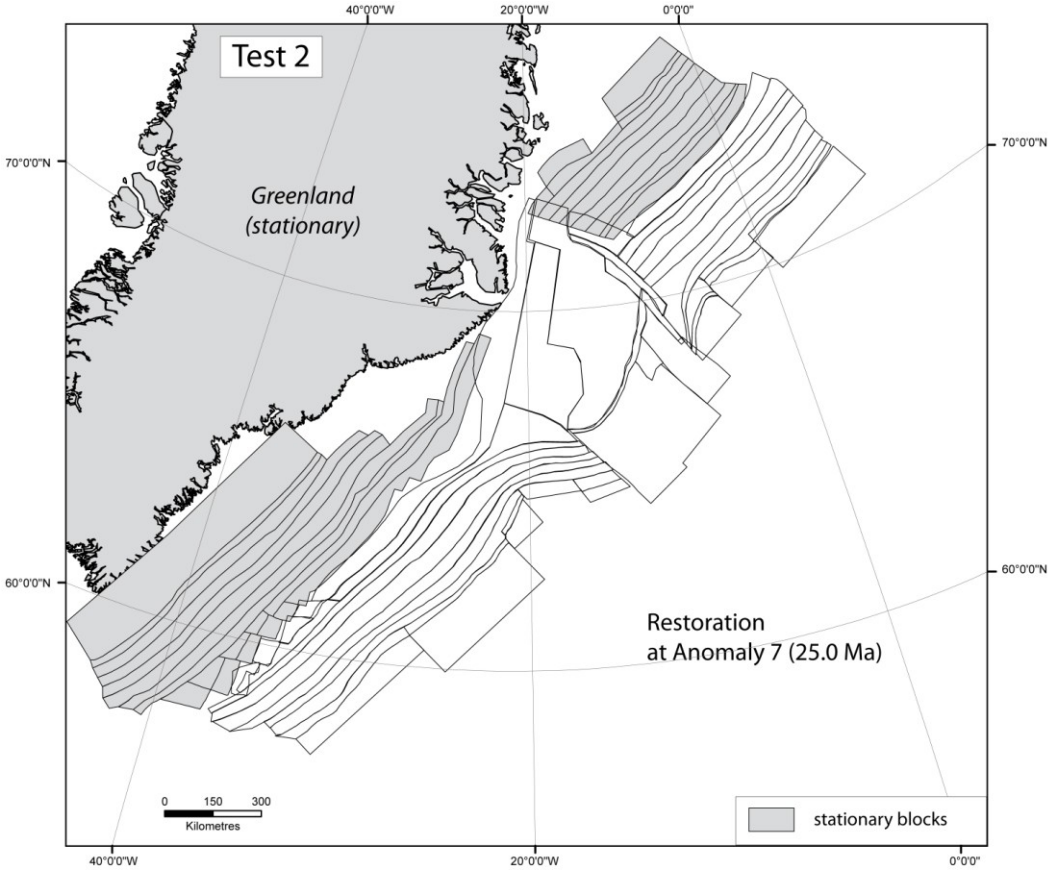

Figure 7 *Restoration at Anomaly 7 (25Ma), after 580 iterations*

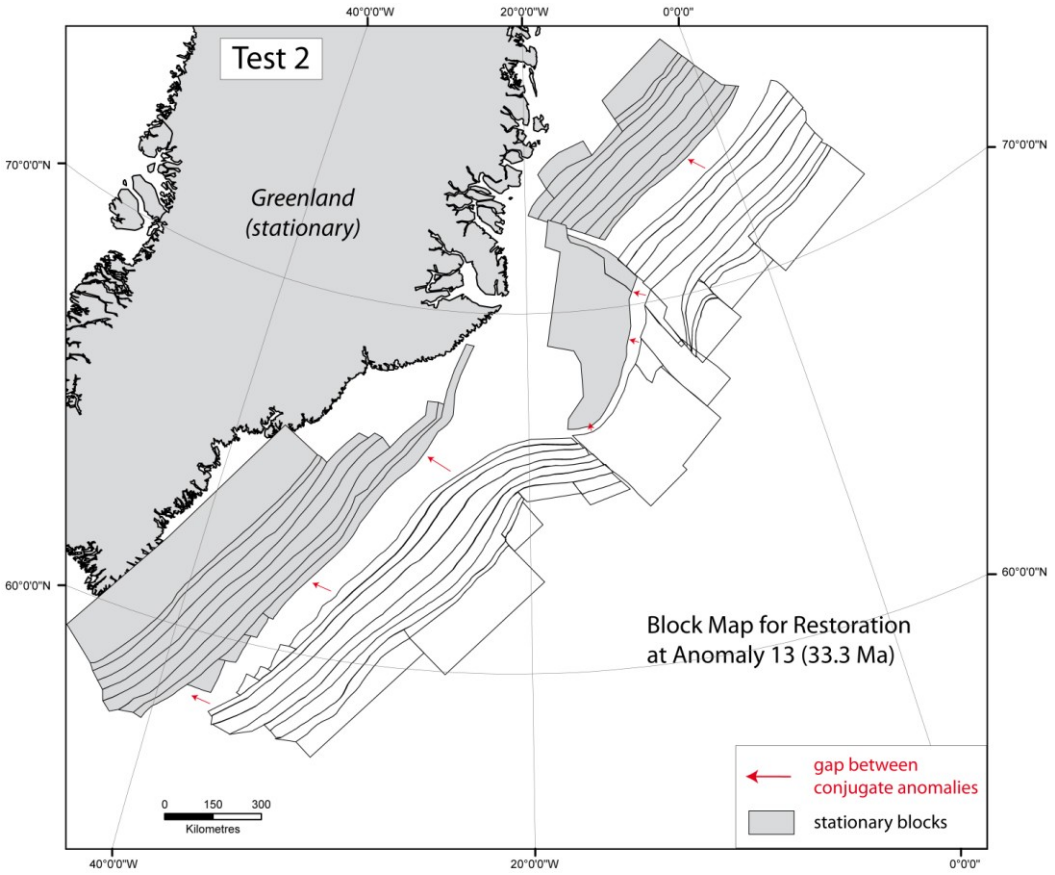

Figure 8 *Block map for restoration at Anomaly 13 (33.3 Ma)*

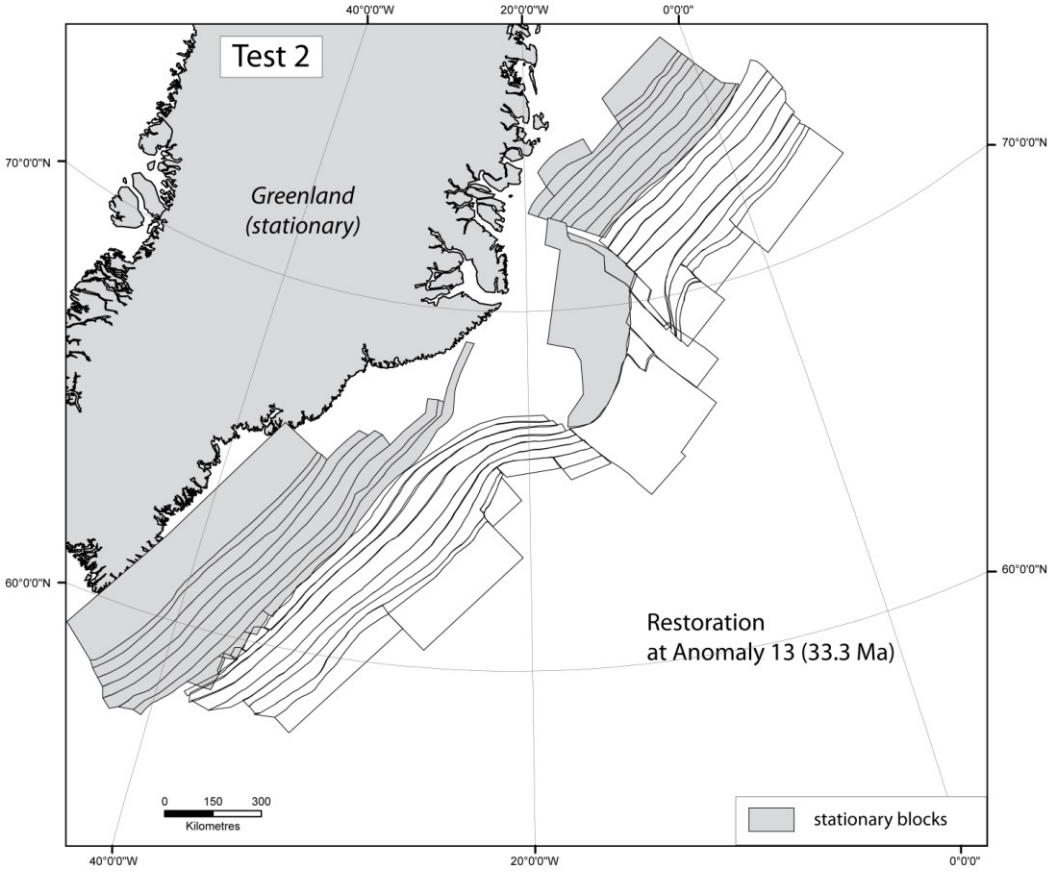

Figure 9 *Restoration at Anomaly 13 (33.3 Ma), after 200 iterations*

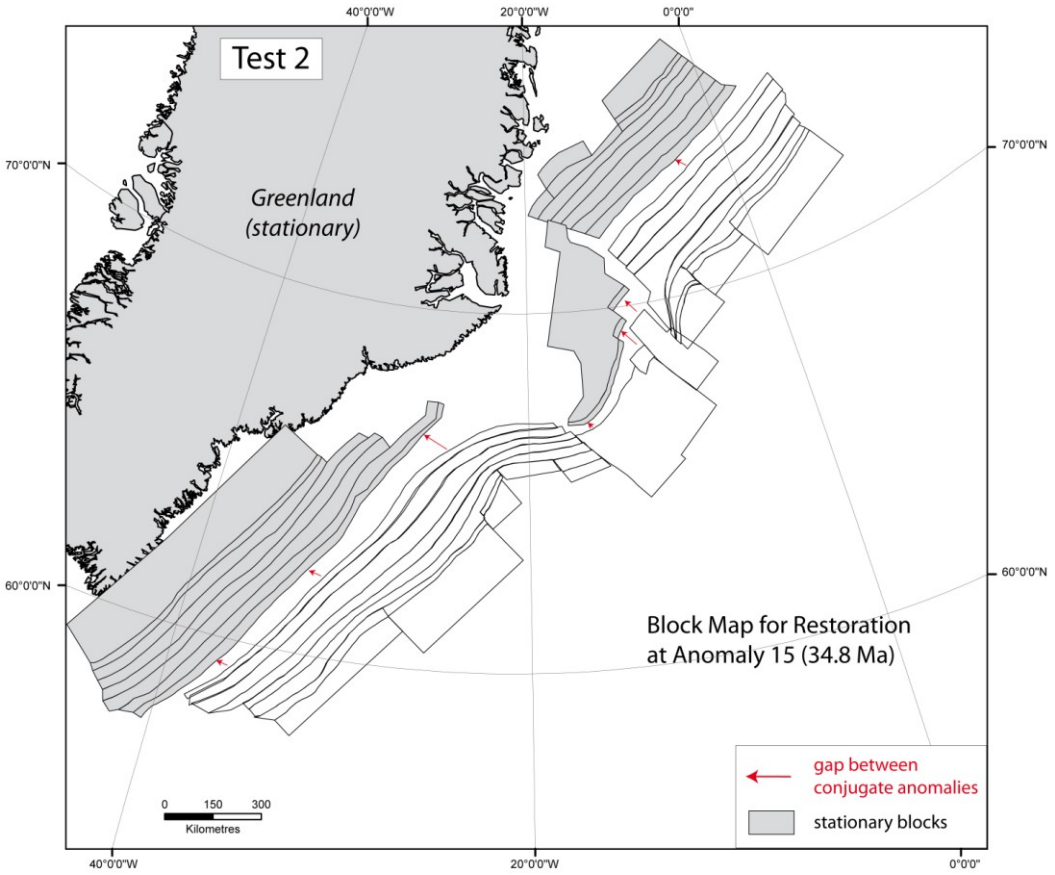

Figure 10 *Block map for restoration at Anomaly 15 (34.8 Ma)*

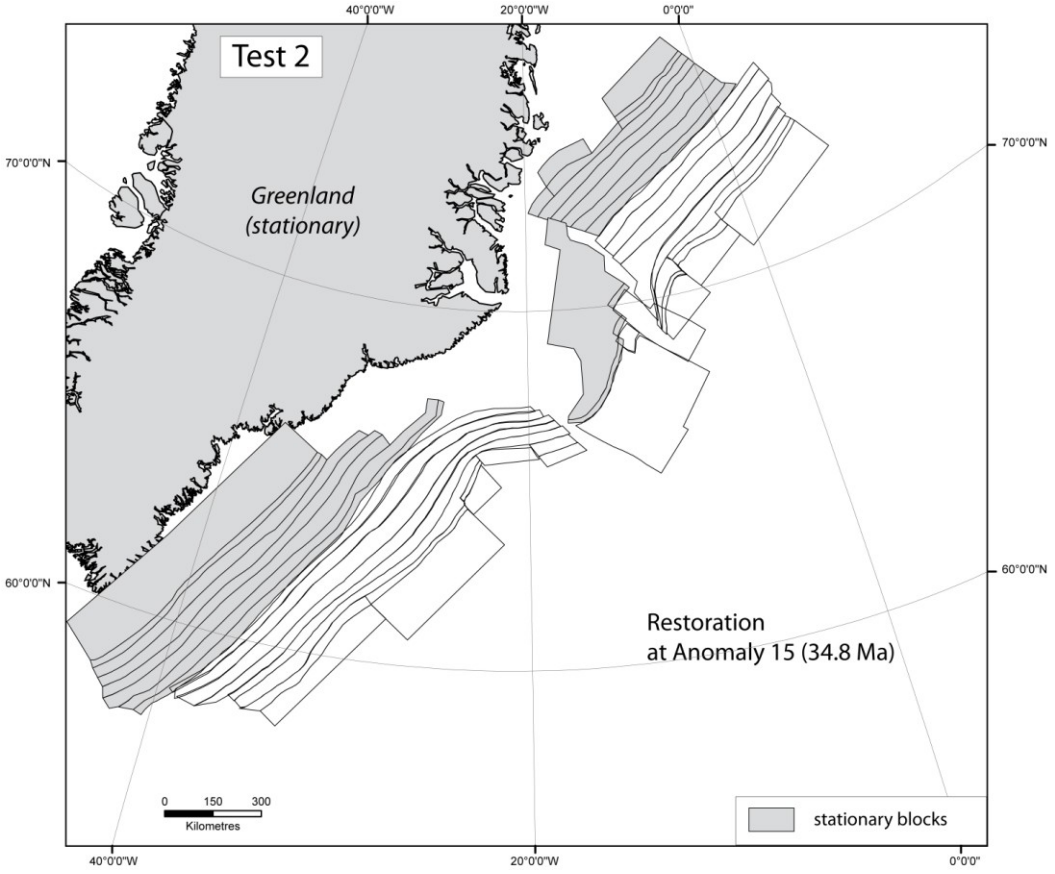

Figure 11 *Restoration at Anomaly 15 (34.8 Ma), after 200 iterations*

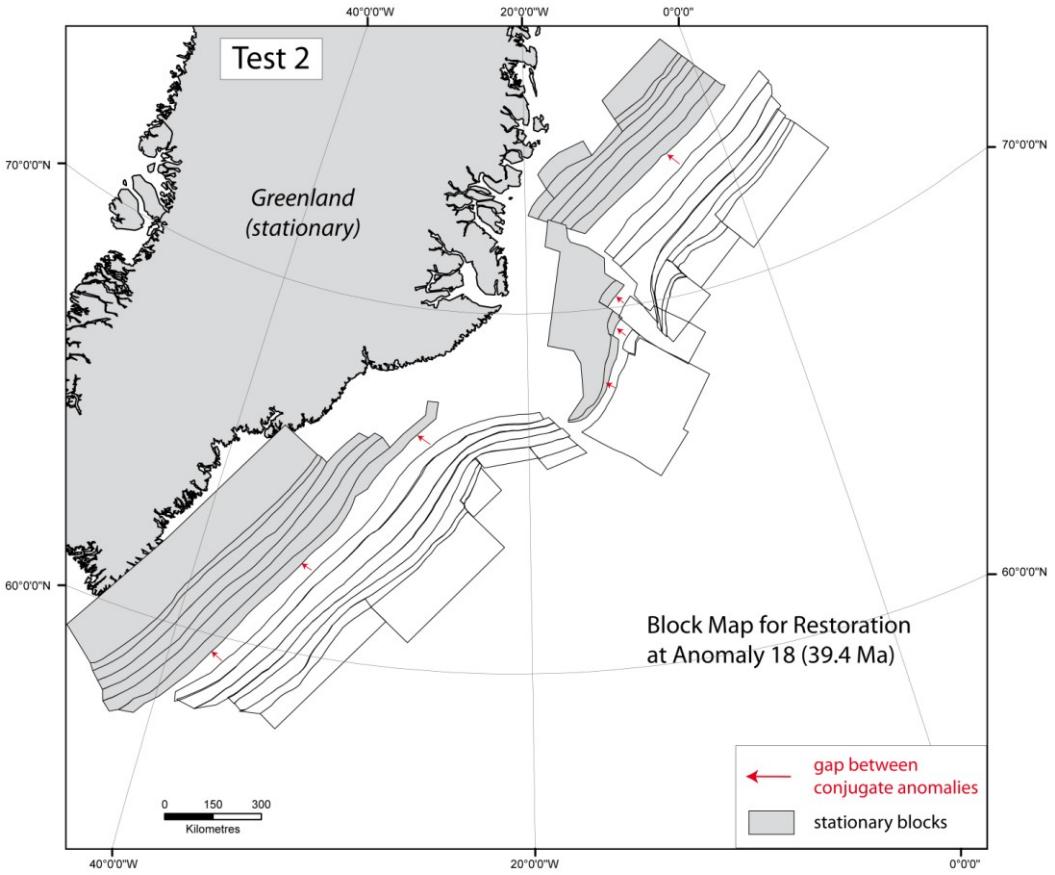

Figure 12 *Block map for restoration at Anomaly 18 (39.4 Ma)*

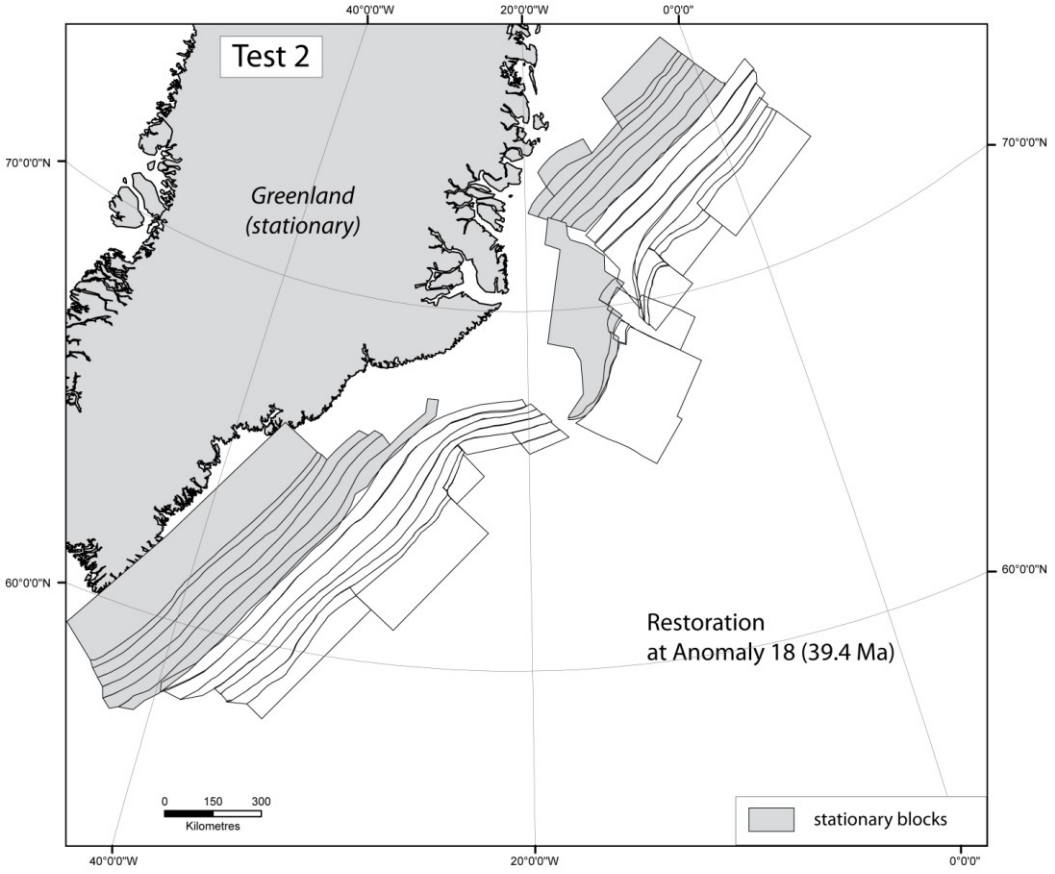

Figure 13 *Restoration at Anomaly 18 (39.4 Ma), after 200 iterations*

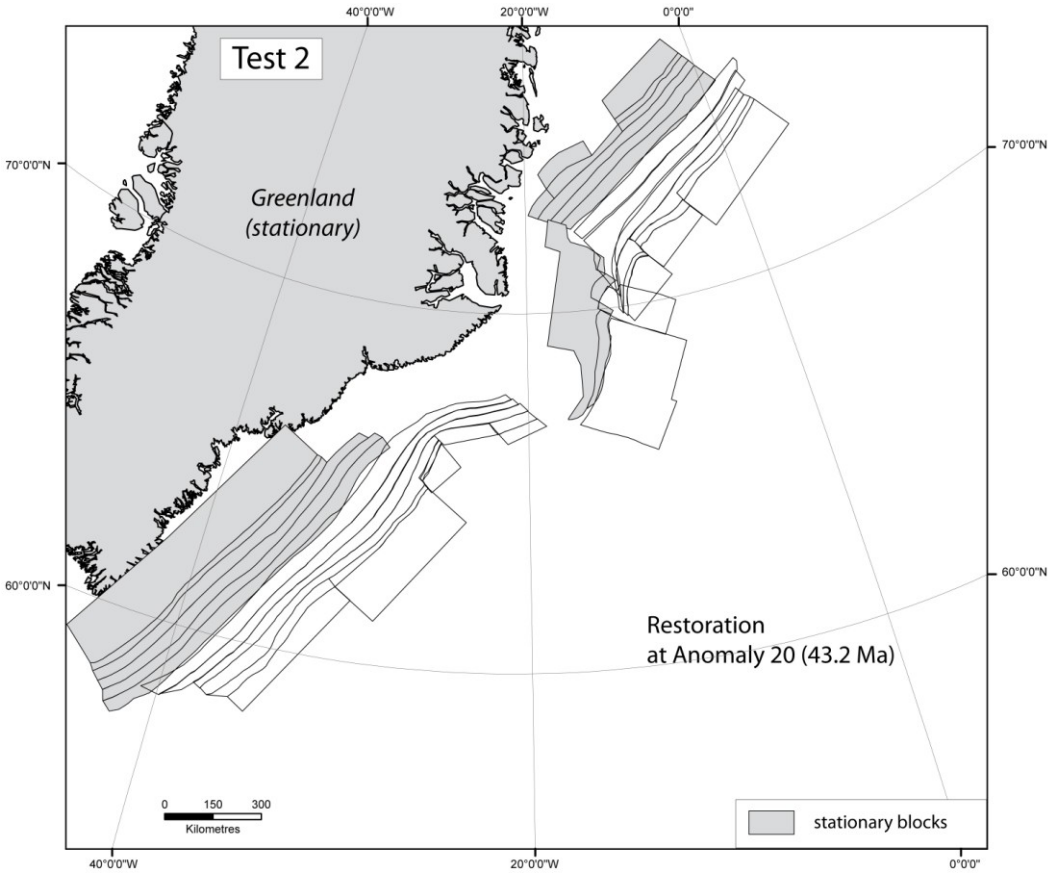

Figure 14 *Block map for restoration at Anomaly 20 (43.2 Ma*)

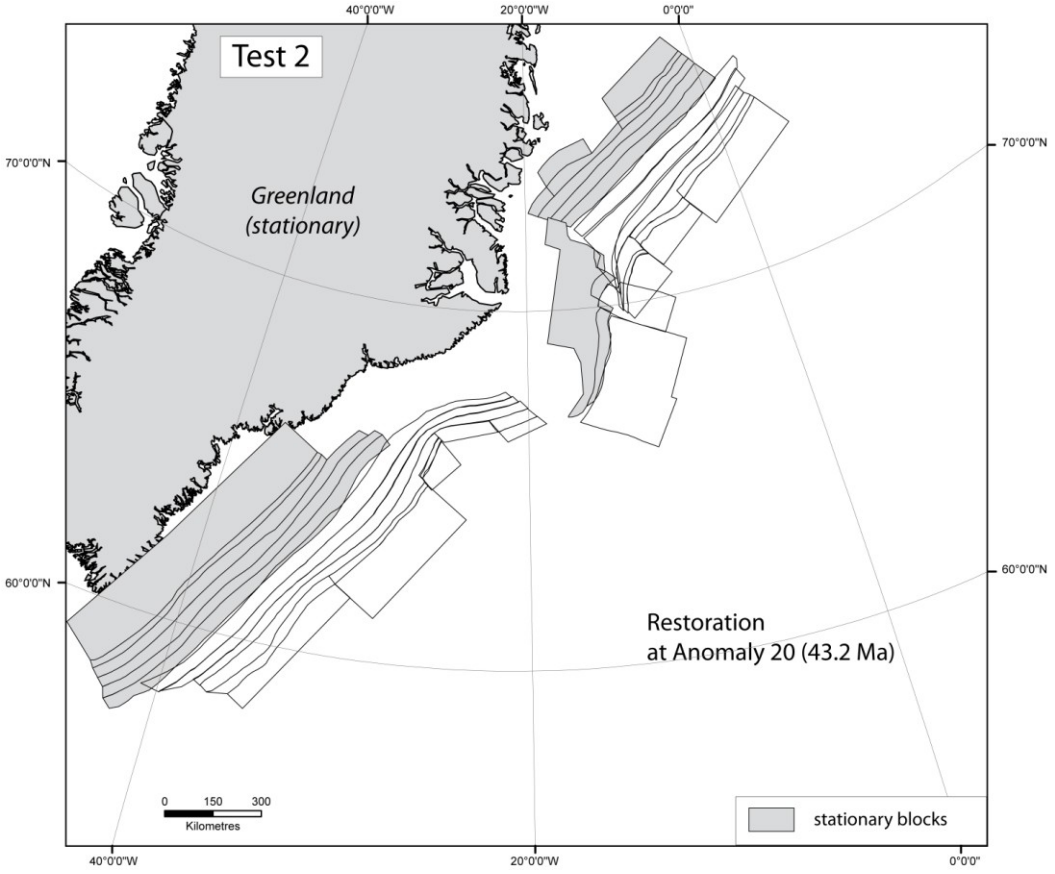

Figure 15 *Restoration at Anomaly 20 (43.2 Ma), after 200 iterations*

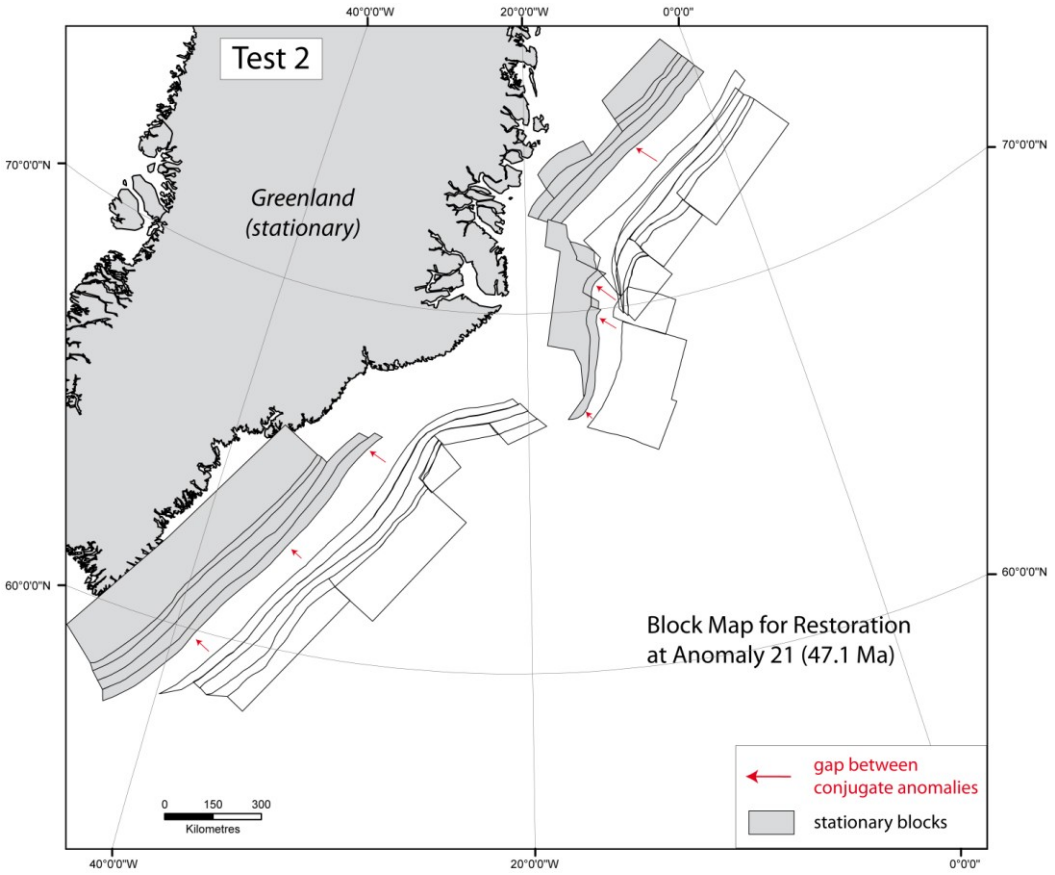

Figure 16 *Block map for restoration at Anomaly 21 (47.1 Ma*)

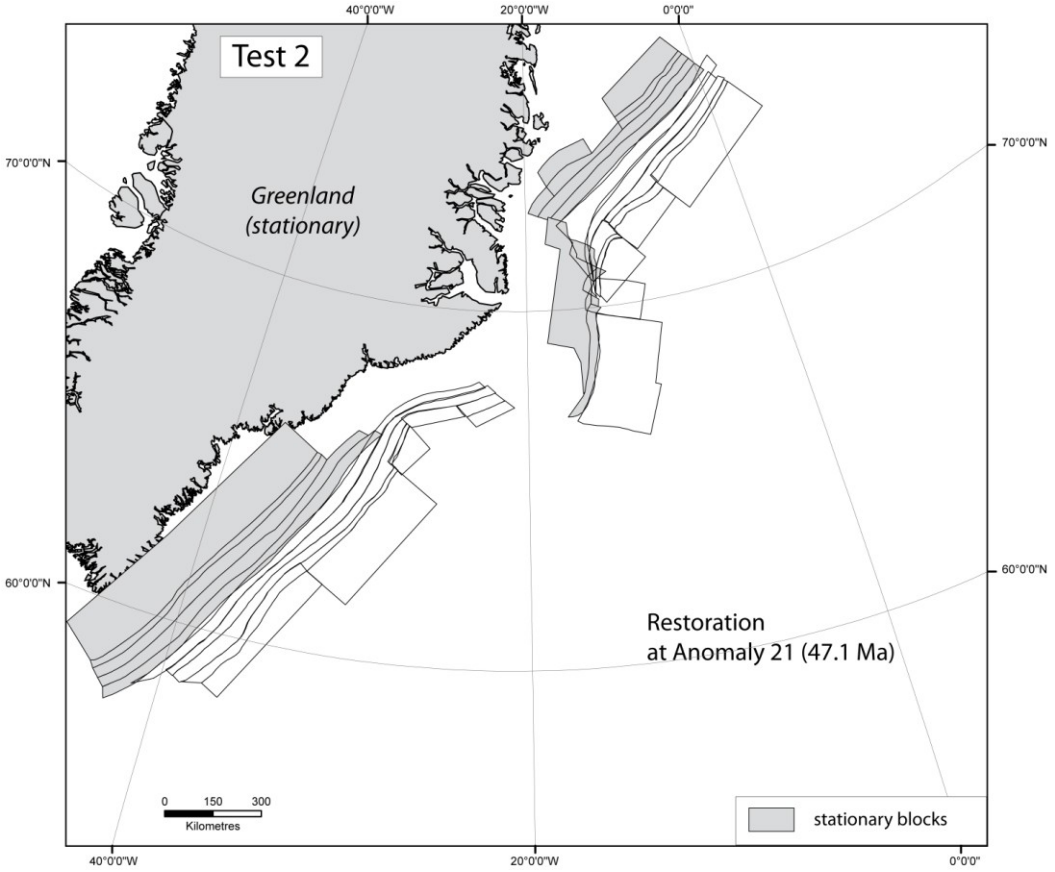

Figure 17 *Restoration at Anomaly 21 (47.1 Ma), after 200 iterations*

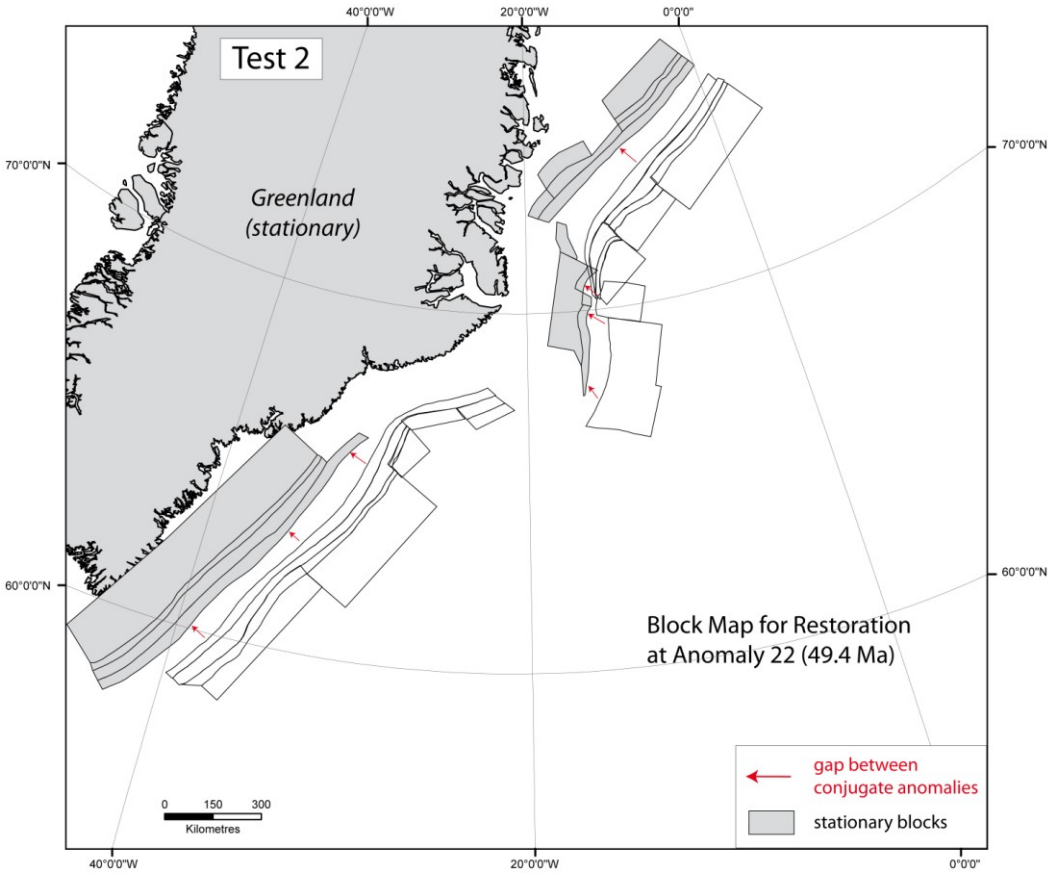

Figure 178 *Block map for restoration at Anomaly 22 (49.7 Ma)*

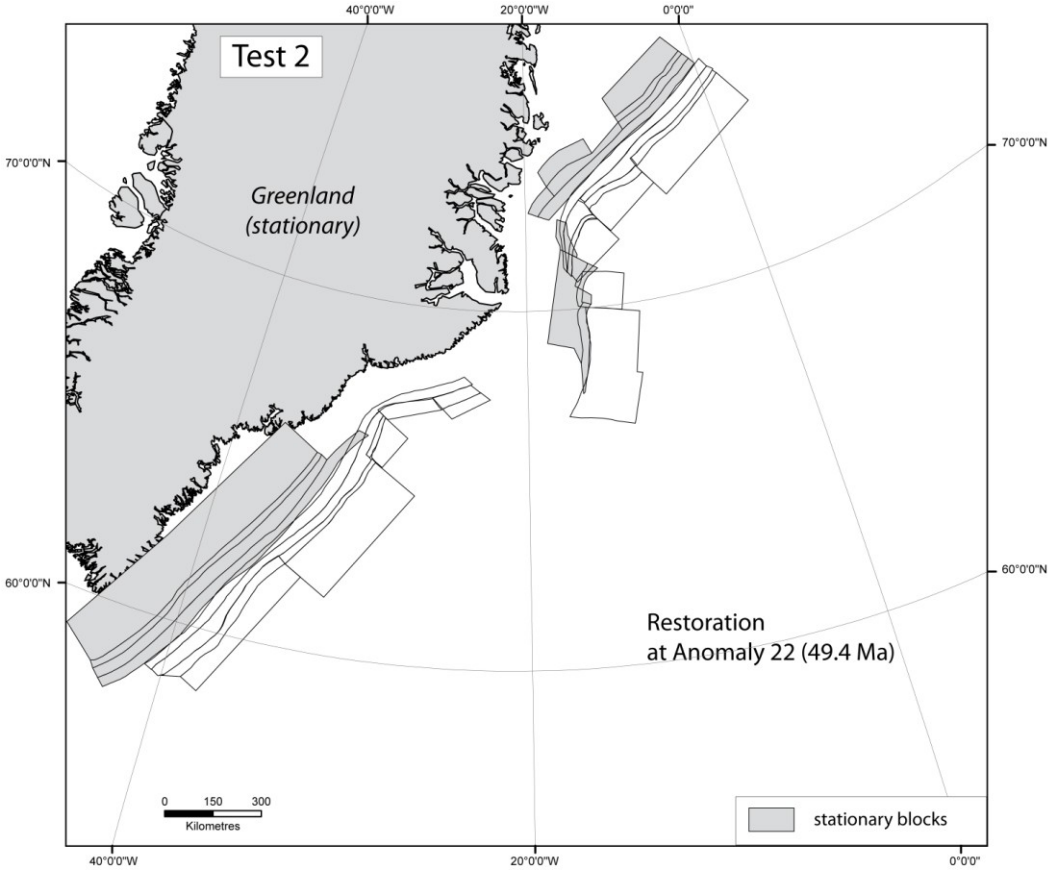

Figure 19 *Restoration at Anomaly 22 (49.7 Ma), after 200 iterations*

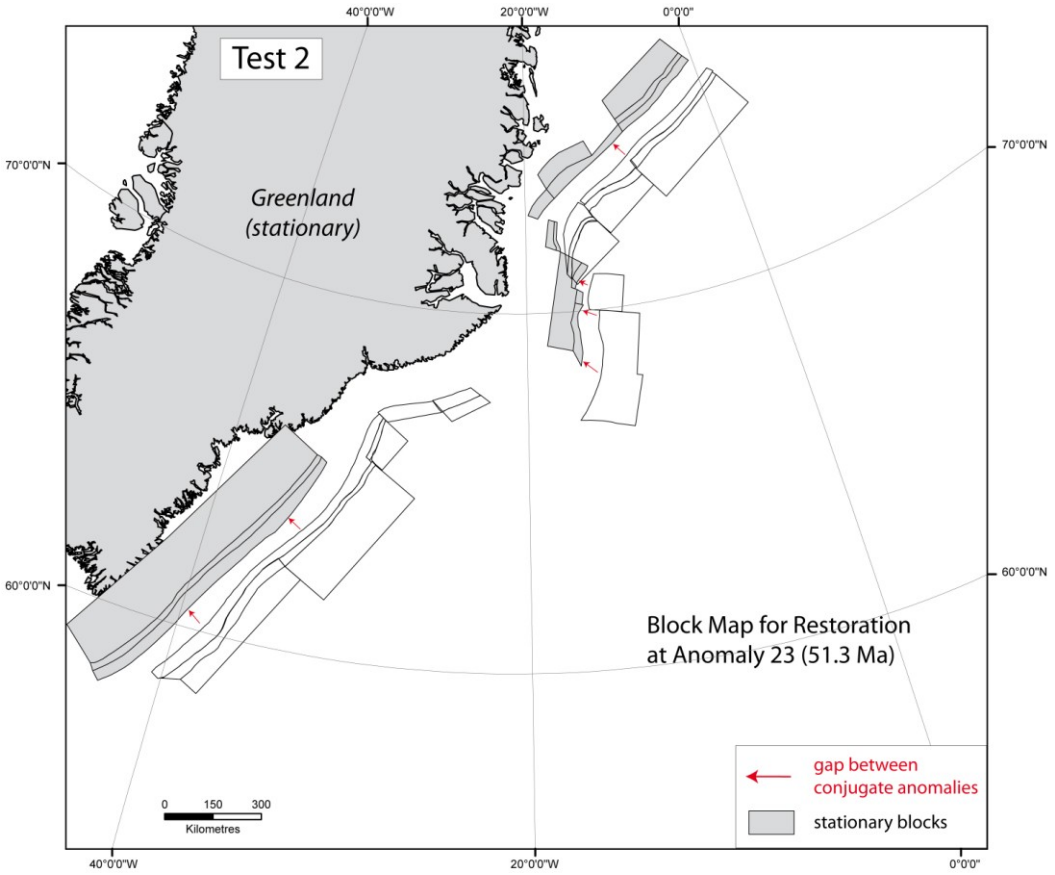

Figure 20 *Block map for restoration at Anomaly 23 (51.3 Ma)*

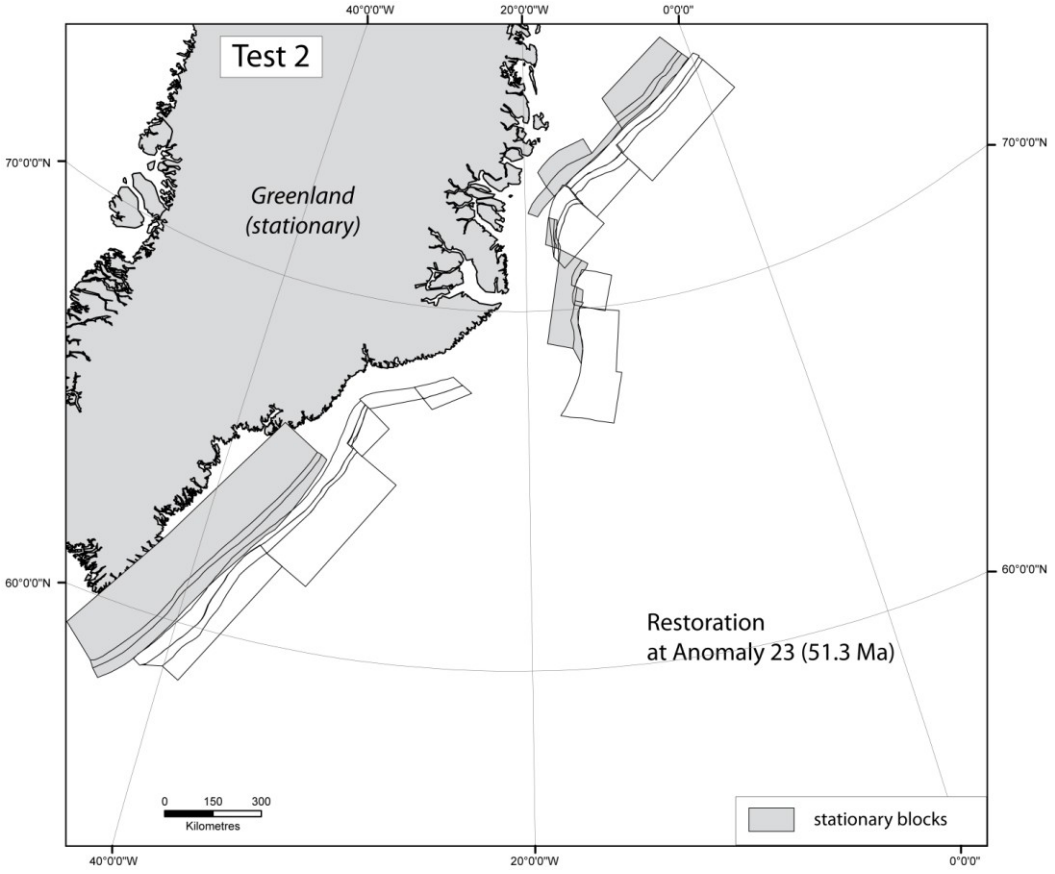

Figure 21 *Restoration at Anomaly 23 (51.3 Ma), after 200 iterations*

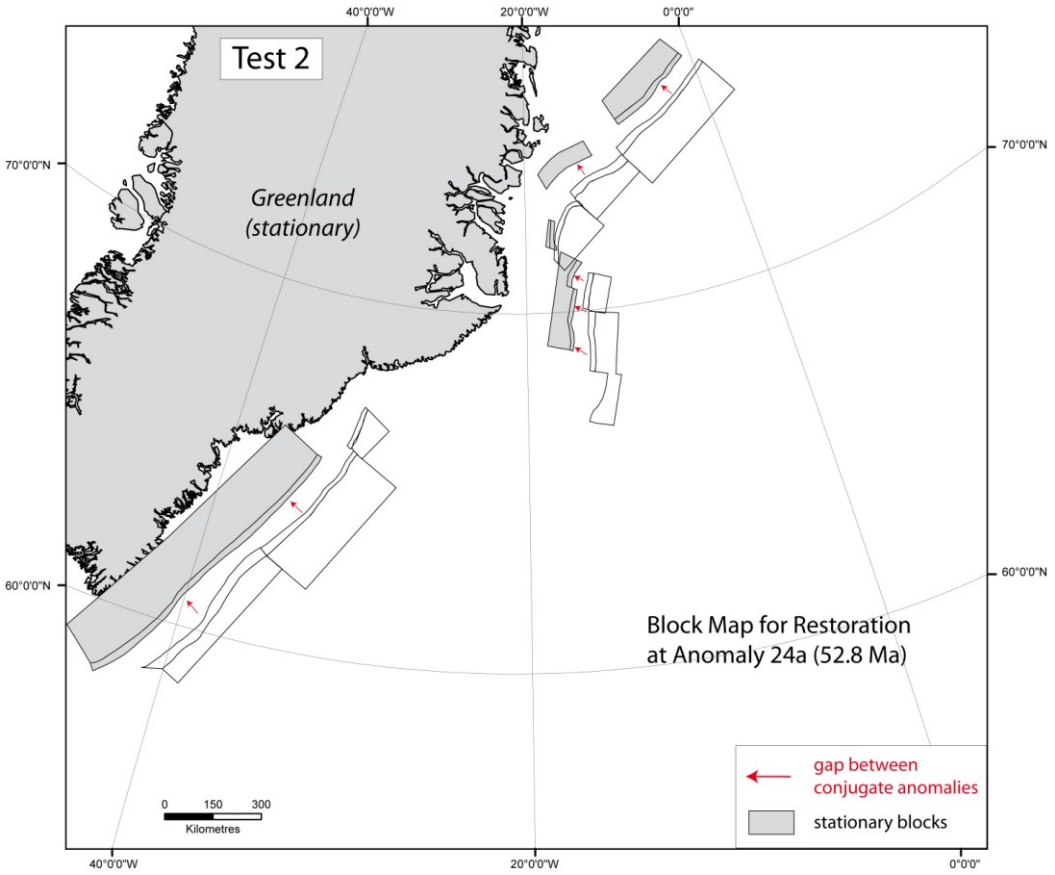

Figure 22 *Block map for restoration at Anomaly 24a (52.8 Ma)*

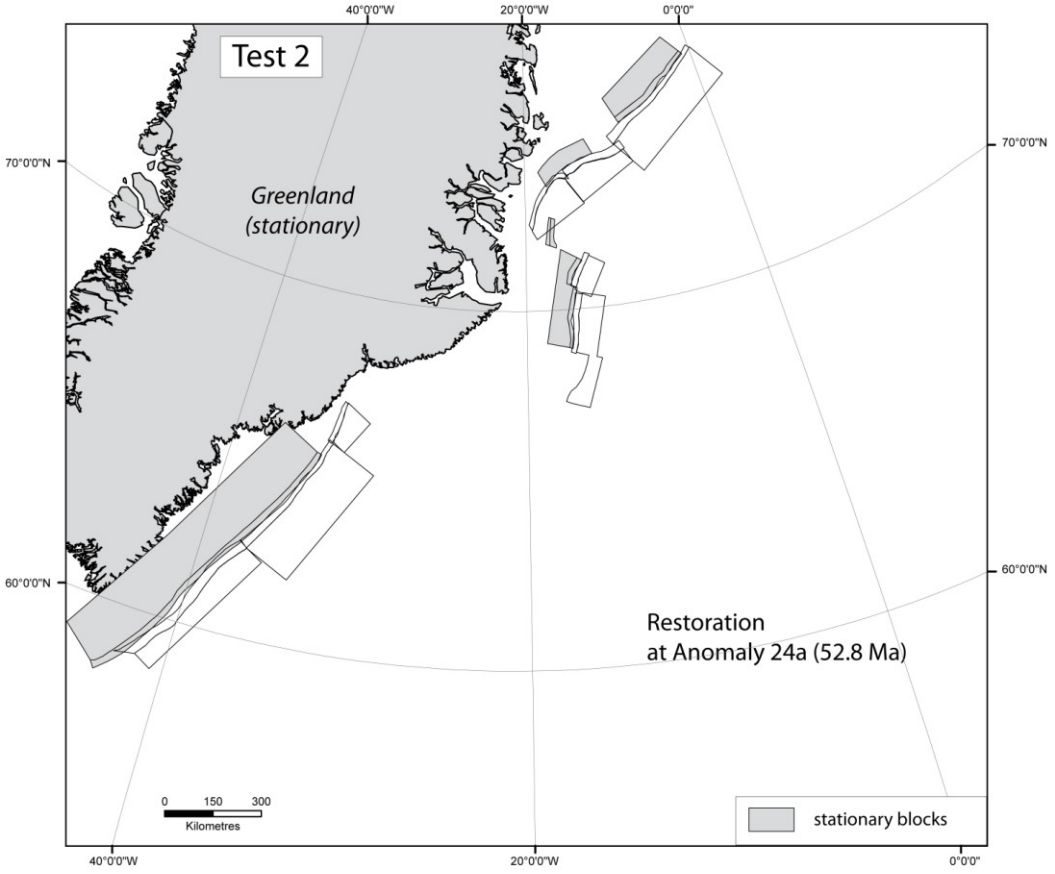

Figure 23 *Restoration at Anomaly 24a (52.8 Ma), after 140 iterations*

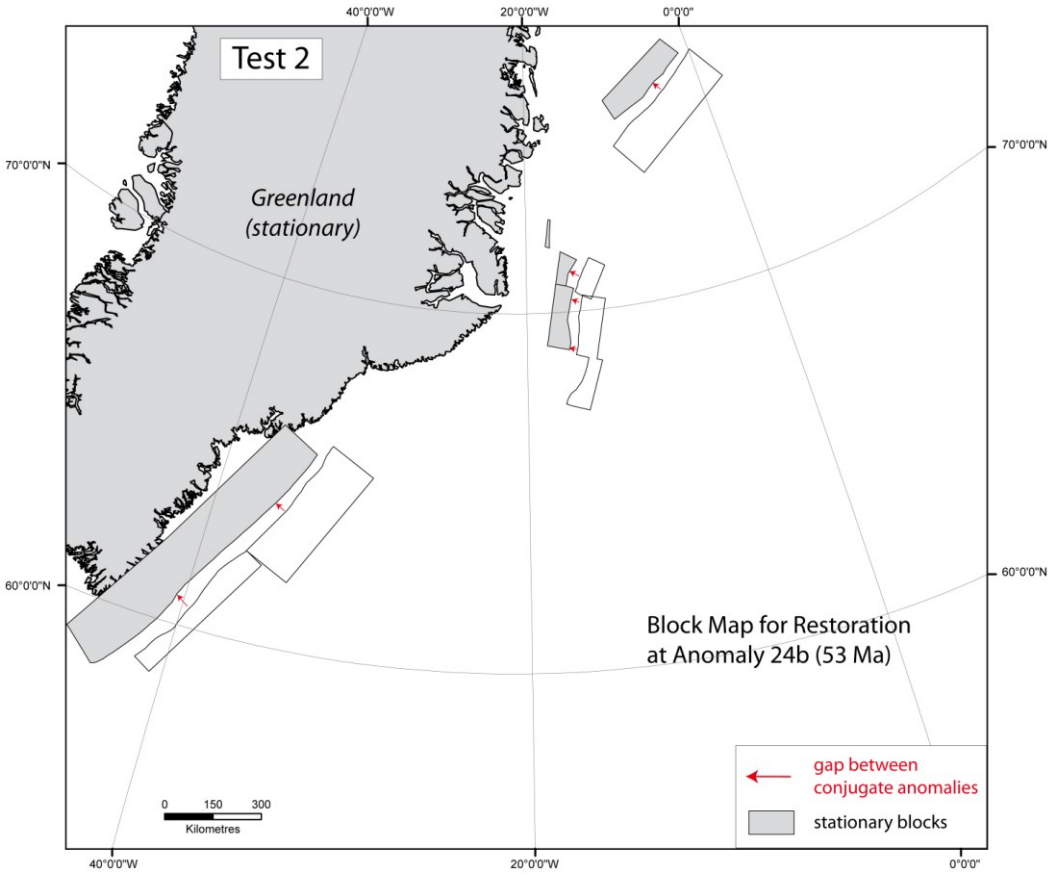

Figure 24 *Block map for restoration at Anomaly 24b (53 Ma)*

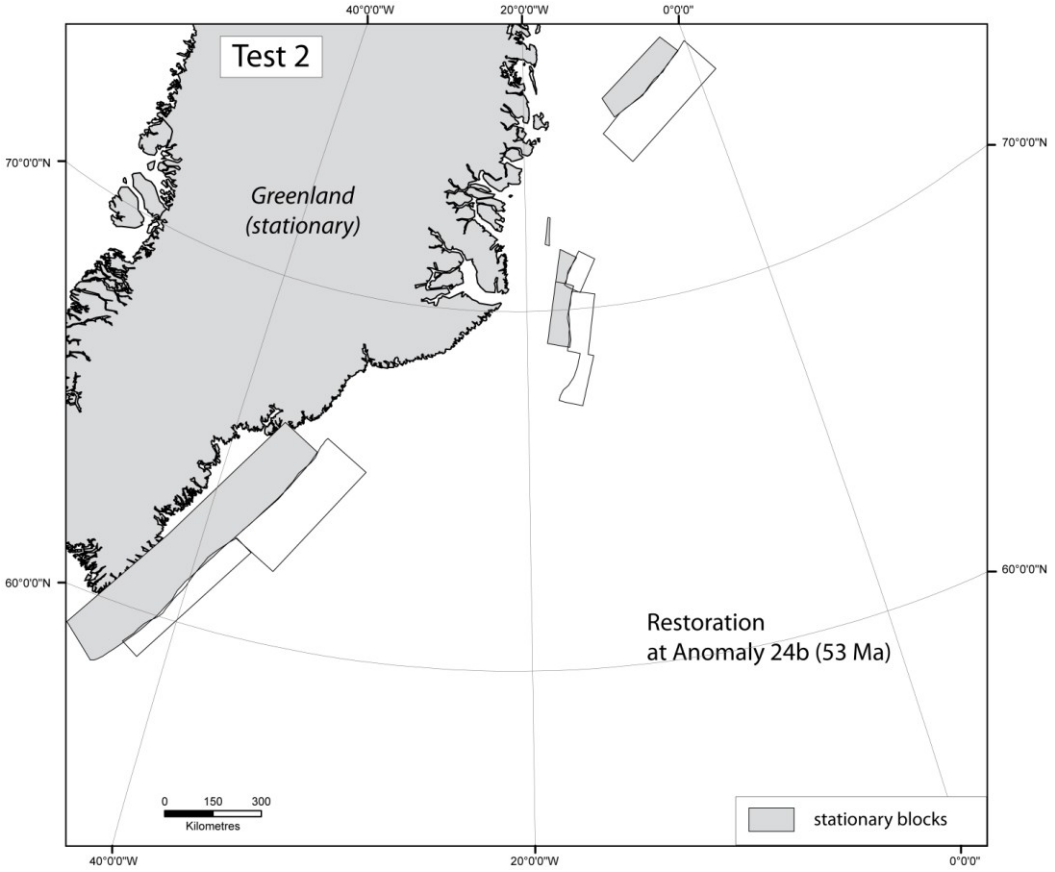

Figure 25 *Restoration at Anomaly 24b (53 Ma), after 50 iterations*

Appendix C: Results of restoration of whole NE Atlantic – TEST 3

The block map includes a boundary between the Reykjanes and Jan Mayen Segment, the Faeroe Fracture Zone and the Europe side of the ridge is assumed stationary

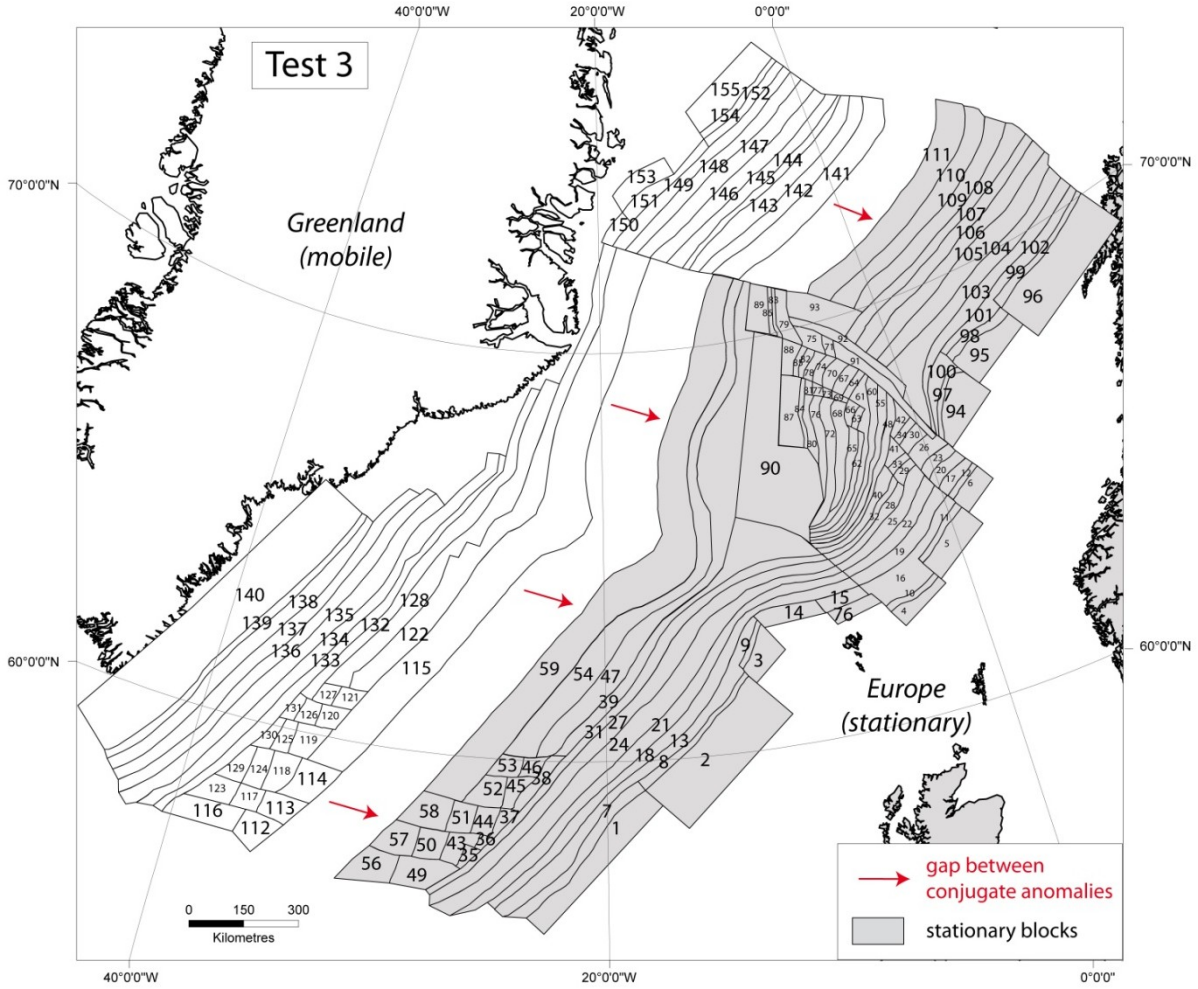

Figure 1 *Initial Block Map of Test 3 that includes a boundary between Reykjanes and Jan Mayen segments along Faeroe Fracture Zone (FFZ). Greenland plate is assumed stationary. Map projection is Universal Transverse Mercator (UTM, WGS 1984, zone 27N).*

As for Test 2, I have simplified the block map around the Aegir Ridge to avoid displacements of the little blocks, which are not supposed to move, and to reduce the calculation time (by reducing the number of blocks). Indeed, once formed, the oceanic crust is assumed as rigid, only relative displacements along fracture zones are possible. Therefore for restoration, for example at Anomaly 7, the little blocks of older magnetic anomalies are not supposed to move and can be grouped into 'bigger' rigid blocks. These 'bigger' blocks are then redrawn at each restoration stage.

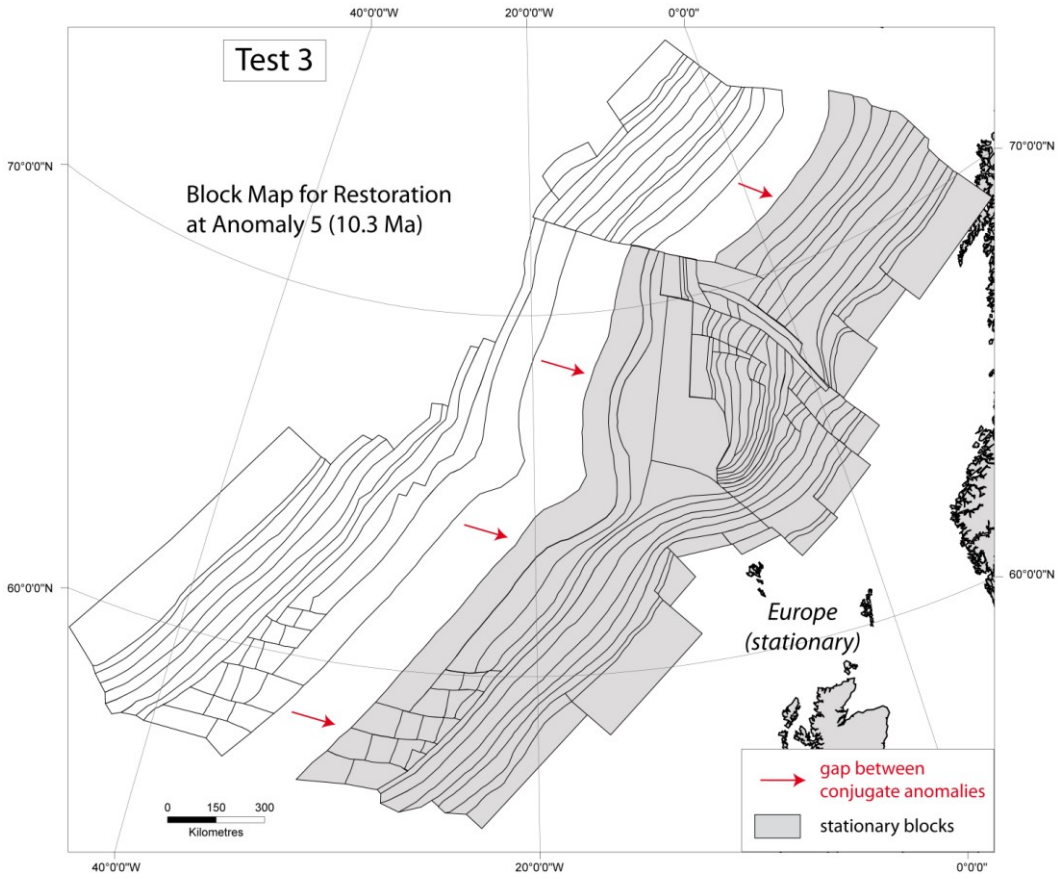

Figure 2 *Block map for restoration at Anomaly 5 (10.3 Ma)*

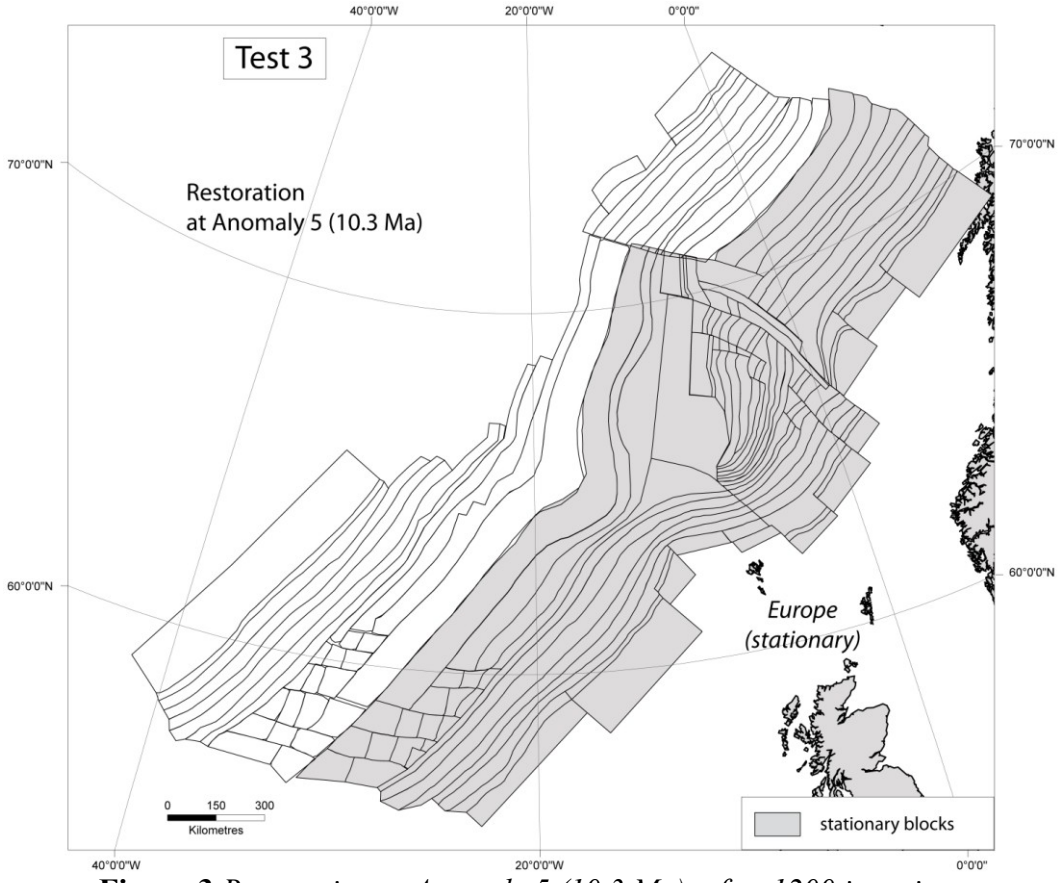

Figure 3 *Restoration at Anomaly 5 (10.3 Ma), after 1200 iterations*

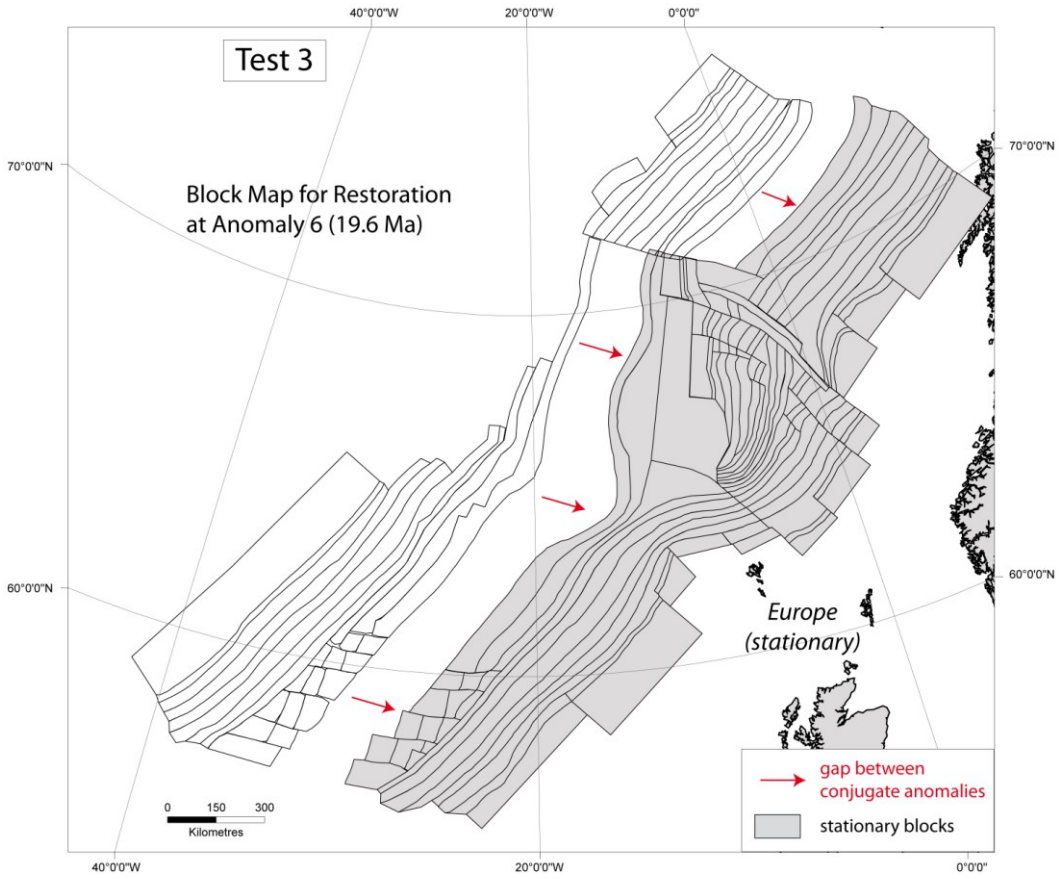

Figure 4 *Block map for restoration at Anomaly 6 (19.6 Ma)*

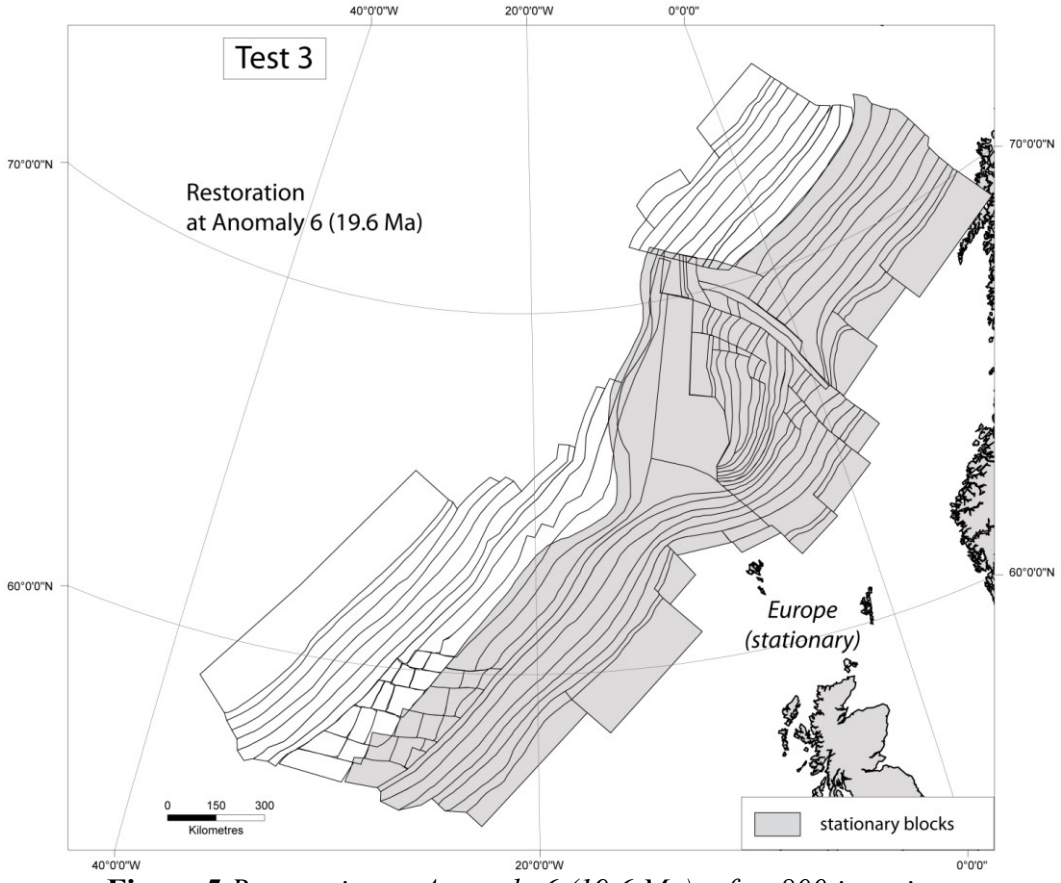

Figure 5 *Restoration at Anomaly 6 (19.6 Ma), after 800 iterations*

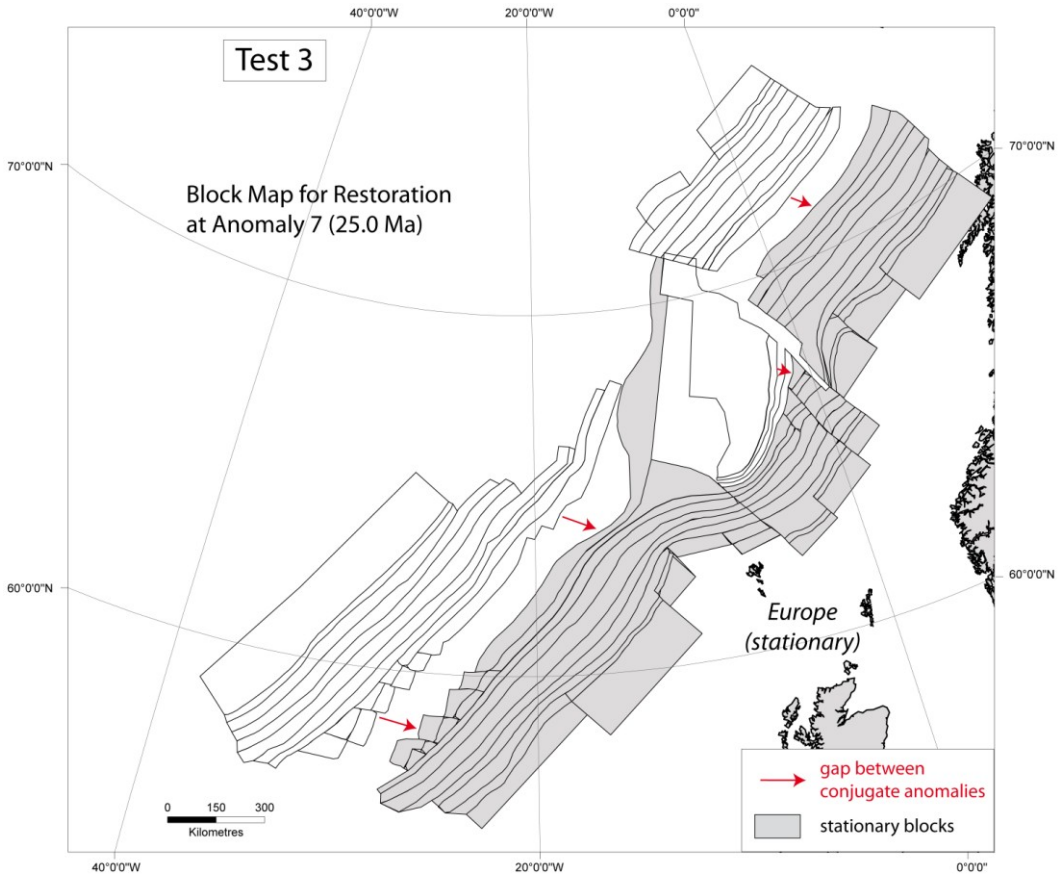

Figure 6 *Block map for restoration at Anomaly 7 (25 Ma)*

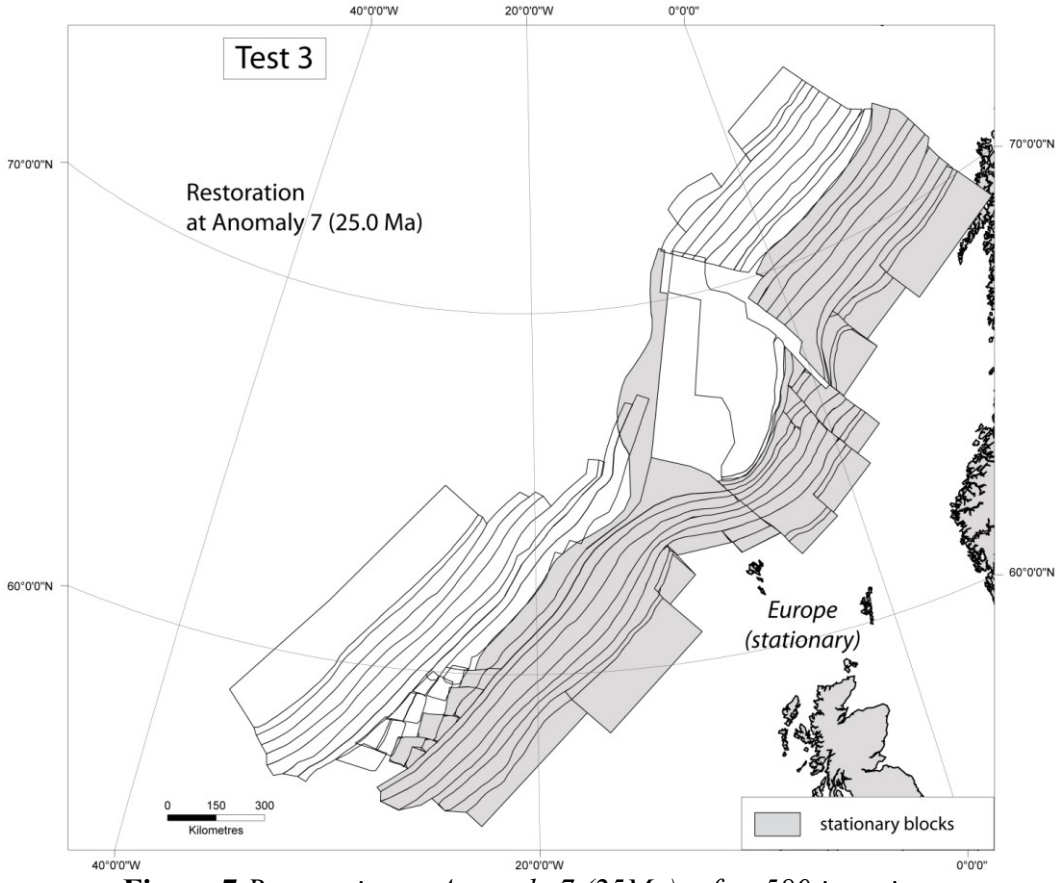

Figure 7 *Restoration at Anomaly 7 (25Ma), after 580 iterations*

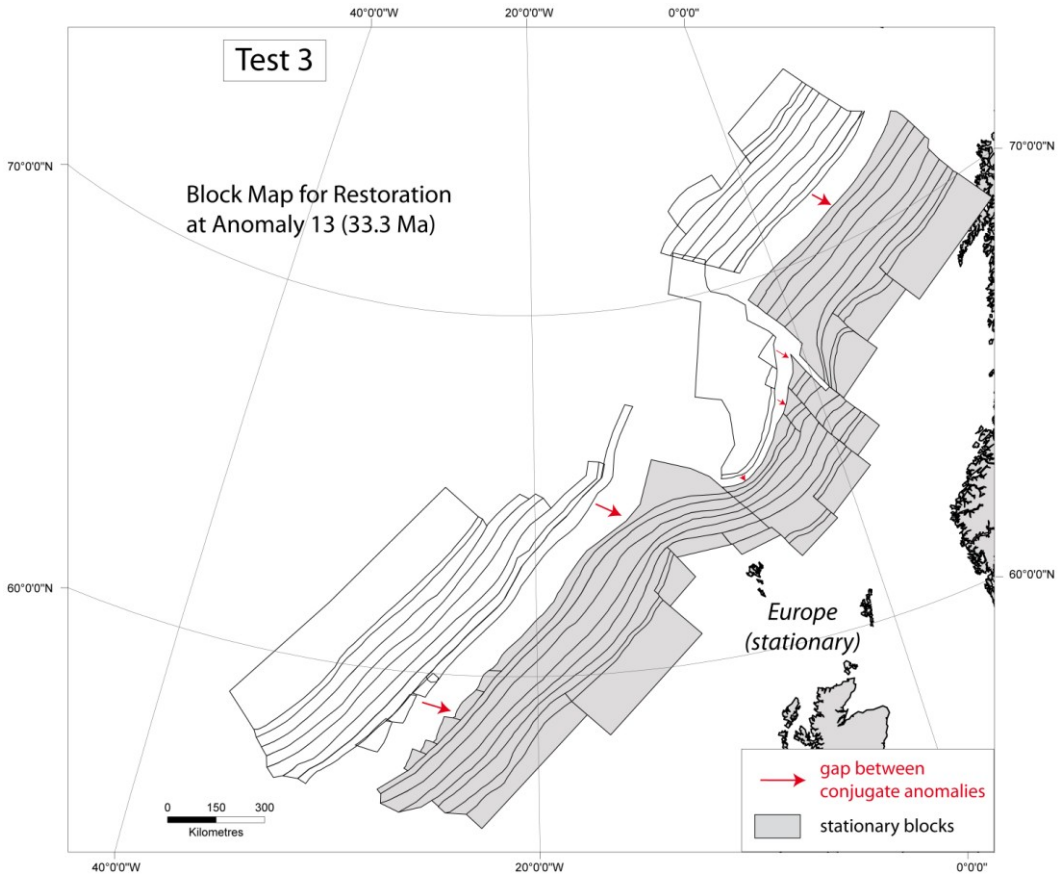

Figure 8 *Block map for restoration at Anomaly 13 (33.3 Ma)*

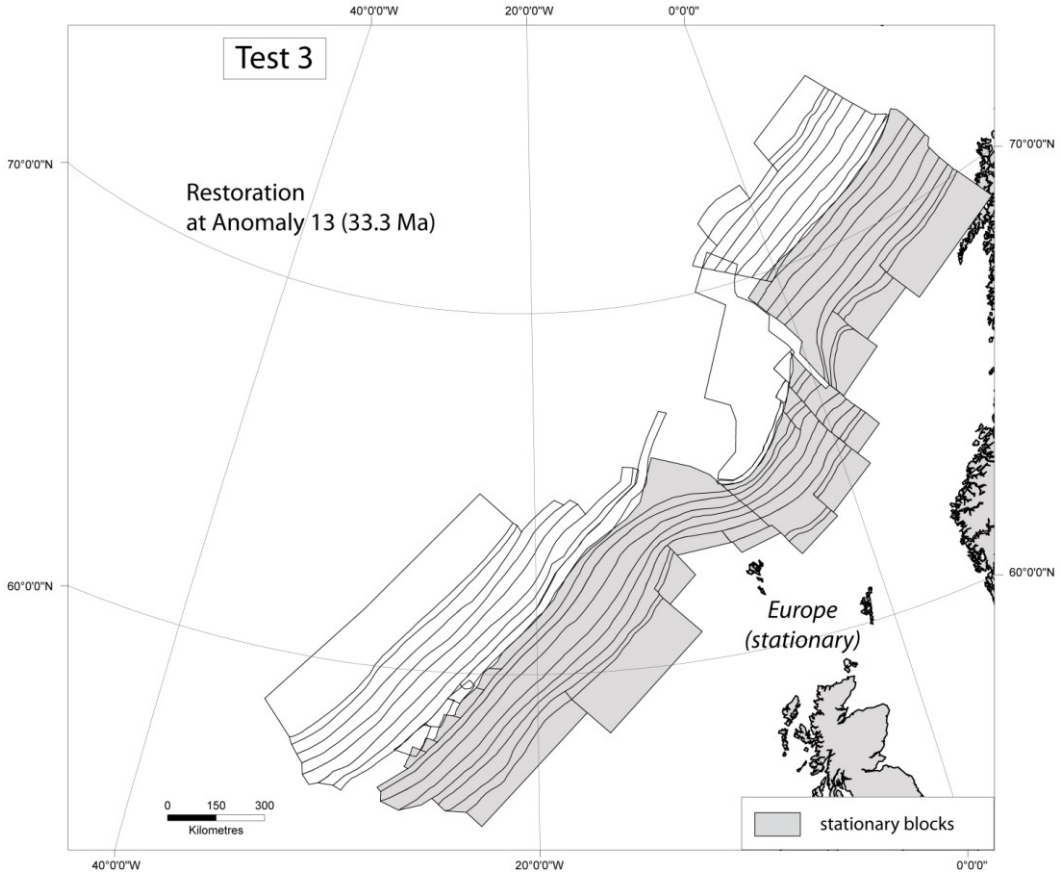

Figure 9 *Restoration at Anomaly 13 (33.3 Ma), after 200 iterations*

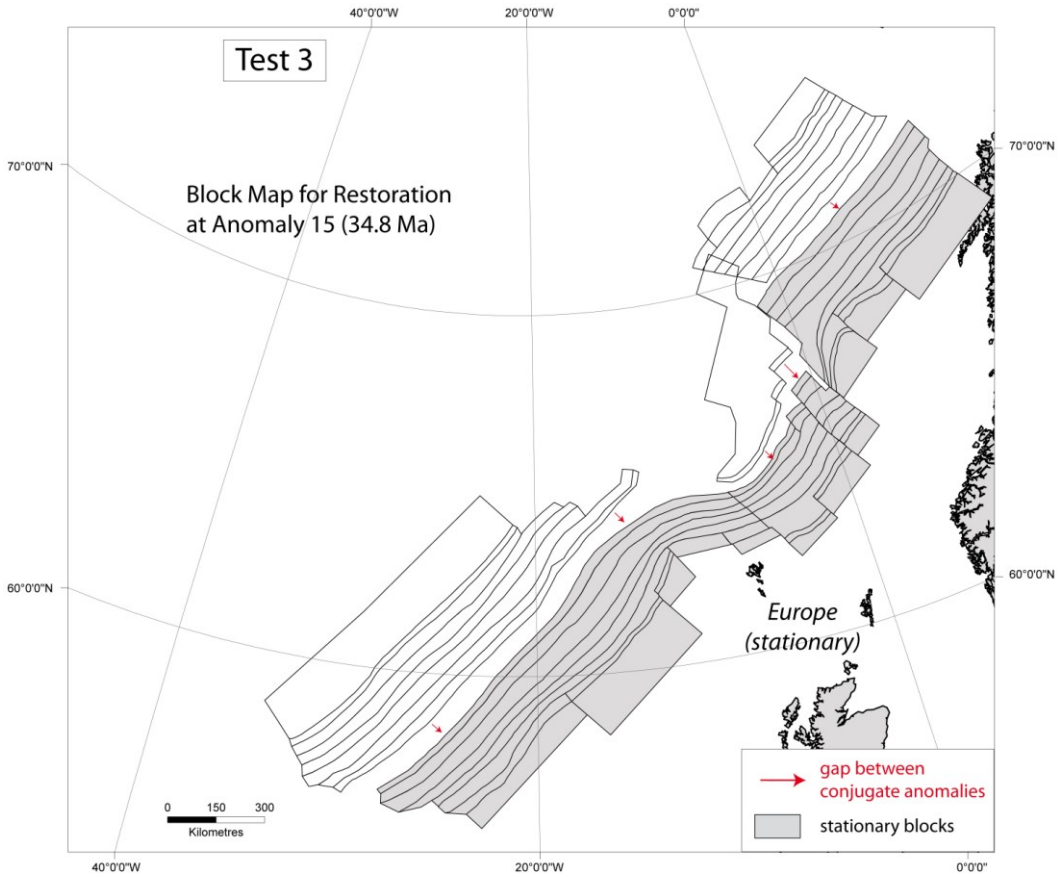

Figure 10 *Block map for restoration at Anomaly 15 (34.8 Ma)*

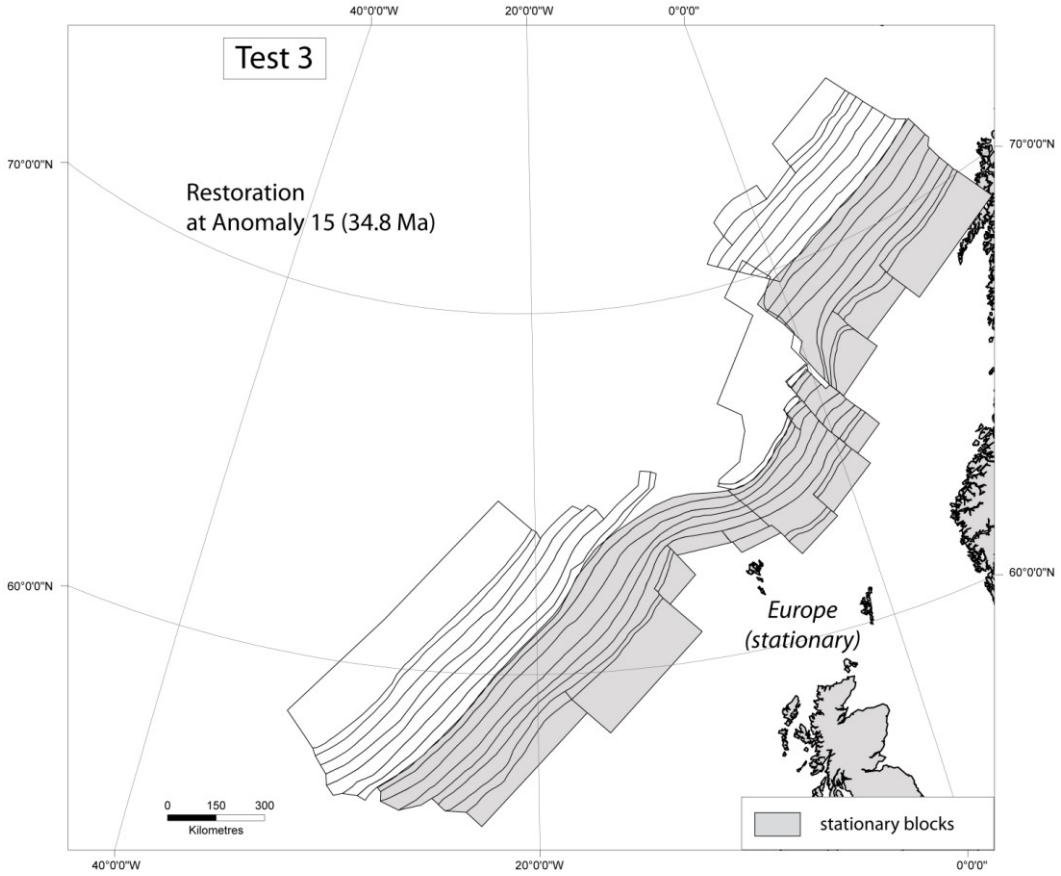

Figure 11 *Restoration at Anomaly 15 (34.8 Ma), after 200 iterations*

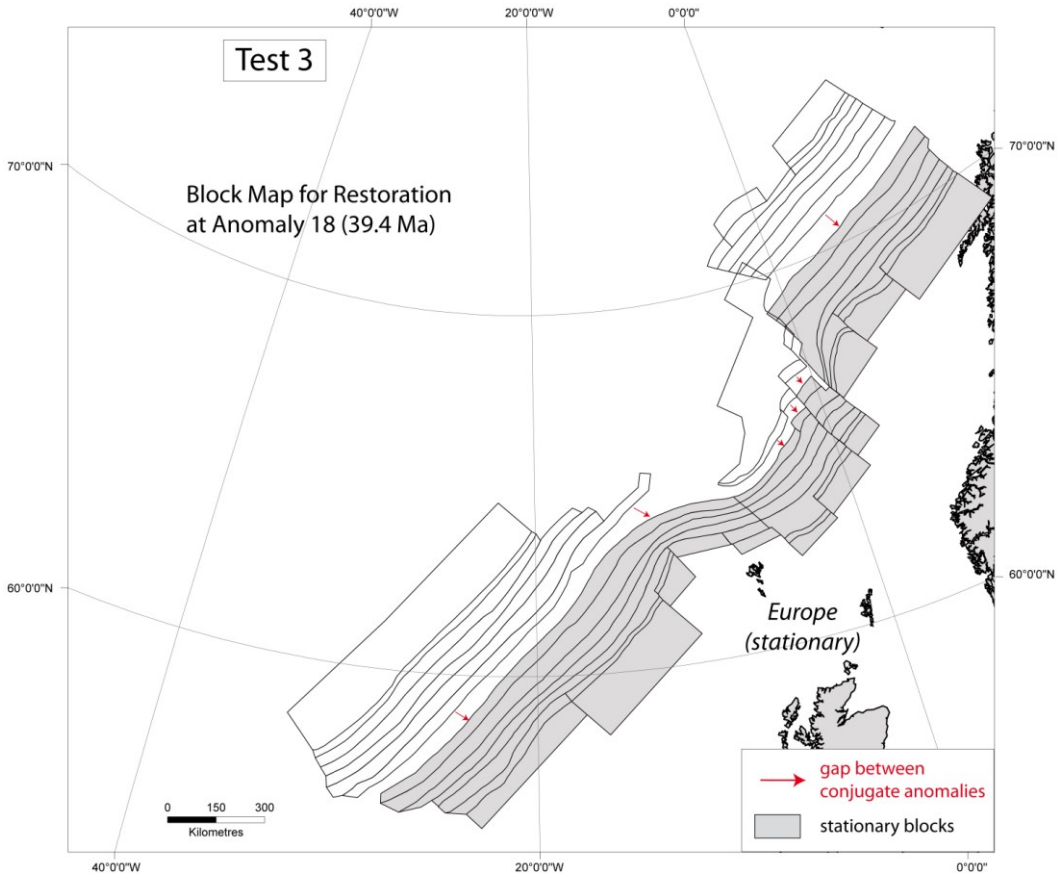

Figure 12 *Block map for restoration at Anomaly 18 (39.4 Ma)*

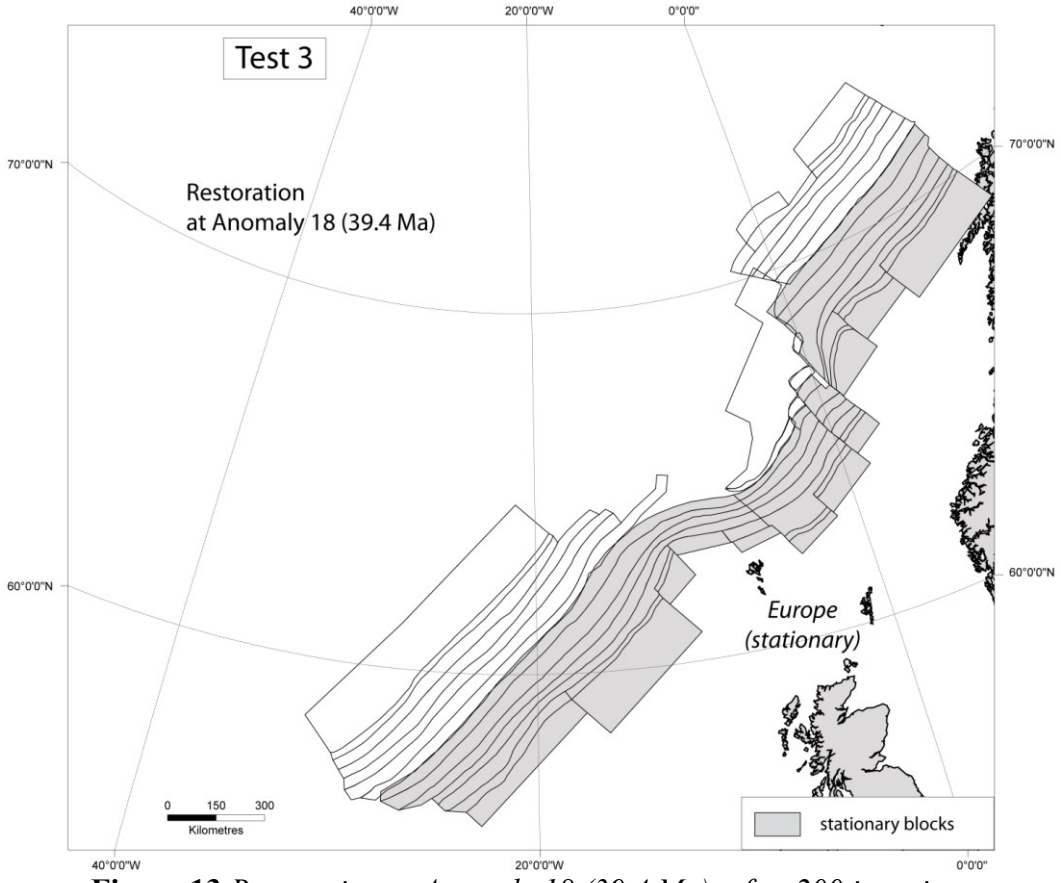

Figure 13 *Restoration at Anomaly 18 (39.4 Ma), after 200 iterations*

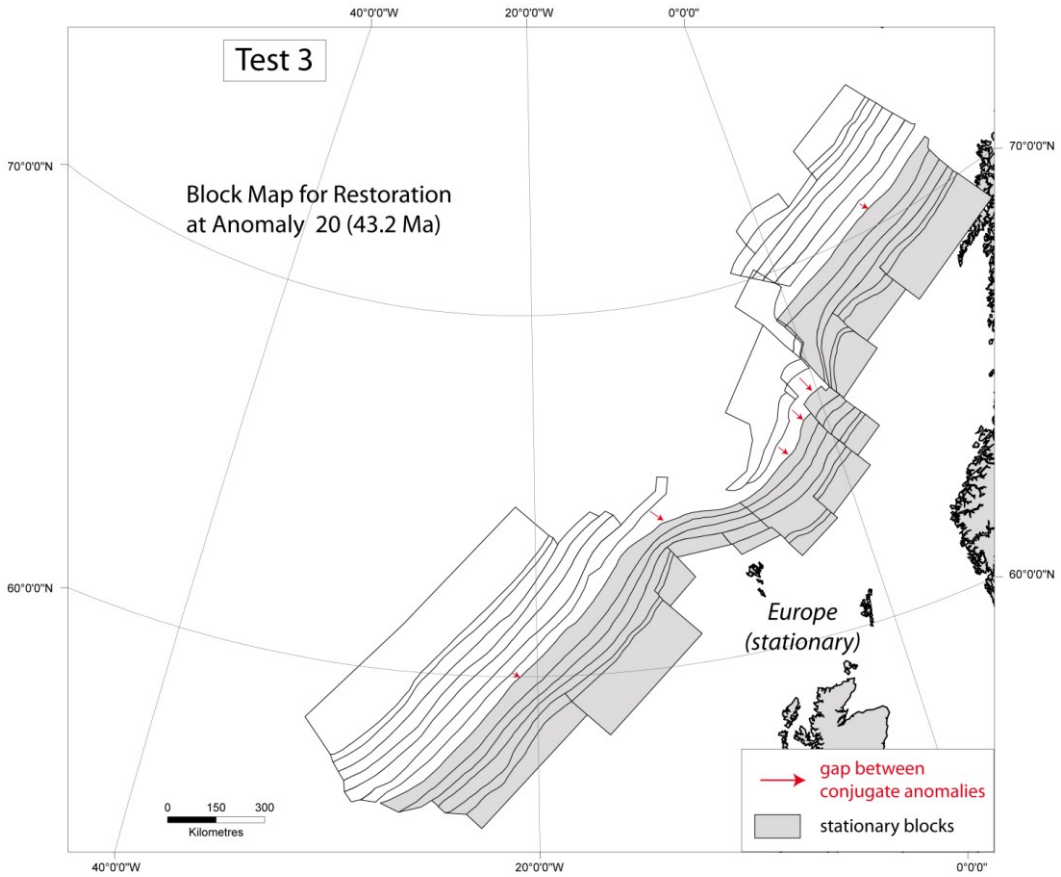

Figure 14 *Block map for restoration at Anomaly 20 (43.2 Ma*)

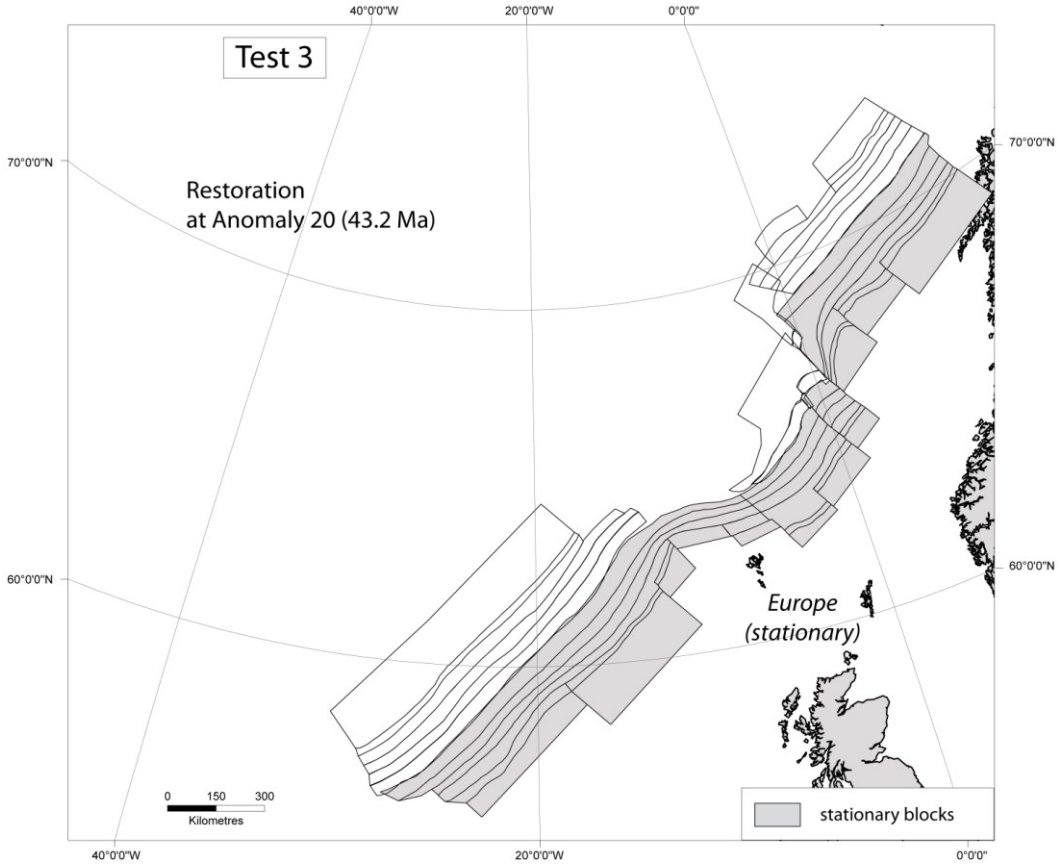

Figure 15 *Restoration at Anomaly 20 (43.2 Ma), after 200 iterations*

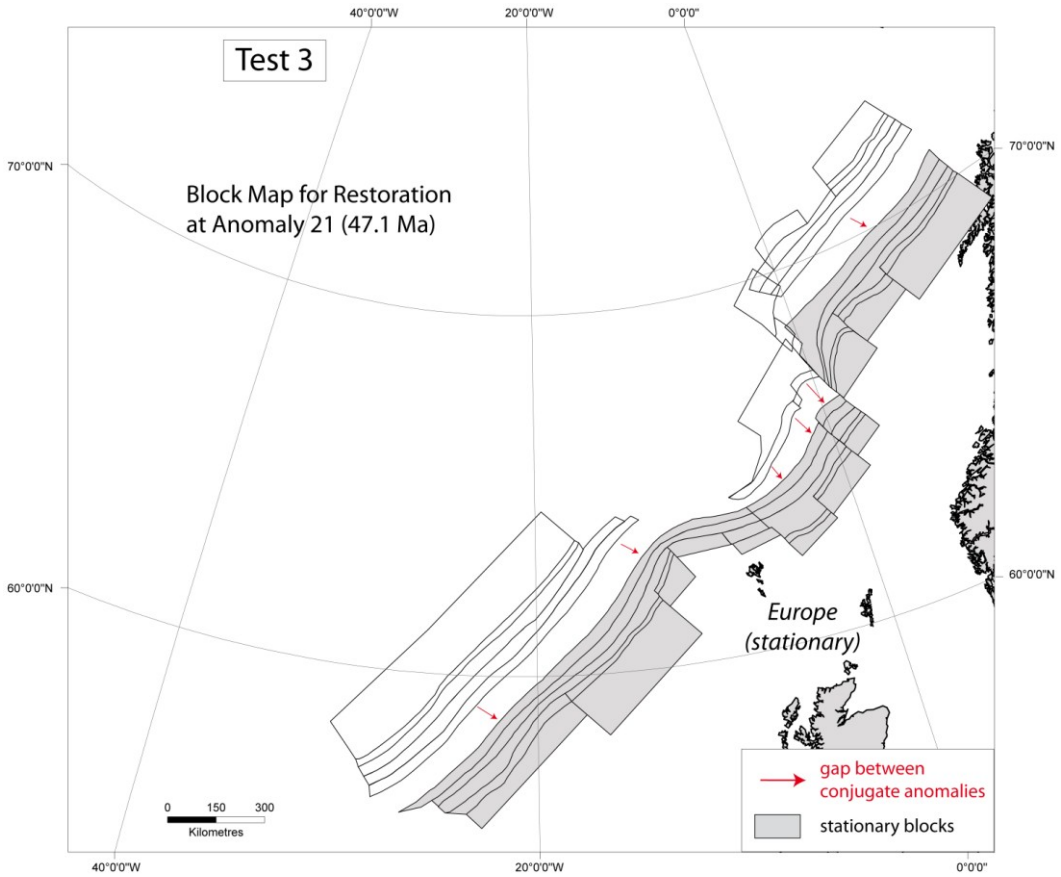

Figure 16 *Block map for restoration at Anomaly 21 (47.1 Ma*)

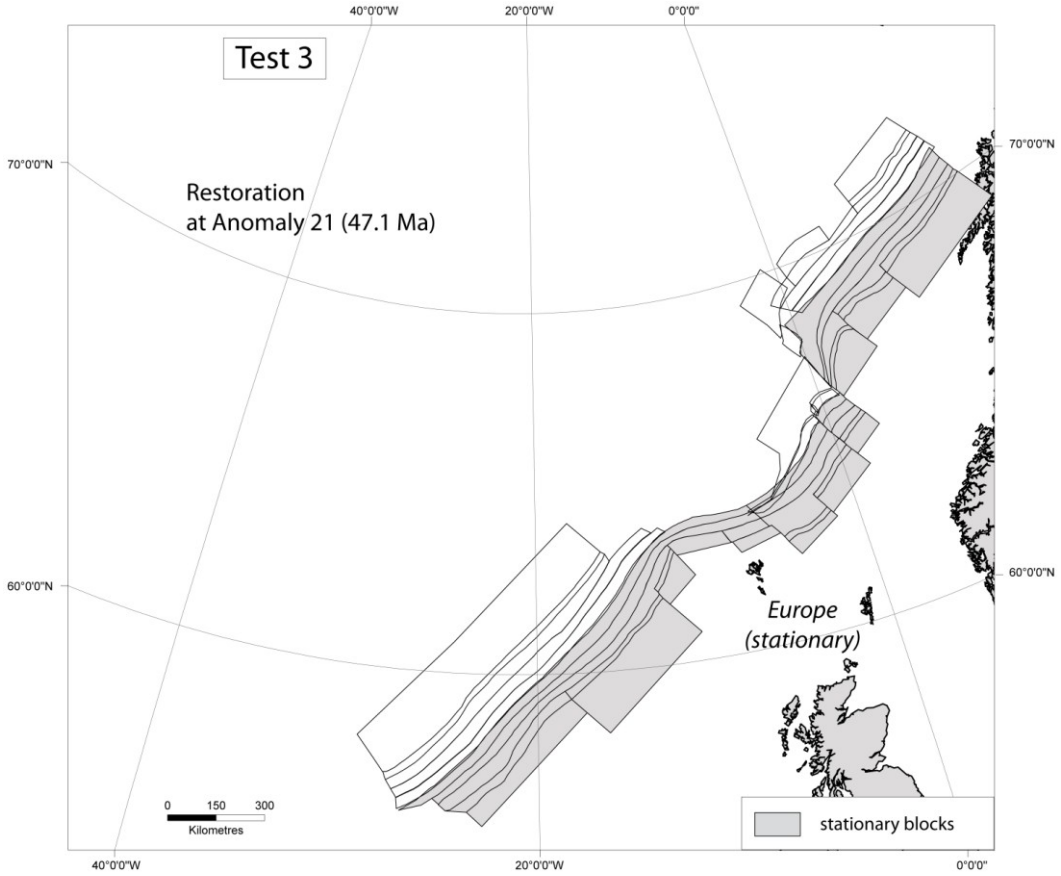

Figure 17 *Restoration at Anomaly 21 (47.1 Ma), after 200 iterations*

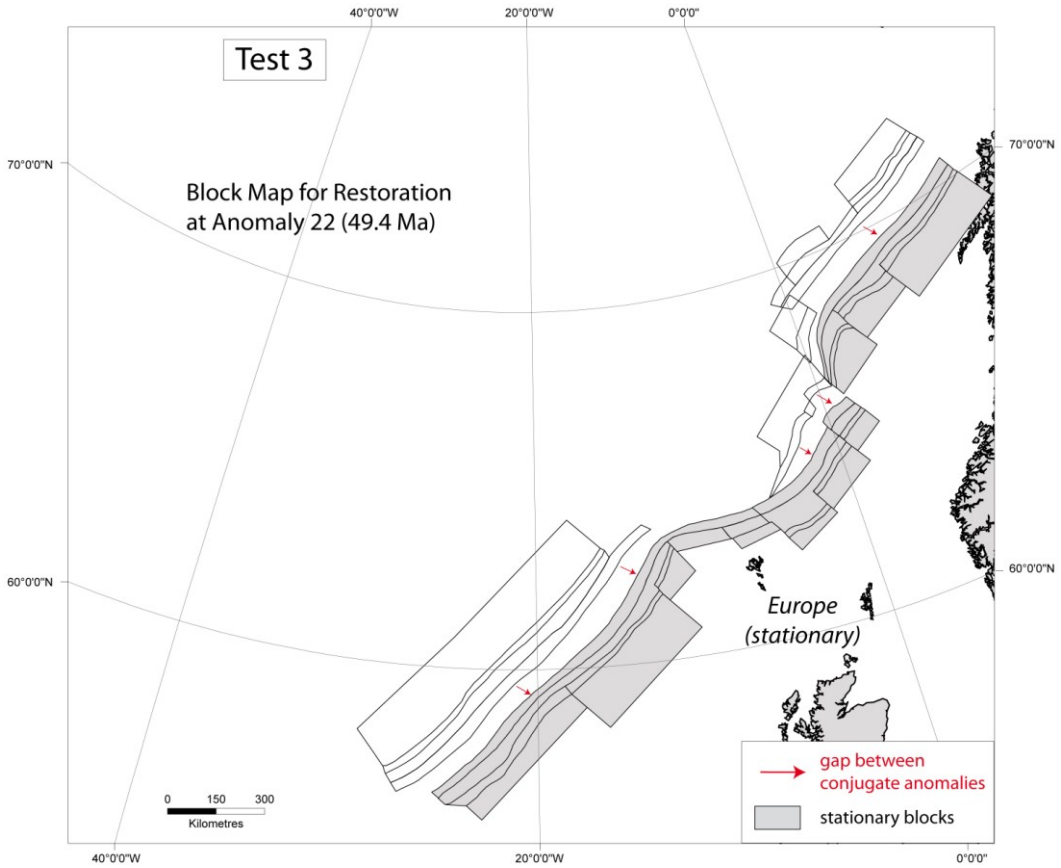

Figure 18 *Block map for restoration at Anomaly 22 (49.7 Ma)*

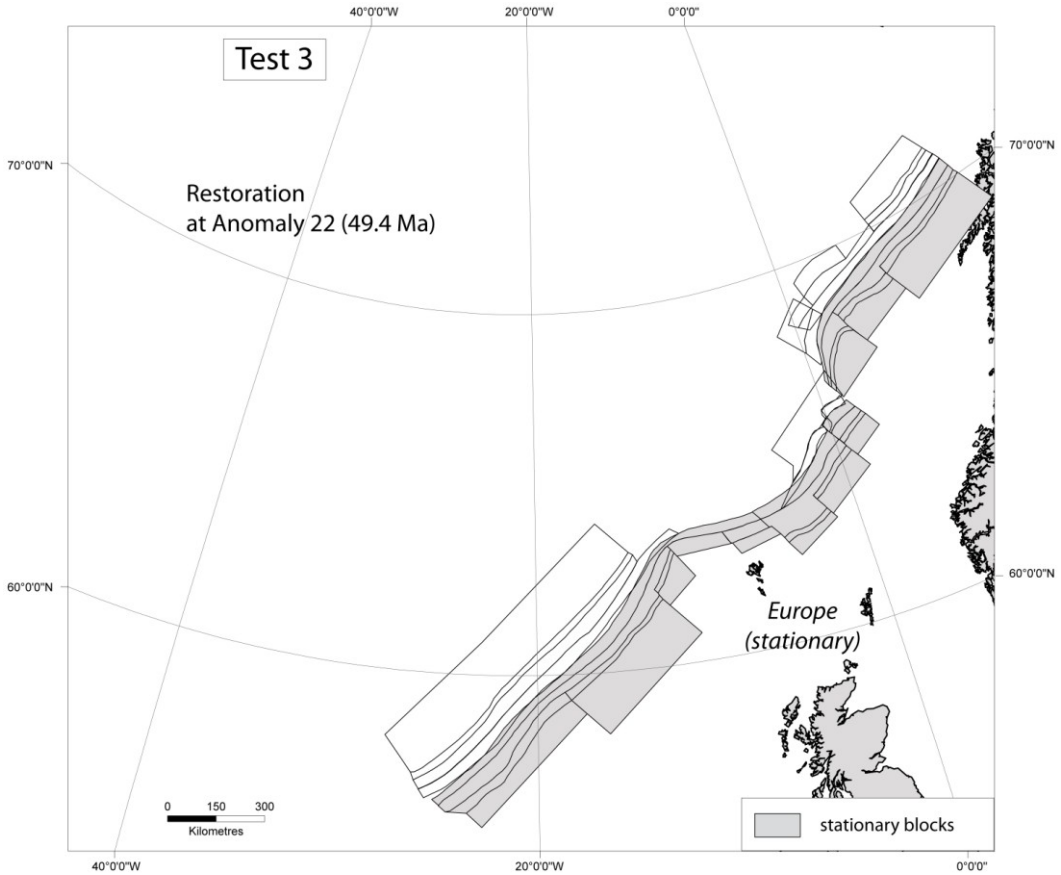

Figure 19 *Restoration at Anomaly 22 (49.7 Ma), after 200 iterations*

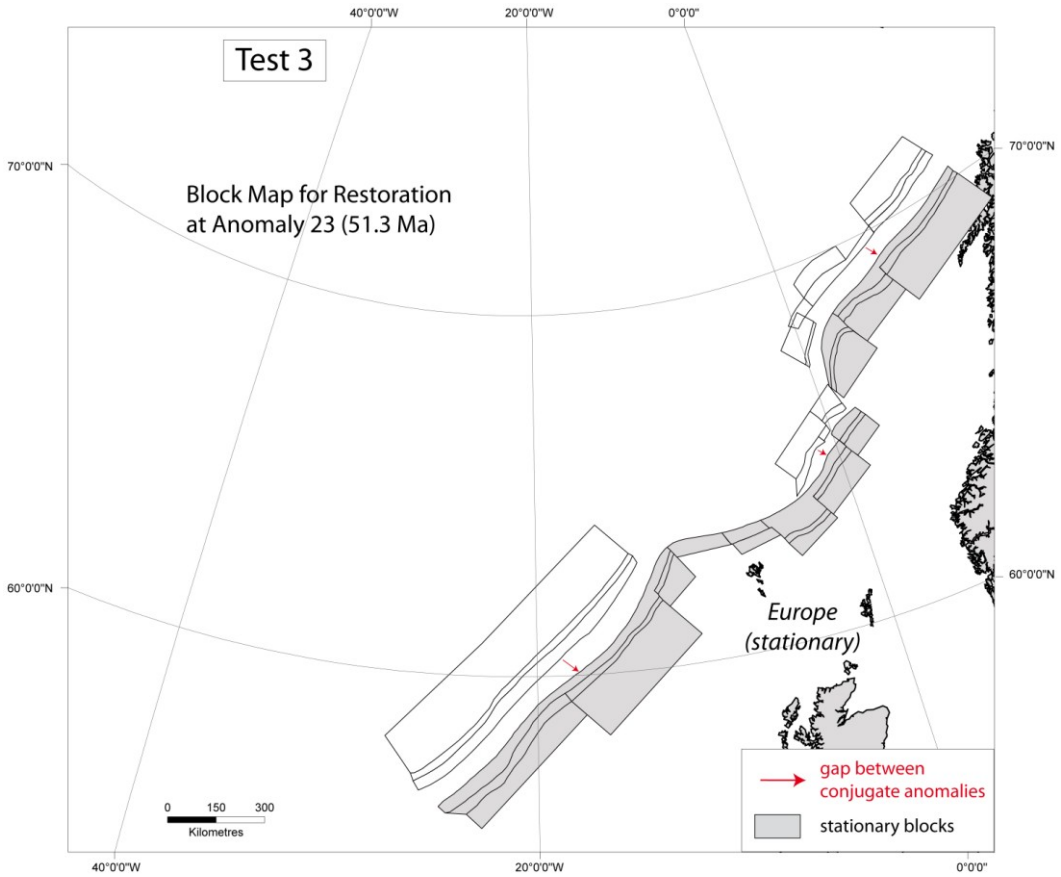

Figure 20 *Block map for restoration at Anomaly 23 (51.3 Ma)*

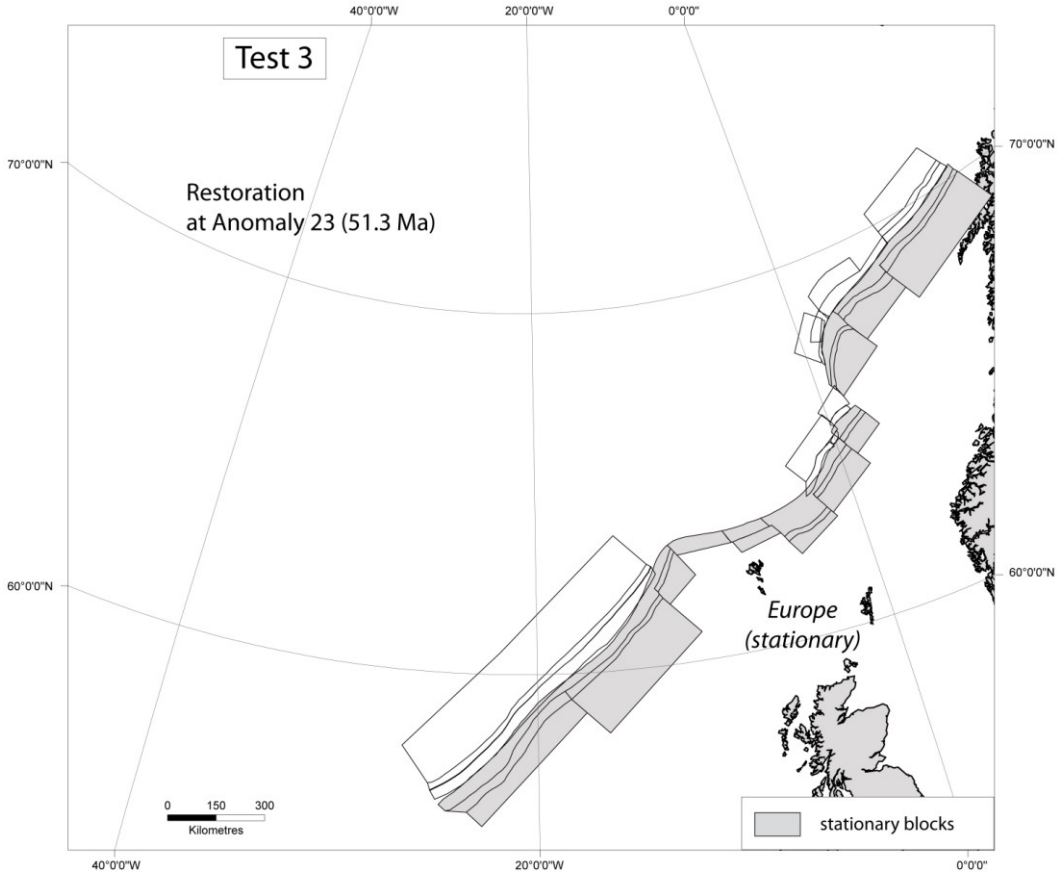

Figure 21 *Restoration at Anomaly 23 (51.3 Ma), after 200 iterations*

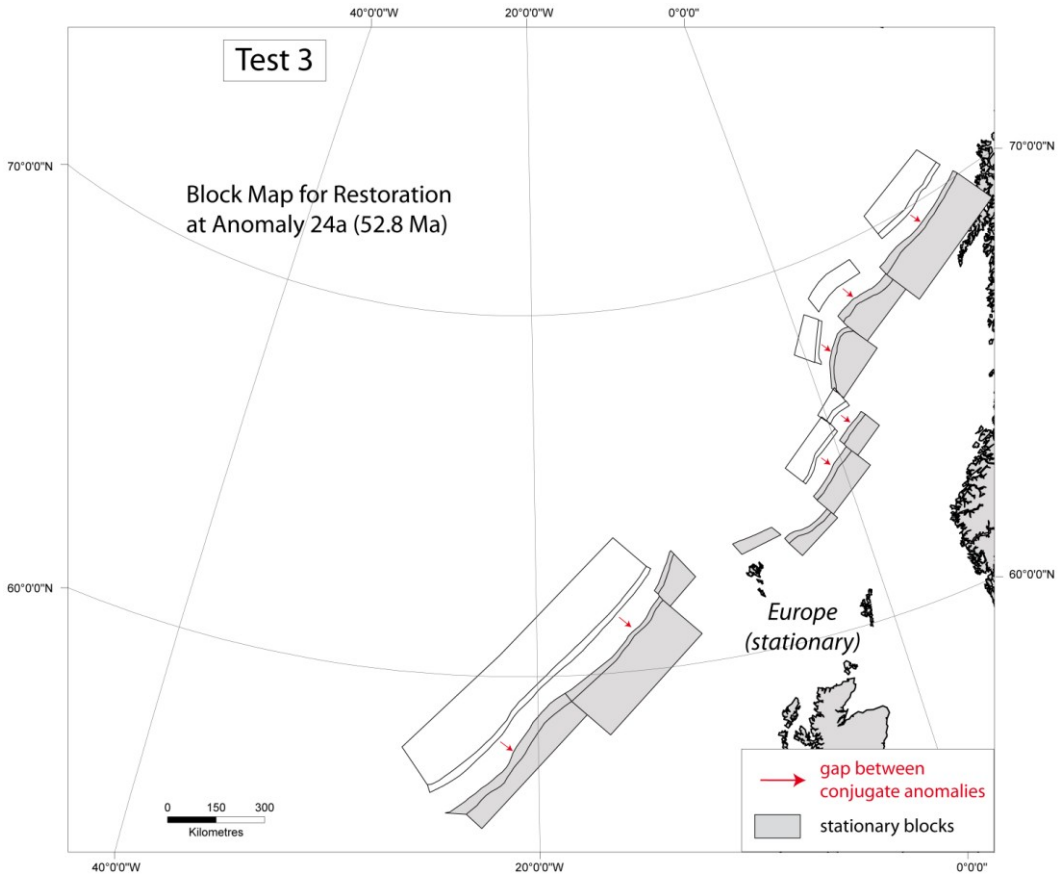

Figure 22 *Block map for restoration at Anomaly 24a (52.8 Ma)*

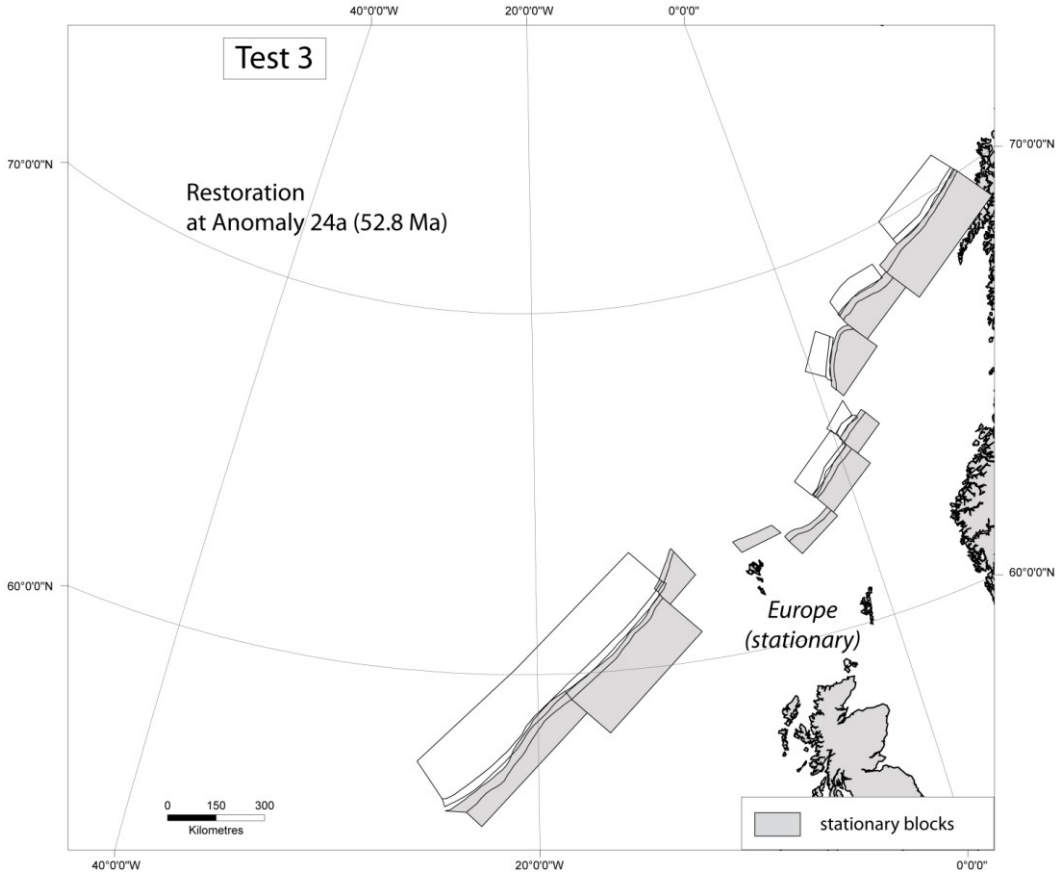

Figure 23 *Restoration at Anomaly 24a (52.8 Ma), after 140 iterations*

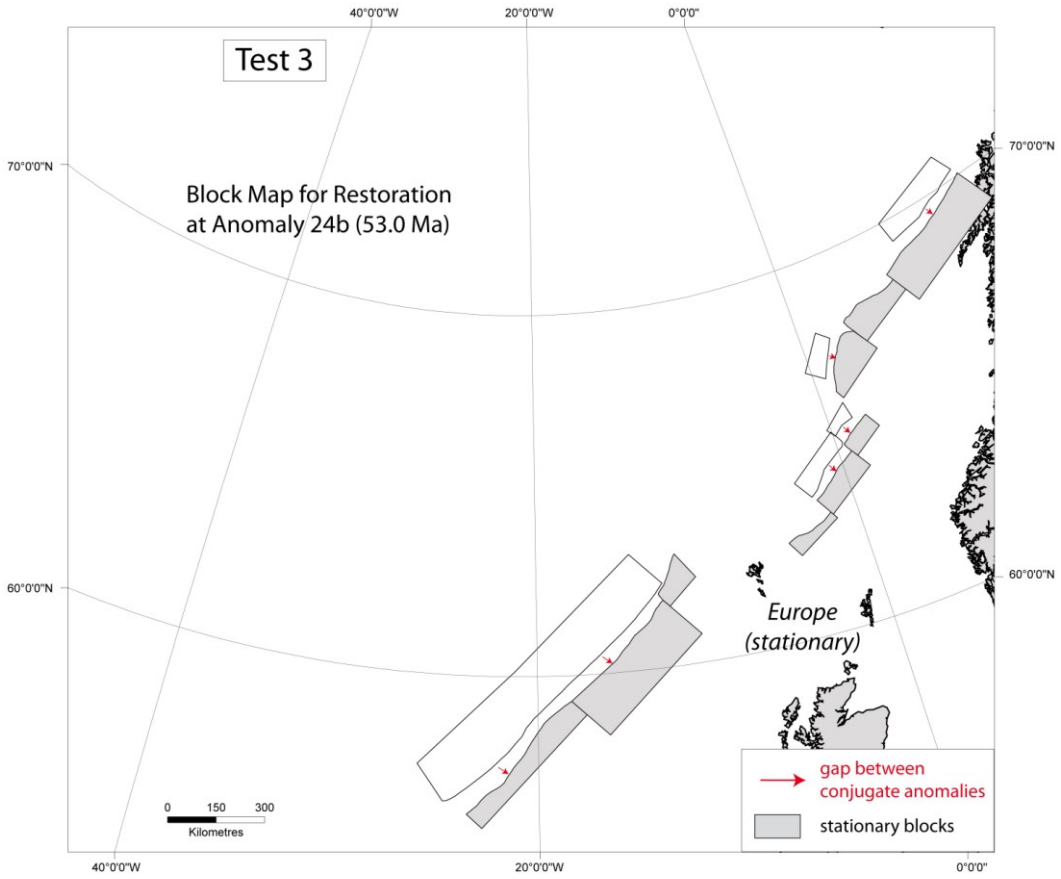

Figure 24 *Block map for restoration at Anomaly 24b (53 Ma)*

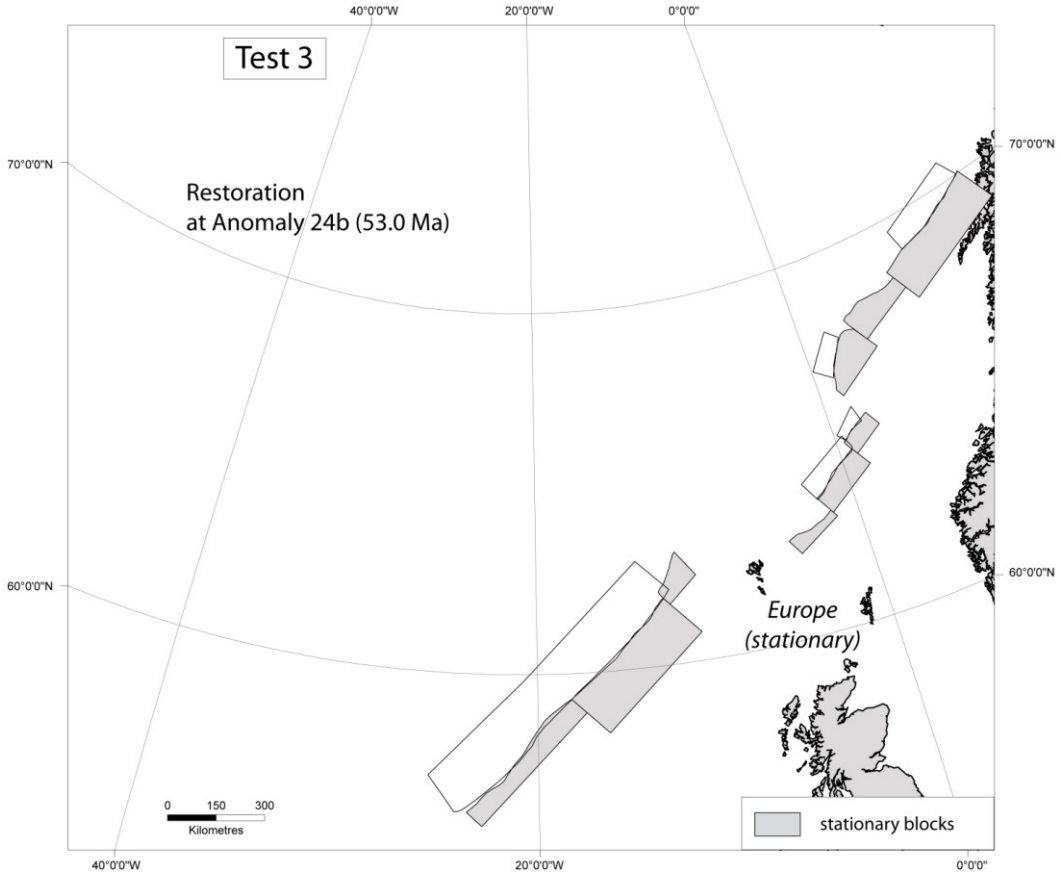

Figure 25 *Restoration at Anomaly 24b (53 Ma), after 50 iterations*

Appendix D: Modification of restoration program
Calculation of rotation equivalent to a translation of a point

(1) Select new Block, by order of increasing block number
Let P be a point (of one block) of geographic coordinates (λ, Φ), with λ the longitude and Φ the latitude (in degree).

(2) Conversion degree into radian
Angle in radian = π*(angle in degree)/180

(3) Conversion of geographic coordinates (λ, Φ) into Cartesian coordinates (x, y, z)

x=R.cosΦ.cosλ
y=R.cosΦ.sinλ
z=R.sinΦ
with R=1 for a sphere

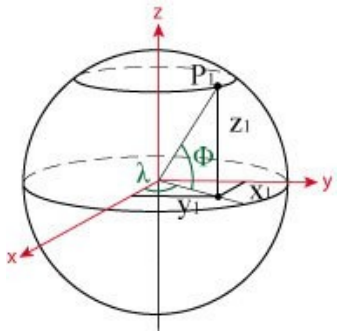

(4) Conversion of Cartesian coordinates (x, y, z) and those of map projection (X, Y)
Chosen map projection: Lambert Azimuthal Equal-Area

$X = \sqrt{\frac{2}{1-z}}\,x$

$Y = \sqrt{\frac{2}{1-z}}\,y$

(5) Calculate translation, using coordinates of map projection (Restoration program on a plane, Appendix C)
Gives a point P' with coordinates (X',Y'), which corresponds to point P after translation

(6) Reverse conversion of coordinates of map projection of P' into Cartesian coordinates (x', y', z') and geographical coordinates (λ', Φ') $x' = \sqrt{1 - \frac{X'^2+Y'^2}{4}}\,X'1$

$y' = \sqrt{1 - \frac{X'^2+Y'^2}{4}}\,Y'1$

$z' = -1 + \frac{X'^2+Y'^2}{2}$

and:

$\Phi' = \text{Arcsin}\left(\frac{z'}{R}\right)$

$\lambda' = \text{Arctan}\left(\frac{y'}{x'}\right)$

with R= radius of the Earth (6371km)

(7) Calculation of the rotation matrix corresponding to the translation
Let be P0 a point at the origin.
The rotation that brings P0 to P and P0 to P' is a combination of two rotations:

- Rotation around the y axis, of angle Φ
- Rotation around the z axis, of angle λ

According to the position of points P and P', these rotations are clockwise or counter-clockwise.
The rotation around the y axis is clockwise if point P or P' is located in the south hemisphere or counter-clockwise in the north hemisphere.
The rotation around the z axis is clockwise if point P or P' is located East of Greenwich or counter-clockwise if West of Greenwich.
The angle Φ is positive is the point is located in the north hemisphere.
The angle λ is positive is the point is located East of Greenwich.
With the trigonometric identity sin(-x) = -sin(x), a single rotation matrix R(λ, Φ), combining a counter-clockwise rotation around y, Ry(Φ), and a clockwise rotation around z, Rz(λ), brings the point P0 to P or P' for any position of point P or P':

$$R=Rz(\lambda).(Ry(\Phi))$$

Ry(Φ) $\begin{pmatrix} cos\Phi & 0 & -sin\Phi \\ 0 & 1 & 0 \\ sin\Phi & 0 & cos\Phi \end{pmatrix}$ *counter clockwise*

Rz(λ) $\begin{pmatrix} cos\lambda & -sin\lambda & 0 \\ sin\lambda & cos\lambda & 0 \\ 0 & 0 & 1 \end{pmatrix}$ *clockwise*

Let be Rot the rotation that bring P to P', Rot is equal to (-R) (R'), that is:

$$\boxed{\textbf{Rot= (R').((R)}^{\textbf{t}}\textbf{)}}$$

R' $\begin{pmatrix} a11 & a12 & a13 \\ a21 & a22 & a23 \\ a31 & a32 & a33 \end{pmatrix}$ $R^t \begin{pmatrix} b11 & b12 & b13 \\ b21 & b22 & b23 \\ b31 & b32 & b33 \end{pmatrix}$ Rot $\begin{pmatrix} R11 & R12 & R13 \\ R21 & R22 & R23 \\ R31 & R32 & R33 \end{pmatrix}$

R(λ', Φ') $\begin{pmatrix} cos\Phi'.cos\lambda' & -sin\lambda' & -sin\Phi'.cos\lambda' \\ cos\Phi'.sin\lambda' & cos\lambda' & -sin\Phi'.sin\lambda' \\ sin\Phi' & 0 & cos\Phi' \end{pmatrix}$

⇨ $a_{11}= cos\Phi'.cos\lambda'$ $a_{12}= -sin\lambda'$ $a_{13}= -sin\Phi'.cos\lambda'$
$a_{21}= cos\Phi'.sin\lambda'$ $a_{22}= cos\lambda'$ $a_{23}= -sin\Phi'.sin\lambda'$
$a_{31}= sin\Phi'$ $a_{32}= 0$ $a_{33}= cos\Phi'$

R^t(λ, Φ) $\begin{pmatrix} cos\Phi.cos\lambda & cos\Phi.sin\lambda & sin\Phi \\ -sin\lambda & cos\lambda & 0 \\ -sin\Phi.cos\lambda & -sin\Phi.sin\lambda & cos\Phi \end{pmatrix}$

⇨ $b_{11}= cos\Phi.cos\lambda$ $b_{12}= cos\Phi.sin\lambda$ $b_{13}= sin\Phi$
$b_{21}= -sin\lambda$ $b_{22}= cos\lambda$ $b_{23}= 0$
$b_{31}= -sin\Phi.cos\lambda$ $b_{32}= -sin\Phi.sin\lambda$ $b_{33}= cos\Phi$

With

$R_{11}=a_{11}b_{11}+a_{12}b_{21}+a_{13}b_{31}$ $R_{12}=a_{11}b_{12}+a_{12}b_{22}+a_{13}b_{32}$ $R_{13}=a_{11}b_{13}+a_{12}b_{23}+a_{13}b_{33}$
$R_{21}=a_{21}b_{11}+a_{22}b_{21}+a_{23}b_{31}$ $R_{22}=a_{21}b_{12}+a_{22}b_{22}+a_{23}b_{32}$ $R_{23}=a_{21}b_{13}+a_{22}b_{23}+a_{23}b_{33}$
$R_{31}=a_{31}b_{11}+a_{32}b_{21}+a_{33}b_{31}$ $R_{32}=a_{31}b_{12}+a_{32}b_{22}+a_{33}b_{32}$ $R_{33}=a_{31}b_{13}+a_{32}b_{23}+a_{33}b_{33}$

(8) Application of this rotation to all the other points of the block (n), let be (n') the points corresponding to (n) after the rotation

$x(n') = R11x(n) + R12y(n) + R13z(n)$

$y(n') = R21x(n) + R22y(n) + R23z(n)$

$z(n') = R31x(n) + R32y(n) + R33z(n)$

(9) Reverse conversion of the Cartesian coordinates to geographical coordinates first in radian, then in degree $(\lambda n', \Phi n')$

⇨ **Return to (1)**

Appendix Chapter 4

Auxilary material for Paper 2011TC003087

Variations in amount and direction of sea-floor spreading along the North East Atlantic Ocean and resulting deformation of the continental margin of North West Europe

E. Le Breton[1]*, P.R. Cobbold[1], O. Dauteuil1, G. Lewis[2]
[1] Geosciences Rennes, Université de Rennes 1, CNRS, 263 Avenue du Général Leclerc, 35042 Rennes, France
[2] Chevron Onshore Europe, Seafield House, Hill of Rubislaw, Aberdeen, AB10 6XL, United Kingdom
*Corresponding author, eline.lebreton@univ-rennes1.fr

Tectonics

Introduction

This appendix contains:
- figures of restoration of the opening of the NE Atlantic for 13 stages, from Chron 5 (10.3Ma) to 55.9 Ma for each restoration, for Model 1 and Model 2; we have indicated the criterion of fit (G) for the restorations of both models on each figure;
- table and a graph of the G values for the restorations of both models;
- tables of the best-fit rotation poles and their uncertainties (total misfit, degrees of freedom, quality factor, number of data points and great circle segments, covariance matrices), for each spreading system, for both models.

Map projection is Universal Transverse Mercator (UTM, WGS 1984, zone 27N).

Figure 1: Restoration at Chron 5 - 10.3 Ma - MODEL 1 *(G = 0.0017)*

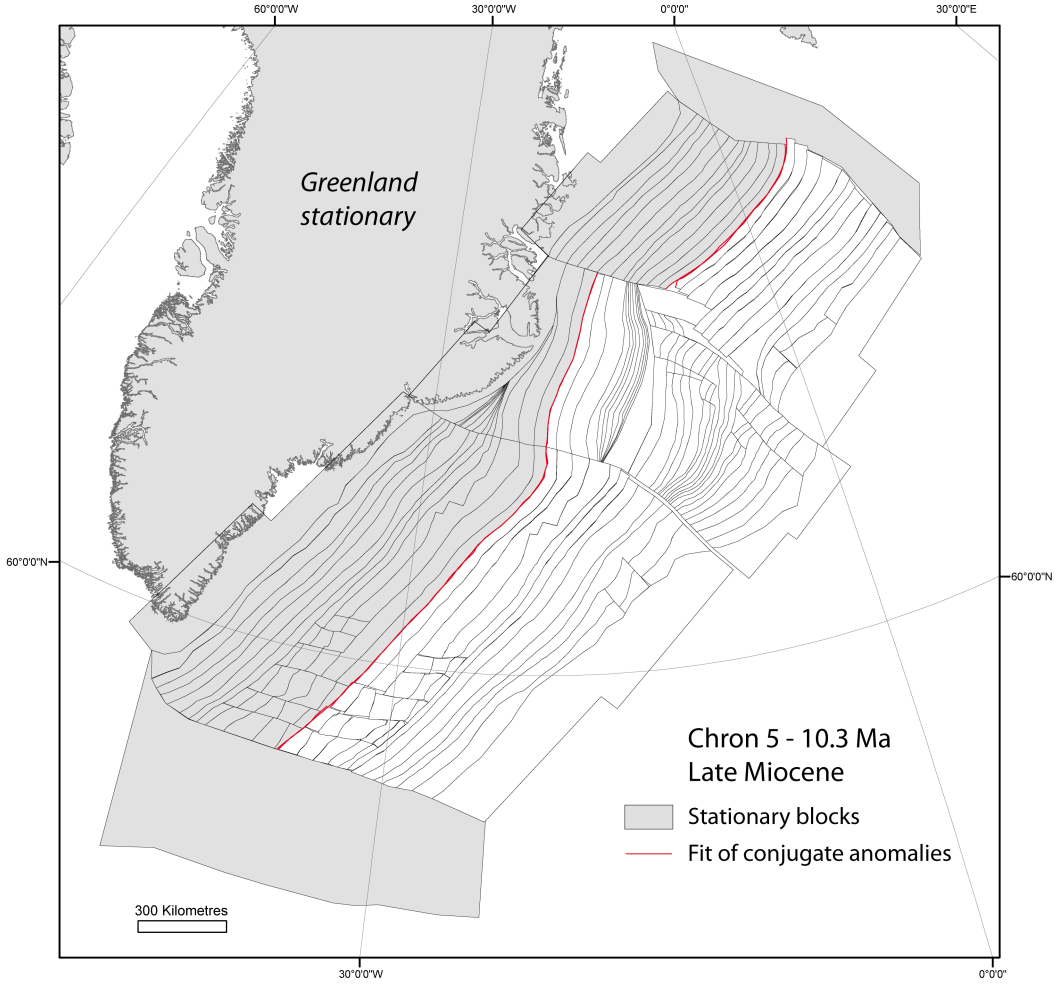

Figure 2: Restoration at Chron 5 - 10.3 Ma - MODEL 2 *(G = 0.0009)*

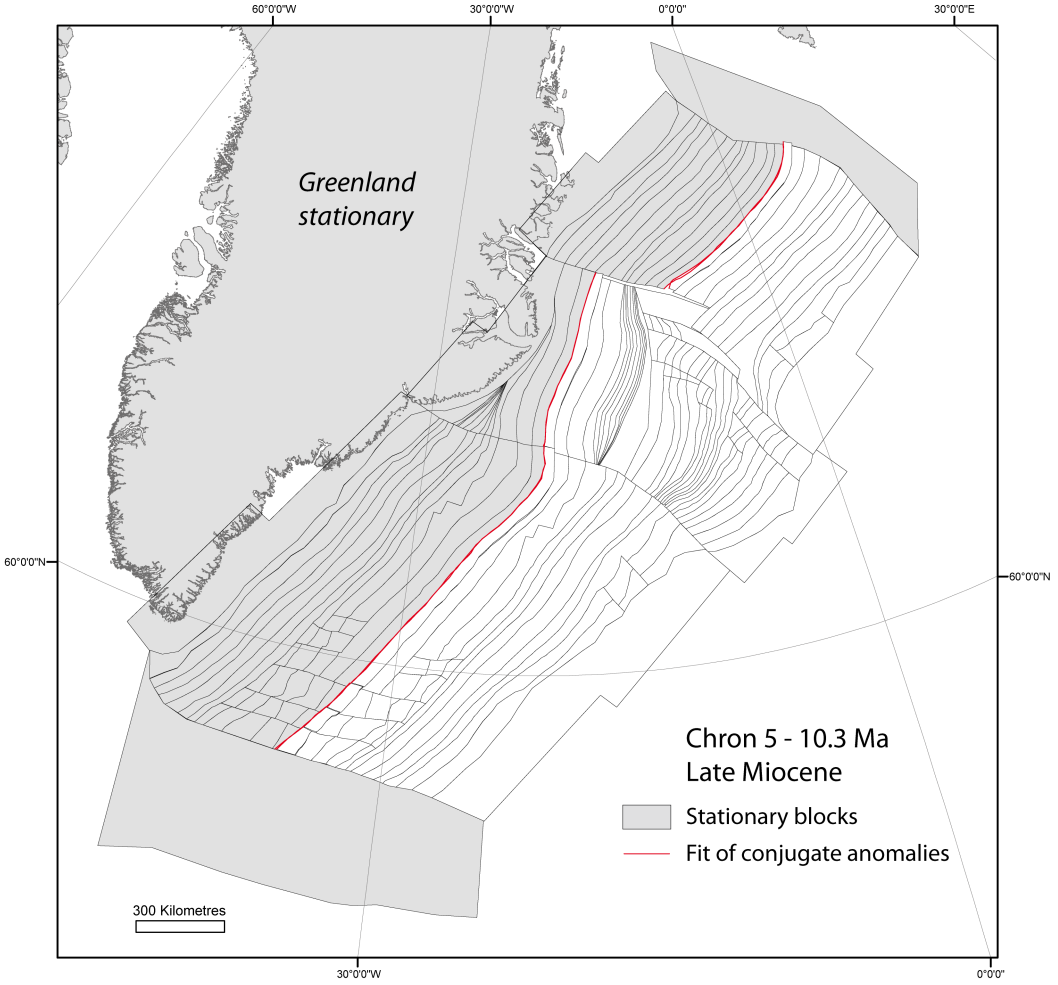

Figure 3: Restoration at Chron 5A - 14.2 Ma - MODEL 1 *(G = 0.0016)*

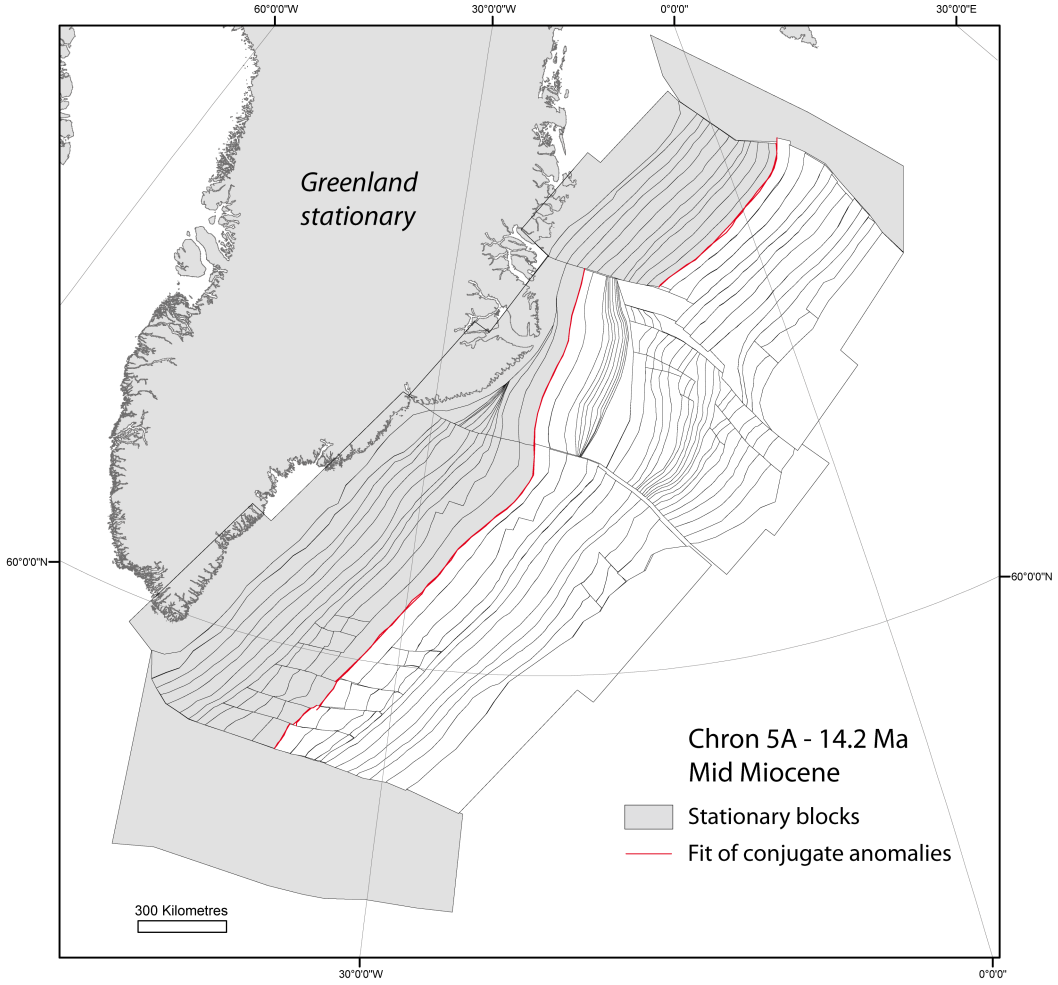

Figure 4: Restoration at Chron 5A - 14.2 Ma - MODEL 2 *(G = 0.0007)*

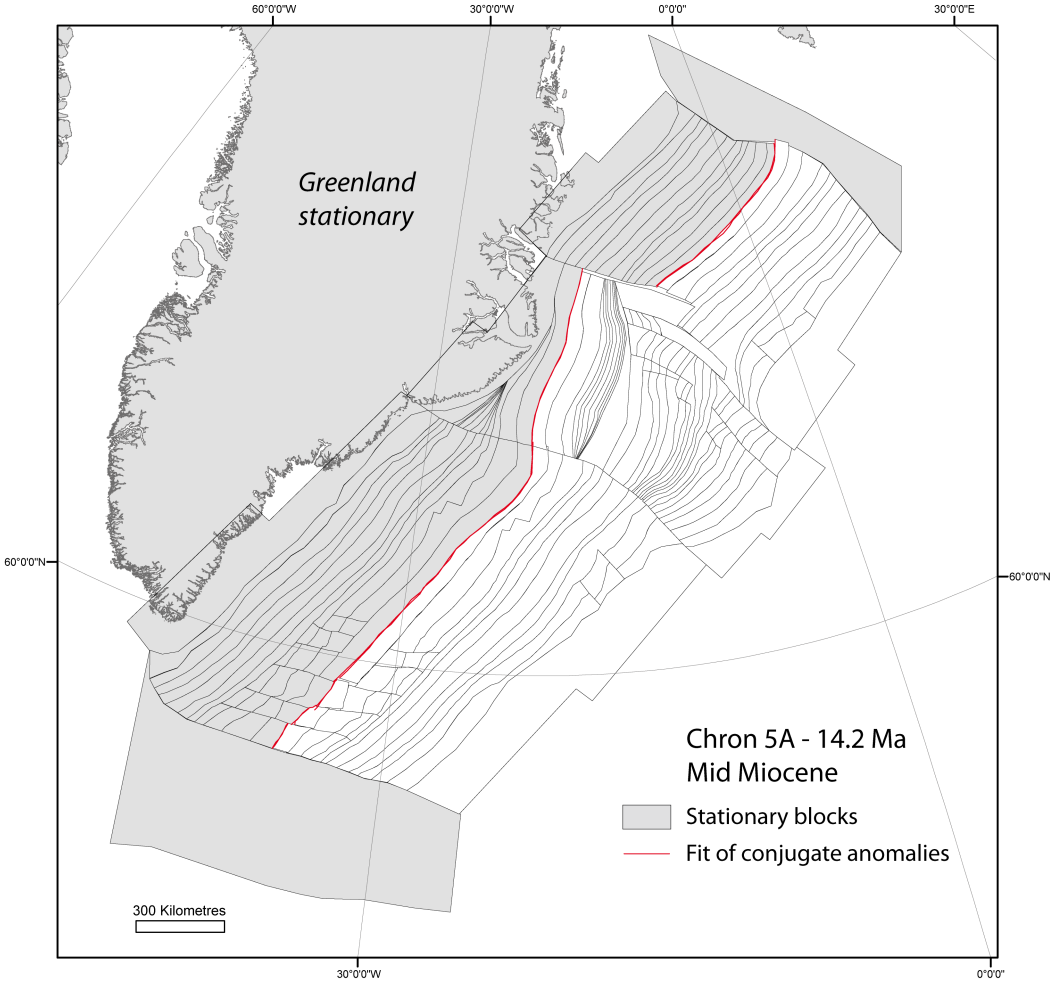

Figure 5: Restoration at Chron 6 - 19.6 Ma - MODEL 1 *(G = 0.0021)*

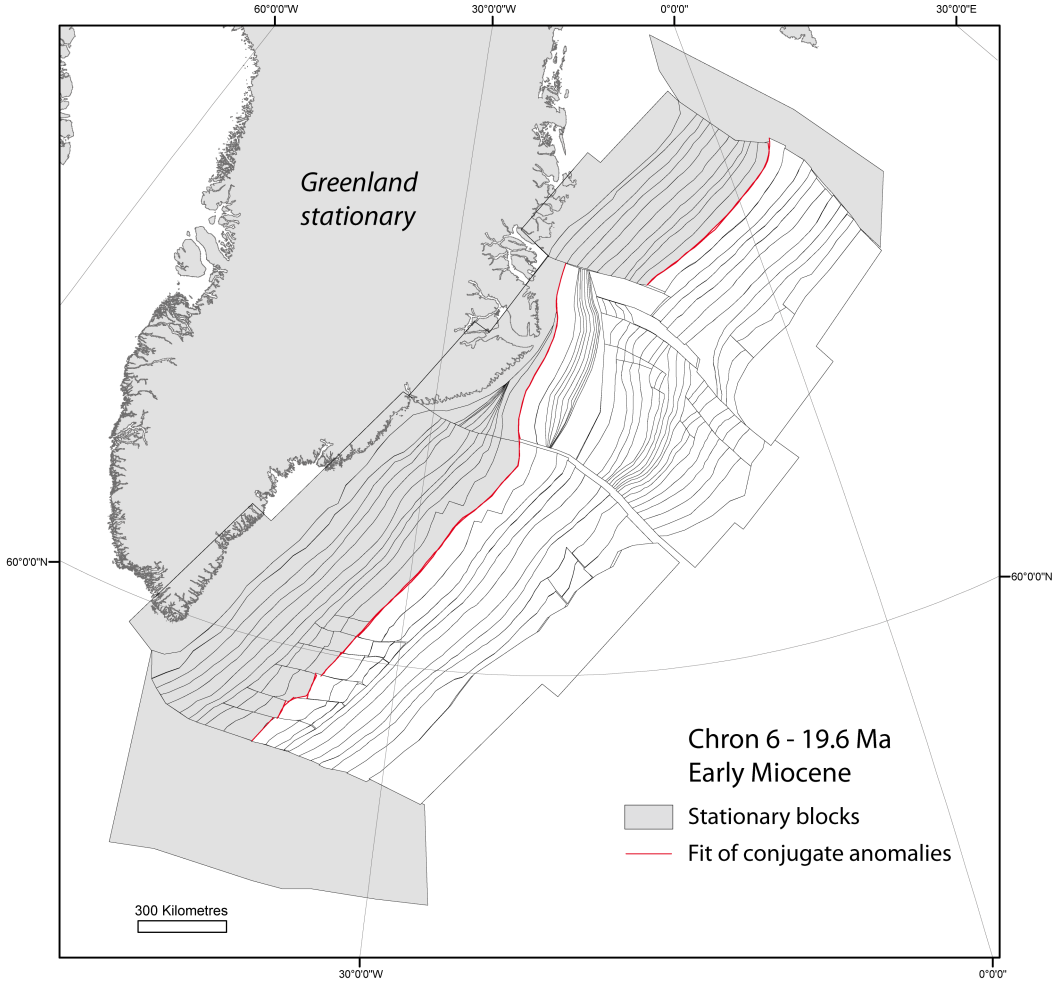

Figure 6: Restoration at Chron 6 - 19.6 Ma - MODEL 2 *(G = 0.0009)*

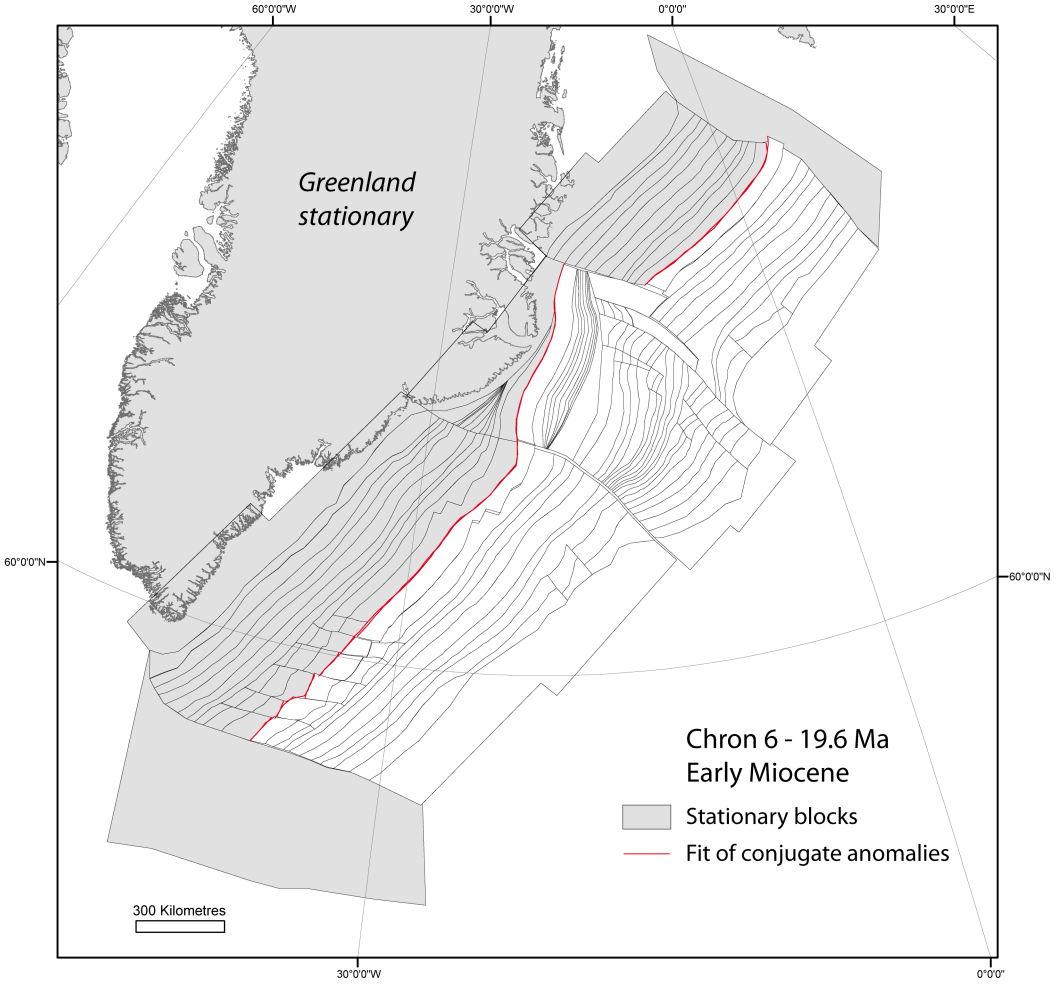

Figure 7: Restoration at Chron 8 - 26.4 Ma - MODEL 1 *(G = 0.0018)*

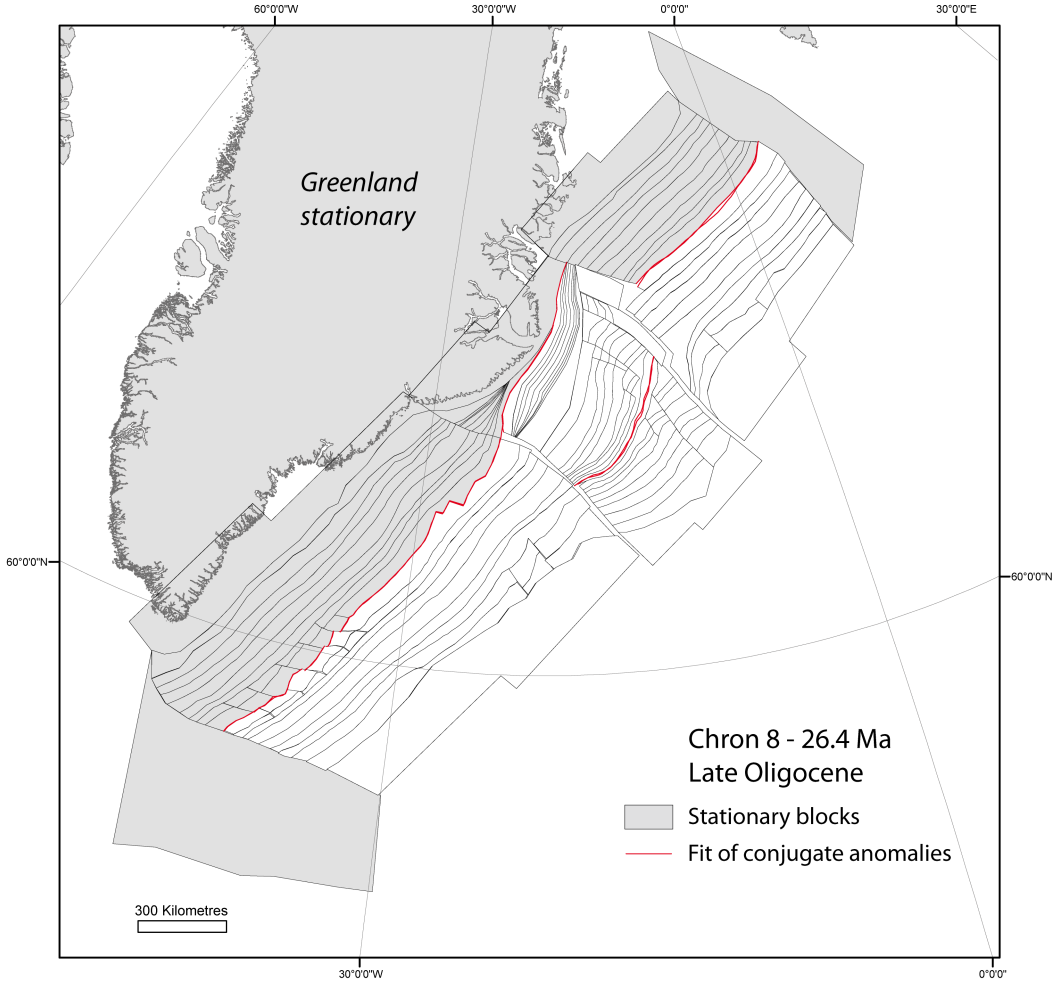

Figure 8: Restoration at Chron 8 - 26.4 Ma MODEL 2 *(G = 0.0024)*

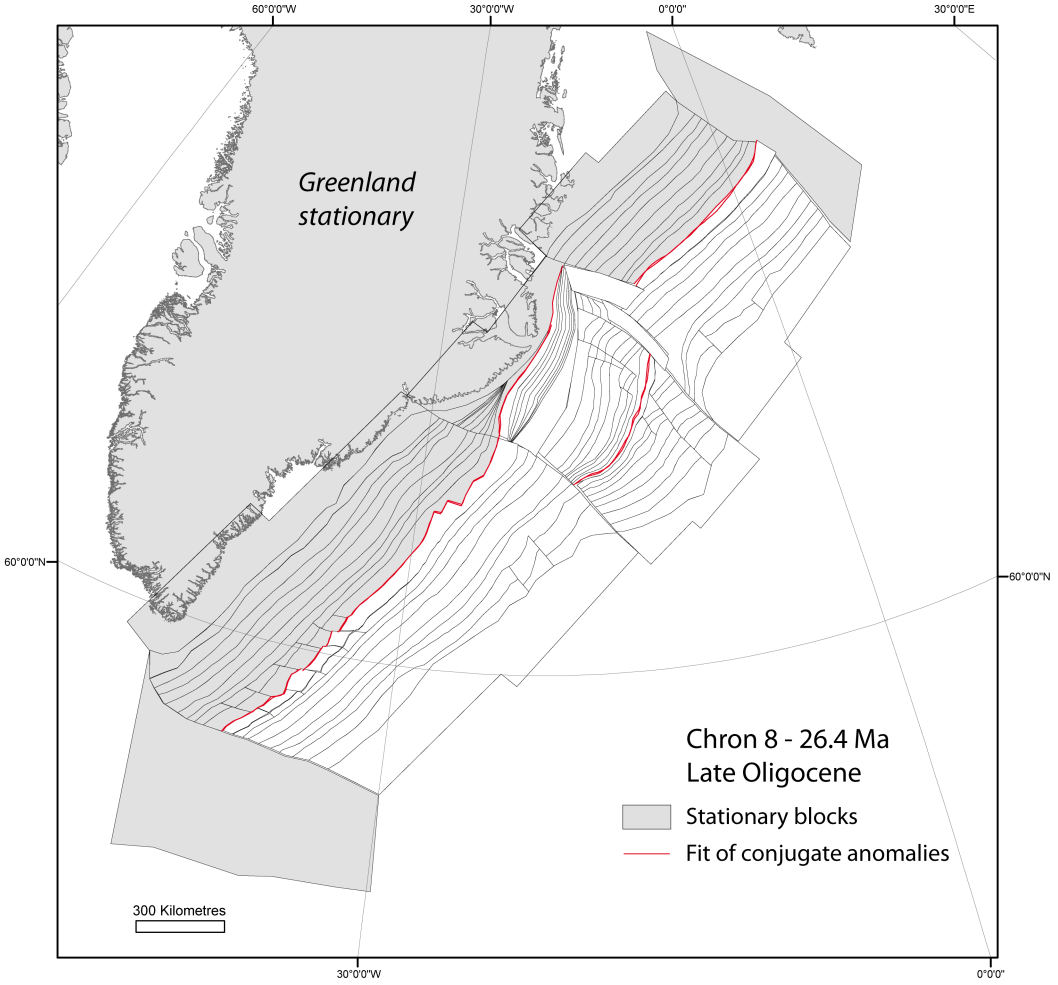

Figure 9: Restoration at Chron 13 - 33.3 Ma - MODEL 1 *(G = 0.0023)*

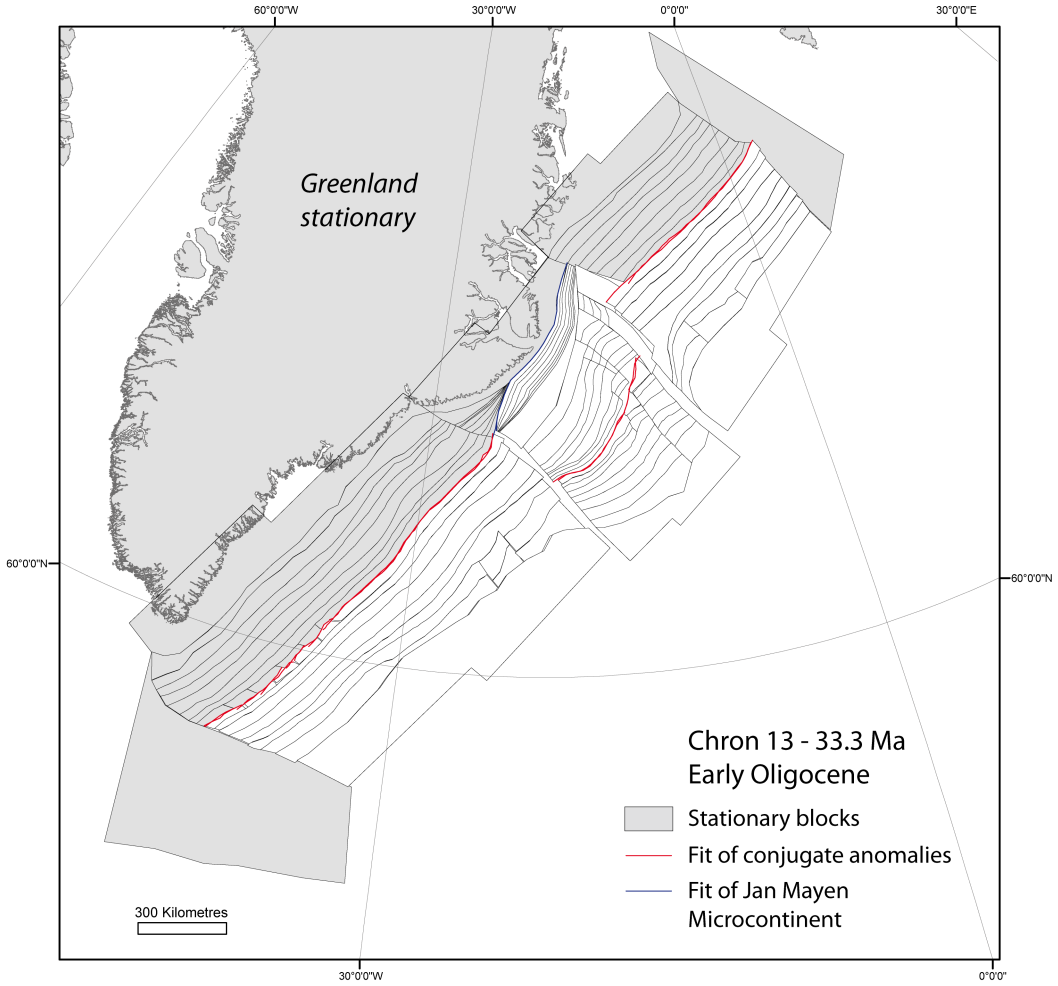

Figure 10: Restoration at Chron 13 - 33.3 Ma - MODEL 2 *(G = 0.0037)*

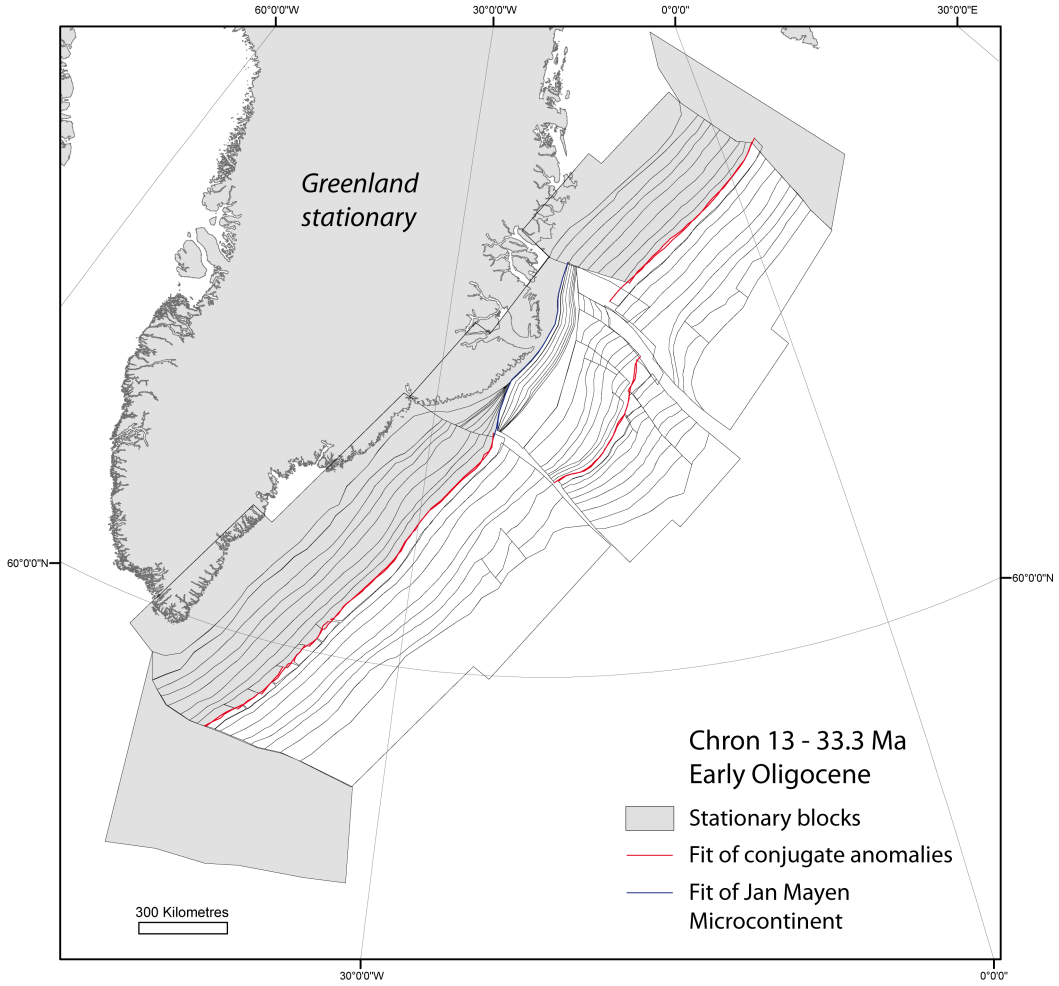

Figure 11: Restoration at Chron 17 - 36.6 Ma MODEL 1 *(G = 0.0026)*

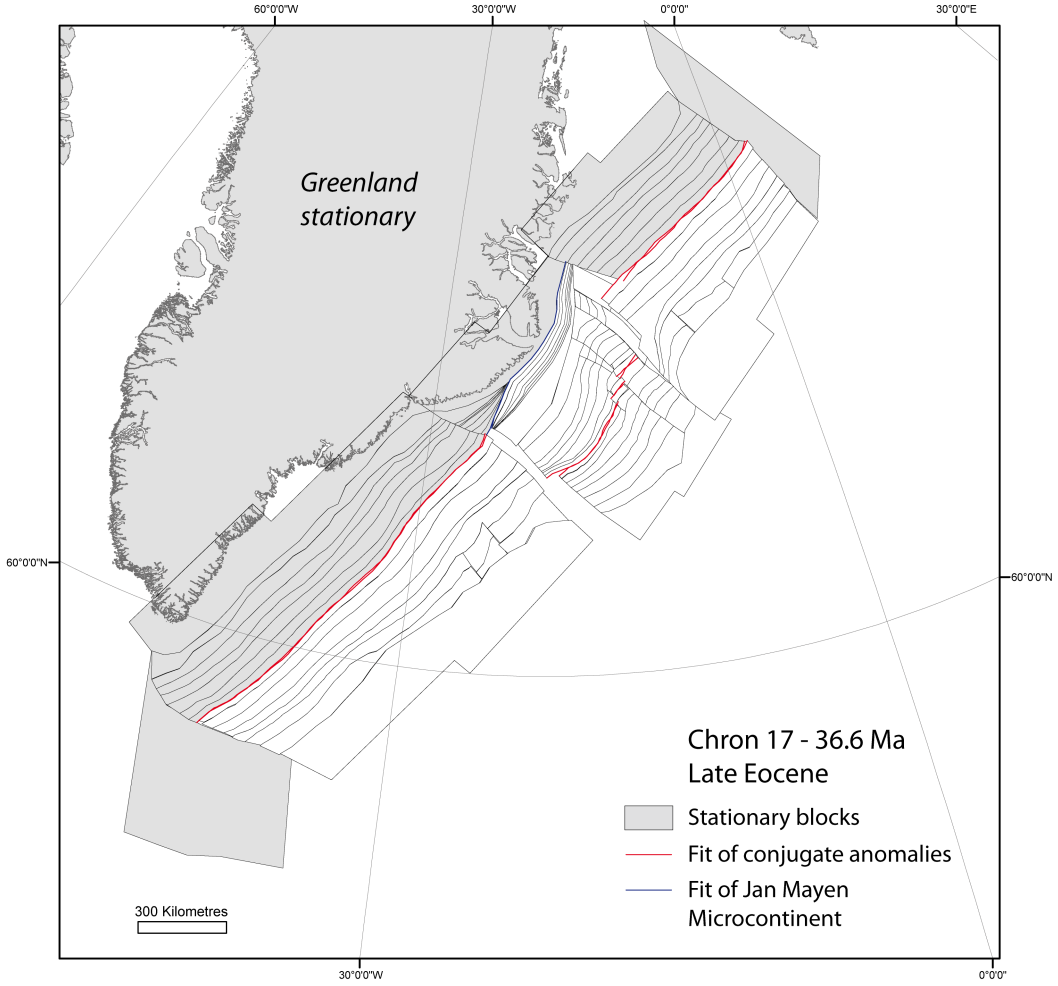

Figure 12: Restoration at Chron 17 - 36.6 Ma - MODEL 2 *(G = 0.0041)*

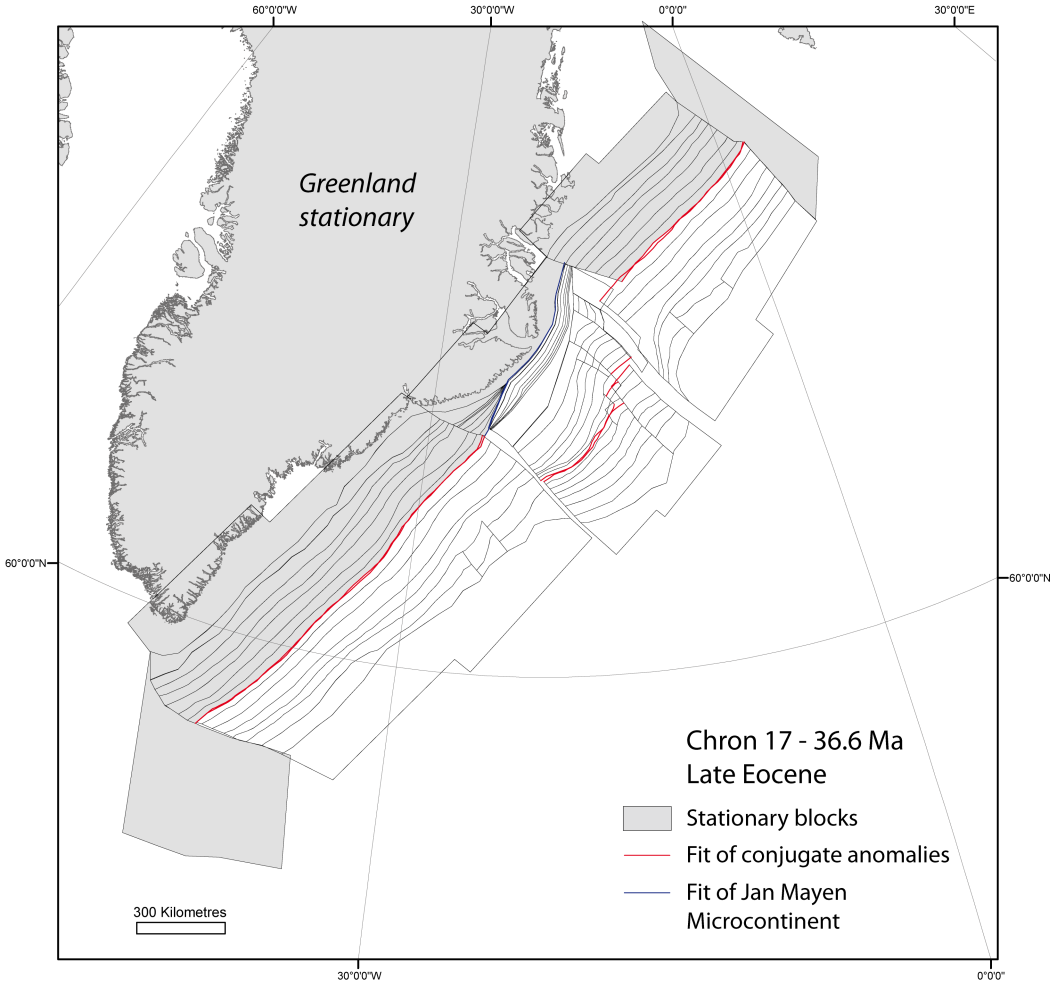

Figure 13: Restoration at Chron 18 - 39.4 Ma - MODEL 1 *(G = 0.0017)*

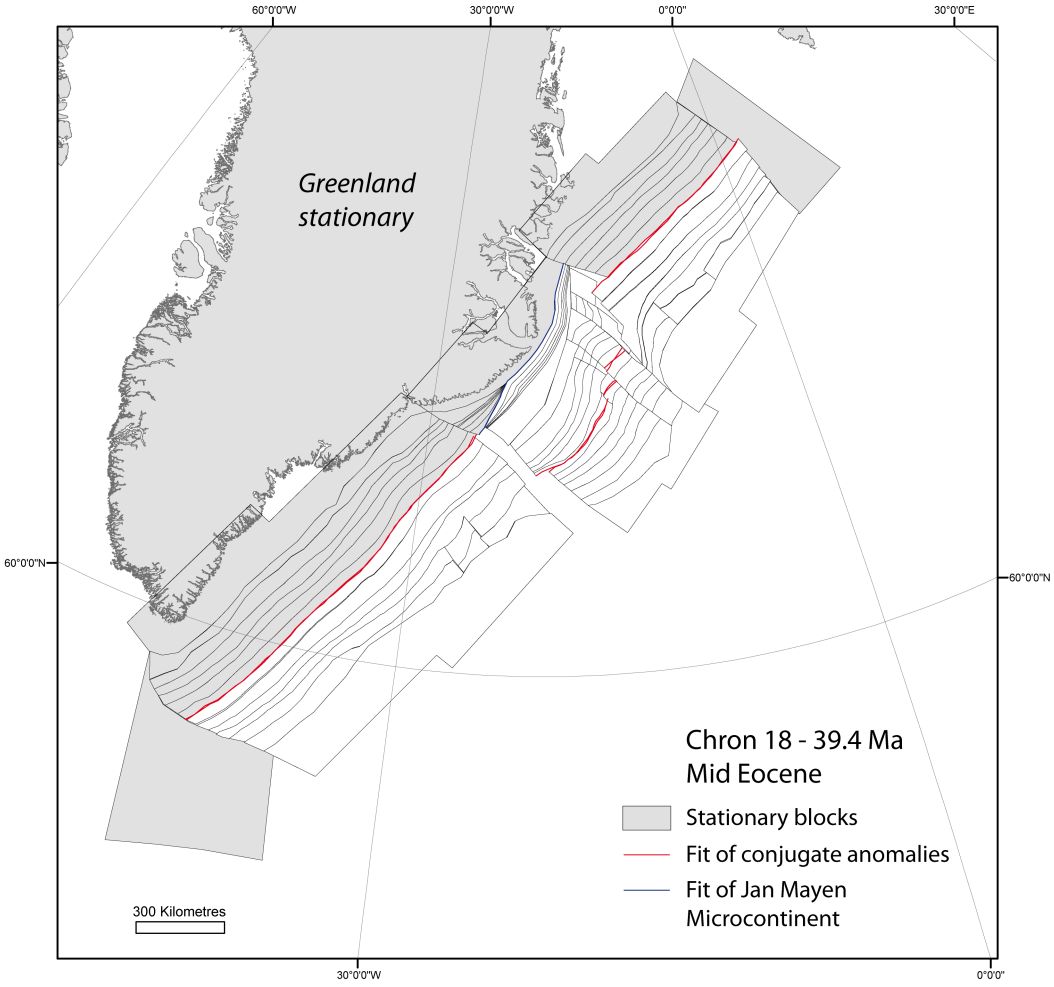

Figure 14: Restoration at Chron 18 - 39.4 Ma - MODEL 2 *(G = 0.0040)*

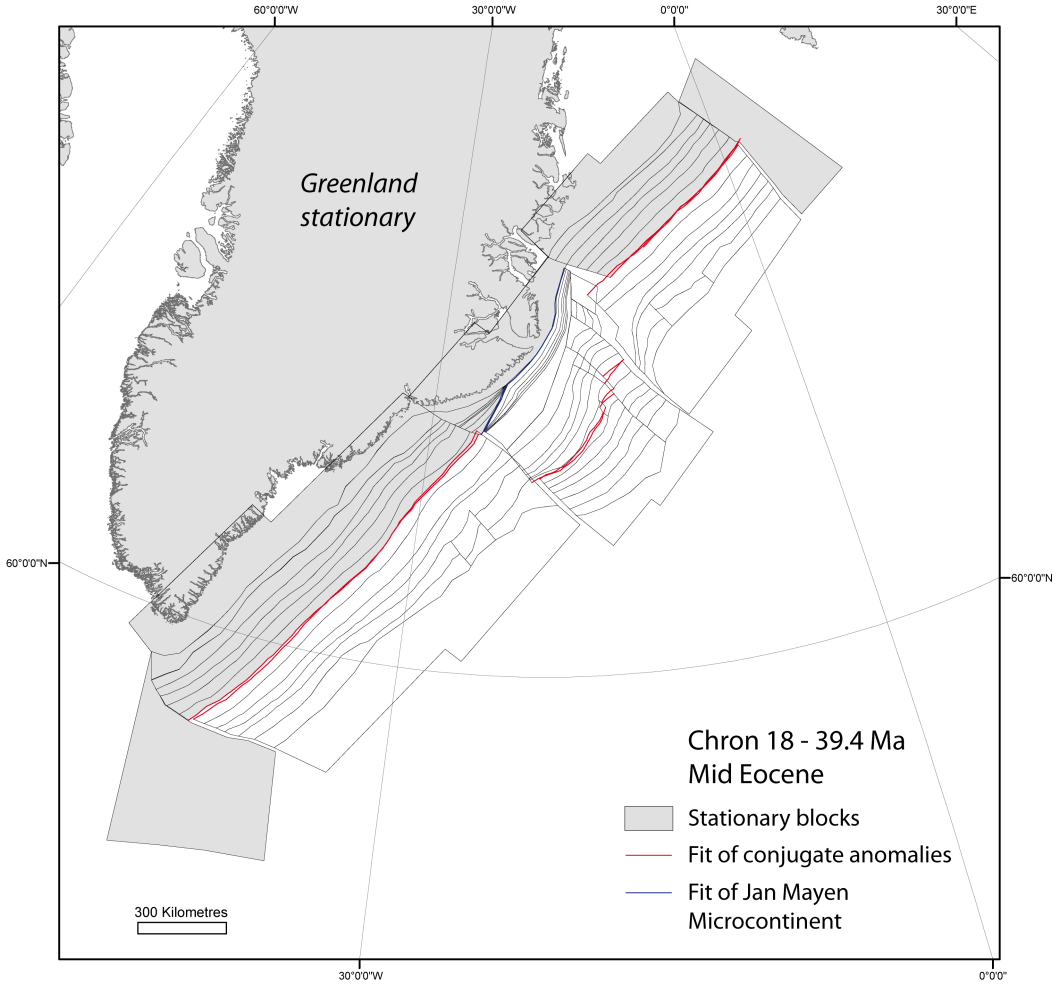

Figure 15: Restoration at Chron 20 - 43.2 Ma - MODEL 1 *(G = 0.0017)*

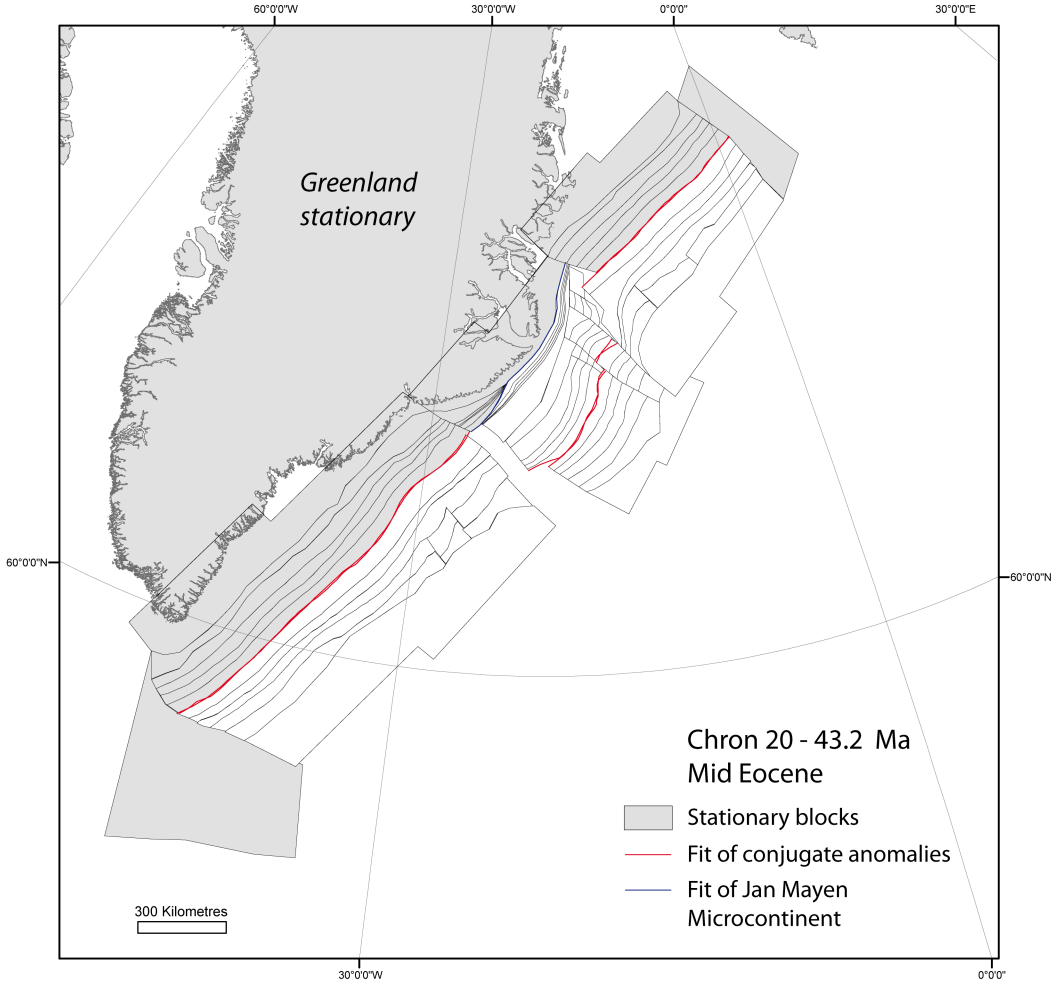

Figure 16: Restoration at Chron 20 - 43.2 Ma - MODEL 2 *(G = 0.0050)*

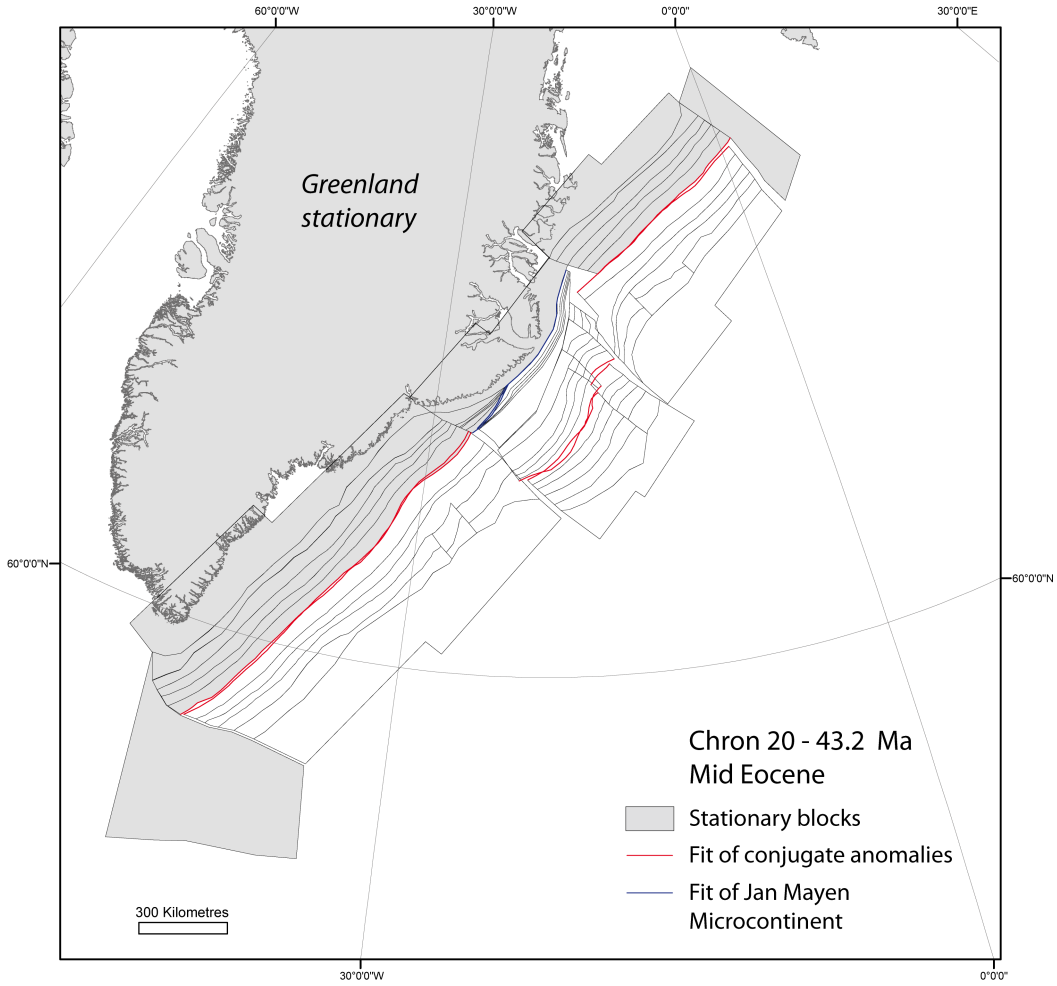

Figure 17: Restoration at Chron 21 - 47.1 Ma - MODEL 1 *(G = 0.0017)*

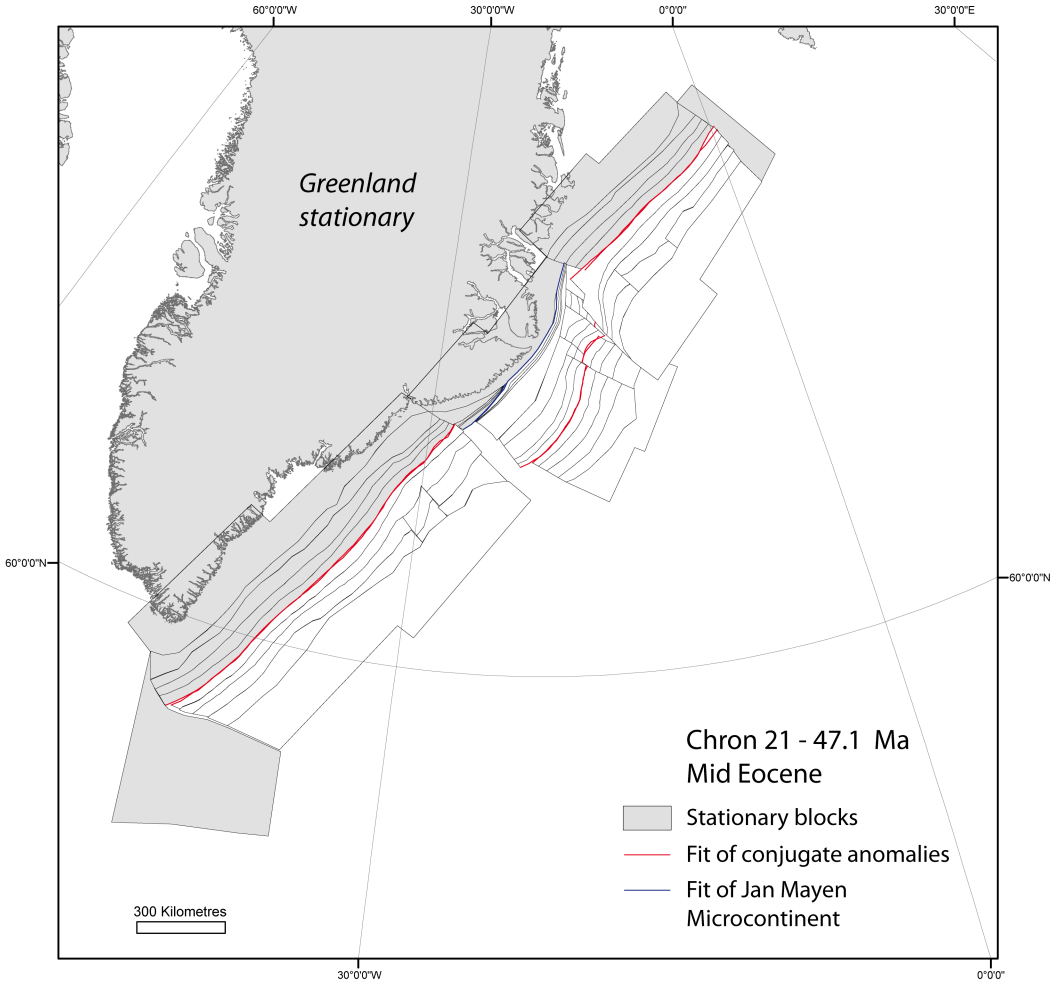

Figure 18: Restoration at Chron 21 - 47.1 Ma - MODEL 2 *(G = 0.0048)*

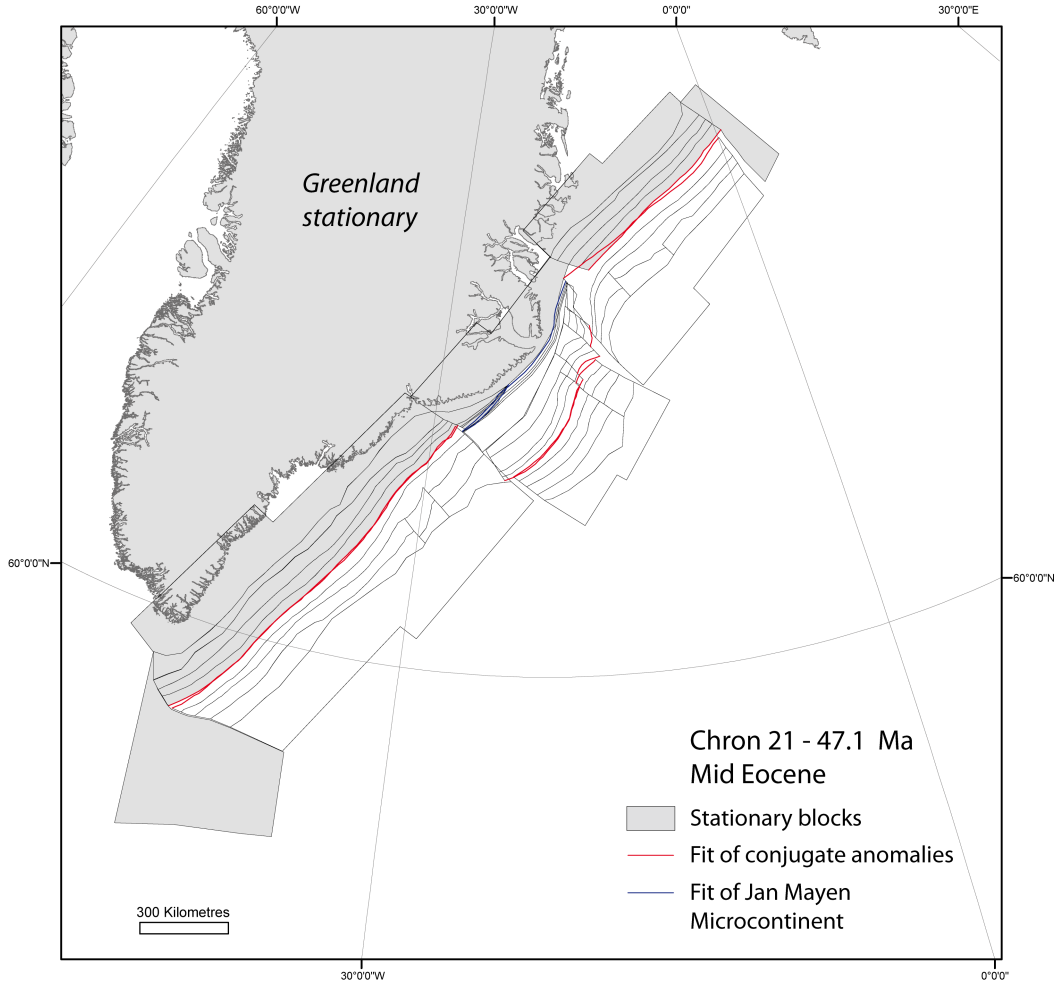

Figure 19: Restoration at Chron 22 - 49.4 Ma - MODEL 1 *(G = 0.0028)*

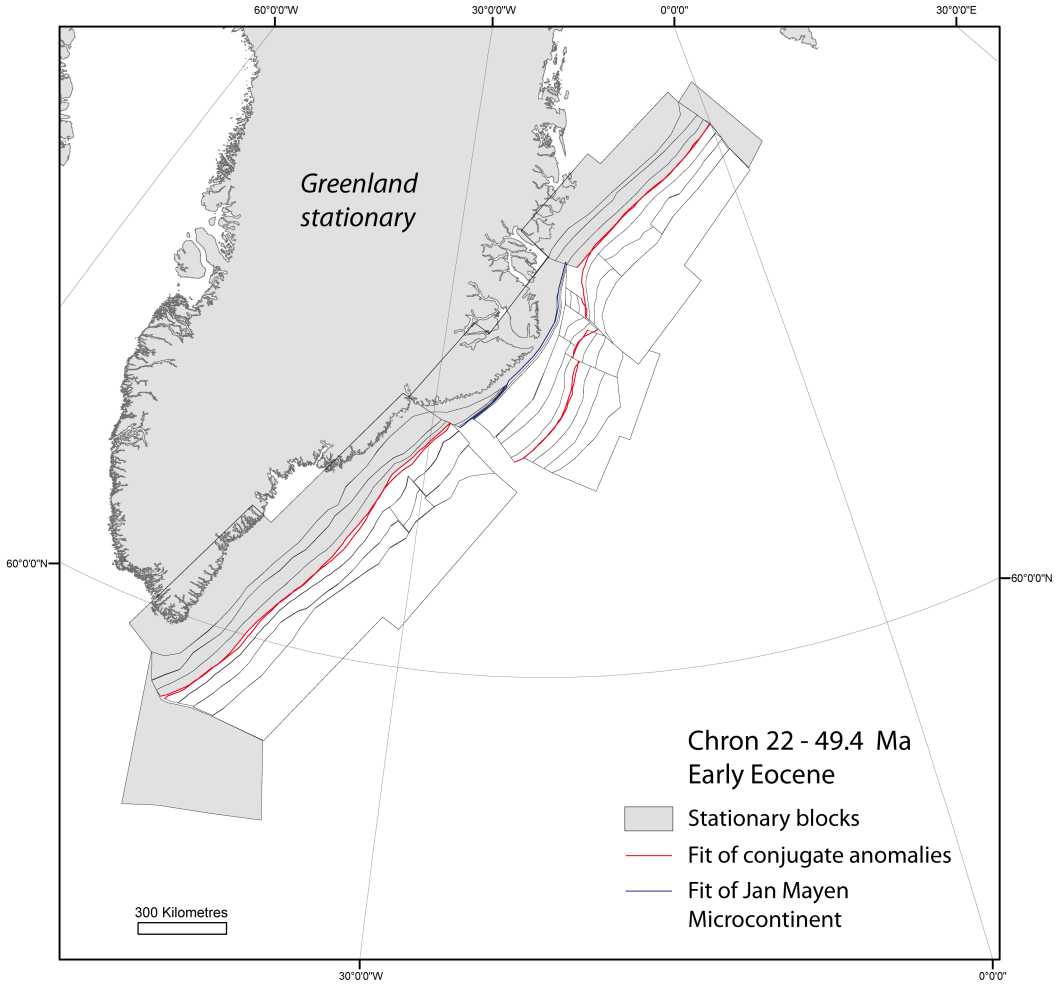

Figure 20: Restoration at Chron 22 - 49.4 Ma - MODEL 2 *(G = 0.0058)*

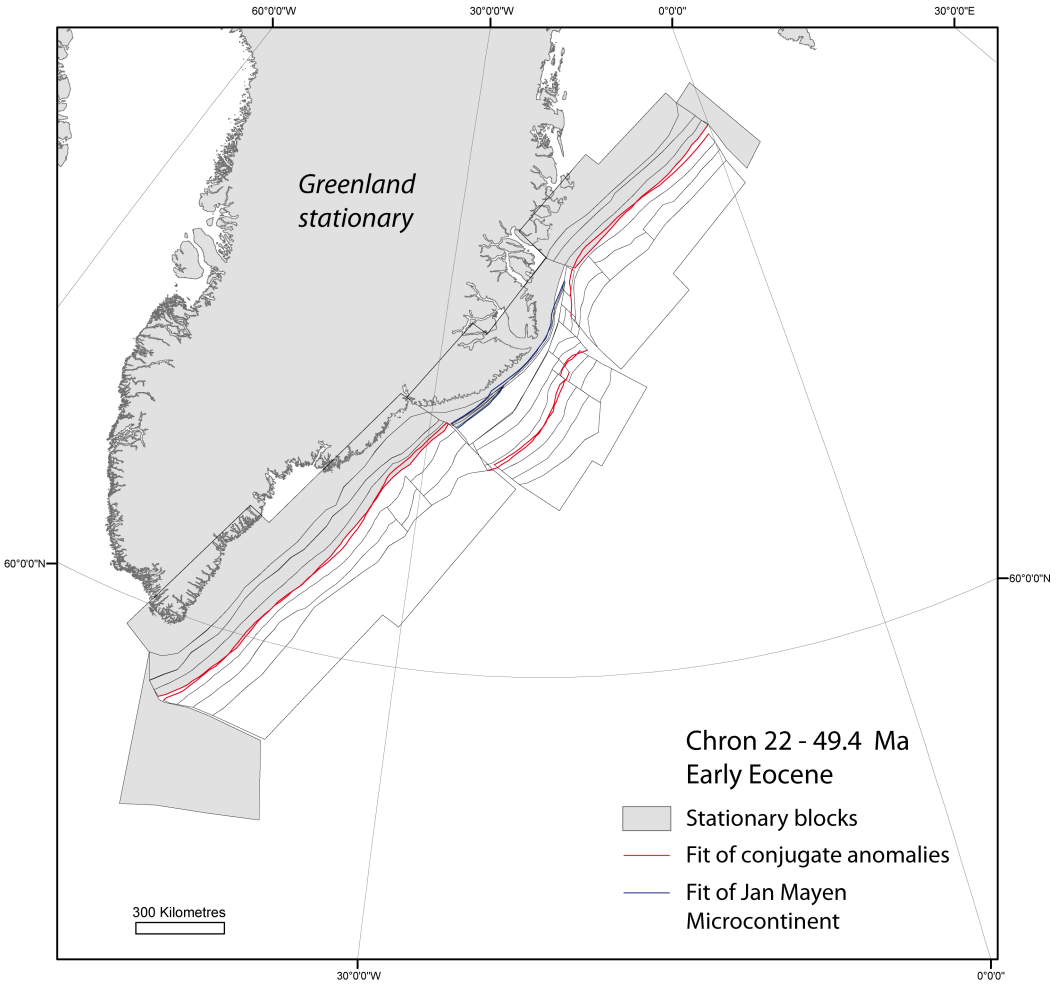

Figure 21: Restoration at Chron 23 - 51.3 Ma - MODEL 1 *(G = 0.0039)*

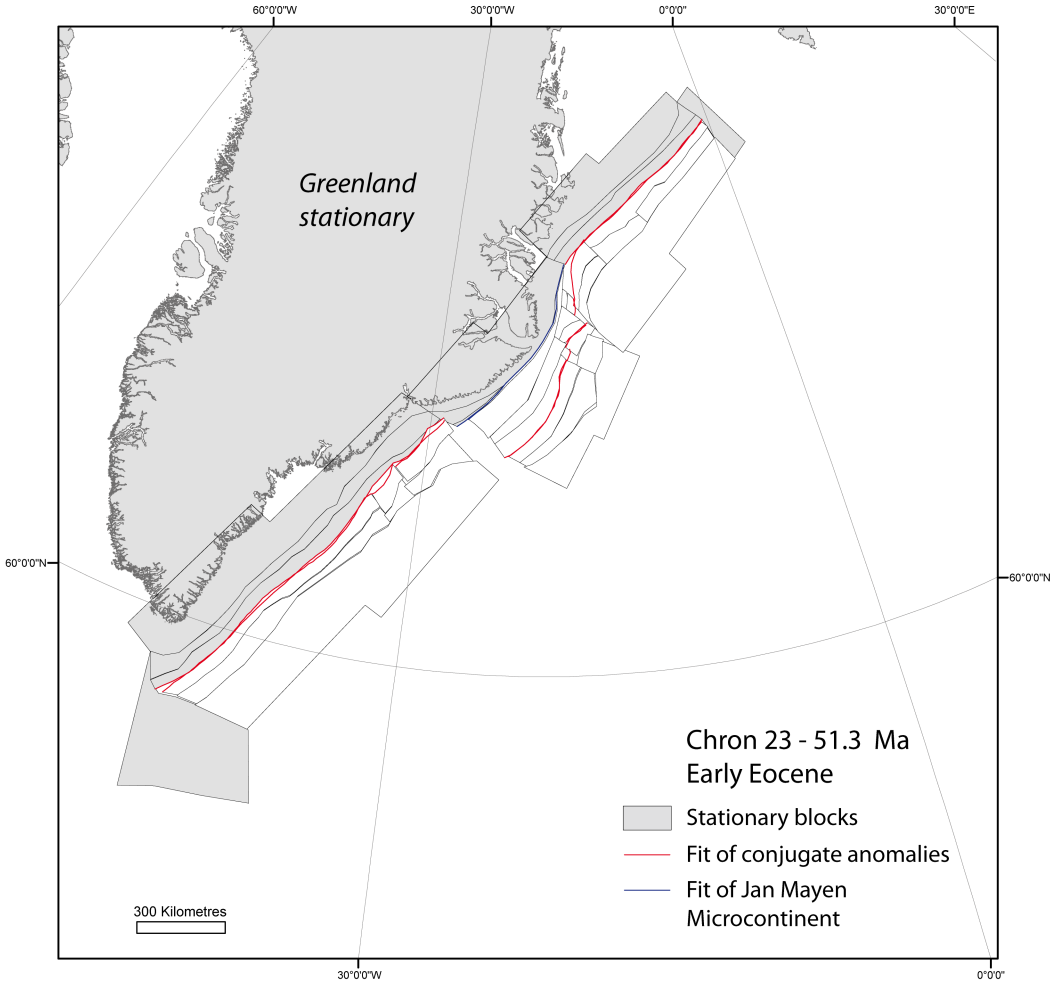

Figure 22: Restoration at Chron 23 - 51.3 Ma - MODEL 2 *(G = 0.0050)*

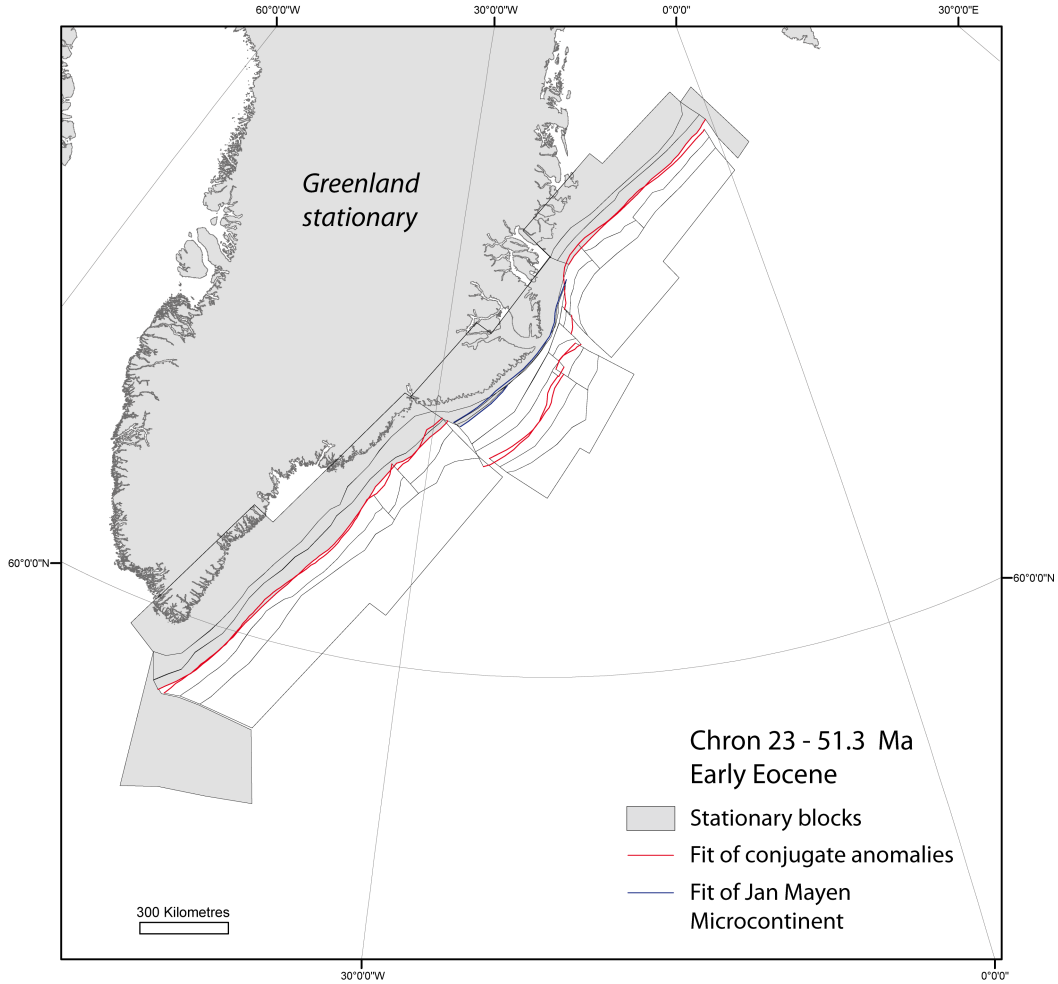

Figure 23: Restoration at Chron 24 - 52.9 Ma - MODEL 1 *(G = 0.0043)*

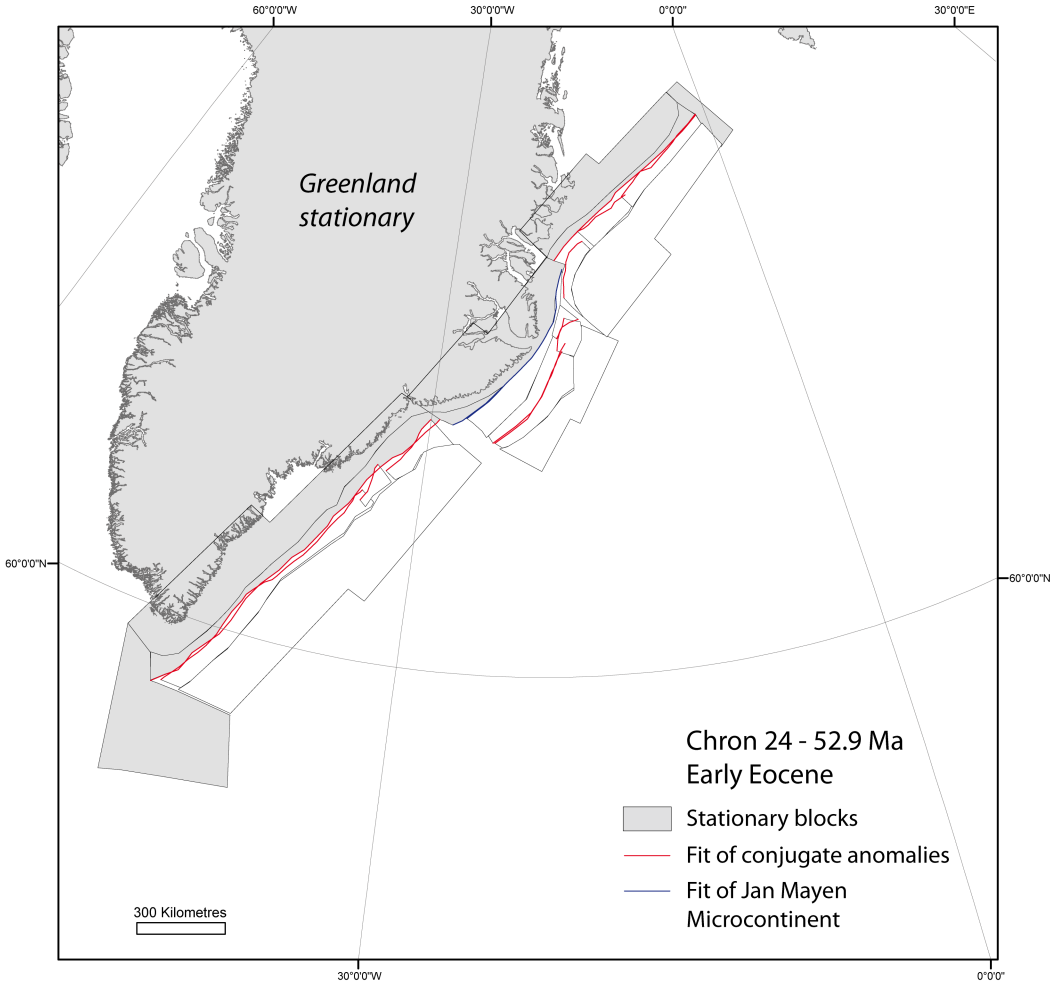

Figure 24: Restoration at Chron 24 - 52.9 Ma - MODEL 2 *(G = 0.0052)*

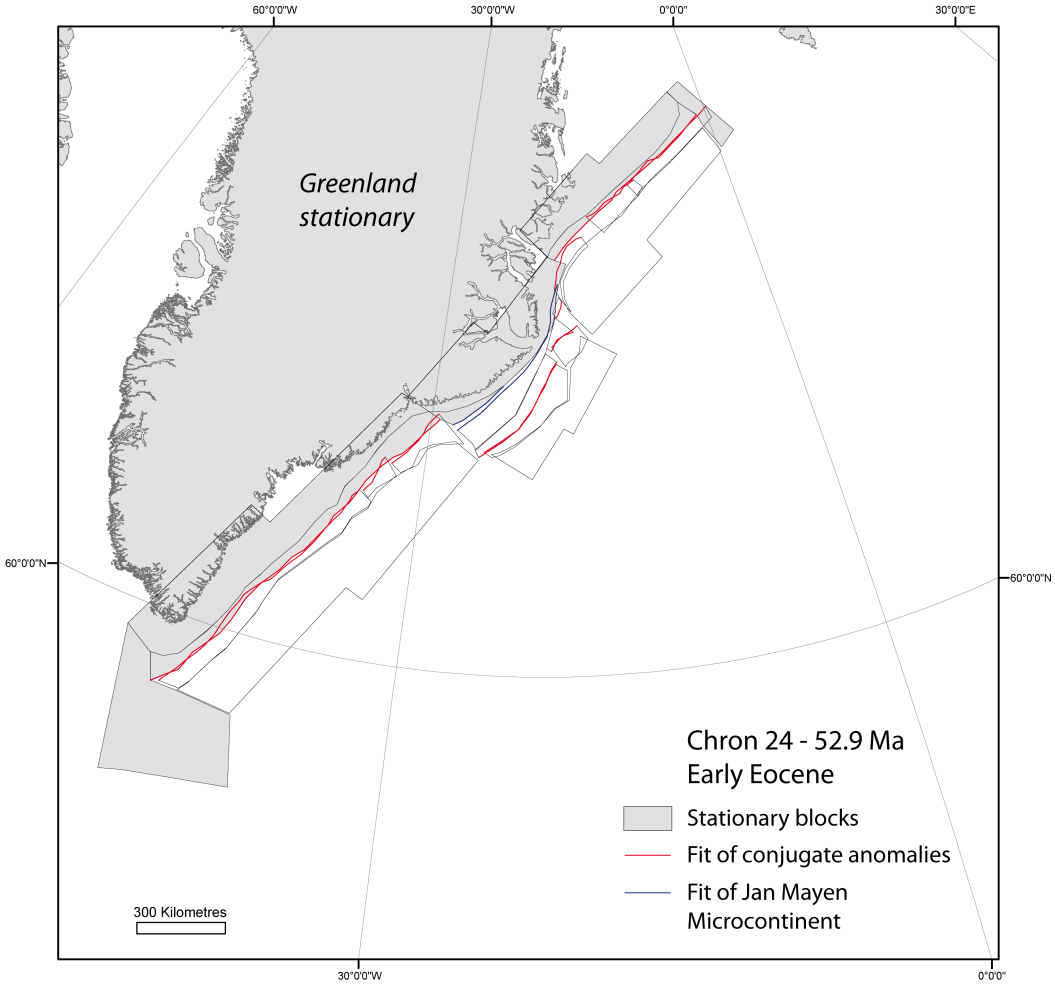

Figure 25: Final Restoration at 55.9 Ma - MODEL 1 *(G = 0.0037)*

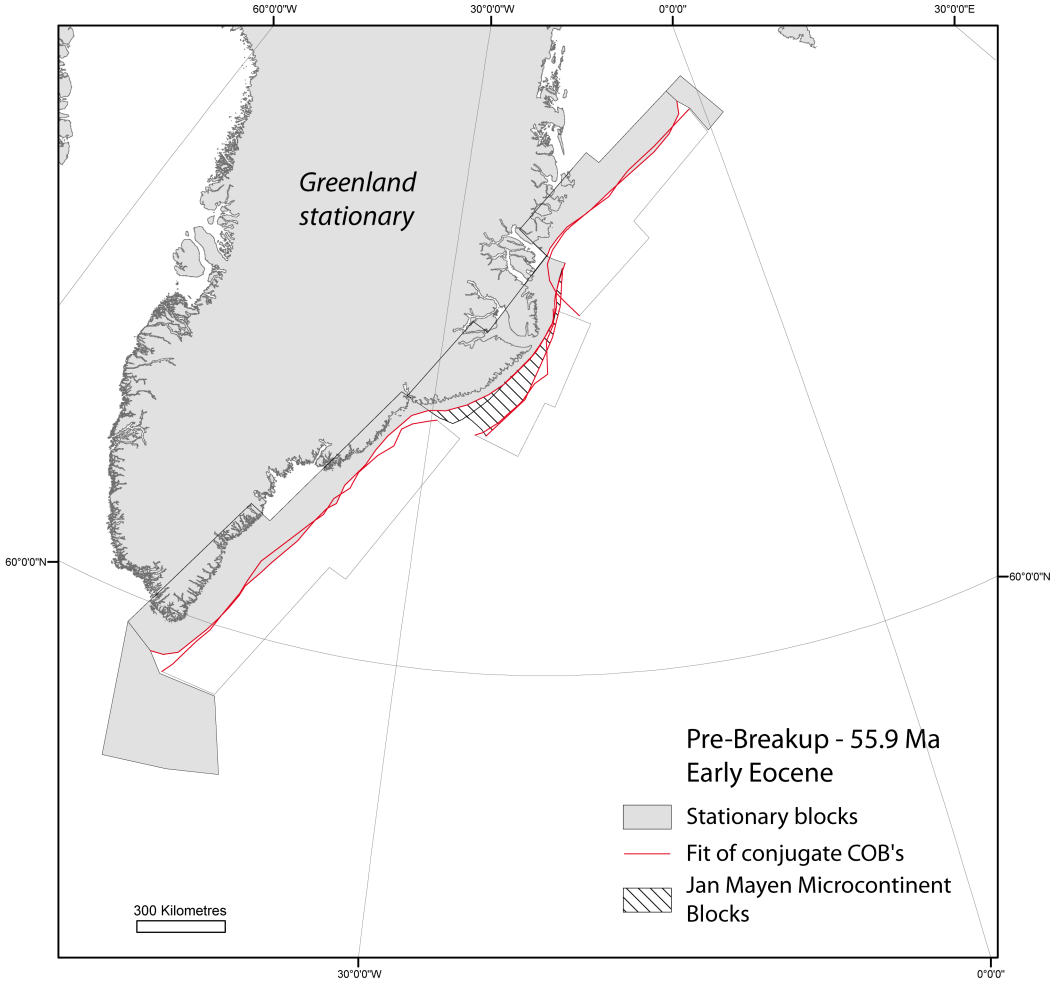

Figure 26: Final Restoration at 55.9 Ma - MODEL 2 *(G = 0.0037)*

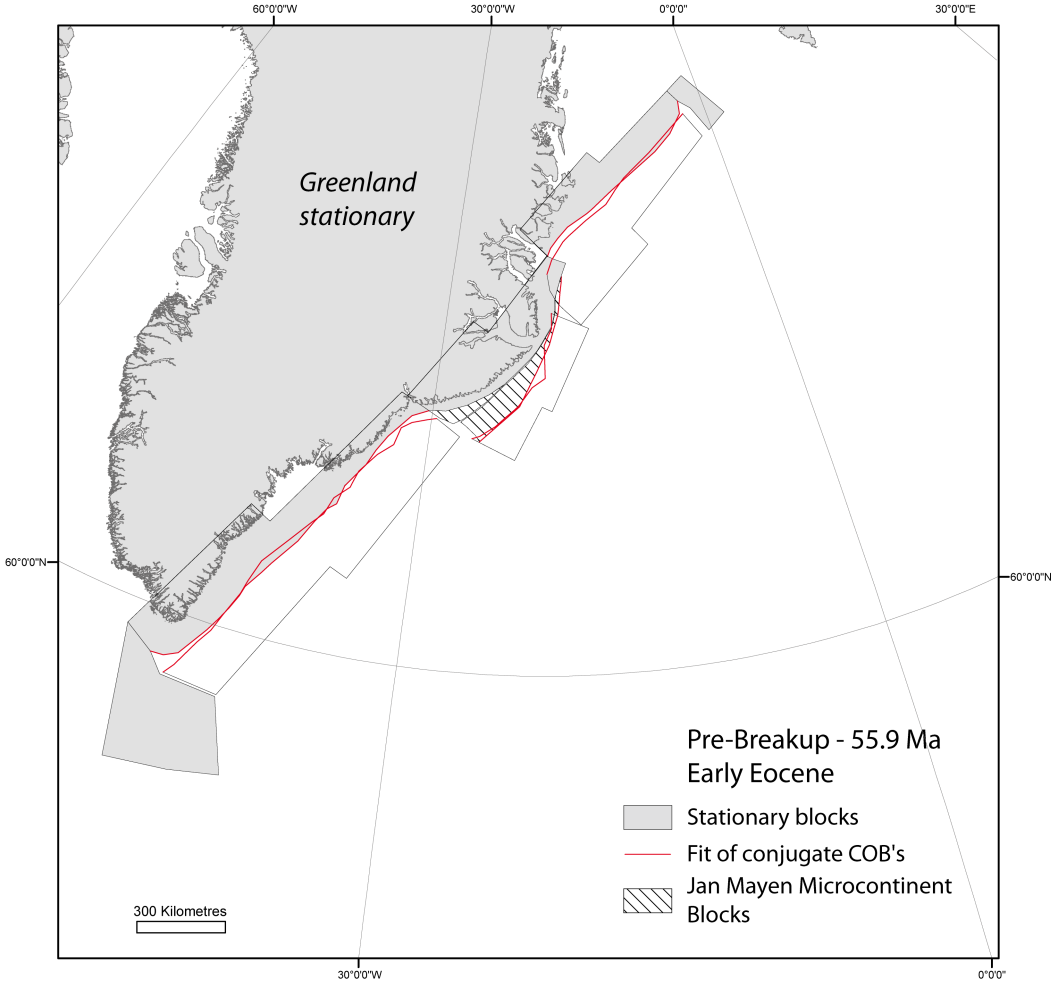

Calculation of criterion G for each restoration stage, for each model

The criterion *G* represents the fractional area of gaps and overlaps:

$$G = S_g/S_b$$

where S_g is the total surface area of all gaps and overlaps, and S_b is the total surface area of all the blocks (*Rouby et al.*, 1993). A good approximation to S_g is:

$$S_g = L^*(D/n)^{1/2}$$

where *L* is the length of a line element, n is the total number of line elements, and $(D/n)^{1/2}$ is the root-mean-square gap width (*Rouby et al.*, 1993).

	Model 1		Model 2	
	G	it	G	it
Chron 5 - 10.3 Ma	0.0017	1000	0.0009	1000
Chron 5A - 14.2 Ma	0.0016	1000	0.0007	1000
Chron 6 - 19.6 Ma	0.0021	500	0.0009	1000
Chron 8 - 26.4 Ma	0.0018	200	0.0024	750
Chron 13 - 33.3 Ma	0.0023	750	0.0037	750
Chron 17 - 36.6 Ma	0.0026	500	0.0041	500
Chron 18 - 39.4 Ma	0.0017	500	0.0040	1000
Chron 20 - 43.2 Ma	0.0017	500	0.0050	600
Chron 21 - 47.1 Ma	0.0017	500	0.0048	700
Chron 22 - 49.4 Ma	0.0028	200	0.0058	500
Chron 23 - 51.3 Ma	0.0039	100	0.0050	250
Chron 24 - 51.3 Ma	0.0043	10	0.0052	50
COB - 55.9 Ma	0.0037	10	0.0037	10
Mean G	0.0025		0.0035	
G minimal	0.0016		0.0007	
G maximal	0.0043		0.0058	

it = number of iteration

MODEL 1

Finite Rotation of the eastern Reykjanes Segment relative to a stationary Greenland plate *(Reykjanes Ridge)*

		Pole of Rotation			Parameters/Uncertainties				Covariance matrix					
Stage	Age (in Ma)	Latitude (°N)	Longitude (°E)	Angle (°)	*r* (km)	*dF*	*K*	(*N*,*s*)	a	b	c	d	e	f
Chron 5	10.3	71.65	136.17	-2.71	0.202	37	183.60	(50,5)	6.90360E-06	-2.34442E-06	1.23087E-05	8.93597E-07	-4.19974E-06	2.24086E-05
Chron 5A	14.2	73.65	128.08	-3.90	0.289	37	128.00	(50,5)	6.69182E-06	-2.45570E-06	1.21442E-05	1.00014E-06	-4.48139E-06	2.25113E-05
Chron 6	19.6	76.27	124.52	-5.71	0.202	37	183.60	(50,5)	6.42987E-06	-2.62878E-06	1.19256E-05	1.17637E-06	-4.90825E-06	2.26015E-05
Chron 8	26.4	71.72	132.23	-6.96	0.397	37	93.21	(50,5)	6.11536E-06	-2.81647E-06	1.16531E-05	1.40164E-06	-5.41070E-06	2.27074E-05
Chron 13	33.3	68.42	133.40	-7.85	0.500	37	74.06	(50,5)	5.84945E-06	-2.92330E-06	1.14228E-05	1.56788E-06	-5.76157E-06	2.28269E-05
Chron 17	36.6	65.01	134.75	-8.16	0.631	37	58.61	(50,5)	5.69249E-06	-2.97719E-06	1.12837E-05	1.66542E-06	-5.96037E-06	2.29002E-05
Chron 18	39.4	58.34	137.60	-8.15	0.708	37	52.27	(50,5)	5.55298E-06	-3.02943E-06	1.11549E-05	1.76216E-06	-6.15119E-06	2.29566E-05
Chron 20	43.2	59.39	135.98	-9.01	0.860	37	43.07	(50,5)	5.35639E-06	-3.08041E-06	1.09756E-05	1.88349E-06	-6.38489E-06	2.30539E-05
Chron 21	47.1	45.18	136.16	-8.88	1.071	37	34.55	(50,5)	5.03877E-06	-3.06258E-06	1.06934E-05	1.97511E-06	-6.58550E-06	2.33005E-05
Chron 22	49.4	46.11	134.91	-9.51	1.338	37	27.65	(50,5)	4.86205E-06	-3.08316E-06	1.05234E-05	2.07127E-06	-6.76670E-06	2.34017E-05
Chron 23	51.3	43.42	134.32	-9.98	1.691	37	21.88	(50,5)	4.66820E-06	-3.09008E-06	1.03334E-05	2.16412E-06	-6.94313E-06	2.35242E-05
Chron 24	52.9	40.97	132.75	-10.56	2.188	37	16.91	(50,5)	4.41898E-06	-3.06708E-06	1.00867E-05	-3.06708E-06	-7.11576E-06	2.37100E-05
COB fit	55.9	33.12	132.41	-11.08	2.906	37	12.73	(50,5)	4.13972E-06	-3.03226E-06	9.79752E-06	2.34679E-06	-7.30847E-06	2.39254E-05

Finite Rotation of the eastern Mohns Segment relative to a stationary Greenland plate *(Mohns Ridge)*

		Pole of Rotation			Parameters/Uncertainties				Covariance matrix					
Stage	Age (in Ma)	Latitude (°N)	Longitude (°E)	Angle (°)	*r* (km)	*dF*	*K*	(*N*,*s*)	a	b	c	d	e	f
Chron 5	10.3	82.19	83.35	-4.71	0.757	37	48.86	(50,5)	1.13846E-05	9.28870E-07	2.78877E-05	2.01685E-07	2.32923E-06	6.89130E-05
Chron 5A	14.2	78.61	106.84	-5.11	1.214	37	30.48	(50,5)	1.10403E-05	6.78475E-07	2.75064E-05	1.66916E-07	1.74043E-06	6.91472E-05
Chron 6	19.6	78.06	104.94	-6.75	1.934	37	19.13	(50,5)	1.06802E-05	3.40517E-07	2.70920E-05	1.35724E-07	9.05389E-07	6.93536E-05
Chron 8	26.4	72.79	123.40	-6.96	2.856	37	12.96	(50,5)	1.02647E-05	-2.25357E-08	2.65984E-05	1.23976E-07	-2.31012E-08	6.95782E-05
Chron 13	33.3	59.49	134.49	-6.11	3.573	37	10.36	(50,5)	9.73399E-06	-2.31960E-07	2.59661E-05	1.28218E-07	-5.84361E-07	6.99629E-05
Chron 17	36.6	56.59	132.89	-6.47	4.033	37	9.18	(50,5)	9.35852E-06	-3.54206E-07	2.55073E-05	1.35866E-07	-9.33766E-07	7.02450E-05
Chron 18	39.4	47.41	135.90	-6.37	4.609	37	8.03	(50,5)	8.97396E-06	-5.11627E-07	2.50199E-05	1.50831E-07	-1.39713E-06	7.05139E-05
Chron 20	43.2	57.53	126.47	-8.39	5.293	37	6.99	(50,5)	8.44346E-06	-6.92658E-07	2.43309E-05	1.79541E-07	-1.97683E-06	7.09050E-05
Chron 21	47.1	48.36	128.60	-8.26	5.919	37	6.25	(50,5)	7.84366E-06	-8.19679E-07	2.35172E-05	2.07606E-07	-2.44145E-06	7.13668E-05
Chron 22	49.4	55.37	121.72	-10.11	6.414	37	5.77	(50,5)	7.35696E-06	-9.31726E-07	2.28314E-05	2.41171E-07	-2.88545E-06	7.17562E-05
Chron 23	51.3	54.30	121.00	-10.66	6.789	37	5.45	(50,5)	6.98572E-06	-1.01454E-06	2.22858E-05	2.70720E-07	-3.23618E-06	7.20436E-05
Chron 24	52.9	55.07	118.30	-11.71	7.153	37	5.17	(50,5)	6.52936E-06	-1.08135E-06	2.15925E-05	3.03147E-07	-3.58362E-06	7.24139E-05
COB fit	55.9	62.94	109.08	-15.24	7.571	37	4.89	(50,5)	6.01707E-06	-1.18949E-06	2.07759E-05	3.62037E-07	-4.13488E-06	7.28101E-05

Parameters: *r*, total misfit; *K*, estimated quality factor; *dF*, degrees of freedom; *N*, number of data points; *s*, number of great circle segments; the unvertainty of fracture zone and magnetic anomaly identification is σ = 5.00 km; ages are after Cande and Kent (1995) timescale.

Covariance matrix:

a	b	c
b	d	e
c	e	f

The units of the matrix elements are radians squared

MODEL 1

Finite Rotation of the eastern Aegir Segment relative to a stationary Greenland plate *(Kolbeinsey Ridge from present-day to Chron 6 ; Aegir Ridge and formation of the Jan Mayen microcontinent from Chron 6 to 55.9 Ma)*

		Pole of Rotation			Parameters/Uncertainties				Covariance matrix					
Stage	Age (in Ma)	Latitude (°N)	Longitude (°E)	Angle (°)	*r* (km)	*dF*	*K*	(*N*,*s*)	a	b	c	d	e	f
Chron 5	10.3	69.45	130.89	-2.57	0.248	37	149.33	(50,5)	3.35120E-05	-2.57099E-06	6.80240E-05	3.04155E-07	-5.18912E-06	1.38574E-04
Chron 5A	14.2	66.23	133.28	-3.35	0.431	37	85.81	(50,5)	3.26758E-05	-3.30713E-06	6.72789E-05	4.41502E-07	-6.78447E-06	1.39032E-04
Chron 6	19.6	63.92	133.63	-4.50	0.732	37	50.57	(50,5)	3.14336E-05	-4.28433E-06	6.61493E-05	6.90794E-07	-8.99812E-06	1.39727E-04
Chron 8	26.4	74.23	123.88	-7.42	1.134	37	32.64	(50,5)	3.03916E-05	-5.62214E-06	6.51054E-05	1.14885E-06	-1.20369E-05	1.39997E-04
Chron 13	33.3	72.14	126.48	-8.15	1.354	37	27.32	(50,5)	2.94412E-05	-6.24277E-06	6.41959E-05	1.43294E-06	-1.36110E-05	1.40519E-04
Chron 17	36.6	-7.60	149.05	-6.25	1.403	37	26.37	(50,5)	2.78213E-05	-5.75421E-06	6.27766E-05	1.29226E-06	-1.29800E-05	1.42263E-04
Chron 18	39.4	-7.65	147.66	-6.67	1.501	37	24.64	(50,5)	2.70598E-05	-5.94188E-06	6.20355E-05	1.40679E-06	-1.36210E-05	1.42847E-04
Chron 20	43.2	-36.96	151.87	-12.08	1.608	37	23.02	(50,5)	2.55566E-05	-5.78563E-06	6.05788E-05	1.40698E-06	-1.37178E-05	1.44294E-04
Chron 21	47.1	-40.63	152.22	-15.12	1.796	37	20.60	(50,5)	2.42245E-05	-6.17182E-06	5.91660E-05	1.66807E-06	-1.50877E-05	1.45259E-04
Chron 22	49.4	-41.72	151.73	-16.92	1.910	37	19.37	(50,5)	2.31476E-05	-6.43141E-06	5.79872E-05	1.88202E-06	-1.61333E-05	1.46058E-04
Chron 23	51.3	-32.22	148.87	-13.97	2.012	37	18.39	(50,5)	2.25475E-05	-7.05571E-06	5.72548E-05	2.30611E-06	-1.79447E-05	1.46179E-04
Chron 24	52.9	-25.96	145.53	-13.31	2.068	37	17.89	(50,5)	2.10777E-05	-7.33247E-06	5.55567E-05	2.65098E-06	-1.93648E-05	1.47273E-04
COB fit	55.9	-27.84	145.32	-15.10	2.093	37	17.68	(50,5)	1.97342E-05	-7.68793E-06	5.39159E-05	3.09584E-06	-2.10572E-05	1.48204E-04

Finite Rotation of the eastern Kolbeinsey Segment relative to a stationary Greenland plate *(Kolbeinsey Ridge from present-day to Chron 6 ; Aegir Ridge and formation of the Jan Mayen microcontinent from Chron 6 to 55.9 Ma)*

		Pole of Rotation			Parameters/Uncertainties				Covariance matrix					
Stage	Age (in Ma)	Latitude (°N)	Longitude (°E)	Angle (°)	*r* (km)	*dF*	*K*	(*N*,*s*)	a	b	c	d	e	f
Chron 5	10.3	70.83	129.69	-2.68	19.778	117	5.92	(132,6)	3.89111E-06	-1.01950E-06	1.05461E-05	3.59204E-07	-2.81065E-06	2.87972E-05
Chron 5A	14.2	67.43	132.17	-3.48	19.825	117	5.90	(132,6)	3.74889E-06	-1.10396E-06	1.03626E-05	4.18531E-07	-3.10401E-06	2.88676E-05
Chron 6	19.6	65.04	132.68	-4.65	19.877	117	5.89	(132,6)	3.54422E-06	-1.20958E-06	1.00915E-05	5.08446E-07	-3.50432E-06	2.89723E-05
Chron 8	26.4	83.13	69.32	-11.00	19.918	117	5.87	(132,6)	3.37296E-06	-1.27921E-06	9.85280E-06	5.84298E-07	-3.82645E-06	2.90655E-05
Chron 13	33.3	81.71	19.99	-16.65	19.921	117	5.87	(132,6)	3.31102E-06	-1.29598E-06	9.76109E-06	6.07226E-07	-3.93254E-06	2.91070E-05
Chron 17	36.6	81.61	18.77	-17.36	19.310	117	6.06	(132,6)	3.19851E-06	-1.27880E-06	9.45614E-06	6.11210E-07	-3.89717E-06	2.82928E-05
Chron 18	39.4	81.11	13.74	-18.87	19.959	117	5.86	(132,6)	3.26734E-06	-1.31686E-06	9.69578E-06	6.31280E-07	-4.02907E-06	2.91253E-05
Chron 20	43.2	80.70	11.23	-20.26	19.935	117	5.87	(132,6)	3.23202E-06	-1.32432E-06	9.64455E-06	6.43425E-07	-4.07911E-06	2.91493E-05
Chron 21	47.1	80.40	9.80	-21.41	19.250	117	6.08	(132,6)	3.18890E-06	-1.32307E-06	9.57186E-06	6.49318E-07	-4.10454E-06	2.91135E-05
Chron 22	49.4	80.12	8.69	-22.43	19.953	117	5.86	(132,6)	3.16746E-06	-1.33034E-06	9.55147E-06	6.59875E-07	-4.14839E-06	2.91997E-05
Chron 23	51.3	79.99	6.63	-23.33	19.956	117	5.86	(132,6)	3.16730E-06	-1.34514E-06	9.54761E-06	6.72477E-07	-4.19484E-06	2.91864E-05
Chron 24	52.9	80.03	7.03	-23.45	19.961	117	5.86	(132,6)	3.15087E-06	-1.34682E-06	9.52418E-06	6.77101E-07	-4.21210E-06	2.91978E-05
COB fit	55.9	80.03	7.03	-23.45	19.961	117	5.86	(132,6)	3.15087E-06	-1.34682E-06	9.52418E-06	6.77101E-07	-4.21210E-06	2.91978E-05

Parameters: *r*, total misfit; *K*, estimated quality factor; *dF*, degrees of freedom; *N*, number of data points; *s*, number of great circle segments; the unvertainty of fracture zone and magnetic anomaly identification is σ = 5.00 km; ages are after Cande and Kent (1995) timescale.

Covariance matrix:

a	b	c
b	d	e
c	e	f

The units of the matrix elements are radians squared

MODEL 2

Finite Rotation of the eastern Reykjanes Segment relative to a stationary Greenland plate *(Reykjanes Ridge)*

		Pole of Rotation			Parameters/Uncertainties				Covariance matrice					
Stage	Age (in Ma)	Latitude (°N)	Longitude (°E)	Angle (°)	*r* (km)	*dF*	*K*	(*N*,*s*)	a	b	c	d	e	f
Chron 5	10.3	68.32	136.10	-2.54	0.198	37	187.04	(50,5)	6.89438E-06	-2.33052E-06	1.23057E-05	8.85047E-07	-4.17941E-06	2.24287E-05
Chron 5A	14.2	64.37	136.08	-3.35	0.294	37	126.00	(50,5)	6.68605E-06	-2.44794E-06	1.21413E-05	9.94685E-07	-4.47069E-06	2.25233E-05
Chron 6	19.6	71.02	131.59	-5.15	0.402	37	92.07	(50,5)	6.42664E-06	-2.62193E-06	1.19244E-05	1.17078E-06	-4.89802E-06	2.26112E-05
Chron 8	26.4	68.65	133.54	-6.57	0.496	37	74.63	(50,5)	6.10898E-06	-2.79759E-06	1.16526E-05	1.38518E-06	-5.38006E-06	2.27312E-05
Chron 13	33.3	61.63	135.43	-7.08	0.560	37	66.07	(50,5)	5.83533E-06	-2.88718E-06	1.14192E-05	1.53445E-06	-5.70318E-06	2.28730E-05
Chron 17	36.6	56.96	135.53	-7.33	0.606	37	61.04	(50,5)	5.66252E-06	-2.92003E-06	1.12715E-05	1.61288E-06	-5.87165E-06	2.29792E-05
Chron 18	39.4	51.64	136.11	-7.50	0.658	37	56.21	(50,5)	5.51124E-06	-2.94792E-06	1.11385E-05	1.68494E-06	-6.02299E-06	2.30701E-05
Chron 20	43.2	53.07	135.80	-8.37	0.802	37	46.13	(50,5)	5.32812E-06	-3.02311E-06	1.09643E-05	1.82607E-06	-6.29393E-06	2.31352E-05
Chron 21	47.1	44.30	136.60	-8.84	1.078	37	34.32	(50,5)	5.04326E-06	-3.06856E-06	1.06968E-05	1.98071E-06	-6.59472E-06	2.32945E-05
Chron 22	49.4	42.99	135.05	-9.32	1.301	37	28.44	(50,5)	4.85047E-06	-3.06388E-06	1.05174E-05	2.05106E-06	-6.73745E-06	2.34346E-05
Chron 23	51.3	41.19	134.30	-9.87	1.660	37	22.28	(50,5)	4.65189E-06	-3.07398E-06	1.03218E-05	2.14971E-06	-6.92425E-06	2.35571E-05
Chron 24	52.9	37.90	133.52	-10.52	2.264	37	16.34	(50,5)	4.39888E-06	-3.07206E-06	1.00647E-05	2.26756E-06	-7.14612E-06	2.37199E-05
COB fit	55.9	30.92	132.71	-11.04	2.885	37	12.82	(50,5)	4.13289E-06	-3.02589E-06	9.79066E-06	2.34095E-06	-7.30097E-06	2.39345E-05

Finite Rotation of the eastern Mohns Segment relative to a stationary Greenland plate *(Mohns Ridge)*

		Pole of Rotation			Parameters/Uncertainties				Covariance matrice					
Stage	Age (in Ma)	Latitude (°N)	Longitude (°E)	Angle (°)	*r* (km)	*dF*	*K*	(*N*,*s*)	a	b	c	d	e	f
Chron 5	10.3	81.60	81.76	-4.81	0.770	37	48.05	(50,5)	1.13319E-05	9.23722E-07	2.78340E-05	2.01224E-07	2.32272E-06	6.89691E-05
Chron 5A	14.2	78.91	103.96	-5.29	1.920	37	19.27	(50,5)	1.10280E-05	6.66715E-07	2.74944E-05	1.65562E-07	1.71174E-06	6.91638E-05
Chron 6	19.6	76.53	112.58	-6.25	1.230	37	30.07	(50,5)	1.06675E-05	3.46215E-07	2.70795E-05	1.35891E-07	9.21729E-07	6.93753E-05
Chron 8	26.4	75.05	118.26	-7.64	2.936	37	12.60	(50,5)	1.02656E-05	-6.35145E-08	2.65978E-05	1.24563E-07	-1.31610E-07	6.95665E-05
Chron 13	33.3	69.52	125.16	-7.80	3.751	37	9.86	(50,5)	9.75633E-06	-3.20938E-07	2.59878E-05	1.34121E-07	-8.26643E-07	6.99097E-05
Chron 17	36.6	66.99	125.60	-8.06	4.191	37	8.83	(50,5)	9.43254E-06	-4.43809E-07	2.55921E-05	1.44255E-07	-1.17880E-06	7.01452E-05
Chron 18	39.4	65.72	124.07	-8.78	4.770	37	7.76	(50,5)	9.02739E-06	-6.03673E-07	2.50832E-05	1.63765E-07	-1.65723E-06	7.04334E-05
Chron 20	43.2	64.46	123.42	-9.70	5.497	37	6.73	(50,5)	8.56063E-06	-8.10647E-07	2.44734E-05	2.00309E-07	-2,30501E-06	7.07401E-05
Chron 21	47.1	66.41	116.71	-11.68	6.177	37	5.99	(50,5)	7.95554E-06	-9.78334E-07	2.36615E-05	2.44867E-07	-2.90832E-06	7.11989E-05
Chron 22	49.4	66.68	112.82	-13.05	6.640	37	5.57	(50,5)	7.45547E-06	-1.07252E-06	2.29623E-05	2.79622E-07	-3.31023E-06	7.15963E-05
Chron 23	51.3	64.28	114.66	-13.19	7.021	37	5.27	(50,5)	7.07384E-06	-1.16068E-06	2.24053E-05	3.15870E-07	-3.68844E-06	7.18865E-05
Chron 24	52.9	65.28	108.62	-14.98	7.302	37	5.07	(50,5)	6.49424E-06	-1.16957E-06	2.15351E-05	3.37248E-07	-3.90018E-06	7.24074E-05
COB fit	55.9	58.19	116.34	-13.49	7.665	37	4.83	(50,5)	6.13795E-06	-1.26115E-06	2.09638E-05	3.84787E-07	-4.33121E-06	7.26627E-05

Parameters: *r*, total misfit; *K*, estimated quality factor; *dF*, degrees of freedom; *N*, number of data points; *s*, number of great circle segments; the unvertainty of fracture zone and magnetic anomaly identification is σ = 5.00 km; ages are after Cande and Kent (1995) timescale.

Covariance matrix:

a	b	c
b	d	e
c	e	f

The units of the matrix elements are radians squared

MODEL 2

Finite Rotation of the eastern Aegir Segment relative to a stationary Greenland plate *(Kolbeinsey Ridge from present-day to Chron 6 ; Aegir Ridge and formation of the Jan Mayen microcontinent from Chron 6 to 55.9 Ma)*

		Pole of Rotation			Parameters/Uncertainties				Covariance matrice					
Stage	Age (in Ma)	Latitude (°N)	Longitude (°E)	Angle (°)	*r* (km)	*dF*	*K*	(*N*,*s*)	a	b	c	d	e	f
Chron 5	10.3	75.53	130.38	-2.95	0.264	37	140.07	(50,5)	3.37604E-05	-2.72202E-06	6.82058E-05	3.26634E-07	-5.47073E-06	1.38286E-04
Chron 5A	14.2	71.95	131.63	-3.79	0.453	37	81.63	(50,5)	3.28785E-05	-3.45890E-06	6.74273E-05	4.71012E-07	-7.06973E-06	1.38781E-04
Chron 6	19.6	70.26	128.88	-5.11	0.752	37	49.22	(50,5)	3.15624E-05	-4.40582E-06	6.62449E-05	7.22443E-07	-9.23033E-06	1.39555E-04
Chron 8	26.4	72.93	125.52	-7.22	1.137	37	32.54	(50,5)	3.02996E-05	-5.60433E-06	6.50295E-05	1.14522E-06	-1.20211E-05	1.40097E-04
Chron 13	33.3	67.49	131.23	-7.41	1.351	37	27.39	(50,5)	2.92846E-05	-6.15803E-06	6.40681E-05	1.40339E-06	-1.34704E-05	1.40714E-04
Chron 17	36.6	58.63	134.63	-7.14	1.499	37	24.69	(50,5)	2.81783E-05	-6.42865E-06	6.30294E-05	1.57448E-06	-1.43812E-05	1.41556E-04
Chron 18	39.4	40.54	141.68	-6.3	1.581	37	23.41	(50,5)	2.76918E-05	-6.57201E-06	6.25567E-05	1.66589E-06	-1.48495E-05	1.41909E-04
Chron 20	43.2	9.07	147.77	-6.77	1.747	37	21.18	(50,5)	2.67469E-05	-6.95227E-06	6.16049E-05	1.91086E-06	-1.60210E-05	1.42518E-04
Chron 21	47.1	-17.37	150.55	-9.54	1.908	37	19.39	(50,5)	2.53132E-05	-7.25509E-06	6.01471E-05	2.18036E-06	-1.72551E-05	1.43598E-04
Chron 22	49.4	-9.26	146.96	-9.38	2.084	37	17.76	(50,5)	2.39508E-05	-7.53782E-06	5.87084E-05	2.47477E-06	-1.85002E-05	1.44619E-04
Chron 23	51.3	-9.34	145.62	-10.04	2.000	37	18.50	(50,5)	2.28652E-05	-7.74116E-06	5.75163E-05	2.72370E-06	-1.95029E-05	1.45426E-04
Chron 24	52.9	-13.14	144.00	-11.09	2.059	37	17.97	(50,5)	2.14892E-05	-7.69752E-06	5.59844E-05	2.86006E-06	-2.00914E-05	1.46651E-04
COB fit	55.9	-26.23	145.51	-14.74	2.106	37	17.57	(50,5)	1.98802E-05	-7.84667E-06	5.40631E-05	3.19841E-06	-2.13921E-05	1.47910E-04

Finite Rotation of the eastern Kolbeinsey Segment relative to a stationary Greenland plate *(Kolbeinsey Ridge from present-day to Chron 6 ; Aegir Ridge and formation of the Jan Mayen microcontinent from Chron 6 to 55.9 Ma)*

		Pole of Rotation			Parameters/Uncertainties				Covariance matrice					
Stage	Age (in Ma)	Latitude (°N)	Longitude (°E)	Angle (°)	*r* (km)	*dF*	*K*	(*N*,*s*)	a	b	c	d	e	f
Chron 5	10.3	74.79	131.33	-2.93	19.779	117	5.92	(132,6)	3.91855E-06	-1.03367E-06	1.05774E-05	3.64884E-07	-2.83859E-06	2.87650E-05
Chron 5A	14.2	70.94	132.21	-3.73	19.812	117	5.91	(132,6)	3.76973E-06	-1.11473E-06	1.03874E-05	4.23204E-07	-3.12510E-06	2.88454E-05
Chron 6	19.6	68.79	130.81	-5.00	19.863	117	5.89	(132,6)	3.55452E-06	-1.21445E-06	1.01044E-05	5.10734E-07	-3.51415E-06	2.89634E-05
Chron 8	26.4	83.83	74.64	-10.88	19.903	117	5.88	(132,6)	3.40840E-06	-1.30832E-06	9.89661E-06	6.01626E-07	-3.88794E-06	2.90161E-05
Chron 13	33.3	81.65	16.52	-17.25	19.908	117	5.88	(132,6)	3.32325E-06	-1.31057E-06	9.77506E-06	6.16955E-07	-3.96893E-06	2.90866E-05
Chron 17	36.6	80.56	8.73	-20.08	19.914	117	5.88	(132,6)	3.29100E-06	-1.32335E-06	9.72599E-06	6.32305E-07	-4.03559E-06	2.91048E-05
Chron 18	39.4	81.25	12.84	-18.91	19.921	117	5.87	(132,6)	3.28140E-06	-1.32943E-06	9.71402E-06	6.39295E-07	-4.05689E-06	2.91086E-05
Chron 20	43.2	80.30	5.28	-21.90	19.936	117	5.87	(132,6)	3.26829E-06	-1.35301E-06	9.68859E-06	6.60805E-07	-4.14300E-06	2.91010E-05
Chron 21	47.1	79.17	-3.80	-26.56	19.933	117	5.87	(132,6)	3.30338E-06	-1.41939E-06	9.71997E-06	7.10129E-07	-4.32307E-06	2.90201E-05
Chron 22	49.4	79.96	-1.14	-25.38	19.942	117	5.87	(132,6)	3.25310E-06	-1.42955E-06	9.65214E-06	7.29963E-07	-4.38724E-06	2.90525E-05
Chron 23	51.3	79.55	0.98	-25.62	19.934	117	5.87	(132,6)	3.20217E-06	-1.38660E-06	9.58804E-06	7.01466E-07	-4.29867E-06	2.91325E-05
Chron 24	52.9	78.15	-5.17	-30.20	19.942	117	5.87	(132,6)	3.24697E-06	-1.40902E-06	9.63906E-06	7.10087E-07	-4.34076E-06	2.90799E-05
COB fit	55.9	78.41	-4.51	-29.79	19.944	117	5.87	(132,6)	3.22662E-06	-1.41396E-06	9.61111E-06	7.18972E-07	-4.36974E-06	2.90920E-05

Parameters: *r*, total misfit; *K*, estimated quality factor; *dF*, degrees of freedom; *N*, number of data points; *s* , number of great circle segments; the unvertainty of fracture zone and magnetic anomaly identification is σ = 5.00 km; ages are after Cande and Kent (1995) timescale.

Covariance matrix:

a	b	c
b	d	e
c	e	f

The units of the matrix elements are radians squared

Appendix Chapter 6

Appendix: Restoration of pre-rift structure of Santos and Campos basins

During an internship at Chevron offices in Houston, I had the opportunity to work on data from the SE Brazilian Margin and to study the rift structure of the Santos Basin. The purpose of this internship was to restore the pre-rift structure of the Santos Basin, using the method of Chapter 3, in order to quantify the amount and direction of extension. I also restored the pre-rift structure of the Campos Basin, using published data. This appendix describes the restorations of the Santos and Campos basins, step by step.

1. Restoration of pre-rift structure of Santos Basin

First Restoration

In order to restore the pre-rift structure of the Santos Basin, I used a structural map at the top of volcanic basement, which provides fault heaves (**Figure 1**). To this map of cut-off lenses, I added artificial faults in order to construct a block map of the Santos Basin (**Figure 2**). **Figure 3** illustrates the restoration after 2000 iterations. The restoration shows two main directions of extension: NNE-SSW and NW-SE, resulting in the sigmoid trend of the faults in map view (**Figure 1**). From this restoration, I estimated the amount of extension in various directions. I estimated the extension (*e*) by comparing the initial length (before rifting, l_0) and final length (after rifting, l_1), thus *e* is equal to $(l_1-l_0)/l_0$.

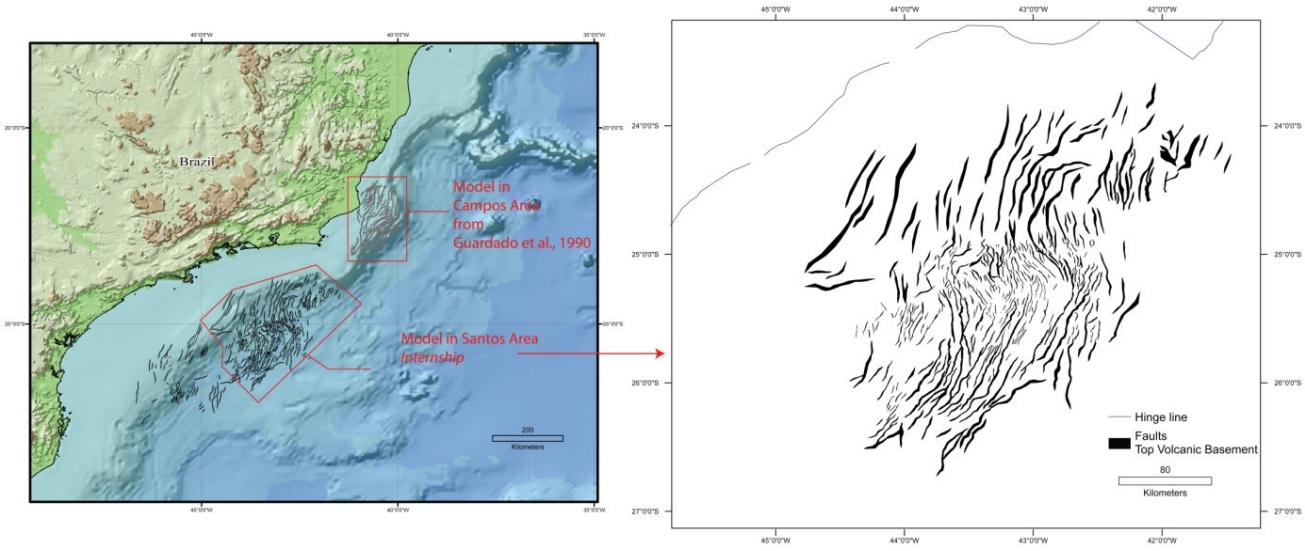

Figure 1. *Structure map of faults in top volcanic basement displaying rift framework of Santos Basin. Provided by Chevron.*

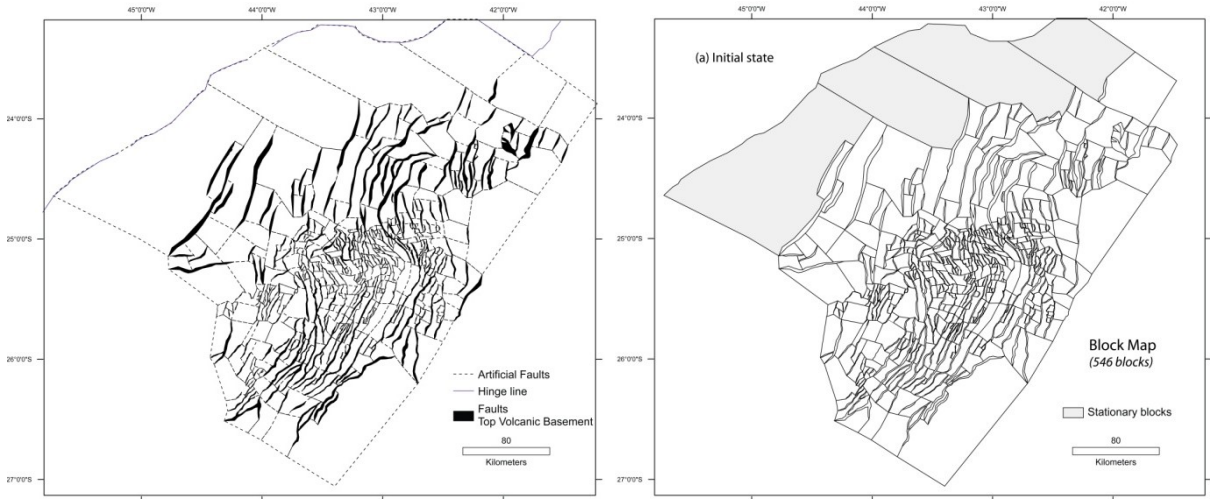

Figure 2. *Right*: *block map showing artificial fault (to the hinge line). Left: block map for top of volcanic basement in Santos Basin.*

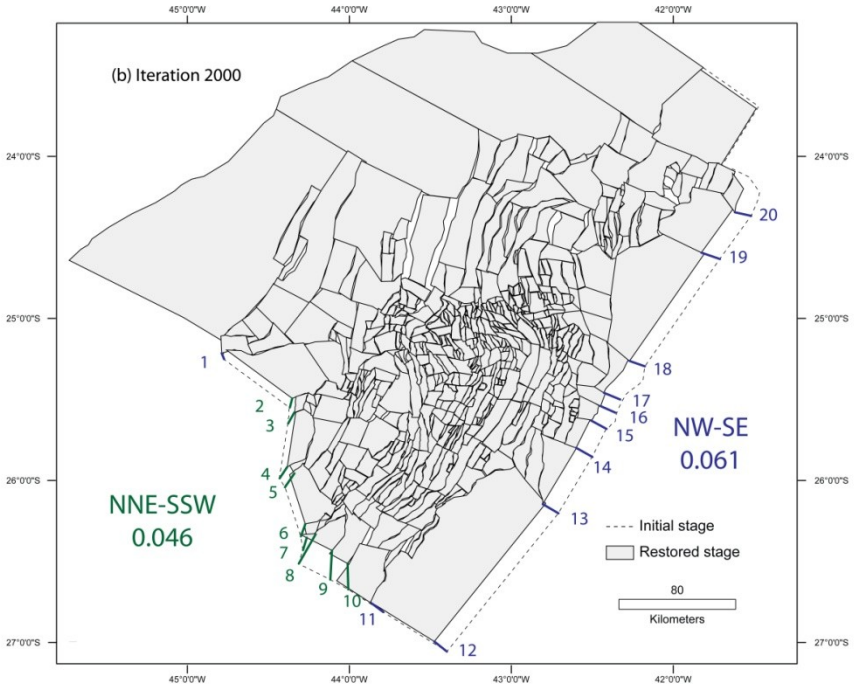

Blocks	Extension	Direction
2	0.039	NNE/SSW
3	0.049	NNE/SSW
4	0.049	NNE/SSW
5	0.041	NNE/SSW
6	0.031	NNE/SSW
7	0.028	NNE/SSW
8	*0.071*	*NE/SW*
9	0.060	N/S
10	0.047	N/S
Average	0.046	NNE/SSW
1	0.028	NNW/SSE
11	0.060	NW/SE
12	0.045	NW/SE
13	0.049	NW/SE
14	0.050	NW/SE
15	0.046	NW/SE
16	0.043	NW/SE
17	0.047	NW/SE
18	0.045	NW/SE
19	0.088	NW/SE
20	0.137	WNW/ESE
Average	0.061	NW/SE

Figure 3. *Results of restoration after 2000 iterations using block map of Figure 2, and amount of extension (table). External boundary is shown for current state (dashed line).*

The calculated amount of extension is very small (0.046 to 0.061). However, some problematic areas are visible in the restoration, where gaps are not closed, and therefore the amount is underestimated. This is mostly due to a difference in acquisition of the data, between 2D and 3D seismic data.

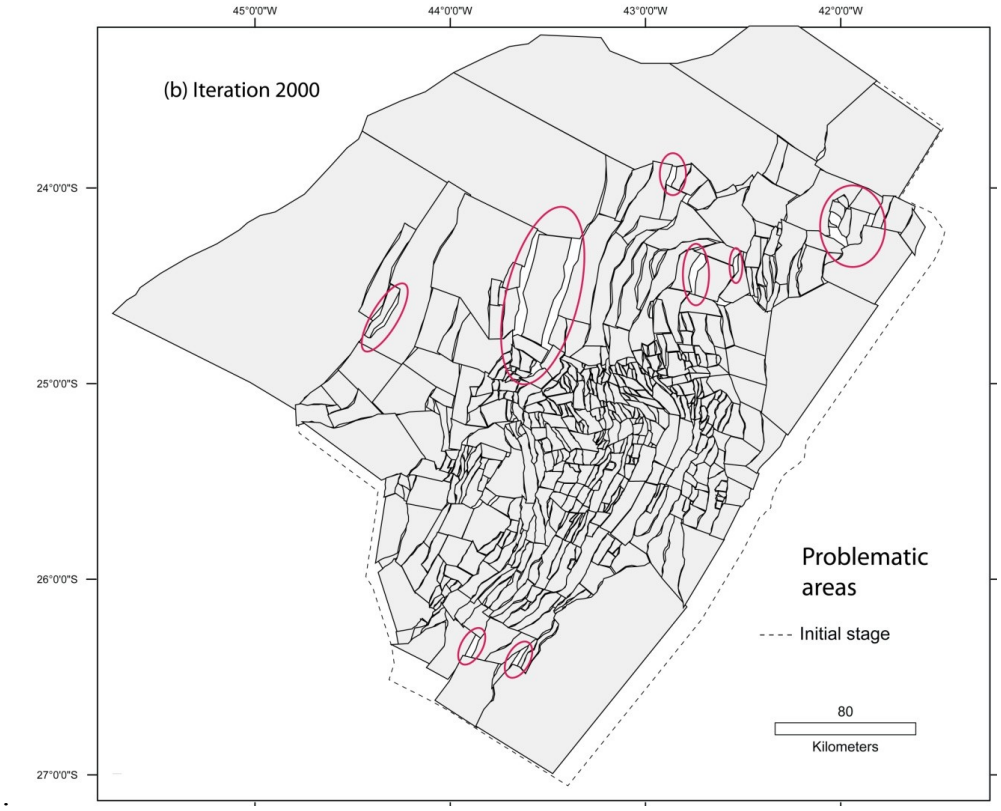

Figure 4. *Problematic areas in restoration (due to 2D vs 3D data), all gaps are not closed; amount of extension is therefore underestimated.*

I drew this block map from the top of volcanic basement. However, on seismic lines, there are deeper horizons in the basement. These deeper horizons may represent more accurately the pre-rift structure of the basin. Therefore, for a small area I mapped these horizons, re-evaluated the fault heave corresponding to each visible horizon and the restoration.

Seismic data: Re-evaluation of fault heave

The first structural map showed the rift framework on top volcanic basement. During my internship, I interpreted seismic lines of an area of the Santos Basin where faults show sigmoid trend (**Figure 5**). I mapped horizons below the top-volcanic basement in the acoustic basement. I mapped two horizons using Seiswork software (**Figure 6**) and estimated the depth and dip of each horizon using Gocad software (**Figures 7, 8, 9**). The heave of the faults changes significantly from the top-volcanic horizon to the deeper horizon, which therefore may change the results of restoration and calculation of extension. Therefore, I constructed block maps form the fault heaves and restore each horizon (**Figures 10-19**).

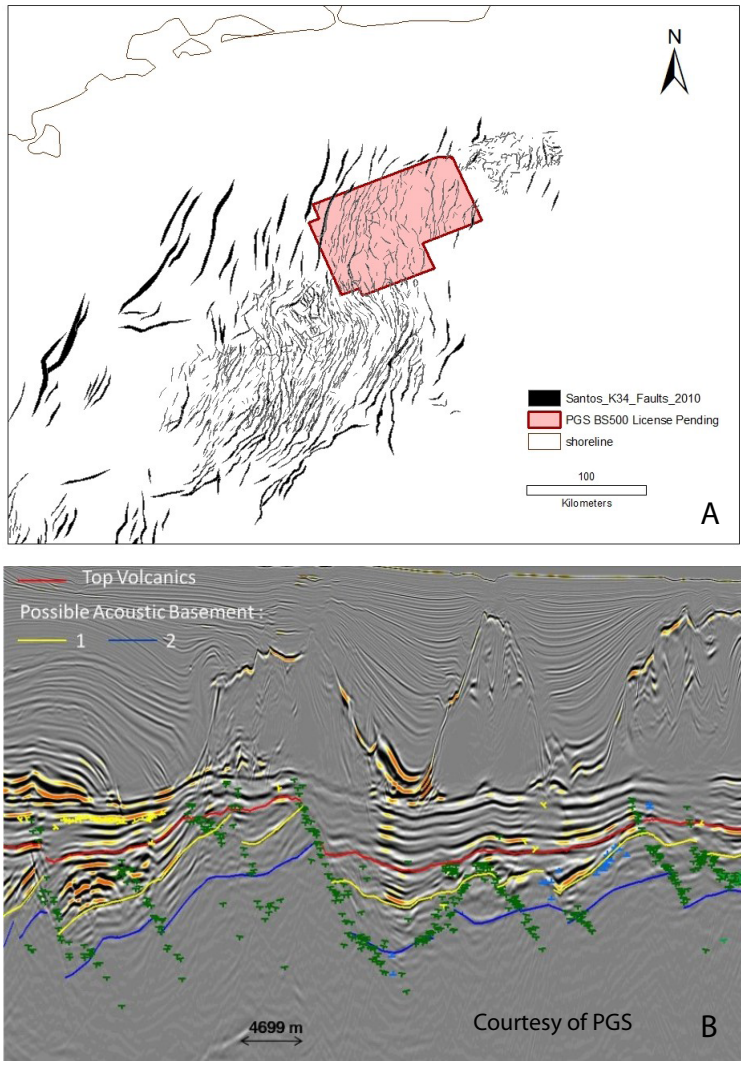

Figure 5. *A) Location of seismic data of Santos Basin used to re-evaluate fault heave in acoustic basement and B) example of cross section showing mapping of horizons in acoustic basement (Provided by Chevron, Courtesy of PGS).*

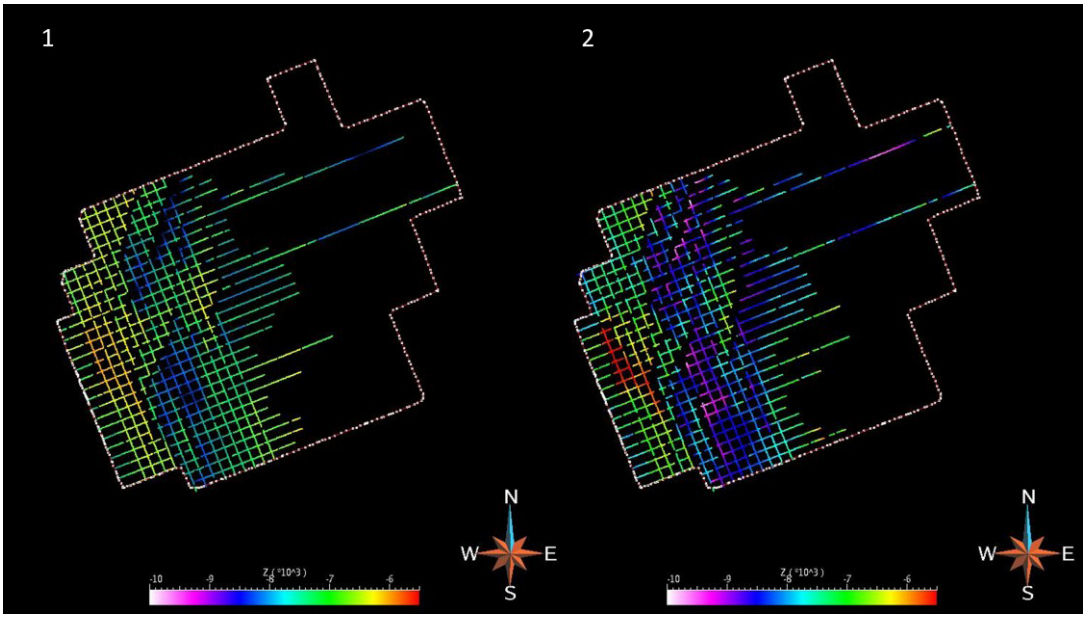

Figure 6. *Seismic Lines where (1) Horizons 1 and (2) Horizon 2 were mapped. Colour bars indicate depth in km.*

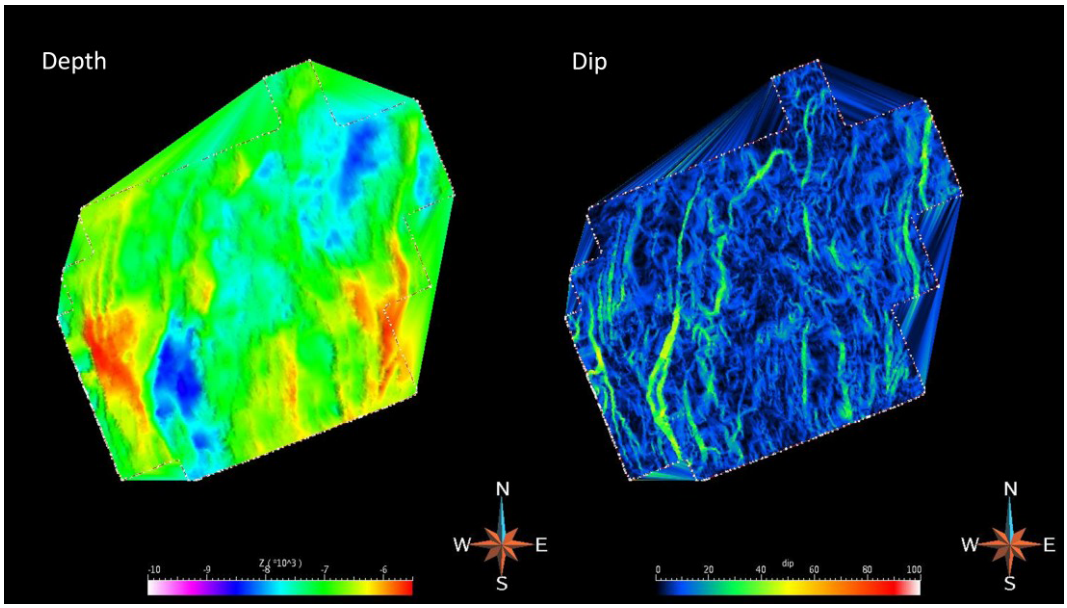

Figure 7.

Depth and dip of Top Volcanic Horizon

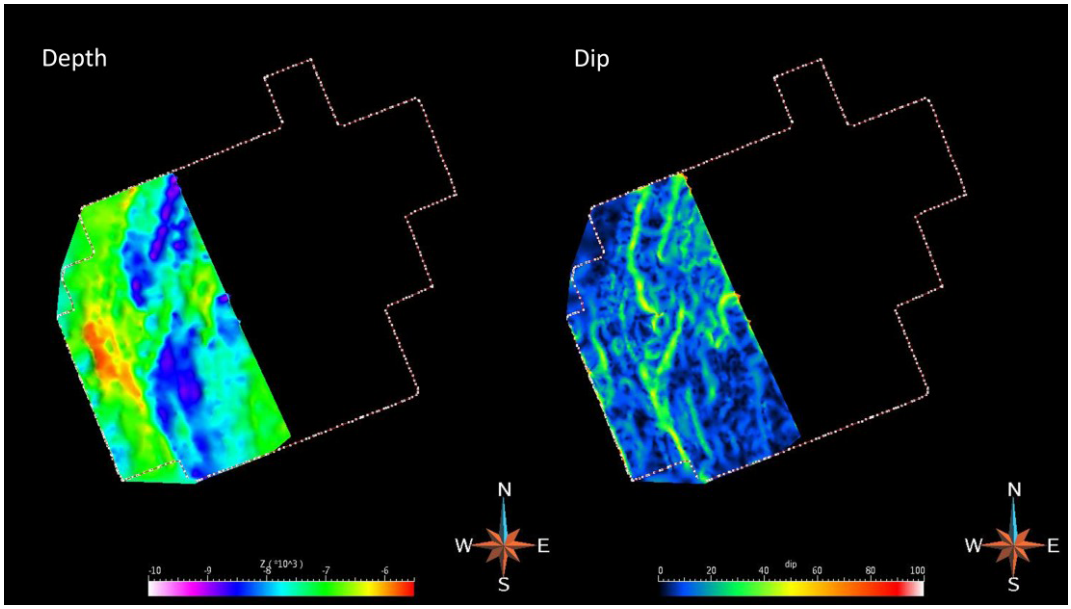

Figure 8.

Depth and dip of Acoustic Basement – Horizon 1

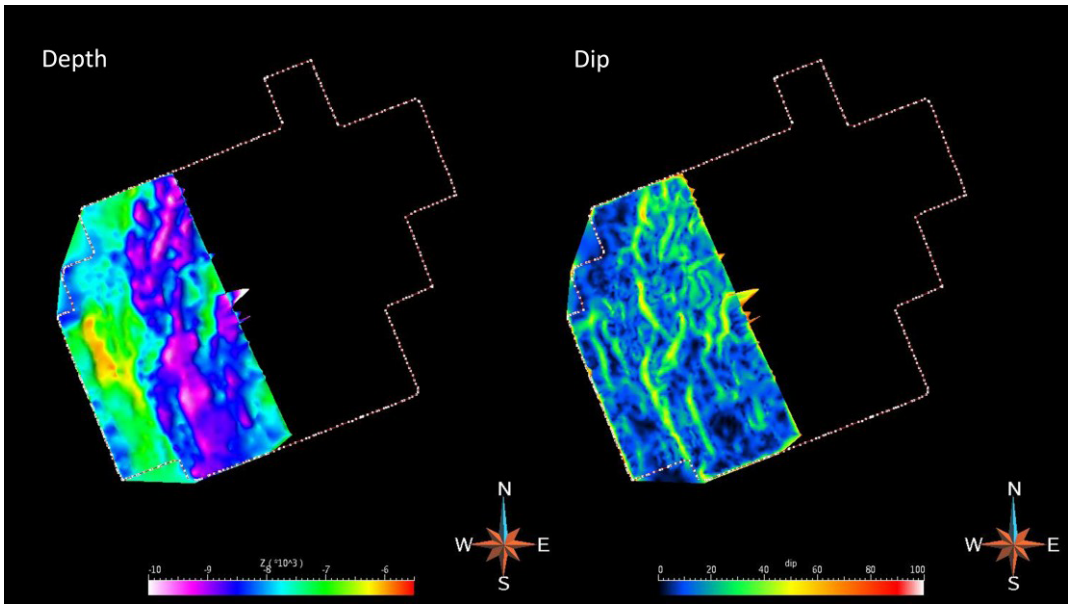

Figure 9.

Depth and dip of Acoustic Basement – Horizon 2

Second Restoration (of three horizons)

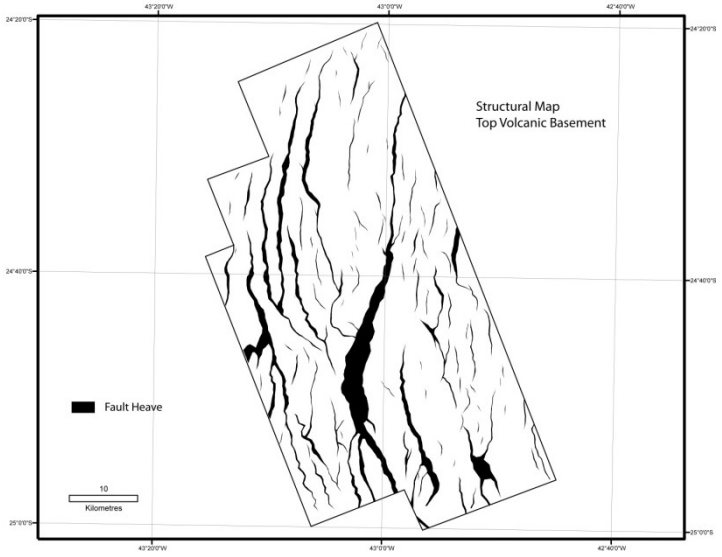

Figure 10.

Map of cut-off lenses of Top volcanic horizon

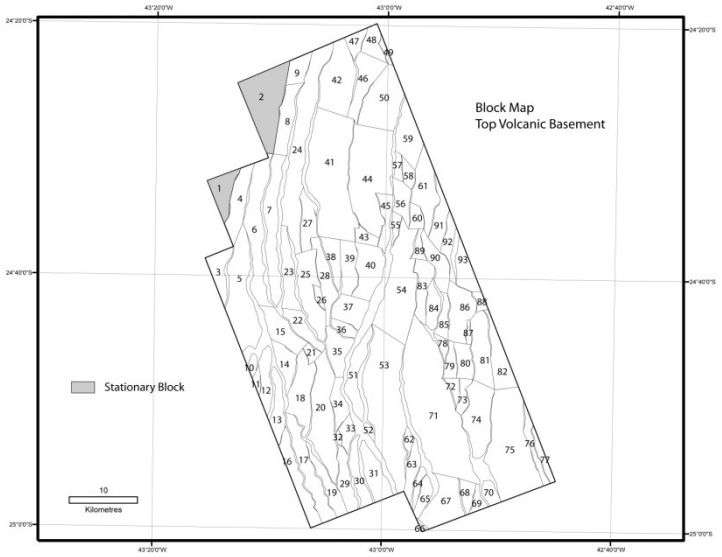

Figure 11.

Block Map of Top Volcanic horizon

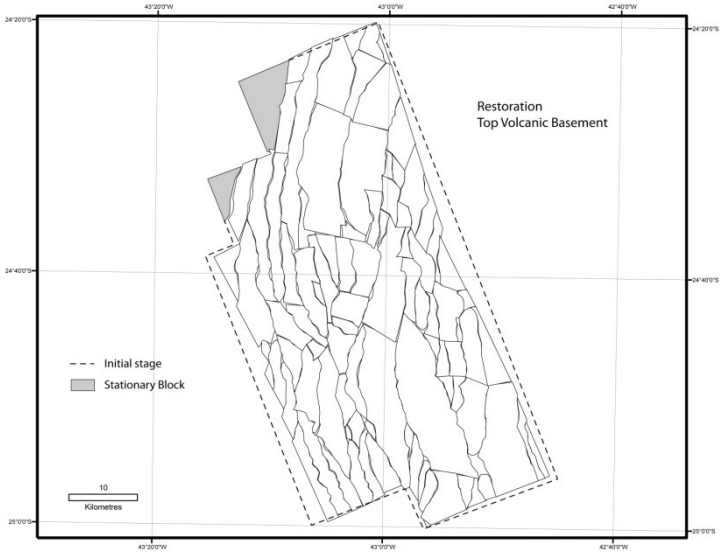

Figure 12.

Restoration of Top Volcanic horizon

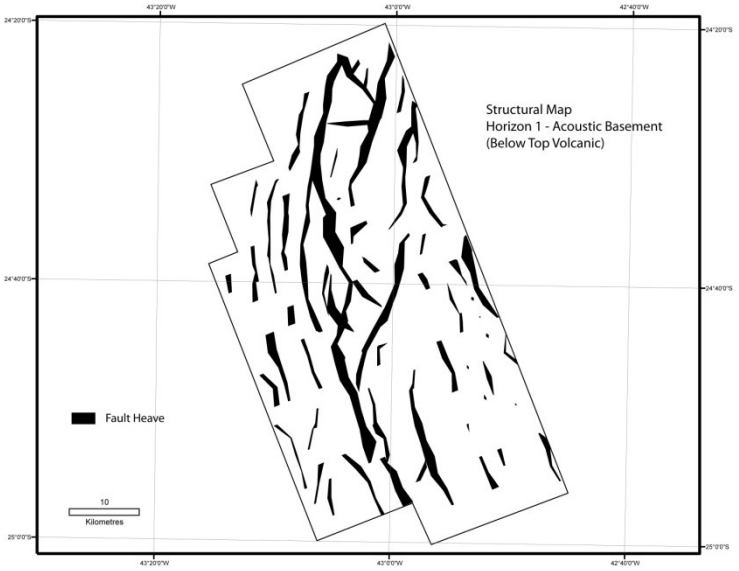

Figure 13.

Map of cut-off lenses of Horizon 1, in acoustic basement below top-volcanic horizon

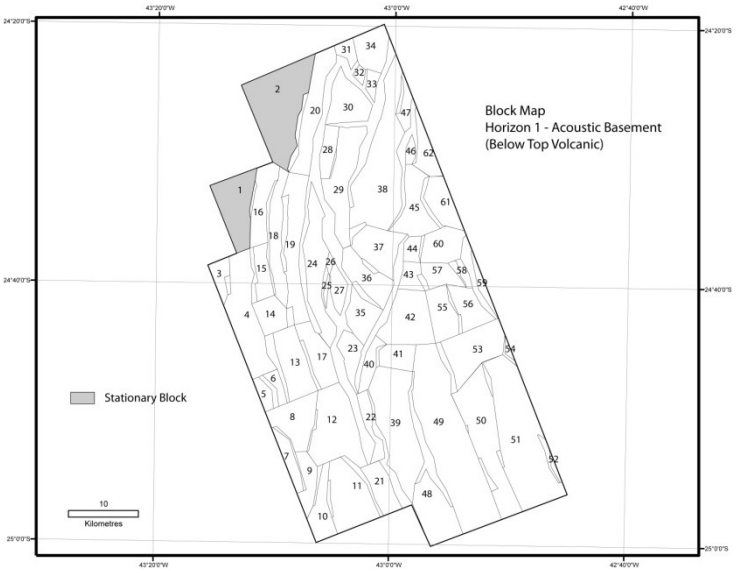

Figure 14.

Block Map of Horizon 1, in acoustic basement below top-volcanic horizon

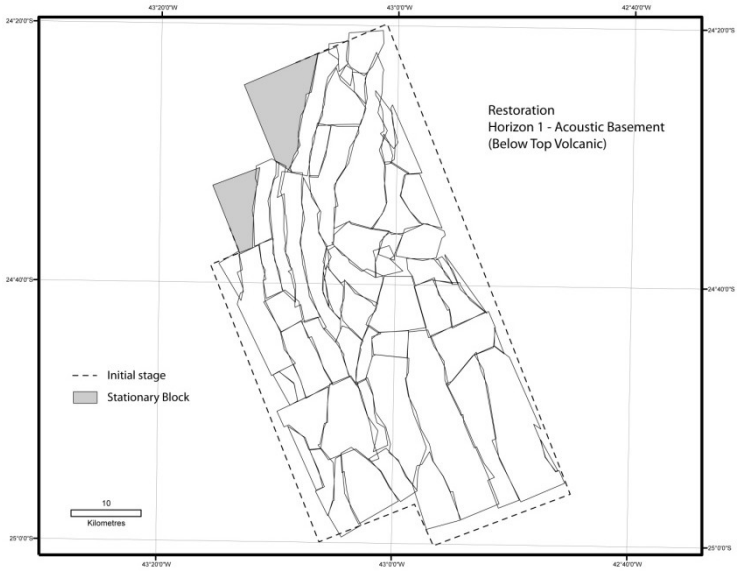

Figure 15.

Restoration of Horizon 1, in acoustic basement below top-volcanic horizon

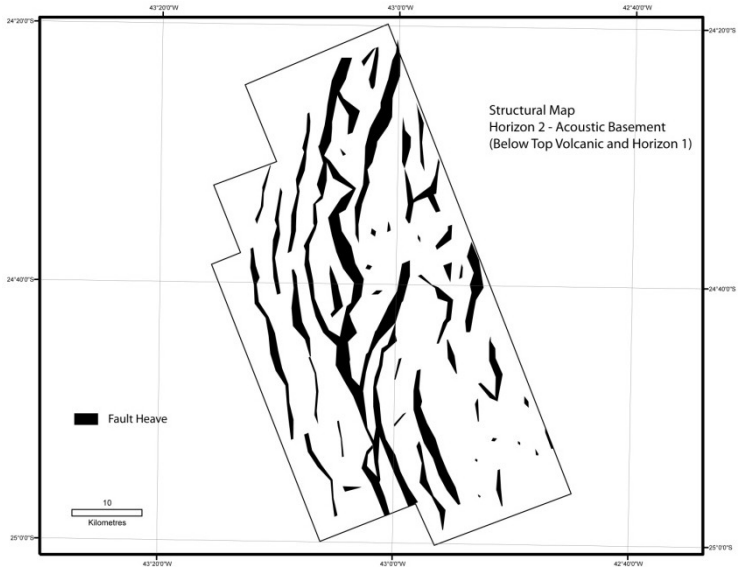

Figure 16.

Map of cut-off lenses of Horizon 2, in acoustic basement below top-volcanic horizon and Horizon 1

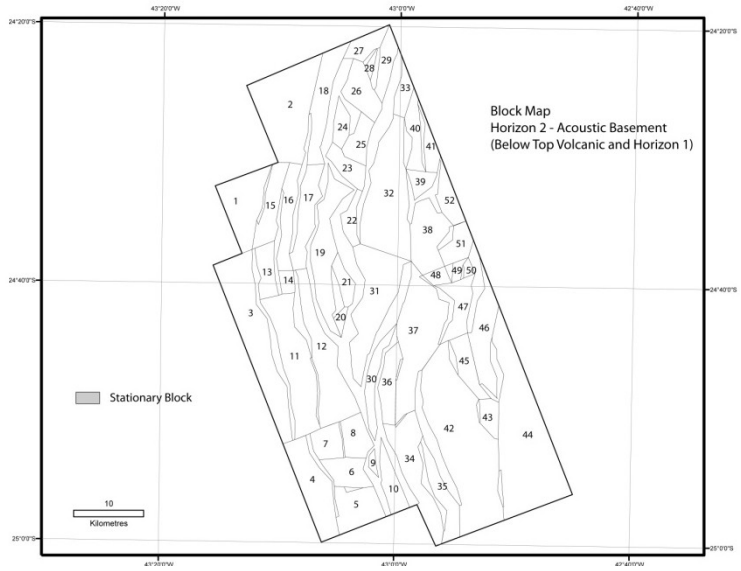

Figure 17.

Block Map of Horizon 2, in acoustic basement below top-volcanic horizon and Horizon 1

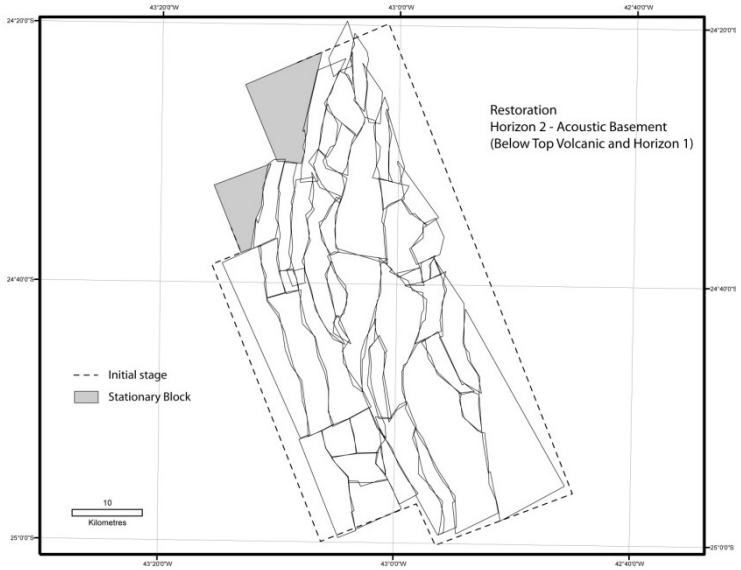

Figure 18.

Restoration of Horizon 2, in acoustic basement below top-volcanic horizon and Horizon 1

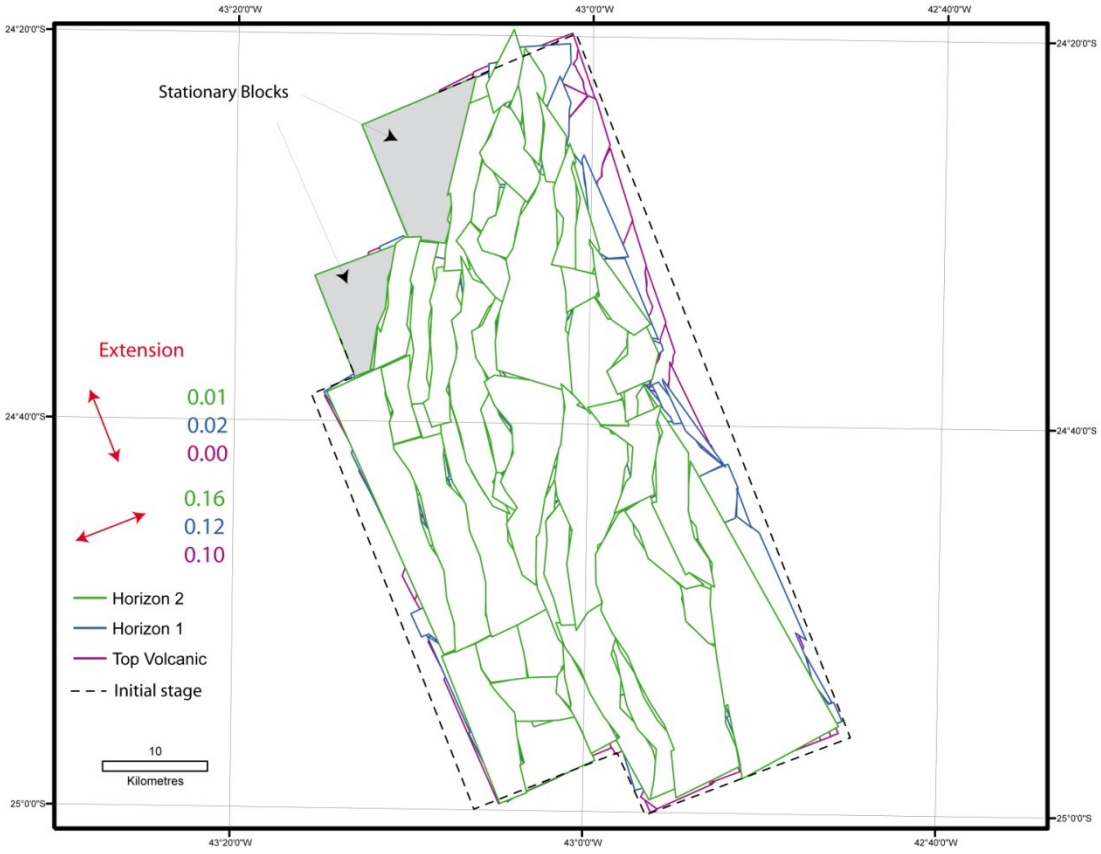

Figure 19. *Calculation of extension from restorations of each horizon*

Restoration of the deeper horizon in the acoustic basement predicts slightly higher amounts of extension in the NE-SW direction (0.16; **Figure 19**). However, this amount of extension is still very low and not enough to explain the total extension on the SE Brazilian Margin. This could reflect differences in weakness between the lower and upper crust, suggesting an asymmetric non-uniform mode of extension. Also, the Santos Basin was subject to magmatic activity from the Tristan da Cunha Plume. It is most likely that dyke emplacement occurred in the basin; it would thus be necessary to estimate the amount of extension that resulted from such magmatic activity. Further studies would be therefore be necessary to re-evaluate the accurate amount of extension in this region.

2. Restoration of pre-rift structure of Campos Basin

I also restored the pre-rift structure of the Campos basin, Brazil, for which structural data (fault location and heave) are in the public domain. I produced a fault-block map of the area, using data from *Guardado et al.* (1990) (**Figure 20**). I digitized the normal faults and their cut-off lenses, and subdivided the area into blocks (**Figure 21**).

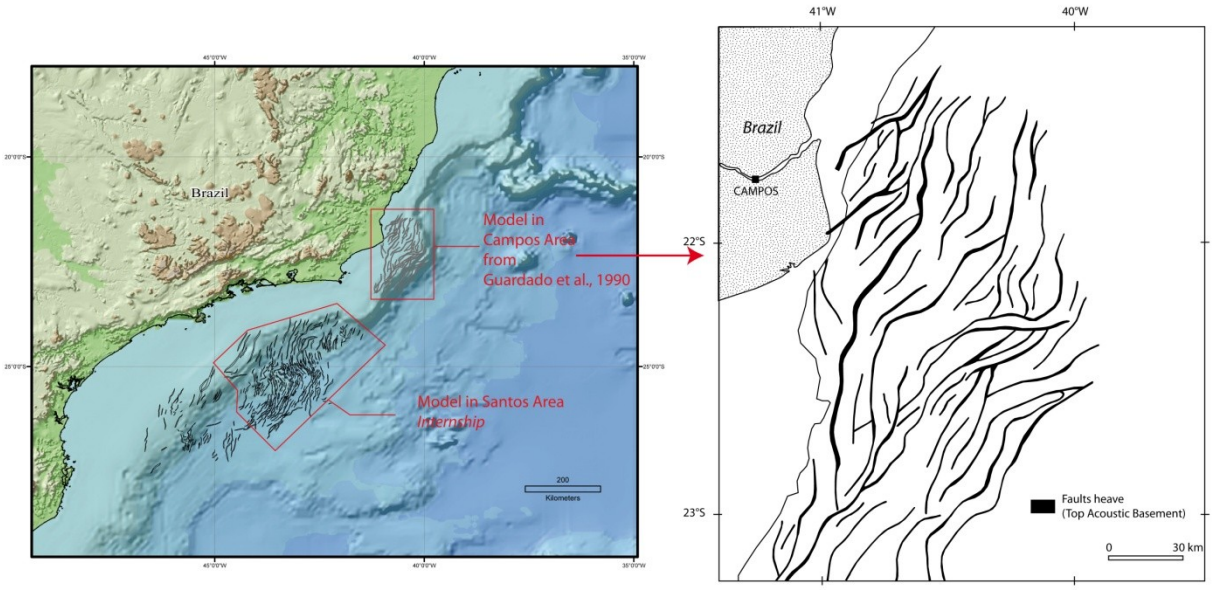

Figure 20. *Structure map on top acoustic Basement, Lower Cretaceous basalts, displaying rift framework of Campos basin (from Guardado et al., 1990).*

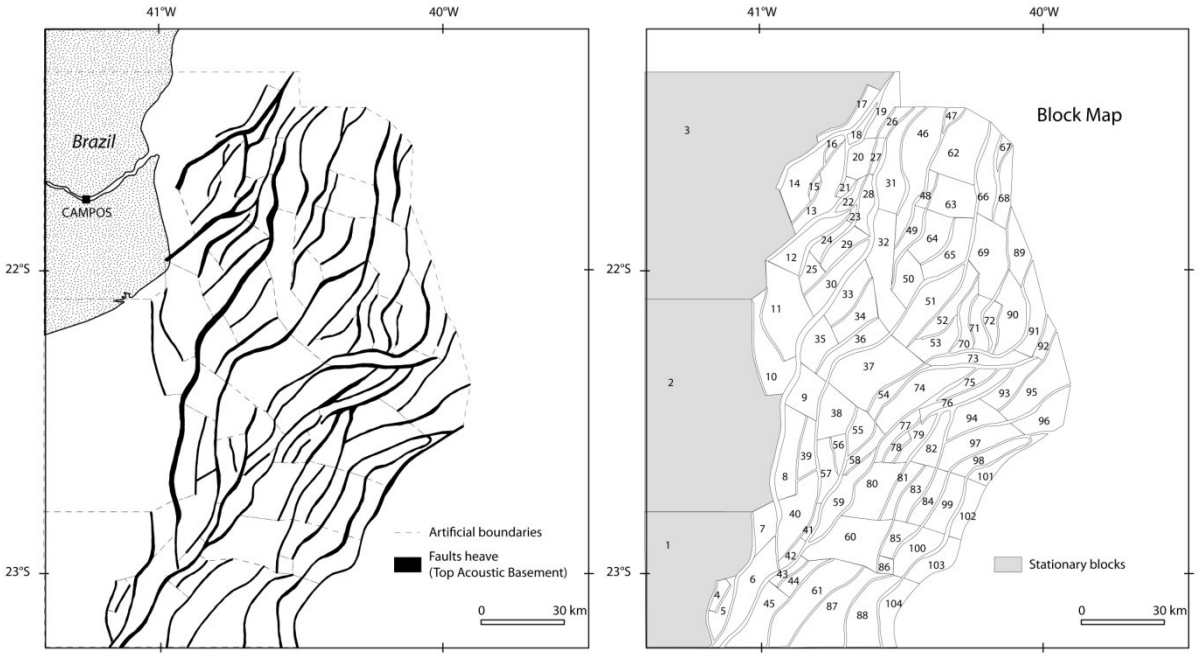

Figure 21. *Fault block map of Campos Basin from data of Guardado et al. (1990). Fault blocks have numbers (1 to 104, blocks 1 to 3 are stationary).*

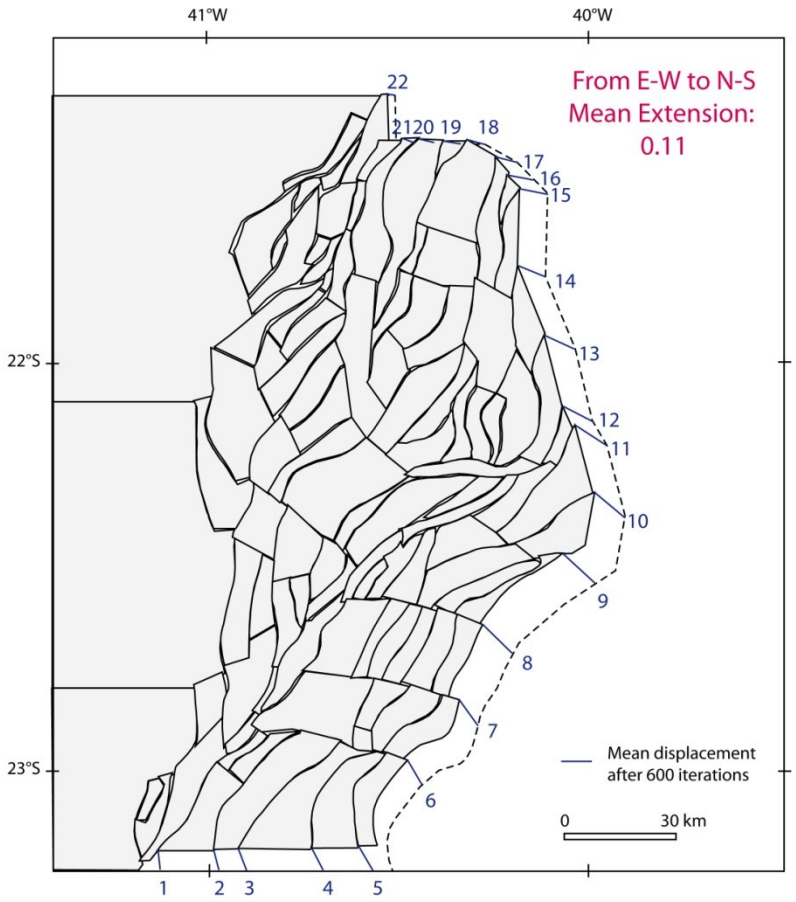

Block	Displacement (in km)	Extension	Direction
1	5	0.204	N-S
2	6	0.040	NNW-SSE
3	6	0.036	NNW-SSE
4	7	0.035	NNW-SSE
5	8	0.037	NNW-SSE
Average	6	0.07	
6	8	0.118	NNW-SSE
7	9	0.118	NW-SE
8	11	0.138	NW-SE
9	12	0.103	NW-SE
10	11	0.091	NW-SE
11	10	0.102	NW-SE
12	10	0.097	NW-SE
13	9	0.095	NW-SE
14	8	0.110	WNW-ESE
15	8	0.138	WNW-ESE
Average	10	0.11	
16	7	0.109	WNW-ESE
17	6	0.120	WNW-ESE
18	5	0.129	WNW-ESE
19	5	0.145	WNW-ESE
20	4	0.161	WNW-ESE
21	4	0.134	WNW-ESE
22	2	0.080	E-W
Average	4	0.13	
Total Average		**0.11**	

Figure 22. *Restoration of pre-rift structure of Campos Basin and amount of extension.*

These restorations brought a first approximation of the amount of stretching of the SE Brazilian Margin. The amount of extension obtained from the restoration of the Campos Basin is in the order of 0.11 (**Figure 22**). This amount is very small, as those of the Santos Basin. Further studies would be necessary to characterize the amount of extension in the whole Santos Basin and compare both regions. It would be also necessary to estimate the amount and distribution of extension in the lower crust during continental rifting.

Bibliography

A

Andersen, O. B., P. Knudsen, and P. a. M. Berry (2010), The DNSC08GRA global marine gravity field from double retracked satellite altimetry, *Journal of Geodesy*, *84*(3), 191-199, doi:10.1007/s00190-009-0355-9.

Anderson, D. L. (2001), Top-down tectonics? *Science, 293*, 2016-2018.

Anell, I., H. Thybo, and I. M. Artemieva (2009), Cenozoic uplift and subsidence in the North Atlantic region: Geological evidence revisited, *Tectonophysics*, *474*(1-2), 78-105, doi:10.1016/j.tecto.2009.04.006.

Archambault, M-F. (1984), *Evolution cinématique post-Eocène de l'Atlantique Nord et Central : Implications sur le fonctionnement des Açores et l'évolution du domaine méditerranéen occidental*, Thèse de doctorat de 3ème cycle, Université de Bretagne Occidentale, 211p.

Argent, J. D., S. A. Stewart, P. F. Green, and J. R. Underhill (2002), Heterogeneous exhumation in the Inner Moray Firth, UK North Sea: constraints from new AFTA(R) and seismic data, *Journal of the Geological Society*, *159*(6), 715-729, doi:10.1144/0016-764901-141.

Arriagada, C. (2004), *Rotations tectoniques et deformation de l'avant arc des Andes centrales au cours du Cénozoïque*, Mémoire de Géosciences Rennes, No. 107, 308 p.

Arriagada, C., P. Roperch, C. Mpodozis, and P. R. Cobbold (2008), Paleogene building of the Bolivian Orocline: Tectonic restoration of the central Andes in 2-D map view, *Tectonics*, *27*(6), 1-14, doi:10.1029/2008TC002269.

Audibert, M. (1991), Déformation discontinue et rotations de blocs, PhD Thesis, 250 pp., Université Rennes 1.

B

Benioff, H. (1949), Seismic evidence for the fault origin of oceanic deeps, *Bulletin of the Geological Society of America, 60*, 1837-1856.

Bird, P. (2003), An updated digital model of plate boundaries, Geochemistry, Geophysics, Geosystems, 4, 1027 , doi:10.1029/2001GC000252.

Bohnhoff, M., and J. Makris (2004), Crustal structure of the southeastern Iceland-Faeroe Ridge (IFR) from wide aperture seismic data, *Journal of Geodynamics*, *37*(2), 233-252, doi:10.1016/j.jog.2004.02.004.

Boldreel, L. O., and M. S. Andersen (1993), Late Pliocene to Miocene compression in the Faeroe-Rockall area, in *Petroleum Geology of Northwest Europe: Proceedings of the 4th Conference*, edited by J. R. Parker, pp. 1025-1034, Geological Society, London, Petroleum Geology Conference series.

Boldreel, L. O., and M. S. Andersen (1998), Tertiary compressional structures on the Faroe – Rockall Plateau in relation to northeast Atlantic ridge-push and Alpine foreland stresses, *Tectonophysics*, *300*, 13-28.

Bonow, J. M., K. Lidmar-Bergström, P. Japsen, J. A. Chalmers, and P. F. Green, (2007), Elevated erosion surfaces in central West Greenland and southern Norway: their significance in integrated studies of passive margin development, *Norwegian Journal of Geology, 87*, 197-206.

Bott, M. H. P. (1982), The interior of the Earth: Its structure, Constitution and Evolution (2nd edn.), Arnold, London.

Bott, M. H. P. (1983), Deep structure and geodynamics of the Greenland-Scotland Ridge: An Introduction Review, in *Structure and development of the Greenland-Scotland Ridge New methods and concepts*, edited by M. H. P. Bott, S. S., M. Talwani, and J. Thiede, NATO Conference Series, Series IV: Marine Sciences, *8*, 3-9.

Bott, M. H. P. (1985), Plate tectonic evolution of the Icelandic Transverse Ridge and adjacent regions, *Journal of Geophysical Research*, *90*(B12), 9953-9960, doi:0148-0227/85/004B-116850.

Bott, M. H. P. (1987), The continental margin of central East Greenland in relation to North Atlantic plate tectonic evolution, *Journal of the Geological Society*, *144*(4), 561-568, doi:10.1144/gsjgs.144.4.0561.

Bott, M. H. P. (1991), Ridge push and associated plate interior stress in normal and hotspot regions, *Tectonophysics, 200*, 17-32.

Bott, M. H. P., J. Sunderland, P. J. Smith, V. Casten, and S. Saxov (1974), Evidence for continental crust beneath the Faeroe Islands, *Nature, 248*, 1974, 202-204.

Bourgeois, O., P. R. Cobbold, D. Rouby, and J.-charles Thomas (1997), Least squares restoration of Tertiary thrust sheets in map view, Tajik depression, central Asia, *Journal of Geophysical Research*, *102*(B12), 24553-27573, doi:10.1029/97JB02477.

Boyden, J. A., R. D. Müller, M. Gurnis, T. H. Torsvik, J. A. Clark, M. Turner, H. Ivey-Law, J. Watson, and J. S. Cannon (2011), Next-generation plate-tectonic reconstructions using GPlates, in *Geoinformatics: Cyberinfrastructure for the Solid Earth Sciences*, edited by G. R. Keller and C. Baru, pp. 95-114, Cambridge University Press.

Breivik, A. J., R. Mjelde, H. Shimamura, Y. Murai, and Y. Nishimura (2003), Crustal structure of the Northern and Southern Jan Mayen Ridge Segments, Norwegian Sea, based on

ocean bottom seismometer data. American Geophysical Union, Fall Meeting 2003, abstract #T12D-0492.

Brekke, H. (2000), The tectonic evolution of the Norwegian Sea Continental Margin with emphasis on the Voring and More Basins, in *Dynamics of the Norwegian Margin*, vol. 167, edited by A. Nottvedt, Geological Society, London, Special Publications, *167*, 327-378,

Brekke, H., S. Dahlgren, B. Nyland, and C. Magnus (1999), The prospectivity of the Vøring and Møre basins on the Norwegian Sea continental margin, in *Petroleum Geology of Northwest Europe: Proceedings of the 5th Conference,* edited by A.J. Fleet and S. A. R. Boldy, Geological Society, London, Petroleum Geology Conference series, *5*, 261-274,

Brodie, J., and N. White (1994), Sedimentary basin inversion caused by igneous underplating: Nortwest European continental shelf, *Geology*, *22*, 147-150.

Bull, J. M., and R. A. Scrutton (1992), Seismic reflection images of intraplate deformation, central Indian Ocean, and their tectonic significance, *Journal of the Geological Society, London*, 149, 955-966.

Bullard, E., J. E. Everett, and a. G. Smith (1965), The Fit of the Continents around the Atlantic, *Philosophical Transactions of the Royal Society A: Mathematical, Physical and Engineering Sciences*, *258*(1088), 41-51, doi:10.1098/rsta.1965.0020.

Butler, R.F. (1992), *Paleomagnetism: Magnetic Domains to Geologic Terranes*, Blackwell Scientific Publications.

C

Callot, J. P., L. Geoffroy, C. Aubourg, J. P. Pozzi, and D. Mege (2001), Magma flow direction of shallow dykes from the East Greenland margin inferred from magnetic fabric studies, *Tectonophysics, 335*, 313–329.

Cande, S. C., and D. V. Kent (1995), Revised calibration of the geomagnetic polarity timescale for the Late Cretaceous and Cenozoic, *Journal of Geophysical Research*, *100*(B4), 6093-6095, doi:10.1029/94JB03098.

Cande, S. C., and D. R. Stegman (2011.), Indian and African plate motions driven by the push force of the Reunion plume head. *Nature*, *475*, 47-52.

Carlson, R. L., T. W. C. Hilde, S. Uyeda (1983), The driving mechanism of plate tectonics: Relation to age of lithosphere at trenches, *Geophysical Research Letters, 10*, 297-300.

Chalmers, J. (2000), Offshore evidence for Neogene uplift in central West Greenland, *Global and Planetary Change*, *24*(3-4), 311-318, doi:10.1016/S0921-8181(00)00015-1.

Chang, T. (1987), On the statistical properties of estimated rotations, *Journal of Geophysical Research, 92*, 6319-6329.

Chang, T. (1988), Estimating the relative rotation of two tectonic plates from boundary crossings, Journal of the American Statistical Association, 83, 1178-1183.

Chang, T., J. Stock, and P. Molnar (1992), The rotation group in plate tectonics and the representation of uncertainties of plate reconstructions, *Geophysical Journal International, 101*, 649-661.

Choukroune, P., Francheteau, J., and Hekinian, R., 1984, Tectonics of the East Pacific Rise near 128509N: A submersible study: Earth and Planetary Science Letters, v. 68, p. 115–127.

Clift, P. D., A. Carter, and A. J. Hurford (1998), The erosional and uplift history of NE Atlantic passive margins: constraints on a passing plume, *Journal of the Geolocal Society, London*, *155*, 787-800.

Cobbold, P. R. (1979), Removal of finite deformation using strain trajectories, *Journal of Structural Geology*, *1*(1), 67-72, doi:10.1016/0191-8141(79)90022-1.

Cobbold, P. R. (2008), Horizontal compression and stress concentration at passive margins: causes, consequences, and episodicity, *33rd International Geological Congress, Oslo*.

Cobbold, P. R., K. E. Meisling, and V. S. Mount (2001), Reactivation of an obliquely-rifted margin, Campos and Santos basins, southeastern Brazil, *AAPG Bulletin, v. 85*, no. 11, p. 1925–1944.

Cobbold, P. R., E. A. Rossello, P. Roperch, C. Arriagada, L. A. Gómez, and C. Lima (2007), Distribution, timing, and causes of Andean deformation across South America, in *Deformation of the continental crust: The legacy of Mike Coward*, edited by A. C. Ries, R. W. H. Butler, and R. H. Graham, Geological Society, London, Special Publications, *272*, 321-343

Coblentz, D. D., and R. M. Richardson (1995), Statistical trends in the intraplate stress field, *Journal of Geophysical Research, Solid Earth, 100*, 20245-20255.

Coffin, M. F., and O. Eldholm (1994), Large igneous provinces: Crustal structure, dimensions, and external consequences, *Reviews of Geophysics*, *32*(1), 1-36, doi:10.1029/93RG02508.

Courtillot, V., A. Davaille, J. Besse, and J. Stock (2003), Three distinct types of hotspots in the Earth's mantle, *Earth and Planetary Science Letters*, *205*(3-4), 295-308, doi:10.1016/S0012-821X(02)01048-8.

Couthinho, J. M. V. (2008), Dyke Swarms of the Paraná Triple Junction, Southern Brazil. *Geol. USP Sér. Cient., São Paulo*, *8*(2), 29-52.

D

Dahlen, F. A. (1981), Isostasy and the ambient state of stress in the oceanic lithosphere. *Journal of Geophysical Research, 86*, 7801–7807.

Darbyshire, F. A., R. S. White, and K. F. Priestley (2000), Structure of the crust and uppermost mantle of Iceland from a combined seismic and gravity study, *Earth and Planetary Science Letters*, *181*(3), 409-428, doi:10.1016/S0012-821X(00)00206-5.

Dauteuil, O., and J-P. Brun, (1996), Deformation partitioning in a slow spreading ridge undergoing oblique extension: Mohns Ridge, Norwegian Sea, *Tectonics, 15*(4), 870-884.

Davies, R., I. Cloke, J. Cartwright, A. Robinson, and C. Ferrero (2004), Post-breakup compression of a passive margin and its impact on hydrocarbon prospectivity: An example from the Tertiary of the Faeroe-Shetland Basin, United Kingdom, *AAPG Bulletin*, *88*(1), 1-20, doi:10.1306/09030303008.

Davison, I., S. Stasiuk, P. Nuttall, and P. Keane (2010), Sub-basalt hydrocarbon prospectivity in the Rockall, Faroe-Shetland and Møre basins, NE Atlantic in *Petroleum Geology: From Mature Basins to New Frontiers - Proceedings of the 7th Petroleum Geology Conference*, edited by B. A. Vinning and S. C. Pickering, Geological Society, London, Petroleum Geology Conference series, *7*, 1025-1032.

Dietz, R. S. (1961), Evolution by spreading of the sea floor, *Nature, 190*, 854.

Doré, A. G. (1991), The structural foundation and evolution of Mesozoic seaways between Europe and the Arctic. *Palaeogeography, Palaeoclimatology, Palaeoecology*, *87*, 441-492.

Doré, A. G., and E. R. Lundin (1996), Cenozoic compressional structures o n the NE Atlantic margin: nature, origin and potential significance for hydrocarbon exploration, *Petroleum Geology*, *2*, 299-311.

Doré, A. G., E. R. Lundin, L. N. Jensen, O. Birkeland, P. E. Eliassen, and C. Fichler (1999), Principal tectonic events in the evolution of the northwest European Atlantic margin service Principal tectonic events in the evolution of the northwest European Atlantic margin, in *Petroleum Geology of Northwest Europe: Proceedings of the 5th Conference*, edited by A. J. Fleet and S. A. Boldy, Geological Society, London, Petroleum Geology Conference series, London, *5*, 41-61.

Doré, A. G., E. R. Lundin, N. J. Kusznir, and C. Pascal (2008), Potential mechanisms for the genesis of Cenozoic domal structures on the NE Atlantic margin: pros, cons and some new ideas, in *The Nature and Origin of Compression in Passive Margins*, vol. 306, edited by H. Johnson, A. G. Doré, R. W. Gatliff, R. Holdsworth, E. R. Lundin, and J. D. Ritchie, Geological Society, London, Special Publications, *306*, 1-26.

E

Eldholm, O., and K. Grue (1994), North Atlantic volcanic margins: Dimensions and production rates, *Journal of Geophysical Research*, *99*(B2), 2955-2968.

Eldholm, O., J. Gladczenko, J. Skogseid, and Planke, S. (2000), Atlantic volcanic Margins: a comparative study, in *Dynamics of the Norwegian* edited by A. Nottvedt, B. T. Larsen, R. H. Gabrielsen, S. Olaussen, H. Brekke, B. Torudbakken, O. Birkeland, and J. Skogseid, Geological Society, London, Special Publications, *167*, 1-14.

Ellen, S. M. O. (2002), *Geological Map of Land and Sea Areas of Northern Europe*, Scale 1:4 000 000, Geological Survey of Norway.

Escher, J. C., and T. C. R. Pulvertaft (1995), *Geological map of Greenland*, scale 1:2 500 000, Geological Society of Denmark and Greenland.

Evans, D., C. Graham, A. Armour, and P. Bathurst (2003), *The Millennium Atlas: petroleum geology of the central and northern North Sea.* Geological Society, London, 389 p.

Eyles, N., and C. H., Eyle (1993), Glacial geologic confirmation of an intraplate boundary, in the Parana basin of Brazil. *Geology*, *21*, 459-462.

F

Fedorova, T., W. Jacoby, and H. Wallner (2005), Crust?mantle transition and Moho model for Iceland and surroundings from seismic, topography, and gravity data, *Tectonophysics*, *396*(3-4), 119-140, doi:10.1016/j.tecto.2004.11.004.

Fidalgo Gonzales, L. (2001), *La cinématique de l'Atlantique Nord : la question de la deformation intraplaque*, Thèse de doctorat de l'Université de Bretagne Occidentale, 260 p.

Firth, C.R., and I. S. Stewart (2000), Postglacial tectonics of the Scottish glacio-isostatic uplift centre. *Quaternary Science Reviews*, *19*, 1469-1493.

Forsyth, D., and S. Uyeda (1975), On the Relative Importance of the Driving Forces of Plate Motion, *Geophysical Journal of the Royal Astronomical Society*, *43*, 163-200.

Foulger, G., and D. Anderson (2005), A cool model for the Iceland hotspot, *Journal of Volcanology and Geothermal Research*, *141*(1-2), 1-22, doi:10.1016/j.jvolgeores.2004.10.007.

Foulger, G. R., Z. Du, and B. R. Julian (2003), Icelandic-type crust, *Geophysical Journal International*, *155*(2), 567-590, doi:10.1046/j.1365-246X.2003.02056.x.

Foulger, G. R., J. H. Natland, and D. L. Anderson (2005), A source for Icelandic magmas in remelted Iapetus crust, *Journal of Volcanology and Geothermal Research*, *141*(1-2), 23-44, doi:10.1016/j.jvolgeores.2004.10.006.

Foulger, G. R., M. J. Pritchard, B. R. Julian, J. R. Evans, R. M. Allen, G. Nolet, W. J. Morgan, B. H. Bergsson, P. Erlendsson, S. Jakobsdottir, S. Ragnarsson, R. Stefansson, K. Vogfjo (2000), The seismic anomaly beneath Iceland extends down to the mantle transition zone and no deeper, *Energy*, 1-5.

Foulger, G. R., M. J. Pritchard, B. R. Julian, J. R. Evans, R. M. Allen, G. Nolet, W. J. Morgan, B. H. Bergsson, P. Erlendsson, S. Jakobsdottir, S. Ragnarsson, R. Stefansson, K. Vogfjo (2001), Seismic tomography shows that upwelling beneath Iceland is confined to the upper mantle, *Energy*, 504-530.

G

Gaina, C., W.R. Roest, and R.D. Müller (2002), Late Cretaceous–Cenozoic deformation of northeast Asia, *Earth and Planetary Science Letters*, *197*(3-4), 273-286, doi:10.1016/S0012-821X(02)00499-5.

Gaina, C., L. Gernigon, and P. Ball (2009), Palaeocene – Recent plate boundaries in the NE Atlantic and the formation of the Jan Mayen microcontinent, *Journal of the Geolocal Society, London*, *166*, 601-616, doi:10.1144/0016-76492008-112.

Ganerød, M., M. a. Smethurst, T. H. Torsvik, T. Prestvik, S. Rousse, C. McKenna, D. J. J. Van Hinsbergen, and B. W. H. Hendriks (2010), The North Atlantic Igneous Province reconstructed and its relation to the Plume Generation Zone: the Antrim Lava Group revisited, *Geophysical Journal International*, *182*(1), 183-202, doi:10.1111/j.1365-246X.2010.04620.x.

Geoffroy, L. (2005), Volcanic passive margins, *Comptes Rendus Geosciences*, *337*(16), 1395-1408, doi:10.1016/j.crte.2005.10.006.

Gernigon, L., J.-C. Ringenbach, S. Planke, and B. Le Gall (2004), Deep structures and breakup along volcanic rifted margins: insights from integrated studies along the outer Vøring Basin (Norway), *Marine and Petroleum Geology*, *21*, 363-372, doi:doi:10.1016/j.marpetgeo.2004.01.005.

Gernigon, L., O. Olesen, J. Ebbing, S. Wienecke, C. Gaina, J. O. Mogaard, M. Sand, and R. Myklebust (2009), Geophysical insights and early spreading history in the vicinity of the Jan Mayen Fracture Zone, Norwegian–Greenland Sea, *Tectonophysics*, *468*(1-4), 185-205, doi:10.1016/j.tecto.2008.04.025.

Gernigon, L., Gaina, C., Péron-Pinvidic, G. and O. Olesen (2010), Spreading evolution of the Norway Basin and implication for the evolution of the Møre rifted margin and its intermediate conjugate system (the Jan Mayen microcontinent), *Central & North Atlantic conjugate margins conference, Lisbon, Portugal*, Extended Abstract, p. 45.

Green, P.F. (1989) Thermal and tectonic history of the East Midlands shelf, onshore UK and surrounding regions assessed by apatite fission track analysis, *Journal of the Geological Society of London, 146*, 755–774.

Green, P. F. (2002), Early Tertiary paleo-thermal effects in Northern England: reconciling results from apatite fission track analysis with geological evidence, *Tectonophysics*, *349*, 131–144.

Greiner, B. (1999), Euler rotations in plate-tectonic reconstructions, *Computers & Geosciences*, *25*(3), 209-216, doi:10.1016/S0098-3004(98)00160-5.

Guardado, L. R., L. A. P. Gamboa, and C. F. Lucchesi (1990), Petroleum geology of the Campos Basin, a model for a producing Atlantic-type basin, in *Divergent/passive margin basins,* edited by Edwards J. D. and P. A. Santogrossi, AAPG Memoir, 48, pp. 3–79.

Gudlaugsson, S. T., K. Gunnarsson, M. Sand, and J. Skogseid (1988), Tectonic and volcanic events at the Jan Mayen Ridge microcontinent, 1988, in the N Atlantic, in *Early Tertiary Volcanism and the Opening of the NE Atlantic*, A. C. Morton, and L. M. Parson, Geological Society, London, Special Publication, *39*, 3-13.

Guedes, E., M. Heilbron, P. M.Vaconcelos, C. de Morisson Valeriano, J. C. Horta de Almeida, W. Teixera, and A. T.Filho (2005), K–Ar and 40Ar/39Ar ages of dikes emplaced in the onshore basement of the Santos Basin, Resende area, SE Brazil: implications for the south Atlantic opening and Tertiary reactivation. *Journal of South America Earth Sciences*, *18*, 371-382.

H

Hall, A., and P.Bishop (2002), Scotland's denudational history: an integrated view of erosion and sedimentation at an uplifted passive margin, in *Exhumation of the North Atlantic Margin: Timing, Mechanisms and Implications for Petroleum Exploration*, edited by A. G. Doré, J. A. Cartwright, M. S. Stoker, J. P. Turner and N. White, Geological Society, London, Special Publications, *196*, 271-290.

Hamann, N. E., R. C. Whittaker, and L. Stemmerik (2005), Geological development of the Northeast Greenland Shelf, in *Petroleum Geology: North-West Europe and Global Perspectives - Proceedings of the 6th Petroleum Geology Conference*, edited by A. G. Doré and B. A. Vining, Geological Society, London, Petroleum Geology Conference series, *6*, 887 -902.

Hansen, K., S. C. Bergman, and B. Henk (2001), The Jameson Land basin (east Greenland): a fission track study of the tectonic and thermal evolution in the Cenozoic North Atlantic spreading regime, *Tectonophysics*, *331*, 307-339.

Hartley, R. a., G. G. Roberts, N. White, and C. Richardson (2011), Transient convective uplift of an ancient buried landscape, *Nature Geoscience*, *4*(8), 562-565, doi:10.1038/ngeo1191.

Hawkesworth, C .J., K. Gallagher, M. Mantovani, D. W. Peate, M. Regelous, and W. Rogers, W. (1992), Parana magmatism and the opening of the South Atlantic. in *Magmatism and*

the causes of continental break-up, edited by B. C. Storey, T. Alabaster, and R. J. Pankhurst R.J., Geological Society, London, Special Publication, *68*, 221–240,

Hawkesworth, C. J., K. Gallagher, L. Kirstein, M. S. M. Mantovani, D. W. Peate, and S. P. Turner (2000), Tectonic controls on magmatism associated with continental break-up: an example from the Parana-Etendeka Province, *Earth and Planetary Science Letters*, *179*, 335-349.

Heidbach, O., M. Tingay, A. Barth, J. Reinecker, D. Kurfeß, and B. Müller (2008), *The World Stress Map database release 2008*, doi:10.1594/GFZ.WSM.Rel2008.

Hellinger, S. J. (1981), The Uncertainties of Finite Rotations in Plate Tectonics, *Journal of Geophysical Research*, *86*(B10), 9312-9318.

Hendriks, B., P. Andriessen, Y. Huigen, C. Leighton, T. Redfield, G.Murrell, K. Gallagher, and S. B. Nielsen (2007). A fission track data compilation for Fennoscandia. *Norwegian Journal of Geology*, *87*, 227-239.

Herron, E. M. (1972), Sea-Floor Spreading and the Cenozoic History of the East-Central Pacific, *Geological Society Of America Bulletin*, *83*, 1671-1692.

Hess, H. H. (1962), History of ocean basins. *Geological Society of America Bulletin; Petrologic Studies: A Volume to Honour A.F. Buddington*, 559-620.

Hillier, R. D., and J. W. Cosgrove (2002), Core and seismic observations of overpressure-related deformation within Eocene sediments of the Outer Moray Firth, UKCS. *Petroleum Geoscience, 8*, 141-149.

Hitchen, K. (2004), The geology of the UK Hatton-Rockall margin, *Marine and Petroleum Geology*, *21*, 993-1012, doi:10.1016/j.marpetgeo.2004.05.004.

Holbrook, W. S., H. C. Larsen, L. Korenaga, T. Dahl-Jense, I. D. Reid, P. B., Kelemen, J. R. Hopper, G. M. Kent, D. Lizarralde, S. Bernstein, and R. S. Detrick (2001), Mantle thermal structure and active upwelling during continental breakup in the North Atlantic, *Earth and Planetary Science Letters*, *190*(3-4), 251-266, doi:10.1016/S0012-821X(01)00392-2.

Holford, S. P., P. F. Green, I. R. Duddy, J. P. Turner, R. R. Hillis, and M. S. Stoker (2009), Regional intraplate exhumation episodes related to plate-boundary deformation, *Geological Society of America Bulletin*, *121*(11-12), 1611-1628, doi:10.1130/B26481.1.

Holford, S. P., P. F. Green, R. R. Hillis, J. R. Underhill, M. S. Stoker, and I. R. Duddy (2010), Multiple post-Caledonian exhumation episodes across NW Scotland revealed by apatite fission-track analysis, *Journal of the Geological Society*, *167*(4), 675-694, doi:10.1144/0016-76492009-167.

Holgate, N. (1969), Palaeozoic and Tertiary transcurrent movements on the Great Glen Fault, *Scottish Journal of Geology*, *5*(2), 97-139.

Holmes, Arthur (1944). *Principles of Physical Geology* (1 ed.). Edinburgh: Thomas Nelson & Sons.

Hopper, J. R., T. Dahl-Jensen, W. S. Holbrook, H. C. Larsen, D. Lizarralde, J. Korenaga, G. M. Kent, and P. B. Kelemen (2003), Structure of the SE Greenland margin from seismic reflection and refraction data: Implications for nascent spreading center subsidence and asymmetric crustal accretion during North Atlantic opening, *Journal of Geophysical Research*, *108*(B5), 1-22, doi:10.1029/2002JB001996.

Hutton, D. H. W., and M. McErlean (1991), Silurian and Early Devonian sinistral deformation of the Ratagain granite, Scotland: constraints on the age of Caledonian movements on the Great Glen fault system, *Journal of the Geolocal Society, London*, *148*, 1-4.

I

Imsland, P. (1978), The geology of the volcanic island Jan Mayen, Arctic Ocean. *Nordic Volcanic Institute Research Report 7813,* 1-74.

Institute of Geological Sciences *(*1973), *Geological Map of Cromarty, Sheet 94, 1:50 000*. British Geological Survey.

Isack, B., Oliver, J., and L. R. Sykes (1968), Seismology and the New Global Tectonics, journal of Geophysical Research, 73(18), 5855-5899.

Ito, G. (2003), Observational and theoretical studies of the dynamics of mantle plume–mid-ocean ridge interaction, *Reviews of Geophysics*, *41*(4), doi:10.1029/2002RG000117.

J

Japsen, P., P. F. Green, and J. a. Chalmers (2005), Separation of Palaeogene and Neogene uplift on Nuussuaq, West Greenland, *Journal of the Geological Society*, *162*(2), 299-314, doi:10.1144/0016-764904-038.

Japsen, P., P. F. Green, L. H. Nielsen, E. S. Rasmussen, and T. Bidstrup (2007), Mesozoic–Cenozoic exhumation events in the eastern North Sea Basin: a multi-disciplinary study based on palaeothermal, palaeoburial, stratigraphic and seismic data, *Basin Research*, *19*(4), 451-490, doi:10.1111/j.1365-2117.2007.00329.x.

Japsen, P., P. F. Green, J. M. Bonow, E. S. Rasmussen, and J. A. Chalmers (2010), Episodic uplift and exhumation along North Atlantic passive margins: implications for hydrocarbon prospectivity, in *Petroleum Geology: From Mature Basins to New Frontiers - Proceedings of the 7th Petroleum Geology Conference*, edited by B. A. Vinning and S. C. Pickering, Geological Society, London, Petroleum Geology Conference series, *7*, 979-1004.

Japsen, P., J. M. Bonow, P. F. Green, P. R. Cobbold, D. Chiossi, R. Lilletveit, L. P. Magnavita, and A. Pedreira (2012), Episodic burial and exhumation in NE Brazil after opening of the South Atlantic, Geological Society of America Bulletin, published online on 13 January 2012 as doi:10.1130/B30515.1.

Johannesson, H., and K. Sæmundsson (1998) *Geological map of Iceland*, scale 1:500 000, Bedrock geology, 2nd edition. Icelandic Institute of Natural History, Reykjavik.

Johnson, C., and K. Gallagher (2000), A preliminary Mesozoic and Cenozoic denudation history of the North East Greenland onshore margin, *Global and Planetary Change*, *24*, 261–274.

Johnson, H., J. D. Ritchie, K. Hitchen, D. B. Mcinroy, and G. S. Kimbell (2005), Aspects of the Cenozoic deformational history of the Northeast Faroe − Shetland Basin , Wyville − Thomson Ridge and Hatton Bank areas, in *Petroleum Geology: North-West Europe and Global Perspectives - Proceedings of the 6th Petroleum Geology Conference*, edited by A. G. Doré and B. A. Vining, Geological Society, London, Petroleum Geology Conference series, 6, 993-1007.

Jolivet, M. (2007), Histoire de la dénudation dans le corridor du loch Ness (Écosse) : mouvements verticaux différentiels le long de la Great Glen Fault, *Comptes Rendus Geosciences*, *339*(2), 121-131, doi:10.1016/j.crte.2006.12.005.

Jones, S. M. (2003), Test of a ridge–plume interaction model using oceanic crustal structure around Iceland, *Earth and Planetary Science Letters*, *208*(3-4), 205-218, doi:10.1016/S0012-821X(03)00050-5.

Jones, S. M., and J. Mclennan (2005), Crustal flow beneath Iceland, *Journal of Geophysical Research*, *110*(B9), 1-19, doi:10.1029/2004JB003592.

Jones, S. M., N. White, B. J. Clarke, E. Rowley, and K. Gallagher (2002a), Present and past influence of the Iceland Plume on sedimentation, in *Exhumation of the North Atlantic Margin: Timing, Mechanisms and Implications for Petroleum Exploration,* edited by A. G. Doré, J. A. Cartwright, M. S. Stoker, J. P. Turner and N. White, Geological Society, London, Special Publications, *196*, 13-25.

Jones, S. M., N. White, and J. Maclenna (2002b), V-shaped ridges around Iceland: Implications for spatial and temporal patterns of mantle convection, *Geochemistry Geophysics Geosystems*, *3*(10), doi:10.1029/2002GC000361.

Jonk, R., D. Duranti, J. Parnell, A. Hurst, and A. E. Fallick (2003), The structural and diagenetic evolution of injected sandstones: examples from the Kimmeridgian of NE Scotland. *Journal of the Geological Society, London*, *160*, 881-894.

Judd, J. W. (1873), The Secondary Rocks of Scotland, *Quarterly Journal of the Geological Society*, *29*(1-2), 97-195, doi:10.1144/GSL.JGS.1873.029.01-02.16.

K

Kimbell, G. S., R. W. Gatliff, J. D. Ritchie, a S. D. Walker, and J. P. Williamson (2004), Regional three-dimensional gravity modelling of the NE Atlantic margin, *Basin Research*, *16*(2), 259-278, doi:10.1111/j.1365-2117.2004.00232.x.

Kimbell, G. S., J. D. Ritchie, H. Johnson, and R. W. Gatliff (2005), Controls on the structure and evolution of the NE Atlantic margin revealed by regional potential field imaging and 3D modelling, in *Petroleum Geology: North-West Europe and Global Perspectives - Proceedings of the 6th Petroleum Geology Conference*, edited by A. G. Doré and B. A. Vining, Geological Society, London, Petroleum Geology Conference series, *6*, 933-945.

Kirkwood, B. H., J.-Y. Royer, T. C. Chang, and R. G. Gordon (1999), Statistical tools for estimating and combining finite rotations and their uncertainties, *Geophysical Journal International*, *137*(2), 408-428, doi:10.1046/j.1365-246X.1999.00787.x.

Kodaira, S., R. Mjelde, K. Gunnarsson, H. Shiobara, and H. Shimamura (1998), Structure of the Jan Mayen microcontinent and implications for its evolution, *Geophysical Journal International*, (132), 383-400.

L

Larsen, H. C. (1990), The East Greenland Shelf, in *The Geology of North America, vol. L, The Arctic Ocean region*, edited by A. Grantz, L. Johnson, and J. F. Sweeney, Geological Society of America, Boulder, Colorado, 185–210.

Larsen, H. C. (2002), The southeast Greenland Volcanic Rifted Margin: Nature of Breakup and Interaction with the Iceland Plume, *AAPG Search and Discovery,* Article #90022.

Larsen, H. C., and S. J. Jakobsdóttir (1988), Distribution, crustal properties and significance of seawards-dipping sub-basement reflectors off East Greenland. In *Early Tertiary volcanism and the opening of the northeast Atlantic*, edited by A. C. Morton, and L. M. Parson, Geological Society Special Publication (London), vol. 39, pp. 95-114.

Lawver, L. A., and R. D. Müller (1994), Iceland Hotspot track, *Geology*, *22*, 311-314.

Le Pichon, X. (1968), Sea-floor spreading and continental drift, *Journal of Geophysical Research, 73,* 3661–97.

Le Pichon, X., J. Francheteau, and J. Bonnin (1973), *Plate tectonics*, Elsevier, Amsterdam, 300 p.

Le Pichon, X., J. C. Sibuet, and J. Francheteau (1977), The fit of continents around the North Atlantic Ocean, *Tectonophysics, 38*, 169-209.

Leroy, M., O. Dauteuil, P.R. Cobbold, (2004), Incipient shortening of a passive margin: the mechanical roles of continental and oceanic lithospheres, *Geophysical Journal International*, *159*, 400–411.

Lundin, E. R., and A. G. Doré (2002), Mid-Cenozoic post-breakup deformation in the "passive" margins bordering the Norwegian - Greenland Sea, *Marine and Petroleum Geology*, *19*, 79-93.

Lundin, E. R., and A. G. Doré (2005), NE Atlantic break-up: a re-examination of the Iceland mantle plume model and the Atlantic – Arctic linkage, in *Petroleum Geology: North-West Europe and Global Perspectives - Proceedings of the 6th Petroleum Geology*

Conference, edited by A. G. Doré and B. A. Vining, Geological Society, London, Petroleum Geology Conference series, *6*, 739-754.

Løseth, H., and S. Henriksen (2005), A Middle to Late Miocene compression phase along the Norwegian passive margin, in *Petroleum Geology: North-West Europe and Global Perspectives - Proceedings of the 6th Petroleum Geology Conference*, edited by A. G. Doré and B. A. Vining, Geological Society, London, Petroleum Geology Conference series, *6*, 845 -859.

M

Mackay, L. M., J. Turner, S. M. Jones, and N. J. White (2005), Cenozoic vertical motions in the Moray Firth Basin associated with initiation of the Iceland Plume, *Tectonics*, *24*(5), 1-23, doi:10.1029/2004TC001683.

Macnab, R., J. Verhoef, W. Roest, and J. Arkani-Hamed (1989), New Database Documents the Magnetic Character of the Artic and North Atlantic, *Eos Trans. AGU*, *76*(45), 449-458.

Maus, S., U. Barckhausen, H. Berkenbosch, N., Bournas, J. Brozena, V. Childers, F. Dostaler, J. D. Fairhead, C. Finn, R. R. B. von Frese, C. Gaina, S. Golynsky, R. Kucks, H. Lühr, P. Milligan, S. Mogren, R. D. Müller, O. Olesen, M. Pilkington, R. Saltus, B. Schreckenberger, E. Thébault, and F. Caratori Tontini (2009), EMAG2: A 2–arc min resolution Earth Magnetic Anomaly Grid compiled from satellite, airborne, and marine magnetic measurements, *Geochemistry Geophysics Geosystems*, *10*(8), doi:10.1029/2009GC002471.

McKenzie, D. (1978), Some remarks on the development of sedimentary basins, *Earth and Planetary Science Letters*, *40*, 25-32.

McKenzie, D. P., and R. L. Parker (1967), The north Pacific, an example of tectonics on a sphere, *Nature, 216*, 1276–80.

McQuillin, R., J. A. Donato, and J. Tulstrup (1982), Development of basins in the Inner Moray Firth and the North Sea by crustal extension and dextral displacement of the Great Glen Fault, *Earth and Planetary Science Letters*, *60*, 127-139.

Meijer, P. T., and M. Wortel (1992), The dynamics of motion of the South American Plate, *Journal of Geophysical Research, 97*, 11915-11931.

Meisling, K. E., P. R. Cobbold, and V. S. Mount (2001), Segmentation of an obliquely rifted margin, Campos and Santos basins, southeastern Brazil, *AAPG Bull., 85***,** 1903–1924.

Mendum, J. R., and S. R. Noble (2010), Mid-Devonian sinistral transpressional movements on the Great Glen Fault: the rise of the Rosemarkie Inlier and the Acadian event in Scotland, in *Continental tectonics and mountain building: the legacy of Peach and Horne*, edited by R. D. Law, R. W. H. Butler, R. E. Holdsworth, M. Krabbendam, R. A. Strachan, Geological Society, London, Special Publications, *335*, 161-187.

Mihalffy, P., B. Steinberger, and H. Schmeling (2008), The effect of the large-scale mantle flow field on the Iceland hotspot track, *Tectonophysics*, *447*(1-4), 5-18, doi:10.1016/j.tecto.2006.12.012.

Miller, H. (1851), *The old red sandstone or, New walks in an old field*, published by Gould and Lincoln, Boston, 288 p., from the 4th London Edition.

Mitchell, A. H., and H. G. Reading (1969), Continental margins, geosynclines, and ocean floor spreading, *The Journal of Geology*, *77*(6), 29-646.

Mjelde, R., T. Raum, Y. Murai, and T. Takanami (2007), Continent-ocean-transitions: Review, and a new tectono-magmatic model of the Vøring Plateau, NE Atlantic, *Journal of Geodynamics, 43*, 374-392.

Mjelde, R., T. Raum, a. J. Breivik, and J. I. Faleide (2008), Crustal transect across the North Atlantic, *Marine Geophysical Researches*, *29*(2), 73-87, doi:10.1007/s11001-008-9046-9.

Mohriak, W. U., B. R. Rosendahl (2003), Transform zones in the South Atlantic rifted continental margins. Intraplate strike-slip deformation belts, in *Intraplate Strike-Slip Deformation Belts*, edited by F. Storti, R. E. Holdsworth, F. Salvini, Geological Society, London, Special Publication, *210*, 211–228.

Mohriak, W. U., M. Nemcok, G. Enciso, (2008). South Atlantic divergent margin evolution: rift-border uplift and salt tectonics in the basins of SE Brazil, in *West Gondwana pre-Cenozoic correlations across the South Atlantic region,* edited by R. J. Pankhurst, R. A. J. Trouw, B. B. Brito Neves, M. J. de Wit, Geological Society, London, Special Publications, *294*, 365–398.

Morgan, W. J. (1968), Rises, trenches, great faults, and crustal blocks, *Journal of Geophysical Research, 73,* 1959–82

Morgan, W. J. (1971), Convection plumes in the lower mantle, *Nature, 230*, 42-43

Mosar, J., G. Lewis, and T. Torsvik (2002), North Atlantic sea-floor spreading rates: implications for the Tertiary development of inversion structures of the Norwegian – Greenland Sea, *Journal of the Geological Society*, *159*, 503-515, doi:110.1144/0016-764901-135.

Müller, R. D., J.-Y. Royer, and L. A. Lawver (1993), Revised plate motions relative to the hotspots from combined Atlantic and Indian Ocean hotspot tracks, *Geology*, *21*, 275-278.

Müller, R. D., W. R. Roest, and J-Y. Royer (1998). Assymetric sea-floor spreading caused by ridge-plume interactions. *Nature*, *396*(6710), 455-459.

Müller, R.D., J.-Y. Royer, S. C. Cande, W. R. Roest, S. Maschenkov, (1999). New constraints on the Late Cretaceous/Tertiary plate tectonic evolution of the Caribbean, in Caribbean Basins, in *Sedimentary Basins of the World series*, edited by P. Mann, Elsevier Science B.V., Amsterdam, *4*, 33–59.

Müller, R. D., C. Gaina, W. R. Roest, and D. L. Hansen (2001), A recipe for microcontinent formation, *Geology*, *29*(3), 203.

Müller, R. D., M. Sdrolias, C. Gaina, B. Steinberger, and C. Heine (2008), Age, spreading rates and spreading asymmetry of the world's ocean crust, *Geochemistry, Geophysics, Geosystems, 9*(4), Q04006, doi:10.1029-2007GC001743.

N

Nadin, P. A., N. J. Kusznir, and M. J. Cheadle (1997), Early Tertiary plume uplift of the North Sea and Faeroe-Shetland Basins. *Earth and Planetary Science Letters*, *148*, 109-127.

Nielsen, S. B., G. E. Paulsen, D. L. Hansen, L. Glemmer, O. R. Clausen, B. H. Jacobsen, N. Balling, M. Huuse, K. Gallagher (2002), Paleocene initiation of the Cenozoic uplift in Norway, in *Exhumation of the North Atlantic Margin: Timing, Mechanisms and Implications for Petroleum Exploration*, edited by A. G. Doré, J. A. Cartwright, M. S. Stoker, J. P. Turner and N. White, Geological Society, London, Special Publications, *196*, 45–65.

Nielsen, S, K. Gallagher, C. Leighton, N. Balling, L. Svenningsen, B. H. Jacobsen, E. Thomsen, O. B. Nielsen, C. Heilmann-Clausen, D. L. Egholm, M. A. Summerfield, O. R. Clausen, J. A. Piotrowski, M. R. Thorsen, M. Huuse, N. Abrahamsen, C. King, H. Lykke-Andersen (2009) ,The evolution of western Scandinavian topography: A review of Neogene uplift versus the ICE (isostasy–climate–erosion) hypothesis, *Journal of Geodynamics, 47*(2-3), 72-95.

Noble, R. H., R. M., Macintyre, and P. E. Brown (1988), Age constraints on Atlantic evolution: timing of magmatic activity along the E Greenland continental margin, in *Early Tertiary Volcanism and the Opening of the NE Atlantic,* edited by A. C. Morton, and L. M. Parson, Geological Society, London, Special Publications, *39*, 201-214.

Nunns, A. G. (1983), Plate tectonic evolution of the Greenland-Scotland Ridge and surrounding regions, in *Structure and development of the Greenland-Scotland Ridge New methods and concepts*, edited by M. H. P. Bott, S. S., M. Talwani, and J. Thiede, NATO Conference Series, Series IV: Marine Sciences, *8*, 11-30.

O

Olesen, O., J. Ebbing, E. Lundin, E. Mauring, J. R. Skilbrei, and T. H. Torsvik (2007), An improved tectonic model for the Eocene opening of the Norwegian – Greenland Sea: Use of modern magnetic data, *Marine and Petroleum Geology*, *24*, 53-66, doi:10.1016/j.marpetgeo.2006.10.008.

Oliver, J., and B. Isacks (1967) Deep Earthquakes Zones, Anomalous Structures in the Upper Mantle, and the Lithosphere, *Journal of Geophysical Research, 72*(16), 4259-4275.

P

Pascal, C., and R. Gabrielsen (2001), Numerical modeling of Cenozoic stress patterns in the mid-Norwegian margin and the northern North Sea, *Tectonics, 20(4),* doi: 10.1029/2001TC900007.

Peate, D.W., (1997). The Parana-Etendeka province, in *Large Igneous Provinces Continental, Oceanic, and Planetary Flood Volcanism*, edited by J. J. Mahoney and M. F. Coffin *Geophysical Monograph*, *100*, 217– 245.

Péron-Pinvidic, G., G. Manatschal, L. Gernigon, and C. Gaina (2010), *The formation and evolution of crustal blocks at rifted margins: new insights from the interpretation of the Jan Mayen microcontinent*, Central and North Atlantic Conjugate Margins Conference, Lisbon 2010, ISBN: 978-989-96923-1-2, *V*, 231-235.

Persano, C., D. N. Barfod, F. M. Stuart, and P. Bishop (2007), Constraints on early Cenozoic underplating-driven uplift and denudation of western Scotland from low temperature thermochronometry, *Earth and Planetary Science Letters*, *263*(3-4), 404-419, doi:10.1016/j.epsl.2007.09.016.

Pitman, W. C., and M. Talwani (1972), Sea-Floor Spreading in the North Atlantic, *Geological Society of America Bulletin*, *83*(3), 619-646, doi:10.1130/0016-7606(1972)83[619:SSITNA]2.0.CO;2.

Planke, S., J. Skogseid, and O. Eldholm (1991), Crustal structure off Norway, 62° to 70° north, *Tectonophysics*, *189*, 91-107.

Praeg, D., M. S. Stoker, P. M. Shannon, S. Ceramicola, B. Hjelstuen, J. S. Laberg, A. Mathiesen (2005), Episodic Cenozoic tectonism and the development of the NW European 'passive' continental margin. *Marine and Petroleum Geology, 22*, 1007–1030.

Price, S., J. Brodie, A. Whitiam, and R.A.Y. Kent, (1997), Mid-Tertiary rifting and magmatism in the Traill Ø region, East Greenland, *Journal of the Geological Society, 154*, 419-434, doi:110.1144/gsjgs.154.3.0419.

R

Redfield, T. F. (2010), On apatite fission track dating and the Tertiary evolution of West Greenland topography, *Journal of the Geological Society London, 167,*261-271.

Redfield, T. F., P. T. Osmunsen, and B. W. H. Hendriks (2005), The role of fault reactivation and growth in the uplift of western Fennoscandia, *Journal of the Geological Society London, 162*, 1013–1030.

Richard, P., B. Mocquet, and P. R. Cobbold (1991), Experiments on simultaneous faulting and folding above a basement wrench fault, *Tectonophysics*, *188*, 133-141.

Richardson, R. M. (1992), Ridge forces, absolute plate motions, and the intraplate stress field, *Journal of Geophysical Research, 97*, 11739-11748.

Riis, F., and W. Fjeldskaar (1992), On the magnitude of the Late Tertiary and Quaternary erosion and its significance for the uplift of Scandinavia and the Barents Sea, in *Structural and Tectonic Modeling and its Application to Petroleum Geology*, edited by R. M., Larsen, H. Brekke, B. T. Larsen, E. Talleraas, Norw. Petrol. Soc. Spec. Publ., *1*, 163-185.

Ritchie, J. D., H. Johnson, and G. S. Kimbell (2003), The nature and age of Cenozoic contractional deformation within the NE Faroe–Shetland Basin, *Marine and Petroleum Geology*, *20*(5), 399-409, doi:10.1016/S0264-8172(03)00075-8.

Ritchie, J. D., H. Johnson, M. F. Quinn, and R. W. Gatliff (2008), The effects of Cenozoic compression within the Faroe-Shetland Basin and adjacent areas, in *The Nature and Origin of Compression in Passive Margins*, edited by H. Johnson, A. G. Doré, R. W. Gatliff, R. Holdsworth, E. R. Lundin, and J. D. Ritchie, Geological Society, London, Special Publications, *306*, 121-136.

Roberts, D. G. (1989), Basin inversion in and around the British Isles, in *Inversion Tectonics*, edited by M. A. Cooper, Geological Society, London, Special Publications, No. 44, pp. 131-150, doi:10.1144/GSL.SP.1989.044.01.09.

Rodrigues, N., P. R. Cobbold, H. Loseth, and G. Ruffet (2009), Widespread bedding-parallel veins of fibrous calcite (‘beef’) in a mature source rock (Vaca Muerta Fm, Neuquen Basin, Argentina): evidence for overpressure and horizontal compression. *Journal of the Geological Society, London*, *166*(4), 695-709.

Rogers, D. A., J. E. A. Marshall, and T. R. Austin (1989), Devonian and later movements on the Great Glen fault system, Scotland, *Journal of the Geolocal Society, London*, *146*, 369-372.

Rohrman, M., P. Van Der Beek, P. Andriessen, and S. Cloetingh (1995), Meso-Cenozoic morphotectonic evolution of southern Norway: Neogene domal uplift inferred from apatite fission track thermochronology, *Tectonics, 14*(3), 704-718.

Rohrman, M., and P. Van Der Beek (1996), Cenozoic postrift domal uplift of North Atlantic margins: An asthenospheric diapirism model *Geology*, *24*(10), 901–904.

Rouby, D. (1994), *Restauration en carte des domains faillés en extension : Méthode et Application*, Mémoires de Geosciences Rennes, No. 58, 230 p.

Rouby, D., P. R. Cobbold, P. Szatmari, S. Demercian, D. Coelho, and J. A. Rici (1993a), Least-squares palinspastic restoration of regions of normal faulting - application to the Campos Basin (Brazil), *Tectonophysics*, *221*(3-4), 439-452, doi:10.1016/0040-1951(93)90172-G.

Rouby, R., P.R. Cobbold, P. Szatmari, S. Demercian, D. Coelho et R. Ricci (1993b), Restauration in map-view of faulted Upper Cretaceous and Oligocene horizons and its bearing on the history of salt tectonics in the Campos Basin (Brazil), *Tectonophysics*, *228*, 435-445.

Rowley, D. B., and A. L. Lottes (1988), Plate kinematic reconstruction of the North Atlantic and Artic, Late Jurassic to Present, *Tectonophysics, 155*, 73-90.

Royer, J-Y, and T. Chang, T. (1991), Evidence for relative motions between the Indian and Australian Plates during the last 20 m.y. from plate tectonic reconstructions: Implications for the deformation of the Indo-Australian Plate, *Journal of Geophysical Research, 96*, 11779-11802.

S

Saunders, A. D., J. G. Fitton, A. C. Kerr, M. J. Norry, and R. W. Kent (1997), The North Atlantic Igneous Province, in *Large Igneous Provinces Continental, Oceanic, and Planetary Flood Volcanism*, edited by J. J. Mahoney and M. F. Coffin, American Geophysical Union, Geophysical Monograph Series, *100*, 45-93.

Saunders, A. D., S. M. Jones, L. A. Morgan, K. L. Pierce, M. Widdowson, and Y. G. Xu (2007), Regional uplift associated with continental large igneous provinces: The roles of mantle plumes and the lithosphere, *Chemical Geology*, *241*(3-4), 282-318, doi:10.1016/j.chemgeo.2007.01.017.

Scotchman, I. C., G. Gilchrist, N. J. Kusznir, N. J., A. M. Roberts, and R. Fletcher (2010), The breakup of the South Atlantic Ocean: formation of failed spreading axis and blocks of thinned continental crust in the Santos Basin, Brazil and its consequences for petroleum system development, in *Petroleum Geology: From Mature Basins to New Frontiers - Proceedings of the 7th Petroleum Geology Conference*, edited by B. A. Vinning and S. C. Pickering, Geological Society, London, Petroleum Geology Conference series, *7*, 855-866.

Scott, R. A. (2000), Mesozoic-Cenozoic Evolution of East Greenland: Implications of a Reinterpreted Continent-Ocean Boundary Location, *Polarforschung, 68*, 83-91.

Scott, R. A., L. A. Ramsey, S. M. Jones, S. Sinclair, and C. S. Pickles (2005), Development of the Jan Mayen microcontinent by linked propagation and retreat of spreading ridges, in *Onshore-Offshore Relationships on the North Atlantic Margin*, vol. 12, edited by B. T. G. Wandas, J. P. Nystuen, E. Eide, and F. M. Gradstein, Norwegian Petroleum Society Special Publications, 69-82.

Selley, R. C. (1992) Petroleum seepages and impregnations in Great Britain. *Marine and Petroleum Geology*, *9*, 226-244.

Sibuet, J-C., S.P. Srivastava, and W. Spakman (2004), Pyrenean orogeny and plate kinematics, *Journal of Geophysical Research*, *109*, B08104.

Skogseid, J. (2001), Volcanic margins: geodynamic and exploration aspects, *Marine and Petroleum Geology, 18*, 457-461.

Skogseid, J., S. Planke, J. I. Faleide, T. Pedersen, O. Eldholm, and F. Neverdal (2000), NE Atlantic rifting and volcanic margin formation, in *Dynamics of the Norwegian Margin*,

edited by A. Nottvedt, B. T. Larsen, R. H. Gabrielsen, S. Olaussen, H. Brekke, B. Torudbakken, O. Birkeland, and J. Skogseid, Geological Society, London, Special Publications, No. 167, pp. 295-326.

Smallwood, J. R. (2004), Tertiary Inversion in the Faroe-Shetland Channel and the Development of Major Erosional Scarps, in *3D Seismic Technology: Application to the Exploration of Sedimentary Basins*, edited by R. J. Davies, J. A., Cartwright, S. A. stewart, M. Lappin, and J. R. Underhill, Geological Society, London, Special Publications, *29*, 187-198.

Soper, N. J., R. A. Strachan, R. E. Holdsworth, R. A. Gayer, and R. O. Geiling (1992), Sinistral transpression and the Silurian closure of Iapetus, *Journal of the Geolocal Society, London*, *149*, 871-880.

Speight, J. M., and J. G. Mitchell (1979), The Permo-Carboniferous dyke-swarm of northern Argyll and its bearing on dextral displacement on the Great Glen Fault, *Journal of the Geolocal Society, London*, *139*, 3-11.

Srivastava, S. P., and C. R. Tapscott (1986), Plate Kinematics of the North Atlantic, in *The Geology of North America, The Western North Atlantic Region*, edited by P. R. Vogt and B. E. Tucholke, Geological Society of America, 379-404.

Srivastava, S. P., and W. R. Roest (1999), Extent of oceanic crust in the Labrador Sea, *Marine and Petroleum Geology*, *16*(1), 65-84, doi:10.1016/S0264-8172(98)00041-5.

Steinberger, B., R. Sutherland, and R. J. O'Connell (2004), Prediction of Emperor-Hawaii semount locations from a revised model of global plate motion and mantle flow, *Nature*, *430*, 167-173, doi:10.1038/nature02660.

Stevenson, D. J., and J. S. Turner (1997), Angle of subduction, *Nature, 270*, 334-336.

Stewart, M., R. E. Holdsworth, and R. A. Strachan (2000), Deformation processes and weakening mechanisms within the frictional ± viscous transition zone of major crustal-scale faults: insights from the Great Glen Fault Zone , Scotland, *Journal of Structural Geology*, *22*, 543-560.

Stewart, M., R. A. Strachan, M. W. Martin, and R. E. Holdsworth (2001), Constraints on early sinistral displacements along the Great Glen Fault Zone, Scotland: structural setting, U-Pb geochronology and emplacement of the syn-tectonic Clunes tonalite, *Journal of the Geological Society*, *158*(5), 821-830, doi:10.1144/jgs.158.5.821.

Stoker, M. S. (2002), Mate Neogene development of the UK Atlantic Margin, in *Exhumation of the North Atlantic Margin: Timing, Mechanisms and Implications for Petroleum Exploration*, edited by A. G. Doré, J. A. Cartwright, M. S. Stoker, J. P. Turner and N. White, Geological Society, London, Special Publications, *196*, 313-329.

Stoker, M. S., R. J. Hoult, T. Nielsen, B. O. Hjelstuen, J. S. Laberg, and P. M. Shannon (2005), Sedimentary and oceanographic responses to early Neogene compression on the NW European margin, *Atlantic*, *22*, 1031-1044, doi:10.1016/j.marpetgeo.2005.01.009.

Stone, P. (2007), *Bedrock geology UK North, An explanation of the bedrock geology map of Scotland, northern England, Isle of Man and Northern Ireland - 1:625 000*, 5th Edition, British Geological Survey, Natural Environment Research Concil.

Storey, M., R. a. Duncan, and C. Tegner (2007), Timing and duration of volcanism in the North Atlantic Igneous Province: Implications for geodynamics and links to the Iceland hotspot, *Chemical Geology*, *241*(3-4), 264-281, doi:10.1016/j.chemgeo.2007.01.016.

Stuevold, L. M., J. Skogseid, and O. Eldholm (1992), Post-Cretaceous uplift events on the Voring continental margin, *Geology*, *20*, 919-922.

Sykes, R. M. (1975), The stratigraphy of the Callovian and Oxfordian stages (Middle-Upper Jurassic) in northern Scotland, *Scottish Journal of Geology*, *11*(1), 51-78.

T

Talwani, M., and O. Eldholm (1977), Evolution of the Norwegian-Greenland Sea, *Geological Society of America Bulletin*, *88*(7), 969-999.

Taylor, F.B. (1910) Bearing of the Tertiary mountain belt on the origin of the Earth's plan. *Geological Society of America Bulletine, 21,* 179–226.

Thiérault, P., and R. J. Steel (1995), Syn-rift sedimentation in the Upper Jurassic (Helmsdale Boulder Beds) of the Inner Moray Firth. in *Sequence Stratigraphy on the Northwest European Margin*, edited by R. J. Steel, V. L. Felt, E. P. Johannessen and C. Mathieu, Norwegian Petroleum Society Special Publication, 365-387.

Thompson, R. N., S. A. Gibson, J. G. Mitchell, A. P. Dickin, O. H. Leonardos, J. A. Brod, and J. C. Greenwood (1998), Migrating Cretaceous–Eocene magmatism in the Serra do Mar alkaline province, SE Brazil: melts from the deflected Trindade mantle plume?: *Journal of Petrology*, *39*, 1493–1526.

Thomson, K., and J. R. Underhill (1993), Controls on the development and evolution of structural styles in the Inner Moray Firth Basin, in *Petroleum Geology of Northwest Europe: Proceedings of the 4th Conference*, edited by J. R. Parker, Geological Society, London, Petroleum Geology Conference series, *4*, 1167-1178.

Thomson, K., and R. R. Hillis (1995), Tertiary structuration and erosion of the Inner Moray Firth, in *The Tectonics, Sedimentation and Palaeoceanography of the North Atlantic Region*, edited by R. A. Scrutton, M. S. Stoker, G. B. Shimmield and A. W. Tudhope, Geological Society, London, Special Publications, *90*. 249-269.

Thomson, K., P. F. Green, A. G. Whitman, S. P. Price, J. R. Underhill (1999), New Constraints on the thermal history of NE Greenland from apatite fission track analysis. *Geological Society of America Bulletin,* 7, 1054–1068.

Torsvik, T. H., and M. A. Smethurst (1999), Plate Tectonic modeling: Virtual Reality with GMAP. *Computer & Geosciences, 25*, 395-402.

Torsvik, T.H., J. Mosar, and E.A. Eide, (2001a), *Cretaceous-Tertiary geodynamics: a North Atlantic exercise, Geophysic. J. Int.*, *146*, 850-866.

Torsvik, T. H., R. Van der Voo, J. G. Meert, J. Mosar, and H. J. Walderhaug (2001b), Reconstructions of the continents around the North Atlantic at about the 60th parallel, *Earth and Planetary Science Letters*, *187*(1-2), 55-69, doi:10.1016/S0012-821X(01)00284-9.

Torsvik, T.H., M. A. Smethurst, K. Burke and B. Steinberger (2006), Large Igneous Provinces generated from the margins of the Large Low Velocity Provinces in the deep mantle, *Geophysical Journal International, 167*, 1447–1460.

Torsvik, T.H., S. Rousse, C. Labails, and M. A. Smethurst (2009), A new scheme for the opening of the South Atlantic Ocean and the dissection of an Aptian salt basin. *Geophysical Journal International, 177*, 1315–1333.

Trewin, N. H., and A. Hurst (2009), *Excursion Guide to the Geology of East Sutherland and Caithness*, Aberdeen Geological Society.

Tuitt, A., J. R. Underhill, J. D. Ritchie, H. Johnson, and K. Hitchen (2010), Timing , controls and consequences of compression in the Rockall – Faroe area of the NE Atlantic Margin, in *Petroleum Geology: From Mature Basins to New Frontiers - Proceedings of the 7th Petroleum Geology Conference*, edited by B. A. Vining and S. C. Pickering, Geological Society, London, Petroleum Geology Conference series, *7*, 963-977.

U

Underhill, J. R. (1991a), Implications of Mesozoic-Recent basin development in the western Inner Moray Firth, UK, *Marine and Petroleum Geology*, *8*, 359-369.

Underhill, J. R. (1991b), controls on Late Jurassic seismic sequences, Inner Moray Firth, UK North Sea: a critical test of key segments of Exxon's original global cycle chart, *Basin Research*, *3*, 79-98.

Underhill, J. R., and J. A. Brodie (1993), Structural geology of Easter Ross, Scotland: implications for movement on the Great Glen fault zone, *Journal of the Geological Society*, *150*(3), 515-527, doi:10.1144/gsjgs.150.3.0515.

Unternehr, P. (1982), *Etude structurale et cinématique de la mer de Norvège et du Groenland. Evolution du microcontinent de Jan Mayen*, Thèse de 3ème cycle de l'Université de Bretagne occidentale, 228 p.

Upton, B. G. J. (1988), History of Tertiary igneous activity in the N Atlantic borderlands, in *Early Tertiary Volcanism and the Opening of the NE Atlantic*, edited by A. C. Morton and L. M. Parson, Geological Society, London, Special Publications, *39*, 429-453.

Upton, B. G. J., C. H. Emeleus, D. C. Rex, and M. F. Thirlwall (1995), Early Tertiary magmatism in NE Greenland, *Journal of the Geological Society, London*, *152*, p. 959-964

V

Vågnes, E., R. H. Gabrielsen, and P. Haremo (1998), Late Cretaceous-Cenozoic intraplate contractional deformation at the Norwegian continental shelf: timing, magnitude and regional implications, *Tectonophysics, 300*, 29–46.

Vink, G. E. (1984), A hotspot model for Iceland and the Vøring Plateau, *Journal of Geophysical Research*, *89* (B12), 9949-9959, doi: 0148-0227/84/004B-0588505.00.

Vine, F. J., and D. H. Matthews (1963). Magnetic anomalies over oceanic ridges. *Nature*, *199*, 947–9.

Vine, F. J., and J. T. Wilson (1965), Magnetic anomalies over a young oceanic ridge off Vancouver Island, *Science, 150*, 485-489.

Vogt, P. R. (1971), Asthenosphere motion recorded by the ocean floor south of Iceland, *Earth Planet. Sci. Lett., 13*, 153–160.

Vogt, P. R., and O. E. Avery (1974), Detailed Magnetic Surveys in the Northeast Atlantic and Labrador Sea, *Journal of Geophysical Research*, *79*(2), 363-389, doi:10.1029/JB079i002p00363.

W

Wadati, K. (1928). Shallow and deep earthquakes. *Geophys. Mag. 1*, 161-202.

Wegener, A. (1912). Die Entstehung der Kontinente. *Geologische Rundschau, 3* (4), 276–292.

Wessel, P., and R. D. Müller (2007), Plate Tectonics, in *Treatise on Geophysics*, edited by G. Schubert, Elsevier, *6*, 49-98.

White, N., and B. Lovell (1997), Measuring the pulse of a plume with the sedimentary record, *Nature*, *387*, 888-891.

White, R., and D. McKenzie (1989), Magmatism at Rift Zones: The Generation of Volcanic Continental Margins and Flood Basalts, *Journal of Geophysical Research*, *94*(B6), 7685-7729, doi:10.1029/JB094iB06p07685.

White, R. S. (1988). A hot-spot model for early Tertiary volcanism, in *The N Atlantic, in Early Tertiary Volcanism and the Opening of the NE Atlantic*, edited by A. C. Morton, and Parson, L. M., Geological Society, London, Special Publication, *39*, 3-13.

White, R. S., and L. K. Smith (2009), Crustal structure of the Hatton and the conjugate east Greenland rifted volcanic continental margins, NE Atlantic, *Journal of Geophysical Research*, *114*(B2), 1-28, doi:10.1029/2008JB005856.

White, R. S., L. K. Smith, A. W. Roberts, P. A. F. Christie, N. J. Kusznir, and the rest of the iDIMM Team (2008), Lower-crustal intrusion on the North Atlantic continental margin, Nature, *452*, 460-464.

Wilson, J. T. (1965) A new class of faults and their bearing on continental drift, *Nature, 207*, 34-347.

Wilson, M. (1993), Plate-moving mechanisms – constraints and controversies, *Journal of the Geological Society, 150*, 923-926.

Wilson, R. C. L., R. B. Whitmarsh, N. Froitzheim, and B. Taylor (2001), Introduction: the land and sea approach, *Non-Volcanic Rifting of Continental Margins: A Comparison of Evidence from Land and Sea*, edited by R. C. L. Wilson, R. B. Whitmarsh, B. Taylor and N. Froitzheim, Geological Society, London, Special Publication, *187*, 1-8.

Wright, J. K., and B. M. Cox (2001), *British Upper Jurassic Stratigraphy (Oxfordian to Kimmeridgian),* Geological Conservation Review Series, Joint Nature Conservation Committee, Peterborough, *21*, 266 p.

Z

Ziegler, P. A. (1987) Evolution of the Western Approaches Trough, *Tectonophysics,137*(1-4), 341-346

Ziegler, P. A. (1988), *Evolution of the Arctic-North Atlantic and the Western Tethys*, American Association of Petroleum Geologists Memoir 43.

Ziegler, P. A. (1989a), Evolution of the North Atlantic—an overview, ,in: *Extensional Tectonics and Stratigraphy of the North Atlantic Margins,* edited by .J. Tankard, H. R. Balkwill, AAPG Memoir, *46*, 111–129.

Ziegler, P. A. (1989b) Geodynamic model for Alpine intra-plate compressional deformation in Western and Central Europe, in *Inversion Tectonics*, edited by M. A. Cooper, Geological Society, London, Special Publications, *44*, 63-85.

Ziegler, P. A. (1993), First- and second-order patterns of stress in the lithosphere: The world stress map project, *Journal of Geophysical Research, 97*, 11703-11728.

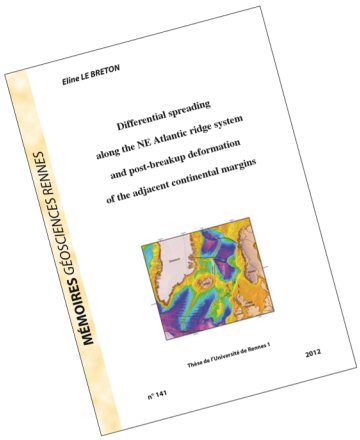

Differential spreading along the NE Atlantic ridge system and post-breakup deformation of the adjacent continental margins

Résumé

La théorie de la tectonique des plaques implique que les plaques lithosphériques soient rigides. Or les reconstructions de l'ouverture de l'océan Atlantique NE, utilisant deux plaques rigides (Eurasie et Groenland), conduisent à des zones de recouvrement. De plus, l'ouverture océanique de la zone située entre l'Islande et la zone de fracture de Jan Mayen (JMFZ) fut très complexe, incluant la formation progressive du microcontinent de Jan Mayen (JMMC) et un saut de ride. J'ai développé une méthode de reconstruction palinspastique d'ouverture de l'Atlantique NE, à partir de données d'anomalies magnétiques et de zones de fracture, méthode qui permet d'obtenir un bon ajustement des anomalies magnétiques. Le modèle prédit des différences de direction et de taux d'ouverture entre les segments océaniques. Cette ouverture différentielle a induit des mouvements décrochants sénestres le long des zones de fractures océaniques, compatibles avec le développement de structures compressives le long de la marge continentale européenne, (1) de l'Éocène inférieur à l'Oligocène supérieur, le long de la zone de fracture des îles Féroé (FFZ), et (2) de l'Éocène supérieur à Oligocène inférieur, et au Miocène, le long de la JMFZ. Aussi, j'ai mis en évidence, par une étude de terrain, une réactivation Cénozoïque en dextre de la Great Glen Fault, en Ecosse, que j'interprète comme étant due aux mouvements senestres le long de la FFZ. Je suggère également que les forces motrices proviennent du point chaud, actuellement sous l'Islande, qui était en mesure de générer une ouverture différentielle de l'Atlantique NE et les déformations compressives de la marge continentale européenne.

Mots Clés:

Atlantique Nord Est, accrétion océanique, microcontinent de Jan Mayen, zones de fracture, réactivation, compression, marge européenne, Great Glen Fault, panache mantellique islandais

Abstract

One of the main assumptions of the theory of plate tectonics is that all lithospheric plates are rigid. However, reconstructions of the opening of the NE Atlantic Ocean, on the basis of two rigid plates (Eurasia and Greenland), lead to gaps and overlaps between the plates. Also, the area between Iceland and the Jan Mayen Fracture Zone (JMFZ) had a complex spreading history, including progressive separation of the Jan Mayen Microcontinent (JMMC) and a ridge jump from the Aegir to Kolbeinsey Ridge. I have developed a method of palinspastic reconstruction of the opening of the NE Atlantic, using magnetic anomalies and fracture zones. The model ensures a good fit of the magnetic anomalies and predicts differences in the direction and rate of sea-floor spreading between the NE Atlantic ridge systems. This differential spreading generated left-lateral strike-slip deformation along oceanic fracture zones: (1) from Early Eocene to Late Oligocene, along the Faeroe Fracture Zone (FFZ); and (2) from Late Eocene to Early Oligocene, and during the Miocene, along the JMFZ. Such motion and relative rotation between the oceanic segments are compatible with the development of inversion structures on the NW European Margin at these times. Furthermore, a field study along the Great Glen Fault (GGF), NE Scotland, provided additional evidence for right-lateral reactivation of the GGF during the Cenozoic. I infer this to be a result of left-lateral slip along the FFZ. I also suggest that the driving forces came from the Iceland Mantle Plume, which was in a position to generate differential sea-floor spreading along the NE Atlantic and resulting deformation of the NW European margin.

Keywords:

NE Atlantic, seafloor spreading, Jan Mayen microcontinent, fracture zones, compression, reactivation, European margin, Great Glen Fault, Iceland plume

UNIVERSITÉ DE RENNES 1

GEOSCIENCES Rennes

Éditions de Géosciences Rennes
Université de Rennes 1 - F - 35042 Rennes Cedex
ISSN 1240-1498
ISBN 2-914375-82-4